

# Using 21st Century Technology to Better Manage Irrigation Water Supplies

*Seventh International Conference  
on Irrigation and Drainage*

Phoenix, Arizona  
April 16-19, 2013



**USCID**

*The U.S. society for irrigation and drainage professionals*

**Edited by**

Brian T. Wahlin  
WEST Consultants, Inc.

Susan S. Anderson  
U.S. Committee on Irrigation and Drainage

**Published by**

U.S. Committee on Irrigation and Drainage  
1616 Seventeenth Street, #483  
Denver, CO 80202  
Telephone: 303-628-5430  
Fax: 303-628-5431  
E-Mail: [stephens@uscid.org](mailto:stephens@uscid.org)  
Internet: [www.uscid.org](http://www.uscid.org)

## USCID

*The Mission of the United States Committee on Irrigation and Drainage is to foster sustainable, socially acceptable and environmentally responsible irrigation, drainage and flood control systems and practices for providing food, clothing and shelter to the people of the United States and the World.*

USCID is a nonprofit professional society whose members share an interest in the planning, design, construction, operation and maintenance of irrigation, drainage and flood control works; agricultural economics; water law; and environmental and social issues affecting irrigated agriculture.

USCID is the United States member of the **International Commission on Irrigation and Drainage (ICID)**, an association of more than 70 countries. Founded in 1950, ICID is a non-governmental organization dedicated to the sound and responsible management of water resources. Its central purpose is to promote the development and application of the sciences and techniques of irrigation, drainage, flood control and river channel stabilization.

USCID publishes the *USCID Newsletter*, proceedings of USCID meetings and special reports; organizes and sponsors periodic technical meetings and Conferences; and distributes ICID publications.

Since 1986, USCID has organized a number of regional, national and international meetings throughout the U.S. These meetings address contemporary issues affecting irrigated agriculture, offering a multi-disciplinary evaluation of problems and solutions.

For additional information about USCID, its meetings, publications and membership, contact

USCID  
1616 Seventeenth Street, # 483  
Denver, CO 80202  
U.S.A.

Telephone: 303-628-5430  
Fax: 303-628-5431  
E-mail: [stephens@uscid.org](mailto:stephens@uscid.org)  
Internet: [www.uscid.org](http://www.uscid.org)

USCID accepts no responsibility for the statements made or the opinions expressed in this publication.

Copyright © 2013, U.S. Committee on Irrigation and Drainage

Printed in the United States of America

Library of Congress Control Number: 2013935703

ISBN 978-1-887903-43-1

## Preface

The papers included in these Proceedings were presented during the **USCID Seventh International Conference on Irrigation and Drainage**, held April 16-19, 2013, in Phoenix, Arizona. The Theme of the Conference was *Using Technology to Better Manage Irrigation Water Supplies*. An accompanying book presents abstracts of each paper.

Since the beginning of the 21st century, advances in agricultural science and technology have been unprecedented. Science and technology can drive increased agricultural productivity and economic growth to alleviate world hunger and poverty. New technologies are critical for developing sustainable agricultural systems that can remain productive in the long run. The focus of this Conference was to emphasize key issues of science and technology transfer for the agricultural industry. The Conference provided an ideal forum for farmers and irrigation districts to learn about new technologies available in the 21st century as well as to share their ideas and experiences with others.

The authors of papers presented in these Proceedings are professionals from academia; international, federal, state and local government agencies; water and irrigation districts; and the private sector.

USCID and the Conference Chairman express gratitude to the authors, session moderators and participants for their contributions.

Brian T. Wahlin  
WEST Consultants, Inc.  
Tempe, Arizona  
Conference Chairman

# Contents

## Plenary Session

- The San Joaquin Valley: 20 Years Later ..... 1  
*James E. Ayars, Blaine R. Hanson and Bakhodir Mirzaev*
- Validation of a Decision Support System for Improving Irrigation System  
Performance..... 13  
*Kristoph-Dietrich Kinzli, David Gensler, Ramchand Oad and Nabil Shafike*
- Analysis of Water Resource Networks Using Parallel Coordinates ..... 33  
*Leah Meeks and David E. Rosenberg*
- Rapid Implementation Program (RIP) to Improve Operational Management and  
Efficiencies in Irrigation Districts in Iraq ..... 45  
*Gabriele Bonaiti and Guy Fipps*
- Impacts of Climate Change and Human Interventions on Lower Indus Basin. .... 59  
*Khero Zarif, Memon Mansoor and Bakhshal Lashari*

## Evapotranspiration

- Estimating Crop Water Use with Remote Sensing: Development of Guidelines  
and Specifications ..... 75  
*Hatim M. E. Geli, Christopher M. U. Neale, James Verdin and Gabriel  
Senay*
- Soil Scouts: Wireless Underground Soil Sensor Nodes ..... 89  
*M. Johannes Tiusanen*
- Role of Hot and Cold Pixel Concept in Remote Sensing Based Single Source  
Surface Energy Balance Algorithms..... 103  
*George Paul, Prasanna H. Gowda, P.V. Vara Prasad, Terry A. Howell,  
Robert M. Aiken and Stacy L. Hutchinson*
- Evaluating the Performance of SEBAL ET Algorithm Under Advective  
Conditions ..... 119  
*Mcebisi M. Mkhwanazi, José L. Chávez and Allan A. Andales*
- Remote Sensing of Evapotranspiration and Root Zone Water Balance  
Modeling to Estimate Groundwater Extraction in the Kaweah River  
Delta of California ..... 129  
*Byron Clark, Lindsay Hall, Larry Dotson and Grant Davids*
- Estimation of Evapotranspiration for a Drip-Irrigated Olive Orchard Using  
Multispectral Satellite Images..... 145  
*Samuel Ortega-Farias, Rodrigo Aguilar, Daniel De la Fuente, Samuel  
Ortega-Salazar, Fernando Fuentes and Carlos Poblete-Echeverría*
- Drip Irrigation Impacts on Evapotranspiration Rates in California's San  
Joaquin Valley..... 155  
*Bryan Thoreson, Deepak Lal and Byron Clark*

Irrigation-Induced Changes to the Near Surface Hydrometeorology for Sustainable Water Management . . . . .	171
<i>V. Sridhar, W.T.A. Jaksa and Korri Anderson</i>	
Sensitivity Analysis of Sensor Accuracy for the ASCE Standardized Evapotranspiration Equation . . . . .	181
<i>Kendall DeJonge</i>	
Development and Distribution of Crop Coefficients via Remote Sensing in California's San Joaquin Valley . . . . .	193
<i>Byron Clark, Deepak Lal, Kris Lynn-Patterson, Blake Sanden and Bryan Thoreson</i>	
Microclimate Effects of Urban-Fringe Irrigated Agriculture in a Desert Environment . . . . .	207
<i>Zohrab Samani, Rhonda Skaggs and Bradley Griggs</i>	

**Water Quality**

Reducing Cost of Water Quality Monitoring in Tile Drainage Outflow Using Electrical Conductivity as a Surrogate . . . . .	213
<i>Xinhua Jia and Thomas F. Scherer</i>	
Grassland Bypass Project Treatment Techniques for Reduction of Salt Discharge to the San Joaquin River . . . . .	227
<i>Joseph C. McGahan and Dennis Falaschi</i>	
The Role of Agriculture in Atmospheric Nitrogen Deposition in the Chesapeake Bay Watershed . . . . .	237
<i>William F. Ritter</i>	
The Use of Recycled Water for Irrigation of Turf and Landscape Plants: A Comparison of the Current State Regulations for Water Reuse . . . . .	249
<i>Anastasia E. M. Chirnside and Stephanie Hahn</i>	
Estimating Production and Crop Water Use of Deficit Irrigated Crops . . . . .	259
<i>Thomas J. Trout and Kedall DeJonge</i>	
Potential Nutrient Trading in the Chesapeake Bay Watershed to Meet TMDL Nutrient Load Reductions . . . . .	269
<i>William F. Ritter</i>	

**Flood Control**

What Happens if the Canal Breaks? Tools for Estimating Canal-Breach Flood Hydrographs . . . . .	281
<i>Tony L. Wahl</i>	
Hurricane Katrina: Its Impacts to the Middle Rio Grande Region of New Mexico . . . . .	297
<i>Subhas K. Shah, Ray A. Gomez and Kristoph Kinzli</i>	
Unique Methodology for Determining Ponding Floodplains Along Irrigation Canal Embankments . . . . .	309
<i>Brian Wahlin, Brent Travis, Riley Asburry and Kathryn Gross</i>	

## Technology

- Potential Savings of Water and Nutrients for the Bear River Canal Company . . . 323  
*Jonna D. van Opstal and Christopher M.U. Neale*
- Using 21<sup>st</sup> Century Technology to Grow One of the Earth’s Most Renewable Resources — Trees, on 10,440 Hectares of Drip Irrigated Tree Farm . . . . . 335  
*Nabil Mohamed*

## New Technology and Flow Measurement

- Mobile Canal Control, an Automatic Administration System for Manual Canal Operations Using Smart-Phone Technology . . . . . 349  
*Peter-Jules van Overloop, Rick Kuijten, Wouter Jan Klerk and Meinte Vierstra*
- Regulating Reservoir and Lateral Improvements Result in Spillage Reduction . . 359  
*Bryan Thoreson, Rick Massa and Tommy Ostrowski*
- Development of a Web-based GIS Management System for Agricultural Authorities in Iraq. . . . . 373  
*Gabriele Bonaiti, Dave Flahive and Guy Fipps*
- “Spot” Measurements of Flow Rate Can Be “Good Enough” for California’s Heightening Agricultural Measurement Requirements . . . . . 383  
*Jeffrey C. Davids, Brandon A. Ertis, Sean P. Early and Lewis E. Bair*
- Colorado Experience with Discharge Measurements at Parshall Flumes and Assessment of Parshall Flume Performance . . . . . 399  
*T. Ley, R. Stroud, B. Tyner, S. Veneman, G. Thrush, C. Bruner, D. Meyer, B. Boughton, L. Cunning, P. Tyler, M. Wild, B. Erosky, D. Ridnour, T. Arnett, M. Rusch, A. Gutierrez, C. Hart, G. Markus, S. Ditmars, L. Conner, J. Jaminet, A. Taillacq, J. Miller, B. Leavesley, P. DeArcos and D. Hutchens*
- Long-Throated Flume Measurement Accuracy Verification and Head Loss Calculation. . . . . 423  
*Guanghua Guan, Changde Wang and Albert J. Clemmens*
- The Use of Low-Cost Pneumatic Sensors for Water Level Detection in Permanent Stream Gauge Stations . . . . . 437  
*Kristoph-Dietrich Kinzli, David Gensler, Matthew Martinez, Aaron Morris and Zach Wohlpert*
- Event-Driven Hierarchical Control of Irrigation Canals . . . . . 457  
*Anna Sadowska, Bart De Schutter and Peter-Jules van Overloop*
- A Prototype Automated Surface Irrigation System. . . . . 473  
*Tom Gill, Dale Lentz and Khaled Bali*
- On-Farm Irrigation Efficiency in New Mexico’s Lower Rio Grande . . . . . 487  
*Rasool Ahadi, Zohrab Samani and Rhonda Skaggs*
- Unique Replogle Flume Installations at the Truckee Carson Irrigation District . . 495  
*Stuart Styles, Brandon Downing and Walter Winder*

# THE SAN JOAQUIN VALLEY: 20 YEARS LATER

James E. Ayars<sup>1</sup>  
Blaine R. Hanson<sup>2</sup>  
Bakhodir Mirzaev<sup>3</sup>

## ABSTRACT

The history of irrigation development and the need for disposal of saline drainage water in the San Joaquin Valley was described to provide background for the drainage water disposal problem that resulted from the closure of the Kesterson Reservoir. A 5 year study developed in-Valley alternatives for disposal of saline drainage water containing toxic trace elements. Eight recommendations were developed with the most effective methods being source control (improved irrigation), drainage water reuse for supplemental irrigation, discharge to the San Joaquin River, and land retirement. Several of these recommendations have been implemented on nearly 95,000 acres on the westside of the San Joaquin Valley. Several lawsuits resulted in the US Bureau of Reclamation preparing alternatives to provide drainage water disposal but did not require the construction of the selected alternatives. There have been nearly 200,000 acres of land retired on the westside of the San Joaquin Valley as part of the selected alternative.

## INTRODUCTION

The history of irrigated agriculture contains many examples of the impact of poor water management and a lack of understanding of the integrated nature of irrigation and drainage water management. From ancient history we have the loss of irrigated agriculture in the Fertile Crescent from the salination of the region between the Tigris and Euphrates Rivers in what is now modern Iraq (Gelbrud 1985). Closer to home we have the loss of thousands of acres of irrigated land on the westside of the San Joaquin Valley (SJV) due to the lack of a drainage outlet (San Joaquin Valley Drainage 1990).

The SJV is the southern portion of the Central Valley of California and is bounded on the east by the Sierra Nevada and the west by the Coast Range. The two principal geologic features of the SJV are the San Joaquin Basin that is drained by the San Joaquin River and the Tulare Basin, a hydrologically closed basin drained by the San Joaquin River only in extremely wet years. The two basins make up roughly the northern and southern halves of the SJV (San Joaquin Valley Drainage 1990).

The SJV is a gently sloping unbroken alluvial plain about 250 miles long and 45 miles wide with a mild dry climate. The combinations of climate, soils, and available water have made this one of the most productive agricultural areas in the world. Soils on the westside of the valley are derived from the marine sediments that make up the Coast Range and are high in salts and trace elements (Se, B, Mo, As) that occur in marine

---

<sup>1</sup> USDA-ARS-SJVASC, 9611 S. Riverbend Ave, Parlier, CA 93648, [james.ayars@ars.usda.gov](mailto:james.ayars@ars.usda.gov)

<sup>2</sup> University of California, Davis, 95616. [brhanson@ucdavis.edu](mailto:brhanson@ucdavis.edu)

<sup>3</sup> #1 Shayhantahur Street, UZ, [Bakhodir.mirzaev@undp.org](mailto:Bakhodir.mirzaev@undp.org)

environments. The region receives an average of 6 inches of rainfall a year and irrigation has increased the rate of dissolution of substances in the soil and the subsequent transport to shallow ground water. This has resulted in extensive areas with shallow ground water that have high concentrations of these constituents.

The conditions associated with drainage are not new and inadequate drainage and salt accumulation have been persistent problems in the Valley. Widespread acreages of grain were first planted on the westside of the valley in the 1870's and 1880's and irrigated with water from the San Joaquin and Kings rivers. This continued until the river water supply was inadequate to meet the demand. Poor natural drainage conditions coupled with rising groundwater levels and increased soil salinity led to land being removed from production and ultimately being abandoned.

Agricultural development in the 1900's was spurred by the development in the 1930's of large turbine pumps that lifted water from hundreds of feet below ground and increased the available water supply fostering increased production. However, the heavy pumping resulted in severe aquifer overdrafts and hydraulic pressure in the aquifers dropped rapidly leading to widespread land subsidence.

Initial facilities of the Federal Central Valley Project (CVP) transported water from Northern California through the Sacramento-San Joaquin Delta and the Delta Mendota canal in 1951 to irrigate 600,000 acres of land in the northern part of the San Joaquin Valley. This water was used to replace and supplement San Joaquin River water that was diverted at Friant Dam to the Southern SJV.

The CVP's San Luis Unit and the State Water Project, each authorized in 1960, began delivering Northern California water to agriculture in the southern SJV in 1968. The projects together irrigated approximately 1 million acres. The San Luis authorization also mandated construction of an interceptor drain to collect drainage water from the irrigation service area and carry it to the Sacramento-San Joaquin Delta for disposal. The feasibility report for the San Luis Unit described the drain as an earthen ditch that had the capacity to drain 96,000 acres. In 1962 the design was changed to a concrete-lined canal serving 300,000 acres. In 1964 an alternative plan added a regulating reservoir (Kesterson) to temporarily store drainage water. By the mid - 70's, the fateful decision was made to use the regulating reservoir to store and evaporate drainage water until the drainage canal was completed to the Sacramento-San Joaquin Delta.

At this same time, questions were raised about the potential effects of untreated agricultural drainage on the water quality in the Sacramento-San Joaquin Delta and the San Francisco Bay. This concern was reflected in a rider added to the CVP appropriations by Congress in 1965, which stated that "... the final point of discharge for the interceptor drain for the San Luis Unit shall not be determined until development by the Secretary of the Interior and the State of California as approved by the Administrator of the Environmental Protection Agency." This proviso remains in effect today (San Joaquin Valley Drainage 1990).

The drain was initially to be a State/Federal project but the State declined to participate and the US Bureau of Reclamation (Reclamation) began construction in 1968. By 1975, 85 miles of the main drain had been completed along with 120 miles of collector drains and the first phase of the regulating reservoir (Kesterson). In 1970 Kesterson Reservoir was included in a new national wildlife refuge managed jointly by Reclamation and U.S. Fish and Wildlife Service. Federal budget constraints and environmental concern about discharging drainage water into the Sacramento-San Joaquin Delta halted work on the drain and reservoir.

The San Joaquin Valley Interagency Drainage program was formed in 1975 to find an economically, environmentally, and politically acceptable solution to the drainage problem. The group's recommendation was to complete the drain to a discharge point near Chipp's Island. This was followed by a 1981 special study by Reclamation to fulfill the requirements for a discharge permit from the State Water Resources Control Board.

The 1983 discovery of deformities and deaths of aquatic birds at Kesterson Reservoir significantly changed the perception of the drainage problems on the westside of the SJV. Selenium poisoning was identified as the probable cause. Contamination-related problems similar to those identified at Kesterson were found in parts of the Tulare Basin, which receives irrigation water from the State Water Project, as well as from other surface and ground water supplies. Wildlife deformities and deaths were observed at several agricultural drainage evaporation ponds as well.

In 1984 the San Joaquin Valley Drainage Program (SJVDP) was established as a joint Federal and State effort to investigate drainage and drainage related problems and to identify possible solutions. The study area was primarily the westside of the SJV from the Sacramento-San Joaquin Delta on the north to the Tehachapi Mountains in the south. The area includes the Federal Delta Mendota-Canal and the San Luis Unit irrigation services area and the State Water Project service area. The principal study area was on the westside of the Valley and was broken into the Northern, Grasslands, Westlands, Tulare and Kern subareas (Fig.1). This was a \$50,000,000 research program that included university and federal scientists and consultants.

In 1985, the Secretary of the Interior ordered that discharge of subsurface drainage to Kesterson be halted, and feeder drains in the Westlands Water District leading to the San Luis Drain and reservoir be plugged. The reservoir was closed, vegetation plowed under and the low-lying areas filled in 1988. Plugging of the feeders resulted in the loss of drainage service on 40,000 acres of land with subsurface drains located south of Mendota, California.

In 1986 farmers in the San Luis Unit sued the federal government for not providing a drain as was mandated in the original plan for the Unit. In 1986 a federal judge directed Reclamation to develop and implement a drainage plan. This ruling is commonly called the Barcellos Judgement.

The final report of the SJVDP “A Management Plan for Agricultural Subsurface Drainage and Related Problems on the Westside San Joaquin Valley” was issued in 1990 with 8 recommendations for management of the drainage and drainage-related problems on the westside of the SJV (San Joaquin Valley Drainage 1990). This report was dubbed the Rainbow Report.

### Recommendations:

1. Source control: This consisted of mainly on-farm irrigation improvements to reduce deep percolation losses and thus total drainage water e.g. improved irrigation scheduling, improved irrigation systems, improved irrigation system management.

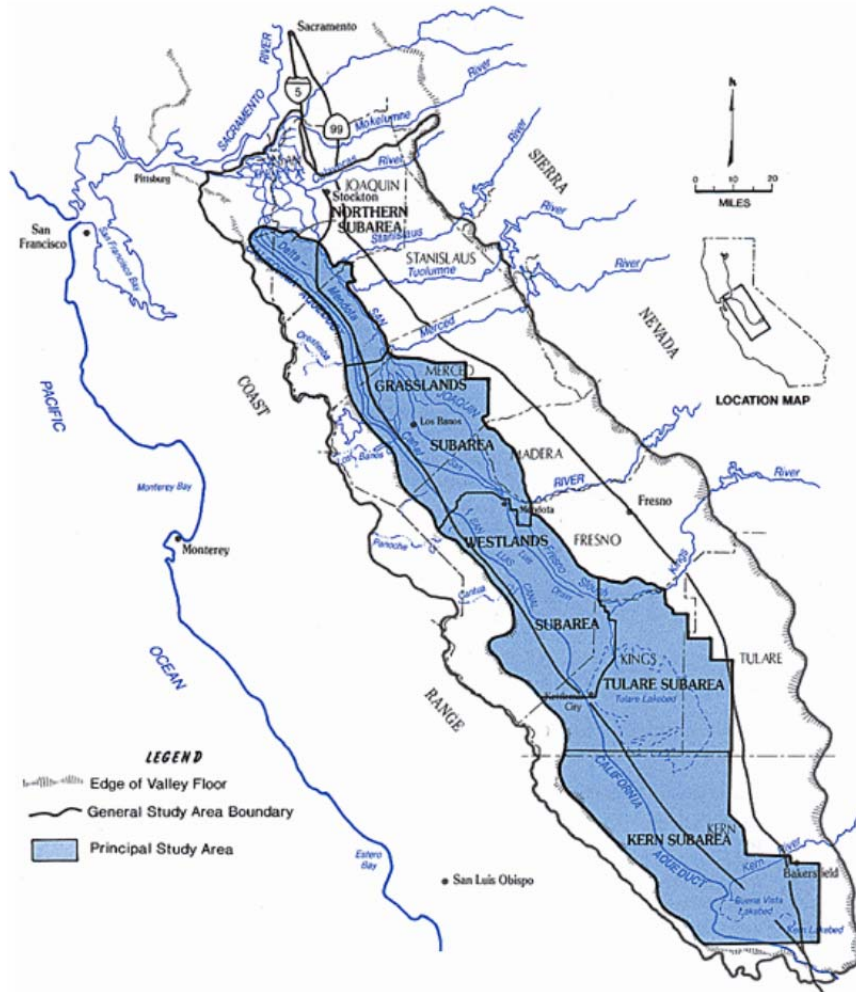


Figure 1. The San Joaquin Valley Drainage Program study area (SJVDP, 1990)

2. Drainage reuse: This is a system of capturing drainage water and reusing for supplemental irrigation on progressively more salt tolerant crops. This can be on a field by field basis or a regional system.

3. Evaporation system: This uses drainage-evaporation ponds planned for storage and evaporation of residual drainage water from the reuse systems.
4. Land retirement: This requires the cessation of irrigation on areas with underlying shallow ground water containing elevated levels of selenium and soils that are difficult to drain.
5. Ground water management: This is planned pumping from deep within the semi-confined aquifer in places where near-surface water tables can be lowered and water pumped that is a suitable quality for irrigation and wildlife habitat.
6. Discharge to the San Joaquin River: This involves controlled and limited discharge of drainage water from the San Joaquin Basin portion of the study area to the San Joaquin River while meeting water quality objectives.
7. Protection, restoration, and provision of substitute water supplies for fish and wildlife habitat: This requires providing freshwater supplies to substitute for drainage contaminated water previously used on wetlands and to allow protection and restoration of contaminated fisheries and wildlife habitat.
8. Institutional change: These changes included tiered water pricing, improved scheduling of water deliveries, water transfers and marketing and formation of regional drainage management organizations to aid in implementing other plan components.

Individual recommendations were proposed for each study area as were deemed appropriated for conditions within the area.

As a follow up to the Rainbow Report, the San Joaquin Valley Drainage Implementation Program was established in 1991 to further encourage and promote the recommendations in the Rainbow report. The participants included Reclamation, US Fish Wildlife Service, US Geological Service, Natural Resource Conservation Service and from California the Department of Food and Agriculture, Department of Water Resources, Department Fish and Game, and State Water Resources Control Board. The agencies signed a Memorandum of Understanding in December agreeing to use the Rainbow report as a guide to correct drainage problems in the SJV. The result of the collaboration was a report in 1998 that evaluated the current conditions and identified action and costs. However, funding sources were not identified.

There have been a series of lawsuits and studies since the completion of the Rainbow report. In 1992 as part of the Barcellos Judgment Reclamation submitted an EIS for the San Luis Drainage Program that suggested several in-valley approaches to the drainage issue. It also stated that “the social and environmental unacceptability of “of completing a drain “precludes further consideration.” The Court rejected the EIS as not complying with the judgment. In 1994 Judge Oliver Wanger of the US District Court ordered Reclamation to apply for a discharge permit for the San Luis Drain to the San Francisco Bay Delta. This was followed in 1995 by an appeal from the Department of Interior,

Contra Costa County, Contra Costa County Water District and environmental groups of the Wanger decision.

In 2000 the US Court of Appeals determined that the Reclamation did not have to build a drain, but must propose a plan to provide drainage service. In 2001 Reclamation developed a plan of action outlining its proposed efforts to provide drainage service considering a range of options. The first phase was a re-evaluation consistent with the Plan of Action that identified a list of preliminary alternatives meeting the Court Order to provide prompt drainage service to the Unit. This resulted in the Preliminary Alternatives Report (PAR), San Luis Unit Drainage Feature Re-evaluation published in 2001. The alternatives described in the PAR would provide the drainage service as required by the Court using proven technologies.

The second phase of the re-evaluation was the preparation of the Plan Formulation Report (PFR) that included the land requiring drainage, and the anticipated quantity and quality of the drainage water requiring service. Alternatives were formulated screened and evaluated. The final set of alternative plans and selected proposed actions were published in 2002. The third phase further refined the components of the alternatives and provided engineering detail and the completion of the environmental review of the alternatives.

In May of 2003 the Westside Regional Drainage Plan was developed as a collaborative effort between the San Luis Unit water districts and the San Joaquin River Exchange Contractors Authority to provide relief in portions of the Unit and adjacent areas. Key elements of the plan include adaptive management to perfect the final drainage management strategy, land retirement of up to 200,000 acres, groundwater management, source control, regional reuse, treatment and salt disposal. The plan calls for identification of sound projects to manage drainage and an accelerated implementation schedule to comply with impending regulatory constraints.

As a result of stakeholder input and the Regional drainage plan, Reclamation broadened the scope of its analysis to include land retirement as a component of drainage service alternatives. In 2004 Reclamation submitted an "Amended Plan of Action for Drainage to the San Luis Unit". The amendment indicated that Reclamation would continue to refine and evaluate all 5 alternatives in the PFR for inclusion in the EIS and would consider land retirement as well as a method to control drainage need. The final EIS provide 7 drainage service Action Alternatives for the Unit and was completed in 2006.

Reclamation's decision was to select the In-Valley/Water- needs, Land-Retirement Alternative which is closely aligned with the Westside Regional Drainage Plan. It includes drainage reduction measures, drainage water reuse, treatment facilities and evaporation ponds as well as retiring 194,000 acres of irrigated land. The Record of Decision was posted in 2007.

Reclamation sent the new Feasibility Report to Congress in July 2008 that presented the relative economic analysis of the drainage plan confirming the need for new authorizing

legislation to increase the appropriations ceiling for funding beyond what was authorized by the 1960 San Luis Act. The estimated cost to fully implement the Record of Decision (ROD) was \$2.7 billion. Selecting the “In-Valley/Water Needs/Land Retirement Alternative” fulfilled the requirements of the Court order that Reclamation has a statutory duty to provide drainage service to the San Luis Unit.

In 2009 as part of the on-going litigation the Department of Justice on behalf of the Department of Interior advised the Court that while Interior could not implement the entire San Luis Unit Drainage ROD, a sufficient appropriation ceiling allowed Interior to construct one sub-unit of the drainage facilities in the Westlands Water District (WWD). A Supplemental Status Report filed in 2011 concluded that a proposed phase approach to providing drainage service in the central sub-unit of the WWD is feasible and support the WWD’s request to proceed with Phase 1 implementation of the construction under the 2007 ROD. As result, a demonstration reverse osmosis plant is being constructed in the Panoche Drainage District as part of the San Luis Drainage Feature Re-evaluation record of decision.

### **CURRENT CONDITIONS**

As was demonstrated in the introduction, the path to providing drainage service to the westside of the SJV has been a contentious and torturous one without an end in sight. The Westside Regional Drainage Plan was developed specifically to cover activities in the Grasslands and Westlands Drainage Areas and the eight recommendations from the Rainbow Report were evaluated and selected for inclusion in drainage water management in each of the sub-units based on existing conditions within the unit.

The Grasslands Drainage Area includes the San Luis Unit of the Central Valley Project (CVP) and the Exchange Contractors subareas with the following units: Broadview Water District, Charleston Drainage District, Firebaugh Canal Water District, Pacheco Water District, Pacheco Drainage District, Widren Water District, and the Camp 13 Drainage District located in part of the Central California Irrigation District. This group was formed initially to implement the Grassland Bypass Project. There are approximately 97,000 acres of irrigated farmland in the area that require drainage service.

Drainage from this area had previously discharged to the San Joaquin River through channels that were used to deliver water to seasonal wetlands that are a part of the Pacific Flyway. The Grasslands Bypass was designed to channel water around the wetlands impacted by the drainage water using a portion of the San Luis Drain that had been closed by order of the Secretary of the Interior. Implementation of the bypass required negotiations between the San Luis and Delta Mendota Authority, US Environmental Protection Agency, USFWS, California Department of Fish and Game, Central Valley Regional Water Quality Control Board, Environmental Defense Fund, Contra Costa County, and Contra Costa Water District. The initial agreement was completed in 1995 for 5 years but that was extended for another 8 years through 2009 and it has subsequently been extended for another 10 years.

The total load being discharge through the bypass is shown in Fig. 2. The data show that with the exception of a wet year in 1998 that the selenium (Se) load goals were met and in fact were below the allocations for discharge into the San Joaquin River. The total maximum monthly load (TMML) values are given for the remaining part of the agreement to 2019 for each of the potential water conditions described in the agreement. The Grasslands Drainage Area is the only entity that has the capability to discharge into the San Joaquin River and it is apparent that the privilege will be eliminated in the next few years.

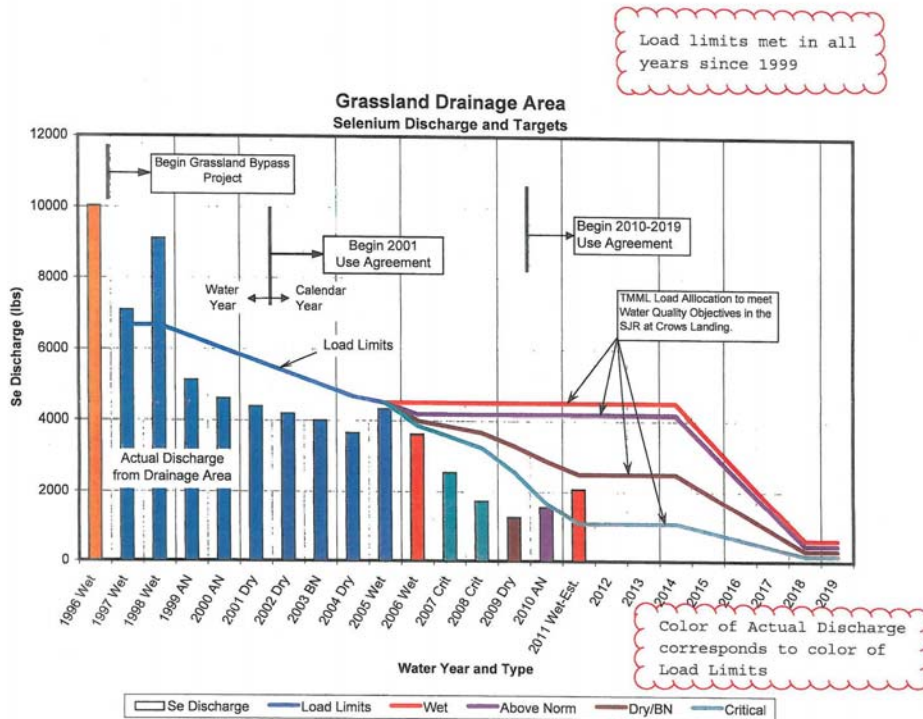


Figure 2 Actual selenium discharge from the Grassland Drainage Area from 1996 to 2011 and the load limits for Wet years, flow above normal (Above Norm), dry below normal (Dry B/N) and Critical low flow years from 2011 to 2019.

As a result, they are developing a water reuse system dubbed the San Joaquin River Water Quality Improvement Project (SJRIIP). This project was begun in 2001 on 1821 acres of land used to irrigate salt tolerant crops. The site is projected to increase in size to approximately 4000 acres to accommodate the loss of drainage to the San Joaquin River. Crops being irrigated include salt tolerant forages and pistachios. The irrigation water is a blend of drainage water and good quality water.

The Panoche Water and Drainage District has been a leader in the implementation of improved drainage water management. They have been managing the Grassland Bypass Project during its existence. The District has seen significant changes in the cropping

patterns and irrigation systems since the beginning of the problem in 1984. In an inventory in 1986 there were approximately 2100 acres irrigated by high pressure sprinkler, 3250 acres with furrow from gated pipe, 36,750 with furrow from a head ditch, and 30 acres by surge flow. Currently, the district is 98% irrigated with drip irrigation. In 1986 there were approximately 20 crops grown with processing tomatoes, cotton, sugar beet, wheat and alfalfa being the principal crops. The current cropping is primarily in permanent horticultural crops e.g. grapes and almonds. The shift has accounted for a significant reduction in drainage flow throughout the District. Panoche is one of the largest districts in the Grasslands Drainage Area and improved water management has been a part of the reduction in total Se load over the years.

Another component in the success of the Grasslands in meeting the discharge limit is land retirement. The Broadview Water District which was contributing to the drainage flow was sold to the Westlands Water District and the entire district (10,000 acres) was fallowed. The water allocation was then transferred to the Westlands Water District and the entire area is available for lease by dry land agriculture.

The Westlands Water District makes up most of the Westland subarea shown in Fig. 1 and contains approximately 600,000 acres of irrigated crop land. Drainage from the District was solely through the San Luis Drain that has been closed. The allocation to the WWD is approximately 2.2 acre-feet per acre prior to the allocation of 20% of the water supply to environmental restoration of the San Joaquin – Sacramento Delta as a result of the Central Valley Project Improvement Act of 1991. The combination of reduced water supply and drought significantly reduced the drainage volumes in the District.

There has been significant adoption of improved irrigation practices and irrigation systems. Subsurface drip irrigation is routinely used on processing tomatoes and horticultural crops. Center pivot irrigation systems have been installed in several areas of the valley. The main strategy has been to change cropping to account for water supply limitations.

The data in Fig. 3 show that crops that are large water users (cotton) with low value were dropped while crops with high economic value (tomato) were retained and in some cases increased (almond). Fallowing of land was also part of the strategy to accommodate reduced water supply. Cotton is irrigated primarily by surface irrigation while tomato is irrigated using drip. This combination results in reduced deep percolation and the need for drainage.

Reuse of saline drainage water is another strategy that was implemented in the WWD on a farm by farm basis. The Red Rock Ranch implemented an integrated on-farm drainage management (IFDM) system on one section as part of a demonstration/research project. Three quarter sections were used to grow salt sensitive crops. Deep percolation was collected from the 3 quarters and used to irrigate the fourth quarter. Water applied to the fourth quarter was used to irrigate halophytic plants. Drainage from the fourth quarter was evaporated on a rock bed.

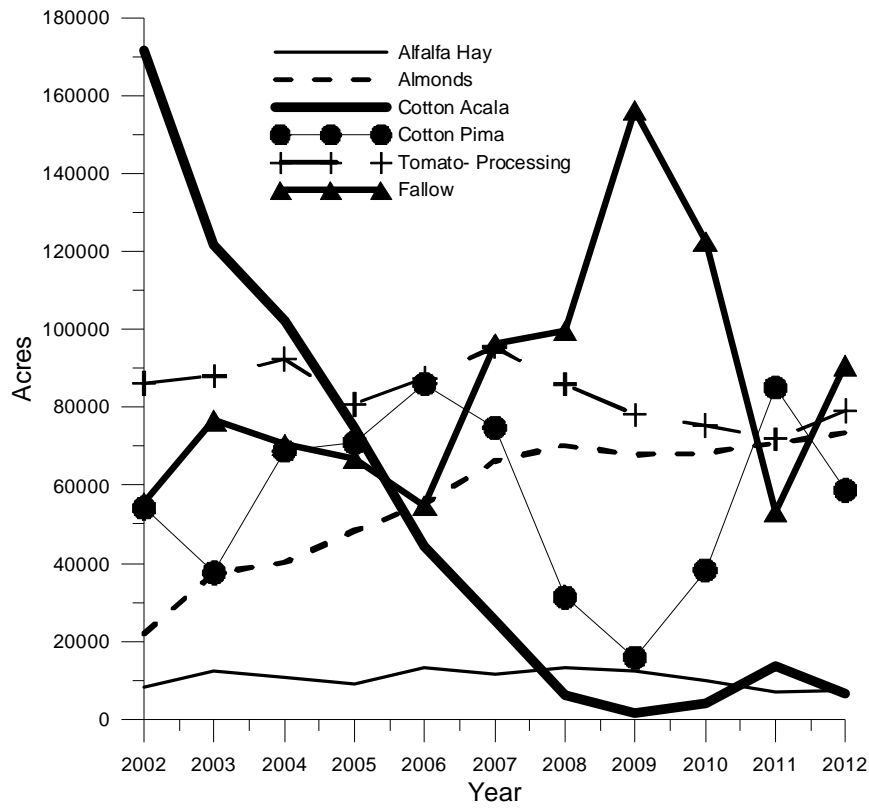


Figure 3. Cropping patterns in Westland Water District from 2002 to 2012.

The total area in the IFDM system devoted to non-productive agriculture was less than 6% of the area being served. This compares to an estimated 10% of land previously considered as necessary for evaporation. The water balance for the IFDM system showed that the drainage flow was approximately 0.7% of the total applied water. The IFDM system was demonstrated to be an effective method for drainage water disposal. The remaining problem is the disposal of the accumulated salt on the evaporation bed.

### SUMMARY

The Grasslands Drainage Area participants and the Westlands Water District have implemented nearly all the recommendations found in the Rainbow Report. Source control, drainage water reuse, and land retirement are the principal actions that were implemented in both areas. The Grasslands Drainage Area is a regional drainage solution. Disposal of water to the San Joaquin River is currently being practiced but this has a limited life span. Institutional arrangements include: improved irrigation scheduling and tiered water pricing being practiced on a limited scale. The Grasslands Drainage Area is investigating the potential for deep ground water pumping to manage shallow groundwater.

Source control, drainage water reuse and land retirement are responsible for reducing the drainage water disposal volumes by nearly 90%. However, there still is the need to develop methods for disposal of the accumulated salt in the soil and in any evaporation structure that is part of the process. This will be particularly true for the brine developed from the reverse osmosis plant that will be treating drainage water. The basic recommendations have wide applicability for implementation in arid irrigated areas throughout the world.

### ACKNOWLEDGEMENTS

The authors relied heavily on several documents when compiling the manuscript and either quoted nearly verbatim or paraphrased paragraphs from those documents. We acknowledge the authors of those reports. In particular, several sections describing the development of agriculture and the problems and geology of the SJV in the final report of the San Joaquin Valley Drainage program were included in the introduction. The reports prepared by the US Bureau of Reclamation were also significant sources for the preparation of the introduction. Panoche Water District also provided information used in the preparation of the manuscript.

“The U.S. Department of Agriculture (USDA) prohibits discrimination in all its programs and activities on the basis of race, color, national origin, age, disability, and where applicable, sex, marital status, familial status, parental status, religion, sexual orientation, genetic information, political beliefs, reprisal, or because all or part of an individual's income is derived from any public assistance program. (Not all prohibited bases apply to all programs.) Persons with disabilities who require alternative means for communication of program information (Braille, large print, audiotape, etc.) should contact USDA's TARGET Center at (202) 720-2600 (voice and TDD). To file a complaint of discrimination, write to USDA, Director, Office of Civil Rights, 1400 Independence Avenue, S.W., Washington, D.C. 20250-9410, or call (800) 795-3272 (voice) or (202) 720-6382 (TDD). USDA is an equal opportunity provider and employer.”

### REFERENCES

Anonymous (2003). Westside Regional Drainage Plan. B. W. D. San Joaquin River Exchange Contractors Water Authority, Panoche Water District, Westlands Water District.

Gelbrud, D. E. (1985). "Managing salinity, lessons from the past." *Journal of Soil and Water Conservation* 40(4): 329-331.

Mirzaev, B. (2009). Drainage Management *..just* Water Use Efficiency, Investigation of Water Management Strategies in Arid Regions San Joaquin Valley, California. Irrigation and Water Engineering Group. Wageningen, Netherlands, Master of Science: 166.

San Joaquin Valley Drainage, P. (1990). The problem. [A Management Plan for Agricultural Subsurface Drainage and Related Problems on the westside San Joaquin](#)

Valley. U. S. D. o. Interior and A. California Resources. Sacramento, California, California Department of Water Resources: 183.

# VALIDATION OF A DECISION SUPPORT SYSTEM FOR IMPROVING IRRIGATION SYSTEM PERFORMANCE

Kristoph-Dietrich Kinzli<sup>1</sup>  
David Gensler<sup>2</sup>  
Ramchand Oad<sup>3</sup>  
Nabil Shafike<sup>4</sup>

## ABSTRACT

To address water shortage and improve water delivery operations, decision support systems have been developed and utilized throughout the United States and the world. One critical aspect that is often neglected during the development and implementation of decision support systems is validation. Neglecting validation can result in flawed water distribution and rejection of the DSS by water users and managers.

This paper presents the results of a significant validation effort for a DSS in the Middle Rio Grande Conservancy District (MRGCD). The validation resulted in a refined application efficiency of 45%, a refined readily available moisture remaining when farmers irrigate value of 20% and a Nash Sutcliffe Modeling Efficiency of 0.86 for soil moisture depletion patterns. Overall, the validation and refinement of input parameters resulted in a DSS model that accurately predicts ET and can be used to schedule water delivery. The refinement of the DSS input parameters resulted in an increased 15,600AF diversion suggested by the DSS, indicating that the original DSS input parameters would have shortchanged farmers in the MRGCD. The study showed that validation of a DSS is crucial if such a program is to be successfully utilized to deliver irrigation water.

## INTRODUCTION

Decision support systems (DSS) for irrigation system management have many benefits that include water savings and development of optimal water delivery schedules, while maintaining and possibly improving farmer productivity. To address water shortage and improve water delivery operations DSS have been developed and utilized throughout the United States and the world (Oad et al. 2009). DSS are most useful in irrigation districts where water rights have not been adjudicated and managers cannot anticipate water demand in advance (Oad et al. 2009). In lieu of adjudicated water rights, DSS can be used to predict crop depletions using weather data and schedule water delivery based on crop demand.

---

<sup>1</sup> Assistant Professor, Department of Environmental and Civil Engineering, Florida Gulf Coast University, Fort Myers, FL; [kkinzli@fgcu.edu](mailto:kkinzli@fgcu.edu) (Corresponding author)

<sup>2</sup> Water Operations Manager, Middle Rio Grande Conservancy District, Albuquerque, NM  
[dgensler@mrgcd.com](mailto:dgensler@mrgcd.com)

<sup>3</sup> Professor, Department of Civil and Environmental Engineering Colorado State University, Fort Collins, CO,  
[oad@engr.colostate.edu](mailto:oad@engr.colostate.edu)

<sup>4</sup> Hydraulic modeler, New Mexico Interstate Stream Commission, Albuquerque, NM [nabil.shafike@state.nm.gov](mailto:nabil.shafike@state.nm.gov)

The Middle Rio Grande Conservancy District (MRGCD) in central New Mexico represents such an un-adjudicated water district. To address water management concerns associated with endangered species and drought, the MRGCD in conjunction with the New Mexico Interstate Stream Commission (NMISC) sponsored the development of a DSS to anticipate and effectively manage water demand (Oad et al. 2009). The DSS for the MRGCD was developed over a period of four years from 2004 to 2008 to organize information about water demand in a service area and then schedule available water supplies to meet irrigation demands. The MRGCD DSS was formulated using three modules. The development of the MRGCD DSS and the formulation of the programming logic are discussed in detail in Oad et al. (2009).

The conceptual problem addressed by the MRGCD DSS for the irrigation system, is how best to route water supply in a main canal to its laterals to best meet predicted or scheduled demand, while minimizing required diversions from the river. The solution to this problem is “demand driven,” in the sense that it is based on a realistic estimation of water demand. The water demand in a lateral canal service area, or for an irrigated parcel, can be predicted using the MRGCD DSS throughout the season by evaluating crop water requirements based on information on the irrigated area, crop type, and soil characteristics. The important demand concepts are: when is water needed for an irrigation (irrigation timing), for how long is the water needed during an irrigation event (irrigation duration), and how often must irrigation events occur for a given service area (irrigation interval) (Oad et al. 2009). In order to develop the MRGCD DSS it was necessary to make several assumptions of input parameters. These assumptions included on farm application efficiency (50%), readily available moisture (RAM) remaining before irrigation occurs (0%), soil moisture depletion patterns, and the rates of canal conveyance loss. These assumptions were necessary because no studies had been completed in the MRGCD to accurately determine the required input parameters (Kinzli, 2010). Although DSS have a huge utility as a water management tool, improperly validated programs often result in flawed management decisions and inequitable water distribution. Flawed water distribution schedules also result in the outright rejection of the DSS as a water management tool when water users are short changed. To make the MRGCD as robust a model as possible input parameters had to be validated.

In order to obtain data necessary to validate the assumptions of on-farm application efficiency, RAM remaining, and soil moisture depletion patterns, a field study was conducted in 2008 and 2009. Canal conveyance loss was determined in a separate study in 2008 by Kinzli et al. (2010).

### **INSTRUMENTATION**

In order to obtain data necessary to validate the assumptions of on-farm application efficiency, RAM remaining at the start of an irrigation event, and soil moisture depletion patterns, field instrumentation was necessary. To measure the DSS input parameters in the MRGCD service area, eight representative farms were chosen in Bernalillo and Valencia Counties. Farmers were asked to volunteer for this study through the MRGCD website, the local newspapers, and their ditch-riders. The fields were chosen based on

the following criteria: that they had a well distinguished permanent head ditch, where the amount of water applied could be measured, and that the field was a basin with no irrigation water leaving the downstream end of the field as surface runoff.

The reason for selecting basins was that the measurement of surface runoff from furrows and borders is difficult and often associated with high error rates. Additionally, the MRGCD irrigation policy states that there should be no surface runoff from fields, and therefore, a majority of the fields in the valley are irrigated basins. Of the eight selected fields, four were planted in alfalfa and four were planted in grass hay. These two crops represent over 85% of the irrigated acreage in the MRGCD.

The selected fields were located across a 50 mile section of the Middle Rio Grande Conservancy District in the Albuquerque and Belen Divisions. Three fields were located in the Albuquerque Division, specifically in Corrales near Alameda, Candelaria Farms, and Prices Dairy in the South Valley. Five fields were located in the Belen Division, specifically in Bosque near Veguita, on the south side of Belen near Highway 6, and three fields were located in Los Lunas/Los Chavez area. The fields were also selected to be on separate laterals in order to validate DSS model assumptions across eight separate service areas (Table 1).

Table 1. Instrumented Farm Fields with Data Logger ID, GPS Coordinates, Associated Lateral, and Acreage

Logger ID	X	Y	Lateral	Acreage
1	1484677.48	1353586.40	New Belen Acequia	9.85
2	1490282.29	1323593.67	Old Jarales Acequia	12.61
3	1486224.65	1358421.17	Gabaldon Acequia	10.78
4	1481349.13	1296901.33	Sabinal 1 Acequia	4.4
5	1515285.83	1515745.08	Summerford lateral	3.655
6	1511950.56	1504210.90	Duranes Acequia	8.97
7	1490862.85	1354494.11	Los Chavez Acequia	4.49
8	1510869.86	1447705.89	Williams lateral	8.08

Each of the eight fields was instrumented with broad crested weirs (designed using the Bureau of Reclamation software Winflume) and Hobo pressure transducers to determine total water volume applied during irrigation events remotely. Additionally, each field was instrumented with ECH2O EC-20 capacitance type soil moisture sensors to monitor crop depletions. The details of the field instrumentation can be found in Kinzli (2012). To ensure that the soil moisture measurements were as accurate as possible a calibration was performed for each sensor installation using the methodology presented by Kinzli et al. (2011). Through the instrumentation of the farm fields it was possible to create a daily water balance for each field and determine on-farm application efficiency, RAM remaining, and quantify farmer practices.

### ON FARM APPLICATION EFFICIENCY

Since the inception of the DSS in 2004, a global value of 50% for the on-farm water application efficiency was assumed as no previous studies had been conducted on application efficiency. From the instrumented fields it was possible to refine this value in the DSS. For the purpose of this analysis the on-farm application efficiency was defined as the water replenished for crop use divided by the total water applied. This definition of application efficiency focuses only on water for crop growth and does not include any water used for leaching salts out of the root zone. The reason that application efficiency was defined in this manner is that the DSS calculates irrigation schedules based on replenishing the soil moisture for crop growth and does not include any leaching requirements. Additionally, soil salinity values in the MRGCD are quite low and leaching salts is not a concern of irrigators.

In order to determine application efficiency the broad crested weirs and pressure transducers installed on the eight farm fields (Kinzli, 2012) were used to determine the total water delivered for each irrigation event during the 2008 and 2009 irrigation seasons. The total water applied for each irrigation event was calculated in cubic feet and inches for 144 irrigation events on the eight instrumented fields during the 2 year study.

Once the total water applied for an irrigation event was calculated, it was possible to calculate the depth of water applied per unit area by dividing the total volume applied by the acreage of the basin that was irrigated. This resulted in a depth of water in inches applied over the monitored field. Additionally, irrigation event number, the date, duration, and average flow rate for each irrigation event were recorded. Table 2 displays the logger ID, irrigation event, irrigation date, total water applied, and inches applied for ten of the 144 irrigation events.

Table 2. Logger ID, Irrigation Event, Date, Total Water Applied and Depth Applied for 10 of 144 Irrigation Events

Logger ID	Irrigation Event	Date	Total Water Applied (ft <sup>3</sup> )	Depth Applied (inches)
1	1	4/14/2008	157190	6.95
1	2	5/5/2008	266004	7.44
1	3	6/1/2008	325216	9.09
1	4	6/24/2008	149748	4.19
1	5	8/6/2008	150338	4.2
1	6	9/12/2008	125121	3.5
1	1	4/13/2009	112475	3.15
1	2	5/11/2009	148812	4.16
1	3	6/18/2009	173791	4.86
1	4	7/20/2009	113443	3.17

The next step in calculating the application efficiency was determining the water available for crop use that was replenished during each irrigation event. This was possible using the data collected from the installed EC-20 soil moisture sensors. The soil moisture sensor data, corrected using laboratory calibration equations for each specific sensor installation, provided the volumetric soil moisture content before the irrigation event and after field capacity was reached (Kinzli et al. 2011). The difference between the volumetric water content before the irrigation event and field capacity represented the amount of water stored in the root zone for beneficial crop use. This data was recorded at both the 8 inch and 24 inch sensor location for each field for each irrigation event. To calculate the water stored in the soil for beneficial crop use in inches the 8 inch sensor was deemed to be representative of the first 16 inches of root depth for both the alfalfa and grass hay fields. The 24 inch sensor was chosen to represent the subsequent 20 inches of root depth for grass hay and the subsequent 32 inches for alfalfa. For grass hay and alfalfa this represented a 36 inch and 48 inch effective total root zone, respectively. These values were chosen based on 12 years of research by Garcia (2008) at the Natural Resource Conservation Service (NRCS), conducted in the Middle Rio Grande and Mesilla Valleys in New Mexico to determine the root depths that were effectively able to utilize and deplete soil moisture.

Once the effective root depth was determined, the root depth associated with each sensor and crop type was multiplied by the difference between the volumetric water content at field capacity and volumetric water content before the irrigation event took place for the 8 inch and 24 inch sensor. This yielded the water available for crop use in inches for the upper 16 inches and either lower 20 inches for grass hay or 32 inches for alfalfa. These two values were added together to give the total water in inches available for crop use applied during the irrigation event. The total water available for crop use was then divided by the total water applied to determine application efficiency. The application efficiency for all 144 irrigation events was calculated from the collected data. Table 3 displays the results of the application efficiency analysis for 10 of the 144 irrigation events.

Table 3. Irrigation Event, Date, Depth Applied, Moisture Applied for Beneficial Crop Use and Application Efficiency for 10 of 144 Irrigation Events

Logger ID	Irrigation Event	Date	Depth Applied (inches)	Moisture Applied for Crop Use (inches)	Application Efficiency (%)
1	1	4/14/2008	6.95	4.64	67%
1	2	5/5/2008	7.44	1.92	26%
1	3	6/1/2008	9.09	3.36	37%
1	4	6/24/2008	4.19	2.24	53%
1	5	8/6/2008	4.2	1.76	42%
1	6	9/12/2008	3.5	2.4	69%
1	1	4/13/2009	3.15	2.56	81%
1	2	5/11/2009	4.16	2.56	62%
1	3	6/18/2009	4.86	2.56	53%
1	4	7/20/2009	3.17	1.12	35%

The data collected displayed significant variability with a range in application efficiency from 8% to 100%. The mean value for all 144 irrigation events was found to be 44.4% with a standard deviation of 24.4%. The calculated mean value represented a slightly lower application efficiency value than the 50% assumed in the DSS.

To examine the variability in the collected data and determine a single value to utilize in refining the DSS, a histogram of the collected data was created. Figure 1 displays the histogram of application efficiency.

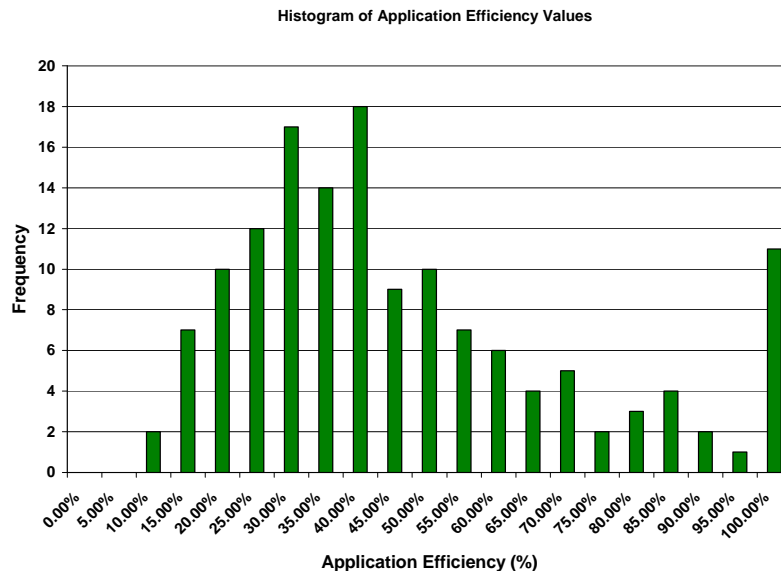


Figure 1. Histogram of Application Efficiency

The developed histogram displayed a nearly normal distribution about the mean value but was skewed slightly to the right due to 11 irrigation events with an application efficiency

of 100%. Irrigation efficiencies of 100% represented farmers that were inadvertently practicing deficit irrigation. From the developed histogram it became clear that the majority of irrigation events exhibited application efficiencies reflected by the calculated mean value.

Using the developed histogram it was possible to calculate the probability that the application efficiency would fall within one standard deviation of the calculated mean. The probability that the application efficiency of an irrigation event would fall within one standard deviation was found to be 112 out of 144 irrigation events resulting in a probability value of 0.78. This indicates that 78% of the irrigation events were within one standard deviation of the calculated mean. Based on the analysis of the histogram a revised value for application efficiency of 45% was incorporated in the DSS, which allowed for more precise representation of farmer practices. During the years of 2008 and 2009 the total irrigation diversion for the MRGCD calculated by the DSS using an application efficiency of 50% was 312,000 acre-feet. The 5% decrease in application efficiency found during this study represents a water volume of 15,600 acre-feet that farmers would not have received using the assumed 50% on-farm application efficiency.

### RAM REMAINING BEFORE IRRIGATION

The assumption used during the development of the DSS for soil moisture remaining before irrigation takes place was that the entire readily available moisture is depleted before farmers in the MRG Valley irrigate their fields. From the data collected during the 2008 and 2009 irrigation season it was possible to calculate the actual RAM remaining at the beginning of irrigation events, as well as the management allowed depletion factor (MAD) used by farmers.

The first step in determining RAM remaining when irrigation occurred was to determine the Total Available Moisture (TAM) for each instrumented field. This was accomplished by subtracting the volumetric water content at the wilting point from the volumetric water content at field capacity and multiplying this value by the root depth represented by each sensor. To calculate the TAM the 8 inch sensor was deemed to be representative of the first 16 inches of root depth for both the alfalfa and grass hay fields (Garcia, 2008). The 24 inch sensor was chosen to represent the subsequent 20 inches of root depth for grass hay and the subsequent 32 inches for alfalfa (Garcia, 2008). For grass hay and alfalfa this represented a 36 inch and 48 inch effective root zone, respectively. This calculation was carried out for the 8 inch and 24 inch sensor. The addition of these values provided the TAM for each field. The equation used to calculate the TAM for each field is displayed as Equation 1.

$$[(FC_{8''} - WP_{8''}) * RZ_{\text{represented by 8'' sensor}} + (FC_{24''} - WP_{24''}) * RZ_{\text{represented by 24'' sensor}}] \quad (\text{Eq. 1})$$

The field capacity used in Equation 1 was determined from the collected soil moisture sensor data, corrected using the developed laboratory calibration equations (Kinzli et al. 2011), as a sharp break in the soil moisture depletion curves was observed as gravitational drainage ceased. The field capacity values were compared to lab results of a pressure plate analysis conducted at the Colorado State University soils lab to ensure accuracy. The wilting point was determined through pressure plate analysis for each individual sensor installation (Kinzli, 2010). The TAM was calculated for a total of 144 irrigation events as the field capacity changed slightly during the irrigation season due to compaction from field trafficking and soil expansion from irrigation events.

The next step was to calculate the TAM utilized by crops between each irrigation event. The difference between the volumetric water content before the irrigation event and field capacity represented the amount of TAM depleted by crops between irrigation events. This value was previously calculated in the analysis of application efficiency as the water available for crop use replenished by irrigation events. Once the TAM and the TAM utilized between irrigations was calculated, it was possible to determine the MAD by dividing the TAM utilized by the total TAM. From the 144 irrigation events it was determined that the mean MAD used by farmers in the MRG Valley was 0.41 for grass hay and 0.34 for alfalfa. This indicates that farmers are averse to stressing their crops and irrigate frequently before a significant amount of the available soil moisture is depleted. These values were used to refine the MAD used under the crop characteristics tab in the DSS. Table 4 displays the MAD values calculated for 10 of 144 irrigation events.

Table 4. Logger ID, Irrigation Event, Date, and MAD Calculated for 10 Irrigation Events

Logger ID	Irrigation Event	Date	MAD
1	1	4/14/2008	0.6
1	2	5/5/2008	0.24
1	3	6/1/2008	0.45
1	4	6/24/2008	0.29
1	5	8/6/2008	0.2
1	6	9/12/2008	0.29
1	1	4/13/2009	0.26
1	2	5/11/2009	0.29
1	3	6/18/2009	0.28
1	4	7/20/2009	0.13

The RAM remaining before irrigation occurred was calculated by first calculating the total RAM. This was done by multiplying the TAM previously calculated for each irrigation event by the MAD calculated for the two crop types of grass hay and alfalfa. The second step was to calculate the RAM utilized by the crop between irrigation events. This was done in the previous analysis of TAM and is the same value as the TAM utilized by the crops between irrigation events. The third step was to calculate the RAM remaining when an irrigation event occurred. This value was calculated by subtracting

the RAM utilized by the crop from the RAM. The final step was to calculate the percent of RAM remaining when irrigation events occurred. This was done by dividing the RAM remaining by the total RAM. Table 5 displays the percent RAM remaining calculated for 10 of 144 irrigation events.

Table 5. Logger ID, Irrigation Event, Date, and % RAM Remaining Calculated for 10 Irrigation Events

Logger ID	Irrigation Event	Date	% RAM Remaining
1	1	4/14/2008	0%
1	2	5/5/2008	26%
1	3	6/1/2008	0%
1	4	6/24/2008	13%
1	5	8/6/2008	39%
1	6	9/12/2008	13%
1	1	4/13/2009	21%
1	2	5/11/2009	12%
1	3	6/18/2009	16%
1	4	7/20/2009	61%

The mean percent of RAM remaining for when irrigation events occur was found to be 23% for the 144 irrigation events with a standard deviation of 24%. It was also observed that there were a significant amount of values representing 0% RAM remaining when irrigation occurred. To analyze the variability and distribution of the data a histogram was developed. Figure 2 displays the histogram of % RAM remaining for the 144 monitored irrigation events.

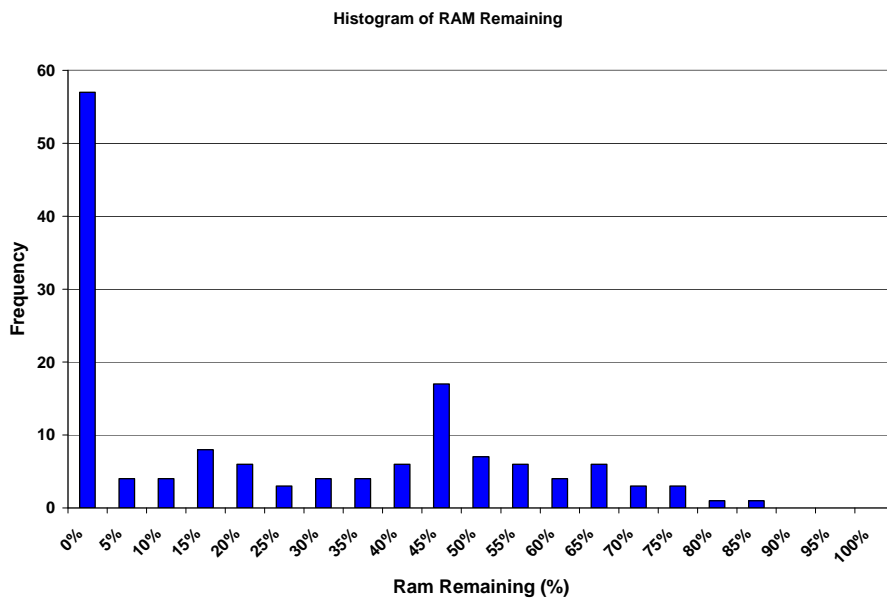


Figure 2. Histogram of % RAM Remaining

The developed histogram displayed a skewed distribution with a skewness coefficient of 0.54. This indicated that the tails of the distribution represented a majority of the irrigation events. This becomes quite apparent upon visual inspection of the histogram as 57 irrigation events exhibited a % RAM remaining of 0%. Using the developed histogram it was also possible to calculate the probability that the % RAM remaining would fall within one standard deviation of the mean value. The probability that the % RAM remaining when irrigation occurred would fall within one standard deviation was found to be 120 out of 144 irrigation events, resulting in a probability value of 0.83. This indicates that 83% of the % RAM remaining values were within one standard deviation of the mean. Based on analysis of the histogram a revised value for % RAM remaining of 20% was incorporated into the DSS. This value was incorporated into the DSS to represent the practice that farmers in the MRG irrigate when there is still a portion of the RAM remaining. In the future the DSS could be revised to include a Monte Carlo simulation of % RAM remaining to represent the variability found during the field experimentation.

The percent of RAM remaining at the start of the irrigation season is another input factor that had not been determined. This value is crucial for developing the first schedules of the season in the DSS. From the collected data it was possible to calculate the percent of RAM remaining at the start of the irrigation season for the 2008 and 2009 irrigation seasons. The mean percent RAM remaining at the beginning of the irrigation season was calculated for both grass hay and alfalfa fields together. The mean percent of RAM remaining in the eight fields monitored was determined to be 7% at the start of the 2008 irrigation season and 11% at the start of the 2009 season. These values will serve as a guide for users of the DSS in inputting appropriate moisture levels at the start of the irrigation season.

### **SOIL MOISTURE DEPLETION PATTERNS**

The modeled soil moisture depletion by growing crops in the DSS was an important aspect that needed to be verified by field experimentation. In the DSS model, the soil moisture depletions are calculated by using the weather-based Penman-Monteith crop ET equation. To evaluate how well the DSS modeled the crop evapotranspiration, the model calculated values were compared to measurements from the instrumented fields to assess the accuracy of the DSS. The data collected for all eight study fields consisted of the volumetric water content collected every 60 minutes at 8 inches and 24 inches of root zone depth. Since the DSS calculates ET from 12:00 AM to 12:00 AM, only the measurements collected at midnight were used to compare the depletion over a 24 hour period. Figure 3 displays the collected depletion data for Field 5 in 2008.

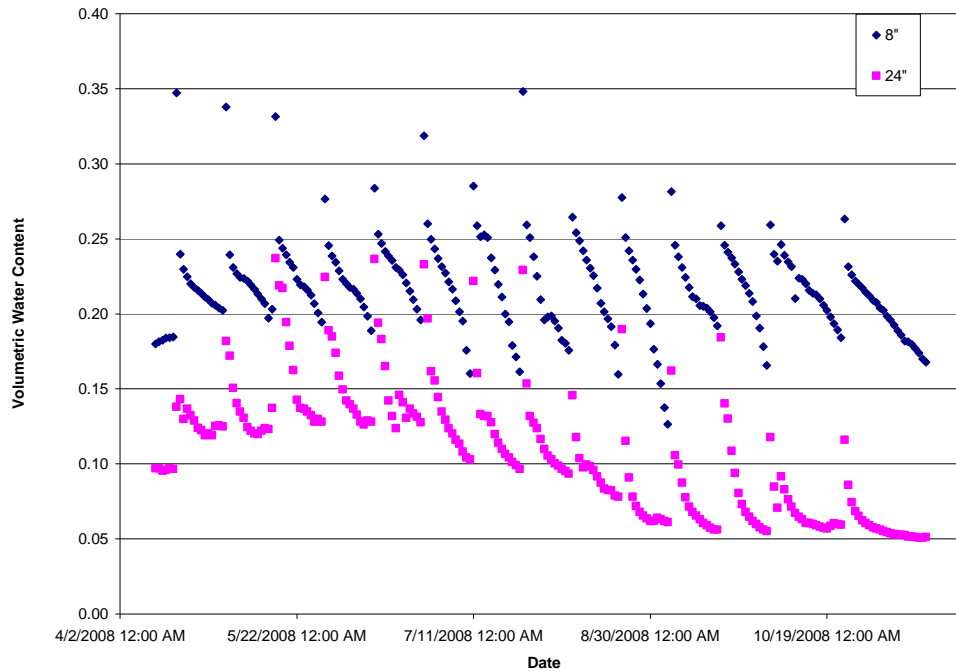


Figure 3. Collected Depletion Data for Field 5 in 2008

The collected data allowed for the creation of a daily water balance for each field to determine the actual evapotranspiration. Since each field contained only two sensors, the depletion from ET could only be calculated between the volumetric water content at field capacity and the volumetric water content directly before the next irrigation. The reason that this methodology was chosen was due to lack of funding for a deeper sensor that could have been used to determine drainage. During this analysis it was also observed that several of the measured fields had groundwater influence that was observed visually in the graphs of the depletion patterns. For these fields the sensor data collected at 24 inches did not significantly decrease throughout the season and displayed values that were indicative of saturation. Once the ET values for these fields were calculated, they were found to be extremely low. This indicates that groundwater was a source contributing to ET that we could not measure with our limited sensor setup. The setup of the sensors was such that a water balance could not be established when groundwater influence was observed, and the measurements showing influence of groundwater were not used in the evaluation of the DSS ET. This resulted in a total of 8 of 16 seasonal measurements that could be utilized to validate the DSS.

To calculate the daily ET from each field in inches the 8 inch sensor was deemed to be representative of the first 16 inches of root depth for both the alfalfa and grass hay fields. The 24 inch sensor was chosen to represent the subsequent 20 inches of root depth for grass hay and the subsequent 32 inches for alfalfa (Garcia, 2008). For grass hay and alfalfa this represented a 36 inch and 48 inch effective total root zone, respectively. The total daily ET was calculated using the volumetric water content readings at midnight shown in Equation 2.

$$[(FC_{8''} - WP_{8''}) * RZ_{\text{represented by 8'' sensor}} + (FC_{24''} - WP_{24''}) * RZ_{\text{represented by 24'' sensor}}] \quad (\text{Eq. 2})$$

The next step in the evaluation of DSS model accuracy consisted of using the DSS to calculate the daily ET values for each of the measured fields so a direct comparison could be conducted. The DSS ET values were calculated for the respective crop of the measured field, either grass hay or alfalfa. The ET values were obtained for the lateral service area that the measured field was in to ensure that spatial variability was addressed and that the DSS modeled ET represented the field location accurately. The modeled values of ET were corrected using an ET correction factor of 0.8 that is currently used in the DSS. This correction factor was determined during a sensitivity analysis of the DSS in 2008 (NMISC, 2008) using ET data collected by Samani et al. (2007). Initially the model ET and the measured ET were compared on a daily basis. Through this analysis it was observed that the measured daily values showed much more variability than the predicted values using the DSS. Figure 4 displays the variability between the measured daily ET and the calculated DSS daily ET for Field 5 in 2008. The variability in Figure 5 was characteristic of the eight seasonal ET measurements used for the evaluation of the DSS.

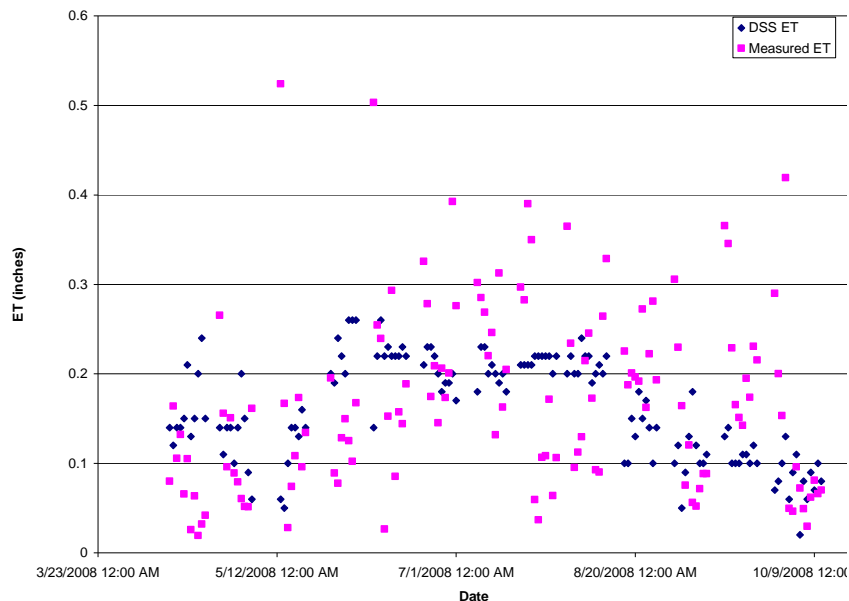


Figure 4. Variability in Measured Daily ET Compared to DSS Predicted Daily ET for Field 5 in 2008.

Since the DSS creates schedules that generally have a two week period between irrigation water deliveries, it was deemed appropriate to compare the cumulative measured ET to the cumulative DSS modeled ET to eliminate the daily variability. Cumulative ET has been used by other researchers to validate predictive models and address the inherent variability in measured daily ET values (DeJonge et al. 2011; Vancloster and Boesten, 2000; Evett and Lascano, 1993; Stroosnijder, 1987; Boesten and Stroosnijder, 1986).

It was found that the measured daily cumulative ET and the DSS predicted daily cumulative ET corresponded well for the eight yearly ET measurements without groundwater influence. Figure 5 displays a graph of the cumulative seasonal ET for both the measured and DSS values for Field 5 in 2009. The other seven comparisons showed similar results to Figure 6. Due to the fact that the sensor set up did not allow for measurements during the period when the soil was draining to field capacity the measurements do not represent a sum of the yearly ET. The time of drainage is represented by the gaps in the data.

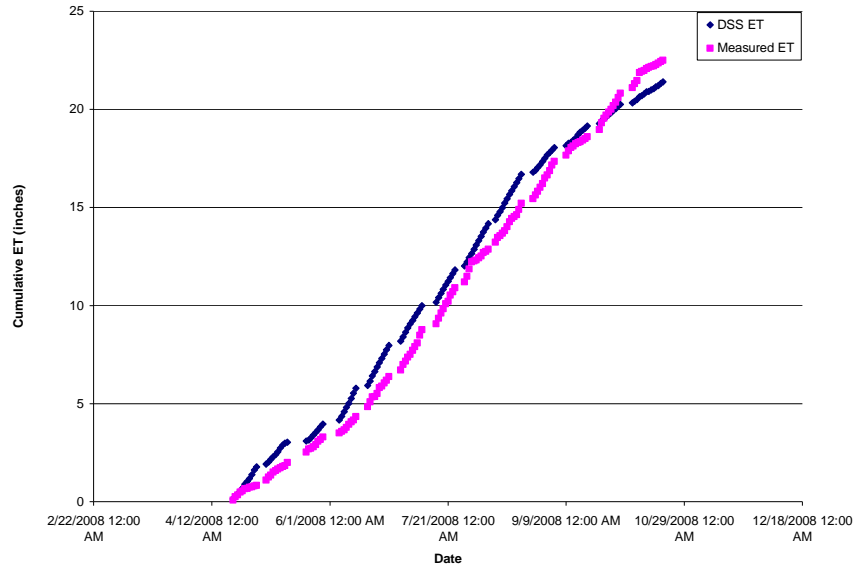


Figure 5. Measured and DSS Predicted Cumulative Seasonal ET for Field 5 in 2008

Since the measured daily cumulative ET and the DSS predicted daily cumulative ET were similar and displayed nearly identical slopes for all eight seasonal measurements it was decided to compare the measured and predicted cumulative ET values utilizing the Nash-Sutcliffe modeling efficiency statistic. The Nash-Sutcliffe model evaluation statistic was first used to compare hydrologic models (Nash and Sutcliffe, 1970). However, it has since been used to evaluate agricultural models (DeJonge et al. 2011), and is widely used to validate various moisture accounting models (McCuen et al. 2006; Downer and Ogden 2004; Birikundavyi et al. 2002). The Nash-Sutcliffe modeling efficiency statistic is also recommended by ASCE (ASCE, 1993) for evaluation of moisture accounting models. The Nash-Sutcliffe model efficiency statistic is defined in Equation 3.

$$E = 1 - \frac{\sum_{t=1}^T (Q_o^t - Q_m^t)^2}{\sum_{t=1}^T (Q_o^t - \overline{Q_o})^2} \quad (\text{Eq. 3})$$

In this equation  $Q_o$  is an actual measurement,  $Q_m$  is the model predicted value, and  $Q_t$  is actual measurement at time  $t$ . Nash–Sutcliffe efficiencies can range from  $-\infty$  to 1. An efficiency of one ( $E = 1$ ) corresponds to a perfect match of modeled values to the observed data. An efficiency of zero ( $E = 0$ ) indicates that the model predictions are as accurate as the mean of the observed data. An efficiency less than zero ( $E < 0$ ) occurs when the observed mean is a better predictor than the model or, in other words, when the residual variance (described by the nominator in the expression above), is larger than the data variance (described by the denominator). The closer the Nash-Sutcliffe model efficiency is to one, the more accurate the model (Moriasi et al. 2007; Nash and Sutcliffe, 1970). In general, a Nash-Sutcliffe value of 0.70 indicates that a model can adequately predict measured values.

The Nash-Sutcliffe modeling efficiency was calculated for all eight fields with valid ET measurements utilizing the measured daily cumulative ET and the DSS predicted daily cumulative ET. Table 6 displays the calculated Nash-Sutcliffe modeling efficiencies.

Table 6. Nash-Sutcliffe Modeling Efficiency for Measured Daily Cumulative ET and the DSS Predicted Daily Cumulative ET

Field	Crop	Year	Nash-Sutcliffe Modeling Efficiency
3	AH	2008	<b>0.94</b>
3	AH	2009	<b>0.97</b>
4	GH	2009	<b>0.99</b>
5	GH	2008	<b>0.98</b>
5	GH	2009	<b>0.52</b>
6	AH	2009	<b>0.54</b>
8	GH	2008	<b>0.98</b>
8	GH	2009	<b>0.95</b>

The analysis of the Nash-Sutcliffe model accuracy statistic indicates that the DSS predicts depletion accurately. The mean statistic of the eight yearly comparisons is 0.86, which indicates a high agreement between actual ET and DSS predicted ET. For six of the yearly comparisons the model efficiency is above 0.94, which is a near perfect agreement. For field 5 in 2009 the value is 0.52 because the field being measured was located in an area where the failure of several weather stations occurred. This resulted in a lower modeled ET than measured. For field 6 in 2009 the value is 0.54 because the field was an old alfalfa field in the last year before reseeding and had a low measured ET. Additionally, the first cut on this field was consumed by geese which further reduced the measured ET. The mean model efficiency for 2008 across both crop types was found to be 0.97 and in 2009 the mean model efficiency for both crop types was 0.80. The variation in modeling efficiency by crop type and year was also examined. Table 7 displays the modeling efficiency by year and crop type.

Table 7. Nash-Sutcliffe Modeling Efficiency by Year and Crop Type

Crop Type	Year	Mean Model Efficiency
Alfalfa	2008	0.94
Alfalfa	2009	0.76
Grass Hay	2008	0.98
Grass Hay	2009	0.82

From the analysis it appears that the DSS model predicts grass hay ET slightly better than the ET for alfalfa in both 2008 and 2009. The results also indicate that the DSS predictions are more accurate for both crops in 2008 than in 2009.

Overall, the values for the Nash-Sutcliffe modeling efficiency indicate that the DSS predicted ET values will match the measured ET values. A modeling efficiency of 0.86 indicates excellent agreement between the actual measured ET and the DSS predicted ET. The obtained mean modeling efficiency is similar to the Nash-Sutcliffe value of 0.89 that has been found for the SWAT (Soil and Water Assessment Tool) model (Spruill et al. 2000).

In addition to the Nash-Sutcliffe modeling efficiency the seasonal sum for measured ET and DSS modeled ET were also compared. Due to the fact that the sensor set up did not allow for measurements during the period when the soil was draining to field capacity the measurements do not represent a sum of the yearly ET. The difference between the measured values and the DSS was calculated by subtracting the sum of DSS ET from field capacity to irrigation from the sum of the measured ET from field capacity to irrigation across all irrigation events during the season for the eight fields. The absolute error was also calculated for the difference in measured ET sums and DSS predicted ET sums. Table 8 displays the values of measured sum ET, DSS sum ET, the difference between the two values, and the absolute error.

Table 8. Measured Sum of ET, Sum of DSS ET, Difference, and Absolute Error

Field	Crop	Year	Measured Sum ET from Field Capacity to Irrigation (in)	Sum DSS ET from Field Capacity to Irrigation (in)	Difference (in)	Absolute Error
3	AH	2008	23.5	22.7	0.8	3.5%
3	AH	2009	31.9	28.3	3.6	11.4%
4	GH	2009	22.1	21.1	0.9	4.3%
5	GH	2008	22.5	21.4	1.1	4.9%
5	GH	2009	16.5	12.2	4.3	26.0%
6	AH	2009	21.6	28.9	-7.3	34.0%
8	GH	2008	18.5	20.3	-1.8	9.9%
8	GH	2009	16.4	15.7	0.8	4.8%

It was found that the mean difference between the measured sum of ET and the DSS predicted sum of ET was 0.3 inches across the eight measurements. The mean absolute difference was found to be 2.6 inches. The mean absolute error across all eight measurements was found to be 12.3%. Work by other researchers suggests that a mean absolute error of 12.3% is an excellent agreement between measured ET values and predicted ET values (Vanclouster and Boesten, 2000; Lascano et al. 1987). In 2008 and 2009 the mean absolute error was found to be 6.1% and 16.1% respectively. This indicates that the DSS predicted the sum of ET more accurately in 2008 than in 2009. The Nash-Sutcliffe model efficiency values also showed this difference between the two years.

Overall, the mean absolute error of 12.3% indicates that the DSS predicts the sum of ET accurately. The completed analysis using modeling efficiency and mean absolute error indicates that the DSS predicts ET depletion accurately in its current form and can be confidently used to determine ET in the Middle Rio Grande Valley.

## DISCUSSION

Through the study of eight farm fields it was possible to determine on-farm application efficiency, % RAM remaining when farmers irrigated and examine DSS depletion against actual measured values. Although it was possible to validate the DSS and improve the modelled water delivery requirements several questions remain. Several irrigation events exhibited an application efficiency of 100% and indicate possible under irrigation or inadvertent deficit irrigation. Such results also point to possible measurement errors and residual moisture that is used by plants but not accounted for in calculations related to an irrigation event. One reason for possible errors could be due to the fact that only one sensor location was installed for each field due to budget constraints (Kinzli, 2012). Spatial variability in soil and topography that could not be measured due to a single sensor station location and could be the cause of uneven water distribution during the irrigation event. Differences in moisture uptake by plants due to spatial root variability could also be the cause this discrepancy. Although the use of a one sensor station setup has proven to be a successful low cost approach (Kinzli, 2012) further studies should be conducted to determine the effects of soil variability and the application uniformity in the MRGCD. Such studies could shed light on irrigation and groundwater interactions. Studies with deeper sensor placement could be used to determine the effects of deep drainage and groundwater and the variability in the groundwater table during the irrigation season. A study with deeper sensors could also be used to validate the work of Garcia (2008) that significant soil moisture depletion does not occur below 32 inches for grass hay and 48 inches for alfalfa.

This study found that there was significant variability in on-farm application efficiency and %RAM remaining before irrigation occurred and this merits further investigation.

In the future the DSS could be revised to include a Monte Carlo simulation of the variability found in the application efficiency values instead of using a single number.

Using a DSS to schedule water presents challenges that include not representing all water users equally. One of the main concerns is that the water users in the MRGCD are represented by large scale commercial farmers and also by “hobby farmers” that irrigate a small pasture. This study was conducted on commercial farms and therefore represents water use practices employed by successful farmers. These same practices might not be utilized by some of the smaller recreational farmers and DSS based water delivery might adversely affect these smaller water users. Other challenges present when using a DSS include the fact that field practices such as fertilizer application are not accounted for. Additionally, the age of alfalfa and grass hay fields is not addressed, a variable that significantly impacts the total ET during an irrigation season.

The numbers for MAD and RAM remaining before irrigation occurs determined during this study are very conservative and indicate that farmers generally irrigate before the RAM is entirely depleted. Since water is not metered, farmers have no incentive to conserve water and watering before the RAM is entirely depleted ensures that crop stress and yield loss does not occur. MAD values could be a function of farmers irrigating when water is available instead of waiting for scheduled turn. This could be due to the cultural practice that farmers in the MRGCD take water when it is there for fear of it not being available when they require it. This culture points toward problems of water reliability in the past. These problems need to be addressed for DSS based water management to be successful.

DSS have been implemented all over the world to aid water managers in delivering irrigation water. Most of these DSS have not been validated. This study elucidates the need for validation and presents the effects that an un-validated DSS could have on water management, in this case short-changing MRGCD farmers by 15,600AF. It is therefore recommended that implemented DSS be validated worldwide and that new DSS be validated during development.

## **CONCLUSION**

Using a low cost approach it was possible to monitor 8 farm fields over a period of two years and refine the DSS input parameters of on-farm application efficiency (45%), RAM remaining when farmers irrigated (20%) and compare modelled and measured moisture depletion patterns.

During the years of 2008 and 2009 the total irrigation diversion for the MRGCD calculated by the DSS using an application efficiency of 50% was 312,000 acre-feet. The 5% decrease in application efficiency found during this study represents a water volume of 15,600 acre-feet that farmers would not have received using the assumed 50% on-farm application efficiency.

The validation of the DSS proved that simply using assumptions for input parameters without proper field measurements results in a flawed model that can short change farmers. The improvement in the on-farm application efficiency number (from 50% to 45%) resulted in farmers receiving 15,600 acre-feet more water than under the previous assumption.

The analysis of model formulation indicated that the DSS was capable of creating real time water delivery schedules capable of meeting crop demand. Additional analysis, that consisted of comparing measured crop depletions to DSS modeled crop depletions, indicated that the DSS accurately modeled crop depletions with a mean Nash Sutcliffe modeling efficiency of 0.86. Overall, the validation effort verified that a DSS can be used to develop water delivery schedules based on real time crop demand. The research effort also clearly elucidated that DSS must be validated before they are utilized to make water management decisions.

### ACKNOWLEDGEMENTS

The authors would like to thank the staff of the Middle Rio Grande Conservancy District, especially Matt Martinez for his assistance in installing the EC-20 probes. The authors would also like to thank the New Mexico Interstate Stream Commission and the Endangered Species Act Collaborative Program for the funding to undertake this research. The advice and assistance of Gaylon Cambell, Doug Cobos, and TJ Clevenger of Decagon Devices are also recognized.

### REFERENCES

- ASCE Task Committee on Definition of Criteria for Evaluation of Watershed Models of the Watershed Management, Irrigation, and Drainage Division (ASCE). 1993. "Criteria for evaluation of watershed models." *J. Irrig. Drain. Eng.*, 119(3): 429–442.
- Birikundavyi, S., Labib, R., Trung, H. T., and Rousselle, J. 2002. "Performance of neural networks in daily streamflow forecasting." *J. Hydrol. Eng.*, 7(5): 392–398.
- DeJonge, K. C., Andales, A. A., Ascough, J. C., & HANSEN, N. (2011). Modeling of full and limited irrigation scenarios for corn in a semiarid environment. *Transactions of the ASABE*, 54(2), 481-492.
- Downer, C. W., and Ogden, F. L. 2004. "GSSHA: Model to simulate diverse stream flow producing processes." *J. Hydrol. Eng.*, 9(3): 161–174.
- Evet, S.R., and R.J. Lascano. 1993. ENWATBAL.BAS: A Mechanistic Evapotranspiration Model Written in Compiled BASIC. *Agronomy Journal* 85: 763-772.
- Garcia, R. 2008. *New Mexico Integrated Water Management Handbook*. United States Department of Agriculture, Natural Resources Conservation Service.
- Gensler, D., Oad, R. and Kinzli, K. 2009. "Irrigation System Modernization: A Case Study of the Middle Rio Grande Valley." *ASCE Journal of Irrigation and Drainage*. 135(2).

Kinzli, K-D. (2012) A Low Cost Remote Monitoring Method for Determining Farmer Irrigation Practices and Water Use. In: Problems, Perspectives and Challenges of Agricultural Water Management. Edited by: Manish Kumar. ISBN 978-953-51-0117-8

Kinzli, K-D., Manana, N., and R. Oad. (2011). A Comparison of Field and Laboratory Calibration of a Soil Moisture Capacitance Probe for Various Soils. ASCE Journal of Irrigation and Drainage. DOI:10.1061/(ASCE)IR.1943-4774.0000418

Kinzli, K-D. (2010). Improving Irrigation System Performance through Scheduled Water Delivery in the Middle Rio Grande Conservancy District. Dissertation. Colorado State University. May.

Kinzli, K. D., Martinez, M., Oad, R., Prior, A., & Gensler, D. (2010). Using an ADCP to determine canal seepage loss in an irrigation district. *Agricultural Water Management*, 97(6), 801-810.

Lascano, R.J., Van Bavel, C.H.M., Hatfield, J.L., and D.R. Upchurch. 1987. Energy and Water Balance of a Sparse Crop: Simulated and Measured Soil and Crop Evaporation. *Soil Science Society of America Journal* 51: 1113-1121.

McCuen, R.H., Knight, Z., and A.G. Cutter. 2006. Evaluation of the Nash-Sutcliffe Efficiency Index. *Journal of Hydrologic Engineering* 11(6): 596-602

Moriasi, D. N. & Arnhold, J. G. & Van Liew, M. W. & Bingner, R. L. & Harmel, R. D. and Veith, T. L. 2007. Model evaluation guidelines for systematic quantification of accuracy in watershed simulations. *American Society of Agricultural and Biological Engineers* 50 (3): 885 – 900.

Nash, J.E. and J.V. Sutcliffe. 1970. River Flow Forecasting through Conceptual Models Part I – A Discussion of Principles. *Journal of Hydrology* 10(3): 282-290.

New Mexico Interstate Stream Commission (NMISC); 2008 (authors Oad, R. Kinzli, K-D. Garcia, L. Patterson, D. and Shafike, N.); Decision Support Systems for Efficient Water Management and Use in the Middle Rio Grande. New Mexico Interstate Stream Commission, August 2008.

Oad, R. Garcia, L. Kinzli, K, Patterson, D and N. Shafike. 2009. Decision Support Systems for Efficient Irrigation in the Middle Rio Grande Valley. *ASCE J. of Irrig. and Drain.* 135(2).

Oad, R., and Kullman, R. (2006). Managing irrigated agriculture for better river ecosystems-A case study of the Middle Rio Grande. *ASCE J. Irrig. Drain. Eng.* 132(6), 579-586.

Samani, Z., Bawazir, A. S., Skaggs, R. K., Bleiweiss, M. P., Piñon, A., & Tran, V. (2007). Water use by agricultural crops and riparian vegetation: an application of remote sensing technology. *Journal of Contemporary Water Research & Education*, 137(1), 8-13.

Spruill, C.A., Workman, S.R., and J.L. Taraba. Simulation of Daily and Monthly Stream Discharge from Small Watersheds using the SWAT Model. *American Society of Agricultural Engineerings* 43: 1431-1439.

Stroosnijder, L. 1987. Soil Evaporation: Test of a Practical Approach under Semi-arid Conditions. *Netherlands Journal of Agricultural Sciences* 35: 417-426.

Vanclooster, M., and J.J.T.T. Boesten. 2000. Application of Pesticide Simulation Models to the Vredepeel Dataset: I. Water, Solute, and Heat Transport. *Agricultural Water Management*. 44: 105-117.

# ANALYSIS OF WATER RESOURCE NETWORKS USING PARALLEL COORDINATES

Leah Meeks, M.E., EIT<sup>1</sup>  
David E. Rosenberg, Ph.D.<sup>2</sup>

## ABSTRACT

The complexity of water resources networks typically requires a large number of computationally intensive simulations to test effects of changes in network structure or management. Current tools can only visualize the effects of a few changes. Here, we introduce a new tool using parallel coordinates to simultaneously visualize large water resources networks and identify nodes that are (1) vulnerable (role depends on the existence of particular nodes), (2) topologically significant (cause other nodes to be vulnerable when removed from the network), and (3) redundant. The tool scales to very large networks and identifies the most promising nodes to subsequently focus computationally-intensive simulation and sensitivity analysis efforts. We apply the tool to identify critical agricultural to urban water transfers in the 56-node lower Bear River water system from southern Idaho to the Great Salt Lake, Utah. The three most topologically significant nodes are Cutler Reservoir, J45-51, and J32-88. Nodes connected to only one other node are the most vulnerable, including Great Salt Lake and Malad River. There are five node pairs with over 96% of the same connections including Cache Valley Irrigation and Cache Valley New M&I service areas. The New Box Elder County Irrigation and South Cache Irrigation service areas have very low topological significance. The three irrigation areas could be sources of water transfers because their removal would have little effect on the Bear River network connectivity. To further analyze agriculture to urban water transfers we recommend including flow direction and magnitude in future network analysis.

## INTRODUCTION

Water resources networks are often large, have numerous water supply, reservoir, diversion, and demand site nodes that are connected through natural and engineered conveyance linkages. Their large size and complexity typically require numerous and computationally intensive simulation runs to test the effects of particular changes in network structure or management. Current network analysis tools can only visualize the effects of two or a few network changes. Here, we introduce a new method and tool using parallel coordinates to automatically identify and rank the key nodes in a network.

---

<sup>1</sup> Graduate Research Assistant, Dept. of Civil & Env. Engineering and Utah Water Research Laboratory, Utah State University Dept. of Civil & Env. Engineering, 4110 Old Main Hill, Utah State University, Logan, UT 84322-4110; c:(435)-881-8697, l.meeks@aggiemail.usu.edu;

<sup>2</sup> Assistant Professor, Dept. of Civil & Env. Engineering and Utah Water Research Laboratory, Utah State University Dept. of Civil & Env. Engineering, 4110 Old Main Hill, Utah State University, Logan, UT 84322-4110; o:(435)-797-8689, f:(435)-797-1185, david.rosenberg@usu.edu.

Parallel coordinate plots (PCP) can simultaneously display a large number of dimensions and are a good way to visualize large networks (Singer and Greenshpan, 2009). PCP draw axes in parallel and allow visualization of an infinite number of dimensions in one figure within the two-dimensional confines of a printed page or screen (Inselberg 1985). PCP contrast with the more traditionally-used Cartesian coordinate plots which can only illustrate two or three dimensions to maintain orthogonality. A point in three-dimensional orthogonal coordinates becomes a vector in parallel coordinates (PC) (Figure 1).

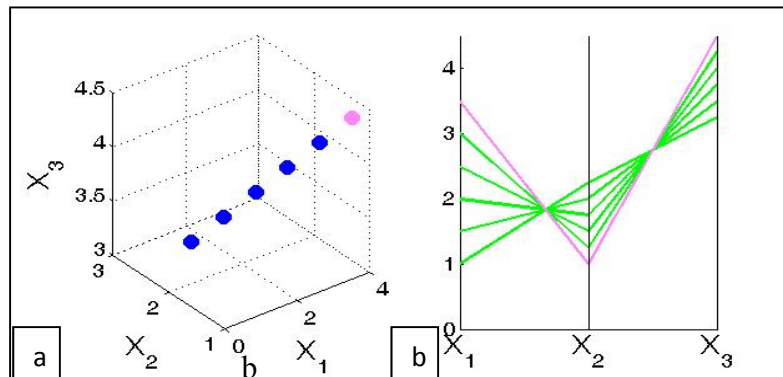


Figure 1. Comparison of data in (a) Cartesian coordinates and (b) parallel coordinates (Rosenberg, 2012). PCP have been used to improve understanding of various systems because of their capacity to display multiple dimensions simultaneously. Albazzaz et al (2005) used PCP to detect abnormal operations in wastewater treatment by tracking 38 variables for 527 days finding 17 abnormal days. PCP were also used to identify errors in raw data through visual inspection of the PCP for lines that did not follow the trends (Edsall 2003).

Choi et al (2008) applied PCP to detect unknown large-scale attacks through internet sources. The plots allowed for visual determination of anomalies in source internet protocol (IP) address, destination IP address, destination port, and average flow packet length of internet network traffic to classify attacks.

PCP can be dynamically linked to geographical maps to help with analysis of geographic phenomena (Edsall 2003). PCP have been used to dynamically update geographic maps to identify dominant attributes (Andrienko and Andrienko 2001). Edsall (2003) used PCP to expand the variables used to classify hurricanes beyond sustained wind speed to include water vapor content, sea surface temperature, and warning systems. In addition, PCP helped scientists identify variables after a hurricane event that were extreme, such as barometric pressure, as well as compare multiple variables at a particular latitude.

Singer and Greenshpan (2009) propose a method using PCP to analyze networks called node extraction visualization (NEVIS) that is included in Inselberg's compilation textbook on parallel coordinates. The NEVIS method systematically removes one node from a network and uses PCP to understand how the removed node influences the rest of the network. Removal of a node can change the centrality (measure of how connected a node is to the network) of other nodes. NEVIS transforms the network nodes into multidimensional points so that node relationships can be identified. Each node is

represented by a different axis on the PCP. For example, a network with 10 nodes requires 10 axes to capture the 45 node interactions (how removing one node affects the others). Singer and Greenspan introduce the terms node topological significance (a node with significant effect on the network's centrality), stability (a node that is not effected by removal of other nodes), and backup (alternate paths bypassing a removed node) to describe a node's function in a network; here, we build upon these terms.

Visual inspection of PCP can add insight to a problem such as connectivity or abnormal data but is also complicated by the large number of variables. Interpretation of PC can be impeded by line density in the plot, the order of the variables, and the peaks and valleys of adjacent variables (Edsall 2003, and Huh and Park 2008). Albazzaz et al (2005) recommended that PC be used for historical database analysis with systems at steady state because of a lack of an automated tool to apply PC.

Here, we introduce a new PC automated method and tool to visualize large water resources networks and identify and rank nodes that are (1) vulnerable (its role in the network is dependent on the existence of particular nodes), (2) topologically significant (when removed or added to the network, it causes other nodes to be vulnerable), and (3) redundant with other nodes. The tool scales to very large networks and identifies the most promising nodes on which to subsequently focus computationally-intensive simulation and sensitivity analysis efforts. We illustrate the approach to identify promising areas for agriculture-urban water transfers in the Lower Bear River basin. Below, we describe steps of the tool and its application to the large Bear River system.

## METHODS

We use and extend the NEVIS method proposed by Singer and Greenspan (2009) to create an algorithm to generate the PCP, identify key nodes, and rank which nodes are most vulnerable, topologically significant, and redundant. To undertake the ranking, we develop performance metrics using matrix manipulation and statistics. In this section, we introduce the programs used to build the tool, define the terms introduced and used within the tool, and then describe how the tool works.

The analysis tool is created using HydroPlatform and Microsoft Excel 2007. HydroPlatform is a geographic open-source software platform that can be used with other modeling software for water management decision support tools. HydroPlatform can output data in multiple forms, including matrices in CSV (comma separated values) that can be imported into Excel. Excel's macro programming capabilities can operate within the spreadsheets for multistep calculations and processes. Visual Basic for Applications (VBA) is a programming language built into Excel which we used to automate the analysis tool.

We created and built upon terminology introduced by Singer and Greenspan (2009). The definition of these terms is very specific to NEVIS and our analysis tool (Table 1).

Table 1. Terms and definitions of parallel coordinate vocabulary.

Term	Definition
Adjacency Matrix	Matrix with each node as a column heading and each node with a row indicating which column nodes are connected by one link with a value of 1
Connectivity Matrix	Matrix with each node as a column heading and each node with a row indicating the number of links between each pair (row and column) of nodes
Extracted Network	A network with one node removed
Centrality Value	Measure of how connected a node is to the network with higher values indicating the node is connected to more nodes
Extracted Centrality	Centrality of a node when calculated from an extracted network
Vulnerability	Measure of how much the extracted centrality values change for a node
Topological Significance	Measure of how much vulnerability a node causes in other nodes when removed from the network
Parallelism	Nodes with similar extracted centrality values
Redundancy	Two nodes that have many of the same connections

The tool has four sequential parts: calculating centrality, creating PCP, calculating pairwise differences, and calculating performance indicators. We describe the calculation steps for each part and present some of the equations utilized in Excel and VBA.

Step 1: Calculate Centrality. First, a user draws the network as a directed graph of nodes and links in HydroPlatform. Then the user exports a square adjacency matrix that identifies the pairs of nodes that are one link apart. We remove one node from the adjacency matrix to create an extracted network. We pivot across and down the adjacency matrix to calculate the smallest number of links between each pair of nodes and populate a corresponding connectivity matrix. We calculate each node's centrality,  $\chi$  (chi), in the extracted network by summing the inverses of the connectivity values associated with all other nodes (a row of values in the connectivity matrix; Equation 1).

$$\chi_i = \sum_{j=1, j \neq i}^n \frac{1}{\text{distance}(\text{node}_i, \text{node}_j)} \quad (\text{Eq. 1})$$

Where:  $\chi$  = centrality value

n = number of nodes in the network

i = row of values

j = column value

distance (node<sub>i</sub>, node<sub>j</sub>) = value in connectivity matrix

We remove one node, creating an extracted network, and calculate the centrality for all network nodes and call them the extracted centrality values. The resulting extracted connectivity values are a matrix with each row being a particular node's extracted chi value when the column node is extracted.

Step 2: Create Parallel Coordinate Plots. We then plot each node's centrality values (y axis) as a horizontal trace across the extracted networks (x axis) to simultaneously show on the same plot the effects of each node extraction. Together, these listings of extracted nodes comprise parallel horizontal axes along which centrality values scale from zero to the largest value observed. The result is a parallel coordinate plot. Each node's extracted centrality value in a horizontal trace shows the node's relationship to other nodes. We visually identify vulnerable nodes as nodes whose traces have vertical drops and topologically significant nodes as locations on the x-axis where extracting a node causes multiple traces to drop.

Step 3: Calculate Pairwise Differences. To quantify the node vulnerability, topological significance, and redundancy we see in the parallel coordinates, we calculate the difference between each pair of extracted network centrality values along a trace, called pairwise differences. By using pairwise differences, the order of the axes does not influence the quantitative results of the analysis. We calculate the cumulative frequency distribution of the pairwise differences for each node. The cumulative frequency distribution has 15 delineations (default values are 1 to 15) that we plot on the x axis of the histogram with the percent of pairwise differences within that delineation on the y-axis. Nodes with similar cumulative frequency distributions are identified in pairs by having similar PCP horizontal traces and are classified as parallel.

Step 4: Calculate Performance Indicators. We average the pairwise differences along a trace as the measure of a node's vulnerability. Higher pairwise differences indicate that the node trace has more drops along its trace. Nodes with the most vulnerability have the highest average pairwise differences.

Topological significance has two factors: the number of drops and the magnitude of each drop. Multiple horizontal trace drops indicate that a particular extracted node causes vulnerability in many nodes. A large drop in a node's trace is a sign of vulnerability at that extracted node. Extracted nodes that cause large numbers of traces to drop and large magnitude drops are topologically significant. We established a minimum drop threshold to count the number of drops that an extracted node causes and measured the magnitude of each drop. We used the average of the pairwise differences for all traces at an extracted node to quantify the magnitude of drop an extracted node causes. We rank each node for number and magnitude. The node having the highest average of number and magnitude of drops has the highest topological significance.

Parallel nodes are a pair of nodes with similar cumulative frequency distributions of the pairwise differences. We compare the connectivity matrix values for each pair of parallel nodes. Node pairs that have similar connectivity along their respective row, a high R%, are redundant pairs (Equation 2).

$$R = \frac{C}{n-2} * 100 \quad (\text{Eq. 2})$$

Where: R = node pair redundancy, as a percent

C = number of common connections between nodes

$n$  = number of nodes in the network  
 $n-2$  = maximum number of common nodes a pair can have; subtract 2 because each node is not connected to itself

This tool is automated with two sets of inputs: adjacency matrix from HydrpPlatform and calculation values. Once the tool has created the PCP, we input a value for PC drop threshold to determine topological significance and a percentage reduction value for the cumulative frequency distribution to determine redundancy. The tool outputs the PCP, each node's rank of vulnerability and topological significance, and lists node pairs that are redundant.

## APPLICATIONS

We use small illustrative networks to demonstrate how the analysis tool works. Later, we apply the tool to the Bear River system that has 56 nodes.

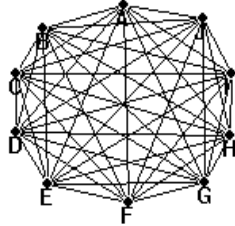
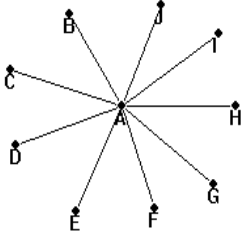
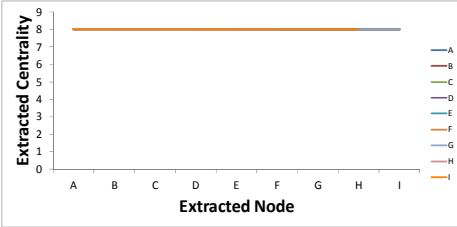
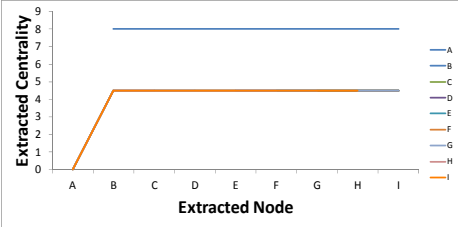
### Illustrative Networks

We present two illustrative networks that are simple in construction with very different structure to introduce how the tool works. These networks help verify that the tool analysis is correct and highlight the relationships among the performance indicators. Each node is described with key findings and then presented in a table for comparison.

Clique. A clique network has all nodes connected to all other nodes. From the directed graph (Table 2), visual inspection indicates that the nodes are likely redundant and no node is topologically significant. In the PCP, all of the traces have straight horizontal lines. None of the nodes are topologically significant or vulnerable while all nodes are redundant with an  $R = 100\%$  for each node pair.

Hub and Spoke. In a hub and spoke network, all nodes (spokes) are connected only to a single node (hub, node A in Table 2). We expect that the hub will be topologically significant with the spokes being vulnerable to the extraction of the hub. The PCP show that all spoke traces (B-J) drop at the hub while the hub trace is a straight horizontal line. From the performance indicators, the spokes are vulnerable, the hub is topologically significant, and all of the spokes are redundant with each other with an  $R = 100\%$ .

Table 2. Parallel coordinate tool applied to illustrative networks.

Network	Clique	Hub & Spoke
Directed Graph		
Parallel Coordinate Plot		
Vulnerability	None	All spokes (B-J)
Topological Significance	None	Hub (A)
Redundancy	All	All spokes (B-J)

**Bear River Network**

The Bear River watershed comprises 7,500 square miles of agricultural, urban, federal, and state lands in southeastern Idaho, northeastern Utah, and southwestern Wyoming and is the largest tributary of the Great Salt Lake with an average annual inflow of 1.2 million acre feet (Mesner and Horsburgh 2012). The primary water uses in the basin are for agriculture, municipal, industrial, power generation, and recreation.

Utah’s population continues to grow increasing urban water demand. Planners are projecting the need to import Bear River along Utah’s Wasatch Front due to urban growth in Salt Lake, Davis, and Weber counties (Mesner and Horsburgh 2012). Increasing water transfers from agricultural to urban use could change how the water system functions.

The Bear River network in this analysis stretches from Southeastern Idaho to the Great Salt Lake in Utah. The Utah Division of Water Resources has developed the Bear River simulation model to look at the sustainability of the system with a 50-year water record (Utah Division of Water Resources, 2004). Figure 2 is the system schematic of the Bear River system comprised of 56 total nodes including 11 reservoirs, 11 service areas, 13 flow junctions, and 74 linkages (Figure 2, Utah Division of Water Resources, 2010).

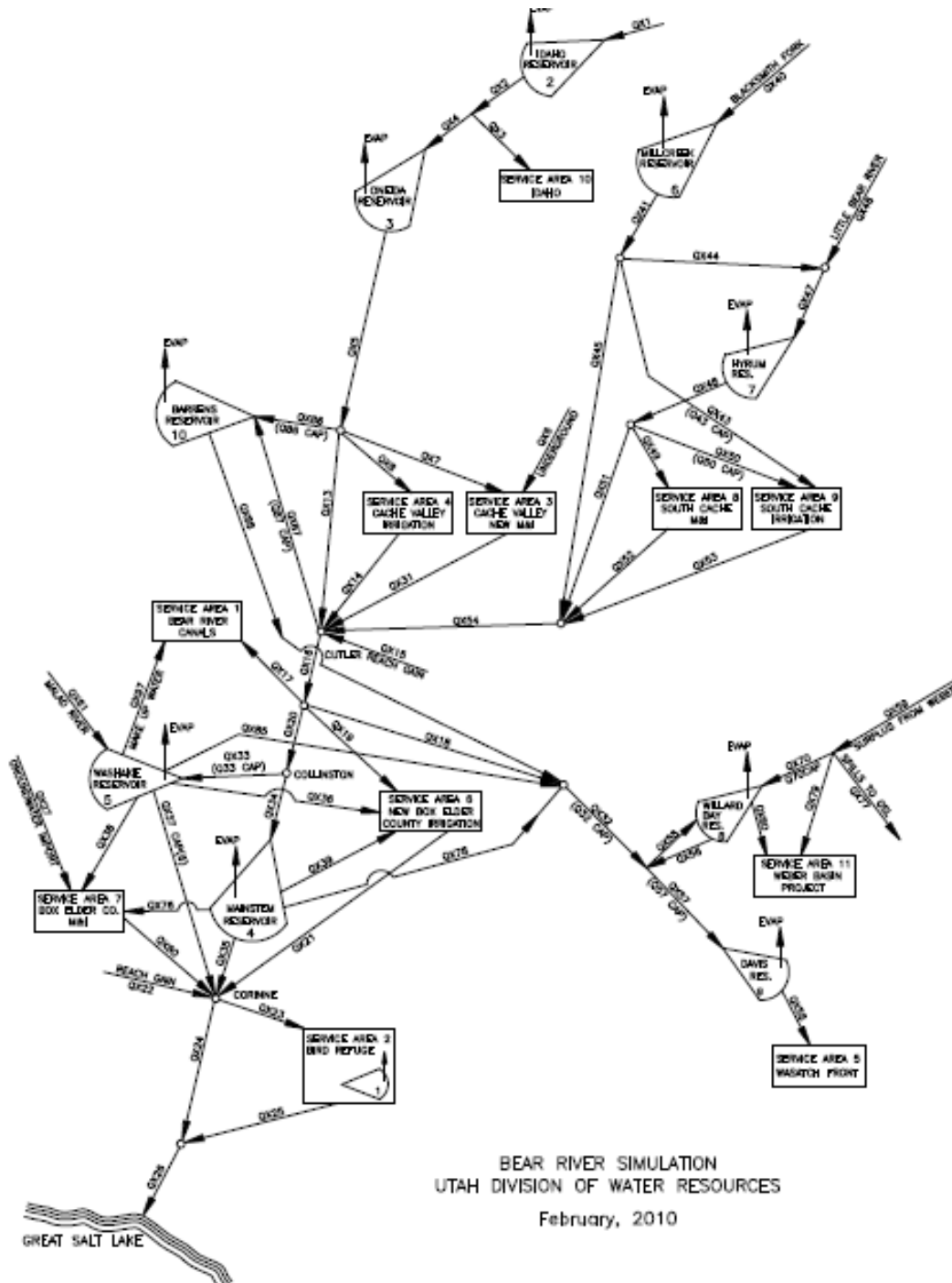


Figure 2. Bear River network used for analysis.

We use the network schematic in Figure 2 to draw the directed graph in HydroPlatform. We input the data into Excel and steps 1 and 2 of the tool to produce the PCP (Figure 3) which show that junctions cause considerable trace drops while individual water sources and sinks have little effect on the rest of the network. Nodes with more connections are less likely to be redundant.

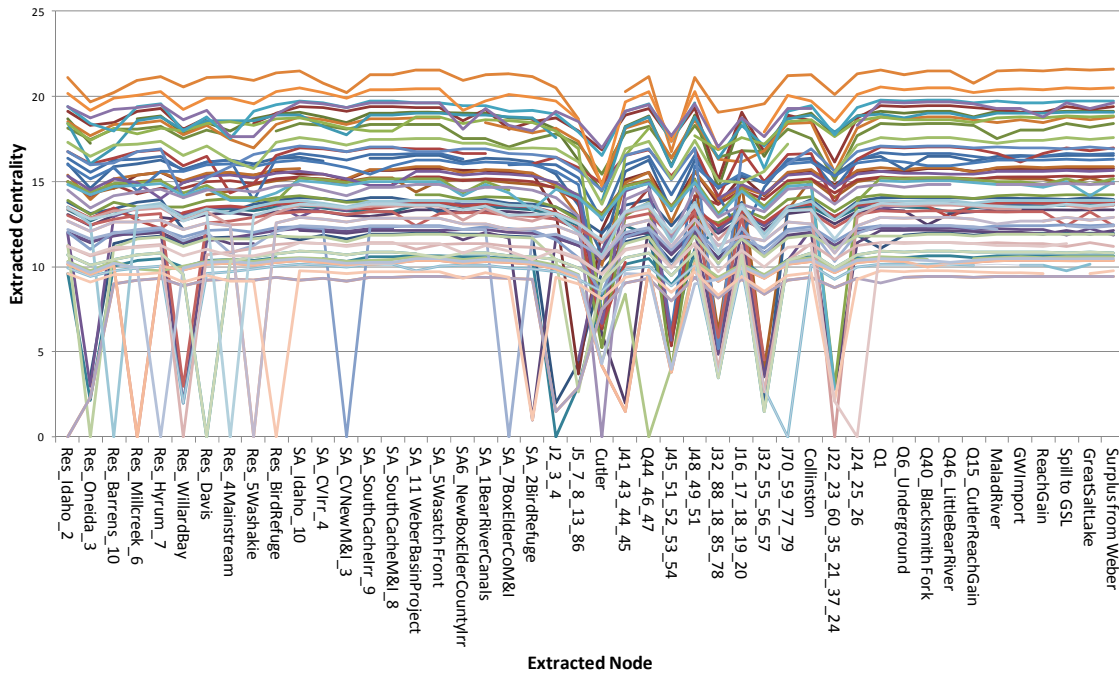


Figure 3. Parallel coordinate plot for Bear River network.

With steps 3 and 4 of the tool, we calculate the performance indicators (Tables 3 and 4). The three most topologically significant nodes are Cutler Reservoir, J45-51, J32-88, and J48-49. Nodes that are connected to only one other node are the most vulnerable, including Great Salt Lake, Malad River, and Evaporation from Hyrum Reservoir. The Cache Valley Irrigation service area was the only network node that was redundant with multiple redundant node pairs.

Table 3. Bear River network most and least vulnerable and topologically significant nodes.

Rank	Vulnerability	Topological Significance
1	Great Salt Lake	Cutler Reservoir
2	Q61 Malad River	Junction 45-51
3	Evaporation from Hyrum Reservoir	Junction 32-88
54	SA7 Box Elder M&I Users	Q15 Cutler Reach Gain
55	Junction 22-60	Collinston
56	Washakie Reservoir	SA1 Bear River Canals

Table 4. Bear River network five most redundant node pairs.

Node 1	Node 2	Redundancy
Spill to GSL	Surplus from Weber	100%
Malad River	Evaporation from Washakie Reservoir	100%
SA4 Cache Valley Irrigation	SA3 Cache Valley New M&I	98%
SA11 Weber Basin Project	Junction 70 and 79	96%
Idaho Reservoir	SA10 Idaho	96%

Most of the Bear River network nodes of interest are in the below Cutler Reservoir (Figure 4).

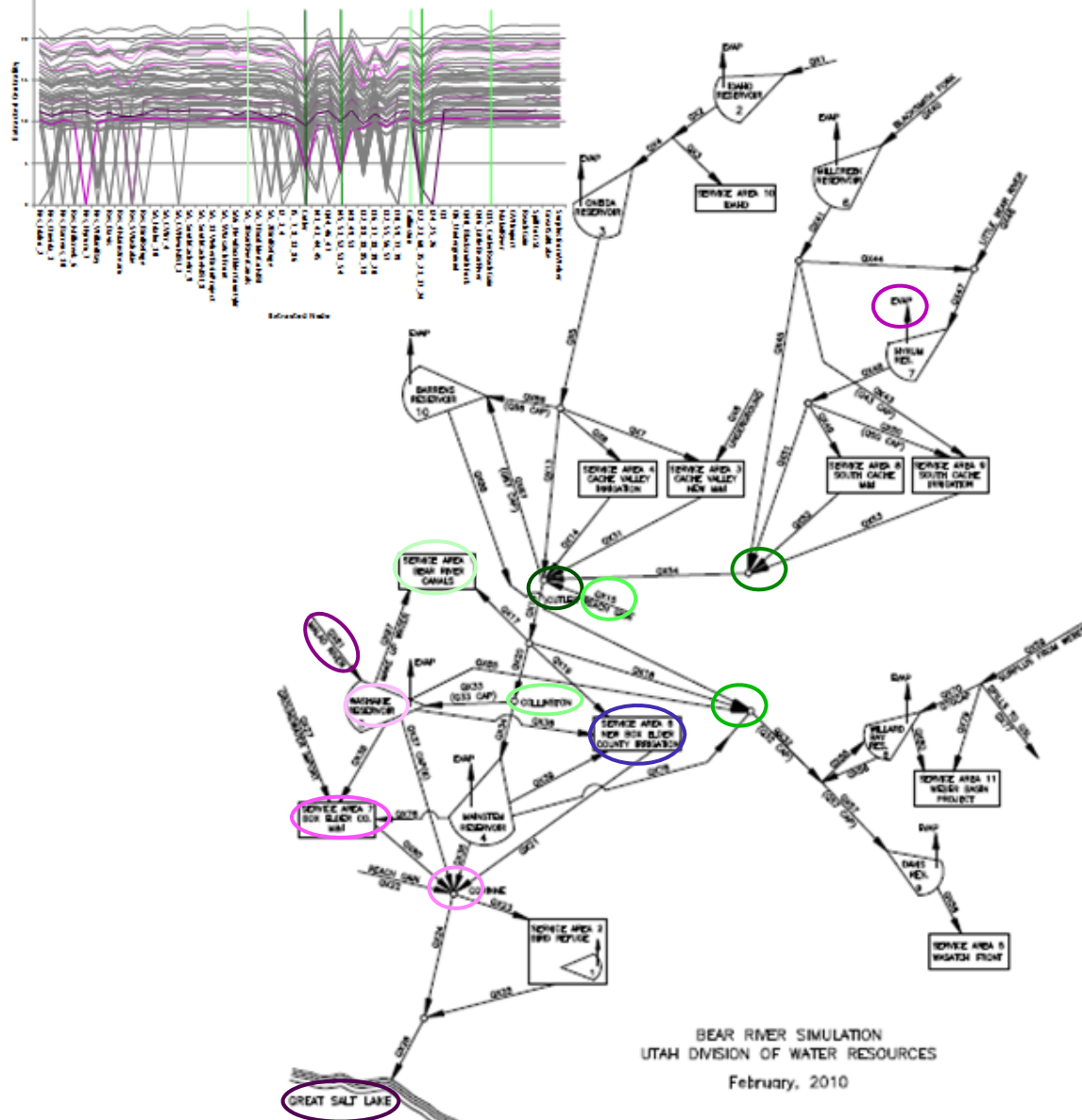


Figure 4. Results from Bear River network using analysis tool (a) parallel coordinate plots with purple as vulnerable and green as topologically significant nodes (three darker as most and three lightest as least) and (b) identification of vulnerable and topologically significant.

## DISCUSSION

The most topologically significant nodes are junctions that connect branches of the Bear River network to the rest of the network. Junction 45-51 and Junction 32-88 are the only way water from the south part of Cache Valley and Weber area, respectively, enter the network. Visual Nodes that are connected to only one node are more likely to be

vulnerable, as is the case for the Bear River network's three most vulnerable nodes (Great Salt Lake, Malad River, and Evaporation from Hyrum Reservoir).

Redundancy can be both positive and negative from a management standpoint. Not all nodes need to be redundant but redundancy does add flexibility for management. The service areas of Cache Valley Irrigation and Cache Valley New M&I are redundant which provides a way to reroute water in the event of delivery system failure at one node. But such redundancy may also be an inefficient use of resources.

Removing nodes that are redundant or not topologically significant will have little effect on the network connectivity. Having a redundant pair means that if one is removed the water can be rerouted through the other. Conversely, removing a topologically significant node will affect many other nodes.

### **Water Transfer Implications**

The transfer of water from agriculture to urban use is represented by the removal of a network node. The Cache Valley Irrigation service area is redundant with three other nodes in the Bear River system which is the largest number of redundancies. The removal of Cache Valley Irrigation will have very little influence on the network connectivity. Its topological significance rank is 53 out of 56. The New Box Elder County Irrigation and South Cache Irrigation have topological significance ranks of 49 and 51, respectively, indicating that their removal will also have little effect on the network.

### **Future Work**

The flow direction and magnitude is not included in the analysis. Both factors would influence the classification of vulnerable, topologically significant, and redundancy. Each nodes water capacity (volume or flow rate) could also be added; nodes may not be redundant if the water would have to change direction or overflow a reservoir to reroute water.

## **CONCLUSION**

Modeling complex water resources networks requires a lot of computational effort. Networks with multiple dimensions, whether it has many nodes or multiple decision variables, are hard to visualize in Cartesian coordinates. We developed an automated parallel coordinate tool to identify key network nodes and plot all nodes simultaneously on one graph. In applying the tool to the 56-node Bear River network in southeastern Idaho and northern Utah, we found that the most vulnerable nodes are those connected to only one other node and topologically significant nodes are often junctions that connect multiple nodes to the rest of the network. The removal of nodes that are redundant has little effect on the network connectivity. Our tool can be scaled to analyze very large networks and can identify the key nodes on which to concentrate time-intensive modeling and sensitivity analysis.

## REFERENCES

- Albazzaz, H., Wang, X.Y., Marhoon, F. (2005). "Multidimensional visualization for process historical data analysis: a comparative study with multivariate statistical process control." *J. of Process Control*, 15(3), 285-294.
- Andrienko, G. and Andrienko, N. (2001). "Exploring spatial data with dominant attribute map and parallel coordinates." *Computers, Environment and Urban Systems*, 25(1): 5-15.
- Choi, H., Heejo, H., Hyogon, K. (2009). "Fast detection and visualization of network attacks on parallel coordinates." *Computers & Security*, 28(1): 276-288.
- Edsall, R.M. (2003). "The parallel coordinates plot in action: design and use for geographic visualization." *Computational Statistics & Data Analysis*, 43(4): 605-619.
- Inselberg, A. (1985). "The plane with parallel coordinates." *The Visual Computer* 1, 69-91.
- Matrosov, E.S., Harou, J.J., Loucks, D.P. (2011). "A computationally efficient open-source water resource system simulator – Application to London and the Thames Basin." *Environmental Modelling & Software*. 26(2011) 1599-1610.
- Mesner, N. and Horsburgh, J. (2012). "Watershed Description." *Bear River Watershed Information System*, <<http://www.bearriverinfo.org>> (Nov. 25, 2012).
- Rosenberg, D.E. (2012). Visualizing high dimensional data. CEE 6930 Hydroinformatics course materials. <https://usu.instructure.com/courses/127332/wiki/lecture-materials> (Dec. 12, 2012).
- Singer, Y. and Greenshpan, O. (2009). Network visualization and analysis with parallel coordinates. *Parallel coordinates: visual multidimensional geometry and its applications*, A. Inselberg, ed., Springer Dordrecht, New York, N.Y., 460-475.
- Utah Division of Water Resources. (2010). Map of Bear River simulation area.
- Utah Division of Water Rights. (2004). Bear River Basin: planning for the future. <<http://www.water.utah.gov/planning/SWP/bear/bearRiver-1A.pdf>> (Dec. 14, 2012).
- Wegman, E.J. (1990). "Hyperdimensional data analysis using parallel coordinates." *J. of the American Statistical Association*, 85(411): 664-675.

# **RAPID IMPLEMENTATION PROGRAM (RIP) TO IMPROVE OPERATIONAL MANAGEMENT AND EFFICIENCIES IN IRRIGATION DISTRICTS IN IRAQ**

Gabriele Bonaiti, Ph.D.<sup>1</sup>  
Guy Fipps, Ph.D., P.E.<sup>2</sup>

## **ABSTRACT**

The Rapid Intervention Program (RIP) was developed over a ten year period by the Texas Agricultural Extension Service, and is a structured and systematic approach for analyzing the distribution network and on-farm irrigation of irrigation schemes, and developing recommendations on improved management strategies. We applied the RIP in two irrigation districts in Iraq in 2012, in collaboration with the United States Agency for International Development to improve efficiency and reduce losses in Iraqi irrigation schemes. In this paper we will present the RIP components, the procedure of applying and adapting it to the Iraqi districts, and some results.

The studied irrigation districts are representative of many others irrigation districts in the Center and South of Iraq, where government support for maintenance and modernizations have been reduced. RIP is designed as a low-cost, user-friendly and versatile approach that takes advantage of the knowledge and experience of the scheme operators and managers, and involves the combination in one single tool of several rating forms: the Head Survey, the Canal and Gate Evaluation, and the On-farm Survey. Included in the RIP is also the building of a GIS map, needed to apply the tools.

A key component of the RIP is the training of collaborators so that they could implement and transfer the RIP to other irrigation schemes in Iraq. We additionally provided training on basic concepts of flow measurement and canal management, and on Excel and ArcGIS for Desktop software. All material is collected into a RIP Manual, including copy in Arabic of all forms, to serve as both a training program and a reference guide to all the steps required in order to successfully apply the RIP.

## **INTRODUCTION**

Irrigation schemes (or irrigation districts) in Iraq and throughout the world are faced with huge challenges as government support for maintenance and modernizations have been reduced. Many irrigation schemes are self-funded through a fee collection that typically is insufficient to cover operating expenses alone. In addition, many irrigation schemes are facing increases in water competition and decreases in water supplies, and often aging and inefficient water distribution systems.

---

<sup>1</sup> Extension Program Specialist, Department of Biological and Agricultural Engineering, 2117 Texas A&M University, College Station, Texas 77843-2117, [gbonaiti@ag.tamu.edu](mailto:gbonaiti@ag.tamu.edu)

<sup>2</sup> Professor and Extension Agricultural Engineer, Department of Biological and Agricultural Engineering, 2117 Texas A&M University, College Station, Texas 77843-2117, [g-fipps@tamu.edu](mailto:g-fipps@tamu.edu)

The Rapid Intervention Program (RIP) was developed over a ten year period by the Texas A&M Extension Service, under the direction of Guy Fipps.

RIP is a structured and systematic approach for analyzing the distribution network and on-farm irrigation of irrigation schemes, and developing recommendations on improved management strategies. RIP is designed as a low-cost, user-friendly and versatile approach that takes advantage of the knowledge and experience of the scheme operators and managers. Components include:

- Inventory of basic data needed to estimate water supply, flows and on-farm irrigation needs;
- Distribution Network Hydraulic Head Survey and Analysis Tool;
- Distribution Network Condition Rating Tool;
- On-farm Head Survey and Analysis Tool;
- Spreadsheets for storage and analysis of data;
- GIS map of the command area;
- Training curriculums for persons implementing the RIP in flow measurement, canal management and basic concepts of surface irrigation.

The objectives of this paper is to describe how we designed a RIP procedure for irrigation schemes in Iraq, and the main components of the RIP manual which is designed to help trained operators to apply it successfully.

### **RIP MANUAL AND GENERAL PROCEDURE**

The RIP manual (Manual) is organized to serve as both a training program and a reference guide to all the steps required in order to successfully apply the RIP. Each of the four major RIP components is discussed in the Manual along with comments and/or observations that the users may find useful. The Manual also includes Appendices which provide:

- A copy of all forms in English and Arabic
- The suggested training curriculum for the specialized skills needed related to GIS mapping, use of spreadsheets and flow measurement.
- Examples of case studies of the application of the RIP to irrigation schemes in Iraq

The Survey and Data Collection Tools were applied according to the following general steps:

- 1) Map the irrigation scheme with GIS. A map with details on canals and irrigated areas is a critical part of the RIP and is used to help organize and analyze the data collected. Usually, any existing maps are used along with recent aerial photographs to create the GIS. The GIS serves as a reference when discussing the data collection forms with the operators.

- 2) Completion of all forms. Typically, this is done in three stages:
  - a. First in the office with assistance of the interviewers using the GIS as a reference, based on the operators' knowledge.
  - b. Then the operators are instructed to go to the field and verify the information.
  - c. The interviewers meet with the operators to verify all information.
- 3) Flow measurements. Actual flow rates required for all canal categories and at the on-farm turnout. Calculated flows based on the original design specifications are not useful for this purpose.
- 4) Enter data into RIP spreadsheets (Excel) and link to GIS as appropriate.
- 5) Analysis and Recommendations. The exact types of analyses that are done will vary from irrigation project to irrigation project due to their differences; thus, some of the spreadsheets and procedures will need to be modified depending on the specific conditions and objectives.

RIP assumes that the persons implementing the program have already had training and basic skills on use of GIS and Excel. However, implementers will need training to review basic concepts, and on how to apply these tools to the RIP. For example, Excel training covers how to use the RIP spreadsheets which are included on the Manual.

Persons who will conduct the flow measurements will need at least some understanding of open channel flow principle. Ideally, they will also have had experience with field instrumentation. Training is usually required on use of portable velocity meters. Even with experienced persons, training will help speeding up the field work and improve accuracy of measurement. Furthermore, speed up of measurement is particularly important when the water level in the canal fluctuates. Other devices, such as portable acoustic meters and flumes may also be used, but are not included in this manual.

## **SURVEYS**

### **Distribution Network Hydraulic Head Survey and Analysis Tool (Head Survey)**

The purpose of the Head Survey is the identification of areas and canals that currently have continuous or intermittent water supply problems, and the identification of the potential causes of these problems. The tools utilized for this survey are Head Survey Rating Forms, and Head Survey Spreadsheets. The Head Survey includes two sections, Head Problem and Drainage Problem.

We applied the survey as follows:

- 1) Obtain map (scale 1:25,000 or larger) of the distribution network and irrigated areas, making sure to identify for each canal the corresponding irrigated areas

- 2) Working with the operators, complete survey forms for canals and command areas, and modify forms as needed
  - a) Train collaborators on how to rate canals and irrigated areas
  - b) Make changes in rating criteria and scale as needed
  - c) Identify canals and irrigated areas to be rated, and assign rating ID
  - d) Jointly complete survey
- 3) Encourage operators to conduct ground truth
- 4) Enter data into spreadsheet
  - a) Train collaborators on data entry (Excel spreadsheets)
  - b) Enter data
- 5) Analyze data and create maps showing results
  - a) Perform data quality control
  - b) Link data to GIS
  - c) Carry out additional analysis as needed
  - d) Review results with operators
- 6) Create reports to include the following:
  - a) Tables of results
  - b) GIS maps with results of rating for canals and irrigated areas

Comments are included in the manual in order to help the user to avoid common mistakes and/or to plan future improvements. For example, with this rating it can happen that the same canal is rated differently when it serves areas that are rated differently. As two records for the same canal ID cannot be joined to the canal shape file but only related, these results cannot be displayed on map but only on tables.

An example of results of the Head Problem Survey application is reported below. Codes are entered in the forms, each of them representing a complete answer. Columns A1, A2, B and C in Table 1 represent the questions “Frequency of head problem during peak period”, “Frequency of head problem during non-peak period”, “Cause of head problem”, and “Severity of head problem” respectively. Figures 1 and 2 show the case of question A1, for which there are four possible answers: Never (0), Sometimes (1), Often (2), Always (3). Figure 3 shows the case of question C, for which there are three possible answers: Minor (0), Moderate (1), Major (2).

Table 1. Example of Head survey data summary (“n.d.” for canals and command areas with no head problems)

HEAD PROBLEM						
Area_ID	Canal_ID	A1	A2	B	C	Notes
B-0/R	B-0/R	n.d.	n.d.	n.d.	n.d.	
B-0_I	B-0_I	n.d.	n.d.	n.d.	n.d.	
B-0_II	B-0_II	3	3	1, 2, 3d	1	
B-1	B-1	n.d.	n.d.	n.d.	n.d.	
B-2_I	B-2_I	n.d.	n.d.	n.d.	n.d.	
B-2_II	B-2_II	3	0	1, 2, 3d	0	
B-2_III	B-2_III	2	1	1, 2, 3d	1	
B-3	B-3	n.d.	n.d.	n.d.	n.d.	
B-4	B-4	n.d.	n.d.	n.d.	n.d.	
C-1_I	C-1_I	n.d.	n.d.	n.d.	n.d.	
C-1_II	C-1_II	3	2	3e, 3f	2	
C-3_I	C-3_I	n.d.	n.d.	n.d.	n.d.	
C-3_II	C-3_II	3	3	3e, 3f	1	
C-5_I	C-5_I	n.d.	n.d.	n.d.	n.d.	
C-5_II	C-5_II	3	2	3e, 3f	1	
BC-3	BC-3	n.d.	n.d.	n.d.	n.d.	
BC-4	BC-4	n.d.	n.d.	n.d.	n.d.	
BC-5	BC-5	n.d.	n.d.	n.d.	n.d.	
BC-6	BC-6	n.d.	n.d.	n.d.	n.d.	
BC-7_I	BC-7_I	n.d.	n.d.	n.d.	n.d.	
BC-7_II	BC-7_II	1	0	3d, 3f	0	
BC-8	BC-8	n.d.	n.d.	n.d.	n.d.	
BC-9	BC-9	n.d.	n.d.	n.d.	n.d.	
BC-9A	BC-9A	n.d.	n.d.	n.d.	n.d.	
BC-11	BC-11	n.d.	n.d.	n.d.	n.d.	
BC-12	BC-12	n.d.	n.d.	n.d.	n.d.	
BC-10_II	BC-10_II	3	3	3b, 3c, 3d, 3f	2	
BC-10_I	BC-10_I	n.d.	n.d.	n.d.	n.d.	
BC-10/13	BC-10/13	3	3	3c, 3d, 3f	2	
BC-19	BC-19	n.d.	n.d.	n.d.	n.d.	
BC-20/1	BC-20/1	n.d.	n.d.	n.d.	n.d.	
BC-20/2	BC-20/2	3	3	3b, 3d, 3f	0	
BC-20/2/2	BC-20/2/2	3	3	3b, 3d, 3f	0	
BC-18	BC-18	3	3	3b, 3d, 3f	0	

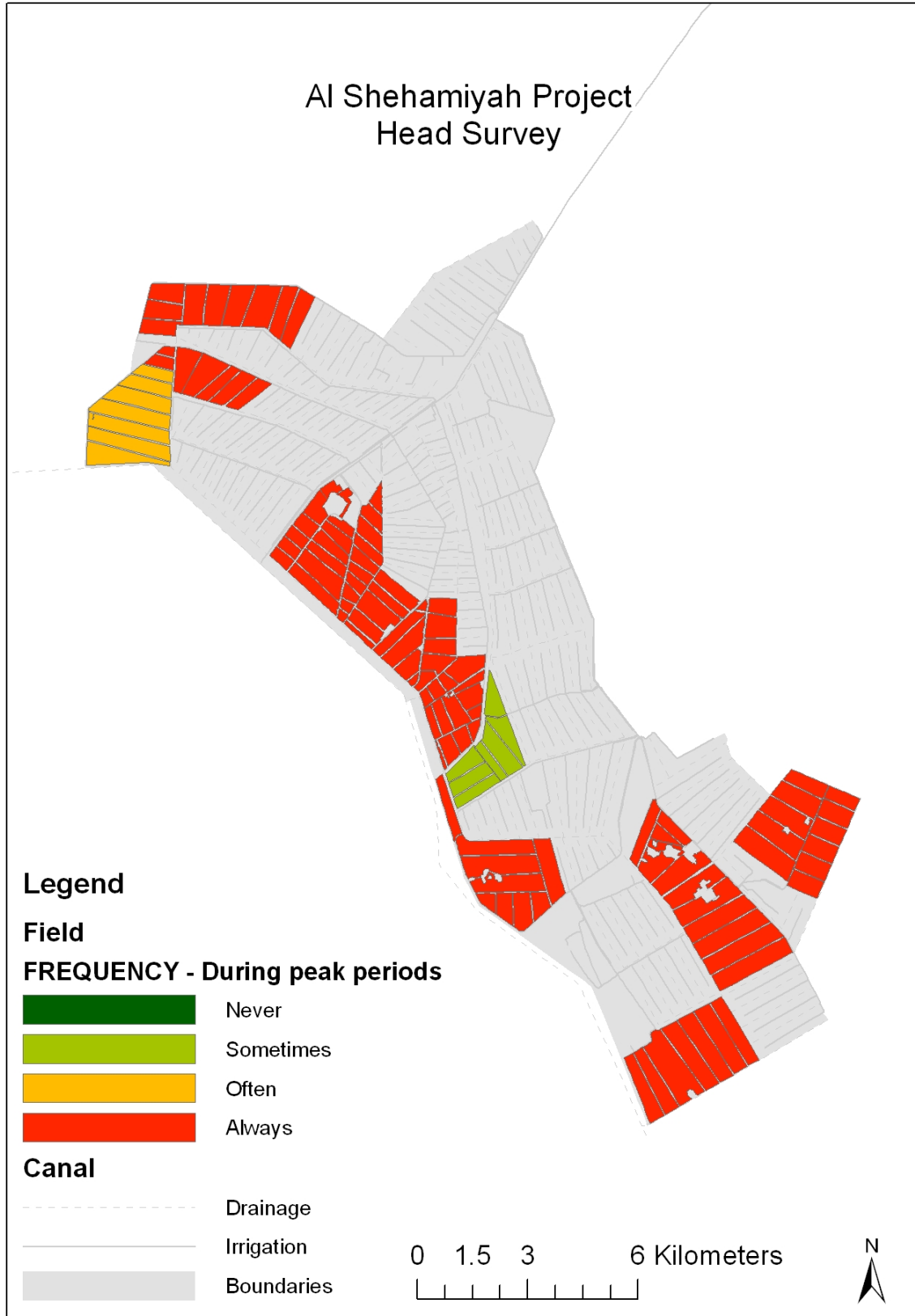


Figure 1. Example result for the Head Survey: Frequency during peak periods (Irrigated area)

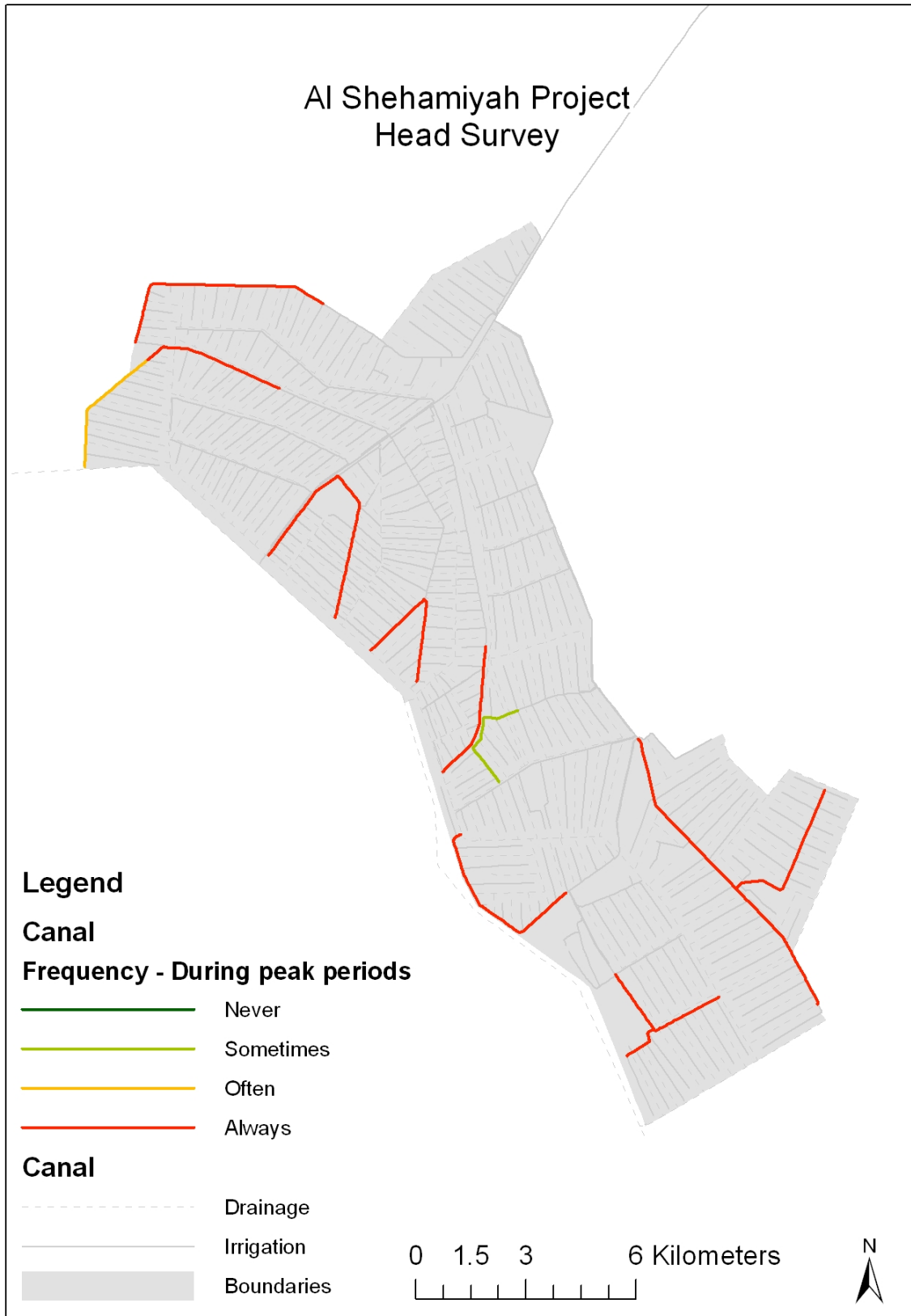


Figure 2. Example result for the Head Survey: Frequency during peak periods (Network)

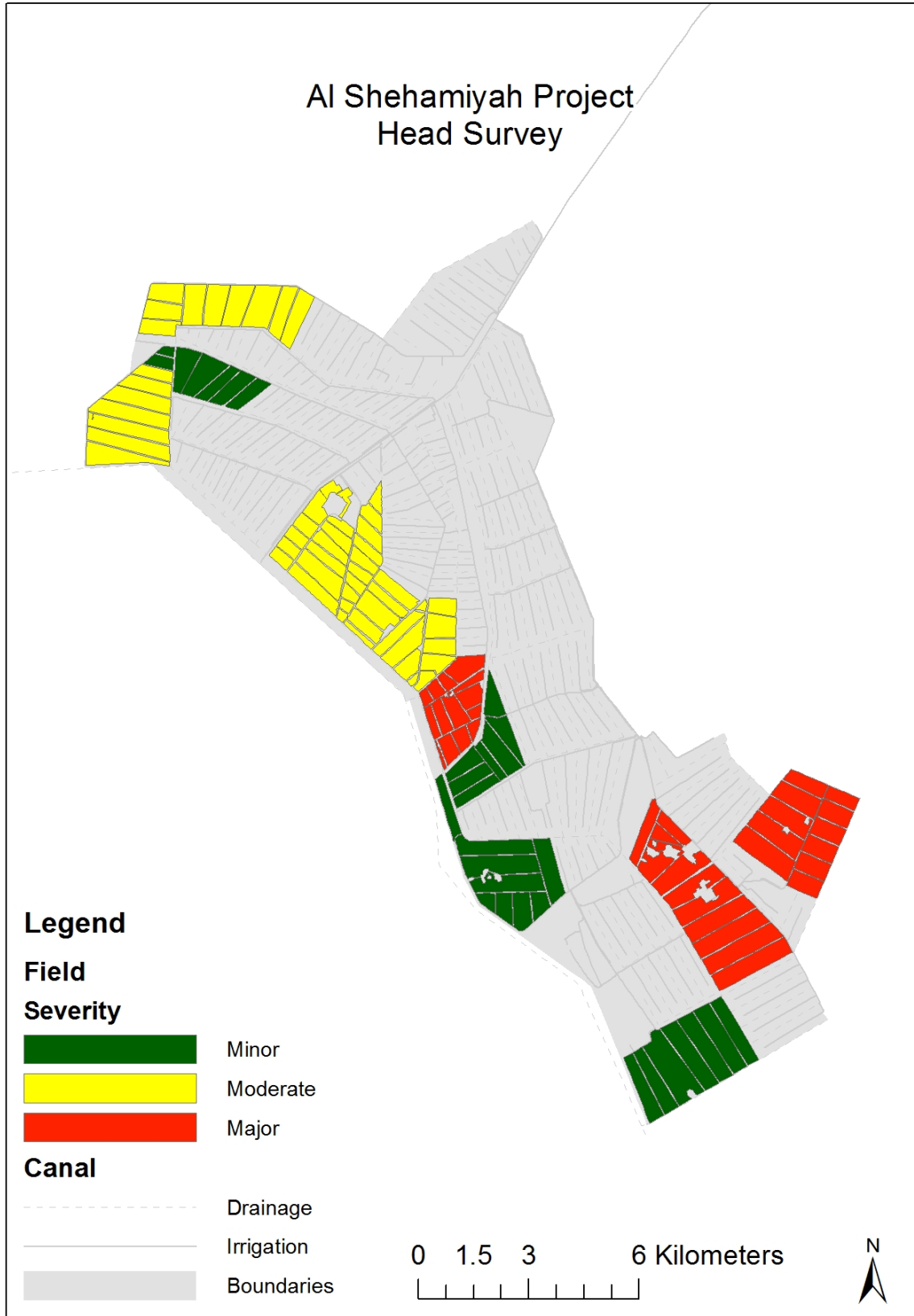


Figure 3. Example result for the Head Survey: Severity of head problem (Irrigated area)

**Distribution Network Condition Rating Tool (Canal and Gate Evaluation)**

The purpose of the Canal and Gate Evaluation is to assess general condition of the irrigation distribution network through a visual rating system to identify segments which need rehabilitation. The tools utilized for this survey are Distribution Network Condition Rating Form/Survey, and Excel Spreadsheet. The Canal and Gate Evaluation includes three sections, General Description, Questions to the Canal Riders, and Field Rating Forms (Concrete Canal, Earthen Canal, Gates).

As for the Head Survey, the Manual reports a suggested procedure and additional comments. For example we recommend to identify segments to be rated using existing hydraulic structures (such as diversion gates, control gates, bridges), and to make sure that segments are fairly homogeneous. For example, a segment will be split in more segments if during the field survey it results having a not homogeneous rating. An example of results of the application of the Concrete Canal Evaluation is reported in Table 2 and Figure 4. In figure we show the rating for the general conditions, i.e. column 10 in the table (0 = Excellent, 1 = Good, 2 = Fair, 3 = Poor, 4 = Serious Problems).

**On-farm Head Survey and Analysis Tool (On-Farm Survey)**

The purpose of the On-Farm Survey is to collect information needed to determine if the current flow at the farm turn-out is sufficient to allow for efficient on-farm irrigation. The tools utilized for this survey are On-Farm Survey Rating Form, and On-Farm Survey Spreadsheet.

As for the previous tools, the Manual reports a suggested procedure and additional comments. For example we recommend that answers should refer to a typical field in the scheduling unit, and during peak irrigation month. An example of results of the application of the On-Farm Survey is reported in Figure 5. Once again, forms are filled using codes.

An On-farm water delivery schedule calculation procedure is also available in the Manual. Additional data are needed to complete this calculation, which can be collected using recommended forms and procedures reported in the Manual.

Table 2. Concrete Canal Evaluation data summary for Main Canal (MC) and Branch Canal (BC). Column 10 is the rating for the general conditions (0 = Excellent, 1 = Good, 2 = Fair, 3 = Poor, 4 = Serious Problems)

QUESTION																							
GENERAL					CANAL RIDER				FIELD														
1_ID	2	3	4	5	6	7	8	9	10	11	12	13	14	15	16	17	18	19a	19b	20	21	22a	22b
MC_0_4	0	4	0	1	1982	0	1	1A	2	2	1	0	2	1	0	0	2	1	2	3	1	1	10
MC_4_10.5	4	10.5	0	0	1982	0	1	1A	2	2	1	0	2	0	0	0	1	1	1	2	0	0	8
MC_10.5_13.5	10.5	13.5	0	0	1982	0	1	1A	2	2	1	0	2	1	0	0	1	1	1	3	1	1	8
MC_13.5_15	13.5	15	0	0	1982	0	1	1A	2	2	1	0	2	1	0	0	1	2	2	3	1	1	4
MC_15_16	15	16	0	0	1982	0	1	1A	2	2	1	0	2	1	1	0	1	1	2	3	1	1	3
MC_16_17.5	16	17.5	0	0	1982	0	1	1A	2	2	1	0	2	0	0	0	1	2	1	3	1	1	2
MC_17.5_19.6	17.5	19.6	0	0	1982	0	1	1A	2	1	1	0	2	0	0	0	1	2	2	3	1	1	4
BC_0_3	0	3	0	0	1982	0	1	1A	2	2	0	0	2	0	0	0	1	1	1	2	1	1	9
BC_3_5.4	3	5.4	0	0	1982	0	1	1A	3	2	1	0	2	0	0	0	1	1	2	2	1	1	15
BC_5.4_6.3	5.4	6.3	0	0	1982	0	1	1A	1	1	0	0	2	0	0	0	1	1	2	2	1	0	1
BC_6.3_6.9	6.3	6.9	0	0	1982	0	1	1A	1	1	0	0	2	0	0	0	1	1	1	2	0	0	0
BC_6.9_11.1	6.9	11.1	0	0	1982	0	1	1A	1	1	0	0	2	0	0	0	1	1	1	2	0	0	6
BC_11.1_12	11.1	12	0	0	1982	0	1	1A	1	1	0	0	2	0	0	0	1	1	1	2	0	0	0
BC_12_12.3	12	12.3	0	0	1982	0	1	1A	3	3	1	0	2	1	0	0	2	2	2	2	1	1	1

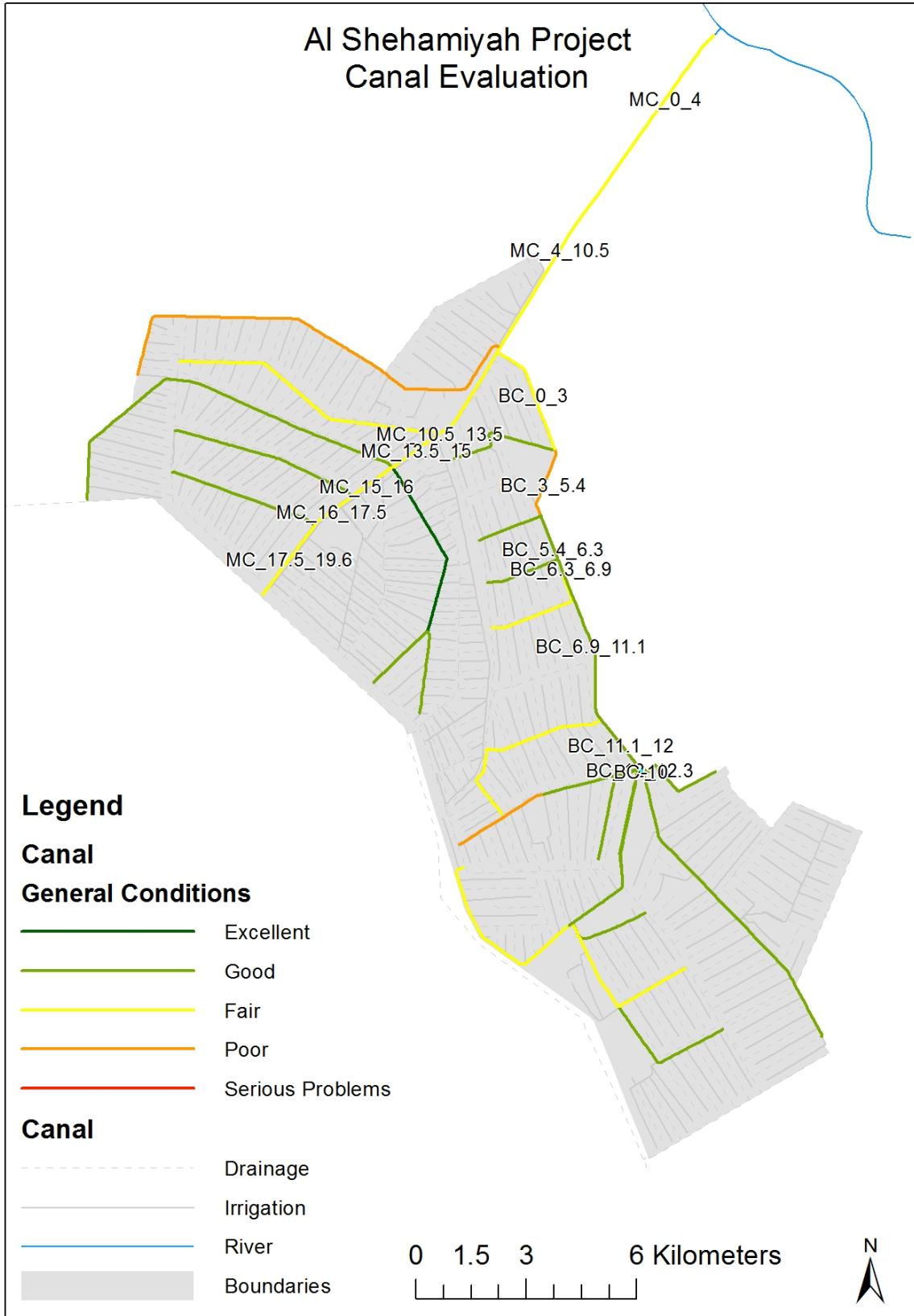


Figure 4. Example result for general conditions in the Canal evaluation (concrete canal). Rating IDs are shown for the Main Canal and the Branch Canal

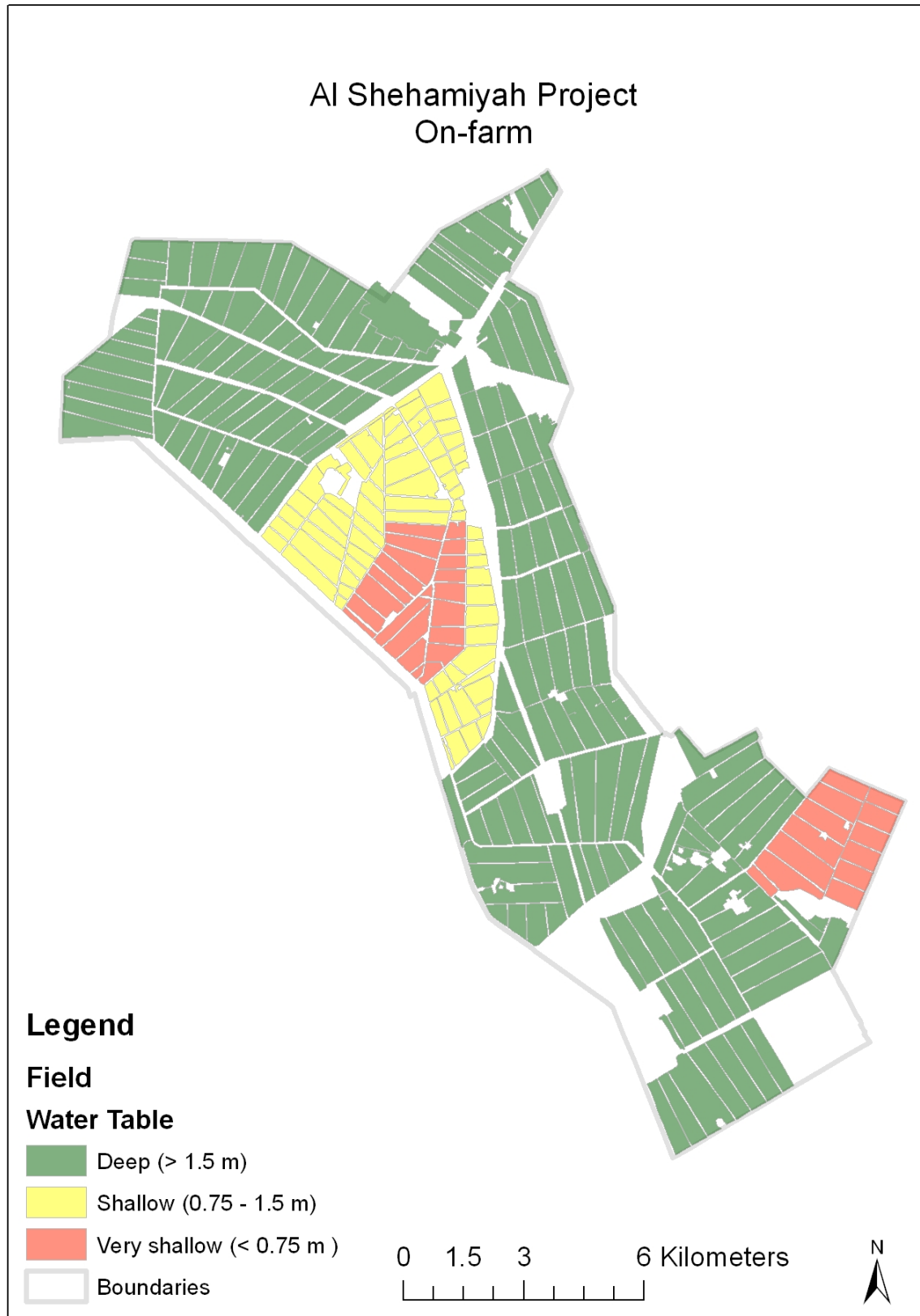


Figure 5. Example result for on farm survey: Water Table depth

## **GIS MAPPING**

GIS is an essential component of the RIP, and irrigation schemes in Iraq have no structured GIS. We recommended a GIS Structure and a procedure to build it. Several comments are also included in the manual to guide the user, such as edit at a scale 1:5,000 or larger, use snap control when creating hydraulic network features, or draw canals features always in the direction of the flow.

## **CONCLUSIONS**

The type of results and benefit of applying the RIP include the setup of an organized structure of data that can be further developed in more complex analysis, and a quick picture of the priorities to be addressed to improve water delivery efficiency. Such structure and analysis are not to be considered a static but dynamic product. This is because all data are interconnected and easily modifiable by a trained person, in such a way that whenever additional data are available or current data change, results can be quickly updated with a minor effort. Additionally, the GIS structure is set up in such a way that different projects can be combined together within the same files, in such a way that the user can simply query the desired irrigation scheme results to be shown.

For example, if periodic field surveys are conducted (head survey, or canal survey, or on-farm survey), the new entered data in the Excel tables will produce automatically new maps and charts to be visually analyzed. Another example can be done for the irrigation scheduling. When detailed flow rate measurements or other field data become available, water delivery scheduling can be recalculated and improved using the available spreadsheets. Furthermore, the user can change all variables that he likes based on local traditions and/or requirements (ex. diversion and irrigation efficiency, time and interval of application, number of borders irrigated at the same time) to set up the best water management scenario desired.



# IMPACTS OF CLIMATE CHANGE AND HUMAN INTERVENTIONS ON LOWER INDUS BASIN

Khero Zarif<sup>1</sup>  
Memon Mansoor<sup>2</sup>  
Bakhshal Lashari<sup>3</sup>

## ABSTRACT

The Lower Indus Basin represents almost 100 percent of the population of Sindh province of Pakistan. It provides water supply to irrigated agriculture (83%), ecology (10%) and domestic and industries (7%) of the province. During the last four to five decades, the changing hydrological behavior at Lower Indus Basin has been noticed. In order to evaluate behavioral change affecting water inflows, sediment flushing, water level rise in floodplain and lag time, the relevant data were collected from the Irrigation Department from 1961 to 2011.

The mass curve developed has shown that the average annual inflows from 1961 to 1999 were 88 million acre feet (MAF) whereas from 1999-2011 it decreased to 51 MAF. These variations in water flows have caused low water and land productivity in irrigated areas of the province. The flow duration curve derived from the data has indicated that 100% of the water supply to canals occurred 25% of the time and 80% of the supply occurred 68% of the time. Further, the supply to irrigation canals from 1961-1999 (human interventions era) ranged between 53 - 95 percent and from 2000-2011 (human interventions era and climate change) was between 48- 76 percent of the design water requirement.

River morphology is dependent on river flows and sediment transport. The sediment sluicing flow factor (i.e., ratio of downstream flow to canal withdrawal at diversion barrages) of the last 50 years was calculated between 0.18-1.54 against design operating requirement of 2. This huge variation has caused shoal formations in all three barrages of Lower Indus Basin. This changing river morphology has resulted in high flood levels along the river embankments and extended lag time from 6 days to 22 days from Sukkur Barrage to Kotri Barrage.

Study concluded that any future interventions should be linked with water availability and climate change effect, thus, there is a dire need to assess water balance in the Indus Basin to protect existing irrigated agriculture of Lower Indus Basin.

---

<sup>1</sup> Executive Engineer, Irrigation Department Government of Sindh, Pakistan, [zarifkhero@gmail.com](mailto:zarifkhero@gmail.com)

<sup>2</sup> Executive Engineer, Irrigation Department Government of Sindh, Pakistan, [memonmansoor4@gmail.com](mailto:memonmansoor4@gmail.com)

<sup>3</sup> Professor, Institute of Water Resources Engineering and Management, Mehran University of Engineering and Technology Jamshoro, Sindh Pakistan email: [bakhshall@yahoo.com](mailto:bakhshall@yahoo.com)

## INTRODUCTION

The irrigation system of Lower Indus Basin covers the command areas of three barrages (Gudu-Sukkur-Kotri) and the coastal area which makes up about 83% of the total arable land of the province. The Indus River Basin hosts a major network of rivers flowing between India, Pakistan, China, and Afghanistan. It is comprised of six shared rivers: Indus, Jhelum, Chenab, Ravi, Beas, and Sutlej [Lower Indus Report (1965), Bashir A. Malik (2005), Dr Nazir Ahmed (1993), The World Bank Report (2005)]. Region-wise and the Country-wise distribution of the land in the Basin is depicted in Figure 2.

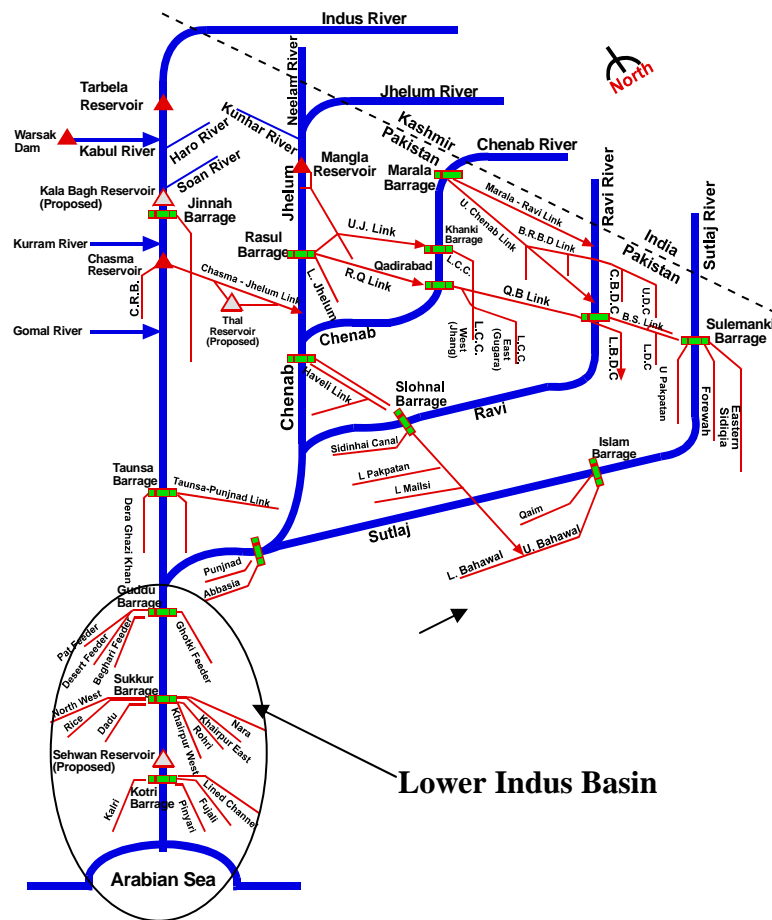


Figure 1. Indus Basin Irrigation System

Pakistan possesses a number of rivers which are tributaries to the Indus. Five main rivers joining its eastern side are the Jhelum, Chenab, Ravi, Beas and Sutlej beside three minor rivers the Soan, Harrow and Siran draining certain sub-mountainous areas. A number of comparatively small rivers join the Indus on the west side. The biggest is the Kabul with its main tributaries, the Swat, Panjkora and Kunar. Kurran, Gomal, Kohat Tai, Tank and several other small streams also join on the right side of the Indus [Appraisal of Flood Management Systems in Pakistan Volume – I&II (1975)]

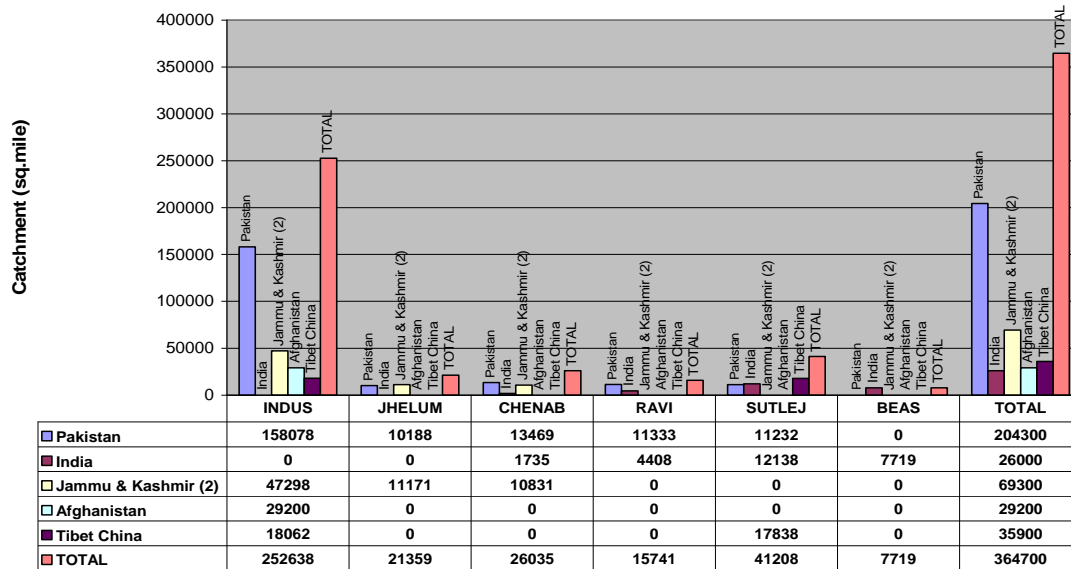


Figure 2. Details of Catchments Area of Indus River System  
(source: Dr Nazir Ahmed 1993)

The total catchment area of the Indus Basin is approximately 1,165,500 km<sup>2</sup> upto the sea and 761,000 km<sup>2</sup> upto Sukkur Barrage. The catchment area lies 56% in Pakistan, 7% in India, 19% in Jammu & Kashmir, 8% in Afghanistan and 10% in Tibet China.

The upper portion of the Indus is fed by snow and glacial melt waters and converges in the Punjab region of Pakistan with the five other rivers in the system. The Lower Indus Basin (LIB) starts just above the Gudu Barrage, the first barrage of Sindh Province, and terminates at the Arabian Sea. It stretches to some 500 km in the southwest to the Arabian Sea, and in the south-east to the border with India in the Rann of Kutch.

The climate of Sindh can simply be described as arid and hot and its average annual rain fall does not exceed 260mm except the rain 2011 which exceeded 1400 mm

Lower Indus Basin System (Gudu-Sea) consists of 3 barrages and 14 irrigation canals which divert about 48 million acre-feet (59 billion cubic meters) of water annually to irrigate 14.391 million acres (5.8 million hectares) of land [Operation & Maintenance Manual (1995)]. To control the river floods 1325 miles of Flood Protective Embankments and 133 miles of Left Bank Outfall Drains (L.B.O.D) are constructed in Sindh province.

Indus Waters Treaty 1960: About 33 million acre-feet of water or the complete run-off of the eastern rivers (Ravi, Beas and Sutlej Rivers) was agreed for the exclusive use of India. The average annual flow of the Indus basin is narrated in Table 2.. To feed the Sutlej Valley Project which was debarred from the water right from its original source, the Treaty provides construction of replacement works to divert the water of Western rivers to affected areas which includes construction of 2 reservoirs of aggregate storage capacity of 10 MAF and 9 inter-river links as shown in Table 1 (a&b).

Table 1(a). Interventions on Indus Basin (Pakistan)

Intervention/ Change	Year of Construction	Initial Capacity (Cusec)	Intervention/ Change	Year of Construction	Initial Capacity (Cusec)
<b>Pre-Indus Basin Treaty IWT-1960 Projects</b>			<b>Post Treaty Project (continue)</b>		
Haveli Project	1939	11,000	Taunsa – Panjnad	1962	12000
Thal Canal	1955	7,500	Chashma – Jhelum	1971	21700
Marala Ravi Link	1956	22,000	<b>Barrages</b>		
Taunsa Barrage	1958	36,501	Sidhnai	1965	14100
<b>Projects Completed under Indus Basin Project (IWT 1960)</b>			Marala	1968	38500
<b>Link Canals</b>			Qadirabad	1967	18600
Trimmu – Sidhnai	1965	11000	Rasul	1967	24300
Sidhnai – Mailsi	1965	10100	Chashma	1971	26700
Mailsi – Bahawal	1965	3900	<b>Dams</b>		<b>L.Storage in MAF</b>
Rasul – Qadirabad	1967	19000	Mangla	1967	4,542 MAF
Qadirabad – Balloki	1967	18600	Tarbela	1976	7.3 MAF
L.C.C Feeder	1967	4100	Chashma – Barrage	1971	0.87 MAF
Baloki – Sulemanki II	1967	6500	Gomal Zam Dam	2012	1.14

Table 1(b). Interventions on Indus Basin (India)

RIVER	INDUS		JHELMUM		CHENAB		TOTAL	
	Completed	Under-Const	Completed	Under-Const	Completed	Under-Const	Completed	Under-Const
<b>NO OF STRUCTURES</b>	12	4	17	6	16	4	<b>45</b>	<b>14</b>
<b>H.P INSTALLED CAPACITY (MW)</b>	100	19.25	1,025.18	369.5	1557.99	1,033	<b>2,683</b>	<b>1,422</b>
<b>G.STORAGE (Acre-Feet)</b>	43,305	0	6,764.15	14,881	617,759	66,641.33	<b>667,828</b>	<b>81,522</b>

This human intervention ultimately affected the water availability to the Lower Indus Basin. To ensure the parity of distribution of the remnant waters of the Western rivers the Water Apportionment Accord 1991 was signed by the chief executives of all provinces and agreed on the water distribution as shown in Table 3.

Table 2. Average Annual River Flows of Indus Basin (Source: IWT-1960)

<b>(Million acre-feet)</b>						
<b>RIVER</b>	<b>April - June</b>	<b>July - September</b>	<b>October - December</b>	<b>January - March</b>	<b>Annual Flow</b>	
Indus	27.9	48.7	7.1	5.8	89.5	<b>135.6</b>
Jhelum	9.9	8.2	1.8	2.7	22.6	
Chenab	6.7	13.1	1.7	2	23.5	
Ravi	1.9	3.3	0.5	0.7	6.4	<b>32.7</b>
Beas	1.9	8.5	1.3	1	12.7	
Sutlej	3.2	8.4	1.2	0.8	13.6	
	<b>51.5</b>	<b>90.2</b>	<b>13.6</b>	<b>13</b>	<b>168.3</b>	

Table 3. Water Apportionment Accord 1991

<b>WATER APPORTIONMENT ACCORD 1991 PROVINCIAL SHARES</b>			
<b>(Million acre-feet)</b>			
<b>PROVINCE</b>	<b>ALLOCATION</b>		
	<b>Kharif</b>	<b>Rabi</b>	<b>Total</b>
<b>PUNJAB</b>	37.07	18.87	55.94
<b>SINDH</b>	33.9	14.82	48.72
<b>NWFP (A)</b>	3.48	2.3	5.78
<b>(B)</b>	1.8	1.2	3.0
<b>BALUCHISTAN</b>	2.85	1.02	3.87
<b>TOTAL</b>	<b>77.34</b>	<b>37.01</b>	<b>114.35</b>
	<b>+</b>	<b>+</b>	<b>+</b>
	1.8	1.2	3.0

The Indus System is largely fed by the snow and glaciers of the Himalayas, Karakoram and the Hindokush ranges of Tibet, Jammu, Kashmir and the northern areas of Pakistan. The flow of the river is determined by the seasons. It diminishes greatly in winter, while flooding its banks in the monsoon months from July to September.

The peak stream flows in July in Upper Indus Basin (UIB) constitutes 32% glacier melt 40% snow melt and 28% rain water which causes major floods in the Basin. The combination of UIB flow and the synchronization of peaks from Western and Eastern rivers cause extremely high floods in the Lower Indus Basin.

### Data collection and analysis

In order to perform the statistical analysis of the data, the main provincial data collection and processing station of the Sukkur Barrage were selected. From the Sukkur Barrage about 60% of the total demand for agriculture and 80% water supply for the urban areas of the Lower Indus Basin is diverted. The barrage is located on the Indus River near the cities of Sukkur and Rohri about 500 km north of Karachi in the upper Sindh area. The geographical coordinates of the barrage are  $68^{\circ} 50' 53''$  E and  $27^{\circ} 40' 50''$  N. Two more barrages on the Indus River within the Lower Indus Basin, Gudu and Kotri, are located respectively about 160 km upstream and 380 km downstream of Sukkur Barrage. The Sukkur Barrage is one of the major structures in irrigation system of Pakistan.

In various countries, guidelines have been formulated for planning of river valley projects for different purposes. For example, according to the practice in India, irrigation projects are planned using 75% dependable flow. Hydropower and drinking water projects are planned with 90% to 100% dependable flows, respectively. The 90% dependability percentage is also used as a measure of groundwater contribution to stream flow. This same value can also be used as measure of run-of-the-river hydropower potential (S.K Jain & V.P Singh, 2003, A. Gustard, A. Bullock and J. M. Dixon 1992, Walter J. Hickel, 1969).

According to Alam (2001), the total quantity of sediment transported annually to the sea by rivers of the world is about  $2 \times 10^{10}$  tons or about  $13.5 \text{ km}^3$  in terms of volume. Of the total, the Indus River contributes only  $480 \times 10^6$  tons into the sea (Holeman 1968). Assuming that all this sediment enters into the reservoirs of the world, it would take about 481 years to fill up the estimated  $6500 \text{ km}^3$  of the storage volume available. The sediment deposits were also found to raise the bed elevations and flood levels in the Yellow River. The accumulation of sediments is one of the principal factors that threaten the longevity of river valley projects.

In order to assess dependable flows, the analysis of the available stream flow data was conducted for the period of 1961-2011. Empirical frequency distributions (flow duration curves) of the river and the off taking canals of Sukkur Barrage are prepared to check the variability of stream flow. To assess the consistency of available flows and the effect of interventions, the mass curve is prepared to check the existing and under planning water resources projects in upper Indus Basin. Analysis envisages the effects of the river regulation, flood control and the sediment load deposition at the barrages and along the River in the Lower Indus Basin. (HIS, Hydrological Project India- July, 2000).

RESULTS AND DISCUSSION

Water Flow Extremes

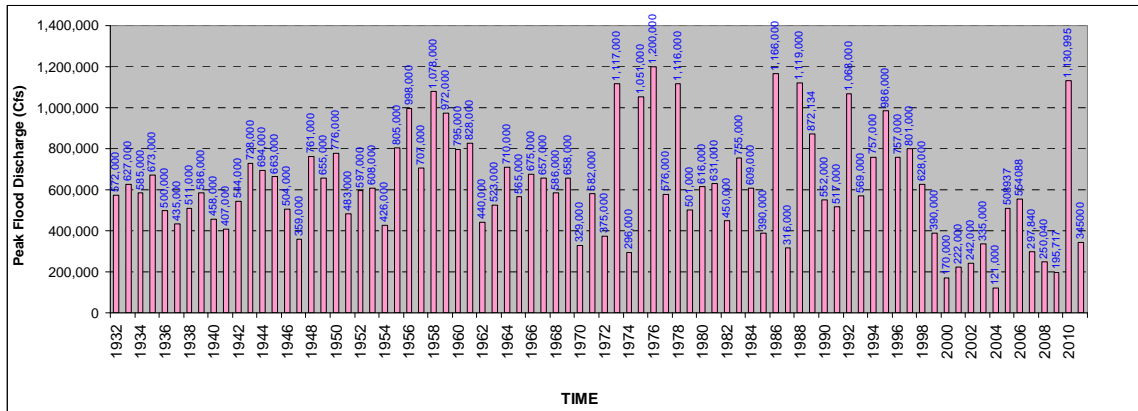


Figure 3. Annual Extreme Floods at Sukkur

Figure 3 describes the extreme flood events from 1932 to 2011. As per flood magnitude classification described by the Irrigation Department, Government of Sindh and), the flood trends from 1932 to 2011 (80 years) shown in (Table 4). From the data it is observed that the difference between the minimum flood peaks (170,000 Cfs in 2000 and 121,000 Cfs in 2004) and the maximum flood peak (1,200,000 Cfs in 1976), is approximately seven to ten times. This large difference between the minimum and maximum annual discharges reflects the unpredictable nature of the hydrological condition/variation and behaviors of the Indus River.

Table 4. Flood Magnitude Classification by Irrigation Department

Flood Severity	Threshold of Discharge (cfs)	Number of floods occurring between 1932 and 2011	Percentage
Super Flood	$Q > 900,000$	12	15%
Very High Flood	$700,000 < Q \leq 900,000$	13	16%
High Flood	$500,000 < Q \leq 700,000$	32	40%
Medium Flood	$350,000 < Q < 500,000$	11	14%
Low Flood	$200,000 < Q \leq 350,000$	9	11%
Normal Flood	$Q \leq 200,000$	3	4%

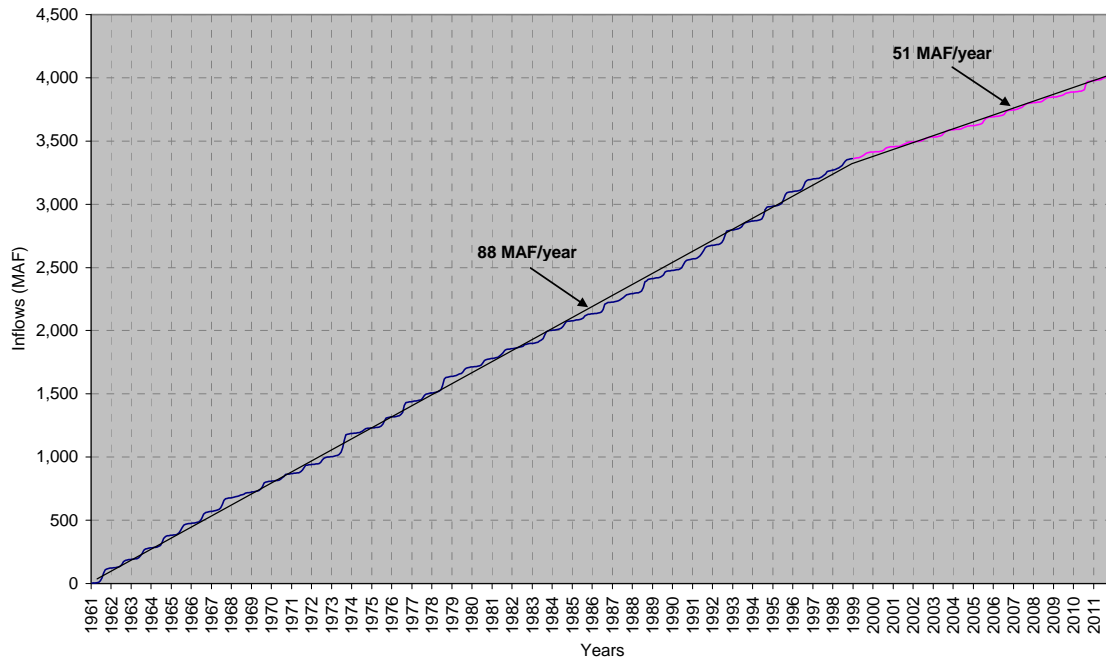


Figure 4. Mass Curve of Monthly Flows at Sukkur Barrage, 1961-2011

Figure 4 describes the cumulative monthly total flows versus time. The average annual inflows which were 88 MAF/year up to 1999, has dropped to 51 MAF in the last 13 years. This indicates matured effect of the interventions in upper Indus Basin and the change in climate.

The reduction in flow and human intervention has caused the sediment deposition along the River bed from Gudu to the Sea. Subsequently the River morphology has changed which causes low flow velocity and high flood level along the River. This is one of the major reasons of extended lag time from average 6 days (medium to high flood) to 17 days (very high to super flood) from Sukkur Barrage to Kotri during the flood time (Figure 5). Overtopping of the flood embankment during 2010 floods on the right side downstream of Gudu Barrage is one such example that caused enormous damages to human life, infrastructure and socio economics of the province of Sindh.

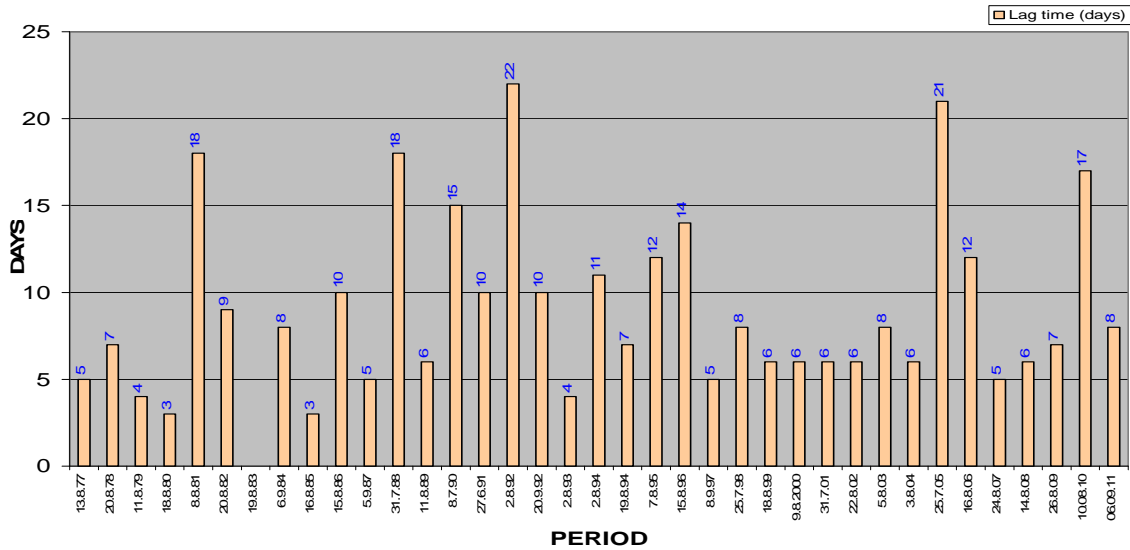


Figure 5. Lag Time of the Peaks between Sukkur & Kotri Barrages

**Flow variability and system performance**

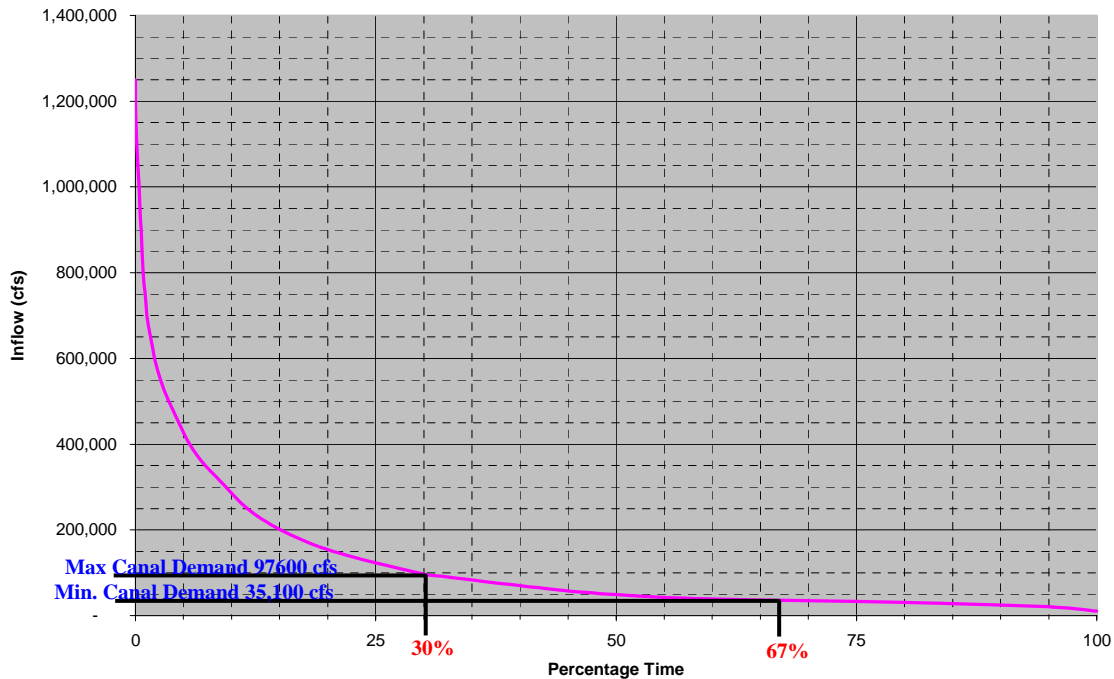


Figure 6. Duration Curve of Daily Flows at Sukkur Barrage, 1961-2011

Figure 6 states the variability of river flows for the last 50 years (1961-2011). The data analysis indicates that the availability of maximum canal demand (Kharif-97,600 Cfs) remained available only for 30 percent of the time and minimum canal demand (Rabi-35,100 Cfs) was available for the period of 67 percent time. The curve trend also

indicates that the low flows prevail for longer times as compared to the flows equal to or higher than the 100% demand. The causes of this reduction in the flows are the human intervention (combined effect of the implementation of Indus Water Treaty 1960, post treaty works) and climate change effects.

The reduction of flows in the River is causing operational and management problems for the canals taking off from barrages in Sindh.

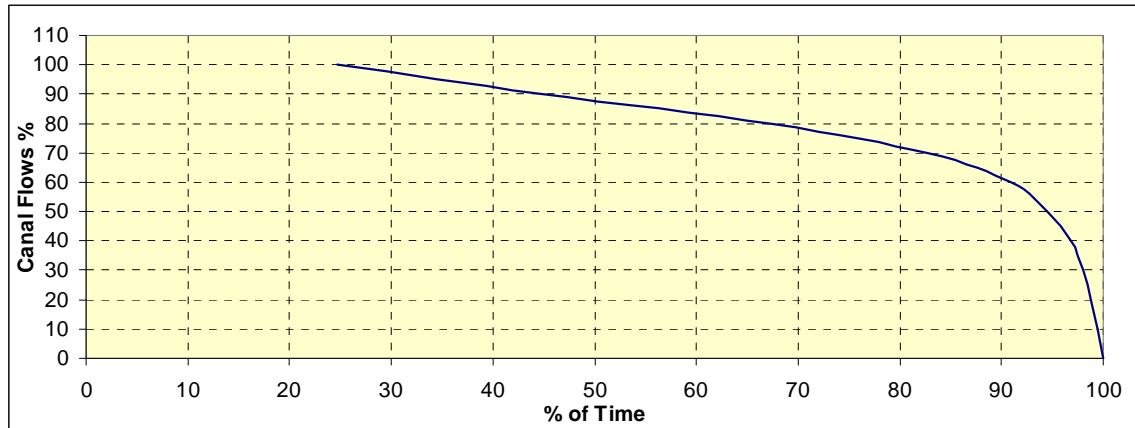


Figure 7. Flow Duration Curve of Sukkur Barrage Canals

The water demand and supply were assessed and are shown in Figure 7. The data analysis expresses that 100% demand of the canals of Sukkur Barrage during last of 50 years (1961-2011) is met only for 25% of time, whereas, the 80% demand of the canals is available only for 68% of time. Thus, the water availability scenario is found below the standard operating requirement for the canal and barrage operations. This phenomenon is causing irreparable damage to crops, canal regime and the overall economy of Lower Indus Basin. Water and Power Development Authority (WAPDA) stated that during shortage periods, the canals should not be stressed beyond 80% of their requirement, as yields are significantly affected beyond this point (Report of the Technical Committee on Water Resources, 2005). Table 5 describes the supply to irrigation canals from 1961-1999 (human interventions era) was ranging between 53 - 95 percent and from 2000-2011 (human interventions era and climate change) was between 48- 76 percent of design water requirement.

Table 5. Average Monthly Demand and Supply to Canals of Sukkur and Kotri Barrages

Month	Average Monthly Demand (MAF)	Water Supplied Through Canals			
		Average of 1961-1999		Average of 2000-2011	
		Water Supplied (MAF)	% of Demand	Water Supplied (MAF)	% of Demand
January	0.71	0.62	87.32	0.34	47.89
February	1.88	1.51	80.32	1.18	62.77
March	1.77	1.57	88.70	1.18	66.67
April	2.427	1.48	60.99	1.26	51.92
May	3.470	1.98	57.06	2	57.64
June	5.253	2.8	53.30	2.82	53.68
July	5.602	3.2	57.12	3.35	59.80
August	4.831	3.14	64.99	2.99	61.89
September	4.950	2.65	53.54	2.72	54.95
October	3.277	2.21	67.43	1.94	59.20
November	1.91	1.83	95.81	1.45	75.92
December	1.81	1.65	91.16	1.28	70.72
Annual	37.890	24.640	71.479	22.510	60.25

Figures 8(a&b) also describe the unpredictable behaviors of the water availability during the crucial cropping periods for the last eleven (11) years.

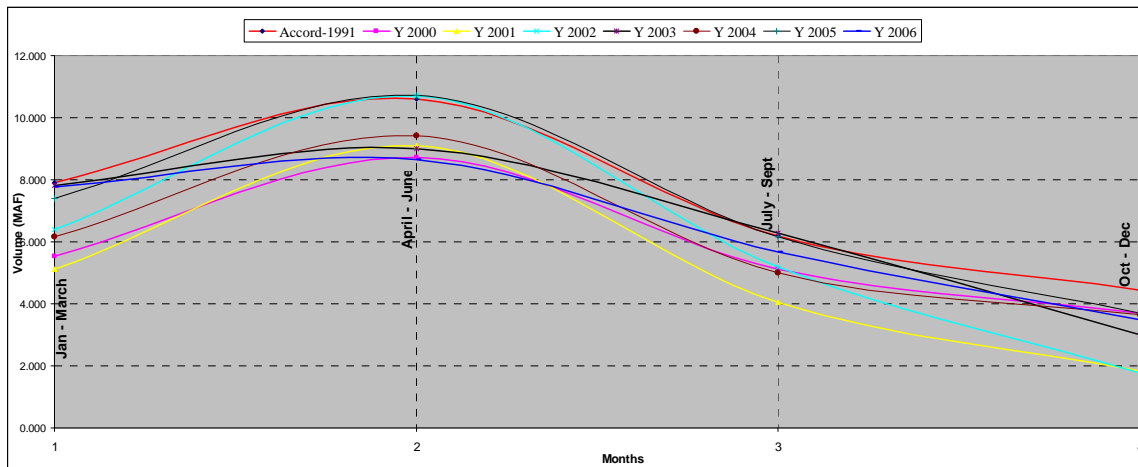


Figure 8 (a). Canal withdrawal and Water Allocation (1991) of Sukkur Barrage, 2000-2006

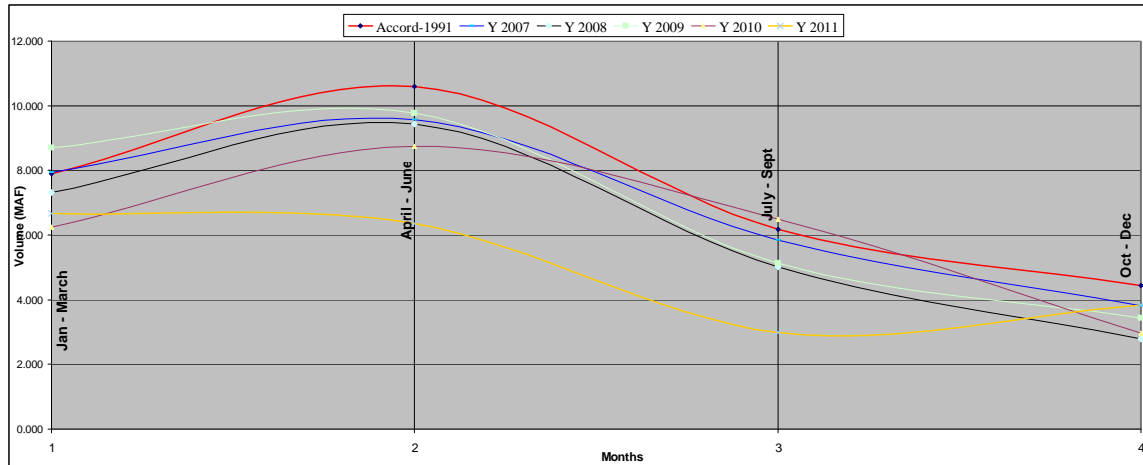


Figure 8 (b). Canal withdrawal and Water Allocation (1991) of Sukkur Barrage, 2007-2011

The Figures 8 (a) & (b) explain that the water withdrawals of the Sukkur Barrage Canals show that the flow is less in all the years than the water demand. It has been observed that the shortages of water has largely influenced the water distribution that includes water equity, reliability and water use efficiency. The distribution in the canal commands is also managed through rotations which have resulted in low yield of major crops causing socio-economic problems in the province.

### **Sediment sluicing**

The sluicing of sediments becomes successful, when discharge through barrage is 2 times the discharge of diversion canals (USBR, 1967: Design Standards No.3 Canals and Related Structures). The sediment sluicing flow factor (i.e., ratio of downstream flow to canal withdrawal at diversion barrages) of last 50 years was calculated between 0.18-1.54 against design operating requirement of 2 (Table 6). This huge variation has caused shoal formations in all three barrages of Lower Indus Basin.

Table 6. Sediment Sluicing Factor at Sukkur Barrage, 1961-2011

Month	Period 1961-2011			Period 2001-2011		
	Average Diverted flows into the Canals (MAF)	Average Downstream flows (MAF)	Ratio of flows / Diverted Flows	Average Diverted flows into the Canals (MAF)	Average Downstream flows (MAF)	Ratio of flows / Diverted Flows
January	0.62	0.80	1.29	0.34	0.52	1.54
February	1.48	0.34	0.23	1.18	0.31	0.27
March	1.56	0.64	0.41	1.18	0.57	0.48
April	1.48	1.46	0.98	1.26	0.82	0.65
May	2.04	2.81	1.38	2.24	1.32	0.59
June	2.87	5.32	1.85	3.13	2.82	0.90
July	3.20	12.90	4.03	3.35	5.99	1.79
August	3.14	20.06	6.39	2.99	11.53	3.86
September	2.65	9.11	3.44	2.72	4.29	1.58
October	2.21	1.59	0.72	1.94	0.92	0.47
November	1.83	0.36	0.20	1.45	0.39	0.27
December	1.65	0.29	0.18	1.28	0.27	0.22

This situation becomes worse in Rabi season, when the ratio of canal diversion flows and river downstream flow drops to as low as 0.18.

## CONCLUSIONS

Flood flow pattern of the last 80 years shows that low to medium floods have been dominating, and that the super floods and high flood patterns were occasional and of low duration. The water availability assessed through mass curve clearly describes that from 1961-1999, the water availability was 88 MAF/year which further reduced to 51 MAF from 1999-2011. These two periods clearly indicate that the human interventions and climate change have significantly influenced the reduction of flow in the Lower Indus Basin System. This reduction is not only causing the management problems but also the destabilization of the canal regime.

The river flows variability assessed through flow duration curve indicates that the water availability at Lower Indus Basin System significantly varies. This fluctuation/variability affects crop sowing, crop water need and alive the ecosystem of Lower Indus Basin and the delta. The last 50 years of data of the canal withdrawals have shown that the full supply (100% of demand) was available to the canals only 25% of the time and the availability of 80% of demand, which is the minimum required canal supply to keep running the canal, was 68% of the time. These two extremes show that the crops do not get the required amount of water when needed. This variability affects water use efficiency, water equity and reliability of the system. Thus, the rotation is the only option for the engineers to run the canals.

The sediment sluicing flow factor (i.e., ratio of downstream flow to canal withdrawal at diversion barrages) of the last 50 years ranged from a minimum 0.18 to a maximum 1.54 which is always less than 2.0. This has been one of the major causes of shoal formations in all three barrages of Lower Indus Basin. Consequently, high flood levels along the river embankments occurred and travel time of high floods extended from Sukkur Barrage to the sea, which resulted in huge loss of infrastructure and livelihood of the people especially in year 2010 flood.

Study concluded that any future interventions should be linked with water availability and climate change effects, thus, there is a dire need to assess water balance in the Indus Basin to protect existing irrigated agriculture and eco system and the delta of Lower Indus Basin.

### ACKNOWLEDGEMENTS

Authors are highly thankful to the Department of Irrigation Government of Sindh for financial support required to present this paper in the international conference. Mr. M Ibrahim Samoon, regional Director ACE Karachi for extending technical help and Mr. Abdul Aziz soomro incharge Sukkur Barrage control room in collecting comparable and dependable data for analysis to complete this paper.

### REFERENCES

- A. Gustard, A. Bullock and J. M. Dixon December (1992), Report No. 108, Low flow estimation in the United Kingdom, Institute of Hydrology Wallingford, U.K
- Alam, S. (2001), A critical evaluation of sedimentation management design practice. Hydropower and Dams, Issue One, 54-59
- An overview & Note on Hydrological Information System, Hydrological Project India-July, 2000.
- Appraisal of Flood Management Systems in Pakistan Volume – I (1975), "Flood Forecasting & Flood Warning Systems, October 1975.
- Appraisal of Flood Management Systems in Pakistan Volume – II (1976) "Existing Flood Control Structures & Recommendations for a Planning Programme, January 1976.
- Bashir A. Malik (2005), Indus Water Treaty in Retrospect
- Dr Nazir Ahmed (1993), Water Resources of Pakistan printed by Miraj Din press, Lahore Sept 1993
- Lower Indus Report (1965), Physical Resources by Hunting Technical Services Ltd. and Sir M. Macdonald & Partners, 1965.

Operation & Maintenance Manual (1995): Irrigation Department Government of Sindh  
Volume 1 & 2, 1995

Report of the Technical Committee on Water Resources (2005)

S.K Jain & V.P Singh (2003), Developments in Water Science (ELSEVIER)

Water Accord (1991), Apportionment of Waters of Indus River System between the  
Provinces of Pakistan - Agreement 1991.

USBR, 1967: Design Standards No.3 Canals and Related Structures

Walter J. Hickel (1969), Manual of Hydrology: Part 2. Low-Flow Techniques.  
Geological Survey Water-Supply Paper 1542-A.

World Bank Report (2005), Pakistan's Water Economy Running Dry, draft of June 2005.

Working Paper No. 48 Flood Protection - Lower Indus Region Study for Right Bank  
Master Plan - December 1990.



# **ESTIMATING CROP WATER USE WITH REMOTE SENSING: DEVELOPMENT OF GUIDELINES AND SPECIFICATIONS**

Hatim M. E. Geli<sup>1</sup>  
Christopher M. U. Neale<sup>2</sup>  
James Verdin<sup>3</sup>  
Gabriel Senay<sup>4</sup>

## **ABSTRACT**

This paper provides a brief overview of a suggested framework that is aimed to provide guidelines and specifications for the application of remote sensing of evapotranspiration (ET). Several models that are available, that if properly applied, can provide spatial estimates of ET with reasonable accuracy. However varying results can also be obtained with a relatively unknown range of uncertainty. There is currently an effort by the USGS to investigate the associated uncertainties of the input data needed for these models as well as model parameterizations on their estimates of ET.

The analysis in this paper focused on two issues: (1) the potential of using gridded weather forcing and input data and (2) their effects on estimates of ET using remote sensing techniques. Comparison of gridded and ground based weather forcing data with preliminary results is provided. Gridded weather forcing data were obtained from the NLDAS-2 and selected stations in and around Utah providing ground data.

The associated uncertainty and bias of using NLDAS-2 forcing data with regard to ground-based measurements was investigated using the two source energy balance (TSEB) model of Norman et al. (1995). Surface energy balance fluxes (SEBF) and ET were estimated over the Palo Verde Irrigation District (PVID), CA. The PVID covers 500 km<sup>2</sup> with predominantly alfalfa and cotton crops. It is surrounded by desert, which provides challenging conditions for the use of gridded weather data. The estimated fluxes were compared with ground-based flux measurements. The analysis was conducted during the summer of 2008 using thermal and multispectral images from the Landsat.

## **INTRODUCTION**

Accurate estimates of crop water use are becoming increasingly important as irrigated agriculture represents the largest consumptive use of water in the western United States. Water lost/used in irrigated agriculture through evapotranspiration (ET) needs to be estimated from field to regional scales. With the advances in the application of remote sensing data and techniques, several methods can be used to provide spatial estimates of ET with a reasonable accuracy. The USGS is required to provide estimates of the consumptive water use as part of the WaterSMART program. Consumptive water use

---

<sup>1</sup> Department of Civil and Environmental Engineering, Utah State University, Logan, UT 84322-4110.

<sup>2</sup> Department of Civil and Environmental Engineering, Utah State University, Logan, UT 84322-4110.

<sup>3</sup> USGS EROS Center, Sioux Falls, South Dakota

<sup>4</sup> NIDIS Program Office, NOAA/ESRL, Boulder, Colorado

was previously reported on a 5-years basis. However there is an increased need for annual evaluations considering limited water resources. Such reporting, whether provided on regional, state or at watershed/basin scale (e.g. Colorado River basin), should be consistent and neighboring states within a basin should agree on methodologies and best practices for ET estimation. Some of the Western States have individually started to explore the use of these methods, sharing the same interest in providing estimates of consumptive water use on a seasonal basis. Currently Western States are using different methods, and there is a need to agree on future approaches and methodology and avoid duplication of effort and most importantly, establish the uncertainties associated with estimates.

This has led to the effort of performing a rigorous analysis on models and estimates to come up with guidelines and a common framework. This will help in standardizing the use of remote sensing data and techniques for providing spatial estimates of ET for crop water use in irrigated areas of the Western US. Within this context and as an ongoing effort, this study is investigating the accuracy and uncertainties of using gridded weather forcing data. Most of the remote sensing models of ET use weather forcing data from ground-based stations assuming that it can reasonably represent local conditions. However, at regional and even watershed scales this assumption might not be applicable and hence investigating other possible approaches to account for the variability of near/at surface weather conditions is warranted. The North American Land Data Assimilation System (NLDAS) (Cosgrove et al. 2003) provides gridded weather forcing data that can potentially be a source for such information. This analysis provides some preliminary comparisons between NLDAS-2 forcing and ground-based stations data to highlight some associated uncertainties.

Estimates of ET at regional scales over agricultural areas provide a means for efficient water resources management and allocation. Different thermal remote sensing-based models can be used to obtain such estimates with reasonable accuracy. Ground-based point measurements are generally used in the application of most of these models. However at such scales, using point weather data might not be representative of local variability. With the availability of the NLDAS one potentially can account for local and regional variability of the weather. On the other hand the NLDAS forcing data is available at  $1/8^{\text{th}}$  degree grid ( $\sim 14 \text{ km} \times 14 \text{ km}$ ), which is considered relatively coarse resolution to represent field to field variability in agricultural areas. Here we are investigating the associated uncertainties and biases of using NLDAS-2 forcing data instead of ground-based measurements. The two source energy balance (TSEB) model of Norman et al. (1995) was used to obtain estimates of surface energy balance fluxes (SEBF) and ET over the Palo Verde Irrigation District (PVID), CA. The PVID is about  $500 \text{ km}^2$  in area covered mostly with alfalfa and cotton crops. Estimates of SEBF/ET obtained using both type of weather data (NLDAS-2 and ground-based) are compared to ground-based eddy covariance flux measurements. The analysis is conducted during the summer of 2007 using thermal and multispectral images from the Landsat.

METHODOLOGY

**Framework Outline**

The ET Framework that is under development will provide technical and scientific specification for the required criteria for the different types of input data needed for application of remote sensing of ET. The input data include a) imagery of land surface reflectance and surface temperature that are generally obtained from the USGS, b) investigation of all possible required weather forcing data in terms of accuracy and uncertainties, c) provide specifications of selected remote sensing models of ET with details on their parameterizations, calibration, areas, and scales of applications, d) study uncertainty associated with the different input variables in the estimates of ET.

Towards achieving these goals, we provided some preliminary analysis with respect to the potential of using gridded weather forcing data and their effects on the estimated ET. A comparison of gridded and ground-based weather data can provide an insight to the quality of the gridded data especially in areas featuring high terrain and surface heterogeneity. The two-source energy balance model of Norman et al. (1995) was used to provide estimates of ET from remote sensing using both types of weather forcing i.e gridded and ground-based data.

**Two-Source Energy Balance Model**

Generally, the TSEB model separates the surface into soil and vegetation canopy components and solves the energy balance equation for each.

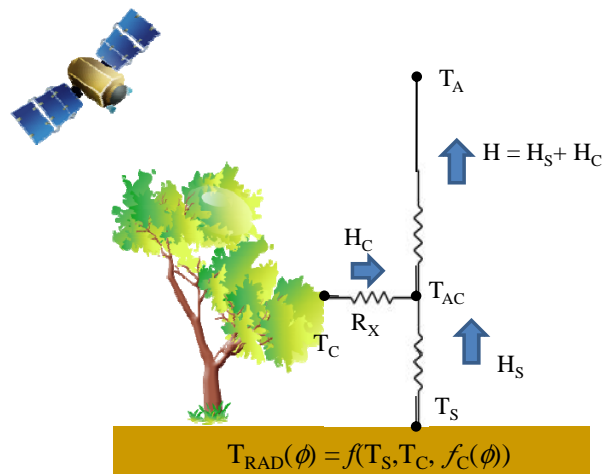


Figure 1. Illustration of a two-source energy balance series resistance formulation model.

The model uses the radiometric surface temperature,  $T_R$ , as the main boundary condition. It decomposes  $T_R$  into soil and canopy surface temperatures components,  $T_s$  and  $T_c$ . The energy balance equation is applied for each component separately as

$$T_R(\phi) \approx [f_c(\phi)T_c^4 + (1 - f_c(\phi))T_s^4]^{1/4} \quad (1)$$

where  $f_c(\phi)$  is the fraction of vegetation cover as a function of the view zenith angle ( $\phi$ ).

Interaction between bare soil and canopy components of  $H$ ,  $H_c$  and  $H_s$ , respectively, is allowed at some level above the ground surface called the air-canopy interface.

$$H_c = \rho C_p \frac{T_c - T_{ac}}{R_x}, \quad (2)$$

$$H = \rho C_p \frac{T_{ac} - T_a}{R_a}, \quad (3)$$

$$H_s = \rho C_p \frac{T_s - T_a}{R_s} \quad (4)$$

where  $R_a$ ,  $R_x$ , and  $R_c$  are the aerodynamic resistance to heat transfer, the total boundary layer resistance of the complete canopy leaves, and the resistance to heat flow in the boundary layer immediately above the soil surface, respectively,  $\rho$  the air density, and  $C_p$  the specific heat of air.

The total latent heat flux,  $\lambda E$ , is estimated as  $\lambda E = \lambda E_s + \lambda E_c$  with  $\lambda E_c$  and  $\lambda E_s$  are the canopy and soil components, respectively. The model uses the Priestley-Taylor approach to estimate canopy  $\lambda E_c$  as

$$\lambda E_c = \alpha_{PTC} f_G \frac{\Delta}{\Delta + \gamma} Rnc \quad (5)$$

where  $\alpha_{PTC}$  is the Priestley-Taylor coefficient in this case defined specifically for canopy. The value of Priestley-Taylor is initially set to 1.3 providing a potential rate for LEC then iteratively adjusted to canopy conditions, the fraction of green vegetation normally set to 1.00,  $\Delta$  the slope of the saturation vapor pressure versus temperature curve, and  $\gamma$  the psychrometric constant ( $\sim 0.066$  kpa C-1).

The soil heat flux,  $G$ , is estimated as  $G = C_g \cdot Rns$ , with  $C_g$  can be set as 0.35. A physically based model developed by Campbell and Norman (1998) is used to estimate the net radiation components  $Rns$  and  $Rnc$ .

The spatial estimates of fluxes were evaluated against measurements obtained by Bowen ratio systems using a 3D footprints analysis. The footprint model by Horst and Weil (1992, 1994) was used to integrate the fluxes.

Extrapolation of instantaneous estimates of  $\lambda E$  to daily values of  $ET$  was achieved using the evaporative fraction (EF) method.

The TSEB was first applied using ground based weather forcing data using a nearby weather station to provide the instantaneous  $R_n$ ,  $G$ ,  $H$  and  $\lambda E$  fluxes and the daily  $ET$ . The model was applied again using the gridded weather forcing data to provide the same results. Both estimates were then compared with ground-based measurements.

## DATA

Gridded weather forcing data were obtained from NLDAS-2 which provided information on 11 variables at  $1/8^{\text{th}}$  of a degree grid ( $\sim 14 \text{ km} \times 14 \text{ km}$ ). In this study we considered only five variables i.e. air temperature ( $T_a$ ) at 2 m above ground level (agl), the zonal and meridional wind speed components  $U$  and  $V$  at 10 m agl, respectively, downward shortwave radiation ( $R_s$ ), and specific humidity ( $q$ ) at 2 m agl.

As described by Cosgrove et al. (2003), the data are a product of running land surface models in an uncoupled mode to produce weather forcing variables at one hour intervals

A full year of hourly NLDAS-2 weather forcing data for 2007 was used in this analysis for the comparison with ground data. To use the NLDAS weather forcing data in remote sensing of ET at field to regional scales with increased confidence it is important to compare it with ground-based observations. Such comparison will help to identify uncertainties and biases. It can also help in quantifying uncertainties in the remote sensing-based model estimates of ET.

The ground data were obtained from selected automated electronic weather station (EWS) in and around Utah (Figure 1). These stations which were maintained by different entities were operated over different surfaces. The study focused on those stations located in irrigated agricultural areas. The total number of stations considered was 24, all providing hourly observations.

Note that the air temperature  $T_a$  measurements at all EWS were made at 2 m above ground, consistent with the NLDAS-2 forcing so no further processing was needed to make the direct comparison. The wind speed,  $u$ , measured at the EWS was at different heights, 2-4 m above ground. Thus to properly be compared with NLDAS-2 grid values, the ground measurements were exponentially extrapolated to 10 m above ground assuming neutral atmospheric conditions. The specific humidity,  $q$ , at all the EWS was not directly reported so it was estimated using the  $T_a$  and  $P$  measured at the weather stations.

To verify the location of the EWS, cropland data were obtained from the US Department of Agriculture USDA, the National Agriculture Statistics Services (NASS) (Boryan et al. 2011). The data are accessible through NASS website (NASS 2012). In 2007 cropland data were not available therefore data for 2008 were used (Figures 2 and 3)

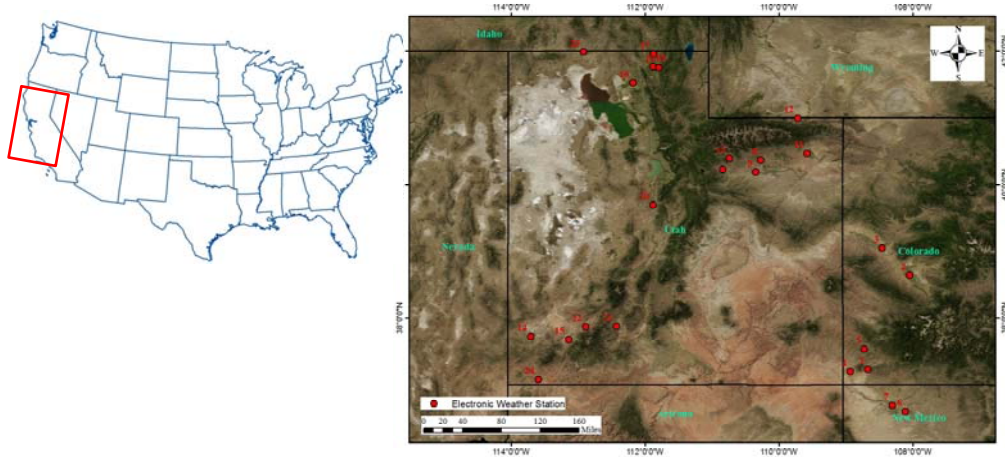


Figure 2. Location of the study area and EWS in and around Utah.

The TSEB model was applied over irrigated agricultural fields at the Palo Verde Irrigation District (PVID) in southern California, (Figure 4). Data from 2008 were processed with crop information and land use as shown in Figure 3. The area is mainly cropped with alfalfa (85%) and cotton (10%) and different kinds of vegetables covering (5%). Landsat 5 images were used to provide surface reflectance and temperature for the 5 dates considered in the analysis including day of year (DOY) 131, 138, in the summer of 2008. Ground-based weather forcing data were obtained from a nearby CIMIS station at Blythe, California; with gridded hourly data obtained for the same period. Ground-based flux measurements were obtained using a Bowen ratio system installed over one of the alfalfa fields, it provided the four main surface energy balance fluxes  $R_n$ ,  $G$ ,  $H$  and  $\lambda E$ .

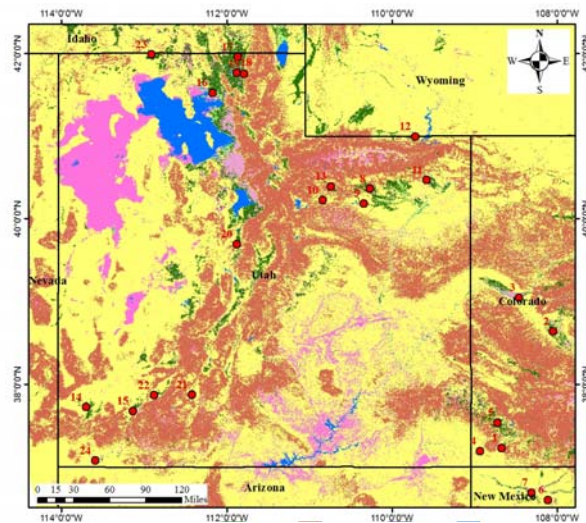
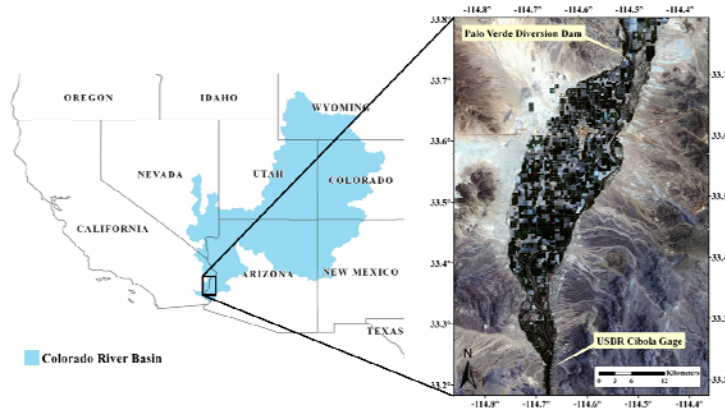
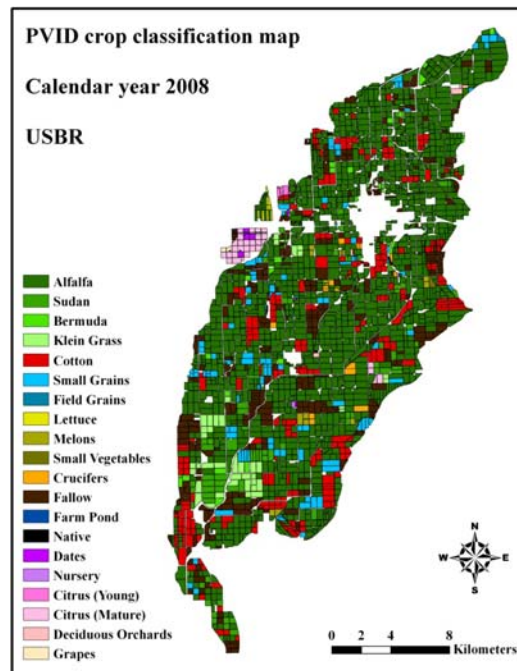


Figure 3. Crop land data in and around Utah for 2008 based on USDA NASS.



(a)



(b)

Figure 4. (a) Location of the agricultural areas PVID in southern California and (b) land use classification.

## RESULTS AND DISCUSSION

### Gridded Weather Forcing

A depiction of the number of pixels of NLDAS that covers PVID is shown in Figure 5 and the results presented in Figure 6 and 7 are for two stations. Figure 6 shows the comparison of  $T_a$  made at Cedar City station named as no. 15. Figure 7 shows the comparison at Parowan station named as no. 22. The statistics used during the analysis are the root mean square difference (RMSD), the bias (BIAS) and the correlation coefficient R.

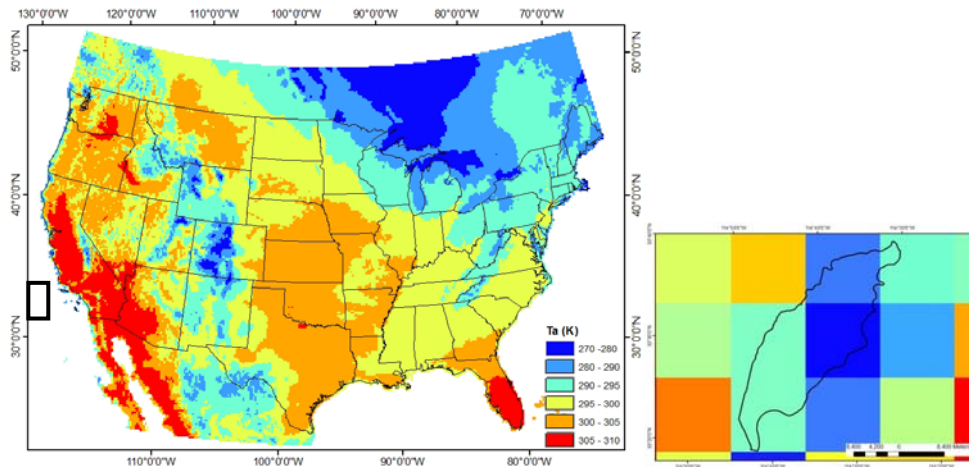


Figure 5. Air temperature  $T_a$  at 2 m above surface (K) at 18:00 GMT during May 17, 2008 with – the PVID overlaid with NLDAS-2 pixels  $\sim 14\text{km} \times 14\text{ km}$ .

Over station 15 NLDAS-2 overestimated  $R_s$  by about  $20\text{ W m}^{-2}$  as indicated by the BIAS however this was not the case over the Parowan station. When including all other stations (results not shown) there was generally a tendency of overestimation by NLDAS-2 by about  $20\text{ W m}^{-2}$  on average. The RMSD at some stations fell within  $85\text{--}95\text{ W m}^{-2}$  but for the majority of the stations was within  $110\text{--}140\text{ W m}^{-2}$ . These RMSD values generally represented over 10% of error for typical ground-based measurements of  $R_s$  values during midday.

The NLDAS-2 forcing of  $T_a$  overestimated the measured values by  $2\text{--}3\text{ }^\circ\text{C}$ . Generally this was the case for the rest of the stations. The RMSD for  $T_a$  over the two stations was about  $5.5\text{ }^\circ\text{C}$  on average. These values may be considered high especially for use in certain remote sensing based ET models that are sensitive to variations and errors in  $T_a$ .

All variables had data scattered around the 1:1 line with varying degrees of dispersion. The least scatter was observed in the specific humidity  $q$  plot and the widest observed in the wind speed  $u$ . These observations were similar for all other stations (results not shown).

As expected in a region comprised of such heterogeneous surfaces as the Western US, the large scatter and variation appears clearly in  $u$  and  $T_a$ . So the use of weather forcing data from NLDAS-2 at a pixel resolution of about 14 km to represent conditions at the surface that has limited or no ground stations might provide significantly different information should be handled with care. Over homogenous areas such as in the study by Luo et al. (2003) that was conducted over the Southern Great Plains, these biases and RMSD are expected to be somewhat lower. The findings in our study generally showed consistent results to those in Luo et al. (2003) with larger biases and scatter in  $u$  and  $T_a$ . Thus it is important to consider local surface heterogeneity and land use, which affect local meteorological conditions, such as irrigated areas with vast surrounding semi-arid and arid areas.

A subset of the data is presented showing comparisons for the same meteorological forcing but for the period between 10 and 11am, typical satellite (e.g. Landsat TM 5) overpass time used in remote sensing of  $ET$ . Some energy balance remote sensing models use data at the overpass time to produce instantaneous fluxes including the latent heat, which are extrapolated to daily  $ET$  values. Figure 8 shows the comparison over Cedar City station. The results indicate lower RMSD values for  $T_a$ . However it indicates underestimation as opposed to the results for the entire day (Figures 6 and 7). Similar results obtained with the wind speed showing the widest scatter around the line 1:1.

### Two-Source Energy Balance Model

Spatial estimates of instantaneous  $R_n$ ,  $G$ ,  $H$ ,  $\lambda E$  fluxes are shown in Figure 9. By visual inspection, generally, a similar spatial pattern can be observed when comparing the results of the individual fluxes using ground and NLDAS gridded weather forcing data. From the maps of  $R_n$ , an underestimation is observed in some area with the use of NLDAS-2 data as it falls in the range between 400-500  $W m^{-2}$  compared to 500-700  $W m^{-2}$  when using ground data as indicated in Figure (9 a and b). The spatial estimates of  $H$  over these same areas showed also a slight underestimation when using the NLDAS-2 data with a range between 50-100  $W m^{-2}$  compared to 100-200  $W m^{-2}$  with the use of ground data. Spatial estimates of  $G$  showed a similar pattern with underestimation with the use of NLDAS-2 data. This has resulted in estimates of  $\lambda E$  and  $ET$  that are apparently not significantly different when using NLDAS-2 and ground weather forcing data.

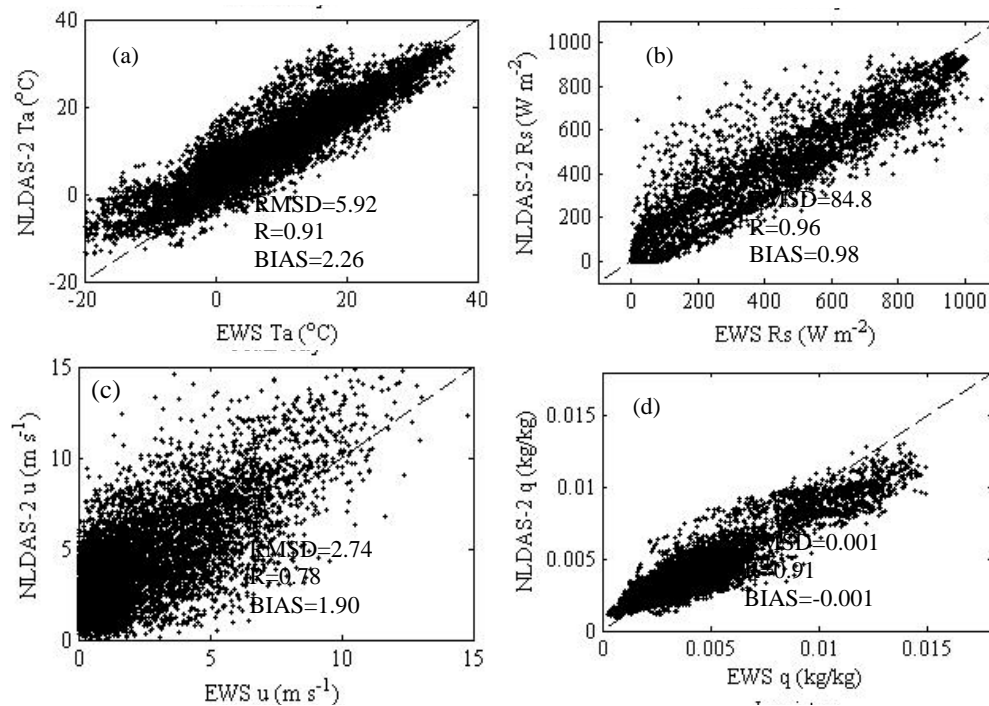


Figure 6. Comparisons of a) 2-m air temperature  $T_a$  ( $^{\circ}C$ ), b) downward shortwave radiation  $R_s$   $W m^{-2}$ , c) 10-m wind speed  $u$  ( $m s^{-1}$ ), and d) specific humidity  $q$  ( $kg/kg$ ) at Cedar City station named as 22 in Figure 3.

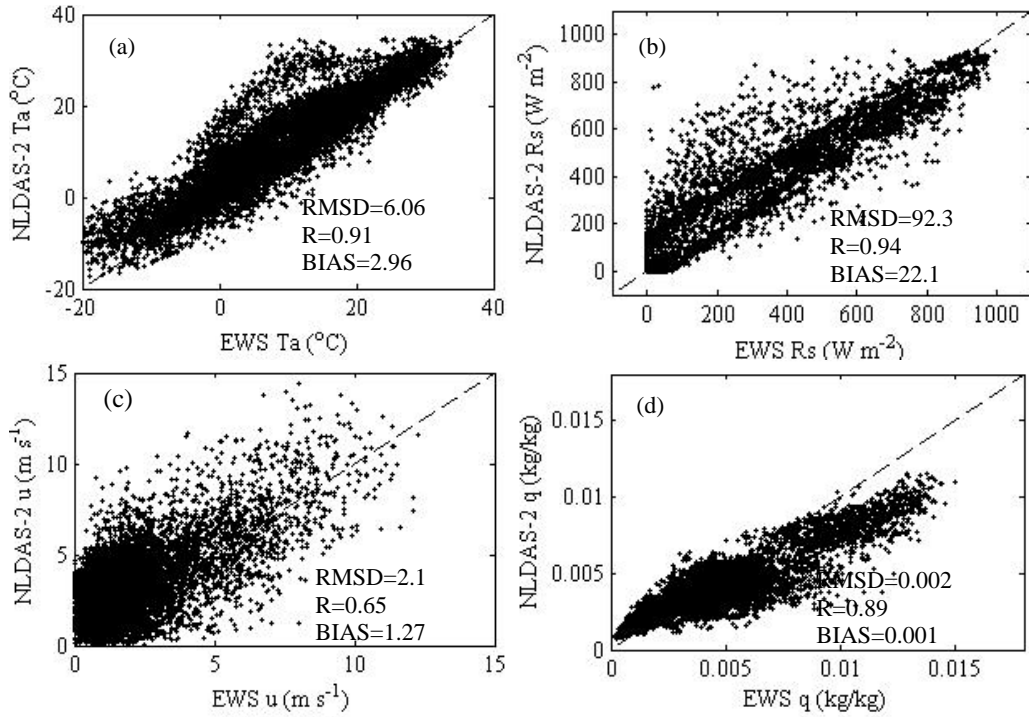


Figure 7. Comparisons of (a) 2-m air temperature  $T_a$ , (b) downward shortwave radiation  $R_s$ , (c) 10-m winds speed  $u$ , and (d) specific humidity,  $q$ , at Parowan station named as 15 in Figure 3.

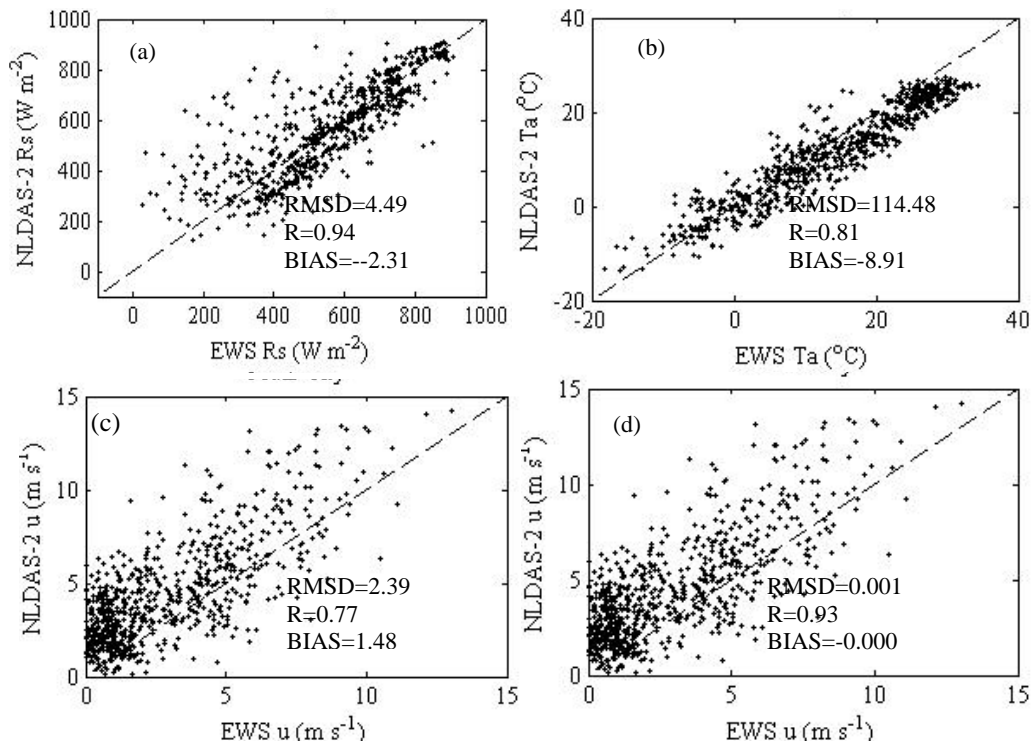


Figure 8. Comparisons of (a) 2-m air temperature  $T_a$ , (b) downward shortwave radiation  $R_s$ , (c) 10-m wind speed  $u$ , and (d) specific humidity  $q$  during 10-11 am at Cedar City station named as 15 in Figure 3.

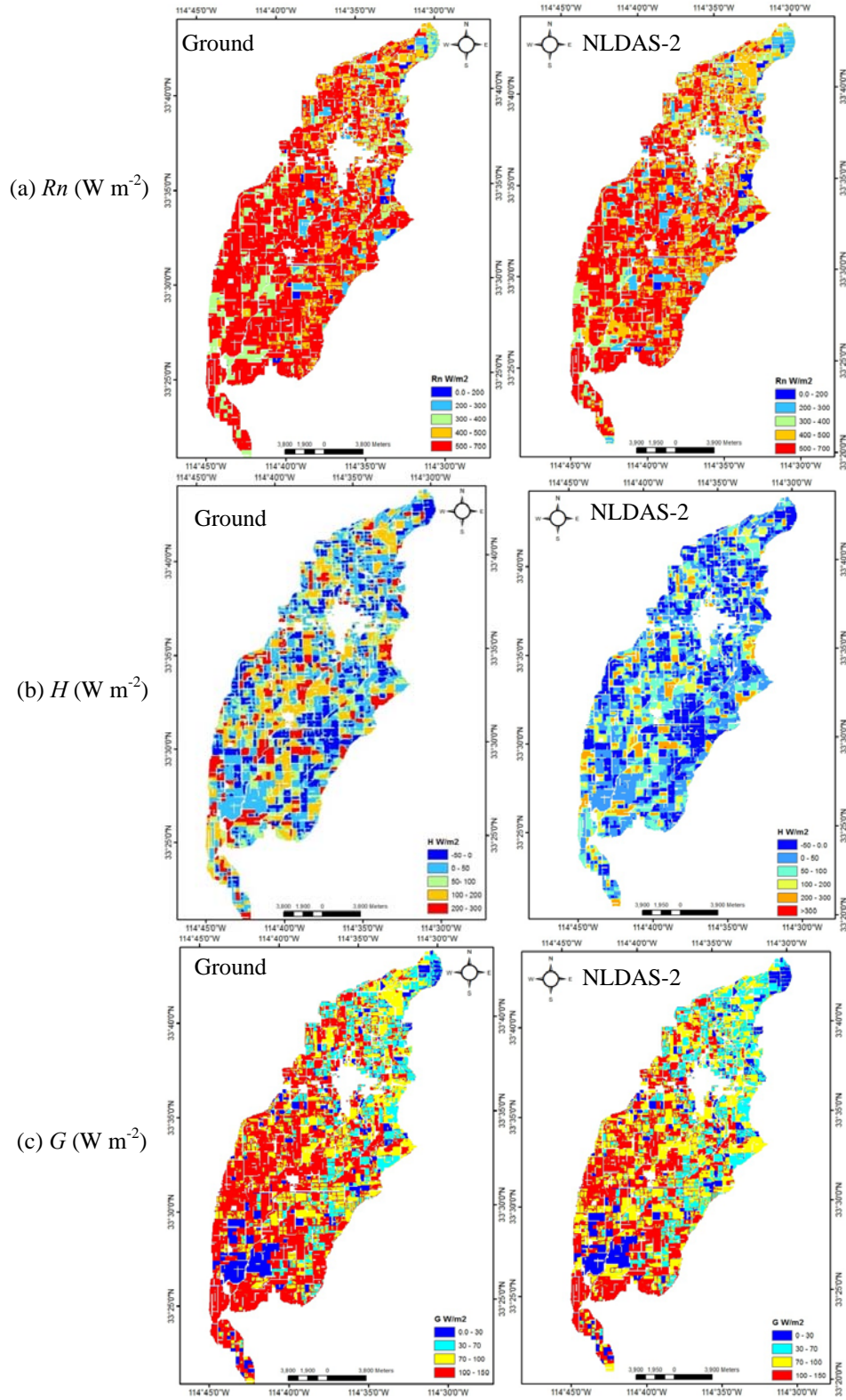


Figure 9. Comparison of spatial a)  $R_n$  b)  $H$ , c)  $G$ , d)  $\lambda E$ , and e) daily  $ET$  estimates of the TSEB model using ground and NLDAS-2 gridded weather forcing data.

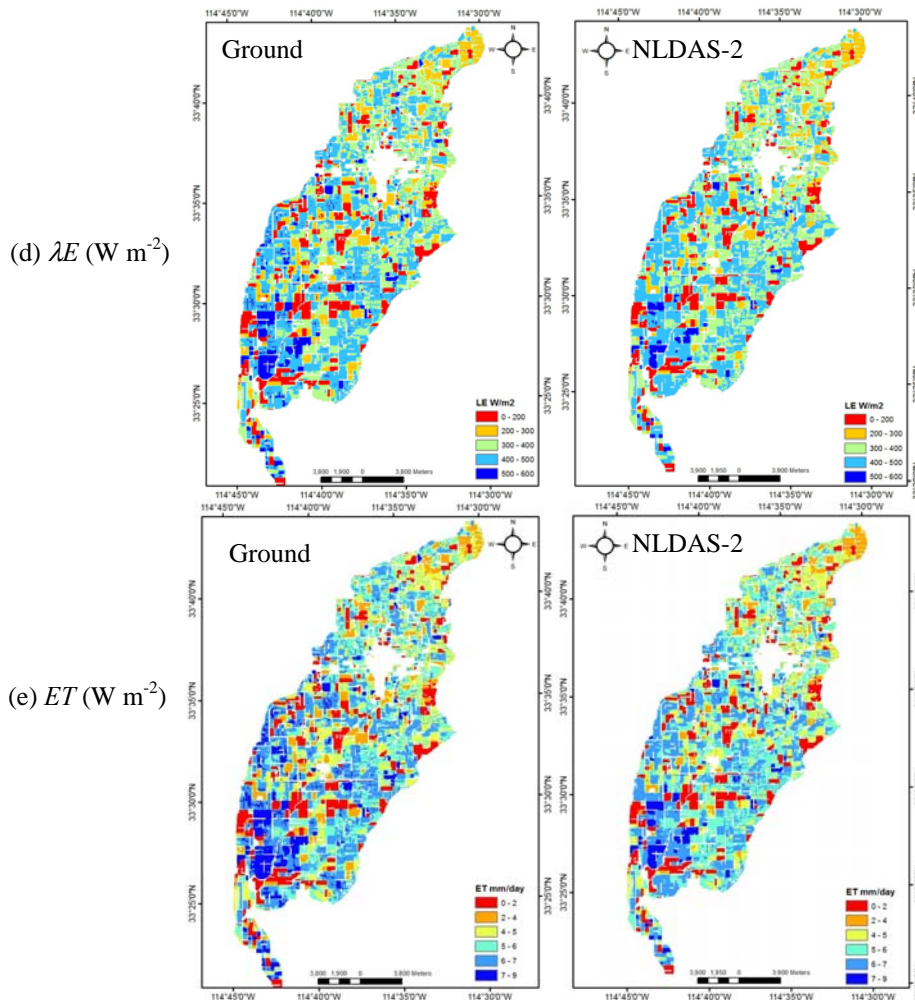


Figure 9 continued.

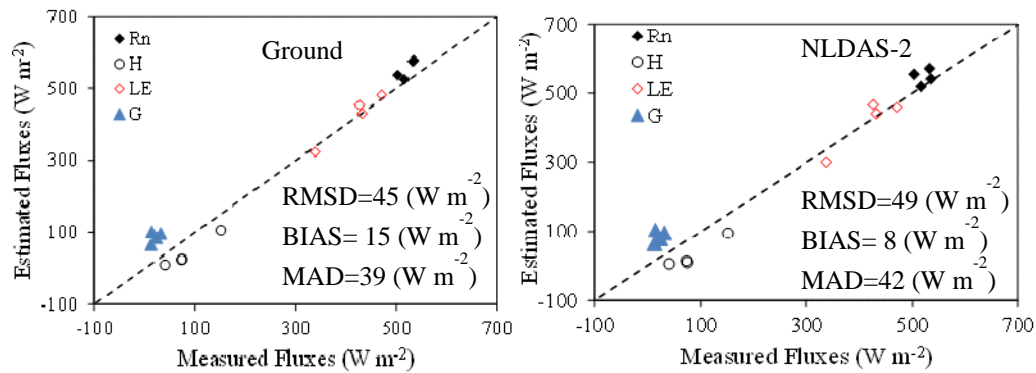


Figure 10. Comparison of surface energy fluxes estimates using a) ground and b) NLDAS-2 weather forcing data with ground based measurements.

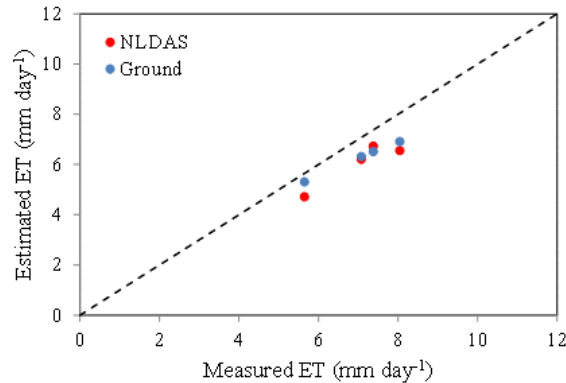


Figure 11. Comparison of daily ET estimates using ground (blue dots) and NLDAS-2 (red dots) with ground based Bowen ratio measurements.

Note that the spatial estimates of the different fluxes are not necessarily representative of the results shown in Figures (10 and 11) with a possible reason could be referred to spatial variation in irrigation patterns. The scatter plot in Figures 10 and 11 are based on comparison of estimates with ground based Bowen ratio measurements made at one single alfalfa field. Based on Figure 10, higher discrepancies can be observed when using the NLDAS-2 compared to ground data as indicated by overall RMSE of  $49 \text{ W m}^{-2}$  to  $45 \text{ W m}^{-2}$ , respectively. However, these differences can be considered insignificant and did not have much effect on the resulting daily ET estimates (Figure 11). It is important to note that these results should not be generalized as they were derived from the analysis of only 4 satellite scenes. Hence more images throughout the growing season need to be included in future analysis in order to have representative seasonal conditions.

## CONCLUSION

This paper presented a brief overview of the guidelines and specification of remote sensing of ET project as an effort by the USGS to standardize estimates of consumptive water use in the Western US. Preliminary results presented showing comparison of gridded and ground based weather forcing data for areas in and around the state of Utah. The paper provided some results on the effects of using this gridded weather forcing data on estimates of ET compared to using ground data.

The large discrepancies between NLDAS-2 forcing and surface values over irrigated areas in semi-arid Utah indicates that the use of these data in remote sensing based energy balance models without adjustments for local surface conditions could lead to large errors. There is a need for research to investigate whether NLDAS data can be adjusted to match surface conditions especially over irrigated agricultural areas surrounded by dry, natural vegetation with low cover. More comparisons of NLDAS weather forcing are needed with ground stations around the western US under different conditions of advection and surrounding surfaces.

A two-source energy balance (TSEB) model was used to study the effects of using the NLDAS-2 gridded weather data. The statistical comparison of the estimated fluxes with ground measured data using the TSEB model were typical of similar studies in irrigated

agricultural areas. Generally, estimate discrepancies at the individual flux level based on NLDAS-2 forcing were slightly higher compared to those estimates using ground data but with similar overall behavior. The estimated  $Rn$  values based on NLDAS-2 were slightly lower than those based on ground forcing. The estimated  $H$  based on NLDAS-2 are slightly lower than those based on ground forcing that might be due to a slightly higher  $T_a$  provided by NLDAS-2. Estimates of  $\lambda E$  based on NLDAS-2 were slightly lower compared to those based on ground data. Daily ET estimates based on NLDAS-2 were slightly lower but not significant.

### ACKNOWLEDGEMENTS

This research is funded by the United States Geological Survey (USGS) Award No. G11AP20229. The project implementation is by the Remote Sensing Services Laboratory, Department of Civil and Environmental Engineering, Utah State University. Support by the Utah Agricultural Experiment Station is also appreciated.

### REFERENCES

- Boryan, C., Yang, Z., Mueller, R., Craig, M., 2011. Monitoring US agriculture: the US Department of Agriculture, National Agricultural Statistics Service, Cropland Data Layer Program. *Geocarto International*, 26(5), 341–358.
- Campbell, G. S. & Norman, J. M., (1998). *An Introduction to Environmental Biophysics*. 2<sup>nd</sup> ed. Springer, 286 pp.
- Cosgrove, B. A., et al. (2003), Real-time and retrospective forcing in the North American Land Data Assimilation System (NLDAS) project, *J. Geophys. Res.*, 108(D22), 8842, doi:10.1029/2002JD003118.
- Horst, T. W. & J. C. Weil, 1994: How far is far enough?: The fetch requirements for micrometeorological measurement of surface fluxes. *J. Atmos. Oceanic Technol.*, **11**, 1018–1025.
- Horst, T. W., & J. C. Weil, (1992). Footprint estimation for scalar flux measurements in the atmospheric surface layer. *Bound.-Layer Meteor.*, **59**, 279–296.
- Luo, L., et al. (2003), Validation of the North American Land Data Assimilation System (NLDAS) retrospective forcing over the southern Great Plains, *J. Geophys. Res.*, 108(D22), 8843, doi:10.1029/2002JD003246.
- NASS, National Agriculture Statistics Services, (accessed 2012), Cropland Data Layer, <http://nassgeodata.gmu.edu/CropScape/>.
- Norman, J. M., W. P. Kustas, & K. S. Humes, (1995). A two-source approach for estimating soil and vegetation energy fluxes in observations of directional radiometric surface temperature. *Agric. Forest Mete.*, 77, 263–293.

# SOIL SCOUTS: WIRELESS UNDERGROUND SOIL SENSOR NODES

M. Johannes Tiusanen<sup>1</sup>

## ABSTRACT

Soil Scouts are palm-size underground wireless soil sensor nodes for monitoring soil parameters such as moisture and temperature. The hourly data packets from underground sensor nodes are received above ground from up to 1 km away and the maintenance free underground sensor nodes will operate for a decade. Two different versions of the system have been applied in true field conditions in 2006 through 2010, with most devices still being operative today. The ability to communicate with a receiver from different depths and distances were observed in both sandy and clay soil. The system is capable of providing real time underground monitoring data still allowing for regular field work above the sensor nodes. A common 402 m radius center pivot irrigation field can be instrumented with Soil Scouts having a single receiving antenna in the center of the field.

## INTRODUCTION

Remote sensing and imaging by aerial and satellite equipment have been applied to agricultural field and crop monitoring. In addition, a number of wireless sensor nodes and measuring stations have been introduced and are commercially available. However, wireless soil condition monitoring and logging has not become routine on many farms. Soil weather stations are expensive, require maintenance and hinder regular farming work by introducing obstacles in the field.

Since 2001 the University of Helsinki has conducted research on soil radio wave interactions in order to develop a wireless and completely underground Soil Scout. Soil Scouts are palm-size sensor nodes for monitoring agriculture soil parameters. For now, the device has been fitted with soil moisture and temperature sensors. The system design was guided by two main criteria; (i) the data packets from underground sensor nodes must be received above ground from up to 1 km away and (ii) the maintenance free underground sensor nodes must operate for a decade. Compared to conventional wired sensors with data loggers wireless devices are easy to install, they do not hinder agricultural soil operations and they produce representative data because the surrounding soil remains undisturbed for several years. The measurement validity is also free of possible influence from cables, which may conduct surface water into wired sensors especially in swelling soil types.

Two prototype populations have now been manufactured and tested in different conditions. The first version in 2006 had a fragile antenna and only 10 mW of transmitting power (Tiusanen, 2007).

---

<sup>1</sup> Department of Agricultural Sciences, University of Helsinki, Finland and Kuokka Agro Innovations (e-mail: johannes.tiusanen@helsinki.fi, address: Suosmerentie 192, 28450 Ulvila, Finland, Europe, mob: +358 44 3659799

The Soil Scout v2 (Fig. 1) was designed and built in 2010. The device became more compact and was fitted with a radio amplifier giving 400 mW transmission power. The power durability was further enhanced through more efficient battery current drain.



Figure 1. Soil Scout v2 prototype without encapsulation.

A model for calculating the attenuation of a radio link from underground (UG) to above ground (AG) was developed and validated by case measurements (Tiusanen, 2005 and 2007). The attenuating phenomena of angular defocusing caused by refraction in the soil-air interface was introduced and verified. The first prototypes of Soil Scouts v1 were installed in 2006 and their data transfer performance reported (Tiusanen, 2007). A wide-band underground printed circuit monopole antenna was developed to provide Soil Scouts an underground single-ended monopole antenna (USEMA). It is capable of staying tuned despite the soil water content altering a radio wave length in soil through changing the complex dielectricity of the media. Some of these v1 devices were serviced and reprogrammed in 2009 and are still operating in December 2012 with minimal battery voltage loss to date.

This paper will a) explain why the Soil Scout system does apply direct communication between a node and the base station; b) present how the Soil Scouts have performed in actual field trials; and c) discuss the case of instrumentating a center pivot irrigation field with Soil Scouts.

### RELATED WORK AND SOIL SCOUT TOPOLOGY

The main challenges for a Wireless Underground Sensor Network (WUSN) concern power management and connectivity, common problems in wireless sensor networks (WSNs) (Akyildiz et al. 2006). Solutions in the complicated underground radio environment differ from terrestrial wireless sensor networks significantly (Sun et al. 2011). Intensive work has been devoted to evaluate communication in the cases of underground (UG)-to-aboveground (AG) link as well as underground-to-underground link (UG-UG). Both stationary and mobile network elements have been considered. Since Soil Scouts only communicate with an AG base station, no actual network is created and

the devices are referred to as wireless underground sensor nodes (WUS) instead of WUSN.

The UG-UG channel was eliminated for reasons related to both hardware restrictions and network topology. Soil Scout development focused on a system, which can monitor a whole agriculture field without any on-soil in-field instruments. In order to achieve adequate sensor coverage this means that data from a sensor node must travel several hundred meters to reach the field boundary.

Soil Scouts employ the European license free 869.4 MHz ISM-band at 400 mW transmitting power, which equals to +26 dBm (decibel of mW). The underground antenna is an advanced omnidirectional underground single-ended monopole antenna, which is diminished in size and improved in mechanical durability compared to the previous v1 design. The system is built around a Nordic Semiconductor nRF9E5 single-chip transceiver micro controller. The measurement and transmission duty cycle is 55 min and the device is powered by a 2500 mAh 3 V lithium battery. During the 400 ms sensing and processing phase the current varies between 0.05 and 32 mA and adds up to 26 nAh per cycle. The time on air for the 11-byte Gaussian frequency-shifting key modulated packet is 2.6 ms, during which 0.5 A current is drawn resulting in 4  $\mu$ Ah per transmission. In sleep state the node draws 2.5  $\mu$ A for 55 minutes, resulting in 2.3  $\mu$ Ah per cycle.

The mean current 6.9  $\mu$ A and battery capacity 2500 mAh results in a theoretical life time of 42 years, but in practice the span is limited by battery internal discharge characteristics. However, the battery is guaranteed a 10-year life span at 30  $\mu$ A discharge current, which is 4 times higher compared to the Soil Scout consumption.

The sensing subsystem consists of a 12-bit analog-to-digital converter, three commercially available Decagon Devices EC-5 sensors and a digital on-board temperature sensor. The sensors and the radio amplifier are powered by a fixed 3.3 V supplied by battery. In addition to individual id number and sensor data, Soil Scouts transfer battery voltage and the error sum of repeated sensor measurements allowing device health diagnostic. Table 1 displays the technical specifications of the Soil Scout.

Table 1. Technical specification of the two design versions.

<i>Parameter</i>	<i>Soil Scout v1</i>	
	<i>(2006)</i>	<i>Soil Scout v2 (2010)</i>
Size excluding moisture sensor, mm	42×90×20	48×68×20
Battery nominal capacity, mAh	1800	2500
Transmitting power, mW	10	400
Duty cycle, min	10	55
Number of moisture sensors	1	3
Max. battery discharge current, mA	32	5
Expected lifetime at 1 h duty cycle, years	4	10..40

The radio wave interaction with soil medium is a complicated phenomenon and guides the radio topology options in many ways, of which the choice of radio frequency has most considerable consequences. In general, both the real and the imaginary part of soil permittivity decrease with increasing frequency at least to 10 GHz (Nyfors et al. 1989). However, because frequency is a factor of the soil attenuation coefficient, lower frequencies will suffer from less attenuation caused by the soil medium. In addition, availability and performance of radio transceiver components in the license free ISM-bands must be observed, since Soil Scouts are not a theoretical scheme but actual devices manufactured for agriculture field property monitoring. The license free 869/915 MHz (Region 1, including Europe/Region 2, including U.S.) band was chosen.

Soil Scout development was given the goal of allowing a 1 km data transfer range. The communication range of an UG-UG radio wave device pair at 10 mW radio power in the 900 MHz frequency range is in general limited to less than 10 m in sandy soils (high content of particles larger than 0.02 mm), in many conditions less than 5 m (Sun et al. 2011). Clay soils (high content of particles smaller than 0.002 mm) have attenuation factors 3-5 times as high, which further reduces range. A travel distance of 1000 m UG-UG would require 100-200 hops. Increasing the power to the regulatory maximum 400 mW would extend the range 6-fold to 30-60 m but the required number of hops would still be about 15-30 in a straight line, and all data beyond a broken link would be lost completely.

Many reported trials have used wireless soil sensor nodes using an UG sensor and AG transmitter (Vellidis et al., 2008), applied systems comprised of UG nodes and near-by AG infrastructure nodes acting as repeaters (Ritsema et al., 2009) or have limited the installation depth in order to keep the soil surface inside the transmitter's one wavelength (Bogena et al. 2009). These approaches are applicable in environments such as golf courses and horticulture structures, but not in open fields where no AG devices are allowed.

## RADIO WAVE ATTENUATION IN SOIL

Papers related to underground radio signal propagation have incorporated a number of different attenuating mechanisms. The four mechanisms regarded in Soil Scout development are shown in Fig. 2. One often disregarded mechanism, when placing an UG transmitter near the soil surface, is the loss due to angular defocusing  $L_{Def}$ . It is a separate phenomenon from the loss due to reflection from the surface interface  $L_{Refl}$ . Soils at different moisture contents have relative permittivity in the range of 5–45, which retards the travelling speed of electromagnetic radiation, but not the frequency. Hence the length of an 869.4 MHz wave in soil is 5–11 cm and a Soil Scout placed 15 cm deep is located about 1.5–3 wavelengths from the soil surface. The wave striking the soil surface interface is spherical and the common plane wave approximation does not apply.

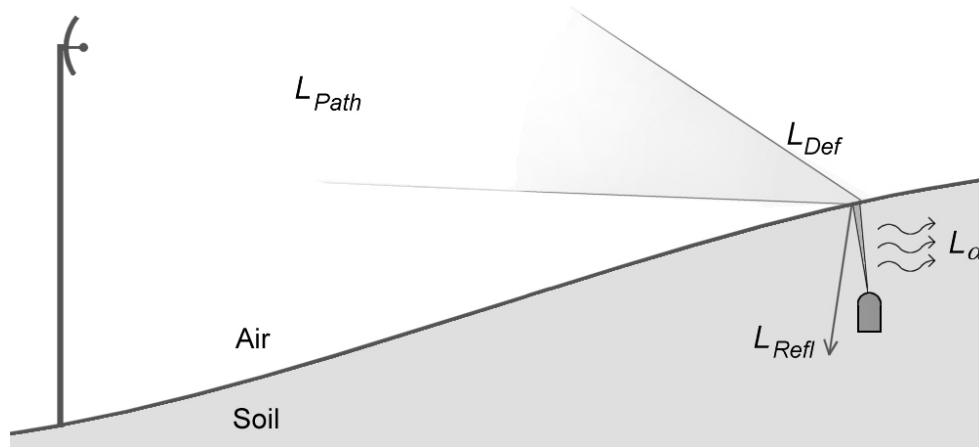


Figure 2. Four mechanisms attenuating an UG-AG radiowave:  $L_{\alpha}$  the loss due to soil medium attenuation;  $L_{Refl}$  due to partial reflection from the surface;  $L_{Def}$  due to angular defocusing; and  $L_{Path}$  free air path loss.

The higher the soil water content is, the more electric field power is absorbed by the soil medium, but the less power is reflected from the soil surface interface. In other words, increasing soil moisture content will increase the loss due to soil medium attenuation  $L_{\alpha}$  but decrease the loss due to partial reflection  $L_{Refl}$ . Thus changes in soil moisture will roughly cause these phenomena to cancel out changes in each other. However, angular defocusing  $L_{Def}$  increases along inclining moisture content. All four mechanisms have been discussed in detail and validated (Tiusanen, 2009; Tiusanen, 2007; Tiusanen, 2005).

One topic in addition to soil radio wave interaction must be addressed here. The receiving antenna significantly affects Soil Scout system performance. The main criterion is antenna directivity, which corresponds to antenna gain. Just like optics, the stronger the signal amplification in one direction becomes, the narrower the beam from which waves can be intercepted. An omnidirectional stick antenna has no gain, which corresponds to +0 dB. The 40 cm wide directive panel antenna used in these experiments has +10 dB gain in the 60° main beam lobe. One 2 m diameter parabolic antenna was also tried out, giving +21 dB gain but only in a narrow 9° sector. So the beam width is always a trade off compared to signal strength gain.

## EXPERIMENT ARRANGEMENTS

As mentioned, two different evolution versions of Soil Scouts have been manufactured and tested in real agriculture conditions. The first 11 Soil Scouts with 10 mW transmitting power were installed in 2006 in a sandy loam where oats was grown (Fig. 3). Here different installation depths (10..45 cm) and distances from the receiving antenna (30...150 m) were used and the transmission probabilities compared to attenuations calculated for each device (Tiusanen, 2007).

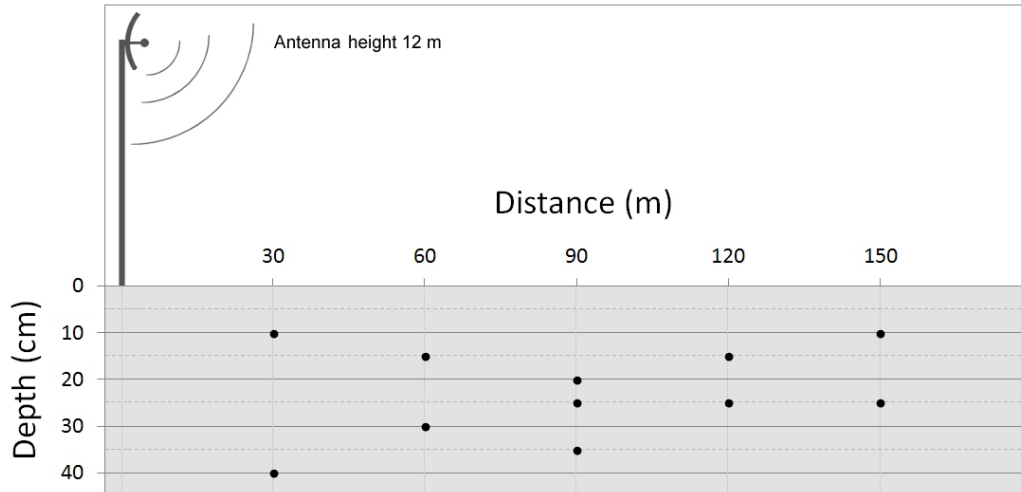


Figure 3. Installation setup with distances and depths for the first 11 Soil Scout prototypes with 10 mW power in sandy loam 2006.

A second generation Soil Scouts v2 with 400 mW radio power were completely re-designed and manufactured in 2010. These were installed in a heavy clay field hillside, where clay (particle size  $< 0.002$  mm) contents were 32-75 % with a mean of 55 %. All prototypes were fitted with three moisture sensors with 15-45 cm long cables in a manner that allowed vertical soil moisture profile monitoring. Here the main focus was on obtaining moisture measurement data to a hydrological model, rather than Soil Scout performance analysis. This is why all Soil Scouts were installed just below soil tillage depth allowing best possible transmission ability. In this experiment, as well as in 2006, all crop farming operations were performed as if no instruments were underground.

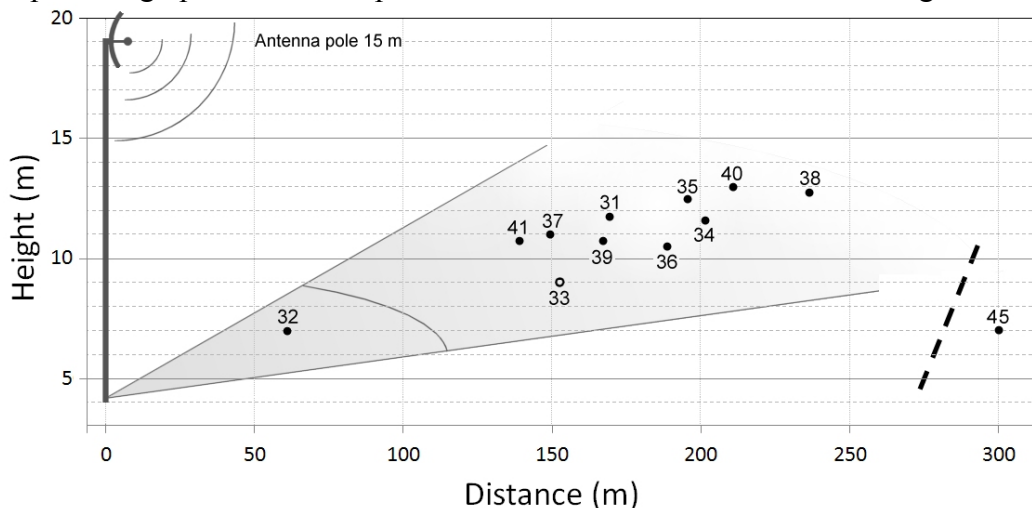


Figure 4. Installation setup with distances and heights for 11 Soil Scout v2 prototypes with 400 mW power in a heavy clay hillside in 2010. All Scouts are installed 15 cm deep. Soil Scout id 45 is installed elsewhere in a sandy loam as a performance reference.

The receiving antenna was connected to a small receiver circuit board using coaxial cable. The receiver then transmitted the packet data to a laptop computer for visualization

and data logging. In the 2010 experiment the logger was also real time accessible through mobile phone network and an internet hypertext interface.

## RESULTS

The results from the Soil Scout v1 experiments in 2006 have been reported (Tiusanen, 2007) and will be presented here only as a matter of comparison to the amplified Soil Scout v2 performance. For the clay soil hillside experiments started in 2010, the detailed comparison between calculated attenuations and performance will be reported in a future paper. The Soil Scout system ability to deliver real time monitoring data from the experimental fields is presented here.

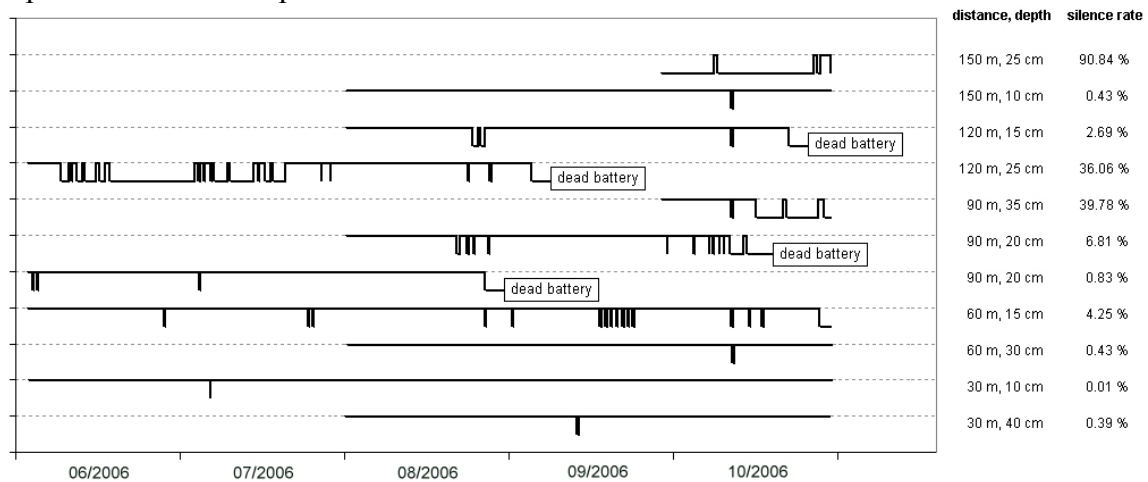


Figure 5. Soil Scout v1 performance in 2006 in a sandy loam soil. Logic “low” values represent a 12-hour break in data transfer.

In 2006 the Soil Scout prototypes were installed on three occasions since the overall system was in an experimental stage. Once heavy rains occurred in late August, many devices started reporting declining battery voltage and died shortly afterwards. All were confirmed to have taken in water due to poor encapsulation, during manufacture.

The system performed well and the observed ability to overcome calculated attenuations was as expected. When the calculated attenuation exceeded -98 dB, it became more likely for a data packet to be lost than received. Fig. 5 shows, that the distance 150 m and depth 10 cm was overcome easily (99.57 % success) regardless of oat vegetation height, but this far 25 cm was too deep (9.16 % success). 120 m away from the receiver 15 cm was overcome but 25 cm was too deep. 90 m away 20 cm was overcome but 35 cm was too deep. At the distances 60 m and 30 m installation depth did not play a significant role.

The data transfer performance was found encouraging but not adequate compared to the system design goals. An interesting observation was, that once the attenuation was close to the system limit, individual data packets was not lost, but the specific Soil Scout was either inside or outside of range for continuous several day periods. Thus having a frequent duty cycle of 10 minutes does not enhance data transfer probability, and a new design approach was chosen in order to significantly increase radio power and reduce the

duty cycle to one hour. In order to ease data post processing, the duty cycle was later set to 55 minutes to exclude the possibility of single missing hourly data points due to timing issues.

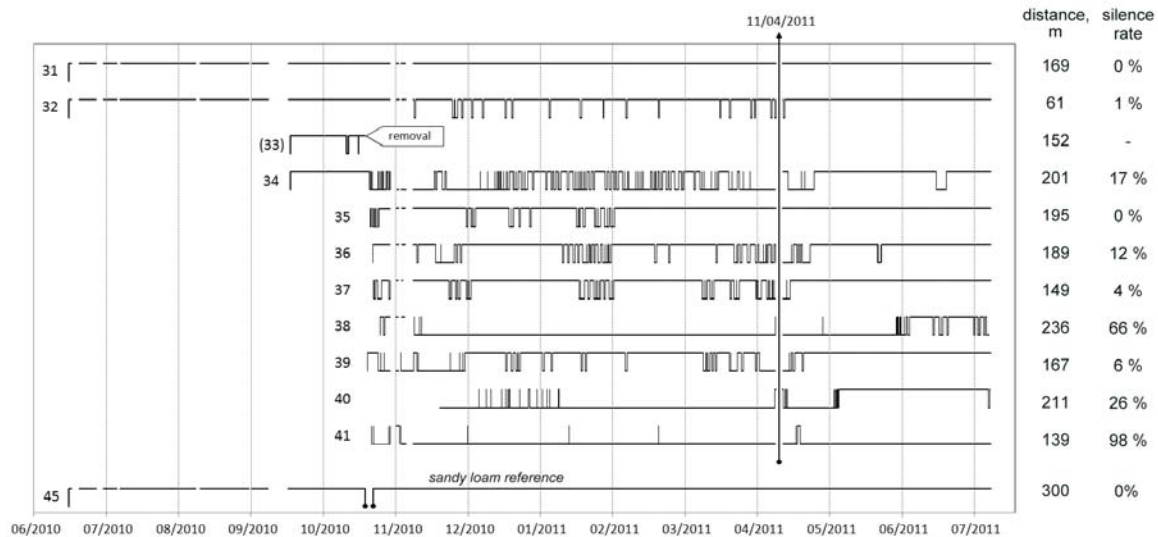


Figure 6. Soil Scout v2 performance in 2010-2011 in a hillside clay soil. Logic “low” values represent a 12-hour break in data transfer. The melting snow in 11/04/2011 restored the soil structure and the silence rates are calculated for the remaining period. Soil Scout id 45 is installed in a separate sandy loam field for reference.

The new Soil Scout v2 production turned out more difficult than expected and the production was first delayed by one year due to design and testing work. The deployment of the prototype series was delayed for another year because of faulty circuit boards from the supplier. Three different kinds of completely new innovative techniques were incorporated all in one design, which in hindsight was not a prudent decision. The winter frost 2009 cancelled any attempts of field installation until the next season.

Confidence in the thorough design and testing led to implementation of the system trial in extreme conditions. MTT Agri Food Research Finland was commencing clay soil hillside nutrient runoff research, and the Soil Scout v2 system was installed there. The research centre provided compatibility for the Soil Scout receiver into their data infrastructure, including on-site backup logging, mobile phone network data transfer and on-line hypertext visualization.

In this heavy clay soil (mean clay content 55 %) the calculated attenuations did not seem to correlate with data transfer ability. The soil structure was more problematic. The first two prototypes (id 31 and 32) performed well over the study period since they were installed in moist and plastic soil conditions. The main group was installed in the fall in mechanically hard soil conditions, and the soil structure could not be restored after installation. The fractured clay rubble introduced a large number of soil-air interfaces and the signals were unable to penetrate into air. However, the snow melting on 11/04/2011 seemed to restore the soil bulk density and thereafter the system started performing well.

Some Soil Scouts (e.g. id 31 and 35) were successful in overcoming attenuations exceeding -110 dB, but others had trouble at -105 dB (e.g. id 38 and 40). The full analysis is yet to be published.

One Soil Scout v2 (id 45) was removed from the clay soil in September 2010 for inspection and re-installed in the flat sandy loam soil of the v1 experiment as a reference. The distance was 300 m and the receiving antenna height 12 m. However, here an omnidirectional quarter-wave monopole antenna without a ground plane was used instead of a directive panel antenna, so this setup introduced a -116 dB path loss. Soil Scout v2 id 45 did not miss one data packet during the period, and whenever the receiver has been started up since, operation has remained constant despite snow cover until now (confirmed 25<sup>th</sup> Feb. 2013). All field work regarding fava bean, spice cumin and now winter wheat sowing has been performed in a normal manner on top of this Soil Scout.

The initial 3.1 V battery voltage of the v2 design declined rapidly to 2.97 V and is now fluctuating between 2.95-3.07 V depending on soil temperature. There are two v1 design prototypes remaining operative today having been reprogrammed to a 55 minute duty cycle and given new batteries in 2009. The current battery voltages have also obtained a stable 0.1 V amplitude fluctuation just below 3.0 V.

### **CENTER PIVOT IRRIGATION FIELD DISCUSSION**

The primary goal was to give a Finnish farmer real-time monitoring data on soil properties to assist in farming decision making. For example frost depth and temperature monitoring combined to information on soil moisture profile at the moment of freezing was not practically possible until now.

The system has not yet been commercialized and one obviously interesting piloting environment would be soil moisture monitoring in a center pivot irrigation field. Agricultural field irrigation is rare in Finland and limited to selected vegetable growers.

The most common center pivot boom length is 402 meters (1/4 mile) and there usually is electricity available in the center. In contrast to the underground node, the receiver must stay operative at all times, and therefore a constant power supply is highly advantageous compared to battery or solar powered systems. The needed power, however, is comparable to a mobile phone in standby.

The range and reliability of UG-AG communication benefits mainly from two setup solutions: 1) receiving antenna height; and 2) receiving antenna directivity or beam width.

If a theoretical receiving antenna would be installed at the level of the soil surface, no radio wave would refract out from the soil, but total reflection would occur. A weak surface wave may be present but will not allow actual communication. The higher the receiving antenna will elevate, the stronger the outgoing radio wave will become. The attenuation due to angular defocusing (Fig. 2) is stronger at low angles as well.

Communicating as far as 402 m will benefit from antenna installation heights 10 m and up, but the requirement is also influenced by choice of antenna type.

A directive antenna beam is not necessary in one direction only. For example in the case of car roof mobile antennas one can assume the base station lies somewhere in the horizon – not up or down, but in whichever direction. A suitable antenna solution will have an omnidirectional pattern around the antenna, but not radiate in vertical directions. This, again, is a tradeoff between beam size and gain. An antenna picking up radiation in a  $25^\circ$  high omnidirectional sector will give +9 dB gain, while a  $30^\circ$  high sector will give +7 dB.

The beam width is not ideal, but the center of the beam is stronger and the outer limits of it weaker. An antenna will pick up some radiation from outside the beam as well. A  $25^\circ$  sector omnidirectional antenna elevated 10 m above ground does not have Soil Scouts installed closer than 45 m inside the main beam, but rather shoot over them (Fig. 7). However, these Soil Scouts will benefit from the short communication distance compared to Soil Scouts further away and will in general be able to communicate.

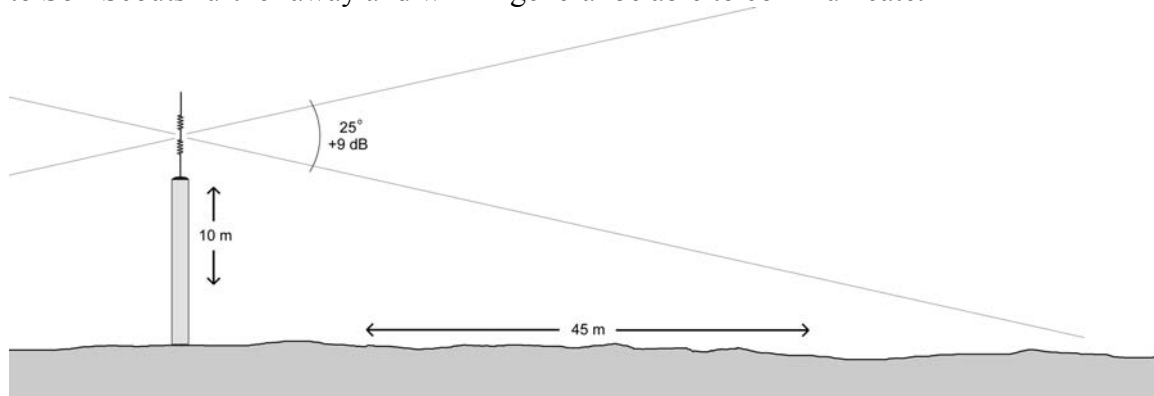


Figure 7. An omnidirectional  $25^\circ$  lobe antenna gives +9 dB gain in the main beam and Soil Scouts installed closer than 45 m may fall in a blind zone. The poor antenna gain below the main beam is compensated by minor attenuation due to short distance.

A receiving antenna height 10 m and gain +9 dB will in sandy soils allow communication with Soil Scouts as far as 700-900 meters away, depending on soil and vegetation. This should cover any center pivot irrigation field radius – or even diameter.

In case of large irregular shaped fields, many arrangements can be used to extend the range even further. A 2 m parabolic dish antenna may be used in order to narrow the directive beam down to  $11^\circ$  in one direction and thus give up to +21 dB gain, but then all Soil Scouts must be installed on this line-of-sight. The base station can be equipped with several directive antennas with individual receiver chips and in special cases an above ground repeater may be used to extend the signal range up to 20 km line-of-sight, although a repeater will require constant power and partly compromise the original underground nature of the Soil Scout system.

## CONCLUSION

Soil Scout technology has here been proven technically feasible in delivering real-time soil measurement data from inside an agriculture field to a base station in most all scenarios. Deciding how valuable the technology is from the agronomic point of view must be reflected against knowledge on similar wired and/or on-soil instruments.

According to Jones (2008) it appears that over half of irrigation decisions are based on guesswork or intuition rather than scientific data. Soil sensors, specifically the Soil Scout can provide this missing data and are readily automated. Lea-Cox (2012) has also found surprisingly many seemingly advanced irrigation scheduling systems functioning only on the basis of time, without any feedback-based sensor systems. However, there is no detailed knowledge on whether the low implementation level of feedback systems is caused by lack of interest towards the technology or perhaps the amount of effort and cost of present on-soil or cabled systems. While some farmers might show interest in wireless underground devices, others might have difficulty accepting their use and implementation. The most probable scenario is that farmers already applying telemetry in irrigation control will find Soil Scouts to be a useful tool in their water management operations. Farmers that were using intuition to schedule irrigation might initiate monitoring encouraged by the level of ease the system introduces.

In his summary on the main sensor techniques that are currently used for irrigation scheduling, Jones (2004) noted that telemetry can give instantaneous data, but because of soil heterogeneity many expensive sensors are required and selecting positions that are representative of the root-zone is difficult. Lea-Cox (2012) added, despite variation in soil water availability being well known, the use of large sensor arrays in order to get high quality representative readings of soil moisture tends to be limited by cost. This could, however, be overcome by sensor placement strategies. The unprecedented possibility of in-field variation monitoring introduced by a large Soil Scout node array may be decisive in transforming soil monitoring from research practice into a farming method.

Jones (2008) proposed that an ideal horticultural irrigation scheduling system should be (1) sensitive to small changes; (2) rapidly and “real time” responsive to these changes, allowing for continual monitoring; (3) readily adaptable to different crops or environments; (4) robust and reliable; (5) user-friendly, requiring little user training; (6) capable of automation, and (7) low cost, both in terms of purchase and running costs. There is no true user interface for the Soil Scout receivers, which presently forward received serial data through both RS232 and USB ports. The system meets most of the proposed requirements, but still requires some development to meet all 7 criteria.

A farmer adapting wireless monitoring is used to installing equipment after sowing and yearly relocating it to the most valuable crop. The added value from underground Soil Scouts is in having them undisturbed for several years, but whether a farmer is prepared to install telemetry instruments more or less permanently, remains unknown. Nevertheless, it is fair to say Soil Scouts are easy to adapt but hard to relocate.

Another issue regarding data transfer reliability is that a Soil Scout user must be prepared to deal with fragmented data. The power saving features have only one-way communication

without retries and the inevitable consequences that individual packets will be lost. On the other hand, comprising the system of a large array, say at least 10 Soil Scouts, will ensure there is always timely and extensive data available. In fact, the inaccurate low power wake up timer onboard the nodes will cause them to wake up every  $55 \pm 2$  minutes, resulting in a horde of transmitters beeping all the time, and individual lost data packets can always be accounted for with simple extrapolating or predicting algorithms.

Lea-Cox et al. (2008) proposed a number of requirements for specifically *wireless* sensor networks, where (1) users should be able to rapidly deploy sensors in any production area; (2) sensor networks should be scalable; (3) nodes should have low power requirements, preferably with rechargeable power options, and (4) sensor data should be reliably transmitted using wireless connections over at least 1000 m. He also made several points regarding the software interface and graphical output in conjunction to decision tools, which do not apply for Soil Scouts, as there presently is no user interface solution, as pointed out.

The Soil Scout system meets all these proposed requirements, but the scalability deserves more detailed discussion. The short data radio burst is optimized to single bit level. The preamble includes a 16-bit address which must match the one programmed into the receiver. In addition, every Soil Scout is assigned with one 8-bit identification byte, which allows up to 255 Soil Scouts to communicate with one receiver. This should be plenty for one field, but if a farmer should own several hundred sensor nodes inside a 1 km radius, they would need to be programmed into separate address groups and would no longer be interchangeable without reprogramming. This, as well as battery recharging, cannot be performed by the customer due to the permanent encapsulation, which on the other hand is justified by the very high 10+ year power durability.

A third version prototype is being designed at the moment. Patenting some of the technical solutions is in progress. Version 3 will feature more self diagnostic data once every 100 measurements; the possibility to wirelessly adjust some performance parameters and will apply some software threshold triggering such as a 12 hour duty cycle during frost temperature and 10 min duty cycle during rapid moisture changes. All trials have so far been conducted in Finland, but piloting opportunities in locations of intensive high-value crop irrigation and co-operation in commercialization are being sought.

## REFERENCES

- Akyildiz, I. F. and Stuntebeck, E. P. 2006. Wireless underground sensor networks: research challenges, *Ad Hoc Networks J.* 4, 669-686.
- Bogena, H. R., Huisman, J. A., Meier, H., Rosenbaum, U., and Weuthen, A. 2009. Hybrid wireless underground sensor networks: quantification of signal attenuation in soil, *Vadose Zone J.* 8 (3), 755-761.
- Jones, H.G. 2004. Irrigation scheduling: Advantages and pitfalls of plant-based methods. *J. Exp. Bot.* 55 (407), 2427-2436.
- Jones, H.G. 2008. Irrigation Scheduling - Comparison of Soil, Plant and Atmosphere Monitoring Approaches. *Acta Hort.* 792, 391-403.

Lea-Cox, J.D., Ristvey, A.G. Arguedas-Rodriguez, F.R., Ross, D.S., Anhalt J. & Kantor. G.F. 2008. A Low-cost Multihop Wireless Sensor Network, Enabling Real-Time Management of Environmental Data for the Greenhouse and Nursery Industry. *Acta Hort.* 801, 523-529.

Lea-Cox, J. D. 2012. Using Wireless Sensor Networks for Precision Irrigation Scheduling. M. Kumar (Ed.) In: *Problems, Perspectives and Challenges of Agricultural Water Management*, 233-258.

Nyfors, E., Vainikainen, P. 1989. *Industrial Microwave Sensors*, Artech House Inc., Norwood USA.

Ritsema, C.J., Kuipers, H., Kleiboer, L. van den Elsen, E., Oostindie, K., Wesseling, J.G., Wolthuis, J.-W. and Havinga, P.J.M. 2009. A new wireless underground network system for continuous monitoring of soil water contents, *Water resources research* 45.

Sun, Z., Akyildiz, I. F. and Hancke, G. P. 2011. Dynamic connectivity in wireless underground sensor networks, *IEEE Trans. Wireless Commun.* 10 (12) 4334-4344.

Tiusanen, J. 2005. Attenuation of a Soil Scout radio signal, *Biosystems Engineering* 90 (2), 127-133.

Tiusanen, J. 2007. Validation and results of the Soil Scout radio signal attenuation model, *Biosystems Engineering* 97, 11-17.

Tiusanen, J. 2009. Wireless soil scout prototype radio signal reception compared to the attenuation model, *Precision Agriculture* 10 (5), 372-381.

Vellidis, G., Tucker, M., Perry, C., Kvien, C., Bednarz, C. 2008. A real-time wireless smart sensor array for scheduling irrigation, *Computers and Electronics in Agriculture* 61 (1), 44-50.



# ROLE OF HOT AND COLD PIXEL CONCEPT IN REMOTE SENSING BASED SINGLE SOURCE SURFACE ENERGY BALANCE ALGORITHMS

George Paul<sup>1</sup>  
Prasanna H. Gowda<sup>2</sup>  
P. V. Vara Prasad<sup>3</sup>  
Terry A. Howell<sup>4</sup>  
Robert M. Aiken<sup>5</sup>  
Stacy L. Hutchinson<sup>6</sup>

## ABSTRACT

Evapotranspiration (ET) mapping with thermal remote sensing data garnered a renewed interest with the inception of SEBAL (Surface Energy Balance Algorithm for Land). Since then, numerous models have been developed along similar concepts that derive near surface temperature gradient,  $dT$ , from a single linear function of surface temperature. The  $dT$  function was derived from two anchor pixels denoting the hydrological extremes, and coined as the hot (dry) and the cold (wet) pixels. Although this concept was revolutionizing, the effects of numerous assumptions and pitfalls associated with it were not well understood. In this study, eight high resolution airborne images acquired during the BEAREX07-08 (Bushland Evapotranspiration and Agricultural Remote Sensing Experiment) campaigns over irrigated and dryland agricultural fields equipped with large precision lysimeters was utilized to test the hot and cold pixel concept. METRIC<sup>TM</sup> (Mapping Evapotranspiration at high Resolution and with Internalized Calibration), a variant of SEBAL, was compared with a generic single source (GSS) algorithm which does not use the hot and cold pixel concept and only differed in its definition and computation of the  $dT$  parameter. METRIC derived ET flux generated an overall relative error of 24%, whereas the GSS produced an 18% relative error. For irrigated conditions, METRIC produced a relative error of 11% against 18% with GSS-ET estimates. However, relative error with METRIC was greater (45%) than that with GSS (20%) for dry land conditions. These results clearly indicated that the use of the  $dT$  function as opposed to the use of classical MOS (Monin-Obukhov similarity) theory while dropping the aerodynamic excess resistance may not perform well for estimating ET over sparse and water limited cropping conditions.

---

<sup>1</sup> Agronomy, 2004 Throckmorton Hall, Kansas State University, Manhattan, KS 66506, USA. Ph (785) 532-7802; Fax (785) 532-6094; email: gpaul@ksu.edu

<sup>2</sup> USDA-ARS Conservation and Production Research Laboratory, P.O. Drawer 10, Bushland, TX 79012, USA. Ph (806) 356-5730; Fax (806) 356-5750 email: Prasanna.Gowda@ars.usda.gov

<sup>3</sup> Agronomy, 2004 Throckmorton Hall, Kansas State University, Manhattan, KS 66506, USA. Ph (785) 532-3746; Fax (785) 532-6094; email: vara@ksu.edu

<sup>4</sup> USDA-ARS Conservation and Production Research Laboratory, P.O. Drawer 10, Bushland, TX 79012, USA. Ph (806) 356-5746; Fax (806) 356-5750; email: Terry.Howell@ars.usda.gov

<sup>5</sup> Northwest Research—Extension Center, Kansas State University, P.O. Box 505, 105 Experiment Farm Road, Colby, Kansas 67701, USA. Ph (785) 462-6281; Fax (785) 462-2315; email: raiken@ksu.edu

<sup>6</sup> Biological and Agricultural Engineering, Kansas State University, Manhattan, KS 66506, USA. Ph: (785) 532-2943, Fax: (785) 532-5825; email: sllhutch@ksu.edu

## INTRODUCTION AND THEORY

Evapotranspiration (ET) is one of the major processes driving the water balance and surface energy balance of earth's hydrosphere, biosphere, and atmosphere. Surface Energy Balance Algorithm for Land (SEBAL) was developed in the early 90's (Bastiaanssen, 1995) for estimating ET using remotely sensed visible and thermal infrared spectral reflectance with auxiliary ground measurements. SEBAL became a widely used algorithm with several variant models such as METRIC (Mapping Evapotranspiration at high Resolution and with Internalized Calibration; Allen et al., 2005), SSEB (Simplified Surface Energy Balance; Senay et al., 2007), ReSET (Remote Sensing of Evapotranspiration; Elhaddad and Garcia, 2008), SEBTA (Surface Energy Balance with Topography Algorithm; Gao et al., 2011), and M-SEBAL (Modified SEBAL; Long and Singh, 2012) built along similar philosophy. A common feature in these algorithms was the concept of deducing the near surface temperature gradient,  $dT$ , as a linear function of surface radiometric temperature. The  $dT$  function was derived from two anchor points (pixels) denoting the hydrological extremes, and coined as the hot (dry) and the cold (wet) pixels. This concept was floated as revolutionizing; however, numerous associated assumptions and pitfalls were never thoroughly examined. The issues related to the  $dT$  concept in SEBAL and its variants can be understood better by investigating the generic bulk parameterizations of sensible heat flux ( $H$ ) based on the Monin and Obukhov (1954) similarity theory (MOST),

$$H = \rho_a C_p \frac{T_o - T_a}{r_{ah}} \quad (1)$$

$$r_{ah} = \frac{1}{k u_*} \left[ \ln \left( \frac{z_{ref} - d_o}{z_{oh}} \right) - \psi_h \right] \quad (2)$$

where  $\rho_a$  is the density of air ( $\text{kg m}^{-3}$ ),  $C_p$  is the air specific heat at constant pressure ( $\sim 1,004 \text{ J kg}^{-1} \text{ K}^{-1}$ ),  $r_{ah}$  ( $\text{s m}^{-1}$ ) is the aerodynamic resistance to heat transfer, and  $T_a$  is the air temperature ( $^{\circ}\text{C}$ ). In Eq.(1),  $T_o$  ( $^{\circ}\text{C}$ ; aerodynamic temperature) is defined as the extrapolation of  $T_a$  down to an effective height within the canopy at which the vegetation component of  $H$  and latent heat (LE) fluxes arise, given by  $d_o + z_{oh}$  (Chehbouni et al., 1996), where  $d_o$  is zero plane displacement height and  $z_{oh}$  (m) is roughness length for heat transport. The other terms in Eq. (2) are von Karman's constant ( $k$ ;  $\sim 0.41$ ), the friction velocity ( $u_*$  in  $\text{m s}^{-1}$ ) and stability correction function for heat ( $\psi_h$ ) as a function of Monin-Obukhov length ( $L$ ). In Eq. (1) the temperature gradient ( $dT$ ) is defined as the difference between  $T_o$  and  $T_a$ . The absence of direct measurement and theoretical nature of  $T_o$  and  $z_{oh}$  made the implementation of Eq. (1) a challenge. The only approach, as an alternative to this limitation was to adopt the radiometric temperature ( $T_s$ ) derived from the thermal sensors and apply the required correction to account for inherent differences between the two temperatures.

SEBAL defined  $dT$  as the near-surface temperature difference between level  $z_1$  and  $z_2$  where  $z_1$  was taken as 0.1 m and  $z_2$  was the reference level ( $T_a$  measurement level usually

2 m) (Bastiaanssen et al., 2005; Allen et al., 2007). This is a serious deviation from the original definition where the position of effective heat source is given by  $z_{oh}$  and not by any arbitrary value of  $z_1$ . How an arbitrary value of 0.1 m for  $z_1$  was reached upon is never found in the SEBAL/METRIC literature. At the same time, numerous studies have reported that  $z_{oh}$  is a highly sensitive parameter when using a MOST formulation (Steward et al., 1994; Liu et al., 2007). The  $dT$  was computed in SEBAL through an indigenous method popularly known as the 'hot and cold pixel' concept. Following Fig. 1,  $dT$  is computed for two points marked as the hot and cold pixel by inverting Eq. (3) and the resulting linear relationship is applied over the study region. There are several assumptions and limitations to this concept which are listed here under two categories:

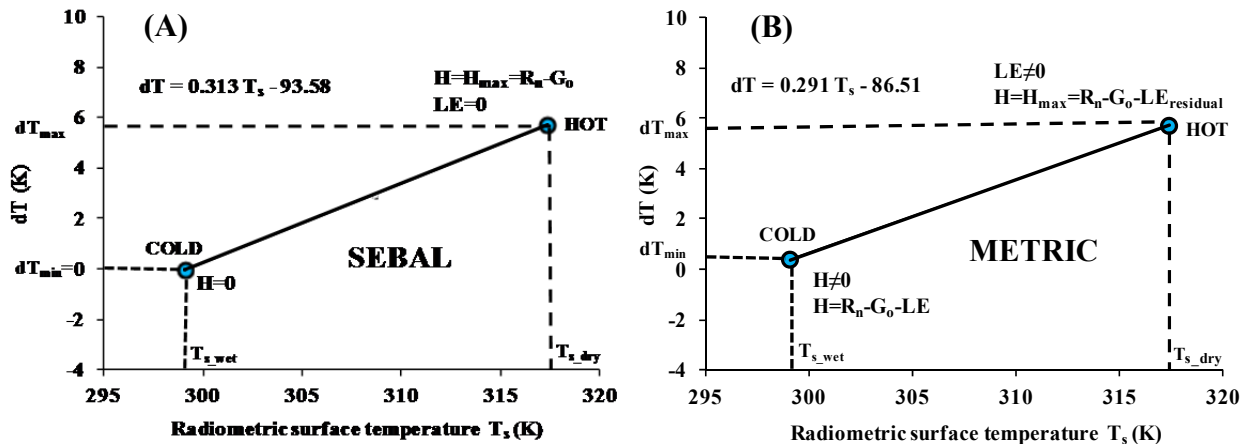


Figure 1. The  $dT$  formulation in SEBAL and METRIC for a July 28, 2008 image acquired over the USDA-ARS Conservation and Production Laboratory, Bushland, Texas. Note the change in the  $dT$  function from SEBAL to METRIC.

(1) assumptions in the validity of  $dT$  vs  $T_s$  relationship across the landscape and (2) assumptions in the selection of hot and cold pixel used for developing the  $dT$  vs  $T_s$  relationship. The first category of assumptions builds the conceptual framework of SEBAL and has several sub-assumptions: (a) a prior existence of relationship between  $dT$  and  $T_s$ ; (b)  $dT$  vs  $T_s$  relationship accounts for the spatial variability of  $z_{oh}$ ; (c) the  $dT$  vs  $T_s$  relationship accounts for the spatial variability of  $T_a$ ; and (d) the  $dT$  vs  $T_s$  relationship accounts for the atmospheric contamination of acquired remote sensing data. The second category of assumptions pertains to the implementation of the concept and has also several sub-assumptions: (a) there exists a hot and a cold pixel in the image; (b) there exists a criterion for the selection of hot and cold pixel; and (c) the selection of hot and cold pixel is invariant of the domain size.

In SEBAL literature, several selection criteria can be found for the selection of hot and cold pixel, example (a) for hot pixel: dry sandy soil (Chandrapala and Wimalasuriya, 2003), bare soil (Allen et al., 2007), maximum temperature (Jacob et al., 2002), scatter plot (Choi et al., 2009, Long and Singh, 2012), and (b) for cold pixel: water body (Bastiaanssen et al., 2005), full vegetation (Allen et al., 2007), minimum temperature (Jacob et al., 2002), scatter plot (Choi et al., 2009, Long and Singh, 2012). Interestingly all these studies generated similar levels of ET accuracy. The METRIC algorithm may be

considered as more conceptually evolved in the hot and cold pixel concept for its physical treatment of end members (Fig 1B), because the METRIC algorithm attempts to attach physical meaning to the hot and cold pixel by stating that at hot pixel some residual moisture is present ( $LE \neq 0$ ) and at cold pixel, vegetation is transpiring at 1.05 times the reference ET ( $H \neq 0$ ). These are deviations from SEBAL (Fig. 1). However, there is no study comparing SEBAL and METRIC to conclude that the physical treatment given to the end member pixels improved performance. Formulation for estimating sensible heat (H) flux in METRIC is given as follows:

$$H = \rho_a C_p \frac{dT_{1-2}}{r_{ah,1-2}} \quad (3)$$

$$r_{ah,1-2} = \frac{1}{ku_*} \left[ \ln \left( \frac{z_2}{z_1} \right) - \psi_h \right] \quad (4)$$

where,  $r_{ah,1-2}$  is aerodynamic resistance ( $s\ m^{-1}$ ) between two near-surface heights,  $z_1$  and  $z_2$  taken as 0.1 and 2 m, respectively, above the zero-plane displacement height. The  $dT_{1-2}$  parameter (K) represents the near-surface temperature difference between  $z_1$  and  $z_2$ . The  $dT_{1-2}$  parameter is computed for the study area using the linear function developed from the hot and cold pixel concept (Fig 1B). The METRIC approach is to fix the source/sink height ( $z_1=0.1$  m) and rely on the  $dT$  from the hot and cold pixel concept to accommodate for the differences between  $T_o$  and  $T_s$ . The  $r_{ah,1-2}$  is computed using  $z_1$  (0.1 m) defined to be at an elevation above  $z_{oh}$ , and thus it eliminates the use of  $z_{oh}$ .

A generic single source (GSS) model formulation is similar to Eq. 1 and 2, except  $T_o$  would be replaced by  $T_s$  and the source/sink height ( $z_{oh}$ ) would be defined as radiometric roughness length for heat.

$$H = \rho_a C_p \frac{T_s - T_a}{r_{ah}} \quad (5)$$

$$r_{ah} = \frac{1}{ku_*} \left[ \ln \left( \frac{z_{ref} - d_o}{z_{oh}} \right) - \psi_h \right] \quad (6)$$

METRIC and GSS differed only in their approach of defining and computing  $dT$  and corresponding  $r_{ah}$ , which would have direct influence on the estimation of H fluxes. The  $z_{oh}$  in Eq. 6 is related to a radiometric excess resistance parameter,  $kB^{-1}$ , (Garratt and Hicks, 1973) as:

$$z_{oh} = z_{om} / \exp(kB^{-1}) \quad (7)$$

It needs to be clarified here that aerodynamic excess resistance parameter ( $kB_a^{-1}$ ) is strictly an aerodynamic term related to the aerodynamic surface temperature. However, it becomes merely a fitting parameter that is no longer connected to its theoretical

background when  $T_o$  is replaced with  $T_s$  (Troufleau et al., 1997; Lhomme et al., 2000). Remote sensing algorithms that use the bulk transfer equations are required to use  $kB^{-1}$  (Verhoef et al., 1997; Lhomme et al., 2000); however, the value of  $kB^{-1}$  can highly vary spatially and diurnally, and parameterization is not easy. Reported  $kB^{-1}$  values ranged between 1–12 (Su et al., 2001) and larger values found to be less sensitive (Troufleau et al., 1997; Verhoef et al., 1997). A widely used constant  $kB^{-1}$  value of 2 proposed by Garrat and Hicks (1973) was too small for most surfaces (Kustas et al., 1989; Stewart et al., 1994; Verhoef et al., 1997; Su et al., 2001; Lhomme et al., 2000) and the fact that the overestimation of  $kB^{-1}$  has less consequence than underestimating it (Troufleau et al., 1997; Verhoef et al., 1997), supports the usage of a value of around 6 (Stewart et al., 1994). Recent developments in conceptualization and parameterization of  $kB^{-1}$  (Su et al., 2001) has proved to be promising in generating spatially variable  $kB^{-1}$  for accurate estimation of  $H$  using  $T_s$  (Kustas and Anderson, 2009). The objective of this study was to analyze the performance of a model that utilizes the hot and cold pixel concept (METRIC) and compares it against an algorithm (GSS) which utilizes the  $kB^{-1}$  parameter.

## MATERIALS AND METHODS

High resolution airborne imagery data from the Bushland Evapotranspiration and Agricultural Remote Sensing Experiments during 2007 and 2008 (BEAREX07 and BEAREX08) was used in this study. Both METRIC and GSS were applied on eight high resolution airborne images acquired during two summer growing seasons for estimating hourly ET and validated against lysimeter data.

### Study area and instrumentations

The BEAREX07 and BEAREX08 field campaigns were conducted at the USDA-ARS Conservation and Production Research Laboratory (CPRL) Bushland, Texas, during the 2007 and 2008 summer growing seasons. This is a semi-arid region with geographic coordinates of 35° 11' N, 102° 06' W and elevation of 1170 m above mean sea level. The CPRL has four large weighing lysimeters (3 m long x 3 m wide x 2.4 m deep) each located in the middle of approximately 4.7 ha fields arranged in a block pattern. The two lysimeter fields located in the east (NE and SE) were managed under irrigated conditions, and the other two lysimeter fields in the west (NW and SW) were under dryland management. Each lysimeter field was equipped with an automated weather station that provided net radiation ( $R_n$ ),  $T_s$ , soil heat flux ( $G_o$ ),  $T_a$ , relative humidity, and wind speed measurements (refer to Chávez et al., 2009 for details of field instrumentation). In addition, a grass reference ET weather station (0.31 ha), which is a part of the Texas High Plains ET Network, was located on the eastern edge of the SE irrigated lysimeter field (Marek et al., 2009). During the BEAREX07 (2007), the NE field was planted with forage sorghum (on 30 May), the SE field was planted to corn (on 17 May). The NW field was planted with grain sorghum in rows (on 6 June), and the SW field was planted with grain sorghum in clumps (on 6 June). During the BEAREX08 (2008), cotton was planted on all lysimeter fields. The planting was done on 21 May and 5 June on irrigated and dryland lysimeters, respectively.

### **Airborne Remote Sensing Data**

Flying expeditions were conducted during the summer field campaign to acquire high resolution remotely sensed imagery using the Utah State University (USU) airborne digital multispectral system. It acquired high resolution imagery in the green (0.545–0.555  $\mu\text{m}$ ), red (0.665–0.675  $\mu\text{m}$ ), near-infrared (0.790–0.810  $\mu\text{m}$ ), and thermal infrared (8–12  $\mu\text{m}$ ) portions of the electromagnetic spectrum. Visible and near infrared images were acquired at 0.5–1 m spatial resolution, and the thermal images were acquired at 1–3 m. Eight images, four in each year, that were acquired close to 12 Noon CST during the mid-cropping season were used in this study. The acquisition dates were 2 July (183), 10 July (191), 26 July (207), 27 July (208) in 2007 and 12 July (194), 20 July (202), 28 July (210), and 5 August (218) in 2008. Description of the post processing including geometric corrections, radiometric calibration, and atmospheric correction that can be found in Neale et al. (2012). Crops in the irrigated field attained a near complete canopy by the last image acquisition date, whereas the dryland fields exhibited relatively less canopy cover. A 12 x 12 ( $\text{m}^2$ ) pixel grid covering the lysimeter location was used in all four lysimeter fields to extract average values of estimated ET,  $R_n$ ,  $G_o$ ,  $T_s$  and aerodynamic parameters for evaluating the performances of METRIC and GSS algorithms.

### **Evaluation Statistics**

Standard and regression statistics (mean, slope, intercept and coefficient of determination), error index statistics (MBE: mean bias error, MAE: mean absolute error and RMSE: root mean square error), and a dimensionless performance statistic (NSE: Nash-Sutcliffe efficiency) were used for model evaluation. All three error indices provide errors in the constituent's unit and could also be expressed as relative error with respect to the mean. These three error indices served a unique purpose and were used in combination to diagnose the performances of the METRIC and GSS algorithms. The MBE was used as the indicator of under/overestimation error, the MAE was used as the primary indicator for average error, and the RMSE was reported as a conventional measure of error, and the MAPD (mean absolute percent difference) was used as a relative error indicator expressed as percentage deviation. Apart from these, the difference between RMSE and MAE was used as an indicator of variance in the individual errors of the dataset. The NSE indicated how well the plot of observed versus model estimated data fit the 1:1 line. Values between 0.0 and 1.0 are generally considered as acceptable levels of performance, whereas values  $<0.0$  indicate unacceptable model performance (Moriassi et al., 2007). Formulations of performance statistics used in this study are provided as footnote in Table 1.

### **Remote Sensing Based Surface Energy Balance Algorithm**

Most algorithms utilize the widely applied residual approach of surface energy balance to estimate ET at different temporal and spatial scales. The net energy coming from the sun and atmosphere in the form of short- and long-wave radiation is transformed and used for (a) heating the soil ( $G_o$ ; soil heat flux into the ground), (b) heating the surface

environment ( $H$ ; sensible heat flux to the atmosphere), and (c) transforming water into vapor ( $LE$ ; latent heat from the crop/soil surfaces). All the energy involved in the soil-vegetation-atmosphere interface can be given as the Energy Balance (EB) equation:

$$R_n = G_o + H + LE \quad (8)$$

where all units expressed in  $W\ m^{-2}$ . Latent heat flux can be expressed as hourly ET (mm) (by dividing  $LE$  by the latent heat of vaporization and the density of water). In METRIC, net radiation ( $R_n$ ) is expressed as an electromagnetic balance of all incoming and outgoing fluxes, and soil heat flux is computed using an empirical relationship developed by Bastiaanssen et al. (1998). Sensible heat flux is estimated as discussed in the previous section using the METRIC approach and the generic approach. The METRIC algorithm with all sub-models and step-wise procedures was adopted as reported in published literature (Allen et al., 2005; Allen et al., 2007; and Allen et al., 2011). The algorithms were coded using Python programming language and executed in Arc-GIS 10.0.

## RESULTS AND DISCUSSION

Performance statistics for estimating  $T_s$ ,  $R_n$  and  $G_o$  are given in Table 1. Estimated  $R_n$  and retrieved  $T_s$ , accuracies were within the typical error limits of instrument measurement uncertainty (5%). A RMSE of  $16\ W\ m^{-2}$  in estimating  $G_o$  amounted to a high relative error of 35% (MAPD); however, the positive NSE (0.12) indicated model's satisfactory performance. Soil heat flux was smallest and relatively low in magnitude as compared with the other components of the energy balance for the present study domain, hence any error in  $G_o$  had minimal influence on the  $LE$  estimation.

Modeled ET from METRIC algorithm plotted against observed instantaneous ET (Fig. 2) showed a lag and large scatter along the regression line in the estimated values. However, a relatively small scatter and a small lag between the GSS-derived ET and observed data points were observed in the regression plot of the GSS model (Fig. 3). Comparison of the METRIC- and GSS-derived ET for irrigated and dryland lysimeter fields indicated a distinct difference in the performance of METRIC in estimating ET (Fig. 2). However, no such distinction could be made for GSS (Fig. 3). Statistical comparison of METRIC-estimated irrigated and dryland ET separately against observed data revealed the performance biases between the two water regimes with relative error of 11% and 45% respectively. The relative errors were 18% and 20% with GSS-estimated ET for irrigated and dryland fields, respectively. In dryland fields with sparsely vegetated surface undergoing frequent water stress, the difference between  $T_s$  and  $T_o$  could exceed  $10^\circ C$  (Chehbouni et al., 1996) whereas, in an irrigated field with well-watered dense homogeneous crops, the differences between  $T_s$  and  $T_o$  is minimal ( $1-2^\circ C$ ; Kustas et al., 1989). Accounting for the large difference between  $T_s$  and  $T_o$  in sparse vegetation water stressed condition is more critical for the model's performance than for the small difference arising under irrigated full canopy cover condition. Thus,  $dT$  is a more sensitive parameter for sparsely vegetated condition than for a dense non-water stressed vegetated condition.

Overall performance of estimated H fluxes from METRIC and GSS were compared against H derived as the residual of the observed components of the energy balance Eq. (8) and tabulated in Table 2. The H estimated from METRIC is marked by a large overestimation error of  $98 \text{ W m}^{-2}$  (MBE), a high relative error of 75% (MAPD) and a NSE value of -0.19, indicating poor performance. The performance of GSS model in predicting H was significantly better with an underestimation error of  $-44 \text{ W m}^{-2}$ ,

Table 1. Performance statistics for retrieved  $T_s$  (Obs. Mean:  $33.3^\circ\text{C}$ ),  $R_n$  (Obs. Mean:  $576 \text{ W m}^{-2}$ ) and  $G_o$  (Obs. Mean:  $34 \text{ W m}^{-2}$ ). Total number of observations - 32.

Parameter	Estimated Mean	MBE <sup>1</sup>	MAE <sup>2</sup>	RMSE <sup>3</sup>	MAPD <sup>4</sup>	NSE <sup>5</sup>	R <sup>2</sup>	slope	y-intercept
$T_s$ ( $^\circ\text{C}$ )	33.4	0.06	0.93	1.2	2.8	0.96	0.97	0.98	0.4
$R_n$ ( $\text{W m}^{-2}$ )	580	3.3	24	29	4.1	0.73	0.75	0.86	81
$G_o$ ( $\text{W m}^{-2}$ )	33	1.5	12	16	35.2	0.12	0.17	0.25	24

$${}^1 \text{ MBE} = \frac{1}{n} \sum_{i=1}^n (M_i - O_i) \quad {}^2 \text{ MAE} = \frac{1}{n} \sum_{i=1}^n |M_i - O_i| \quad {}^3 \text{ RMSE} = \sqrt{\frac{1}{n} \sum_{i=1}^n (M_i - O_i)^2}$$

$${}^4 \text{ MAPD} = \frac{\sum_{i=1}^n |M_i - O_i|}{\sum_{i=1}^n O_i} \times 100 \quad {}^5 \text{ NSE} = \frac{\sum_{i=1}^n (O_i - \bar{O})^2 - \sum_{i=1}^n (M_i - O_i)^2}{\sum_{i=1}^n (O_i - \bar{O})^2}$$

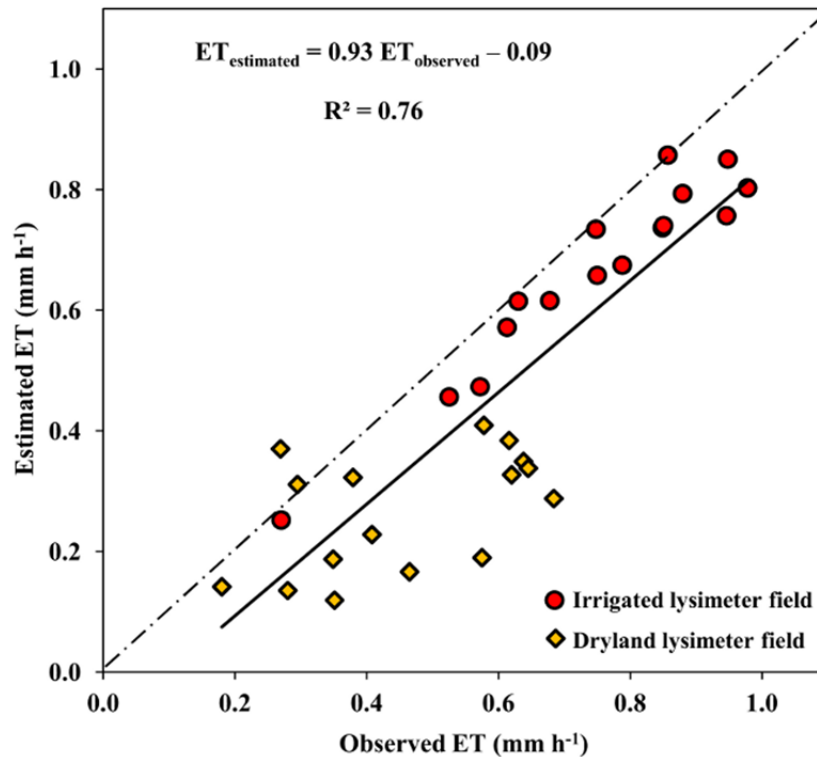


Figure 2. Observed versus METRIC-estimated instantaneous ET ( $\text{mm h}^{-1}$ )

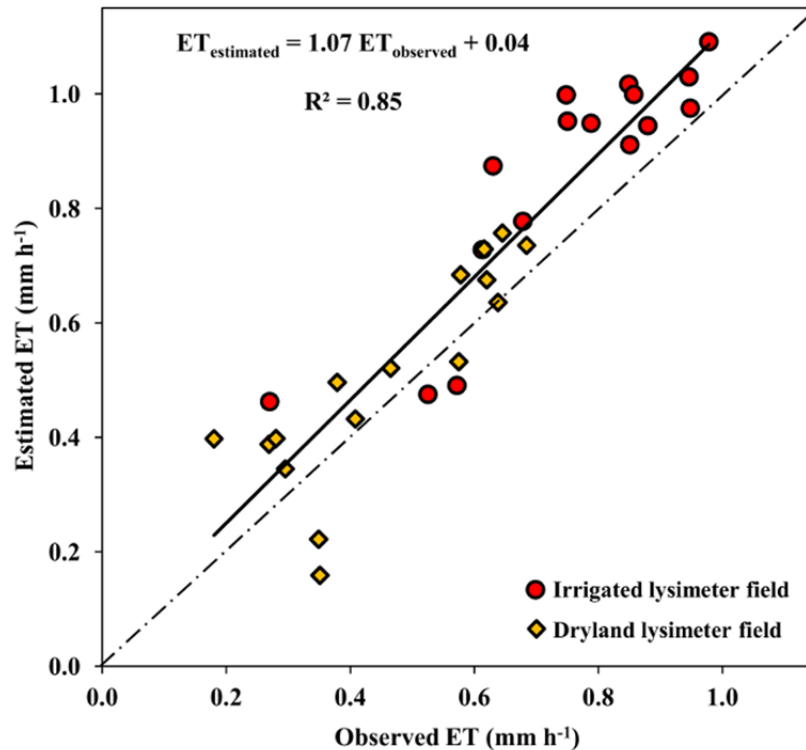


Figure 3. Observed versus GSS-estimated instantaneous ET ( $\text{mm h}^{-1}$ )

relative error of 42.6% and a positive NSE value of 0.63. The overestimation error in the METRIC-estimated H fluxes translated into same magnitude of underestimation error in the estimation of LE fluxes. Interestingly, the greater relative error of 75% in the METRIC-estimated H fluxes corresponded to a nominal error of 24% in the estimated LE fluxes, and this is attributed to the unequal partitioning of the available energy into the H (mean:  $144 \text{ W m}^{-2}$ ) and LE (mean:  $405 \text{ W m}^{-2}$ ) fluxes under the energy non-limiting and water sufficient conditions. The GSS overestimated LE with a relative error of 18% which had its origin traced back to the underestimation in corresponding H estimates. (Table 2). The GSS-LE estimates outperformed the METRIC-LE estimates in all the performance measures. The difference between RMSE and MAE ( $\text{RMSE} - \text{MAE}$ ) was almost double in the case of the METRIC-estimated LE fluxes as compared with GSS estimates indicating a larger variance in the individual errors, substantiating the large scatter illustrated in Fig. 2. The LE or ET underestimation errors in SEBAL and SEBAL-like algorithms is reported by various studies (French et al., 2005; Long and Singh 2012, Choi et al., 2009) and is the direct consequence of overestimation of H fluxes. Transformation of overestimation errors in METRIC-H to underestimation error in GSS-H (evident from Figs. 1 and 2, and Table 2) provides an adequate reason to conclude that  $dT$  is the parameter responsible for this biased behavior. The performance statistics for instantaneous ET evaluated for METRIC and GSS are provided in Table 2.

Table 3 gives the  $dT$  and  $r_{ah}$  values from METRIC and GSS approaches for two soil moisture regimes on two image acquisition dates. The H is a function of  $dT$  and  $r_{ah}$  as described by Eqs. 3 and 4 for METRIC and Eqs. 5 and 6 for GSS. Both  $dT$  and  $r_{ah}$  are

intrinsically related, hence only a qualitative analysis is possible for the  $dT$  and  $r_{ah}$  values derived from the two approaches and reader may refer to Liu et al. (2007) for their ranges. Nevertheless, it could be concluded that GSS derived  $dT$  and  $r_{ah}$  are more accurate since it produced significantly better  $H$  estimates. Some of the critical observations inferred from Table 3 are: (a) negative  $dT$  for the irrigated field in the GSS model (b)  $dT$  for irrigated fields are always smaller than that for dryland field, (c) the differences in the magnitude of  $dT$  and  $r_{ah}$  between the two models and (d) relatively small values of  $z_{oh}$  in GSS model compared with a constant value of  $z_1$  (0.1) used in METRIC.

Table 2. Performance statistics for  $H$  (Obs. Mean:  $144 \text{ W m}^{-2}$ ),  $LE$  (Obs. Mean:  $405 \text{ W m}^{-2}$ ), and  $ET$  (Obs. Mean:  $0.60 \text{ mm h}^{-1}$ )

Estimated Fluxes	Mean	MBE	MAE	RMSE	MAPD	NSE	$R^2$	slope	y-intercept
$H_{\text{METRIC}}$	242	98	108	125	75.1	-0.19	0.61	0.80	126
$LE_{\text{METRIC}}$	313	-92	97	122	23.9	0.34	0.76	0.93	-65
$ET_{\text{METRIC}}$	0.46	-0.14	0.14	0.18	23.9	0.34	0.76	0.93	-0.09
$H_{\text{GSS}}$	100	-44	61	70	42.6	0.63	0.85	1.10	-56
$LE_{\text{GSS}}$	459	53	75	87	18.5	0.67	0.85	1.08	18
$ET_{\text{GSS}}$	0.68	0.08	0.11	0.13	18.5	0.67	0.85	1.07	0.04

Table 3. Temperature gradient,  $dT$ , and aerodynamic resistance,  $r_{ah}$ , values from METRIC and GSS approach

Date	Field <sup>†</sup>	METRIC		GSS		
		$dT$	$r_{ah}^*$	$dT$	$r_{ah}$	$z_{oh}$
July 28, 2008	NE	0.83	9.15	-3.54	34.85	0.00030
	SE	1.06	9.47	-2.74	36.81	0.00025
	NW	3.52	11.69	5.75	51.21	0.00003
	SW	3.01	11.34	3.98	47.44	0.00005
July 27, 2007	NE	1.30	11.05	-4.53	71.48	0.00067
	SE	1.24	9.88	-4.68	67.91	0.00071
	NW	3.40	13.85	1.31	70.94	0.00035
	SW	3.68	14.25	2.10	71.53	0.00029

\*  $z_{oh}$  in METRIC is replaced by empirical level  $z_1$  with a fixed value of 0.1 m.

<sup>†</sup> NE & SE are irrigated fields and NW & SW are dryland fields

## SUMMARY

The  $dT$  as defined in METRIC and computed from the hot and cold pixel concept may not represent and account for the non-unique relationship existing between  $T_o$  and  $T_s$ . The GSS model with an empirical correction in the form of excess resistance parameter,  $kB^{-1}$ , accounts for the difference between  $T_o$  and  $T_s$ . Hence an improvement in the overall performance and negligible bias between irrigated and dryland fields can be achieved.

The influence of  $dT$  cannot be seen under well-watered, densely cropped, energy non-limiting conditions. Because under such a condition, the LE fluxes are much greater than H fluxes and errors in H fluxes would have limited influence on the LE estimation. In other words, H is a relatively insensitive parameter for the estimation of LE flux in irrigated conditions.

The overall relative error in METRIC-estimated ET was 24% whereas from GSS it was 18%, while this difference might not seem large yet this difference is solely the attribute of the  $dT$  parameter and got modulated depending on the partitioning of available energy (between H and LE). For dryland fields, the relative error in ET from METRIC was 45% whereas from GSS it was 20%, once again indicating the uncertainty in using the hot and cold pixel based  $dT$  parameter. More profound and direct impact of  $dT$  is seen in the H flux estimation where METRIC performance was poor with negative NSE values.

The  $dT$  is physically linked to  $r_{ah}$ , however, the non-availability of  $T_o$  and the theoretical nature of  $z_{oh}$  forces adoption of empiricism. The accuracy of H fluxes depends on appropriate  $dT$  and corresponding  $r_{ah}$ . METRIC approach fails in producing appropriate  $dT/r_{ah}$  under heterogeneous, sparse and water limited vegetation conditions. Meanwhile, the GSS approach of adopting a constant radiometric excess resistance parameter ( $kB^{-1}$ ) not only produced significantly improved results but also reduced bias between irrigated and dryland fields proving that this approach accommodates for the discrepancy between  $T_o$  and  $T_s$ .

The selection criteria for the hot and cold pixel or even the physical treatment of the hot and cold pixels has limited and uncertain influence on the performance of METRIC and SEBAL-like models. However, the developers have put great emphasis on this highly subjective selection process, adding that the algorithm should be executed by trained experts alone (Allen et al., 2007; Batiaanssen et al., 2010; Allen et al., 2011), again a subjective requirement. The process of selection of the hot and cold pixel is highly uncertain and operator dependent, hence it becomes difficult to ascertain any form of sensitivity for the  $dT$  parameter. Often a trial and error method is adopted to select the pixels to match the requirements.

## CONCLUSIONS

The two algorithms (METRIC and GSS) examined in this study only differed in their approach of computing the  $dT$  value. Hence any inconsistency in model performance in estimating ET should solely be attributed to the approaches used in calculating this

parameter. The GSS model outperformed METRIC in all the performance statistics. The claims that the  $dT$  parameter computed using the hot and cold pixel concept considers for the atmospheric attenuations,  $T_o - T_s$  difference, spatial variability of  $z_{oh}$ , and the spatial variability of  $T_a$  is implausible especially when the existence of  $dT$  versus  $T_s$  relationship is questionable and never been tested thoroughly. Too much is at stake from a regression equation developed from merely two subjective points. Numerous studies reported the high sensitivity of  $dT$  and termed it as the backbone of SEBAL and SEBAL-like models; however, the large subjectivity and uncertainty attached to  $dT$  computation cannot allow a fair sensitivity analysis. SEBAL-like models including the METRIC model never fully evaluated independently the validity of  $dT$  versus  $T_s$  relationship. The high degree of ambiguity in the selection of hot and cold pixel lead to large variations in the  $dT$  function, thus making the process a trial and error method. The hot and cold pixel approach should be considered as an empirical method for estimating the  $dT$  parameter over a relatively homogeneous and well managed landscape, and any physical treatment given to the end member pixel may not warrant performance augmentation. Finally, the approach of deducing  $dT$  from the hot and cold pixel concept has been exploited beyond its limited capacity and detail studies should be carried out to address the several drawbacks and uncertainties when applying over heterogeneous spatial domain.

#### ACKNOWLEDGMENTS

This research was supported by the Ogallala Aquifer Program, a consortium between USDA–Agricultural Research Service, Kansas State University, Texas A&M AgriLife Research, Texas A&M AgriLife Extension Service, Texas Tech University, and West Texas A&M University. This is contribution number 13-258-A from the Kansas Agricultural Experiment Station.

#### REFERENCES

- Allen, R. G., Irmak, A., Trezza, R., Hendrickx, J. M. H., Bastiaanssen, W., and Kjaersgaard, J., (2011), Satellite-based ET estimation in agriculture using SEBAL and METRIC, *Hydrol. Process.*, 25, 4011–4027, doi: 10.1002/hyp.8408.
- Allen, R. G., Tasumi, M., and Trezza, R., (2007), Satellite-Based Energy Balance for Mapping Evapotranspiration with Internalized Calibration (METRIC)-Model, *J. Irrig. Drain. Eng.*, 133(4), 380–394, doi:10.1061/(ASCE)0733-9437(2007)133:4(380).
- Allen, R. G., Tasumi, M., Morse, A., and Trezza, R., (2005), A Landsat-based Energy Balance and Evapotranspiration Model in Western US Water Rights Regulation and Planning, *Irrig. Drain. Syst.*, 19, 251–268, doi:10.1007/s10795-005-5187-z.
- Bastiaanssen, W., Thoreson, B., Clark, B., David, G., (2010), Discussion of “Application of SEBAL Model for Mapping Evapotranspiration and Estimating Surface Energy Fluxes in South-Central Nebraska” by Ramesh K. Singh, Ayse Irmak, Suat Irmak, and Derrel L. Martin, *J. Irrig. Drain. Eng.*, 134 (3), 282–283, doi: 10.1061/(ASCE)0733-9437(2008)134:3(273)

Bastiaanssen, W. G. M., Noordman, E. J. M., Pelgrum, H., Davids, G., Thoreson, B. P., and Allen, R. G., (2005), SEBAL model with remotely sensed data to improve water-resources management under actual field conditions, *J. Irrig. Drain. Eng.*, 131(1), 85–93, doi: 10.1061/(ASCE)0733-9437(2005)131:1(85)

Bastiaanssen, W. G. M., (1995), Regionalization of surface flux densities and moisture indicators in composite terrain: A remote sensing approach under clear skies in Mediterranean climates, 273 pp., Ph.D. thesis, Wageningen Agric. Univ., Den Haag, Netherlands.

Bastiaanssen, W. G. M., Menenti, M., Feddes, R. A., and Holtslag, A. A. M., (1998), A remote sensing surface energy balance algorithm for land (SEBAL)—1. Formulation, *J. Hydrol.*, 212 (1-4), 198–212, doi:10.1016/S0022-1694(98)00253-4.

Chandrapala, L., and Wimalasuriya, M., (2003), Satellite measurement supplemented with meteorological data to operationally estimate evapotranspiration in Sri Lanka, *Agric. Water Manage.*, 58(2), 89–107, doi:10.1016/S0378-3774(02)00127-0.

Chehbouni, A., Seen, D. L., Njoku, E. G., and Monteny, B. M., (1996), Examination of the difference between radiative and aerodynamic surface temperatures over sparsely vegetated surfaces, *Remote Sens. Environ.*, 58(2), 177–186, doi:10.1016/S0034-4257(96)00037-5.

Chávez, J. L., Gowda, P. H., Howell, T. A., Neale, C. M. U., and Copeland, K. S., (2009), Estimating hourly crop ET using a two-source energy balance model and multispectral airborne imagery, *Irrig. Sci.*, 28 (1), 79–91, doi:10.1007/s00271-009-0177-9.

Choi, M., Kustas, W. P., Anderson, M. C., Allen, R. G., Li, F., and Kjaersgaard, J. H., (2009), An intercomparison of three remote sensing-based surface energy balance algorithms over a corn and soybean production region (Iowa, U.S.) during SMACEX, *Agric. For. Meteorol.*, 149(12), 2082–2097, doi:10.1016/j.agrformet.2009.07.002.

Elhaddad, A., and Garcia, L. A., (2008), Surface energy balance-based model for estimating evapotranspiration taking into account spatial variability in weather, *J. Irrig. Drain. Eng.*, 134(6), 681–689, doi:10.1061/(ASCE)0733-9437(2008)134:6(681).

French, A. N., Jacob, F., Anderson, M. C., Kustas, W. P., Timmermans, W., Gieske, A., Su, Z., Su, H., McCabe, M. F., Li, F., Prueger, J., Brunsell, N., (2005), Surface energy fluxes with the Advanced Spaceborne Thermal Emission and Reflection radiometer (ASTER) at the Iowa 2002 SMACEX site (USA), *Remote Sens. Environ.*, 99(1-2), 55–65, doi:10.1016/j.rse.2005.05.015.

Garrat, J. R., and Hicks, B. B., (1973), Momentum, heat and water vapour transfer to and from natural and artificial surfaces, *Quart. J. Roy. Meteorol. Soc.*, 99(422), 680–687, doi:10.1002/qj.49709942209

Gao, Z. Q., Liu, C. S., Gao, W., and Chang, N. B., (2011), A coupled remote sensing and the Surface Energy Balance with Topography Algorithm (SEBTA) to estimate actual evapotranspiration over heterogeneous terrain, *Hydrol. Earth Syst. Sci.*, 15(1), 119–39, doi:10.5194/hess-15-119-2011.

Jacob, F., Olioso, A., Gu, X. F., Su, Z., Seguin, B., (2002), Mapping surface fluxes using airborne visible, near infrared, thermal infrared remote sensing data and a spatialized surface energy balance model. *Agronomie*, 22(6), 669–680, doi:10.1051/agro:2002053.

Kalma, J. D., and Jupp, D. L. B., (1990), Estimation of evaporation from pasture using infrared thermometry: evaluation of a one-layer resistance model, *Agric. For. Meteorol.*, 51(3-4), 223–246, doi:10.1016/0168-1923(90)90110-R.

Kustas, W. P., Choudhury, B. J., Moran, M. S., Reginato, R. J., Jackson, R. D., Gay, L. W., Weaver, H. L., (1989), Determination of sensible heat flux over sparse canopy using thermal infrared data, *Agric. For. Meteorol.*, 44(3-4), 197–216, doi:10.1016/0168-1923(89)90017-8.

Kustas, W., and Anderson, M., (2009), Advances in thermal infrared remote sensing for land surface modeling, *Agric. For. Meteorol.*, 149(12), 2071–2081, doi:10.1016/j.agrformet.2009.05.016.

Liu, S., Lu, L., Mao, D., and Jia, L., (2007), Evaluating parameterizations of aerodynamic resistance to heat transfer using field measurements, *Hydrol. Earth Syst. Sci.*, 11(2), 769–783.

Long, D., and Singh, V. P., (2012a), A modified surface energy balance algorithm for land (M-SEBAL) based on a trapezoidal framework, *Water Resour. Res.*, 48, W02528, doi:10.1029/2011WR010607.

Lhomme, J. P., Chehbouni, A., and Monteny, B., (2000), Sensible heat flux-radiometric surface temperature relationship over sparse vegetation: Parameterizing  $B^{-1}$ , *Boundary-Layer Meteorol.*, 97(3), 431–457, doi:10.1023/A:1002786402695.

Monin, A. S., and Obukhov, A. M., (1954), Basic laws of turbulent mixing in the ground layer of the atmosphere, *Tr. Akad. Nauk. SSSR Geofiz. Inst.*, 24(151), 163–187.

Moriasi, D. N., Arnold, J. G., Liew, M. W. V., Bingner, R. L., Harmel, R. D., Veith, T. L., (2007), Model evaluation guidelines for systematic quantification of accuracy in watershed simulations, *Tran. ASABE*, 50(3), 885–900.

Marek, T. H., Porter, D. O., Howell, T. A., Kenny, N., Gowda, P. H., (2009), Understanding ET and its use in irrigation scheduling (a TXHPET Network series user manual). Texas AgriLife Research at Amarillo, Publication No. 09-02, Texas A&M University, Amarillo, 6 Texas, 60 pp.

- Neale, C. M. U., et al., (2012), Soil water content estimation using a remote sensing based hybrid evapotranspiration modeling approach, *Adv. Water Resour.*, 50, 152–161, doi:10.1016/j.advwatres.2012.10.008
- Norman, J. M., Anderson, M. C., Kustas, W. P., (2006), Are single-source, remote-sensing surface-flux models too simple? In: G. D'Urso, M.A.O. Jochum, & J. Moreno, (Eds.). Proceedings of the international conference on earth observation for vegetation monitoring and water management. *American Institute of Physics*, 852, 170–177.
- Senay, G. B., Budde, M., Verdin, J. P., and Melesse, A. M., (2007), A coupled remote sensing and Simplified Surface Energy Balance approach to estimate actual evapotranspiration from irrigated fields, *Sensors*, 7(6), 979–1000, doi:10.3390/s7060979.
- Su, Z., Schmugge, T., Kustas, W. P., and Massman, W. J., (2001), An evaluation of two models for estimation of the roughness height for heat transfer between the land surface and the atmosphere, *J. Appl. Meteorol.*, 40(11), 1933–1951, doi:10.1175/1520-0450(2001)040<1933:AEOTMF>2.0.CO;2.
- Stewart, J. B., Kustas, W. P., Humes, K. S., Nichols, W. D., Moran, M. S., De Bruin H. A. R., (1994), Sensible heat flux-radiometric surface temperature relationship for eight semi arid areas, *J. Appl. Meteorol.*, 33, 1110–1117, doi: [http://dx.doi.org/10.1175/1520-0450\(1994\)033<1110:SHFRST>2.0.CO;2](http://dx.doi.org/10.1175/1520-0450(1994)033<1110:SHFRST>2.0.CO;2).
- Troufleau, D., Lhomme, J. P., Monteny, B., Vidal A., (1997), Sensible heat flux and radiometric temperature over sparse Sahelian vegetation. I. An experimental analysis of kB-1 parameter, *J. Hydrol.*, 189(1-4), 815–838, doi:10.1016/S0022-1694(96)03172-1.
- Verhoef, A., DeBruin H. A. R., Van den Hurk B. J. J. M., (1997), Some practical notes on the parameter  $kB^{-1}$  for sparse vegetation, *J. Appl. Meteorol.*, 36(5), 560–572. doi: 10.1175/1520-0450(1997)036<0560:SPNOTP>2.0.CO;2



# EVALUATING THE PERFORMANCE OF SEBAL ET ALGORITHM UNDER ADVECTIVE CONDITIONS

Mcebisi M. Mkhwanazi<sup>1</sup>  
José L. Chávez<sup>2</sup>  
Allan A. Andales<sup>3</sup>

## ABSTRACT

The Surface Energy Balance Algorithm for Land (SEBAL) is one of several remote sensing-based crop evapotranspiration (ET) models. While the use of remote sensing (RS) has several noted advantages in the estimation of ET, SEBAL has an added advantage of requiring minimal climate data. However, its downside is that in the presence of advection, it may grossly underestimate ET. This is partly due to the use of the evaporative fraction (EF), in SEBAL, to extrapolate instantaneous ET (e.g., hourly) to daily ET values. When using the EF function, SEBAL assumes that the ratio of latent heat flux to available energy, at time of satellite overpass, is constant throughout the day, and therefore useable to estimate daily ET. However such an assumption does not hold in areas where there is usually afternoon advection. A study was therefore carried out to evaluate the performance of SEBAL under varying climatic and environmental conditions in a semi-arid area of eastern Colorado. A total of 13 Landsat 7 ETM+ images (2010-2012) were downloaded and processed, and ET estimated for an alfalfa field near Rocky Ford in Eastern Colorado. Results were compared with lysimeter-based ET readings. Results showed that during the days where there was advection, SEBAL underestimated ET even by as much as 5 mm/day, which translated into model error of 47 % in this study.

## INTRODUCTION

The increase in water scarcity in most parts of the world has necessitated improved management of this scarce resource. Most sectors that utilize water, for example irrigation, have developed methods to apportion water according to the needs. For agricultural water, this requires an accurate estimate of evapotranspiration. Several methods have been devised to quantify how much water is being used by crops. Remote sensing (RS) is one of the methods. This is an indirect method of measuring ET, as it uses the land surface energy balance equation:

$$R_n = LE + G + H \quad (1)$$

where  $R_n$  is net radiation,  $LE$  is latent heat flux,  $G$  is soil heat flux and  $H$  is sensible heat flux. In this method, satellite sensed radiances are converted into surface properties;

---

<sup>1</sup> Civil and Environmental Engineering Department, Colorado State University, Fort Collins, CO 80523  
Tel: (970) 818-1159, Email: [mcebisi.mkhwanazi@colostate.edu](mailto:mcebisi.mkhwanazi@colostate.edu)

<sup>2</sup> Civil and Environmental Engineering Department, Colorado State University, Fort Collins, CO 80523  
Tel: (970) 491-6095. Email: [jlchavez@rams.colostate.edu](mailto:jlchavez@rams.colostate.edu)

<sup>3</sup> Department of Soil and Crop Science, Colorado State University, Fort Collins, CO 80523, Tel: (970) 491-6516, Email: [Allan.Andales@colostate.edu](mailto:Allan.Andales@colostate.edu)

albedo, vegetation indices, surface emissivity, surface temperature. These properties are then used to estimate the various components of the energy balance model i.e.  $R_n$ ,  $H$ ,  $G$ , then  $LE$  as a residual (Gowda et al., 2011). A major advantage that RS methods have is that they provide spatially distributed estimates of  $ET$ , from field to regional scales (Elhaddad et al., 2011) unlike most methods that measure  $ET$  at point or at best local scale.

There are several RS models that have been developed; Surface Energy Balance Algorithm for Land (SEBAL; Bastiaanssen et al., 1998), Mapping Evapotranspiration at high Resolution with Internalized Calibration (Allen et al., 2007), Remote Sensing of Evapotranspiration (ReSET; Elhaddad and Garcia, 2008), Analytical Land Atmosphere Radiometer Model (ALARM; Suleiman et al., 2009), Surface Aerodynamic Temperature (SAT; Chavez et al., 2005) and many others.

The SEBAL model is widely used because of its ability to estimate  $ET$  without prior knowledge of the soil, crop, and management conditions (Bastiaanssen et al., 2005). It also requires minimal weather data, only wind speed for time of image capture, and sometimes daily solar radiation for days when there is occasional cloud cover. It is therefore a suitable model to be used in areas where there might not be adequate weather data due to lack of instrumentation.

Wang et al. (2009) reports that SEBAL accuracy varies from 67% to 95% for instantaneous  $ET$  estimates and from 70% to 98% for 1-10 day  $ET$  estimates. He further classifies the errors in  $ET$  estimates as resulting from algorithm error, instrumental error, and temporal sampling error. One source of error that has been identified in SEBAL is its lack of response to advection. This is first in the calculation of  $H$ , with the assumptions associated with the cold pixel, one of them being that  $H$  at the cold pixel is zero, which would not be accurate when there is advection (Wang et al., 2009). Secondly is when instantaneous  $ET$  is extrapolated to hourly and daily  $ET$ , in which case it is assumed the evaporative fraction ( $EF$ ) is constant throughout the day, an assumption which according to Stewart (1996) may cause error in some cases. Both assumptions are discussed later in the paper. The paper therefore seeks to discuss how these assumptions affect the accuracy of the SEBAL model when there is advection.

## MATERIALS AND METHODS

### Study Area

This research was carried out at the Colorado State University (CSU) Arkansas Valley Research Center (AVRC) near Rocky Ford, in eastern Colorado. Irrigated fields in Eastern Colorado are shown in Figure 1 surrounded by dry area. The study area has geographic coordinates  $38^{\circ} 02' N$ ,  $103^{\circ} 41' W$ , with an elevation of 1,274 m above mean sea level (amsl). The area receives an average annual precipitation of about 300 mm, with 65 % falling in May through September. The summer average temperature is  $23.6^{\circ} C$ , and the average daily maximum is  $33^{\circ} C$ . The average relative humidity in the mid-afternoon is 25% in summer, and average wind speed is  $4.4 m s^{-1}$  ([www.wcc.nrcs.usda.gov/ftpref/support/climate/soil.../mlra-69.doc](http://www.wcc.nrcs.usda.gov/ftpref/support/climate/soil.../mlra-69.doc)).

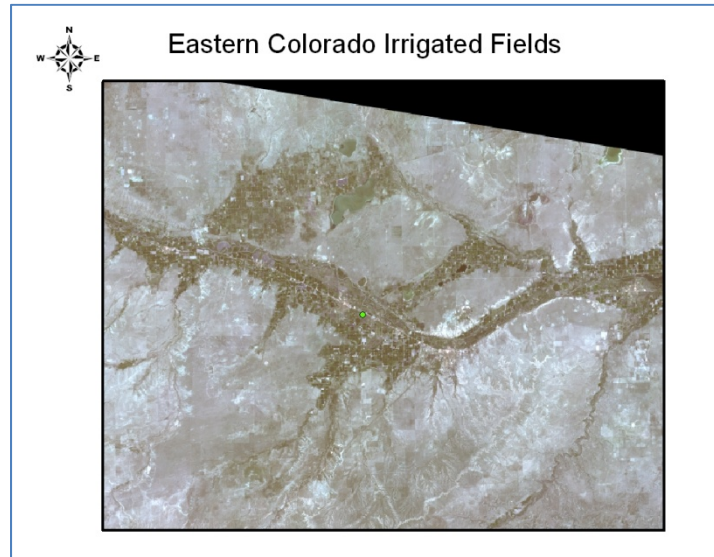


Figure 1. Study area, one of fields surrounded by dry area

The field of study is planted to alfalfa which is irrigated using a furrow irrigation system supplied by siphons and a head ditch. The field is 160 m by 250 m. Close to the center of the field is a large monolith weighing lysimeter (3 m x 3 m x 2.4 m). The field is also equipped with a net radiometer (REBS, Campbell Scientific International (CSI), Logan, Utah, U.S.A.). There is also an infra-red thermometer (IRT, Apogee model S1-111, CSI, Logan, Utah, U.S.A.) to measure crop radiometric surface temperature. Soil heat plates (REBS model HFT3, CSI, Logan, Utah, U.S.A.) are buried in the ground at locations proximal to the measurements of net radiation at a depth of about 10 cm, along with soil temperature and soil water content sensors, for the estimation of soil heat flux.

### **Landsat Satellite Datasets and Processing**

Landsat 7 Enhanced Thematic Mapper Plus (ETM+) cloud free satellite images were downloaded from the USGS Earth Explorer site [<http://earthexplorer.usgs.gov/>] for the 2010-2012 growing seasons. The acquisition dates were as follows: June 15, July 1, August 2, August 18, September 19 and October 5 for 2010, then June 18, July 4, August 5 and August 21 for 2011, then June 4, June 20 and July 22 for 2012. These dates were when the field studied was part of the image without swaths of missing data. The images were processed using the ERDAS Imagine 2010 software (ERDAS, Norcross, Georgia, U.S.A.).

### **SEBAL Algorithms**

As discussed earlier in the paper, most RS models, including SEBAL, estimate ET through the land surface energy balance (EB) method as shown in equation 1.

Net radiation. This is calculated by summing up the net shortwave radiation and net longwave radiation, and is given by equation 2 below:

$$R_n = (1 - \alpha) R_s + \varepsilon_a \sigma T_a^4 - \varepsilon_o \sigma T_s^4 - (1 - \varepsilon_o) \varepsilon_a \sigma T_a^4 \quad (2)$$

where  $R_s$  is incoming shortwave radiation,  $\alpha$  is the surface albedo,  $\epsilon_a$  is the air emissivity,  $T_a$  is air temperature,  $T_s$  is surface temperature,  $\epsilon_o$  is surface emissivity and  $\sigma$  is the Stefan Boltzmann constant.

Soil Heat Flux, G. The soil heat flux is the rate of heat flow into the soil and vegetation due to conduction (Gowda et al., 2011). Different empirical equations have been developed, based on extensive soil heat flux measurements made in experimental fields (e.g., Singh et al. (2008), Bastiaanssen et al. (1998)). The one used in this study (Eq. 3) was published by Bastiaanssen et al. (1998):

$$G/R_n = T_s/\alpha (0.0038\alpha + 0.0074\alpha^2) (1 - 0.98NDVI^4) \quad (3)$$

where  $\alpha$  is the surface albedo, which is the ratio of reflected to incident solar incident at the surface.  $T_s$  is the radiometric surface temperature (K) which is obtained by making use of the thermal band of the electromagnetic spectrum. NDVI is the Normalized Difference Vegetation Index, and is computed using the reflectance of bands 3 and 4 in Landsat 7 which are the red and near infra-red bands, respectively.

Sensible heat flux. The basic calculation of H is performed by using the bulk aerodynamic method as shown in equation 4 below:

$$H = \rho_a C_{pa} (T_o - T_a)/r_{ah} \quad (4)$$

where  $\rho_a$  is the density of moist air ( $\text{kg/m}^3$ ),  $C_{pa}$  is specific heat of dry air ( $\sim 1004 \text{ J/kg/K}$ );  $T_a$  is average air temperature (K) at screen height (typically at 2 m),  $T_o$  is the average surface aerodynamic temperature (K), and  $r_{ah}$  is the aerodynamic resistance to heat transfer. However  $T_o$  may be difficult to estimate, therefore SEBAL replaces  $(T_o - T_a)$  by a  $dT$  function, which is defined as the temperature difference at two levels at near surface, and the levels are 2 m and 0.1 m (Allen et al., 2011).

In the process of determining the  $dT$  function, two extreme pixels, a wet and dry pixel, are selected. In the selection of a wet pixel, it would be a pixel that would have a low temperature; with the assumption that the low temperature is so because the available energy ( $R_n - G$ ) is only used to evaporate water and not to warm the surface. Therefore SEBAL assumes that at the wet/cold pixel H equals zero. That rules out the possibility of a negative H which is a possible occurrence in arid regions where there could be advection. Traditionally in SEBAL, a water body is selected (Allen et al, 2011); however in its absence or by preference an agricultural field of good growth can be selected. The value of  $dT$  in the wet pixel is assumed to be zero.

For the selection of the dry pixel, a pixel with a high temperature would be a candidate since it would indicate dryness. In addition, the pixel should have low biomass or leaf area index value. Care should be taken that man-made surfaces such as highways are not selected. A dry agricultural area (possibly fallow) or bare soil is recommended. This pixel is assumed to have ET of zero, and a large value of  $dT$ . Once the dry/hot pixel is identified, the value of H can be calculated using  $R_n$  and G from the image for the pixel. The  $dT$  value can then be calculated using equation 5.

$$dT_{hot} = \frac{(R_n - G)r_{ah\ hot}}{\rho_{air\ hot} C_p} \quad (5)$$

SEBAL then assumes a linear relation of  $dT$  to radiometric surface temperature and the relationship is explained by the use of coefficients  $a$  and  $b$  whereby:

$$dT = aT_s + b \quad (6)$$

where:

$$a = \frac{dT_{hot} - dT_{cold}}{T_{s\ hot} - T_{s\ cold}} \quad b = dT_{hot} - a \times T_{s\ hot}$$

24 hour evapotranspiration. When  $R_n$ ,  $G$  and the final value of  $H$  have been established, with the latter obtained after an iterative process to consider atmospheric stability effects,  $LE$  is then calculated as a residual. This is the energy equivalent of the instantaneous  $ET$  at the time of satellite overpass. Then the evaporative fraction ( $EF$ ) for each pixel is calculated where:

$$EF = \frac{LE}{R_n - G} \quad (7)$$

All the fluxes are instantaneous. Since this fraction is assumed to remain constant throughout the day, it is then used in the extrapolation of  $LE$  obtained for short periods to hourly and daily values, therefore giving the daily  $ET$  to be:

$$ET_{24} = \frac{86,400 \times EF \times (R_{n24} - G_{24})}{\lambda} \quad (8)$$

86,400 is the conversion from seconds to a day.  $R_{n24}$  is the average net radiation for the day;  $\lambda$  is the latent heat of vaporization used to convert the energy to mm of evaporation and is a function of temperature.  $G_{24}$  is assumed to be zero for vegetation and soil surfaces.

The assumption of a conserved  $EF$  has been widely accepted and generally used (Nichols and Cuenca, 1993; Crago and Brutsaert, 1996; Gowda et al., 2008; Suleiman et al., 2009). However, Gentine et al. (2011) states that  $EF$  is rarely constant, though more likely to be constant under conditions of higher relative humidity (75-90%). In semi-arid regions, the  $EF$  constancy may not apply. Lhomme and Elguero (1999) also state that the assumption of a constant diurnal  $EF$  results in significant error in conditions of advection.

### **Data Analysis**

Four performance indicators were used to evaluate the SEBAL model. The measured daily  $ET$  (lysimeter) was compared with estimated daily (SEBAL)  $ET$ . The coefficient of determination ( $R^2$ ), Mean Bias Error (MBE), Root Square Mean Error (RMSE) and the Nash-Sutcliffe Coefficient of Efficiency (NSCE) were the indicators used.

## RESULTS AND DISCUSSIONS

When SEBAL ET values were compared with the lysimeter, there was a large negative MBE of 2.6 mm/d (-34 %) and RMSE of 3.2 mm/d. The  $R^2$  was 0.63, and the NSCE was a good 0.98. This showed that for most days, the model was significantly underestimating ET, as also indicated in Figure 2; most points are below the 1:1 line.

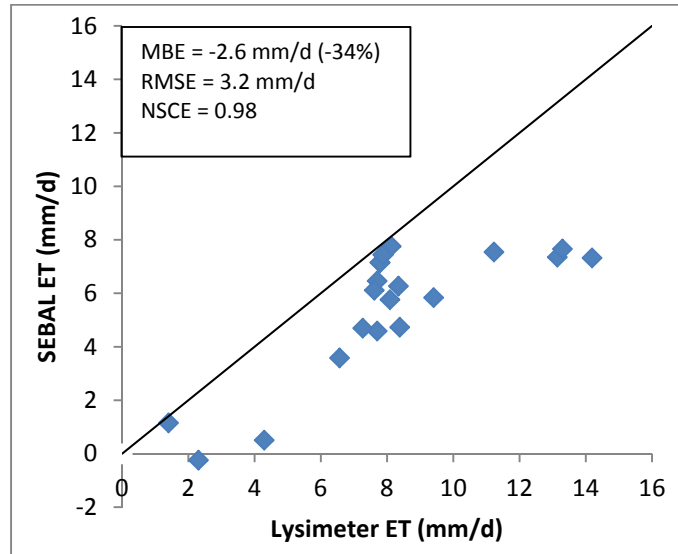


Figure 2. SEBAL-modeled vs. Lysimeter-measured daily alfalfa ET

To attempt to identify the source of error, the daily average evaporative fraction ( $EF_{24}$ ) was determined. This was obtained by first calculating the daily average latent heat flux ( $LE_{24}$ ) by using the lysimeter measured ET. The daily average net radiation ( $Rn_{24}$ ) and daily average soil heat flux ( $G_{24}$ ) were obtained from the net radiometer and soil heat flux plates respectively. These daily averages were calculated from measurements of the various fluxes taken from the field every 15 minutes.  $EF_{24}$  was therefore calculated as follows:

$$EF_{24} = LE_{24} / (Rn_{24} - G_{24}) \quad (9)$$

A relationship was then drawn between  $EF_{24}$  and SEBAL % error for conditions of no water stress. These were identified by having an instantaneous EF ( $EF_{inst.}$ ) of at least 0.96. Figure 3 shows a polynomial relating the  $EF_{24}$  to % error, with the error increasing with increasing EF. EF of more than 1 suggests advective conditions as the latent heat exceeds the available energy, which means the excess energy, would be coming from outside the area of interest.

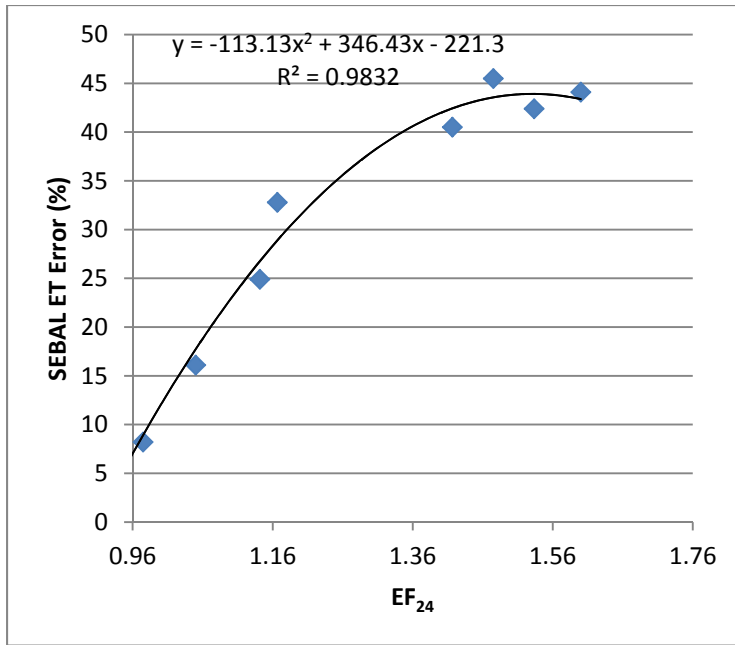


Figure 3. Relationship between average daily EF and % error

The lysimeter-measured ET was then adjusted so that the resulting EF would be 1, in that case removing the advective component of the total LE. This was carried out for the conditions of no water stress, and the performance indicators were recalculated, for both the unadjusted and the adjusted lysimeter ET, and Table 1 shows the results.

Table 1. Performance indicators for lysimeter ET adjusted for advection compared with unadjusted

Indicator	SEBAL vs. Lysimeter ET	SEBAL vs. adjusted Lysimeter ET
MBE (mm/d and %)	-3.0 (29%)	0.11 (2%)
RMSE (mm/d)	3.6	0.54
NSCE	0.97	0.97
R <sup>2</sup>	0.67	0.94

The results show significant improvement in performance when the contribution of advection is taken out of the total evapotranspiration.

### CONCLUSION

In this study, SEBAL showed poor performance under conditions of advection. The more the advected energy, the more error incurred by SEBAL. The error seemed to result from the assumption that EF is constant throughout the day. However, this assumption would

only be reasonable in calm conditions, not in arid windy areas like Rocky Ford. The study area being arid, and at the same time irrigated, encouraged advection in most days. The observations confirm what has been stated about the non-constancy of EF throughout the day, and consequently SEBAL's inaccuracy under conditions of advection. It is therefore recommended that an improvement be made on SEBAL, but still maintaining the advantageous aspect of the model to use as minimal data as possible.

### ACKNOWLEDGEMENTS

This study was possible thanks to the support of Colorado State Agricultural Experiment Station and Fulbright. We also want to thank the following individuals for their collaboration in the project: Lane Simmons and Dale Straw.

### REFERENCES

- Allen A, Irmak A, Trezza R, Hendrickx JMH, Bastiaanssen W, Kjaersgaard J, 2011: Satellite-based ET estimation in agriculture using SEBAL and METRIC. *Hydrol. Process.* 25, 4011-4027.
- Bastiaanssen WGM, Menenti M, Feddes RA and Holtslag AAM, 1998: Remote sensing surface energy balance algorithm for land (SEBAL): 1. Formulation. *J. Hydrol.*, 212-213(1-4), 198-212.
- Bastiaanssen WGM, Noordman EJM, Pelgrum H, Davids G, Thoreson BP, Allen RG, 2005: SEBAL Model with remotely sensed data to improve water resources management under actual field conditions. *Journal of Irrigation and Drainage Engineering*, 131 (1):85-93.
- Crago RD and Brutsaert W, 1996: Daytime evaporation and the self-preservation of the evaporative fraction and the Bowen ratio. *J. Hydrol.*, 178, 241-255.
- Chávez JL., Neale, CMU, Hips LE, Prueger, JH, and Kustas, WP (2005). "Comparing aircraft-based remotely sensed energy balance fluxes with eddy covariance tower data using heat flux source area functions." *J. of Hydromet.* 6(6), 923-940.
- Elhaddad A and Garcia LA, 2008: Surface energy balance-based model for estimating evapotranspiration taking into account spatial variability in weather. *Journal of Irrigation and Drainage Engineering*, 134 (6):681-689.
- Elhaddad A, Garcia LA, Chávez JL, 2011: Using surface energy balance model to calculate spatially distributed actual evapotranspiration. *Journal of Irrigation and Drainage Engineering*. 137(1). Gowda PH, Chavez JL, Colaizzi PD, Evett SR, Howell TA, Tolk AT, 2008: ET mapping for agricultural water management: present status and challenges. *Irrigation Science*. 26: 223-237.

Gowda PH, Howell TA, Paul G, Colaizzi PD, Marek TH, 2011: SEBAL for estimating hourly ET fluxes over irrigated and dryland cotton during BEAREX08. World Environmental and Water Resources Congress. ASCE.

Lhomme JP and Elguero E, 1999: Examination of evaporative fraction diurnal behavior using a soil-vegetation model coupled with a mixed-layer model. *Hydrology and Earth System Sciences*, 3(2):259-270.

Nichols WE and Cuenca RH, 1993: Evaluation of the evaporative fraction for parameterization of the surface energy balance. *Wat. Resour. Res.*, 29, 3681-3690.

Singh RK, Irmak A, Irmak S, Martin DL, 2008: Application of SEBAL Model for mapping evapotranspiration and estimating surface energy fluxes in South-Central Nebraska. *Journal of Irrigation and Drainage Engineering*, 134 (3): 273-285

Suleiman AA, Bali KM, Kleissl J, 2009: Comparison of ALARM and SEBAL Evapotranspiration of Irrigated Alfalfa. 2009 ASABE Annual International Meeting.  
Wang J, Sammis TW, Gutschick VP, Gebremichael M, Miller DR, 2009: Sensitivity analysis of the surface energy balance algorithm for land (SEBAL). Transactions of the ASABE 2009 Vol. 52 No. 3 pp. 801-811.



# REMOTE SENSING OF EVAPOTRANSPIRATION AND ROOT ZONE WATER BALANCE MODELING TO ESTIMATE GROUNDWATER EXTRACTION IN THE KAWEAH RIVER DELTA OF CALIFORNIA

Byron Clark<sup>1</sup>  
Lindsay Hall<sup>2</sup>  
Larry Dotson<sup>3</sup>  
Grant Davids<sup>4</sup>

## ABSTRACT

Remote sensing approaches that rely on surface energy balance analysis provide an opportunity to determine actual evapotranspiration (ET) over large areas with a degree of accuracy difficult or impossible to achieve using traditional crop coefficient approaches. Combining energy balance analysis with root zone water balance modeling can be used to improve estimates of total actual ET and the amount of ET derived from precipitation versus applied irrigation water, as well as estimates of total applied irrigation water (when combined with estimates of application efficiency).

To leverage existing datasets describing actual ET developed using the Surface Energy Balance Algorithm for Land (SEBAL), a methodology was developed for the Kaweah Delta Water Conservation District in California's southern San Joaquin Valley to estimate actual ET based on remotely-sensed vegetation indices combined with root zone water balance modeling. Specifically, a relationship between the Normalized Difference Vegetation Index (NDVI) and the actual basal crop coefficient was established using SEBAL data for 2007, 2008, and 2009 and applied in a daily root zone water balance model across twelve years (1999 through 2010) to provide improved estimates of actual ET, ET of applied water, and total applied irrigation water.

Aggregate actual ET over the growing season estimated using the root zone water balance model agreed with SEBAL results within one percent for each of the three years evaluated as part of validation (2007, 2008, and 2009), with a mean absolute error for individual fields of approximately 13% of the mean total actual ET from the SEBAL datasets. Crop coefficients derived from modeled ET estimates are compared to typical, published crop coefficients used in the region, and a confidence interval analysis of actual ET and total applied irrigation water is presented for approaches using typical crop coefficients and the combined approach described herein.

---

<sup>1</sup> Davids Engineering, Inc. 1772 Picasso Avenue, Suite A, Davis, CA 95618, 530.757.6107; byron@de-water.com

<sup>2</sup> Davids Engineering, Inc. 1772 Picasso Avenue, Suite A, Davis, CA 95618, 530.757.6107, lindsay@de-water.com

<sup>3</sup> Kaweah Delta Water Conservation District. 2975 N. Farmersville Blvd., Farmersville, CA 93223, 559.747.5601; ldotson@kdwcd.com

<sup>4</sup> Davids Engineering, Inc. 1772 Picasso Avenue, Suite A, Davis, CA 95618, 530.757.6107, grant@de-water.com

## BACKGROUND

The Kaweah Delta Water Conservation District (KDWCD) was formed in 1927 to develop and preserve local water supplies. As part of its groundwater management role, the District serves as a designated monitoring agency for the Kaweah Groundwater Subbasin under the California Statewide Groundwater Elevation Monitoring (CASGEM) program. KDWCD prepares annual reports as part of its groundwater management plan and has developed a numerical groundwater model to support management of the subbasin. As part of its efforts, the District estimates annual groundwater pumping for six defined hydrologic units within the basin.

The KDWCD service area is located on the floor of California's San Joaquin Valley and comprises 340,000 gross acres (Figure 1), of which 250,000 net acres are cropped. Agriculture generally consists of dairy support crops, field crops, and orchards. Primary crops include corn, cotton, alfalfa, walnuts, winter grains, citrus, and vineyards. Surface water supplies within KDWCD consist of the Kaweah River, including Lake Kaweah, and imported surface water from the Friant Division of the federal Central Valley Project. The Kaweah River watershed and Delta include approximately 1.04 million acres, of which 446,000 acres overlie the Kaweah Groundwater Subbasin.

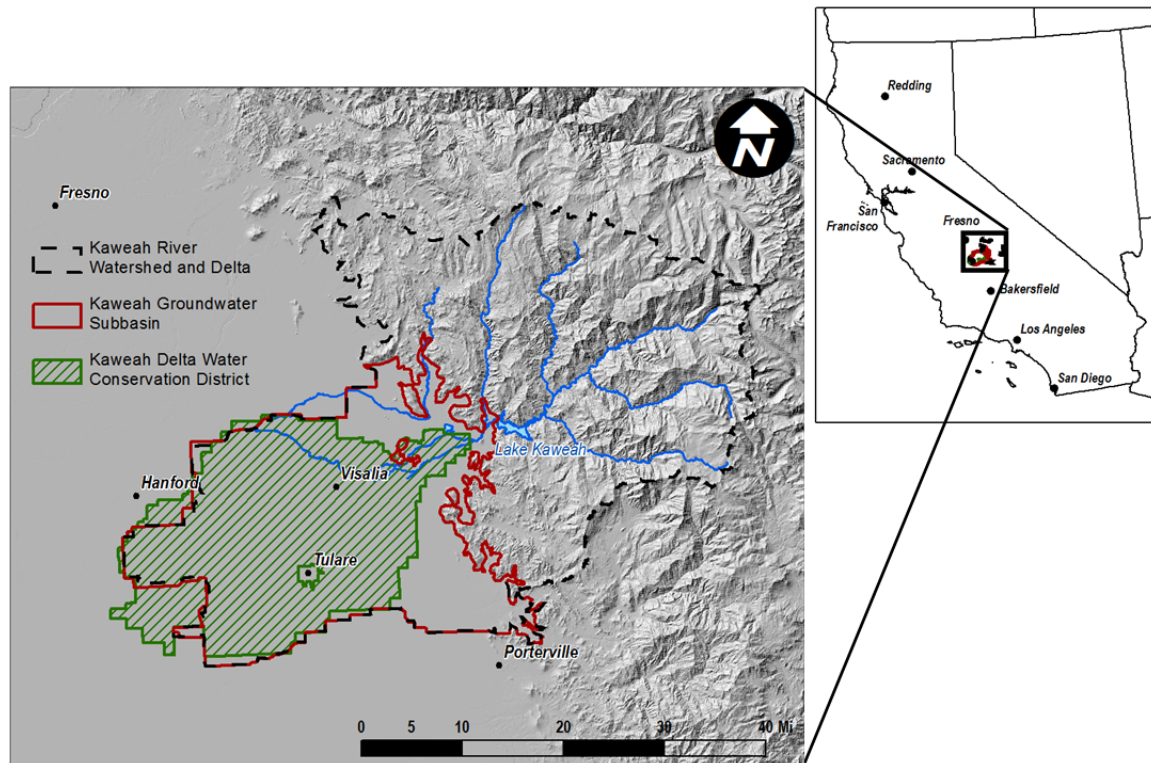


Figure 1. Kaweah River Watershed, Kaweah Groundwater Subbasin, and KDWCD Service Area.

Previous estimates of crop evapotranspiration have relied upon a traditional single crop coefficient approach using published crop coefficients for use in California (Goldhamer and Snyder, 1988) with empirical estimates of effective precipitation developed by the

Natural Resources Conservation Service (NRCS, 1993). Applied irrigation water is estimated based on an assumed consumptive use fraction (CUF), which represents the ratio of ET of applied water ( $ET_{aw}$ , defined as total crop ET minus effective precipitation) to total applied water. Then, groundwater demand is calculated as total applied water minus available surface water supply.

Key uncertainties in the traditional approach to estimating crop ET, effective precipitation, total applied irrigation water, and groundwater demand include infrequent land use surveys; difficulty accounting for double- and, in some cases, triple-cropping; differences between idealized and actual growing conditions (i.e., the effects of stress, disease, and other factors that affect actual crop water use); and difficulty in estimating CUF based on limited information describing applied water at the field scale.

## METHODOLOGY

In order to overcome some of the uncertainties in the traditional approach to estimating surface layer fluxes of ET, effective precipitation (a.k.a. ET of precipitation or  $ET_{pr}$ ), total applied irrigation water, deep percolation of applied water and precipitation, and groundwater demand, the analysis presented herein estimated crop ET, the primary driver of agricultural water demand, using a combination of remote sensing and simulation of irrigation events using a daily root zone water balance model. Total applied irrigation water was then calculated based on estimates of the CUF by general crop type and irrigation method. Fluxes to the groundwater system from deep percolation of precipitation ( $DP_{pr}$ ) and deep percolation of applied water ( $DP_{aw}$ ) were estimated based on daily root zone water balance results at the field scale.

Time series estimates of surface layer fluxes were developed for the KDWCD service area from 1999 through 2010. Demand was quantified at the field scale for approximately 8,000 individual fields using the daily root zone water balance model, allowing aggregation to monthly time steps by hydrologic unit or other spatial scale to support refined groundwater modeling and conjunctive management of available surface water and groundwater supplies by KDWCD.

A fundamental feature of the approach is that a relationship between the Normalized Difference Vegetation Index (NDVI) and basal crop coefficient ( $K_{cb}$ ) from available Surface Energy Balance Algorithm for Land (SEBAL, Bastiaanssen et al. 2005, SNA 2009) data for 2007, 2008, and 2009 was developed and used to estimate the transpiration component of total crop ET for the full 12-year analysis period. Key benefits of the approach include the following:

- Reduces dependence on year-to-year cropping data
- Provides spatial sensitivity across fields of the same crop type
- Accounts for double- and triple-cropping
- Accounts for effects of weather and other factors that influence ET
- Leverages available energy balance results to estimate ET over multiple years, resulting in less cost than applying an energy balance approach each year

These advantages result in more reliable estimates of crop ET and  $ET_{aw}$ ; however, the approach presented herein remains subject to uncertainties in CUF, which affect estimates of total applied water and total groundwater extraction. These uncertainties do not greatly influence estimates of net groundwater extraction (defined as total groundwater extraction for irrigation minus deep percolation of precipitation and applied water).

### **Relationship between NDVI and Basal Crop Coefficient**

The relationship between NDVI and  $K_{cb}$  was developed based on review of results of SEBAL analyses. Specifically, an empirical relationship between NDVI and actual crop coefficients from SEBAL ( $K_{cs}$ ) was developed. An equation of the form published by Er-Raki et al. (2007) was parameterized based on the SEBAL results (Equation 1).

$$K_{cb} = K_{cb,max} \cdot \left[ 1 - \left( \frac{NDVI_{max} - NDVI_{observed}}{NDVI_{max} - NDVI_{min}} \right)^{1.56} \right] \quad (1)$$

In Equation 1,  $K_{cb}$  is the basal crop coefficient, representing the transpiration component of ET,  $K_{cb,max}$  is the basal crop coefficient at full cover, which corresponds to  $NDVI_{max}$ .  $NDVI_{min}$  is the NDVI value at which transpiration is zero, and  $NDVI_{observed}$  is the NDVI value for a given field on a given date, estimated as described later in this Section. The relationship of NDVI to  $K_{cs}$  is shown in Figure 2 for eight SEBAL images from late April through early August 2007. As indicated, the parameters of Equation 1 were estimated for the “base” of the relationship, representing the transpiration component of ET and attempting to avoid the effects of evaporation. The  $K_{cb,max}$  value was subsequently adjusted for general crop-irrigation method groups as part of the model calibration process.

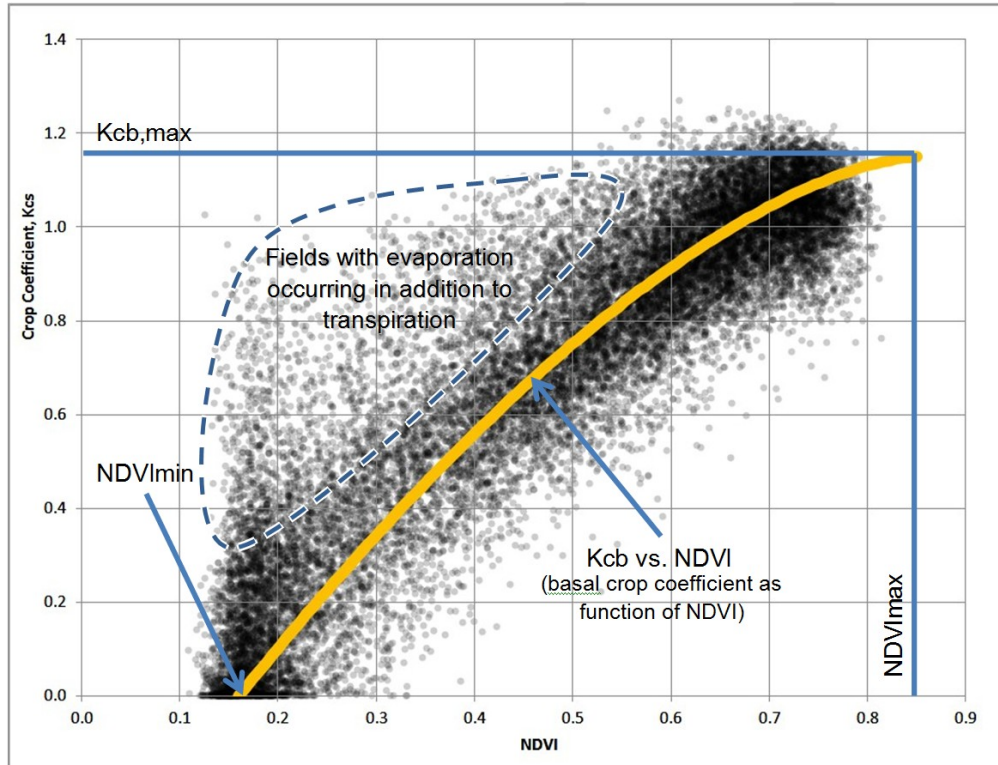


Figure 2. Relationship of Basal Crop Coefficient to NDVI, Estimated from 2007 SEBAL Analysis.

### Development of NDVI Time Series by Field

In order to estimate  $K_{cb}$  over time for individual fields as input to the daily root zone water balance model, 141 individual Landsat 5 and Landsat 7 images acquired between September 1998 and December 2010 were utilized to develop daily time series of NDVI for each field, along with 13 MODIS images for periods without cloud-free Landsat imagery. NDVI values for individual fields were linearly interpolated between image dates to estimate daily NDVI. The objectives of image selection were to minimize cloud gaps within the analysis area while providing adequate coverage throughout each year. A sample of interpolated NDVI values for a selected field from 2002 to 2010 is shown in Figure 3. Based on the figure, it is apparent that a single crop was present each year, with the exception of 2009, for which the field was double-cropped. It is also apparent that in years with single cropping the timing and characteristic of crop growth varied substantially from year to year.

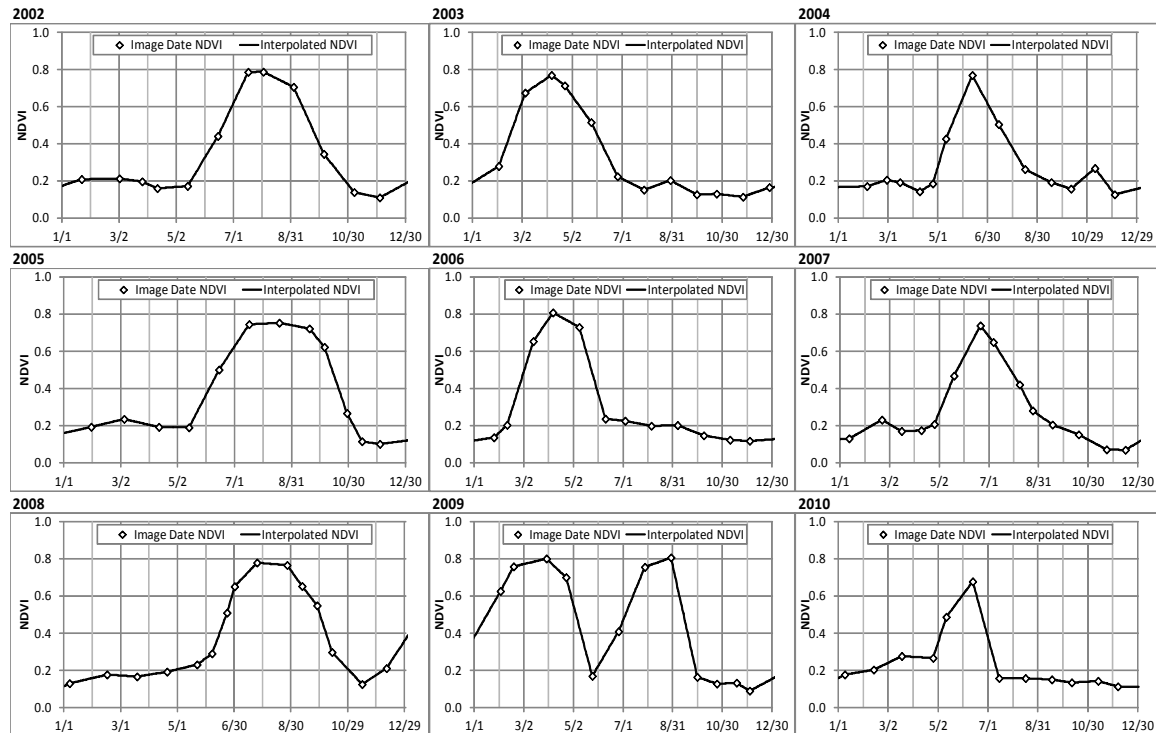


Figure 3. Time Series of NDVI from 2002 to 2010 for Sample Field with Field and Truck Crops.

### Root Zone Water Balance Model

A daily root zone water balance model was developed based on the dual crop coefficient approach of FAO Irrigation and Drainage Paper 56 (Allen et al., 1998) to estimate daily total crop ET, as well as other surface layer fluxes as depicted in Figure 4. The model was parameterized to simulate irrigation to meet crop ET driven by the transpiration estimates from NDVI and also served to estimate the daily evaporation component of ET. As indicated in Figure 4, the following fluxes were estimated:

- Rain (Precipitation): Estimated based on daily rainfall records from nearby weather stations.
- $ET_{aw}$ : ET of applied water, estimated as the portion of daily total ET derived from irrigation water, based on the relative portion of total root zone stored soil moisture of applied water.
- $ET_{pr}$ : ET of precipitation, estimated as the portion of daily total ET derived from precipitation, based on the relative portion of total root zone stored soil moisture of precipitation.
- $RO_{rain}$ : Runoff of precipitation, estimated using the NRCS curve number method.
- Applied Water: Applied irrigation water, estimated based on  $ET_{aw}$  and assumed CUF by irrigation method. Irrigation events were triggered based on estimated soil waterholding capacities and crop-specific management allowable depletions.
- $T_{a,aw}$ : Tailwater (surface runoff) of applied irrigation water, assumed to be zero based on knowledge of local irrigation practices.

- $Sub_{in}$  and  $Sub_{out}$ : Subsurface inflows and outflows, respectively, assumed to be zero.
- $DP_{rain}$ : Deep percolation of precipitation, estimated as the portion of daily total deep percolation derived from precipitation, based on the relative portion of total root zone stored soil moisture of precipitation.
- $DP_{aw}$ : Deep percolation of applied water, estimated as the portion of daily total deep percolation derived from applied irrigation water, based on the relative portion of total root zone stored soil moisture of applied water.

Additionally, changes in soil moisture storage and relative portions of stored precipitation and applied water were estimated over time.

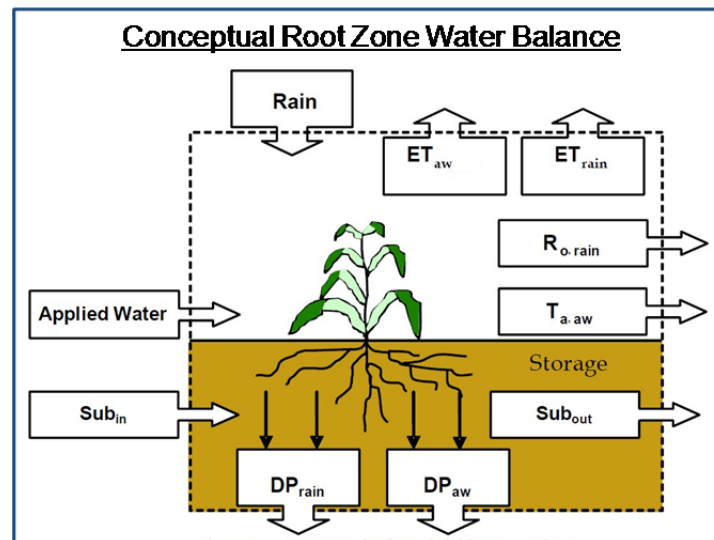


Figure 4. Conceptual Root Zone Water Balance.

### Reference ET and Precipitation

Reference evapotranspiration ( $ET_o$ ) was estimated based on the California Irrigation Management Information System (CIMIS) station at Porterville. Quality control procedures were applied according to Allen et al. (2005). Daily precipitation was estimated based on review of local weather stations from CIMIS and the National Weather Service (NWS).

## RESULTS

### Sample Field Results

An example of daily model results of basal crop coefficient ( $K_{cb}$ ), crop coefficient ( $K_c$ ), transpiration, evaporation, irrigation, and applied water for a selected field is provided in Figure 5 for 2010. The field was double-cropped, consisting of a winter grain crop, followed by corn.

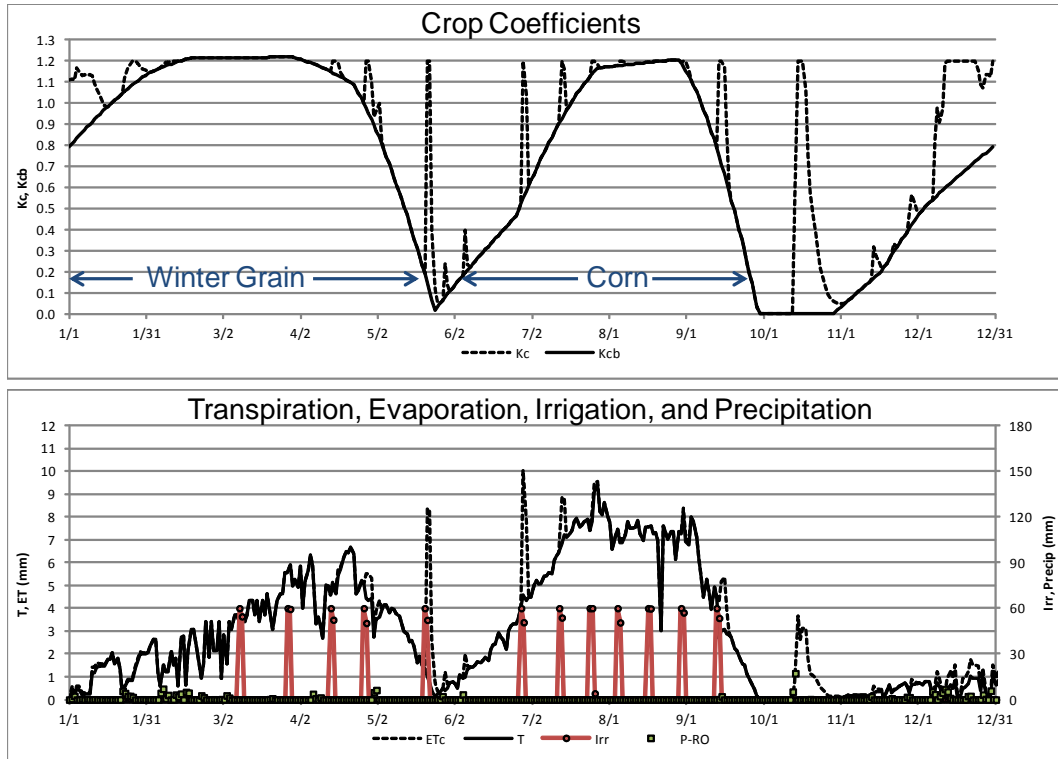


Figure 5. Example Root Zone Model Results for Double-Cropped Grain and Corn, 2010.

### Calibration and Validation

To calibrate the estimation of total crop ET, estimated values of  $K_{cb,max}$  from the NDVI- $K_{cb}$  relationship described previously were iteratively adjusted by comparing root zone model results in aggregate by general crop-irrigation method group to available SEBAL datasets from 2007, 2008, and 2009. A total of seven crop-irrigation method groups were parameterized in the model and simulated<sup>5</sup>. One half of the fields in the analysis area were selected randomly for calibration. Once the ET results for the calibration set matched the SEBAL results in aggregate for each crop-irrigation method group, the model was applied to the remaining fields to validate model calibration.

Results of model validation at the field scale for each year are presented in Figure 6, along with aggregate validation results across all fields for each year. As shown, field scale results from the root zone water balance model agreed generally with SEBAL total ET for each of the years for which SEBAL results were available. The average absolute error at the field scale was 4.3 in, or approximately 13 percent of total ET.

<sup>5</sup> These groups included deciduous orchards with microirrigation, deciduous orchards with surface irrigation, field and truck crops with surface irrigation, pasture with surface irrigation, citrus with microirrigation, vineyards with microirrigation, and vineyards with surface irrigation.

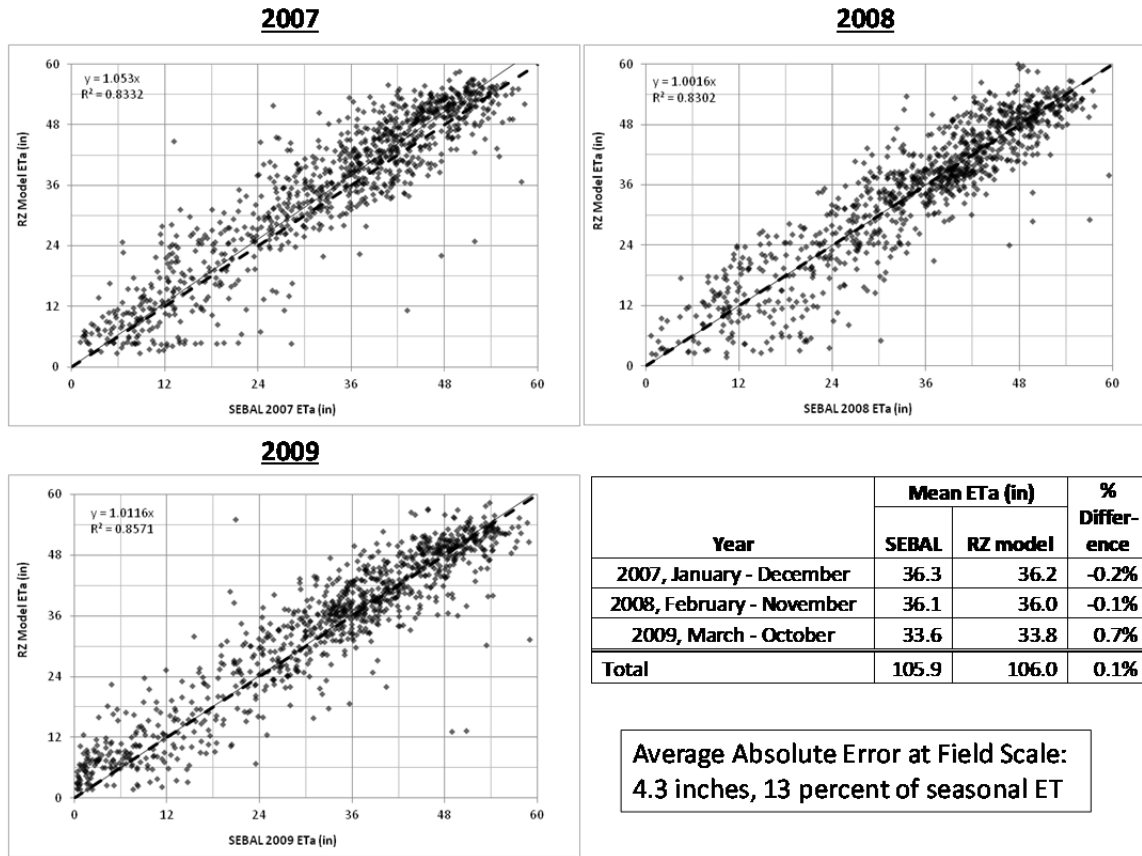


Figure 6. Comparison of Root Zone Model ET Results to Available SEBAL ET Estimates for Validation Fields<sup>6</sup>.

**Comparison of Root Zone Model Results to Standard Crop Coefficients**

Root zone model estimates of crop coefficients and total crop ET were compared to standard values to evaluate both the variability in actual crop coefficients and potential biases in estimating crop ET using a traditional single crop coefficient approach based on published crop coefficient ( $K_c$ ) values. Comparisons for alfalfa, citrus, deciduous orchards (primarily walnuts), fallowed fields, cotton, field crops (primarily grain-corn double-cropping), pasture, and vineyards are provided in Figures 7 through 14, respectively. In each figure, the blue bars represent the crop coefficient estimated from published values based on KDWCD’s previous Water Resources Investigation (denoted “WRI”), along with 10<sup>th</sup> percentile, 90<sup>th</sup> percentile, and mean (denoted “RS-RZ”) crop coefficients from the remote sensing-root zone water balance approach.

<sup>6</sup> For 2007, the SEBAL analysis represents 14 images from January to December. For 2008, the SEBAL analysis represents 14 images from February to November. For 2009, the SEBAL analysis represents 8 images from March to October.

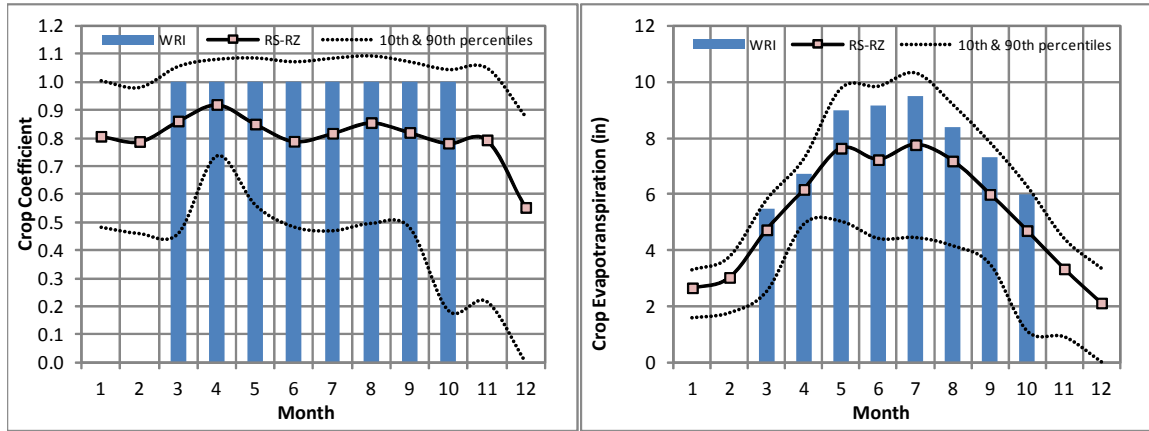


Figure 7. Comparison of Traditional and Remotely-Sensed Crop Coefficients for Alfalfa.

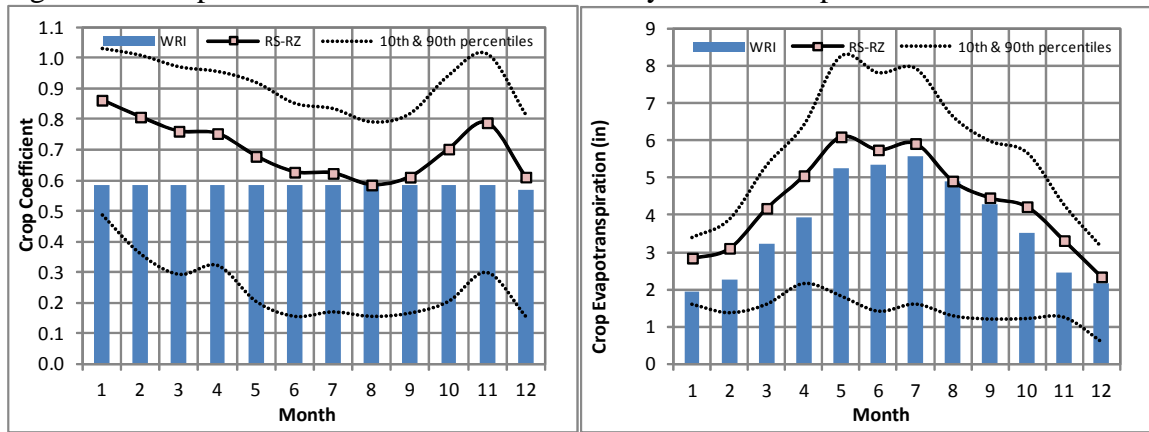


Figure 8. Comparison of Traditional and Remotely-Sensed Crop Coefficients for Citrus.

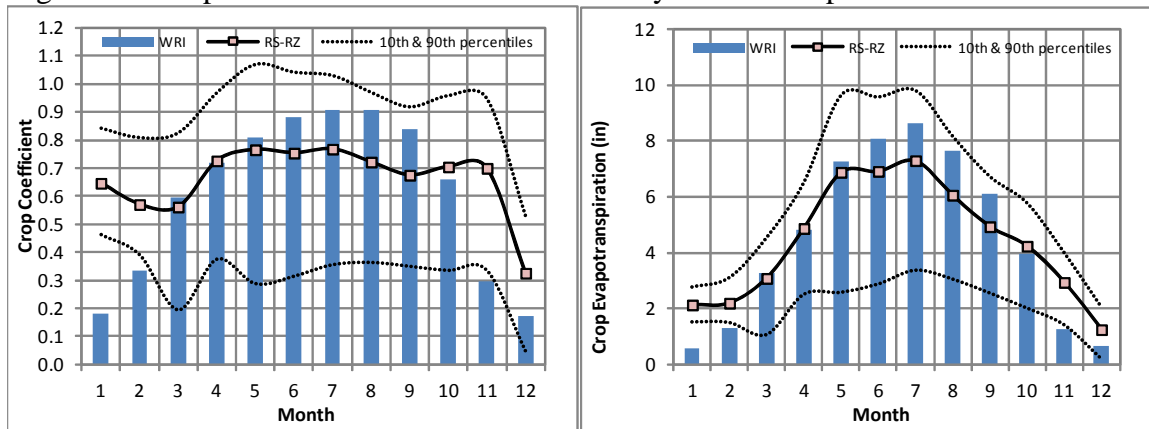


Figure 9. Comparison of Traditional and Remotely-Sensed Crop Coefficients for Deciduous Orchards (Primarily Walnuts).

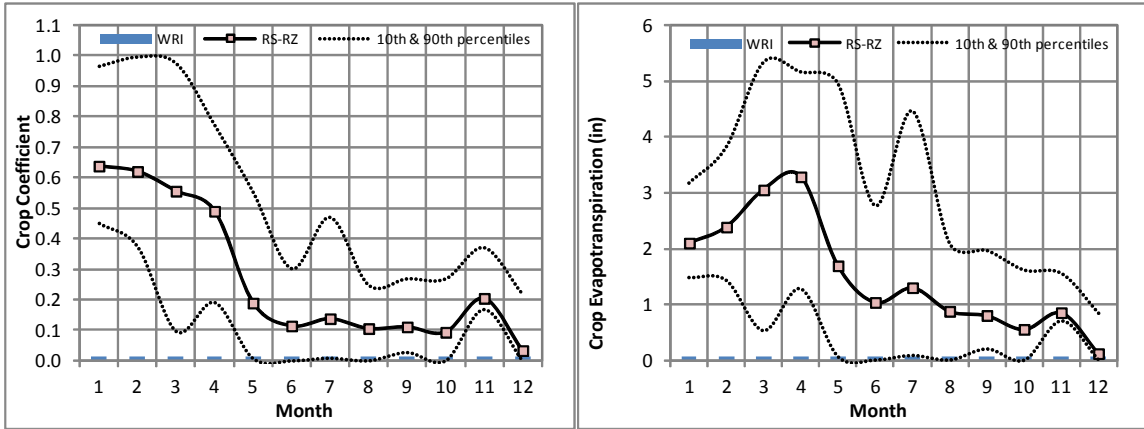


Figure 10. Comparison of Traditional and Remotely-Sensed Crop Coefficients for Fallow Fields.

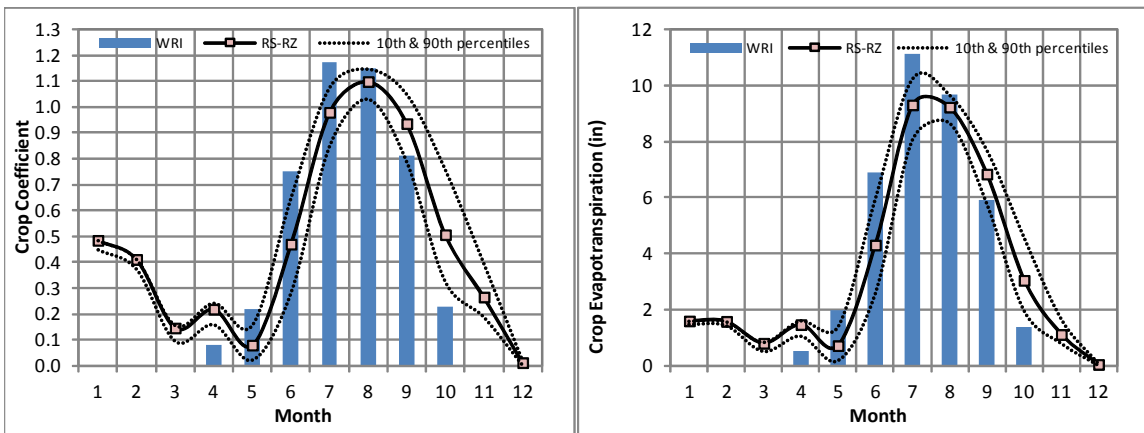


Figure 11. Comparison of Traditional and Remotely-Sensed Crop Coefficients for Cotton.

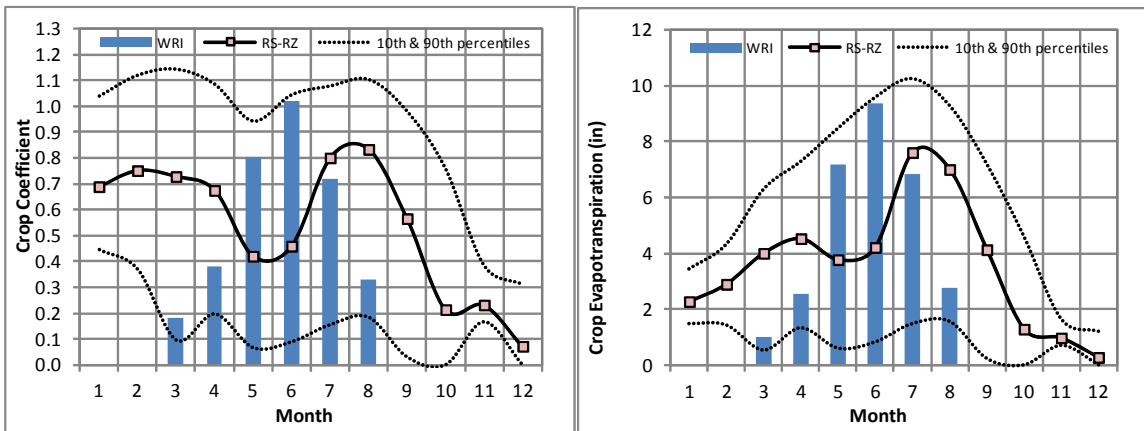


Figure 12. Comparison of Traditional and Remotely-Sensed Crop Coefficients for Field Crops (Primarily Double-Cropped Grain-Corn).

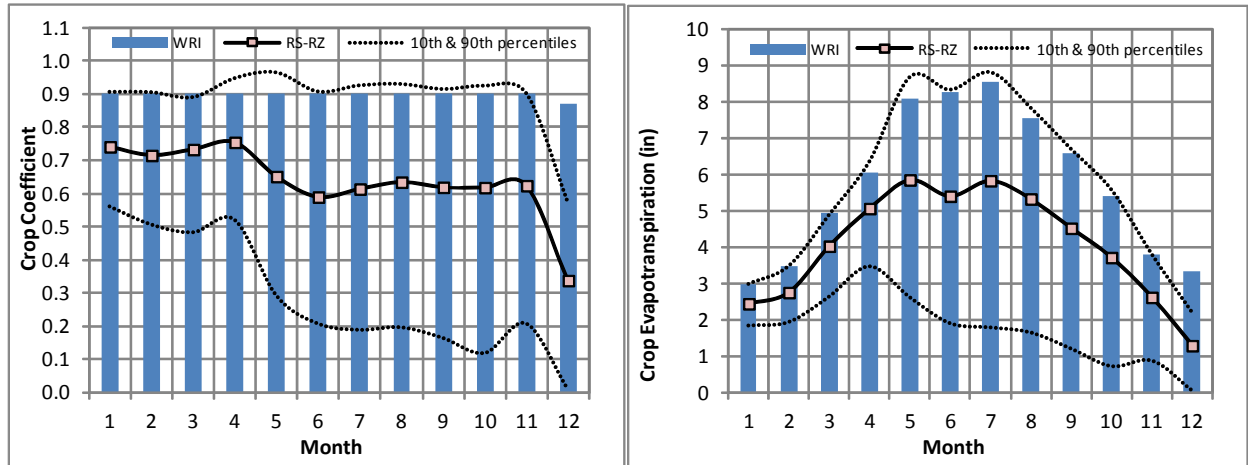


Figure 13. Comparison of Traditional and Remotely-Sensed Crop Coefficients for Pasture.

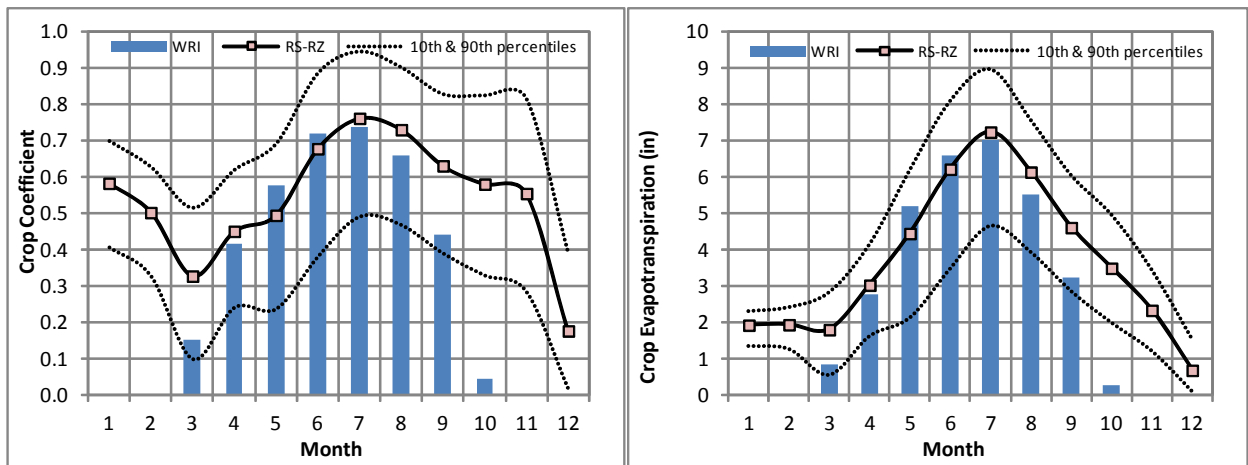


Figure 14. Comparison of Traditional and Remotely-Sensed Crop Coefficients for Vineyards.

In general, the use of published crop coefficients, along with the assumption that crop coefficients and corresponding ET are zero during the winter months (i.e., November through February) appears to result in overestimation of crop ET for KDWCD, with the following notable exceptions:

- Actual crop coefficients and ET for citrus are generally greater than estimated using traditional crop coefficients for the study area.
- The assumption that ET is zero for fallowed fields may result in underestimation of total ET.
- The use of standard crop coefficients for cotton may result in accurate estimates of total seasonal ET, though the timing of actual crop ET within the year may differ.
- Prior estimates of crop coefficients and ET for miscellaneous field crops (which are dominated by double-cropped grain-corn in the study area) do not appear to accurately depict the actual timing or amount of actual ET.

- Prior estimates of crop coefficients appear to result in overestimation of actual ET for pasture.
- Prior estimates of crop coefficients appear to underestimate actual ET between September and March for vineyards.

### **Uncertainty Analysis**

The uncertainty in estimates of surface fluxes from the analysis presented herein relative to traditional approaches using published crop coefficients was evaluated by performing a confidence interval analysis. The uncertainty in components of the calculations for each of the approaches is presented, along with an estimate of overall uncertainty. Calculated uncertainties are based on the assumption of normally-distributed, random errors as described by Clemmens and Burt (1997).

Actual ET for both approaches is estimated based on the product of  $ET_o$  and crop coefficients. For the traditional approach, published crop coefficients are used. For the approach presented herein, crop coefficients developed based on remote sensing are used. For each approach, estimated uncertainties are assumed to represent approximately the 95 percent confidence interval. Uncertainty in actual ET using traditional crop coefficients is estimated to be on the order of 15 percent (Allen, 1999). Uncertainty in actual ET using the remote sensing approach (i.e., SEBAL) is estimated to be on the order of 5 percent (Bastiaanssen et al., 2005). For purposes of evaluation, the uncertainty in  $ET_{pr}$  using the NRCS (1993) approach is assumed to be 25 percent, and the uncertainty in  $ET_{pr}$  using the daily root zone model at the field scale is assumed to be 15 percent. Due to the relatively small magnitude of  $ET_{pr}$ , the analysis is relatively insensitive to these assumptions. For both approaches, the uncertainty in CUF is assumed to be 10 percent.

Table 1 presents the analysis of relative uncertainties in total ET,  $ET_{pr}$ ,  $ET_{aw}$ , CUF, Applied Water, and  $DP_{aw}$  for the two analysis approaches described herein. The magnitude of each parameter is estimated based on the 1999 to 2010 average results from the remote sensing/root zone water balance model for the KDWCD study area. By assuming the same magnitude for each flux, the uncertainty analysis describes the relative uncertainties between approaches.

In reality, application of the two approaches could result in different estimates of the magnitude of each flux; however, similar magnitudes are assumed here for purposes of comparison of the relative uncertainties of each approach. As indicated, based on assumptions regarding the uncertainty in total ET and  $ET_{pr}$  between approaches, the relative uncertainty in  $ET_{aw}$  using a remote sensing approach is approximately one third of the uncertainty for the traditional crop coefficient approach. Similarly, the relative uncertainties in applied water and  $DP_{aw}$  are approximately 1/2 of the uncertainty for the traditional crop coefficient approach.

Table 1. Estimated Uncertainties in ET, ET<sub>aw</sub>, Applied Water, and DP<sub>aw</sub> by Approach.

Approach	Component	Estimated Magnitude (in/yr)	Estimated Uncertainty		Source
			Percent	Absolute (in)	
Traditional, Published Crop Coefficients	Total ET	32.8	15%	4.9	Estimated
	ET <sub>pr</sub>	5.2	25%	1.3	Estimated
	ET <sub>aw</sub>	<b>27.6</b>	<b>18%</b>	<b>5.1</b>	<b>Calculated</b>
	CCUF	0.7	10%	0.1	Estimated
	<b>Applied Water</b>	<b>40.5</b>	<b>21%</b>	<b>8.5</b>	<b>Calculated</b>
	<b>DP<sub>aw</sub></b>	<b>13.2</b>	<b>75%</b>	<b>9.9</b>	<b>Calculated</b>
Remote Sensing, Coupled with Daily Root Zone Water Balance	Total ET	32.8	5%	1.6	Estimated
	ET <sub>pr</sub>	5.2	15%	0.8	Estimated
	ET <sub>aw</sub>	<b>27.6</b>	<b>7%</b>	<b>1.8</b>	<b>Calculated</b>
	CUF	0.7	10%	0.1	Estimated
	<b>Applied Water</b>	<b>40.5</b>	<b>12%</b>	<b>4.9</b>	<b>Calculated</b>
	<b>DP<sub>aw</sub></b>	<b>13.2</b>	<b>39%</b>	<b>5.2</b>	<b>Calculated</b>

1. Estimated magnitude for each approach is based on remote sensing analysis to provide a direct comparison of relative uncertainties.

## DISCUSSION AND CONCLUSIONS

The combination of energy balance modeling, vegetation indices, and daily root zone water balance modeling provides advantages over other approaches to develop time series estimates of surface fluxes for agricultural systems. These advantages include limited dependence on detailed cropping data, improved spatial sensitivity, and the ability to account for actual field conditions that affect ET. Additionally, the ability to leverage available energy balance results over multiple years reduces the cost of developing detailed ET estimates on an annual basis over time.

The use of published crop coefficients can lead to biases in the estimate of annual ET for some individual crops. These biases may result from differences between actual growing conditions and those under which the crop coefficients were developed, or may result from difficulties identifying individual crops or double- or triple-cropping over time. Application of a remote sensing approach can help to avoid biases in ET estimates.

By calibrating the relationship between NDVI and  $K_{cb}$  and estimates of total ET using available energy balance results, similar levels of accuracy can be achieved using the approach presented herein and applying an energy balance approach each year. Because ET represents the largest outflow from the surface layer (i.e. root zone), improved accuracy in ET estimates compared to approaches that rely on standard crop coefficients substantially reduces uncertainty in other fluxes, including ET<sub>aw</sub>, applied water, and deep percolation.

## REFERENCES

- Allen, R.G. 1999. Using the FAO-56 dual crop coefficient method over an irrigated region as part of an evapotranspiration intercomparison study. *Journal of Hydrology*. 229 (2000), 27-41.
- Allen, R.G., Pereira, L.S., Raes, D., and Smith, M. 1998. *Crop Evapotranspiration. Irrigation and Drainage Paper No. 56.* Food and Agriculture Organization of the United Nations. Rome, Italy.
- Allen, R.G., Walter, I.A., Elliot R., Howell, T., Itenfisu, D., and Jensen M. 2005. *The ASCE Standardized Reference Evapotranspiration Equation.* American Society of Civil Engineers. Reston, Virginia.
- Bastiaanssen, W.G.M., Noordman, E.J.M., Pelgrum, H., Davids, G., and Allen, R.G. 2005. SEBAL Model with Remotely Sensed Data to Improve Water Resources Management under Actual Field Conditions. *Journal of Irrigation and Drainage Engineering*. 131(1), 85-93.
- Clemmens, A.J. and Burt, C.M. 1997. Accuracy of Irrigation Efficiency Estimates. *Journal of Irrigation and Drainage Engineering*. 123(6), 443-453.
- Er-Raki, S., Chehbouni, A., Guemouria, N., Duchemin, B., Ezzahar, J., and Hadria, R. 2007. Combining FAO-56 model and ground-based remote sensing to estimate water consumptions of wheat crops in a semi-arid region. *Agricultural Water Management* 87 (41-54).
- Goldhamer, D.A. and Snyder R.L. (eds.). 1989. *Irrigation scheduling: A guide for efficient on-farm water management.* U.C. Publication 21454.
- Natural Resources Conservation Service (NRCS). 1993. *Irrigation Water Requirements.* Chapter 2. Part 623. *National Engineering Handbook.*
- SEBAL North America, Inc. (SNA). 2009. *Spatial Mapping of ET in the Kaweah Delta Water Conservation District Using SEBAL® (version 2009).* Davis, CA.



# ESTIMATION OF EVAPOTRANSPIRATION FOR A DRIP-IRRIGATED OLIVE ORCHARD USING MULTISPECTRAL SATELLITE IMAGES

Samuel Ortega-Farias, Rodrigo Aguilar, Daniel De la Fuente, Samuel Ortega-Salazar, Fernando Fuentes, and Carlos Poblete-Echeverría<sup>1</sup>

## ABSTRACT

A field experiment was carried out to evaluate the METRIC model to estimate instantaneous latent heat flux (LE) and evapotranspiration (ET) over a drip-irrigated olive orchard located in the Péncahue Valley, Maule Region, Chile (Lat. 35° 23' S; Long. 71° 44' W; 96 m above sea level). For estimating LE and ET using the METRIC model, nine satellite images (Landsat 7 ETM+) were used from the 2009/10 and 2010/11 seasons. A constant canopy size was maintained during the two study periods with a leaf area index (LAI) and fractional cover ( $f_c$ ) ranging between 1.29-1.34  $m^2 m^{-2}$  and 0.29-0.31, respectively. Also, the olive orchard was maintained under non-water stress conditions with a midday stem water potential greater than -1.96 MPa. Values of LE and ET obtained from an eddy covariance (EC) system were used to evaluate the performance of the METRIC model. Results indicated that the METRIC model underestimated LE and ET by about 11 and 10%, respectively. Also, the root mean square error (RMSE) was 29  $W m^{-2}$  for LE and 0.46  $mm day^{-1}$  for ET. Main errors of the METRIC model were associated with the selection of the cold pixels, which were difficult to obtain for some satellite images.

## INTRODUCTION

In Chile, new drip irrigated olive orchards are planted under Mediterranean climate conditions, where the low water availability for irrigation is generally the major limiting factor for the olive oil industry. Under these conditions, irrigation water management is required to optimize water use efficiency and maintain sufficient levels of productivity and quality (Ortega-Farias et al., 2009). To achieve these targets, it is necessary to have a reliable method to quantify the olive water requirements or evapotranspiration (ET). The correct determination of ET is a main factor for improving water use efficiency (WUE) and establishing irrigation strategies such as the regulated deficit irrigation (RDI) which has been successfully applied to increase WUE and olive oil quality (Flores and Ortega-Farias, 2011; Patumi et al., 2002; Tognetti et al. 2005).

In this regard, Carrasco-Benavides et al. (2012) and Samani et al. (2009) indicated that remote sensing energy balance (RSEB) models can be used to simulate ET in sparse canopies such as orchards and vineyards. RSEB algorithms are found to be useful to account for the spatial and seasonal variability of ET (Bastiaanssen et al., 2005; Chávez et al., 2005; Gowda et al., 2008). Furthermore, RSEB systems can potentially be employed to assist in tracking irrigation management decisions, to monitor spatially distributed crop water use (as an aid in scheduling irrigations, in general hydrologic

---

<sup>1</sup> Research and Extension Center for Irrigation and Agroclimatology (CITRA), University of Talca, Chile. Avenida Lircay s/n, Talca, Chile. Corresponding author: Samuel Ortega-Farias [sortega@utalca.cl](mailto:sortega@utalca.cl)

models and water rights monitoring) and to assess the overall irrigation project efficiency (Allen et al., 2004; Bastiaanssen et al., 2005; Gowda et al., 2008).

Several RSEB algorithms that vary in complexity are available in the literature to estimate the different components of the energy balance (EB) equation (Allen et al., 2007; Bastiaanssen 1998; Carrasco-Benavides et al., 2012; Galleguillos et al., 2011; Gowda et al., 2007, 2008; Su, 2002, Tasumi, 2005; Teixeira et al., 2009). To estimate ET, the RSEB algorithms use remotely sensed radiometric temperature from an infrared (IR) thermal band and surface reflectance in the visible (VIS) and near-infrared (NIR) regions of the electromagnetic spectrum (Gowda et al., 2008). These satellite data are then converted into land surface characteristics such as albedo, leaf area index, vegetation indices, surface emissivity and surface aerodynamic temperature to estimate the EB components such as net radiation ( $R_n$ ), soil heat flux ( $G$ ) and sensible heat flux ( $H$ ). Finally, RSEB models compute the instantaneous ET as a residual from the EB equation.

One widely applied RSEB algorithm is METRIC (Mapping EvapoTranspiration at high Resolution with Internalized Calibration) (Allen et al., 2007) which has been tested with positive results in several fully covered crops such as alfalfa, bean, pea, potato, sugar beet, spring grain, winter grain, corn, soybean and sorghum (Allen et al., 2007; Singh and Irmak, 2009; Tasumi et al., 2005). However, little research exists on the application of METRIC to estimate ET of olive orchards. Thus, the main objective of this study was to evaluate the METRIC model for computing instantaneous latent heat flux (LE) and daily ET over a drip-irrigated olive orchard in the Talca Valley, Region del Maule, Chile.

## MATERIALS AND METHODS

The experiment was conducted during the 2009/10 and 2010/11 growing seasons on a drip-irrigated olive orchard (*Olea europaea* L. cv. Arbequina) for oil production. This homogeneous and almost flat orchard (average slope was 1.6%) is located in the Penciahue Valley, Maule Region, Chile (Lat. 35° 23' S; Long. 71° 44' W; 96 m above sea level). Trees were planted 5 m apart, with 1.5 m within-row spacing (1,333 trees per hectare) with a tree height of 3.2 m and canopy width of 1.55 m. For the two seasons, the average values of leaf area index (LAI) and fractional cover ( $f_c$ ) ranged between 1.29-1.34  $m^2 m^{-2}$  and 0.29-0.31, respectively. The climate in this area corresponds to a typical Mediterranean semiarid climate with a daily average temperature of 14.8 °C between September and May. Average annual rainfall in the region is 602 mm, concentrated mainly during the winter months. The summer period is usually dry (3.5 % of annual rainfall) and hot with a very high atmospheric demand for water vapour.

The soil at the orchard is classified as Quepo series with a clay loam texture. For this soil type, the water application was done twice a week using 4 L  $hr^{-1}$  drippers spaced at intervals of 1.5 m. Olive trees were maintained under non-water-stress conditions with measured values of midday stem water potential ( $\psi_x$ ) > -1.96 MPa (Pérez-López et al., 2010).

A tower of 5.5 m of height was installed over the drip-irrigated olive orchard to measure latent heat flux (LE), sensible heat flux (H), net radiation (R<sub>n</sub>) and soil heat flux (G). R<sub>n</sub> was measured by a four-way net radiometer (CNR1, Kipp&Zonen Inc., Delft, Netherlands). LE and H were measured using an eddy covariance (EC) system oriented towards the predominant wind direction (North-South). The EC system consisted of a fast response open-path infrared gas analyzer (LI-7500 IRGA; LI-COR, Inc., Lincoln, Nebraska, USA) and a three dimensional sonic anemometer (CSAT, Campbell Sci., Logan, UT). The minimum fetch-to-instrument-height ratio was about 200 m, sufficiently large to preclude horizontal advection. G was estimated using eight flux plates installed on either side of the rows. The flux plates of constant thermal conductivity (HFT3, Campbell Sci., Logan, UT) were placed at a 0.08 m depth. At depths of 0.02 and 0.06 m, two averaging thermocouple probes (TCAV, Campbell Sci., Logan, UT) were installed above each flux plate to measure soil temperature (T<sub>soil</sub>). The configuration, data processing and energy balance closure are described by Ortega-Farias and Lopez-Olivari (2012)

Also, an automatic weather station (Adcon Telemetry, A733GSM/GPRS, Klosterneuburg, Austria) was installed over a well-irrigated grass (1 ha) to measure hourly variables of air temperature (T<sub>a</sub>), relative humidity (RH), wind speed (u<sub>2</sub>) and solar radiation (R<sub>si</sub>). These variables were used to compute the reference evapotranspiration (ET<sub>o</sub>) using the Penman-Monteith model (ASCE-EWRI, 2005).

Nine satellite images (Landsat 7, ETM+) were downloaded from USGS Glovis (<http://glovis.usgs.gov>). Scenes used in this research considered only days with less than 30% cloud cover. Additionally, taking into account that since 2003, the ETM+ images have shown gaps owing to failures in the satellite scan line corrector (slc-off), only scenes without gaps at the experimental plot were processed. All Landsat scenes used in this research were acquired including a default standard terrain correction (Level 1T). Each satellite scene was processed by using the model maker toolbox of the ERDAS Imagine software (ERDAS Inc. USA).

The METRIC model computes ET at high spatial resolution (e.g. 30m for Landsat scenes) as follow:

$$ET_M = ET_o * F_o \quad (1)$$

$$F_o = \frac{ET_i}{ET_{oh}} \quad (2)$$

where ET<sub>M</sub> is the daily ET computed for each pixel (mm day<sup>-1</sup>); ET<sub>o</sub> is the daily Penman-Monteith reference evapotranspiration (mm day<sup>-1</sup>) (ASCE-EWRI, 2005); F<sub>o</sub> is the reference evapotranspiration fraction at the time of satellite overpass; ET<sub>oh</sub> is the hourly Penman-Monteith reference evapotranspiration for short grass surface (mm h<sup>-1</sup>) and ET<sub>i</sub> is the pixel-by-pixel evapotranspiration (mm h<sup>-1</sup>). Values of ET<sub>i</sub> for each pixel are computed as a residual of the surface energy balance (RSEB) equation:

$$\lambda ET_i = LE_M = R_n - H - G \quad (3)$$

where  $\lambda$  is the latent heat of vaporization ( $\text{J kg}^{-1}$ );  $LE_M$  is latent heat flux ( $\text{W m}^{-2}$ );  $R_n$  is net radiation ( $\text{W m}^{-2}$ );  $G$  is soil heat flux ( $\text{W m}^{-2}$ ) and  $H$  is sensible heat flux ( $\text{W m}^{-2}$ ). Instantaneous values of  $R_n$ ,  $LE_M$ ,  $H$ , and  $G$  were computed at the time of satellite overpass (11:28h). For more details about METRIC, refer to Allen et al., (2007) and Carrasco-Benavides et al. (2012).

Instantaneous latent heat flux (LE) and olive evapotranspiration (ET) computed by the METRIC model ( $LE_M$  and  $ET_M$ ) were compared with those obtained by the eddy covariance system ( $LE_{EC}$  and  $ET_{EC}$ ). Instantaneous and daily comparisons included the  $LE_M/LE_{EC}$  ( $r_{LE}$ ) and  $ET_M/ET_{EC}$  ( $r_{ET}$ ) ratios, index of agreement ( $I_a$ ), root mean square error (RMSE) and mean absolute error (MAE). Also, the t-test was used to check whether the values of  $r_{LE}$  and  $r_{ET}$  were significantly different from unity at the 95% confidence level.

## RESULTS AND DISCUSSION

The statistical analysis indicated that the METRIC model predicted the instantaneous latent heat flux with a RMSE and MAE equal to 29 and 26  $\text{W m}^{-2}$ , respectively. The t-test indicates that  $LE_M/LE_{EC}$  ratio ( $b=0.89$ ) was significantly different from unity at 95% confidence level, suggesting that METRIC underestimated latent heat flux by approximately 11% (Table 1). This is depicted in Fig. 1a where the points were evenly distributed around the 1:1 line. In this study, values of LE ranged between 74-155  $\text{W m}^{-2}$  for the METRIC model and between 43-167  $\text{W m}^{-2}$  for the EC system with a maximum difference between  $LE_M$  and  $LE_{EC}$  of 50  $\text{W m}^{-2}$  (Fig. 1b). On a daily basis, results indicate that the METRIC model was able to simulate ET with RMSE of 0.46  $\text{mm day}^{-1}$  and MAE of 0.39  $\text{mm day}^{-1}$ . The t-test indicates that  $ET_M/ET_{EC}$  ratio ( $b=0.90$ ) was significantly different from unity suggesting that the METRIC model underestimated olive ET by about 10%. In this case, Fig. 2a indicates that  $ET_M$  was underestimated by METRIC for  $ET_{EC}$  values  $> 2.5 \text{ mm day}^{-1}$ . Also, results indicated that METRIC presented indexes of agreement of 0.79 and 0.75 for the LE and ET, respectively.

Table 1. Statistical validation of latent heat flux (LE) and actual evapotranspiration (ET) over a drip-irrigated olive orchard estimated by the METRIC model.

	RMSE	MAE	$r_{LE}$ or $r_{ET}$	$I_a$
LE	29 $\text{W m}^{-2}$	26 $\text{W m}^{-2}$	0.89	0.79
ET	0.46 $\text{mm day}^{-1}$	0.39 $\text{mm day}^{-1}$	0.90	0.75

RMSE = root mean square error; MAE = mean absolute error;  $I_a$  = index of agreement;  $r_{LE} = LE_M/LE_{EC}$ ;  $r_{ET} = ET_M/ET_{EC}$

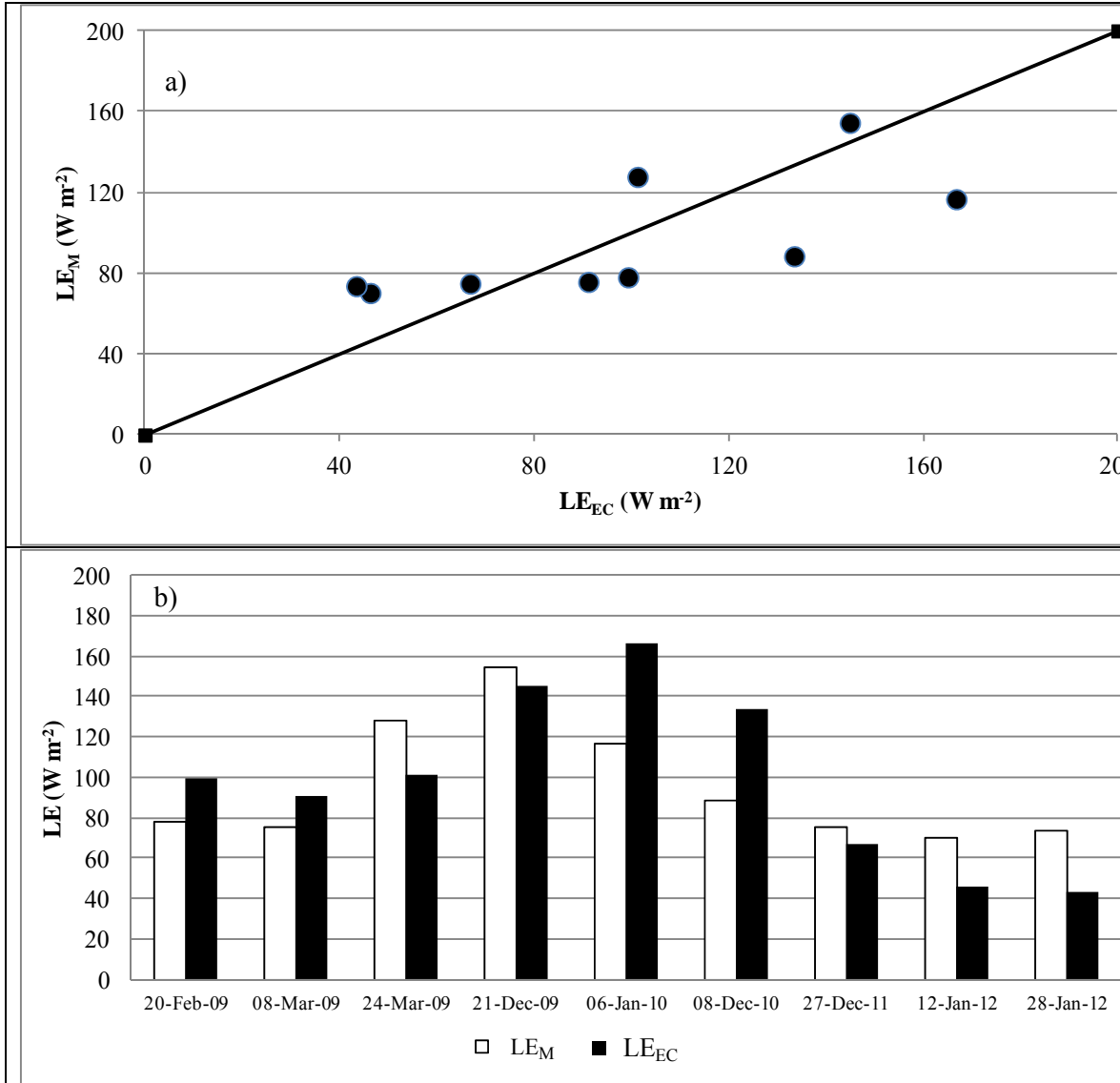


Figure 1. Comparison between latent heat fluxes at the time of satellite overpass obtained using the eddy covariance system method ( $LE_{EC}$ ) and computed using the METRIC model ( $LE_M$ ).

Daily values of olive evapotranspiration (ET) estimated by the METRIC model ( $ET_M$ ) and measured by the EC system ( $ET_{EC}$ ) for the nine satellite images (Landsat 7, ETM+) are presented in Fig. 2b. This Figure shows  $ET_{EC}$  ranged between 0.7 and 2.7  $mm day^{-1}$  and  $ET_M$  was between 1.1 and 2.1  $mm day^{-1}$  for the drip-irrigated olive orchard. The best agreement between  $ET_M$  and  $ET_{EC}$  was observed on 27 December 2011 where the difference between  $LE_M$  and  $LE_{EC}$  was 20  $W m^{-2}$ . The greatest disagreement was observed on 06 January 2010 when  $ET_M$  and  $ET_{EC}$  were 2.1 and 2.7  $mm day^{-1}$ , respectively (Fig. 2b) while  $LE_M$  and  $LE_{EC}$  were 117 and 167  $W m^{-2}$ , respectively (Fig. 1b). Errors observed in this study were most likely associated with the selection of cold pixels which were difficult to obtain for some satellite images.

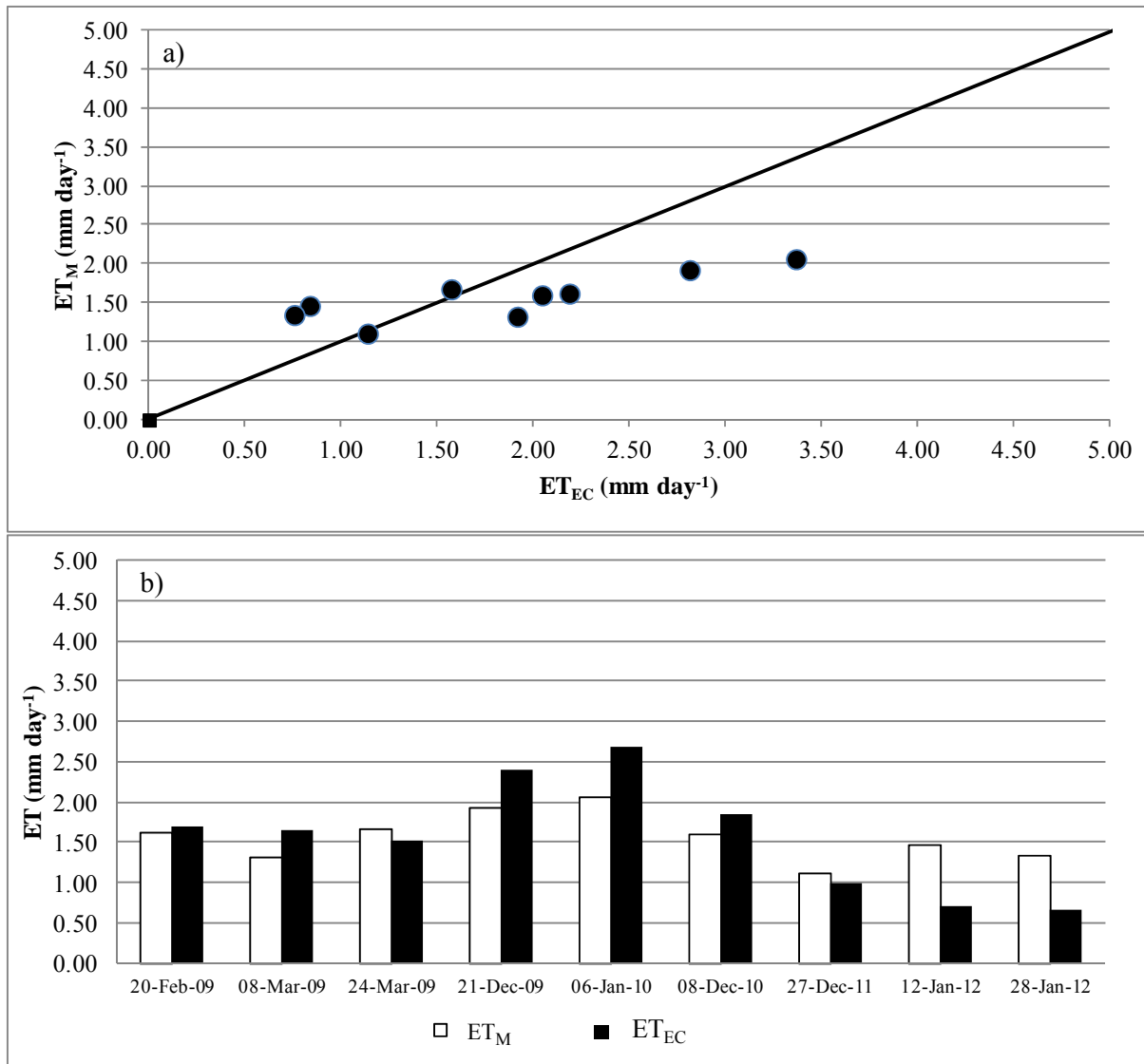


Figure 2. Comparison between olive evapotranspiration (ET) obtained using the eddy correlation method ( $ET_{EC}$ ) and computed using the METRIC model ( $ET_M$ ).

These results are considered reasonable because common errors reported in literature are between 5 and 20% in the estimation of daily or seasonal ET of several fully covered crops such as alfalfa, bean, pea, potato, sugar beet, spring grain, winter grain, corn, soybean and sorghum (Allen et al., 2007; Gowda et al., 2008; Singh and Irmak, 2009; Tasumi et al. 2005). For a drip-irrigated vineyard, Carrasco-Benavides et al. (2012) indicated that the METRIC model overestimated ET by about 9% with a RMSE and MAE of 0.62 and 0.50 mm day<sup>-1</sup>, respectively. The main limitation of METRIC algorithm is associated with the calibration of H. This limitation may produce significant errors in the quantification of ET, especially for heterogeneous canopy such as drip-irrigated olive orchards where H generated at the soil surface can be the main component of equation 3. At the time of satellite overpass (11:28h), H and LE accounted for 44 and 19 % of  $R_n$  during the two study periods, respectively. Under this condition, H

generated at the soil surface can be an important contributor to the orchard energy balance, which plays a key role in tree transpiration. In such a case, the energy absorbed by the vegetation and/or soil surface depends on canopy size, leaf area index and fractional cover (Ortega-Farias and López-Olivari, 2012).

### CONCLUSION

For a drip-irrigated olive orchard under well-irrigated conditions (midday  $\Psi_x > -1.96$  MPa) the METRIC model underestimated LE and ET by about 11 and 10%, respectively. RMSE and MAE values were 29 and 26  $\text{W m}^{-2}$  for LE while those were 0.46 and 0.39  $\text{mm day}^{-1}$  for ET, respectively). Major errors found in this study were associated with the selection of the cold pixels, but they did not significantly affect the overall performance of METRIC model during the study period. Future research will focus on the detection of variables that most significantly affect the performance of METRIC model, considering canopy geometry, LAI and the parameterization of surface energy balance components.

### ACKNOWLEDGEMENTS

The research leading to this report was supported by the Chilean government through the project FONDECYT N° 1100714.

### REFERENCES

- Allen RG, Tasumi M, Trezza R (2007). Satellite-Based Energy Balance for Mapping Evapotranspiration with Internalized Calibration (METRIC) Model. *J Irrig Drainage Eng-ASCE* 133 (4):380-394.
- Allen, RG, Tasumi M, Morse A, and Trezza R (2004). A Landsat-based Energy Balance and Evapotranspiration Model in Western US Water Rights Regulation and Planning. *J. of Irrig. and Drain. Sys.*, 19:251-268.
- ASCE-EWRI (2005) The ASCE Standardized Reference Evapotranspiration Equation. Report of the ASCE-EWRI Task Committee on Standardization of Reference Evapotranspiration.
- Bastiaanssen WGM, Noordman EJM, Pelgrum H, Davids G, Thoreson BP, and Allen RG (2005). SEBAL model with remotely sensed data to improve water-resources management under actual field conditions. *J. of Irrigation and Drainage Engrg., ASCE*, 131(1):85-93.
- Bastiaanssen WGM, Menenti M, Feddes RA, Holtslag AAM (1998) A remote sensing surface energy balance algorithm for land (SEBAL) - 1. Formulation. *J Hydrol* 213 (1-4):198-212
- Carrasco-Benavides M, Ortega-Farías S, Lagos, LO, Kleissl J, Morales L, Poblete-Echeverría C, and Allen RG. (2012). Crop coefficients and actual evapotranspiration for

a drip-irrigated Merlot vineyard using multispectral satellite images. *Irrig. Sci*, 30: 537-553.

Chávez JL, Neale CMU, Hippias LE, Prueger JH and Kustas WP (2005). Comparing aircraft-based remotely sensed energy balance fluxes with eddy covariance tower data using heat flux source area functions. *Journal of Hydrometeorology*, AMS. 6(6):923-940.

Flores F, and Ortega-Farías S. (2011). Effect of three levels of water application on oil yield and quality for an olive (cv. Picual) orchard. *Acta Hort. (ISHS)* 889:317-322.

Galleguillos M, Jacob F, Prevot L, Lagacherie P, Liang SL 2011. Mapping Daily Evapotranspiration Over a Mediterranean Vineyard Watershed. *IEEE Geosci Remote Sens Lett* 8 (1):168-172

Gowda P, Chavez J, Colaizzi P, Evett S, Howell T, Tolk J (2008). ET mapping for agricultural water management: present status and challenges. *Irrig Sci* 26 (3):223-237

Gowda PH, Chávez JL, Colaizzi PD, Evett SR, Howell, A (2007) Remote Sensing Based Energy Balance Algorithms for Mapping ET: Current Status and Future Challenges. *Trans ASABE* 50 (5):1639-1644

Pérez-López D, Gijón M, Mariño J, and Moriana A. 2010. Water relation response to soil chilling of six olive (*Olea europaea* L.) cultivars with different frost resistance. *Span J. Agric. Res.* 8(3): 780-789.

Patumi M, D'Andria R, Marsilio V, Fontanazza G, Morelli G, Lanza B (2002). Olive and olive oil quality after intensive monocone olive growing (*Olea europaea* L., cv. Kalamata) in different irrigation regimes. *Food Chemistry* 77: 27-34.

Ortega-Farías S, Irmak S, Cuenca R (2009). Special issue on evapotranspiration measurement and modeling. *Irrig Sci* 28 (1):1-3.

Ortega-Farías S. and López-Olivari R (2012). Validation of a two-layer model to estimate latent heat flux and evapotranspiration over a drip-irrigated olive orchard. *Transactions of the ASABE*, Vol. 55(4): 1169-1178

Samani Z, Bawazir AS, Bleiweiss M, Skaggs R, Longworth J, Tran VD, Pinon A (2009) Using remote sensing to evaluate the spatial variability of evapotranspiration and crop coefficient in the lower Rio Grande Valley, New Mexico. *Irrig Sci* 28 (1):93-100

Singh RK, and Irmak A (2009) Estimation of Crop Coefficients Using Satellite Remote Sensing. *J Irrig Drainage Eng-ASCE* 135 (5):597-608

Su Z (2002) The Surface Energy Balance System (SEBS) for estimation of turbulent heat fluxes. *Hydrol Earth Syst Sci* 6 (1):85-99

Tasumi M, Allen RG, Trezza R, Wright JL (2005). Satellite-Based Energy Balance to Assess Within-Population Variance of Crop Coefficient Curves. *J Irrig Drainage Eng-ASCE* 131 (1):94-109

Teixeira A, Bastiaanssen WGM, Ahmad MD, Bos MG (2009) Reviewing SEBAL input parameters for assessing evapotranspiration and water productivity for the Low-Middle Sao Francisco River basin, Brazil Part A: Calibration and validation. *Agric For Meteorol* 149 (3-4):462-476.

Tognetti R, d'Andria R, Morelli G, Alvino A. (2005). The effect of deficit irrigation on seasonal variations of plant water use in *Olea europaea* L. *Plant Soil* 273: 139



# **DRIP IRRIGATION IMPACTS ON EVAPOTRANSPIRATION RATES IN CALIFORNIA'S SAN JOAQUIN VALLEY**

Bryan Thoreson<sup>1</sup>  
Deepak Lal<sup>2</sup>  
Byron Clark<sup>3</sup>

## **ABSTRACT**

The acreage irrigated using drip irrigation continues to increase in California and the West. In addition to the increase on orchards and vineyard crops, more and more field crop acreage is coming under drip irrigation due to the increased production that growers are able to achieve with the increased distribution uniformity and improved water and nutrient management possible. When compared to surface irrigation methods, growers are able to increase production with the same, or often less, water applied. Research plot and analytical studies have shown increased evapotranspiration (ET) rates for drip irrigated field crops. Even with less water applied, increased ET rates equal more water consumed. Should the public be concerned about conversion to drip irrigation because water consumption may increase and supplies may be depleted, or should we be advocating conversion to drip/micro because we get more production per unit of water? This study addresses one technical aspect of this question by comparing ET rates over a large area of commercial production agriculture in California's San Joaquin Valley using remotely sensed ET data together with field based land use information.

Using GIS-based crop and irrigation method data and SEBAL ET results, the evapotranspiration rates of populations of selected crop-irrigation method combinations will be compared and contrasted. Statistical tests will be applied to differences in the mean ET rates and within field ET rate variability between selected crop-irrigation method groups. The statistical comparisons will focus on the differences between ET rates of drip irrigation and other irrigation methods.

## **INTRODUCTION**

The cropped area using drip and micro irrigation systems (drip/micro) in California has increased by about thirty-one percent from 1972 to 2001 (Orang, et al., 2008). A corresponding decrease in surface irrigation use has also occurred. These researchers also report an increase in the area planted to orchards and vineyards and a decrease in the area planted to field crops. However, much of the increase in drip/micro irrigation systems results from conversion of surface irrigated orchards and field crops to

---

<sup>1</sup> Corresponding author, Davids Engineering, Inc., 1772 Picasso Avenue, Suite A, Davis, CA 95618, [www.davidsengineering.com](http://www.davidsengineering.com), [bryan@davidsengineering.com](mailto:bryan@davidsengineering.com).

<sup>2</sup> SEBAL North America, Inc., 1772 Picasso Avenue, Suite E, Davis, CA 95618, [www.sebal.us](http://www.sebal.us), [deepak@sebal.us](mailto:deepak@sebal.us).

<sup>3</sup> Davids Engineering, Inc., 1772 Picasso Avenue, Suite A, Davis, CA 95618, [www.davidsengineering.com](http://www.davidsengineering.com), [byron@davidsengineering.com](mailto:byron@davidsengineering.com).

drip/micro. Understanding the effect of this continuing shift in irrigation methods on actual crop evapotranspiration ( $ET_a$ ) is important for water planning and management.

Numerous researchers have estimated the differences in seasonal  $ET_a$  between crops irrigated with drip/micro systems and the same crops irrigated with surface irrigation systems. Burt, et al., (2002) estimated that orchard crop  $ET_a$  in the San Joaquin Valley was six to 10 percent higher under drip/micro irrigation compared to surface or sprinkler irrigation. That study estimated the Transpiration (T) and Evaporation (E) components of ET using the FAO 56 (Allen, et al, 1998) dual crop coefficient method for various types of irrigation systems and irrigated areas of California. The study found total ET for furrow, sprinkle, and subsurface drip irrigation (SDI) to be nearly the same. However, the proportions of T and E comprising ET were different depending on the irrigation method, with SDI having the least evaporation of applied irrigation water (4% of seasonal  $ET_a$ ) and sprinkle irrigation having the most (8% of  $ET_a$ ). Hsiao et al. (2007) describe a systematic and quantitative approach to improve water use efficiency in agriculture. They describe water use efficiency in agriculture in terms of a chain of efficiencies and discuss the reduction of E as one way to increase transpiration efficiency. In this discussion, they cite Bonachela et al. (2001), who notes that in tree crops, especially those with sparse canopy cover, E reductions achieved by localized irrigation (i.e., drip and micro) can be substantial.

Ward and Pulido-Velazquez (2008) analyze water conservation policies on an integrated, basin-scale linking biophysical, hydrologic, agronomic, economic, policy, and institutional dimensions. Based partly on large  $ET_a$  increases ranging from 22 to 29 percent resulting from conversion from surface irrigation to drip irrigation, their results conclude that water conservation subsidies are unlikely to reduce water use. Their study demonstrates the importance of understanding changes in  $ET_a$  resulting from conversion from surface to drip/micro irrigation. For example, if  $ET_a$  does not increase substantially, and yield increases typically associated with drip/micro irrigation are due to a change in the partitioning of ET into E and T, the above mentioned study's conclusions would not be valid.

Increases in  $ET_a$ , or consumptive use of water, as the use of drip/micro increases throughout California could impact future water supplies. The objective of this paper is to further the knowledge and understanding of the changes in  $ET_a$  resulting from changes in irrigation methods. This is approached by comparing seasonal  $ET_a$  for a range of commercially produced crops irrigated with surface and drip/micro irrigation methods, and the statistical evaluation of the  $ET_a$  differences.

Remotely sensed determination of actual  $ET_a$  rates developed using a surface energy balance algorithm provide reliable seasonal estimates for individual fields under production conditions (Bastiaanssen et al., 2005). For this analysis, the SEBAL<sup>®</sup> (Surface Energy Balance Algorithm for Land) model, utilizing satellite-based remotely sensed data together with ground-based weather station data, was used to estimate  $ET_a$  across a large area in the San Joaquin Valley of California. The remainder of this paper describes the  $ET_a$  estimation method; the methodology for obtaining, comparing, and

statistically evaluating the differences between field average seasonal  $ET_a$  values for various crops under surface and drip/micro irrigation methods; and the results of the analysis and the conclusions reached.

### **$ET_a$ ESTIMATION METHOD**

Conservation of energy at the Earth's surface denotes a balance between net radiation reaching the Earth's surface from the Sun and the sum of soil, sensible, and latent heat fluxes. Latent heat flux (energy per unit area per unit time) can be easily converted into ET flux (volume of water per unit area per unit time) based on the latent heat of vaporization and density of water. ET flux can be estimated as a closure term from estimates of the remaining fluxes (Equation 1).

$$ET_a = \frac{1}{\lambda \rho_w} [R_n - (G + H)] \quad (1)$$

where  $\lambda$  is the latent heat of vaporization of water,  $\rho_w$  is the density of water,  $ET_a$  is the actual  $ET_a$ ,  $R_n$  is the net radiation flux at the Earth's surface,  $G$  is the soil heat flux, and  $H$  is the sensible heat flux.

### **Description of SEBAL**

The SEBAL model applies radiative, aerodynamic, and energy balance physics in a series of 25 computational steps to estimate  $ET_a$  from the energy balance.  $ET_a$  is calculated at the pixel-scale using multispectral satellite imagery with a thermal band. The key input data consist of radiances in the visible, near infrared, and thermal infrared regions sensed by earth observing satellites; ground based weather data from agricultural or other weather stations; and land use data describing general vegetation types, when available. Knowledge of specific crop types is not needed to solve the energy balance. SEBAL is internally calibrated for each image to estimate sensible heat flux between the surface and the atmosphere, avoiding the need for absolute calibration of the surface temperature of each pixel. A detailed explanation of the algorithm is provided by Bastiaanssen et al. (1998).

SEBAL has been continually updated over time based on advances in surface energy balance science. These advances include both published and non-published refinements. The 2009 version of SEBAL used for this study includes the following updates from the originally published version of the model:

- Topographic correction of extraterrestrial solar radiation based on actual surface slope and aspect,
- Lapse rate correction of observed surface temperatures prior to calibration of sensible heat flux to normalize for elevation effects on surface temperature,
- Use of spatially distributed weather surfaces from MeteoLook for improved representation of actual surface conditions within the image area,

- Advection correction based on comparison of instantaneous and daily evaporative fractions estimated for a hypothetical grass reference surface assumed to be 0.12 m tall, having a surface resistance of 70 s and an albedo of 0.23 (Allen et. al., 1998) , which is used to compute a theoretical advection correction factor, which is then adjusted based on the actual instantaneous evaporative fraction for each pixel within the image,
- Atmospheric correction and calibration (as needed) of albedo , and
- Improved soil heat flux estimation based on a combination of LAI, and soil moisture.

### **Validation of SEBAL**

SEBAL was developed through 20 years of research and validation. Validation is ongoing due to periodic refinements, sensitivity of model results to analyst judgments related to internal calibration, and interest in further quantifying the accuracy of the approach. The algorithm has been applied in 15 countries, including 11 states mostly in the western United States. Comparisons have been made to six different ET estimation methods for a variety of landscapes including irrigated pasture, sugar beets, riparian vegetation, playas, olives, rice, palm trees, cotton, wheat, sunflower, peaches, almonds, tomatoes, bare soil, grassland and forest.

Recent validations of SEBAL, summarized by Bastiaanssen et al. (2005), have shown seasonal  $ET_a$  results generally fall within five percent of seasonal  $ET_a$  determined from reliable ground-based measurements.  $ET_a$  results from a 2002 SEBAL analysis for the Southern San Joaquin Valley were compared to lysimeter measurements on alfalfa and peaches (Cassel, 2006) and surface renewal measurements on tomatoes (Roberson, 2006). In each comparison, the difference between the SEBAL  $ET_a$  and the ground-based estimates was five percent or less (Figure 1).

Additionally, SEBAL estimates of district-wide  $ET_a$  for the Imperial Irrigation District were compared to an independent water balance (Thoreson et al. 2009). Annual  $ET_a$  was calculated for the 1998 water year (October 1997 – September 1998) based on measured inflows and outflows. Total consumptive use from SEBAL was found to agree with the annual water balance within 1 percent.

### **Input Data**

A combination of satellite, ground-based meteorological, topographic, and land cover classification data are utilized to quantify spatially distributed  $ET_a$ . For this study, these datasets were obtained from the U.S. Geological Survey (USGS), CIMIS, and the U.S. Department of Agriculture (USDA). These data are described in greater detail in the following paragraphs.

### Satellite Images

Seven Landsat 5TM and one Landsat 7 ETM multispectral images encompassing the period from late March to early November for Path 35/Row 42 were obtained from USGS for 2009 (Table 1). Cloud-free images were selected to achieve a temporal frequency of one image per month for each growing season.

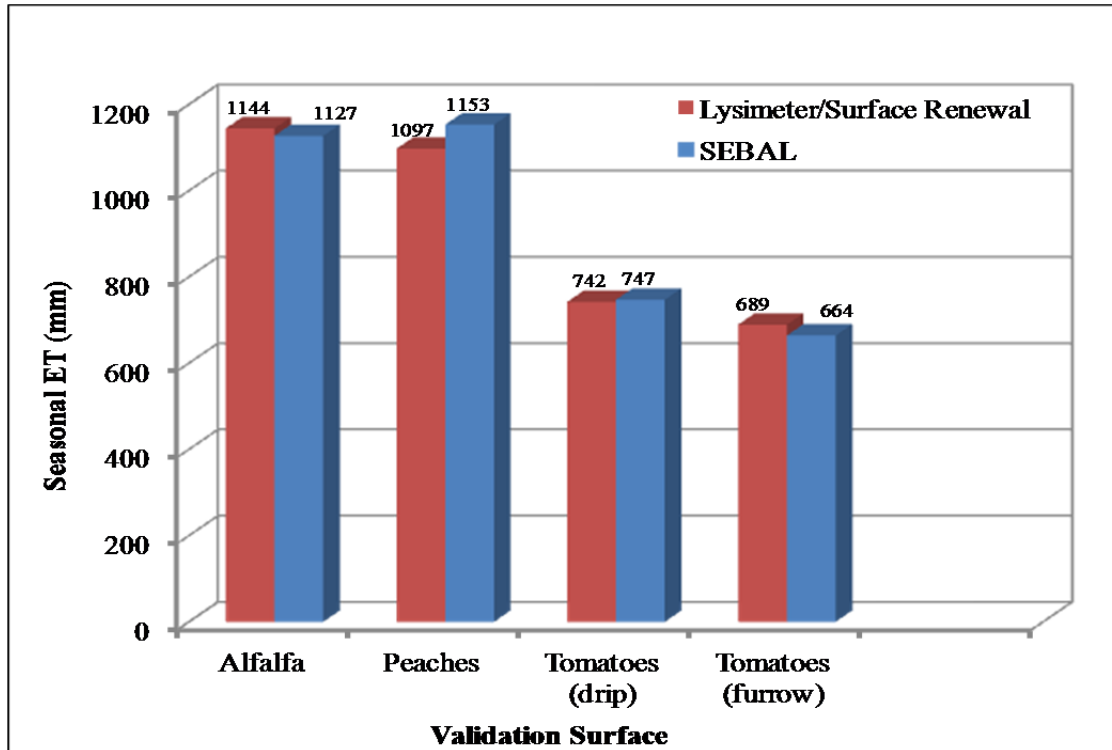


Figure 1. Seasonal SEBAL ET<sub>a</sub> Results Compared to Lysimeter and Surface Renewal Results.

Table 1. SEBAL Datasets Used for 2009 Growing Season ET Analysis.

Region	Satellite Platform	Row/Path	Thermal Resolution	Image Dates	Images
Southern San Joaquin Valley (2009 season)	Landsat 7 ETM	42/35	60 m	3/30/2009	1
Southern San Joaquin Valley (2009 season)	Landsat 5	42/35	120 m	4/23, 5/25, 6/26, 7/28, 8/29, 9/30, 11/1/2009	7

### Meteorological Data

Measurements of incoming solar radiation ( $R_s$ ), relative humidity (RH), air temperature ( $T_a$ ) and wind speed (WS) were available as hourly averages for the time of image acquisition. Daily (average for the image date), and period (average for the days

represented by an individual image) measurements were also available. Eight CIMIS stations falling within or on the edge of the study area were used to develop a spatially varying weather surface prior to the SEBAL image processing. Weather data were quality checked according to the guidelines specified in Appendix-D of the ASCE Task Committee Report on the Standardized Reference Evapotranspiration Equation (Allen et al., 2005).

Weather data were spatially interpolated using MeteoLook, a collection of algorithms developed to interpolate point weather observations based on the surface and terrain characteristics coupled with physically-based models (Voogt, M.P., 2006). Processes that influence surface weather conditions such as elevation, surface roughness, albedo, incoming radiation, land wetness, and distance to water bodies are represented in MeteoLook. This improved spatial distribution of weather data improves the ability to estimate surface conditions influencing the surface energy balance.

### **Landuse Data and Digital Elevation Model (DEM)**

Information describing land use types within the southern San Joaquin Valley was obtained from the statewide land use data provided by the USDA National Agricultural Statistics Service (NASS) (available at [datagateway.nrcs.usda.gov](http://datagateway.nrcs.usda.gov)) for the year 2009. The NASS land use map utilized is a raster grid derived primarily from multiple satellite images obtained from RESOURCESAT – 1 (IRS – P6) across the 2009 growing season. The NASS land use map was resampled from its original spatial resolution of 56 meters to 30 meters to be consistent with other inputs for SEBAL. This land use data was used to estimate obstacle heights for different surfaces within the study area. These data have been developed by various means including analysis of satellite images along with inspection of aerial photographs and ground-surveys.

A DEM of one arc-second resolution (approximately 30 meters) was obtained from USGS and was used in SEBAL to incorporate the effects of the slope, aspect and elevation of the land into the energy balance.

## **METHODOLOGY**

Two general data sources were utilized in this study. An existing SEBAL dataset provided  $ET_a$  estimates at the pixel scale derived from Landsat imagery. Field boundaries, crops and irrigation methods were identified using cropping data from the California Department of Water Resources (DWR) land use survey for east Fresno County for 2009.

Field-scale average seasonal  $ET_a$  in inches was calculated for field groups defined based on crop, irrigation method, and estimated fractional canopy cover in the east Fresno County area covered by the DWR land use survey (Figure 2). Field boundaries were buffered inward to identify areas in which  $ET_a$  estimates were not affected by heat transfer processes occurring outside of the field (thermal contamination). Then, seasonal  $ET_a$  for each pixel within each field of interest was averaged to estimate field-scale seasonal  $ET_a$ . The data were filtered to remove fields with low NDVI during critical

growth periods (suggesting very young crops or miss-classification) and to group fields based on estimates of fractional ground cover, so that comparisons could be made across fields of similar maturity, canopy structure, and/or cover crop presence. Finally, differences in average field-scale  $ET_a$  were compared, and tested for statistical significance.

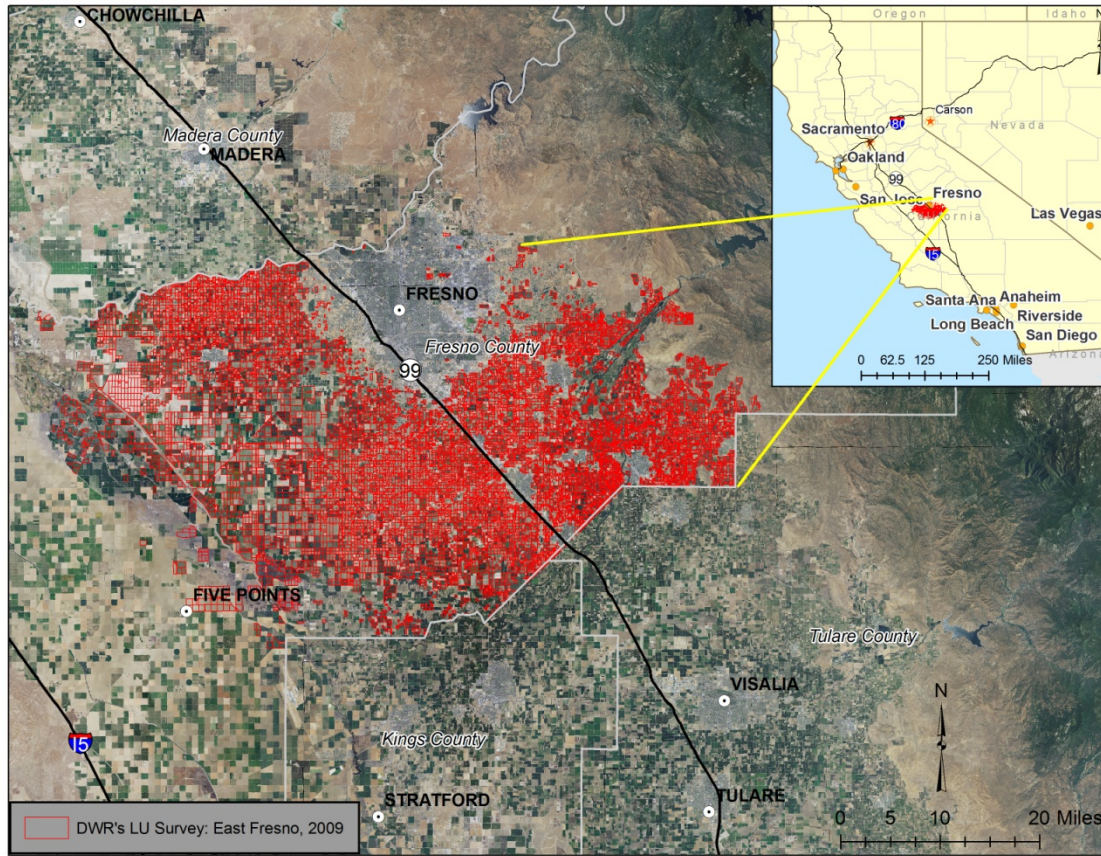


Figure 2. Location of Fields with Land Use Data.

### **Buffering of Field Boundaries**

Field boundaries were buffered inward to identify cropped areas that were not affected by thermal contamination. Thermal contamination within field pixels occurs when lower resolution thermal pixels cross the field boundary and are affected by heat transfer processes outside of the field. For such pixels, the thermal radiance represents a weighted average of the radiance of the pixel area outside the field and the pixel area inside the field. To reduce the thermal contamination on field edges to acceptable levels, field boundaries were buffered 30 meters inward, and all fields with an area of less than five acres after buffering were dropped from the analysis.

Seasonal  $ET_a$  and June 26, 2009 (mid-season) image NDVI values for each pixel within the buffered areas were extracted and imported to a Microsoft Access database for calculation of field averages.

### Filtering of Field Data Based on NDVI

Field  $ET_a$  values were filtered prior to the calculation of average seasonal  $ET_a$  based on mid-season NDVI. Filters were applied primarily to separate fields of tree and vine crops into fractional cover classes based on NDVI presumably representing similar maturity, canopy structure, and/or cover crop presence.

Threshold NDVI values for the filters were estimated based on a relationship estimating fractional canopy cover from NDVI (Equation 2) after the form of Choudhury et al. (1994):

$$f_c = 1 - \left( \frac{0.8 - NDVI}{0.8 - 0.125} \right)^{0.7} \quad (2)$$

Threshold NDVI values corresponding to 10 percent incremental changes in fractional cover ( $f_c$ ) were derived from Equation 2 and are given in Table 2. Fractional cover estimates may also provide insight into the effect of varying ground shading on crop  $ET$ . As fractional cover increases, shading increases leading to a decrease in  $E$ .

Table 2. Threshold NDVI Values Corresponding to Estimated 10 Percent Fractional Cover Increments from Equation 2.

$f_c$	$NDVI$	$f_c$	$NDVI$
0.20	0.310	0.50	0.550
0.30	0.395	0.60	0.618
0.40	0.475	0.70	0.680

## RESULTS AND DISCUSSION

Eleven crops in the area bounded by the intersection of the 2009 East Fresno County DWR Land Use Survey and the SEBAL dataset had more than 1,000 acres irrigated by drip/micro irrigation methods (Table 3). Including processing tomatoes, 74 percent of which are irrigated with buried drip systems, these 12 crops accounted for just over 400,000 irrigated acres. Notably 44 percent of the area was irrigated with drip or micro irrigation. When buried drip, sprinklers and other methods are included, 49 percent of the area is irrigated with methods other than the traditional surface irrigation methods of furrow, border strip and basin.

As described previously, a 30 meter buffer was applied to the field boundaries, and pixels impacted by clouds and scan line gaps<sup>4</sup> as well as all remaining fields less than five acres

<sup>4</sup> Gaps present in the Landsat 7 image acquired March 30<sup>th</sup> result from a malfunction of the Scan Line Corrector (SLC) that occurred in May 2003 in the ETM+ imaging sensor onboard the satellite. Due to the gaps, approximately 22% of the data is missing from a typical Landsat 7 image. These gaps vary in width from one pixel or less in the center of the image to 14 pixels towards the edges of the image. Despite the gaps in the data, the Landsat 7 image was used in the analysis to provide adequate temporal coverage.

were removed from the analysis. This led to a field data set for consideration for the statistical analysis (Table 4). For the succeeding analyses, crop-irrigation method groups with the number of fields greater than 30 and the total acreage greater than 1,000 acres were included.

Table 3. Crops with Area Irrigated by Drip/Micro Greater Than 1,000 Acres.  
Source: East Fresno County DWR Land Use Survey, 2009

Crop	Total Acres	Drip/Micro Irrigation Methods, Acres	Surface Irrigation Methods, Acres	Buried Drip Irrigation Methods, Acres	Sprinklers and Other Irrigation Methods, Acres
Vineyards	202,167	88,250	106,170	215	7,532
Almonds	67,668	29,499	37,404	39	725
Oranges	35,303	29,122	5,802	0	379
Peaches and Nectarines	33,253	3,585	29,128	0	540
Pistachios	18,732	17,222	1,496	0	14
Plums	14,613	2,858	11,554	0	201
Tomatoes (processing)*	10,688	649	968	7,947	1,124
Mixed	6,397	1,293	4,244	583	278
Walnuts	6,183	1,152	4,966	0	65
Miscellaneous deciduous	5,917	2,526	3,023	0	367
Olives	1,329	1,119	210	0	0
Lemons	1,077	1,026	51	0	0
Totals	403,326	178,301	205,015	8,785	11,225
Percent		44%	51%	2%	3%

\*Processing tomatoes are included as a crop of interest even though most of the acreage was irrigated with buried drip systems.

Table 4. Crop-Method Combination Areas Remaining After Buffering, Removing Pixels Impacted by Clouds and Scan Line Gaps (Landsat 7 ETM) and Removing Fields Less Than 5 Acres.

Crop-Method Group	No. of Fields	Acres
Vineyards, drip/micro	1,610	32,391
Vineyards, surface	1,861	31,771
Oranges, drip/micro	761	15,789
Peaches and Nectarines, surface	746	11,172
Almonds, drip/micro	370	8,731
Almonds, surface	423	7,641
Plums, surface	346	4,124
Oranges, surface	194	2,628
Peaches and Nectarines, drip/micro	113	1,447
Plums, drip/micro	88	1,034
Pistachios, surface	18	270
Pistachios, drip/micro	16	236
Tomatoes (processing), drip/micro	11	206
Tomatoes (processing), surface	1	20
Totals	6,558	117,461

The larger areas of drip/micro irrigated almond and orange orchards and vineyards in the lower fractional cover classes indicate a grower preference for drip/micro irrigation compared to surface irrigation (Table 5).

Table 5. Crop-Method Combination Areas and Number of Fields by Fractional Cover Range.

Crop-Method Group	Fractional Cover Class	NDVI Range	Drip/micro Irrigation Method		Surface Irrigation Method	
			No. of Fields	Acres	No. of Fields	Acres
Almonds	< 0.3	< 0.395	112	1,948	96	1,309
Almonds	0.3 - 0.4	0.395 to 0.475	71	1,448	79	1,247
Almonds	0.4 - 0.5	0.475 to 0.55	89	2,195	102	1,852
Almonds	0.5 - 0.6	0.55 to 0.618	81	2,492	114	2,546
Almonds	> 0.6	>0.618	17	648	32	687
Oranges	< 0.3	< 0.395	307	6,109	75	954
Oranges	0.3 - 0.4	0.395 to 0.475	223	4,327	66	1,025
Oranges	0.4 - 0.5	0.475 to 0.55	190	4,522	43	535
Oranges	0.5 - 0.6	0.55 to 0.618	37	788	8	99
Oranges	> 0.6	>0.618	4	43	2	14
Peaches and Nectarines	< 0.3	< 0.395	19	196	66	837
Peaches and Nectarines	0.3 - 0.4	0.395 to 0.475	15	262	77	1,075
Peaches and Nectarines	0.4 - 0.5	0.475 to 0.55	27	333	197	2,934
Peaches and Nectarines	0.5 - 0.6	0.55 to 0.618	38	465	224	3,600
Peaches and Nectarines	> 0.6	>0.618	14	191	182	2,725
Plum	< 0.3	< 0.395	24	241	51	614
Plum	0.3 - 0.4	0.395 to 0.475	12	137	37	432
Plum	0.4 - 0.5	0.475 to 0.55	18	257	85	1,095
Plum	0.5 - 0.6	0.55 to 0.618	23	300	102	1,225
Plum	> 0.6	>0.618	11	99	71	758
Vineyards	< 0.3	< 0.395	866	17,630	842	13,635
Vineyards	0.3 - 0.4	0.395 to 0.475	359	7,585	581	11,138
Vineyards	0.4 - 0.5	0.475 to 0.55	128	2,815	219	3,865
Vineyards	0.5 - 0.6	0.55 to 0.618	82	1,565	123	1,887
Vineyards	> 0.6	>0.618	175	2,796	96	1,246

Average  $ET_a$  for surface irrigated fields was greater than the average  $ET_a$  for drip or micro irrigated for 21 of 25 crop-irrigation method-fractional cover groups. (Table 6). The 0.4 to 0.5 fractional cover group for oranges and plums had average  $ET_a$  of drip or micro fields greater than the average  $ET_a$  of surface irrigated fields. The two smallest fractional cover classes for peaches and nectarines were found to have an average  $ET_a$  of drip or micro irrigated fields slightly larger than average  $ET_a$  of the surface irrigated fields. With the notable exceptions of almonds and peaches and nectarines, the average  $ET_a$  of the surface irrigated fields exceeded average  $ET_a$  of drip/micro irrigated fields by the greatest amount in the smaller fractional cover groups. This is likely due to greater evaporation from surface irrigation of the younger trees. For all groups, the  $ET_a$  difference between surface and drip or micro irrigated fields was less than the standard deviation.

Table 6. Crop-Method Combination Average  $ET_a$  and Standard Deviation by Fractional Cover Range.

Crop-Method Group	Fractional Cover Class	NDVI Range	Drip/micro Irrigation Method		Surface Irrigation Method		Surface - Drip
			Avg. $ET_a$ , in	StdDev, in	Avg. $ET_a$ , in	StdDev, in	Avg. $ET_a$ , in
Almonds	< 0.3	< 0.395	16.6	4.2	18.2	4.2	1.6
Almonds	0.3 - 0.4	0.395 to 0.475	34.0	4.7	35.7	4.7	1.8
Almonds	0.4 - 0.5	0.475 to 0.55	41.9	5.1	43.7	5.3	1.7
Almonds	0.5 - 0.6	0.55 to 0.618	47.6	5.5	49.6	4.9	2.0
Almonds	> 0.6	>0.618	54.0	4.4	55.9	4.3	1.9
Oranges	< 0.3	< 0.395	16.5	4.1	19.6	3.8	3.1
Oranges	0.3 - 0.4	0.395 to 0.475	32.4	4.7	34.8	4.5	2.4
Oranges	0.4 - 0.5	0.475 to 0.55	38.3	4.6	38.1	4.7	-0.2
Oranges	0.5 - 0.6	0.55 to 0.618	42.4	4.2	44.1	4.8	1.6
Oranges	> 0.6	>0.618	42.9	3.7	45.0	4.0	2.1
Peaches and Nectarines	< 0.3	< 0.395	22.1	5.0	19.6	4.9	-2.5
Peaches and Nectarines	0.3 - 0.4	0.395 to 0.475	31.8	6.2	31.5	5.5	-0.3
Peaches and Nectarines	0.4 - 0.5	0.475 to 0.55	35.4	5.5	38.8	4.7	3.3
Peaches and Nectarines	0.5 - 0.6	0.55 to 0.618	39.6	5.2	43.6	4.1	4.0
Peaches and Nectarines	> 0.6	>0.618	45.5	4.7	48.8	3.9	3.3
Plum	< 0.3	< 0.395	16.1	4.8	18.1	5.1	2.1
Plum	0.3 - 0.4	0.395 to 0.475	27.5	5.7	31.0	4.8	3.6
Plum	0.4 - 0.5	0.475 to 0.55	37.9	4.2	37.2	4.6	-0.7
Plum	0.5 - 0.6	0.55 to 0.618	42.2	3.8	43.0	4.6	0.8
Plum	> 0.6	>0.618	47.7	5.2	48.5	3.6	0.8
Vineyards	< 0.3	< 0.395	13.6	3.6	17.0	4.3	3.4
Vineyards	0.3 - 0.4	0.395 to 0.475	21.1	3.6	25.0	4.4	3.9
Vineyards	0.4 - 0.5	0.475 to 0.55	29.2	4.1	30.9	3.9	1.6
Vineyards	0.5 - 0.6	0.55 to 0.618	35.6	3.7	35.9	3.3	0.3
Vineyards	> 0.6	>0.618	41.0	3.1	42.4	3.0	1.4

Statistical hypotheses were tested regarding the differences of the means of each group. Walpole and Myers (1978) define a statistical hypothesis as “an assumption or statement which may or may not be true, concerning one or more populations.” For the fifty populations considered in this study, a statistical hypothesis that the mean  $ET_a$  of surface irrigated fields was equal to the mean  $ET_a$  of drip/micro irrigated fields for each crop fractional cover category was formulated and tested as to whether it should be rejected at the  $\alpha = 0.05$  level of confidence. This hypothesis is called the null hypothesis ( $H_0$ ). The rejection of this hypothesis leads to the acceptance of the alternative hypothesis ( $H_1$ ) that the means are not equal. This null hypothesis was rejected for four of the five crop-method-fractional cover groups for almonds and vineyards, the two crops with the greatest area and number of fields (Table 7). Overall all 25 crop-method-fractional cover groups, the null hypothesis was rejected for 13 groups accounting for 98,411 acres and accepted for 12 groups accounting for 18,318 acres. The null hypothesis that the means were equal was not rejected for all five groups of plums, the crop with the smallest area in the study.

Table 7. Crop-Method Combination Test Statistic and Statistical Hypothesis Test Results.

Crop-Method Group	Fractional Cover Class	NDVI Range	Surface - Drip Avg. ET <sub>a</sub> , in	Z test Statistic	Z <sub>0.05/2</sub>	Reject Null Hypothesis (Alpha = 0.05)
Almonds	< 0.3	< 0.395	1.6	2.732	1.96	<b>Yes</b>
Almonds	0.3 - 0.4	0.395 to 0.475	1.8	2.283	1.96	<b>Yes</b>
Almonds	0.4 - 0.5	0.475 to 0.55	1.7	2.288	1.96	<b>Yes</b>
Almonds	0.5 - 0.6	0.55 to 0.618	2.0	2.594	1.96	<b>Yes</b>
Almonds	> 0.6	>0.618	1.9	1.428	1.96	<b>No</b>
Oranges	< 0.3	< 0.395	3.1	6.215	1.96	<b>Yes</b>
Oranges	0.3 - 0.4	0.395 to 0.475	2.4	3.840	1.96	<b>Yes</b>
Oranges	0.4 - 0.5	0.475 to 0.55	-0.2	-0.269	-1.96	<b>No</b>
Oranges	0.5 - 0.6	0.55 to 0.618	1.6	0.898	1.96	<b>No</b>
Oranges	> 0.6	>0.618	2.1	0.618	1.96	<b>No</b>
Peaches and Nectarines	< 0.3	< 0.395	-2.5	-1.950	-1.96	<b>No</b>
Peaches and Nectarines	0.3 - 0.4	0.395 to 0.475	-0.3	-0.178	-1.96	<b>No</b>
Peaches and Nectarines	0.4 - 0.5	0.475 to 0.55	3.3	3.011	1.96	<b>Yes</b>
Peaches and Nectarines	0.5 - 0.6	0.55 to 0.618	4.0	4.510	1.96	<b>Yes</b>
Peaches and Nectarines	> 0.6	>0.618	3.3	2.562	1.96	<b>Yes</b>
Plum	< 0.3	< 0.395	2.1	1.697	1.96	<b>No</b>
Plum	0.3 - 0.4	0.395 to 0.475	3.6	1.946	1.96	<b>No</b>
Plum	0.4 - 0.5	0.475 to 0.55	-0.7	-0.588	-1.96	<b>No</b>
Plum	0.5 - 0.6	0.55 to 0.618	0.8	0.918	1.96	<b>No</b>
Plum	> 0.6	>0.618	0.8	0.484	1.96	<b>No</b>
Vineyards	< 0.3	< 0.395	3.4	17.382	1.96	<b>Yes</b>
Vineyards	0.3 - 0.4	0.395 to 0.475	3.9	14.802	1.96	<b>Yes</b>
Vineyards	0.4 - 0.5	0.475 to 0.55	1.6	3.590	1.96	<b>Yes</b>
Vineyards	0.5 - 0.6	0.55 to 0.618	0.3	0.612	1.96	<b>No</b>
Vineyards	> 0.6	>0.618	1.4	3.709	1.96	<b>Yes</b>

These results contradict the increased ET<sub>a</sub> attributed to drip/micro irrigation reported by other investigators (Burt, 2002 and Ward, 2008). Four possible reasons for this are:

1. The more precise irrigation management possible on drip/micro irrigated fields provides increased opportunities to practice irrigation management strategies that result in lower ET<sub>a</sub>.
  - a. Vineyards on drip/micro are more likely to be deficit irrigated resulting in reduced ET<sub>a</sub>,

- b. Almonds irrigated with drip/micro systems are more likely to be managed utilizing Regulated Deficit Irrigation (RDI) (Goldhammer, 2005) practices with irrigation restricted during certain growth periods leading to reduced  $ET_a$
2. A reduction in E resulting from conversion to drip or micro, without an offsetting increase in T (T may increase, but not as much as E decreases).
3. Differences in the practice of using cover crops in orchards depending on the use of drip/micro or surface irrigation methods.
4. If surface systems tend to occur in surface water areas with relatively abundant supplies and drip/micro tends to occur in GW areas or water short areas in general, it is possible that differences in water supply source explain the outcome that drip  $ET_a$  is not greater than surface  $ET_a$ .

### CONCLUSION

Mean  $ET_a$  from production fields irrigated with surface irrigation methods was found to be greater than mean  $ET_a$  from fields irrigated with drip/micro for 13 of 25 crop-irrigation method-fractional cover groups. This result is surprising given the conventional wisdom supported by findings of some researchers that  $ET_a$  from drip/micro irrigated fields is more than that from surface irrigation. To obtain the increased yield reported from the drip/micro irrigated fields, it is likely that the partitioning of E and T has changed with the volume of E from drip/micro irrigated fields being less than the E from surface irrigated fields. Additional research into seasonal  $ET_a$  for drip/micro and surface irrigated fields is necessary to confirm or refute this preliminary conclusion. However, if proven to hold true by additional research, this indicates that conversion to drip/micro irrigation on orchard crops in the San Joaquin Valley of California is not substantially increasing the consumptive use of water. Thus, installation of drip/micro irrigation may, in many cases, increase transpiration efficiency by reducing the volume of evaporation without increasing overall  $ET_a$ . Other changes resulting from installation of drip/micro irrigation systems may include reduction of deep percolation. Future studies are required to evaluate differences in  $ET_a$  from surface irrigated and drip/micro irrigated field crops such as tomatoes and alfalfa.

### REFERENCES

- Allen, R.G., Pereira, L.S., Raes, D., and Smith, M. (1998). Crop Evapotranspiration. Irrigation and Drainage Paper No. 56. Food and Agriculture Organization of the United Nations. Rome, Italy.
- Allen, R.A., Walter, I.A., Elliot, R., Howell, T., Itenfisu, D. and Jensen, M. (2005). The ASCE Standardized Reference Evapotranspiration Equation. ASCE. Reston, VA.
- Bastiaanssen, W.G.M., Menenti, M., Feddes, R.A., and Holtslag, A.A.M. (1998). A Remote Sensing Surface Energy Balance Algorithm for Land (SEBAL): 1. Formulation. *Journal of Hydrology*, 212-213: 198-212.

- Bastiaanssen, W.G.M., Noordman, E.J.M., Pelgrum, H., Davids, G., B.P. Thoreson and Allen, R.G. (2005). SEBAL Model with Remotely Sensed Data to Improve Water Resources Management under Actual Field Conditions. *Journal of Irrigation and Drainage Engineering*. 131(1), 85-93.
- Bonachela, S.F, Orgaz, F., Villalobos, F.J, and Fereres, E. (2001) Soil evaporation from drip-irrigated olive orchards. *Irrig Sci*. 20:65–71. Cited in Hsiao, et al. 2007.
- Burt, C. M., Mutziger, A., Howes, D. J., and Solomon, K. H. (2002). “Evaporation from irrigated land in California.” *Rep. R02-001*. Irrigation Training and Research Center, California Polytechnic State Univ., San Luis Obispo, Calif. (<http://www.itrc.org/reports/reportsindex.html>).
- Cassel, F. (2006). Remote Sensing of Evapotranspiration for Verification of Regulated Deficit Irrigation. USBR final project report. pp. 58.
- Choudhury, B.J., Ahmed, N.U., Idso, S.B., Reginato, R.J., and Daughtry, C.S.T. (1994). Relations Between Evaporation Coefficients and Vegetation Indices Studied by Model Simulations. *Remote Sensing of Environment*. 50, 1-17.
- Goldhammer, D.A. and Fereres, E . (2005). The Promise of Regulated Deficit Irrigation in California’s Orchards and Vineyards. California Water Plan, 2005. California Department of Water Resources, Sacramento, CA.
- Hsiao, T. C., Steduto, P., and Fereres, E. (2007). A systematic and quantitative approach to improve water use efficiency in agriculture. *Irrig Sci*. 25:165–188
- Orang, M.N., Matyac, J.S., and Snyder, R.L. (2008). “Survey of irrigation methods in California in 2001.” *Journal of Irrigation and Drainage Engineering*, 134 (1), 96-100.
- Roberson, M. (2006). Personal communication.
- Thoreson, B., Clark, B., Soppe, R., Keller, A., Bastiaanssen, W., and Eckhardt. J. (2009). Comparison of Evapotranspiration Estimates from Remote Sensing (SEBAL), Water Balance, and Crop Coefficient Approaches. In *Great Rivers. Proceedings from an EWRI Congress*, Kansas City, MO.
- Voogt, M.P. (2006). Meteolook, a Physically Based Regional Distribution Model for Measured Meteorological Variables. MSc Thesis, TU Delft, the Netherlands.
- Ward, F.A. and Pulico-Velazquez, M. (2008). Water Conservation in Irrigation Can Increase Water Use. *Proceedings National Academy of Sciences*. November 25, 2008 Vol. 105 No. 47, 18215-18220.
- Walpole, R.E. and Myers, R.H. (1978). *Probability and Statistics for Engineers and Scientists*. Macmillan Publishing Co., Inc. New York, NY.



# IRRIGATION-INDUCED CHANGES TO THE NEAR SURFACE HYDROMETEOROLOGY FOR SUSTAINABLE WATER MANAGEMENT

V. Sridhar<sup>1</sup>  
W.T.A. Jaksa<sup>2</sup>  
Korri Anderson<sup>3</sup>

## ABSTRACT

Irrigation and land use change substantially alters the feedback mechanism between the land and atmosphere. Therefore, it becomes critical to include these anthropogenic-induced changes, i.e., irrigation, when computing the surface fluxes and boundary layer properties that has direct implications on the regional evolution of hydrometeorology. The North American Regional Reanalysis (NARR) data set is available at a coarse resolution (32 km) for surface and atmospheric layers. By disaggregating this data set to 4 km, we evaluate the impact of irrigation using the Noah Land Surface Model and other energy balance approaches in the Snake River Basin in Idaho. Our simulation extends for the period in the growing season to assess the irrigation induced cooling on the surface energy balance. Understanding this near surface cooling is directly useful for sustainable water management under changing climate conditions in the future. We present simulated latent and sensible heat fluxes as well as air temperature, relative humidity and the depth of the planetary boundary layer (PBL) over the region.

## INTRODUCTION

Treating the land-atmosphere interaction as an integrated physical system in weather and climate modeling is necessary to quantify the surface energy balance components and crop evapotranspiration (ET). In general, current generation weather and climate models generally addressed changes of atmospheric composition and the associated feedbacks to the climate system, yet have neglected to account for human-induced changes to the Earth's land surface explicitly and the associated physical characteristics on local and regional scales (Pielke et al., 2011). In a warming world that is also stressed with population growth, providing food, fiber and water assumes extraordinary significance. Inclusion of the role of land-use, land-cover (LULC) change that has been mostly ignored from the climate models for the assessment reports by the Intergovernmental Panel on Climate Change (IPCC) (Pielke et al., 2011) will provide the impacts due to climate change on water resources and agriculture comprehensively. This research seeks to understand the role of irrigation on the semi-arid land surface under a changing climate in Southern Idaho.

---

<sup>1</sup> Department of Civil Engineering, Boise State University, Boise, Idaho 83725-2060, Phone 208-426-3710, Fax 208-426-2351, [vsridhar@boisestate.edu](mailto:vsridhar@boisestate.edu)

<sup>2</sup> Department of Civil Engineering, Boise State University, Boise, Idaho 83725-2060, Phone 208-426-3710, Fax 208-426-2351, [ryshala@gmail.com](mailto:ryshala@gmail.com)

<sup>3</sup> Department of Civil Engineering, Boise State University, Boise, Idaho 83725-2060, Phone 208-426-3710, Fax 208-426-2351, Department of Civil Engineering, Boise State University, Boise, Idaho 83725-2060, Phone 208-426-3710, Fax 208-426-2351

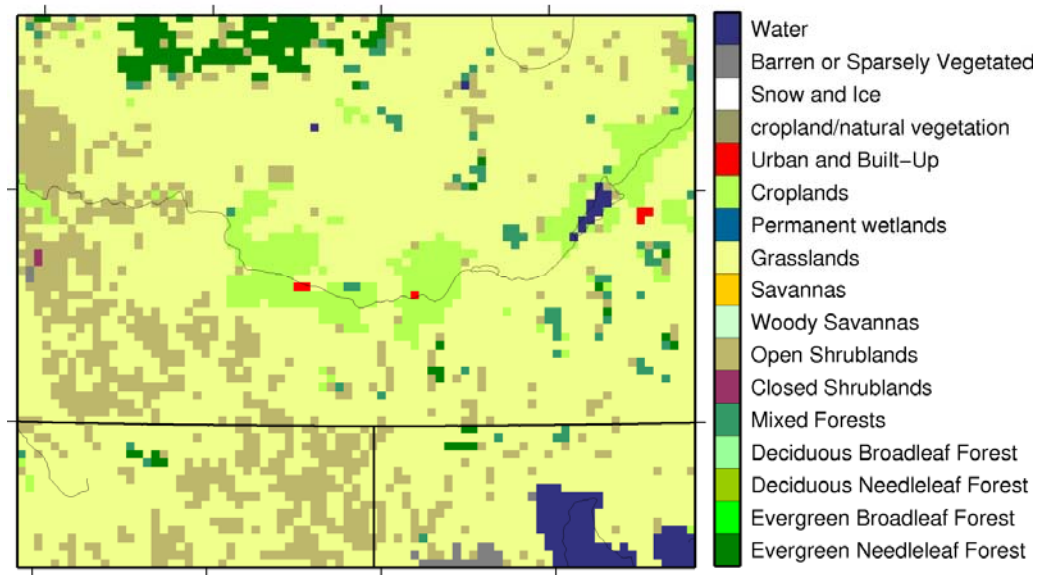


Figure 1. Vegetation map of the study area at 4-km resolution adopted from the MODIS-based classification. Approximately the domain is covers by 71% of grasslands, 15% of shrublands, 7% of croplands and 4% of forests.

## STUDY AREA

The study was performed in the Snake River basin in south central Idaho. The Snake River basin covers a semiarid region of southern Idaho that extends into parts of Oregon, Nevada, Wyoming, Montana and Washington. Cold winters and hot, dry summers typically represent the climatology of this basin. Snow in the winter and precipitation in the fall and early spring is the main source for recharge of the ground water (Kjelstrom, 1995). The main source of water for irrigation diversions during the growing season is from the snowmelt-induced runoff off of the mountains in the headwater region. The region is dominated by grasslands, shrublands, agricultural lands and forests (Figure 1). Various irrigation methods such as flood and center-pivot, sprinkler techniques during the growing season provide required water for crop growth (USGS Water Use in the United States, 2005).

## METHODOLOGY

### Modeling Approach

We used the Noah LSM in the High Resolution Land Data Assimilation System (HRLDAS) framework to simulate the surface fluxes, evapotranspiration, soil moisture, and soil temperature. The Noah LSM consists of four soil layers, one canopy layer and one snow layer. The soil layer depths are 10, 30, 60 and 100 cm from top to bottom. We have implemented this model in our earlier studies for the basin (Jaksa and Sridhar, in review; Jaksa 2011). The model is widely used in many studies (Radell and Rowe 2008; Hogue et al. 2005; Chen et al. 2003; Sridhar et al. 2002) and since it is also part of the

operational modeling system with the Weather and Forecasting (WRF) model (Sridhar, in review).

In order to evaluate the surface fluxes without the atmospheric component, the Noah LSM can also be implemented in the uncoupled within the HRLDAS platform (Chen et al., 2007). Input parameters required for HRLDAS are soil data, land cover types, green vegetation fraction and time invariant deep soil temperature. State Soil Geographic (STATSGO) database available at 1 km spatial scale is used as the input to define soil attributes. Moderate Resolution Imaging Spectroradiometer (MODIS) land cover dataset is used to define the land cover types. Green vegetation fraction (GVF) was based on 5 year monthly averages of Normalized Difference Vegetation Index (NDVI) calculated using 0.15° Advanced Very High Resolution Radiometer (AVHRR) data (Chen et al., 2007). The North American Regional Reanalysis (NARR) data of 32 km resolution provided all the meteorological and initialization data at 3 hourly intervals. Our Noah LSM implementation also included representation of irrigation in the Snake River basin since the current operational Noah LSM does not account for irrigation (Sridhar, in review).

We divided the study area in the model with 81 x 66 cells at 4 km resolution. All the meteorological and initialization data were interpolated spatially into model resolution and temporally into 1 hour by the HRLDAS platform. Model simulations were carried out for a 30-year period from 1 January 1979 to 31 December 2010 at hourly time steps, initializing at 00 hour of 1 January 1979. First two years, 1979 and 1980 were considered as a spin-up period. Spin-up time required for the LSM depends on the soil layer depth, hydraulic conductivity, root depth and persistence of snow cover in addition to other meteorological controls (Rodell et al. 2005). We analyzed the results for 30 years (1981-2010) to understand the hydroclimatology of evapotranspiration and other fluxes. Since Noah LSM is an uncoupled model which produces only land surface processes, results from the WRF model was used to study the near surface atmospheric properties, potential temperature, specific humidity and planetary boundary layer depth.

### **Irrigation Method**

The novel method of irrigation in the Noah LSM adds water to the first soil layer (0-10cm) to replenish soil moisture during the growing season from April to October. For the cells that are classified as irrigated cropland in the land use categories the model applies water periodically. In order to initiate irrigation, three parameters are used in the model. They are: 1) minimum percentage of soil moisture (MinPCT), which serves as an irrigation trigger, 2) the start date of the irrigation season, and 3) the end date. The thin first soil layer of 10 cm is subjected to direct evaporation and hence the first layer dries up faster than the other layers. Therefore the available soil moisture of the second soil layer (10-40 cm) was used to trigger irrigation which was compared with minimum soil moisture (MSM) to determine if irrigation was required. MSM is defined by

$$MSM = (\theta_{ref} - \theta_{wilt}) \times MinPCT + \theta_{wilt}$$

Where,  $\theta_{ref}$  and  $\theta_{wilt}$  are reference soil moisture (field capacity) and the soil moisture at the wilting point. In a step by step approach, firstly it was checked if the simulation date is within the irrigation season and if the grid is classified as an irrigated cropland. In the subsequent step, the available soil moisture is compared with MSM to decide if any irrigation is required at this time step. If the available soil moisture is below MSM, the soil moisture of the first soil layer is saturated at this time step as done by Adegoke et al. (2003) and Evans and Zaitchik (2008). The minimum percentage (MinPCT) used in this study is 50% which is a recommended threshold limit for many crops as the depletion level at which to start irrigation. We saturate the top layer and by gravity flow the soil layers below will receive the water. The water loss from runoff and losses during irrigation are not accounted here and it is assumed that enough water is available for fulfilling the demand.

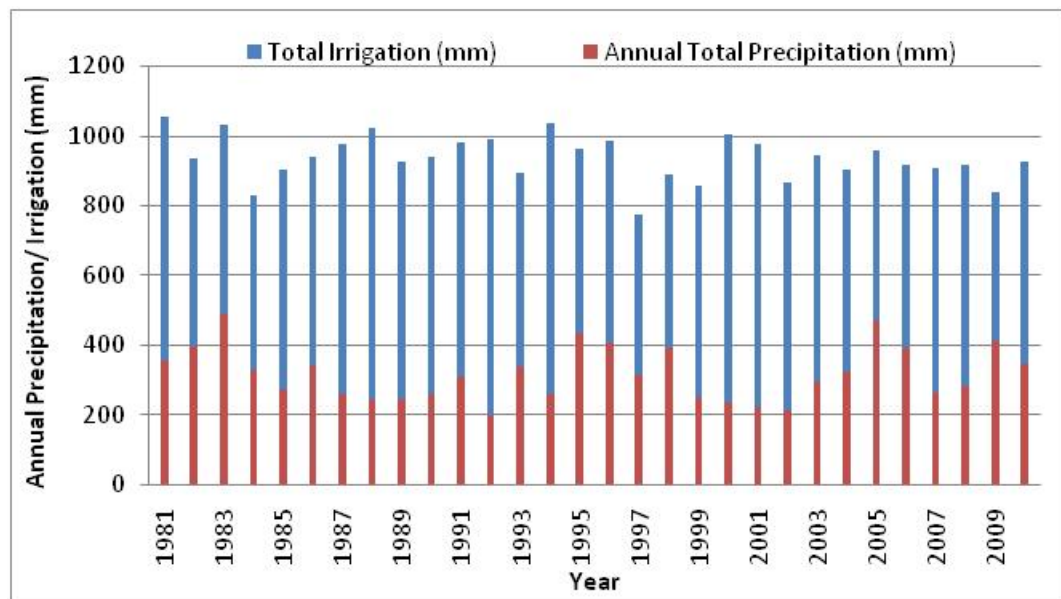


Figure 2. Noah LSM irrigation and precipitation as an average for croplands for the last 30 years (1981-2010).

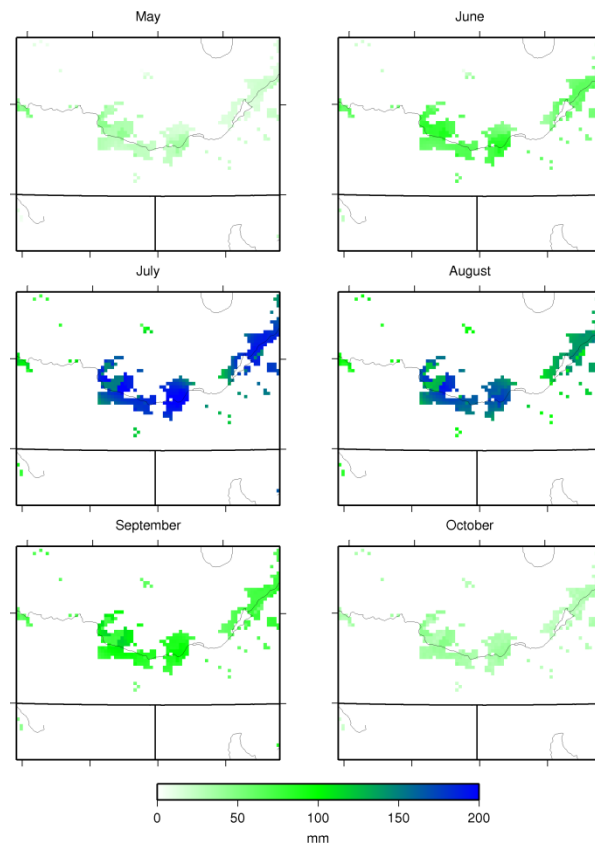


Figure 3. Differences in Monthly Total ET in Millimeters. The Values were Obtained by Subtracting ET Without Irrigation (NI) from ET With Irrigation (I): (I Minus NI) (Jaksa, 2011)

## RESULTS AND DISCUSSION

### Irrigation Demand

We analyzed the impacts of irrigation on the surface fluxes and ET. To avoid the cells with extreme cases, the area average values of all the variables over croplands were computed. Figure 2 shows the annual precipitation and irrigation averaged for the cropland cells in the domain. The total amount of irrigation water applied was approximately 620 mm per year over the past 30 years (1981- 2010) averaged over croplands which varied with the amount of total precipitation. When there was less precipitation, the model applied more water. In other words, the maximum amount of irrigation which was approximately 790 mm was recorded when the total annual precipitation was the minimum. It was in 1992 when precipitation was around 200 mm. However, when the maximum precipitation occurred in 1983, the applied irrigation was 540 mm which was not the minimum. It was because the most of precipitation within that year has occurred during November (80 mm) which was after the growing season. Therefore, the irrigation amount was not affected much as expected. Irrigation usually peaked in July and August with maximum number of events. Minimum irrigation was 430 mm in 2009 where precipitation was 410 mm.

### **Effects of Irrigation on Surface Fluxes and Evapotranspiration**

From the study area, the seasonal totals of ET substantially increased because of irrigation. Figure 3 shows the increment (Irrigated- NonIrrigated) of monthly total ET in the months during the growing season. The average increment over croplands is 169 mm in July. Throughout the whole irrigation period in 2010, an increased in ET by 540 mm was simulated. Added soil moisture due to irrigation within that year was 580 mm. Most of the water applied through irrigation has been converted to ET. It was also reported by Ozdogan et al (2010) that an increase in ET of up to 100% with irrigation was evident in some parts of United States. Even though the maximum increment was visible in July, as a percentage increase, August had the maximum percentage of increase in ET. The components of surface energy balance are affected by irrigation through soil moisture.

Increased soil moisture by irrigation changes the energy partitioning between the latent (LH) and sensible heat fluxes (SH). Since the irrigation induced changes happened only over croplands and there were no feedbacks provided to the atmosphere from the uncoupled LSM, the irrigation induced effects were limited only to the irrigated areas. The addition of irrigation water increased LH over agricultural areas which also increased ET. As a result SH was reduced over the same area. As an example, in July, LH was increased by  $11 \text{ W m}^{-2}$  while SH was decreased by  $10 \text{ W m}^{-2}$  averaged for the region. Changes in  $R_n$  and GH were minimal with increases up to  $1.6 \text{ W m}^{-2}$  and  $0.15 \text{ W m}^{-2}$ , respectively. Net radiation change could be attributed to surface cooling and increased near surface humidity (Cook et al. 2010).

Irrigation has cooled the surface with increased ET which possibly caused reduction in outgoing longwave radiation. Increased humidity resulted from increased ET created more downward longwave radiation. Due to these situations, net longwave radiation increases resulted in simultaneous increase in net radiation. Ground heat flux showed very small variations due to the cooled surface compared to other surface fluxes. Ground heat flux has increased up to July and decreased subsequently. The effects were pronounced during the peak growing months in this area, in July and August, when intensive irrigation takes place. Ozdogan et al. (2010) also showed the effects were significant mostly during July and August when considering the entire United States. According to the results the number of irrigation events was the maximum during July or August.

As average changes over the irrigated cropland during the growing season (April-October), LH increased by  $72 \text{ W m}^{-2}$  (193%), SH decreased by  $62 \text{ W m}^{-2}$  (91%), ground heat increased by  $0.34 \text{ W m}^{-2}$  (16%), and net radiation increased by  $11 \text{ W m}^{-2}$  (10%) in 2010.

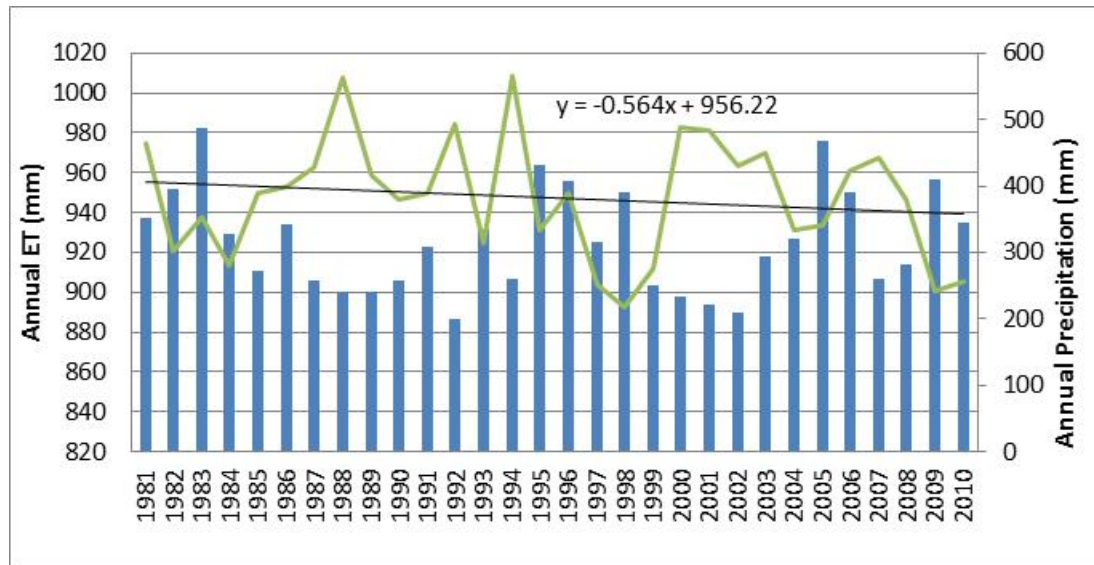


Figure 4. Annual Total ET and Precipitation in Croplands for the Past 30 Year Period from 1981- 2010. Annual Precipitation is Shown by Blue Bars, Annual ET is Shown by the Green Line and Black Line is the Trend Line for Annual ET. Equation for the Trend Line is Mentioned in the Figure (Jaksa, 2011).

### **Long Term Climatology of Surface Fluxes and Evapotranspiration**

Long term climatology of mean annual fluxes was analyzed for the past 30 years (Figure 4). Trends in radiation components for the domain show that solar radiation has increased by  $0.073 \text{ W m}^{-2} \text{ year}^{-1}$  over the past 30 year while long wave radiation has decreased by  $0.163 \text{ W m}^{-2} \text{ year}^{-1}$ . This can be caused by the reduction in cloud cover over this area. However, these effects can be related to the decreasing trend in net radiation ( $R_n$ ). There is also increase in temperature over the same period. This causes LH to increase (by  $0.074 \text{ W m}^{-2} \text{ year}^{-1}$ ) and to counterbalance this effect, SH reduced during the same time (by  $0.218 \text{ W m}^{-2} \text{ year}^{-1}$ ).

In order to study the inter-annual variations in surface fluxes, monthly average fluxes were studied by taking the spatial average values. Monthly mean fluxes calculated as averages for the whole domain for the 30 years. Variation in LH was higher during the summer especially in June and July when the LH was limited by the soil moisture, i.e. LH was most dependent on the precipitation. During the other seasons except summer, variation in  $R_n$  was very small and soil moisture was not limiting LH. Therefore the variation in LH was small. September and October show the least variation in SH for the past 30 years.  $R_n$  and GH showed least inter-annual variations for the past 30 years in terms of energy units. GH showed most variation during the cold months (in fall, winter and spring).

ET showed increasing trends for the natural vegetations in the region. As mentioned before, in dry natural ecosystems, the main driving force of ET during the summer was precipitation. Summer precipitation was greatly correlated with the summer ET in the

whole domain except some cells in high elevations. Hamlet et al. (2007) also found that the trends in warm season ET were more strongly influenced by the trends in warm season precipitation. Temperature is another driving force for ET which aids the uplift of atmospheric water/vapor creating or increasing the vapor pressure deficit. However, only croplands showed a positive relationship between temperature and ET while grasslands and shrublands did not show a strong response to the temperature change.

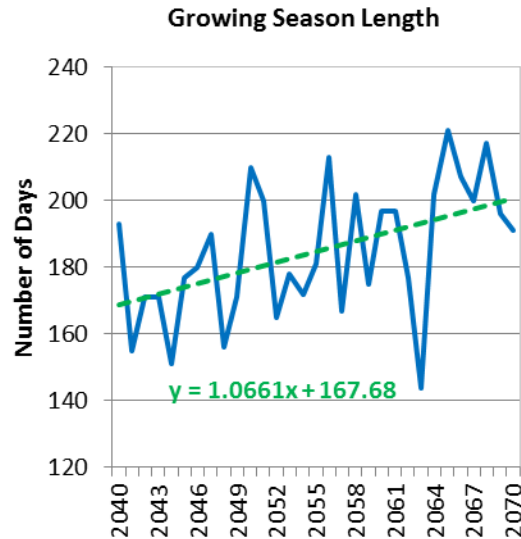


Figure 5. Increasing growing season lengths for the period between 2040-2070 in the Snake River Basin.

Growing season days, number of days where maximum temperature exceeded 90°F and minimum temperature dropped below 32°F and 0°F were examined from 2040-2070. Growing degree days with a base of 50°F were calculated and the growing season length exhibits an increase of +1.06 day/year (Figure 5). The number of days per year where the maximum temperature exceeded 90°F exhibited an increasing trend of +0.47 days/year. Lastly, the number of days per year where the minimum temperature dropped below 32°F displayed a decreasing trend of -0.70 days/year.

## CONCLUSIONS

Using an irrigation algorithm in Noah LSM, this study analyzed the impacts of irrigation and long term climatology of ET and surface fluxes. Average irrigation water added during the whole growing season for the past 30 years was 620 mm. This addition of moisture affected the surface energy budget mainly by increasing LH and decreasing SH.  $R_n$  increased slightly and GH was least affected. In 2010, total ET during the growing season was increased by 540 mm. The long term trends of ET increased by 0.78 mm year<sup>-1</sup> for the past 30 year over the whole domain. Two natural vegetation types, grasslands and shrublands had increasing trends of ET while croplands showed decreasing trends. The overall increasing trend in the domain can be explained with the majority of the natural vegetation with increasing trends. During the first decade (1981 – 1990), ET from grasslands and shrublands were decreasing and after that (1991 – 2010)

ET showed an increasing trend. However, in natural vegetation regions, ET was more related with annual precipitation where in croplands, main moisture input was from irrigation and ET did not depend on the precipitation. In the croplands, summer ET showed a great correlation with the summer temperature indicating the influence of summer temperature on summer ET.

Quantifying these long term trends in crop ET is relevant to manage our water resources sustainably. Also, the natural ecosystem's ET trends will help understand if it would have an impact on recharge of the aquifer system underneath the Snake River Plain.

## REFERENCES

- Adegoke, J.O., R.A. Pielke, J. Eastman, R. Mahmood, and K.G. Hubbard, 2003. Impact of irrigation on midsummer surface fluxes and temperature under dry synoptic conditions: A regional atmospheric model study of the U.S. High Plains. *Monthly Weather Review* 131: 556-564.
- Chen, F., D.N. Yates, H. Nagai, M.A. Lemone, K. Ikeda, and R.L. Grossman, 2003. Land surface heterogeneity in the cooperative atmosphere surface exchange study (CASES-97). Part I: Comparing model surface flux maps with surface-flux tower and aircraft measurements. *Journal of Hydrometeorology* 4: 196-218.
- Chen, F., K.W. Manning, M.A. LeMone, S.B. Trier, J.G. Alfieri, R. Roberts, M. Tewari, D. Niyogi, T.W. Horst, S.P. Oncley, J.B. Basara, and P.D. Blanken, 2007. Description and evaluation of the characteristics of the NCAR high-resolution land data assimilation system. *Journal of Applied Meteorology and Climatology* 46: 694-713.
- Cook, B.I., M.J. Puma, and N.Y. Krakauer, 2010. Irrigation induced surface cooling in the context of modern and increased greenhouse gas forcing. *Climate Dynamics* DOI: 10.1007/s00382-010-0932-x.
- Evans, J.P., and B.F. Zaitchik, 2008. Modeling the large-scale water balance impact of different irrigation systems. *Water Resources Research* 44: W08448, doi:10.1029/2007WR006671.
- Hamlet, A.F., P.W. Mote, M.P. Clark and D.P. Lettenmaier, 2007. Twentieth-century trends in runoff, evapotranspiration, and soil moisture in the Western United States. *Journal of Climate* 20: 1468-1486.
- Hogue, T.S., L. Bastidas, H. Gupta, S. Sorooshian, K. Mitchell, and W. Emmerich, 2005. Evaluation and transferability of the Noah land surface model in semiarid environments. *Journal of Hydrometeorology* 6: 68-84.
- Jaksa, W.T.A., 2011. Assessing the surface energy-balance components in the Snake River Basin, M.S Thesis, Department of Civil Engineering, Boise State University, pp 180.

- Jaksa, W.T.A., and V. Sridhar, 2013. Simulating long-term evapotranspiration climatology using the offline Noah Land Surface Model, *Journal of Contemporary Water Research and Education*, (in review)
- Kjelstrom, L.C., 1995. Streamflow gains and losses in the Snake River and ground-water budgets for the Snake River Plain, Idaho and eastern Oregon. *US Geological Survey Water-Resources Investigation Report: 03-4244*.
- Ozdogan, M., M. Rodell, H.K. Beaudoin, and D.L. Toll, 2010. Simulating the effects of irrigation over the United States in a land surface model based on satellite-derived agricultural data. *Journal of Hydrometeorology* 11: 171-184.
- Pielke, R. A., A. Pitman, D. Niyogi, R. Mahmood, C. McAlpine, F. Hossain, and N. De Noblet, 2011. Land use/land cover changes and climate: modeling analysis and observational evidence. *Wiley Interdisciplinary Reviews-Climate Change*, 2(6), 828–850. doi:10.1002/wcc.144
- Radell, D.B., and C.M. Rowe, 2008. An observational analysis and evaluation of land surface model accuracy in the Nebraska Sand Hills. *Journal of Hydrometeorology* 9: 601-621.
- Rodell, M., P.R. Houser, A.A. Berg, and J.S. Famiglietti, 2005. Evaluation of 10 methods for initializing a land surface model. *Journal of Hydrometeorology* 6: 146-155.
- Sridhar, V., 2013. Tracking the influence of irrigation on land surface fluxes and boundary layer climatology, *Journal of Contemporary Water Research and Education*, (in review)
- Sridhar, V., R.L. Elliott, F. Chen, and J.A. Brotzge, 2002. Validation of the NOAH\_OSU land surface model using surface flux measurements in Oklahoma. *Journal of Geophysical Research* 107: 4418, doi:10.1029/2001JD001306.

# SENSITIVITY ANALYSIS OF SENSOR ACCURACY FOR THE ASCE STANDARDIZED EVAPOTRANSPIRATION EQUATION

Kendall DeJonge<sup>1</sup>

## ABSTRACT

Quantification of evapotranspiration (ET) in arid and semi-arid climates is becoming of increasing importance throughout the world, thus understanding input variability of relevant sensors is of paramount importance as well. The Colorado Agricultural and Meteorological Network (CoAgMet) utilizes an array of sensors to acquire micrometeorological data (temperature, humidity, wind speed, and solar radiation) and uses the ASCE Standardized Reference ET Equation to determine geographically local reference ET values. Previous studies have relied on “local” or single-factor sensitivity analysis to determine the effect of input parameter variability; however these methods do not take into account the interactions between variables, nor have used quantified accuracy bounds set by sensor instrumentation. The objective of this study is to evaluate manufacturer quoted accuracy using local sensitivity analysis, and to compare seasonal potential variability or bias caused by sensor error. Fifteen years of data were used from a micrometeorological station near Greeley, Colorado. Local sensitivity results were shown in terms of daily potential bias of computed reference ET, separated by monthly averages. The reference ET equation was most sensitive to wind input accuracy with seasonal (April – September) potential bias of 60mm, followed by solar radiation with potential bias of 30mm. Effects of temperature and humidity (which are obtained by the same sensor) combined for a potential seasonal bias of 20mm. Global sensitivity analysis results are given in the presentation.

## INTRODUCTION

In irrigated agriculture, accurate and consistent estimates of crop evapotranspiration ( $ET_c$ ) are very important in terms of water management. At the field scale accurate estimates of ET can be used for irrigation scheduling, whereas at regional scales knowledge of ET consumption can be used to evaluate irrigation water resources planning and distribution. However, because ET is very difficult to measure directly, it is often estimated using models based on climactic inputs, which can be highly variable.

### **ASCE-ET Equation**

The most common method to estimate  $ET_c$  is to transform a reference evapotranspiration ( $ET_o$  or  $ET_r$ ) by multiplying with a crop coefficient ( $K_c$ ). The  $K_c$  is unique to each crop, and can vary with several factors affecting ET such as leaf area, soil and climate conditions, and crop stresses to name a few (Doorenbos and Kassam, 1979). While many methods exist to calculate reference ET, physically based approaches (e.g., FAO56 P-M, (Allen et al., 1998)) require more input data but are generally accepted as the most accurate estimation. In 2005, the ASCE-EWRI created a standardized version of this

---

<sup>1</sup> USDA-ARS Water Management Research Unit, Fort Collins, CO. [kendall.dejonge@ars.usda.gov](mailto:kendall.dejonge@ars.usda.gov)

equation for reference ET calculation (ASCE, 2005), which lends the advantages of bringing increased commonality to the methodology for using and evaluating reference ET data, and using a standardized calculated evaporative demand for the transferability of  $K_c$  values (Irmak et al., 2006).

### **Field Sensor Accuracy**

Field sensor accuracy is of paramount importance when determining reference ET using a physical model. Droogers and Allen (2002) evaluated reference ET estimates using both the P-M (Allen et al., 1998) and Hargreaves (Hargreaves and Riley, 1985) methods, and concluded that the more data intensive P-M method is recommended if accurate weather data collection is expected, but if data was suspect the simpler Hargreaves method should be considered. While issues such as station siting, proper fetch, and maintaining adequate reference conditions are very important in creating consistent measurement conditions, bias or other measurement errors associated with the sensors themselves can cause tremendous error in the final outputs of the equations. Therefore, it is desirable to fully understand the potential influence of measurement error on the final reference ET calculation.

Manufacturers of measuring devices typically quote an “accuracy” of the device, often in terms of  $\pm$  a percentage or static value. While it is generally accepted that any measurement from the device will fall within this range, it is rarely specified what the probability is that the measurement accuracy will fall within the range given. For example, if the quoted accuracy of a temperature sensor is  $\pm 2$  °C, it is unclear whether this is true all of the time, 99.9% of the time, 95% of the time, etc. Furthermore, because these quoted accuracy limits are not given a quantified probability, neither is the distribution of potential error. One may assume that the mean of all relative error values would be zero and that the error may be normally distributed around this value, the lack of information suggests that the distribution could just as likely be assumed uniform.

### **Sensitivity Analysis**

Saltelli et al. (2004) defined sensitivity analysis (SA) as “the study of how uncertainty in the output of a model (numerical or otherwise) can be apportioned to different sources of uncertainty in the model input.” The aim of SA is to determine how sensitive the output of a model is with respect to the elements of the model which are subject to uncertainty or variability. SA methods are typically classified as local (i.e., derivative-based) or global (Saltelli et al., 2008). When the purpose of the SA is to study the effects of several input parameters on the model output responses, local SA (e.g., one-factor-at-a-time or OAT) is more simple but less useful than global sensitivity analysis (GSA) where the output variability is evaluated while the input factors vary in their individual uncertainty domains (Monod et al., 2006). GSA methods, such as Morris (1991), Fourier Amplitude Sensitivity Test (FAST, (Saltelli et al., 1999)), and Sobol’ (1993) can determine not only sensitivity to individual factors, but sensitivity to interactions between factors as well.

Several studies have performed SA on ET estimation equations, but results vary by location and none have conducted a variance-based global sensitivity analysis. Ley et al. (1994a) conducted a model sensitivity analysis of the 1982 Kimberly Penman alfalfa ET<sub>r</sub> model to errors in parameters and weather data in Washington state, and in a companion paper (Ley et al., 1994b) evaluated the effects of sensor measurement variability in the equation, finding that at the limits of accuracy specification, the greatest ET error was from solar radiation measurement error, followed by dewpoint, maximum temperature, and finally wind speed measurement errors. However, in most other relevant studies, variability of inputs was chosen without basis on actual sensor accuracy. Liang et al. (2008) used a non-dimensional local sensitivity coefficient to evaluate Penman-Monteith monthly and annual ET<sub>o</sub>, evaluating six meteorological stations in Northeastern China. They found that humidity was the most influential input, closely followed by temperature in the summer. Porter et al. (2012) performed a local and two-input semi-global (temperature and wind) SA using fourteen years of data in Bushland, TX, finding that ET is most sensitive to errors in wind speed and air temperature. Bakhtiari and Liaghat (2011) evaluated linear sensitivity of daily ET<sub>o</sub> in semi-arid Iran, determining that ET<sub>o</sub> was most sensitive to vapor pressure deficit (which can be derived from humidity), followed by wind.

### **Objective**

Many recent studies have explored local SA of climatic input variables in evapotranspiration models. However, these studies have varying results, and few of them have used sensor accuracy limits as the basis for their comparison. Thus, the objective of this study is to evaluate manufacturer quoted accuracy using local sensitivity analysis, and to compare seasonal potential variability or bias caused by sensor error, using the ASCE Standardized Reference Evapotranspiration Equation.

## **METHODS**

### **ASCE-ET Standardized Reference ET Equation**

The ASCE Standardized Reference Evapotranspiration Equation is intended to simplify the full form ASCE Penman-Monteith method:

$$ET_{SZ} = \frac{0.408\Delta(R_n - G) + \gamma \frac{c_n}{T + 273} u_2 (e_s - e_a)}{\Delta + \gamma(1 + C_d u_2)} \quad (1)$$

where  $ET_{SZ}$  is the standardized reference crop ET rate for short ( $ET_{os}$ ) or tall ( $ET_{rs}$ ) surfaces ( $\text{mm d}^{-1}$ ),  $R_n$  the net radiation flux density at the surface ( $\text{MJ m}^{-2} \text{d}^{-1}$ ),  $G$  the sensible or soil heat flux density from the surface to the soil ( $\text{MJ m}^{-2} \text{d}^{-1}$ ),  $\gamma$  the psychrometric constant ( $\text{kPa } ^\circ\text{C}^{-1}$ ),  $T$  is mean air temperature ( $^\circ\text{C}$ ),  $U_2$  is wind speed ( $\text{m s}^{-1}$ ) at 2 m above the ground (relative humidity and dew point are also assumed to be measured at this height),  $e_s$  is mean saturated vapor pressure (kPa) computed as the mean vapor pressure as calculated at the daily minimum and maximum temperature,  $e_a$  the actual vapor pressure of the air (kPa), and  $\Delta$  the slope of the saturation vapor pressure

versus temperature curve ( $\text{kPa } ^\circ\text{C}^{-1}$ ).  $C_n$  and  $C_d$  are constants that change with reference type and calculation time step: for hourly time steps  $C_n$  is 37 for short reference and 66 for tall reference, whereas  $C_d$  is 0.24 (day) or 0.96 (night) for short reference and 0.25 (day) and 1.7 (night) for tall reference (ASCE, 2005). Variables  $\Delta$  and  $e_s$  are calculated from temperature, and  $e_a$  can be determined by temperature and relative humidity. A VBA model was created to calculate  $\text{ET}_{os}$  (short crop grass-based reference ET) based on hourly inputs, and was verified using RefET v3.1 software (Allen, 2011).

### CoAgMet Station and Sensors

The Colorado Agricultural Meteorological Network (CoAgMet) is a network of automated weather stations (Figure 1) distributed across the state of Colorado (<http://ccc.atmos.colostate.edu/~coagmet/>). Dating back to 1992 for select stations, the website provides weather and crop water use data in several formats, including hourly, daily, or monthly summaries (Andales et al., 2009). A main intent of the network is to provide crop water use or ET estimates for irrigation scheduling, using the ASCE Standardized Reference ET Equation for a tall reference crop (similar to 50 cm tall alfalfa), and crop coefficient ( $K_c$ ) values obtained from past experiments in Colorado.

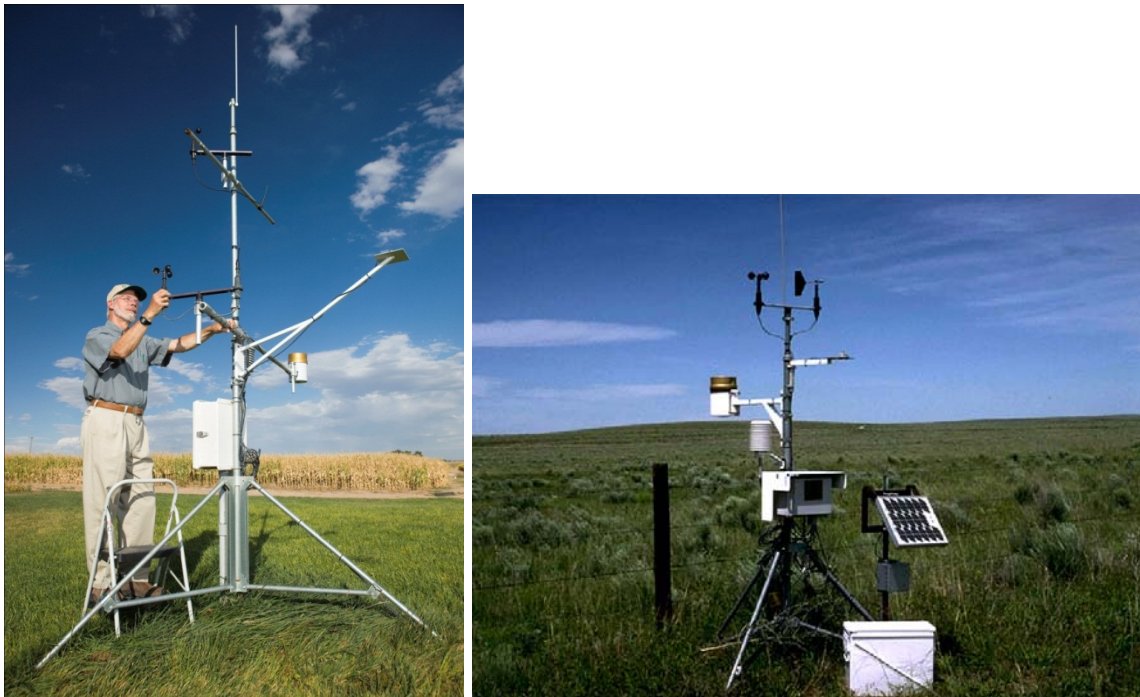


Figure 1. Example Siting of CoAgMet Stations GLY04 (left) and HYK02 (right).

Data was taken from GLY03 station near Greeley, CO. Hourly data used was from 1993-2005, or 15 total years. Any missing data was replaced with nearby Lucerne station, and in some rare cases where Lucerne was unavailable, missing data was replaced with the same day of year (DOY) 2011 or 2012 data from the similarly located GLY04 station, also near Greeley, CO. Erroneous wind data, often during freezing temperatures where the anemometer could freeze, was replaced with data for the same DOY created by

WindGen software (Skidmore and Tatarko, 1990). A list of station sensors and quoted accuracies is given (Table 1 and Figures 2 and 3).

Table 1. Sensors and Rated Accuracies (www.campbellsci.com).

Sensor	Reading	Unit	Quoted Accuracy
Vaisala HMP45C	Temperature	°C	$\pm[0.2+(T-20)*0.005]$ (from Fig. 2)
	Humidity	%	$\pm 2\%$ RH (0 to 90% RH) $\pm 3\%$ RH (90 to 100% RH)
			Temperature dependence: $\pm 0.05\%$ RH/°C
R.M. Young Wind Sentry	Wind Speed	$\text{m s}^{-1}$	$\pm 0.5 \text{ m s}^{-1}$
LI-COR LI200X	Solar Radiation	$\text{kW m}^{-2} \text{ min}^{-1}$	$\pm 5\%$ maximum $\pm 3\%$ typical

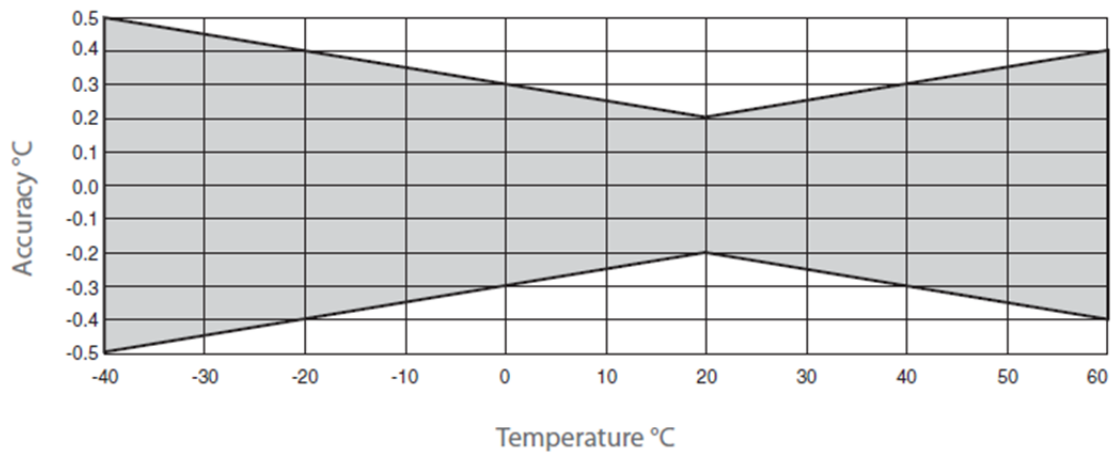


Figure 2. Temperature Accuracy Variability.

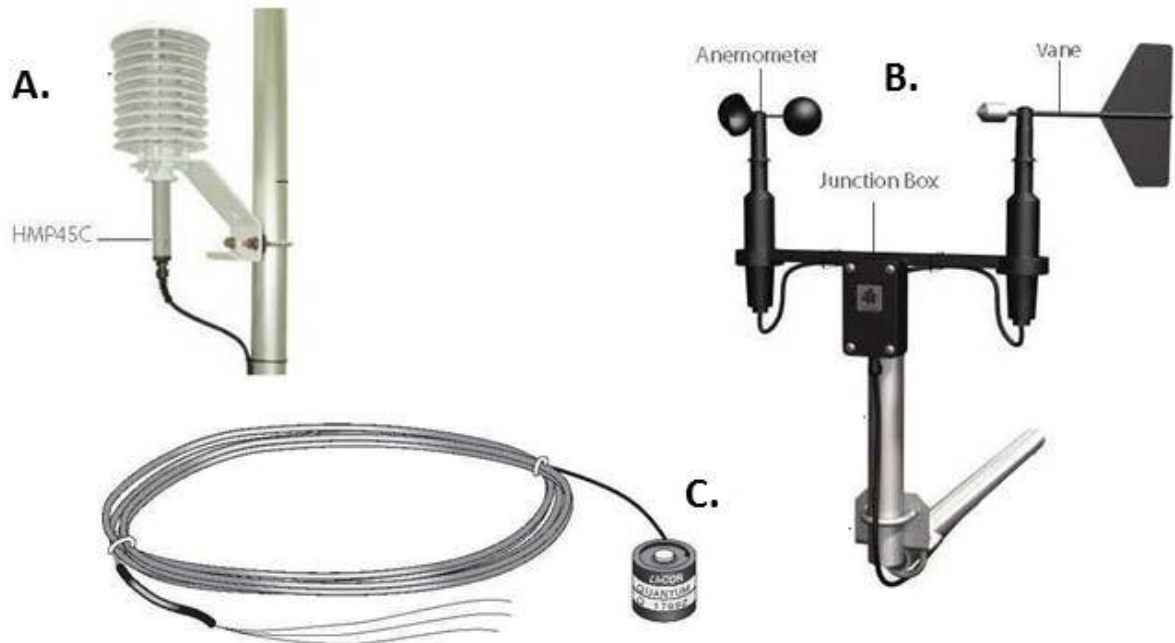


Figure 3. Sensors Analyzed in Study: **A.**Vaisala HMP45C with protective cover. **B.** R.M. Young Wind Sentry. **C.** LI-COR LI200X.

While the ASCE manual suggests data QA/QC to look for systematic or bias error, in the case of this study it was not performed. This systematic error is different than random sensor error, which is described in Table 1 and is the focus of this study. A few exceptions were made for numerical stability reasons, for example relative humidity, wind speed, and solar radiation have physical limits that may be prone to measurement error (for example, all relative humidity measurements over 100% are set to 100%, and all wind and solar radiation measurements less than zero are set to zero). Monthly trends for the input dataset are shown in Figure 4, and  $ET_{os}$  as determined from the model and input dataset is shown in Figure 5.

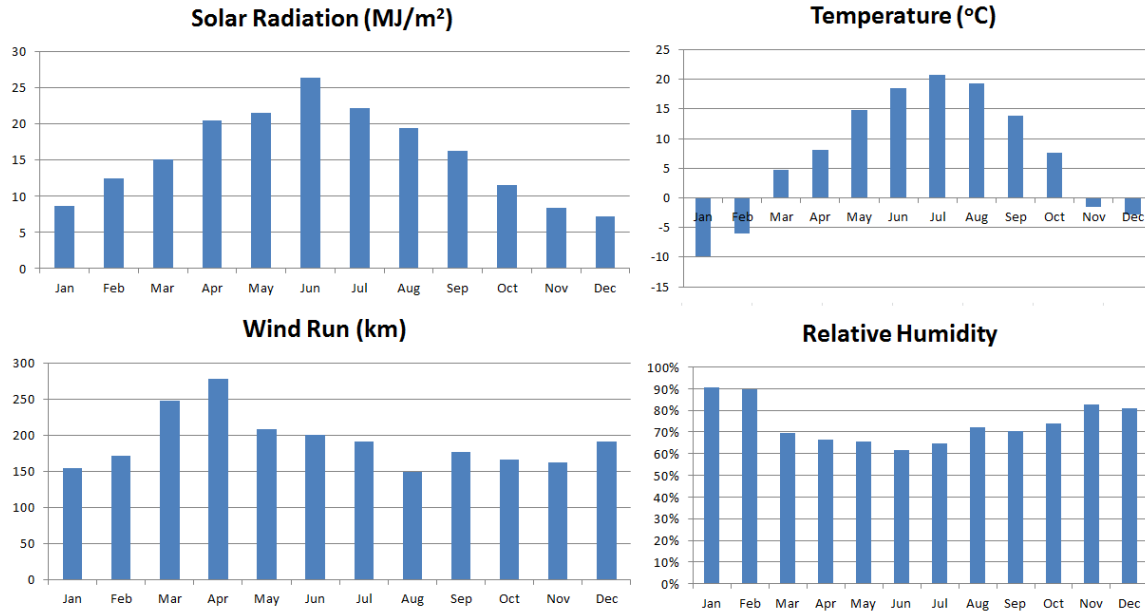


Figure 4. Average Daily Meteorological Inputs by Month for Input Dataset.

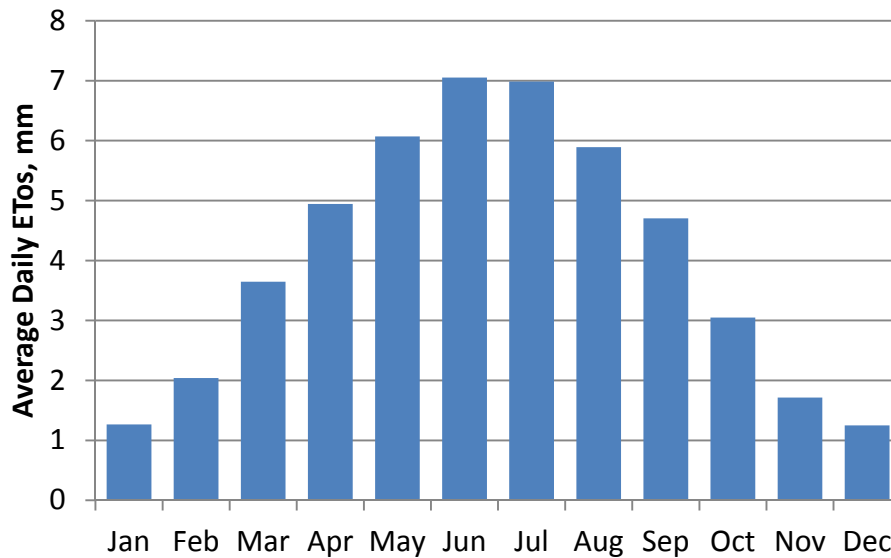


Figure 5. Average Daily ET<sub>os</sub> by Month.

### Sensitivity Analysis and Evaluation

In general, SA is the study of how the variation of the output of a model can be apportioned to different sources of variation of input data (Saltelli et al., 2000). Sensitivity analyses are typically classified as either local sensitivity analysis or global sensitivity analysis (Saltelli et al., 2000). Local SA examines the local response of model output responses by varying input parameters one at a time while holding other parameters at fixed values. GSA characterizes methods that possess two basic properties (Saltelli et al., 2000): (i) multiple parameters are varied simultaneously, and (ii)

sensitivity is measured over the entire range of each input factor. In this early print version of the study, only results of local SA are shown, preliminary results of GSA will be shown in the oral presentation.

For local sensitivity, each of the sensors' outputs were biased by values within the quoted accuracies shown in Table 1, specifically at maximum and half maximum levels of accuracy for temperature, humidity, temperature dependent humidity, and wind. For solar radiation, "maximum" accuracy of  $\pm 5\%$  and "typical" accuracy of  $\pm 3\%$  were evaluated, as well as  $\pm 1\%$  of base values. All hourly values in the input parameter of interest were adjusted (biased), and daily  $ET_{os}$  was calculated based on this new dataset. To evaluate daily mean bias in simple terms, daily results were averaged by month (for example, the average  $ET_{os}$  of a July day, found from all July days in the 15 year dataset). Monthly total bias was found by multiplying the total days in the month by the daily mean bias for that month.

## RESULTS

Monthly potential random error for each input parameter, with limits based on quoted accuracy estimates (Table 1), are shown in Figure 6. Temperature (a), relative humidity (b), and relative humidity as a function of temperature (c) individually had relatively small error due to sensor accuracy, with respective  $\pm 1.0$ ,  $\pm 1.5$ , and  $\pm 1.5$  mm/month error in the month of July (the month with the highest  $ET_o$ ). However, considering that these three graphs are likely interactive and that they all come from the same Vaisala HMP45C sensor, it was worthwhile to combine these three figures into an additive potential error (d) which shows the greatest potential monthly error as  $-4.2$  and  $4.1$  mm.  $ET_o$  showed the highest linear sensitivity to wind input accuracy (e), with monthly potential error of  $-14.1$  and  $13.1$  mm for July. Solar radiation was also an influential input, with monthly potential error of  $-6.7$  and  $7.0$  mm in July at "maximum" error levels, and  $-4.0$  and  $4.2$  mm for "typical" error levels.

On a seasonal basis, one can get a better sense of the potential random error within a growing season. For example, if one considers that many summer seasonal crops are grown between the months of March and September, finding the potential error over this time will help compare the magnitude of relative sensitivities. The combined effects of temperature and relative humidity have seasonal total error limits of  $-21.5$  and  $21.3$  mm, whereas the same limits are  $-62.2$  and  $59.9$  mm for wind, and  $-29.9$  and  $31.9$  mm for solar radiation.

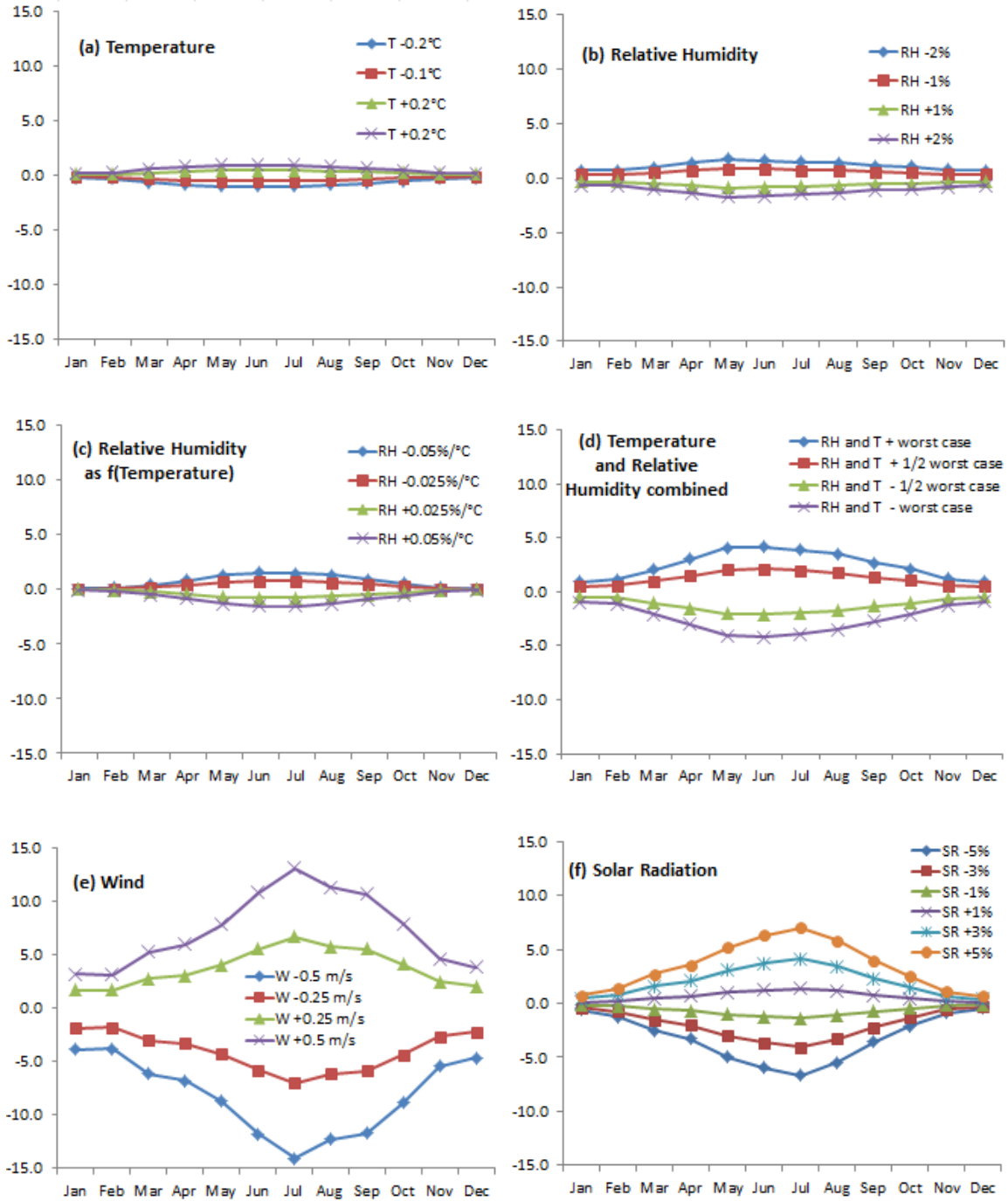


Figure 6. Monthly Total Potential Error (mm) in  $ET_{os}$  From Percentage Error of Accuracy Estimates Shown in Table 1.

## CONCLUSIONS

In a multiple-input model such as the ASCE Standardized Reference Evapotranspiration Model, it is important to understand potential errors of input data. Considering the quoted manufacturer accuracy of the three sensors (with four relevant inputs and five separate sources of error), it is desirable to rank these sensors in order of importance and potential error in calculating reference  $ET_{os}$ . Sensitivity analysis was completed, with monthly sensitivities weighted by the monthly average  $ET_{os}$  experienced over a 15-year dataset.

Linear sensitivity analysis showed wind to be the input in the equation that contributes to the most potential random error, with seasonal (April-September) potential error of over 60 mm. Solar radiation was the next most important input, with seasonal potential error over 30 mm. Temperature and humidity themselves have relatively small potential error, but by combining the effects of these two inputs (which is logical considering they are part of the same physical sensor), seasonal potential error can be as high as 21 mm.

Global sensitivity analysis results are in progress, and preliminary results will be shown in the oral presentation for the USCID Conference.

## REFERENCES

Allen, R.G., 2011. Ref-ET: Reference evapotranspiration calculation software for FAO and ASCE standardized equations, University of Idaho, pp. 76.

Allen, R.G., Pereira, L.S., Raes, D. and Smith, M., 1998. Crop evapotranspiration: guidelines for computing crop water requirements, FAO irrigation and drainage paper. Food and Agriculture Organization of the United Nations, Rome.

Andales, A.A., Bauder, T.A. and Doesken, N.J., 2009. The Colorado Agricultural Meteorological Network (CoAgMet) and Crop ET Reports, Colorado State University Extension.

ASCE, 2005. The ASCE standardized reference evapotranspiration equation, ASCE-EWRI, Reston, VA.

Bakhtiari, B. and Liaghat, A.M., 2011. Seasonal Sensitivity Analysis for Climatic Variables of ASCE-Penman-Monteith Model in a Semi-arid Climate. *Journal of Agricultural Science and Technology*, 13: 1135-1145.

Doorenbos, J. and Kassam, A.K., 1979. Yield Response to Water, FAO, United Nations, Rome.

Droogers, P. and Allen, R.G., 2002. Estimating Reference Evapotranspiration Under Inaccurate Data Conditions. *Irrigation and Drainage Systems*, 16(1): 33-45.

- Hargreaves, G. and Riley, J., 1985. Agricultural Benefits for Senegal River Basin. *Journal of Irrigation and Drainage Engineering*, 111(2): 113-124.
- Irmak, S., Martin, D., Irmak, A. and Howell, T., 2006. Sensitivity analyses and sensitivity coefficients of standardized daily ASCE-Penman-Monteith equation. *Journal of Irrigation and Drainage Engineering*, 132(6): 564-578.
- Ley, TW, RW Hill, and DT Jensen, 1994a. Errors in Penman-Wright Alfalfa Reference ET Estimates: I. Model Sensitivity Analyses. *Transactions of ASAE*, 37(6): 1853-1861.
- Ley, TW, RW Hill, and DT Jensen, 1994b. Errors in Penman-Wright Alfalfa Reference ET Estimates: II. Effects of Weather Sensor Measurement Variability. *Transactions of ASAE*, 37(6): 1863-1870.
- Liang, L., Li, L., Zhang, L., Li, J. and Li, B., 2008. Sensitivity of penman-monteith reference crop evapotranspiration in Tao'er River Basin of northeastern China. *Chinese Geographical Science*, 18(4): 340-347.
- Monod, H., Naud, C. and Makowski, D., 2006. Uncertainty and sensitivity analysis for crop models. In: D. Wallach, D. Makowski and J.W. Jones (Editors), *Working with Dynamic Crop Models*. Elsevier, Amsterdam, The Netherlands, pp. 55-99.
- Morris, M.D., 1991. Factorial sampling plans for preliminary computational experiments. *Technometrics*, 33(2): 161-174.
- Porter, D. et al., 2012. Sensitivity of grass- and alfalfa-reference evapotranspiration to weather station sensor accuracy. *Applied Engineering in Agriculture*, 28(4): 543-549.
- Saltelli, A., Chan, K. and Scott, E.M., 2000. *Sensitivity Analysis*. Wiley series in probability and statistics. Wiley, Chichester, England.
- Saltelli, A. et al., 2008. *Global Sensitivity Analysis: The Primer*. John Wiley, Chichester, England.
- Saltelli, A., Tarantola, S., Campolongo, F. and Ratto, M., 2004. *Sensitivity Analysis in Practice: A Guide to Assessing Scientific Models*. Wiley, Chichester ;.
- Saltelli, A., Tarantola, S. and Chan, K.P.S., 1999. A quantitative model-independent method for global sensitivity analysis of model output. *Technometrics*, 41(1): 39-56.
- Skidmore, E.L. and Tatarko, J., 1990. Stochastic wind simulation for erosion modelling. *Transactions of ASAE*, 33: 1893-1899.
- Sobol', I.M., 1993. Sensitivity analysis for non-linear mathematical models. *Mathematical Modelling and Computer Experiments*, 1: 407-414.



## DEVELOPMENT AND DISTRIBUTION OF CROP COEFFICIENTS VIA REMOTE SENSING IN CALIFORNIA'S SAN JOAQUIN VALLEY

Byron Clark<sup>1</sup>  
Deepak Lal<sup>2</sup>  
Kris Lynn-Patterson<sup>3</sup>  
Blake Sanden<sup>4</sup>  
Bryan Thoreson<sup>5</sup>

### ABSTRACT

A web-based map interface has been developed that provides historical information describing crop water use (evapotranspiration) for individual fields in the southern San Joaquin Valley of California for the 2008 irrigation season. The data and map interface were developed by the GIS team at the University of California Kearney Agricultural Research and Extension Center in cooperation with the University of California Cooperative Extension and SEBAL North America. For individual fields, growers can review the actual evapotranspiration (ET) by the crop present at the field and compare ET rates and crop coefficient against fields with the same crop in the region.

Time series graphs of crop coefficients and actual daily evapotranspiration are provided based on analysis of 14 Landsat satellite images spanning February to November 2008 using the Surface Energy Balance Algorithm for Land (SEBAL). A crop is selected, and time series of crop coefficients and evapotranspiration rates for similar fields are shown for comparison to the field of interest. This tool allows growers to review historical water use for their fields and crops to support evaluation of irrigation practices and planning of future irrigation water application amounts and timing. In the future, the interface could be updated to include more recent data or to include additional growing regions.

Comparison of SEBAL-based crop coefficients to standard crop coefficients used for irrigation scheduling of mature crops demonstrates a wide degree of variability in ET among fields of the same crop. Additionally, published crop coefficients may require adjustment to more accurately account for actual growing conditions in some cases to support both field-scale irrigation management and estimation of regional ET. There may be opportunities to increase water use efficiency (defined herein for discussion purposes as the ratio of crop yield to total applied irrigation water) at the field scale in some cases, depending upon the field-specific factors affecting crop ET and existing irrigation practices.

---

<sup>1</sup> Davids Engineering, Inc., 1772 Picasso Avenue, Suite A, Davis, CA 95618, [www.davidsengineering.com](http://www.davidsengineering.com), [byron@de-water.com](mailto:byron@de-water.com)

<sup>2</sup> Davids Engineering, Inc., 1772 Picasso Avenue, Suite A, Davis, CA 95618, [deepak@sebal.us](mailto:deepak@sebal.us)

<sup>3</sup> University of California, Kearney Agricultural Research and Extension Center, 9240 S. Riverbend Ave. Parlier, CA 93648, [klynn@ucanr.edu](mailto:klynn@ucanr.edu)

<sup>4</sup> University of California, Kern County Cooperative Extension, 1031 South Mount Vernon Avenue, Bakersfield, CA, 93307, [blsanden@ucdavis.edu](mailto:blsanden@ucdavis.edu)

<sup>5</sup> Davids Engineering, Inc., 1772 Picasso Avenue, Suite A, Davis, CA 95618, [bryant@de-water.com](mailto:bryant@de-water.com)

## INTRODUCTION

The University of California Kearney Agricultural Research and Extension Center and Kern County Cooperative Extension worked with SEBAL North America to develop crop coefficients based on satellite remote sensing in the southern San Joaquin Valley of California. This applied research project applied remote sensing to develop crop coefficients based on a large area of crops and actual growing conditions. Crop coefficients from SEBAL were quantified by crop and general soil type for more than 59,000 individual fields representing approximately 3 million acres. Additionally, ground based estimates of ET and crop coefficients were developed using (1) eddy covariance, (2) surface renewal, and (3) soil water content depletion and applied irrigation minus deep percolation analysis of ET for several fields. The remotely-sensed crop coefficients, disseminated through a web-based user interface developed as part of the project, can be applied to improve ET estimates at multiple scales from individual fields to the region as a whole.

Approximately 70% of water applied for irrigation in the southern San Joaquin Valley is consumed as evaporation or transpiration and lost to the atmosphere (DWR, 2010). The remaining 30% leaves the field as surface runoff or deep percolation. In some cases, reduction in irrigation could result in increased water supply, better control of available supplies, improved water quality in downstream surface or groundwater bodies, and/or energy conservation.

The purpose and objective of this project was to improve understanding of the amount of water consumed by crops for individual fields and to make the information available to irrigators and water planners. To satisfy the project objective, a remote sensing analysis of crop consumption of water (i.e., “evapotranspiration” or ET) was conducted using the Surface Energy Balance Algorithm for Land (SEBAL) for the southern San Joaquin Valley in 2008. ET values for individual fields were converted to crop coefficients based on reference ET ( $ET_0$ ) and are available to irrigators and water planners through a web-based map interface ([webgis.uckare.org/prop50](http://webgis.uckare.org/prop50)) (Figure 1).

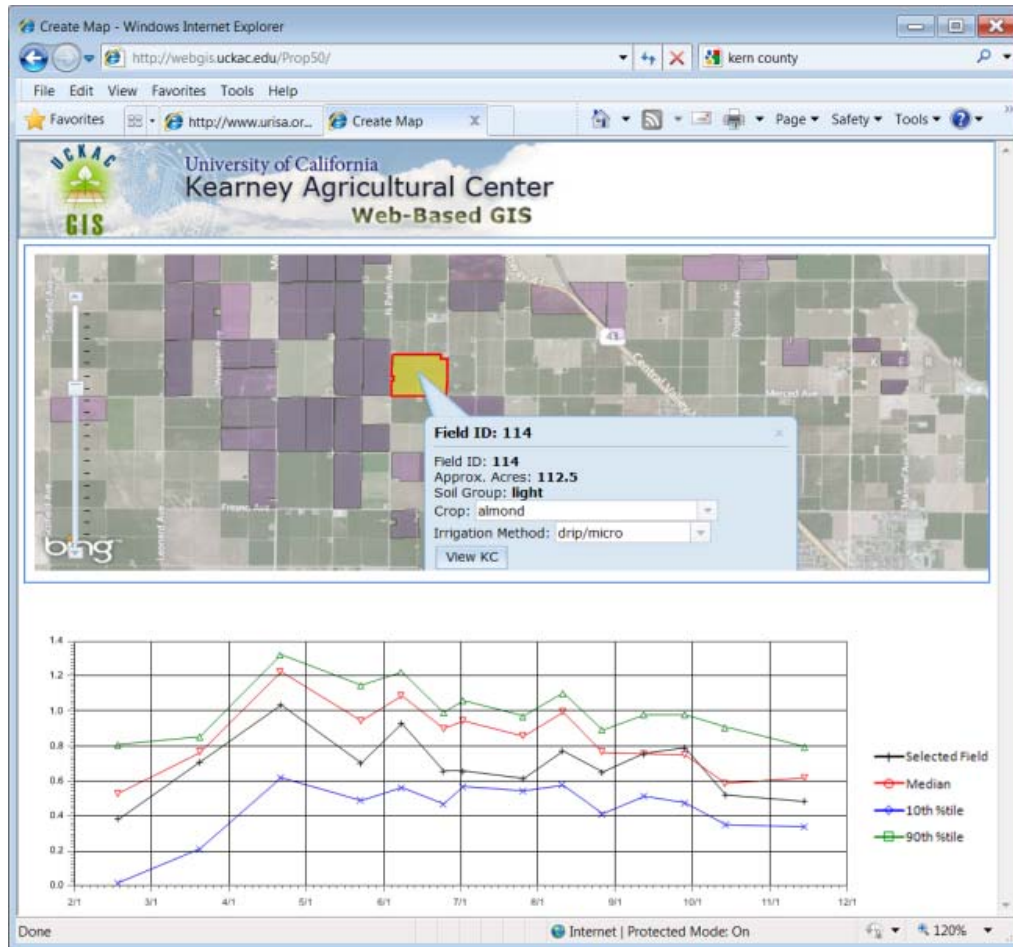


Figure 1. Web Interface to Distribute Field-Specific Crop Coefficients.

## METHODOLOGY

The consumptive use of water by crops or evapotranspiration (ET) represents the combined process of evaporation and transpiration. ET is typically expressed as a depth of water over a given area for a specified time period. In this study actual ET ( $ET_a$ ), which reflects the ET rate for individual fields under actual growing conditions (as compared to potential ET estimated based on published estimates of crop coefficients multiplied by  $ET_o$ ), was estimated using the Surface Energy Balance Algorithm for Land (SEBAL, Bastiaanssen et al. 2005) for the southern San Joaquin Valley for 2008. SEBAL solves the energy balance at the Earth's surface, accounting for all major sources (net Radiation,  $R_n$ ) and sinks (latent heat flux, LE; sensible heat flux, H; and soil heat flux, G) of energy (Figure 2). LE, which is equivalent to  $R_n - G - H$ , is converted to ET based on the latent heat of vaporization ( $\lambda$ ) and density ( $\rho_w$ ) of water.

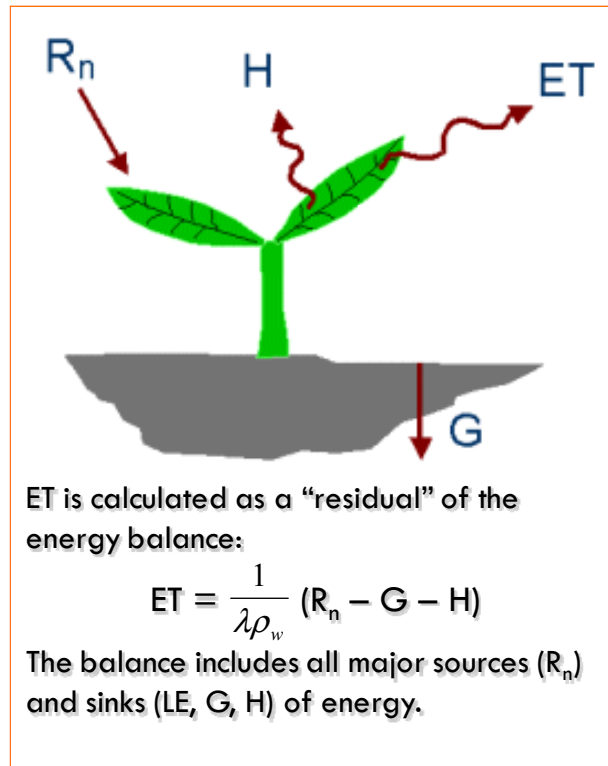


Figure 2. Conceptual Representation of Surface Energy Balance.

SEBAL is applied using multispectral Landsat satellite imagery representing the visible and infrared regions of the electromagnetic spectrum, a digital elevation model, surface roughness estimated from gridded land use data, and gridded weather data. The primary output is actual evapotranspiration ( $ET_a$ ) at the pixel scale. For the analysis presented herein, thirteen Landsat 5 images and one Landsat 7 image spanning the period February to November 2008 were selected and analyzed. For the Landsat 7 image corresponding to 7/1/2008, a gap-filled image from USGS was utilized to overcome scan line corrector gaps.

SEBAL has been updated over time based on advances in surface energy balance science. These advances include both published and un-published refinements. The 2009 version of SEBAL used for this study includes the following updates from the originally published version of the model:

- Topographic correction of incoming solar radiation based on actual surface slope and aspect;
- Lapse rate correction of observed surface temperatures to normalize for elevation effects;
- Use of spatially distributed weather surfaces integrating multiple weather stations for improved representation of actual surface conditions;
- Advection correction based on comparison of instantaneous and daily evaporative fractions estimated for a grass reference surface at each pixel, which is used to

compute an advection correction factor, which is then adjusted based on the actual instantaneous evaporative fraction;

- Atmospheric correction and calibration of albedo; and
- Improved soil heat flux estimation based on a combination of LAI and estimated soil moisture.

ET<sub>o</sub> was estimated based on a combination of ground-based weather stations included in the California Irrigation Management Information System (CIMIS) and gridded ET<sub>o</sub> estimates developed as part of the Spatial CIMIS program (Figure 3). Quality control procedures as described by Allen et al. (2005) were applied to eight selected CIMIS stations, and the Spatial CIMIS grids were fitted to the quality-controlled station values for individual image dates to estimate variability in ET<sub>o</sub> across the study area.

For purposes of the study, it was assumed that quality-controlled daily ET<sub>o</sub> from selected CIMIS stations is more reliable than the raw Spatial CIMIS ET<sub>o</sub> grids. To fit the Spatial CIMIS grids to the ET<sub>o</sub> values for the eight selected stations for each image date, differences between the daily gridded ET<sub>o</sub> and weather station ET<sub>o</sub> were calculated. These differences at the station locations were then interpolated using inverse distance weighting in ArcGIS to develop an ET<sub>o</sub> “difference grid” for each image date for the study area. The difference grid was then subtracted from the original Spatial CIMIS grid to obtain adjusted, spatially distributed ET<sub>o</sub> (Figure 4). Interpolation techniques developed and applied as part of the Spatial CIMIS data development effort are described at <http://www.cimis.water.ca.gov/cimis/cimiSatModel.jsp>.

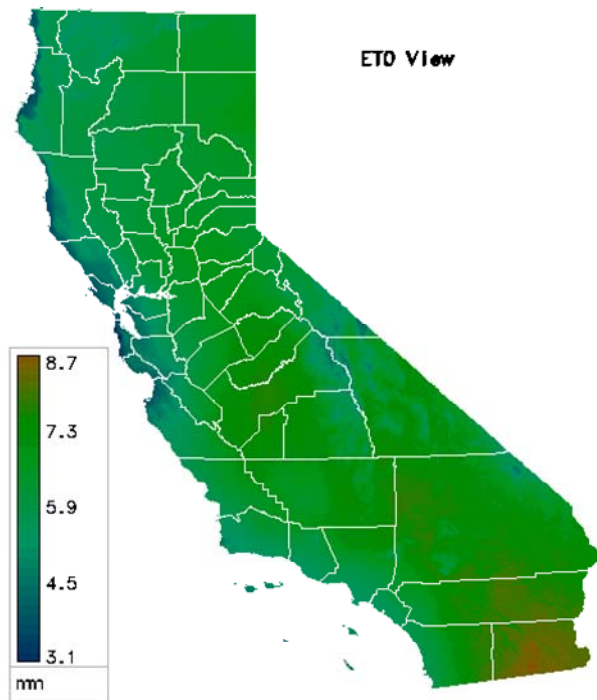


Figure 3. Sample Spatial CIMIS ET<sub>o</sub> Grid for July 25, 2008 (goes.casil.ucdavis.edu/cimis).

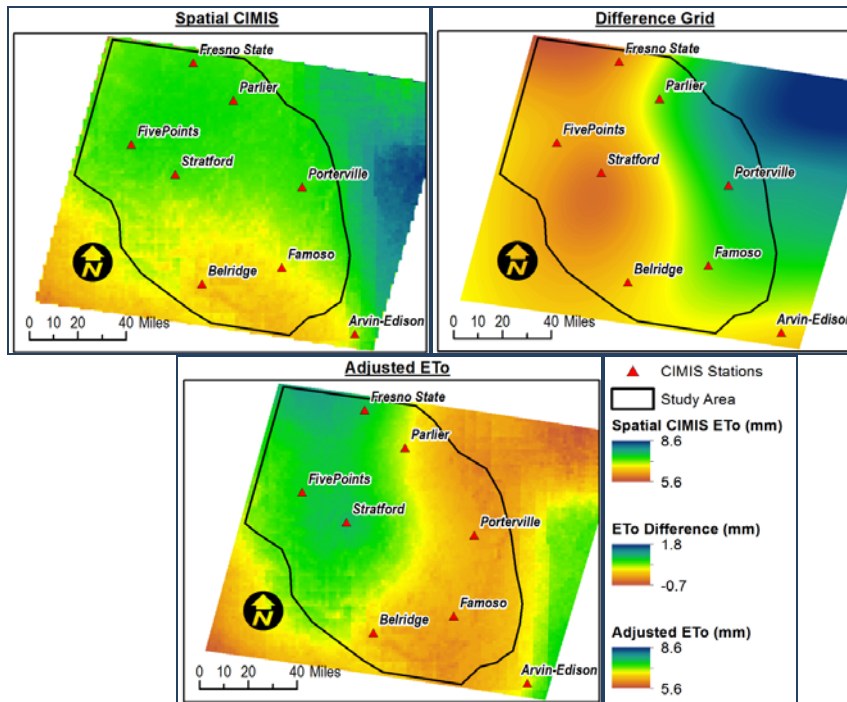


Figure 4. Selected CIMIS Stations, Spatial CIMIS  $ET_0$ , Difference Grid, and Adjusted  $ET_0$  for July 25, 2008.

Following the estimation of spatially distributed  $ET_0$  by image date, crop coefficients were calculated by dividing the  $ET_a$  grids from SEBAL by the spatially distributed  $ET_0$  grids to calculate actual crop coefficients ( $K_{cs}$ ), which incorporates the effects of stress, if any, as illustrated in Figure 5. In Figure 5,  $ET_a$  and  $ET_0$  values range from approximately 0 to 0.4 in/day (0 to 10 mm/day). Crop coefficients range from 0 to 1.4.

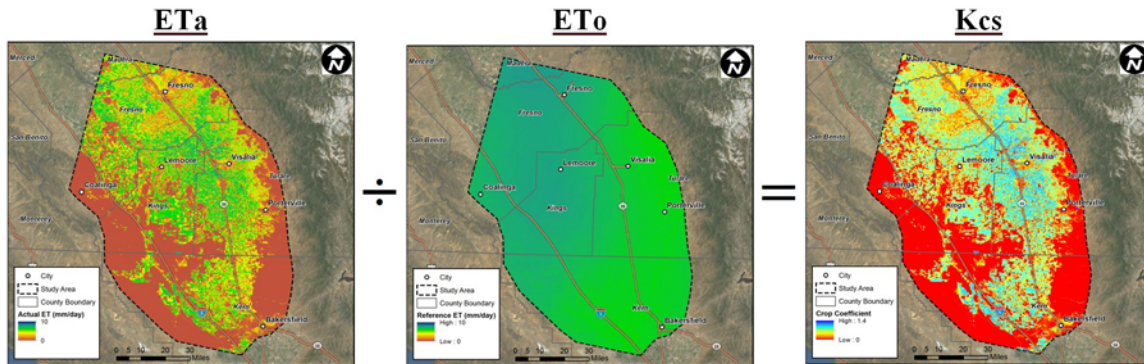


Figure 5. Illustration of Crop Coefficient Calculation for July 25, 2008.

Following the development of estimated crop coefficients by image date, variability in crop coefficients over time was evaluated for 15 major crop types grown in the Southern San Joaquin Valley. The analysis was performed for individual fields, identified based on field boundaries defined by GIS files representing Common Land Units (CLUs) developed by the USDA Farm Services Administration (FSA). The dominant crop type for each CLU was assigned based on a coverage of crop types in the study area developed

as part of the USDA National Agricultural Statistics Service (NASS) Cropland Data Layer for California for 2008. Prior to extracting average crop coefficients for each field and image date, the fields were buffered inward by 60 meters to reduce the impact of thermal pixel overlap along field boundaries. Fields ranged in size from 7 to 1000 acres with an average field size of 50 acres. The frequency distribution of field sizes by number of fields and total acres is shown in Figure 6.

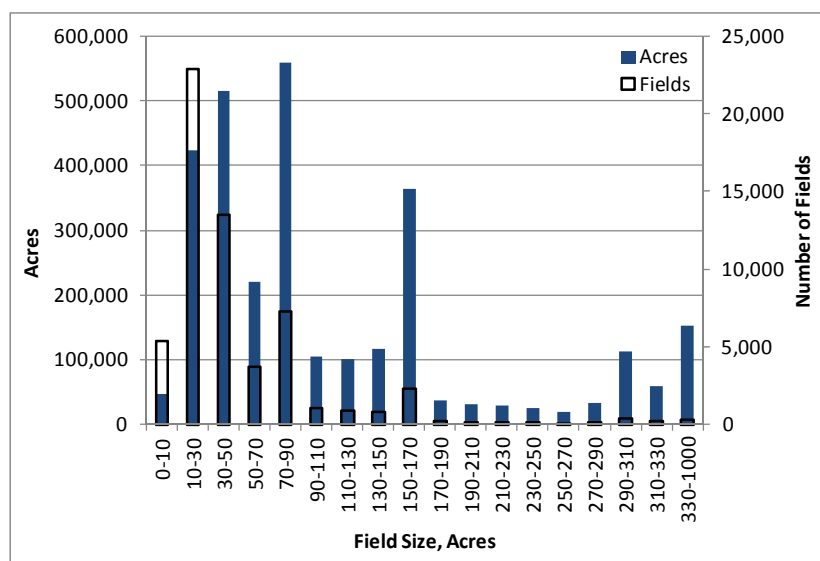


Figure 6. Frequency Distribution of Field Sizes by Number of Fields and Total Acres.

### RESULTS

Crop coefficients estimated using SEBAL have been compared to standard values estimated based on the Basic Irrigation Scheduling (BIS) model developed by the University of California and the California Department of Water Resources (Snyder et al., 2007). The model relies on standard published crop coefficients, combined with estimates of bare soil evaporation from precipitation and irrigation to estimate daily crop coefficients and crop ET to support irrigation scheduling.

Comparisons of SEBAL to BIS estimated crop coefficients are provided for alfalfa, almonds, olives, and vineyards. For each crop, the 10<sup>th</sup> percentile, mean, median, and 90<sup>th</sup> percentile crop coefficients by image date from the SEBAL analysis are provided, along with the relative frequency distribution of crop coefficients rotated 90-degrees along the image date axis, similar to Tasumi et al. (2005). BIS crop coefficients are shown as a red dashed line.

There may be some bias in the remote sensing crop coefficients due to limitations of the land use data used to evaluate crop coefficients by individual crop type. For example, using a satellite based approach to determine crop type, as is done for the NASS CDL data used for this study involves misidentification of some crops. Additionally, in some cases, fields identified as being cropped may not be irrigated. Such potential biases could

be eliminated through the availability of ground-based land use surveys, such as those developed historically by DWR for individual counties over time.

Alfalfa. Alfalfa crop coefficients from SEBAL are presented for 3,818 fields representing 211,070 acres in Figure 7.

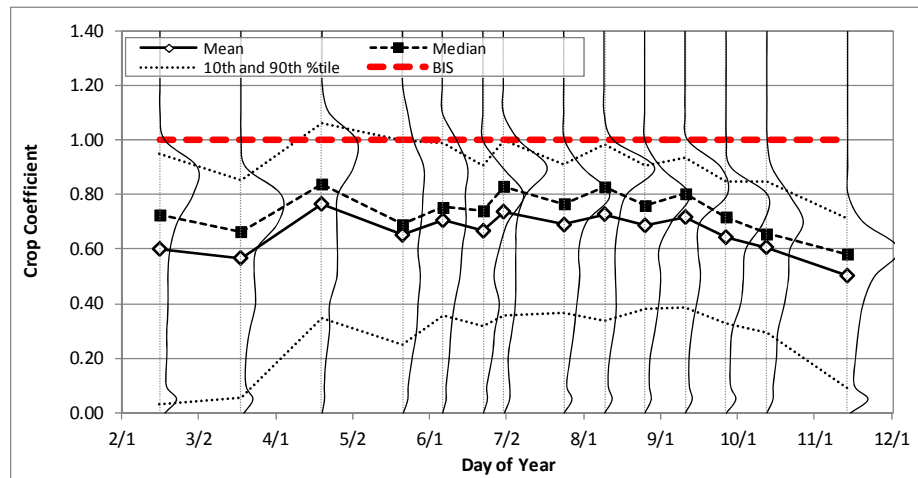


Figure 7. Comparison of SEBAL and BIS Crop Coefficients for Alfalfa, Averaged for Cutting Effects<sup>6</sup>, 2008.

In general, the crop coefficients estimated using SEBAL ranged from zero to 1.2 with 10<sup>th</sup> and 90<sup>th</sup> percentile values during mid-season of 0.4 and 1.0, respectively. Mean and median values were approximately 0.7 and 0.8 during mid-season, respectively. Crop coefficients from BIS, representing the expected average of cutting effects, were estimated to be 1.0. The difference between median crop coefficients from SEBAL and crop coefficients from BIS for alfalfa may represent differences between actual growing conditions and conditions under which the standard crop coefficients were developed. Factors affecting actual ET could include fertility, salinity, water quality, irrigation timing and amount, crop age, pests and disease, grazing practices, and other factors.

In general, the 90<sup>th</sup> percentile crop coefficients from SEBAL are similar to the BIS crop coefficients. The relative frequency distributions of alfalfa  $K_{cs}$  are skewed to the right, reflecting the impact of cutting for hay: following cutting, the crop coefficient drops substantially, gradually returning to the full cover value as regrowth occurs.

Note that for an individual field, satellite images (which were acquired on an 8-, 16-, 24-, or 32-day interval) may capture a given field before cutting, following cutting, or during the regrowth stage. Thus, for irrigation scheduling purposes, a grower wishing to evaluate past ET rates for a given alfalfa field must consider when the image dates were acquired relative to the cutting cycle. An example of crop coefficients for three alfalfa fields is provided in Figure 8.

<sup>6</sup> An overall average crop coefficient that averages the crop coefficients for both before and following cuttings (Allen et al., 1998).

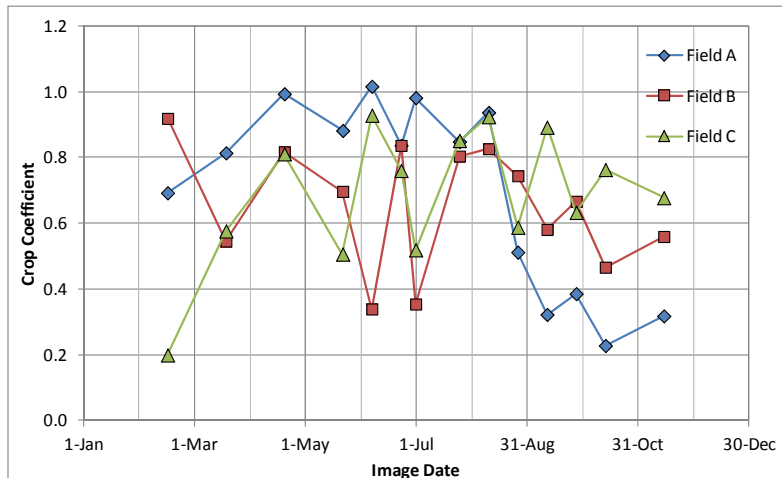


Figure 8. Estimated Crop Coefficients by Image Date for Three Alfalfa Fields Selected at Random.

Using soil water content depletion and applied irrigation minus deep percolation estimates of ET, ground-based data from 16 monitoring sites arrayed across two alfalfa fields in Kern County yielded average seasonal crop coefficients of 0.82 and 0.83 for a sandy loam and a clay soil, respectively, ranging from a site low of 0.70 to a high of 1.02. A ground-based estimate for another field computed by surface renewal using estimates of latent heat flux (ET) with a frequency of 30-minutes yielded a crop coefficient of 0.94 (Snyder, unpublished data).

Almonds. Almond crop coefficients from SEBAL are presented for 5,514 fields representing 239,631 acres in Figure 9.

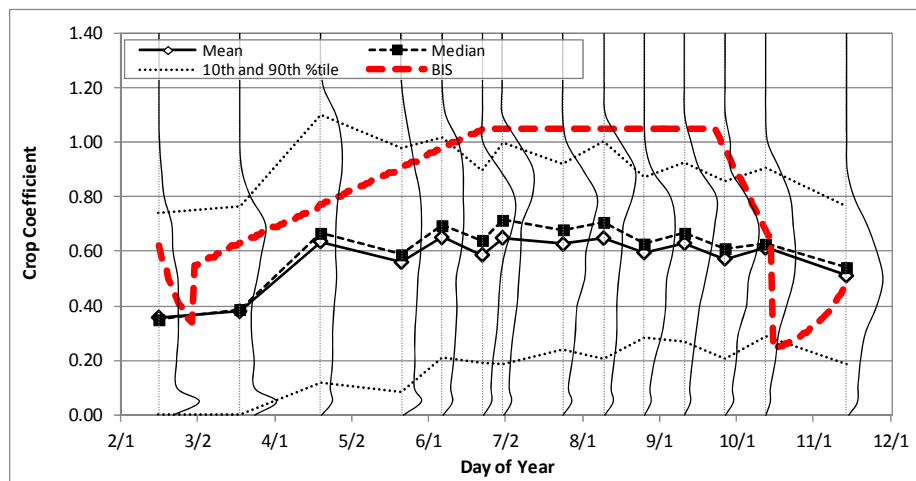


Figure 9. Comparison of SEBAL Crop Coefficients for Almonds of All Maturities and BIS Crop Coefficients for Mature Almonds, 2008.

In general, the crop coefficients estimated using SEBAL ranged from zero to 1.2 with 10<sup>th</sup> and 90<sup>th</sup> percentile values during mid-season of 0.2 and 1.0, respectively. Mean and median values were approximately 0.6 and 0.7 during mid-season, respectively. Crop

coefficients from BIS were estimated to be 1.05 during mid season. The difference between median crop coefficients from SEBAL and crop coefficients from BIS for almonds may represent differences between actual growing conditions and conditions under which the standard crop coefficients were developed, as well as differences in orchard maturity. The SEBAL-based crop coefficients represent all fields identified as almonds, while the BIS crop coefficients represent mature orchards.

In general, the 90<sup>th</sup> percentile crop coefficients from SEBAL are similar to the BIS crop coefficients early in the summer but decrease slightly late in the growing season. Early (prior to June) and late (after September) in the growing season, the 90<sup>th</sup> percentile crop coefficients from SEBAL (which may generally represent mature orchards without ET reduction due to stress or other factors) significantly exceed the BIS crop coefficients, suggesting that adjustments to the timing and magnitude of early and late season standard crop coefficients may be warranted to better represent actual growing conditions.

Using soil water content depletion and applied irrigation minus deep percolation estimates of ET, ground-based data from 38 monitoring sites arrayed across 5 mature almond orchards in Kern County yielded average seasonal orchard crop coefficients of 0.63 to 1.01 for sandy loam to sandy clay loam soils, ranging from a site low of 0.57 to a high of 1.07. A ground-based estimate of the seasonal crop coefficients computed by eddy covariance and surface renewal using 30-minute measurements of latent heat flux/ET yielded a crop coefficient of 0.97 for the orchard with the average site crop coefficient of 1.01 (Snyder, unpublished data). SEBAL seasonal estimates of the crop coefficient for these same fields were above the 90<sup>th</sup> percentile, averaging 1.01 with a low of 0.97 to a high of 1.05.

Olives. Olive crop coefficients from SEBAL are presented for 627 fields representing 13,655 acres in Figure 10.

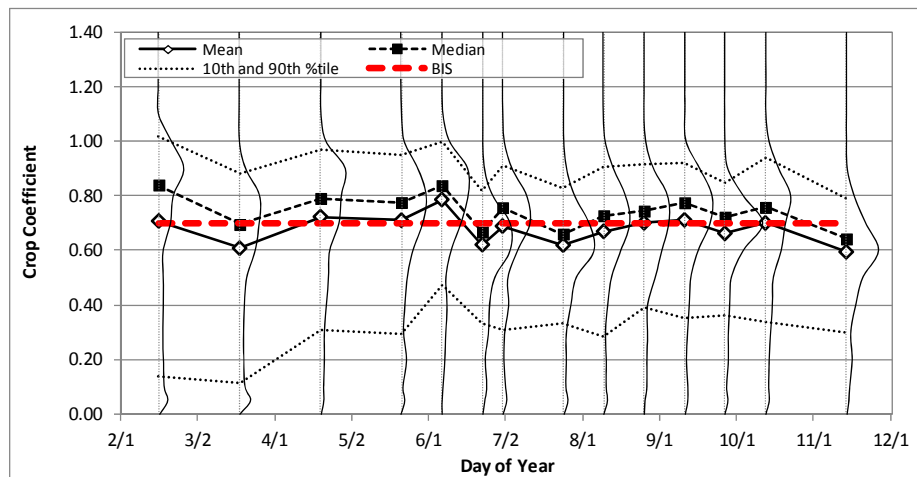


Figure 10. Comparison of SEBAL Crop Coefficients for Olives of All Maturities and BIS Crop Coefficients for Mature Olives, 2008.

In general, the crop coefficients estimated using SEBAL ranged from zero to 1.0 with 10<sup>th</sup> and 90<sup>th</sup> percentile values during mid-season of 0.3 and 0.9, respectively. Mean and median values were approximately 0.7 during mid-season. Crop coefficients from BIS were estimated to be 0.7. Median crop coefficients from SEBAL and crop coefficients from BIS for olives agreed closely throughout the analysis period, however, as for other crops, values for individual fields vary widely. The relatively large number of orchards with low crop coefficients may reflect young orchards planted in recent years as California's olive oil industry grows. The results also suggest that for orchards with full cover and limited stress, crop coefficients of 0.9 to 1.0 may be appropriate for irrigation scheduling.

Vineyards. Vineyard crop coefficients from SEBAL are presented for 3,578 fields representing 117,570 acres in Figure 11.

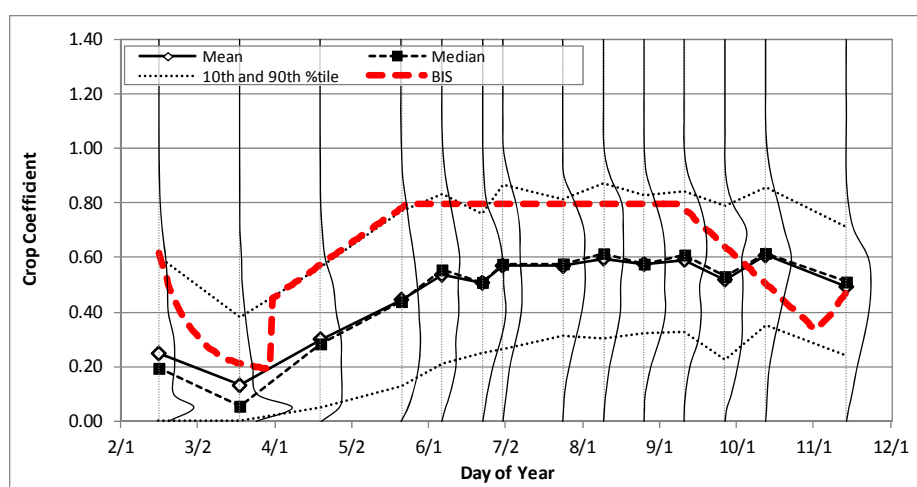


Figure 11. Comparison of SEBAL Crop Coefficients for Vineyards of All Maturities to and BIS Crop Coefficients for Mature Vineyards, 2008.

In general, the crop coefficients estimated using SEBAL ranged from 0.1 to 1.0 with 10<sup>th</sup> and 90<sup>th</sup> percentile values during mid-season of 0.3 and 0.8, respectively. Mean and median values were approximately 0.6 during mid-season. Crop coefficients from BIS were estimated to be 0.8 during mid season. The difference between median crop coefficients from SEBAL and crop coefficients from BIS for vineyards may represent differences between actual growing conditions and conditions under which the standard crop coefficients were developed, as well as differences in vineyard maturity. The SEBAL-based crop coefficients represent all fields identified as vineyards, while the BIS crop coefficients represent mature vineyards.

In general, the 90<sup>th</sup> percentile crop coefficients from SEBAL agree well with the BIS crop coefficients through mid-September. Late in the growing season (after mid-September), the 90<sup>th</sup> percentile crop coefficients from SEBAL (which may generally represent mature vineyards without ET reduction due to stress or other factors) significantly exceed the BIS crop coefficients, suggesting that adjustments to the timing and magnitude of late

season standard crop coefficients may be warranted to better represent actual growing conditions.

## DISCUSSION AND CONCLUSION

Field-scale crop ET varies substantially for fields of the same crop due to a variety of factors that can affect actual ET rates. Caution should be applied in using remote-sensing based crop coefficients summarized for multiple fields. Despite these considerations, the information provided by this study could be used to assist growers in more accurately estimating ET rates for individual fields. Specifically, growers can use the web-based interface developed as part of the study to estimate actual ET rates and crop coefficients for each field they irrigate. In order to most effectively support ongoing irrigation management, the data presented on the website would need to be updated over time; however, review of historical data can provide insight into water use characteristics for individual fields, particularly mature orchards and vineyards.

The first question a grower might ask upon reviewing ET and crop coefficient estimates for a field, assuming the field is consuming water at a rate less than or greater than observed for nearby fields of the same crop, is “Why are my ET rates low?” or “Why are my ET rates so high?” Depending upon the answer to this question, there may be the potential to increase water use efficiency (defined herein for discussion purposes as the ratio of crop yield to total applied irrigation water) and/or reduce the amount of water applied.

If a field’s ET rate is substantially less than the amount of water applied, factors other than water stress are likely to explain the reduced ET relative to other, similar fields. Such factors could include differences in canopy cover from differences in cultural practices or crop maturity, soil fertility, salinity stress, infiltration problems, irrigation system non-uniformity, insufficient irrigation frequency, and/or effects of pests and disease. In some cases, the amount of applied irrigation water could potentially be reduced, subject to considerations of necessary leaching amounts, the distribution uniformity of the irrigation system, and other factors.

For fields with ET substantially less than the amount of water applied, reductions in applied water may not necessarily reduce crop yield and ET. For example, improved irrigation uniformity and scheduling could result in less applied irrigation water and less leaching of nutrients, resulting in subsequent increases in yield and ET. This would actually increase field water use efficiency. To the extent that existing losses to tailwater or deep percolation are recovered by downstream surface water or groundwater users, reduced applied water would not lead to an increase in local or regional water supply. To the extent that the water quality of surface or subsurface runoff from a field is degraded, reduction in the losses could lead to improvements in the quality of receiving water bodies.

Some fields with excessive salinity in the soil and irrigation water will also exhibit limited ET due to the osmotic stress from the salts, but in this case it could be disastrous

for a grower to reduce applied water and, thereby, the leaching fraction necessary to prevent salts from reaching toxic levels.

If a field's ET rate approaches or exceeds the amount of water applied, water stress may be limiting crop growth and ET. In such cases, the presence of water stress could be verified in the field using soil moisture monitoring or other techniques, which could result in increases in applied irrigation water. Such increases in applied water that increase crop ET and yield could lead to increases in water use efficiency, despite the increased irrigation amount.

In summary, differences in total crop ET between fields of the same crop should not be interpreted as a potential reduction in applied water, assuming actual crop coefficients would be applied for irrigation scheduling without consideration of the factors that affect ET and existing irrigation management. Field-specific evaluation must be performed to achieve water use efficiency improvements. Many growers scheduling irrigations based on estimation of crop ET likely adjust standard crop coefficients to better represent field-specific conditions. The availability of actual crop coefficients for individual fields provides the potential to support irrigators in increasing water use efficiency.

Remotely-sensed estimates of crop coefficients in this study agree well in general with ground based estimates. Comparison of SEBAL-based crop coefficients to standard crop coefficients used for irrigation scheduling of mature crops demonstrates a wide degree of variability in ET among fields of the same crop. Additionally, published crop coefficients may require adjustment to accurately estimate regional ET, to the extent that they are used for this purpose.

### **ACKNOWLEDGEMENTS**

The authors would like to thank the California Department of Water Resources for funding this project through a Proposition 50 Water Use Efficiency Research Grant.

### **REFERENCES**

- Allen, R.G., Pereira, L.S., Raes, D., and Smith, M. 1998. Crop Evapotranspiration. Irrigation and Drainage Paper No. 56. Food and Agriculture Organization of the United Nations. Rome, Italy.
- Allen, R.G., Walter, I.A., Elliot R., Howell, T., Itenfisu, D., and Jensen M. 2005. The ASCE Standardized Reference Evapotranspiration Equation. American Society of Civil Engineers. Reston, Virginia.
- Bastiaanssen, W.G.M., Noordman, E.J.M., Pelgrum, H., Davids, G., and Allen, R.G. 2005. SEBAL Model with Remotely Sensed Data to Improve Water Resources Management under Actual Field Conditions. *Journal of Irrigation and Drainage Engineering*. 131(1), 85-93.

California Department of Water Resources (DWR). 2010. California Water Plan Update 2009: Integrated Water Management. Bulletin 160-09.

Snyder, R.L., Orang, M., Bali, K., and Eching, S. 2000. Basic Irrigation Scheduling (BIS). University of California. [biomet.ucdavis.edu/irrigation\\_scheduling/bis/BIS.htm](http://biomet.ucdavis.edu/irrigation_scheduling/bis/BIS.htm). Revised 2007.

Snyder, R.L. Unpublished estimates of crop ET based on eddy covariance and surface renewal techniques.

Tasumi, M., Allen, R.G., Trezza, R., and Wright, J. 2005. Satellite-Based Energy Balance to Assess Within-Population Variance of Crop Coefficient Curves. *Journal of Irrigation and Drainage Engineering*. 131(1), 94-109.

# MICROCLIMATE EFFECTS OF URBAN-FRIDGE IRRIGATED AGRICULTURE IN A DESERT ENVIRONMENT

Zohrab Samani<sup>1</sup>  
Rhonda Skaggs<sup>2</sup>  
Bradley Griggs<sup>3</sup>

## ABSTRACT

Change in land use can affect the energy balance at the ground surface and thus play an important role in the microclimate of an area. Land use change from agricultural to urban influences local land surface and air temperatures and can contribute to decreased quality of life. When the agricultural landscape is an irrigated oasis located in an arid, desert environment, the agricultural landscape can be noticeably more comfortable relative to nearby built-up landscapes, and the cooler temperature can reduce summer energy costs. The microclimate benefits of local irrigated agriculture are an important characteristic of urban-fringe agriculture, and our research in New Mexico's Middle Rio Grande Valley has characterized the relationship between land cover, air temperature, and surface temperature in the region. The present study uses remotely sensed imagery from Landsat 5 Thematic Mapper (TM) and Landsat 7 Enhanced Thematic Mapper (ETM+) to correlate normalized difference vegetation index (NDVI) to land surface temperature (LST) and air temperature (Ta). Results of the research contribute to better understanding of the multifunctional nature of urban-fringe agriculture in an arid desert environment and the contributions of the agricultural landscape to residents' quality of life.

## INTRODUCTION

As the discussion and concern over global warming intensifies, one issue that is often overlooked is the effect of land use on the microclimate and air temperature in general. Crop production activities can have a significant impact on the microclimate of an area, particularly if crops are grown under irrigation. The Albuquerque, New Mexico's South Valley is a transitional zone between the rapidly growing urban landscape and the agricultural zones located south of the city center along the Rio Grande. This study was undertaken to evaluate the impact of urbanization on the micro climate of the South Valley. The typical source of climate data is a single meteorological station which provides data for a discrete location. A single data collection point is incapable of capturing the diversity of temperature or the impact of different land uses on microclimates in the area supposedly represented by the station. For example, it is generally known that plants transpiring water act as a natural evaporative cooler and have a microclimatic cooling effect.

The objectives of this study were to explore relationships between air temperature and land use/land cover (LULC) in the South Valley area of Albuquerque, NM. Land Surface

---

<sup>1</sup> Professor, Civil Engineering, New Mexico State University, Las Cruces, NM, USA.

<sup>2</sup> Professor, Agricultural Economics, New Mexico State University, Las Cruces, NM, USA.

<sup>3</sup> Former Graduate Student, Applied Geography, New Mexico State University, Las Cruces, NM, USA.

Temperature (LST), Albedo and Normalized Difference Vegetation Index (NDVI) derived from Landsat 5 Thematic Mapper™ and Landsat 7 Mapper (ETM+) were used to calculate evapotranspiration (ET), sensible heat, and sensible air temperature. The Regional ET Estimation Model (Samani et al. 2009) was used to calculate sensible air temperature from the sensible heat flows of the energy balance.

### THEORY

The energy balance equation on the land surface can be described as

$$R_n - G - LE = H \quad (1)$$

where, LE is the latent heat flux,  $R_n$  is the net radiation flux at the surface, G is the soil heat flux and H is the sensible heat flux which heats up the air.

Daily net radiation over the crop canopy can be calculated using methodology developed by Samani et al. (2007) as:

$$R_n = R_{ni} \left( \frac{R_s}{R_{si}} \right) \left( \frac{T_a}{T_i} \right)^4 \quad (2)$$

where,  $R_n$  is the daily net radiation in MJ/m<sup>2</sup>/day,  $R_{ni}$  is instantaneous clear sky net radiation (W/m<sup>2</sup>),  $R_s$  is daily short wave solar radiation (MJ/m<sup>2</sup>/day),  $R_{si}$  is the instantaneous short wave solar radiation (W/m<sup>2</sup>),  $T_a$  is average daily temperature in Kelvin (K), and  $T_i$  is the instantaneous air temperature (K).

Instantaneous net radiation ( $R_{ni}$ ) was calculated from the following equation

$$R_{ni} = (1 - \alpha)R_{si} + RL \downarrow - RL \uparrow - (1 - \epsilon_o)RL \downarrow \quad (3)$$

where,  $R_{ni}$  is instantaneous net radiation (W/m<sup>2</sup>),  $R_{si}$  is instantaneous incoming short wave radiation (W/m<sup>2</sup>),  $RL \downarrow$  is instantaneous incoming long wave radiation (W/m<sup>2</sup>),  $RL \uparrow$  is instantaneous outgoing long wave radiation (W/m<sup>2</sup>),  $\alpha$  is surface albedo (dimensionless), and  $\epsilon_o$  is surface emissivity (dimensionless).  $RL \downarrow$  and  $RL \uparrow$  are calculated as follows:

$$RL \downarrow = \epsilon_a \times \sigma \times T_i^4 \quad (4)$$

where,  $\epsilon_a$  is atmospheric emissivity calculated using the following equation (Bastiaanssen 1995):

$$\epsilon_a = 0.85 \times (-\ln \tau_{sw})^{0.09} \quad (5)$$

where,  $\sigma$  is Stefan-Boltzman constant ( $5.67 \times 10^{-8}$  W/m<sup>2</sup>/K<sup>4</sup>),  $T_i$  is instantaneous near surface air temperature (K),  $\tau_{sw}$  is the atmospheric transmissivity calculated from elevation (Allen et al. 1998) and

$$RL \uparrow = \epsilon_o \times \sigma \times T_s^4 \quad (6)$$

where,  $\epsilon_0$  is surface emissivity (dimensionless) calculated as  $\epsilon_0 = 0.95 + 0.01 \text{ LAI}$  when  $\text{LAI} < 3$  and  $\epsilon_0 = 0.98$  when  $\text{LAI} \geq 3$ , LAI is leaf area index, and  $T_s$  is surface temperature (in K). The LAI is the ratio of total upper leaf surface area of vegetation divided by the surface area of the land on which the vegetation grows ( $\text{m}^2/\text{m}^2$ ).

Satellite data from Landsat-5 (2010) and Landsat-7 (2010) were used to calculate Normalized Difference Vegetation Index (NDVI), albedo, and surface temperature for the study site. As equation (1) shows, the residual net energy which has not been used for latent heat is used to heat up the air. The amount of energy which is used to heat the air (H) can be related to surface and air temperature using the equation developed by Monteith (1973) as:

$$H = \rho C_p (T_o - T_a) / r_a \quad (7)$$

Where, H is the sensible heat flux ( $\text{W}/\text{m}^2$ ),  $\rho$  is the density of air ( $\text{kg}/\text{m}^3$ ),  $C_p$  is the air specific heat at constant pressure ( $1004 \text{ J}/\text{kg}/\text{K}$ ),  $T_o$  is the surface temperature (K),  $T_a$  is the ambient air temperature (K), and  $r_a$  is the aerodynamic resistance ( $\text{s}/\text{m}$ ). In this study surface temperature values were calculated using Landsat-5 and Landsat-7 images. The air temperature was calculated using the following methodology.

A relationship was developed between temperature gradient ( $T_o - T_a$ ) and surface temperature ( $T_s$ ) using the following equation:

$$dT = aT_s + b \quad (8)$$

where, dT is the temperature gradient,  $T_s$  is land surface temperature, a and b are coefficients from the above equation. The empirical coefficients were calculated by combining the Monteith (1973) equation with Monin-Obukhov similarity theory as described by Samani et al. (2009). Rearranging equation (8), the air temperature for all pixels can be calculated as:

$$T_a = (1-a) T_s - b \quad (9)$$

## RESULTS AND DISCUSSION

Figure 1 shows the surface temperature in Albuquerque, New Mexico's South Valley at midday for June 14<sup>th</sup>, 2010. The ground surface temperature varies from 85 °F in heavily vegetated area to 120 °F in areas with bare surface. The high ground temperature results in comparatively elevated air temperature. In this study, values of ground surface temperature were used to calculate air temperature values. The results showed that the air temperature and ground temperature are directly correlated as shown in equation (9). Figure 2 shows the difference in air temperature between built-up urban Albuquerque area north of the South Valley and the South Valley for 29 July 2010. The air temperature varied between 31°C in densely vegetated area to 38 °C. in areas with bare surface

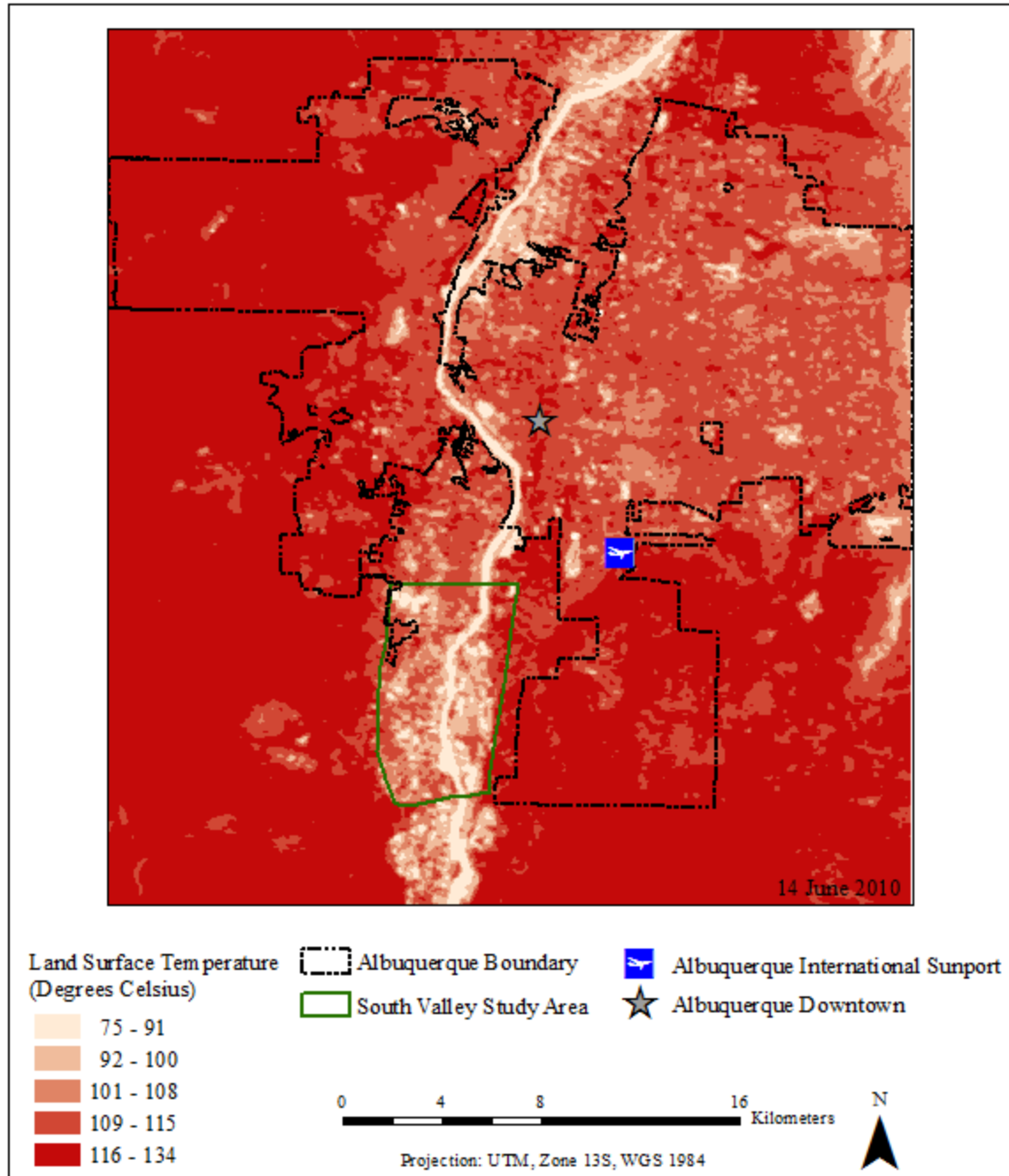


Figure 1. Land Surface Temperature, Albuquerque, New Mexico, USA Metropolitan Area, 14 June 2010.

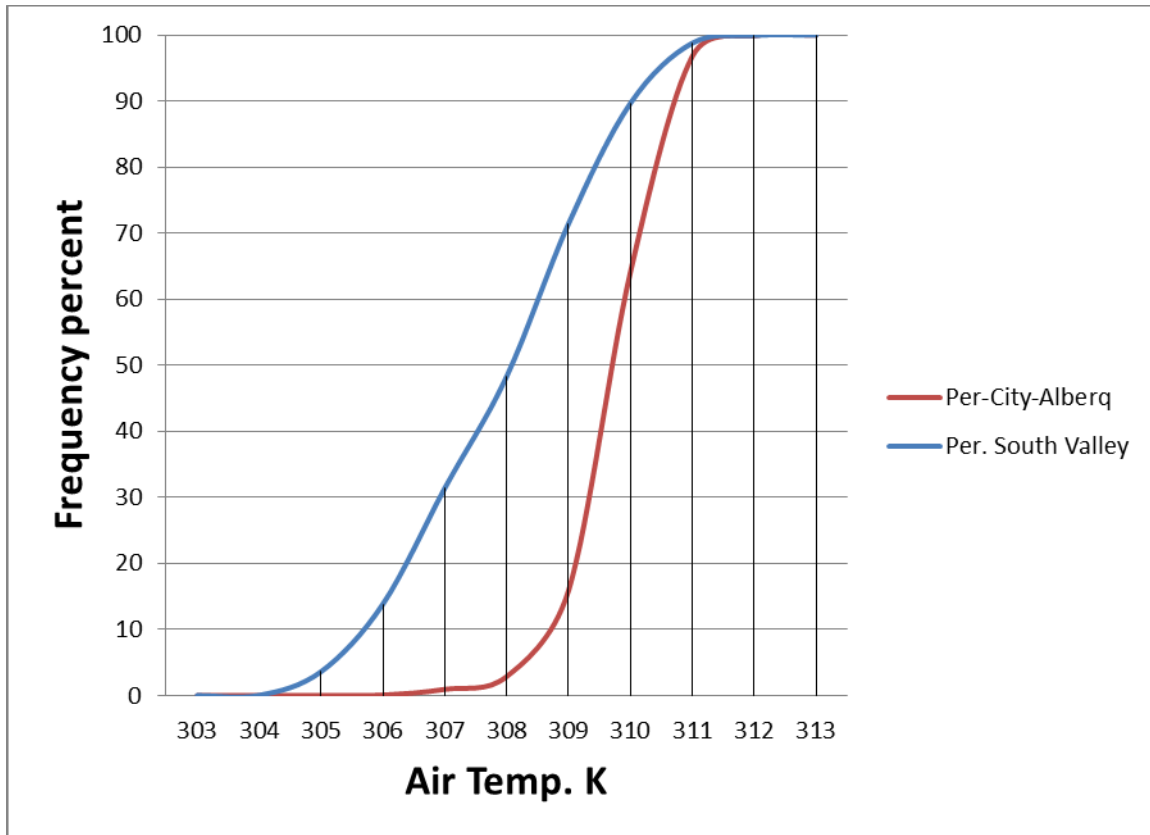


Figure 2. Comparison of Temperature Difference for Various Points within the City of Albuquerque's Urban Built-Up Area and Albuquerque's South Valley for 29 July 2010.

### CONCLUSION

The study shows that urbanization has a significant impact on the microclimate of the area. Densely urbanized areas such as the City of Albuquerque contributes to elevated air temperature especially during the hot summer months. The peri-urban area south of city of Albuquerque has lower air temperature due to the cooling effect of the irrigated agriculture in the area. In addition, high ground surface temperature in urban area is indication of large heat storage in the ground during day time which can translate into higher night time temperature.

The air temperature affects quality of life, productivity and contributes to higher energy cost for cooling during hot summer months.

### ACKNOWLEDGEMENTS

This research was supported by the New Mexico Agricultural Experiment Station, State of New Mexico State Appropriation Fund for south Valley Land Use Feasibility Study, and USDA-CSREES Small and Medium Size Farm Prosperity Agreement No. 2009-55618-05096.

## REFERENCES

Allen, R.G., L.S. Pereira, D. Raes, and M. Smith. 1998. Crop evapotranspiration: Guidelines for computing crop water requirements. Food and Agriculture Organization. FAO Irrigation and Drainage Paper No.56. Rome, Italy.

Bastiaanssen, W.G.M.. 1995. Regionalization of surface flux densities and moisture indicators in composite terrain: A remote sensing approach under clear skies in Mediterranean climates. Ph.D. dissertation, Landbouwniversiteit te Wageningen, The Netherlands. Published as Report 109 of DLO Win and Staring Centre, Wageningen, The Netherlands.

Montieth, J.L. 1973. Principles of environmental physics. Great Britain: Whittdtable Litho Ltd. Whitstable, Kent.

Samani, Z., A.S. Bawazir, M. Bleiweiss and R. Skaggs. 2007. Estimating net radiation over vegetation canopy. ASCE J. Irrig. and Drain. Engrg. 133(4): 291-297.

Samani, Z., A.S. Bawazir, M. Bleiweiss, R. Skaggs, J. Longworth, V.D. Tran and A. Piñon. 2009. Using Remote Sensing to Evaluate the Spatial Variability of Evapotranspiration and Crop Coefficient in the Lower Rio Grande Valley, New Mexico. Irrigation Science 28:93-100.

# REDUCING COST OF WATER QUALITY MONITORING IN TILE DRAINAGE OUTFLOW USING ELECTRICAL CONDUCTIVITY AS A SURROGATE

Xinhua Jia<sup>1</sup>  
Thomas F. Scherer<sup>2</sup>

## ABSTRACT

A three year research study was conducted on a 22-hectare tile-drained field in southeast North Dakota. A pumped lift station was used as outlet for drainage and inlet for subirrigation using groundwater from wells. The drainage outflow and subirrigation inflow were both measured continuously. Water samples were collected bimonthly from the lift station. A total of 38 water quality parameters were analyzed or calculated by the North Dakota Department of Health Environmental Analysis Laboratory during the three-year period (2008-2010). Electrical conductivity (EC) can be measured continuously, and thus can be used as an inexpensive surrogate to determine the concentration of certain minerals in order to reduce the cost of water quality monitoring. For all water quality parameters in the tile drainage outflow (23 out of 38 samples), we found that EC showed good agreement with the dominant cations and anions. EC was linearly related to total dissolved solids, sulfate, hardness, magnesium, and sodium with  $R^2$  values of 0.99, 0.97, 0.96, 0.92, and 0.89, respectively. The  $R^2$  for the other parameters (e.g. phosphorus, nitrate-nitrite, and calcium) was less than 0.5. When both drainage and irrigation samples were analyzed, we found the regression of EC with total dissolved solids, sulfates, hardness, magnesium, and sodium to have  $R^2$  values of 1.00, 0.99, 0.99, 0.95, and 0.83, respectively. For calcium, phosphorus, percent exchangeable sodium, and nitrate-nitrite the  $R^2$  values were 0.85, 0.67, 0.66, and 0.63, respectively. No regression relationships were found for trace metals or micronutrients, most likely due their low concentrations.

## INTRODUCTION

Due to a wet weather cycle since 1993 in the Red River Valley of the North watershed between Eastern North Dakota and Northwest Minnesota, above normal precipitation has resulted in excess soil moisture, raised water tables, increased soil salinity, and interfered with timely planting and harvest. Tile drainage, a process to remove excess moisture from the soil profile and crop root zone using perforated plastic tubing, has become very popular in the region in the last decade. The removal of excess moisture from the root zone allows the landowners to plant and harvest on time, while crop yields are often increased due to higher evapotranspiration rates and better moisture conditions (Rijal et al., 2012; Tan et al., 2002).

Though a tile drainage system is necessary for farmers, discharge of drainage effluent is often the cause of public criticism for its perceived negative impact on the environment,

---

<sup>1</sup> Department of Agricultural and Biosystems Engineering, North Dakota State University, NDSU Dept 7620, PO Box 6050, Fargo, ND 58108. Phone: 701-231-6453. Email: [Xinhua.jia@ndsu.edu](mailto:Xinhua.jia@ndsu.edu).

<sup>2</sup> Department of Agricultural and Biosystems Engineering, North Dakota State University, NDSU Dept 7620, PO Box 6050, Fargo, ND 58108. Phone: 701-231-7239. Email: [Thomas.scherer@ndsu.edu](mailto:Thomas.scherer@ndsu.edu).

particularly to surface water systems. More nutrients and soluble salts enter the surface water via tile drainage, compared to non-tiled fields (Gilliam et al., 1999; Jayawardane et al., 2001). These excess nutrients can cause water quality problems, e.g. eutrophication, decrease of dissolved oxygen, and fish kills, in the surface water systems (Gibson et al., 2000; Wilson, 2009). In order to minimize the negative impacts, a weir or control structure can be added to the outlet of the drainage system, so that the drainage outflow can be regulated and drainage water is discharged only when it is needed to control the water table position. When drainage outflow is reduced, the nutrient loss or water quality impact to surface water is diminished. During the summer time when the crop is in need of additional water, subirrigation via the same tile drainage system can be applied to meet the crop water requirement. The combination of controlled drainage and subirrigation is regarded as a best agricultural water management practice that can benefit both the producers and the environment.

In order to quantitatively determine the impact of tile drainage and subirrigation on water quality, chemical analysis of the water samples is required, but the cost of the analysis can be very expensive. For example, in 2008 – 2010, a tile drainage and subirrigation study conducted in southeastern North Dakota by Jia et al. (2012) analyzed water samples for a suite of water quality parameters, including nutrients (e.g. nitrate nitrogen, ammonium, phosphate), major cations (e.g. sodium, calcium, magnesium), major anions (sulfate, chloride), trace metals (e.g. boron, zinc, selenium), and pesticides (in 2009 only). The cost for each water sample chemical analysis was several hundred dollars, which limits the sampling frequency to minimal levels. Such low sampling frequency made it difficult to determine water quality changes after heavy rainfall events when the outflow was high (Gali et al., 2012), and a simple parameter, such as electrical conductivity, can help separate the hydrographs between different rainfall events (Pellerin et al., 2008). Therefore, it is necessary to identify some key parameters that can adversely affect water quality, and relate these key parameters to some simple and continuous measurement parameters, a surrogate. Miguntanna et al. (2010) developed a set of surrogates to assess water quality parameters and found that total dissolved solids had a good potential for total dissolved nitrogen estimates, and total solids (total dissolved solids plus suspended and settleable solids in water) demonstrated a good potential for total phosphorus. Marttila and Klove (2012) used turbidity to estimate suspended solids and nutrient loads with only 8% error. Smeti et al. (2009) used electrical conductivity as one of the two parameters to discriminate the water source from water treatment plants and the result provided a simple and fast way to identify the origin of the water quality problem. Hayashi et al. (2012) found that electrical conductivity as well as dissolved oxygen and pH values in a pre-alpine river showed a diurnal change due to photosynthesis and calcite precipitation. Iwanyshyn et al. (2009) used the relationship between electrical conductivity and major ions to provide a promising “cost-effective real-time estimation of river concentrations for major ions and nutrients for surface water quality monitoring”.

Electrical conductivity is a measure of the ability of the water to transfer an electrical charge (ASABE, 2008), and is strongly affected by the amount of dissolved inorganic ions present in the water. The electrical conductivity of a water sample is dependent on the geology of the area, the size of the watershed, and the sources of water contributing to

the discharge. Therefore, EC represents the water quality of the specific area, not universally for any area.

In this study, we used water samples collected and analyzed from 2008 – 2010 to determine whether EC can be used as a surrogate for major water quality parameters at this location, and whether a strong relationship can be developed based on EC and the key water quality parameters. Calibration and validation of water quality parameters with the surrogate (e.g. electrical conductivity) is needed to ensure that this simple approach works.

## MATERIALS AND METHODS

### Experimental Site

The experimental site is located at Fairmount, Richland County, in the southeastern corner of North Dakota. Since the Red River of the North flows north into Canada, the site is located in the upper part of the watershed. As detailed in Jia et al. (2012) and Rijal et al. (2012), the experimental field totals 44 ha, with 22 ha tile drained and 22 ha non-tiled. The outlet for the tile water is a pumped lift station. For the 22 ha tile drained section, 11 ha in the eastern part of the field are subirrigated with groundwater introduced into the sump of the lift station. The western 11 ha does not receive subirrigation water due to increasing elevation (Jia et al., 2012). The experiment was conducted from 2008 – 2010. Corn was planted to the entire 44 ha field in 2008 and 2009 and soybean was planted in 2010.



Figure 1. Experimental location and field layout

### **Water Quality Parameters and Analysis**

Typically in this region, tile drainage outflow can occur from late March to the end of November, depending on precipitation amounts. Due to Red River flooding during spring snowmelt, some local water boards (such as the one where the experiment is located) recommend that tile drainage lift stations be turned off to avoid any negative hydrologic impacts from tile drainage outflow. Therefore, water sampling is scheduled when the tile drainage system is running from April to November. In the summer, when controlled drainage or subirrigation is practiced, no water is drained from the structure. From 2008 to 2010, a total of 38 grab water samples were collected on a bimonthly schedule when water was present at the outlet, and among them, 23 samples were during drainage periods, and 15 samples were during the subirrigation periods. The water samples were delivered to the North Dakota Department of Health laboratory for chemical analysis of 38 parameters, including nutrients, major cations and anions, and trace metals. The chemical analysis followed the standard procedures set forth by the Environmental Protection Agency as detailed in Jia et al. (2012).

### **Statistical Analysis**

A three factor, partially nested statistical analysis of major water quality parameters (Jia et al., 2012) indicated that water management practices did not cause significant differences in water quality in the field, instead, the soil heterogeneity, or the local geology of the area, caused significant water quality differences in the field. At the outlet, the major water quality difference was caused by the sources of water, either drainage outflow or subirrigation inflow. Therefore, using EC as a surrogate is appropriate because EC can clearly identify the water sources. Simple linear regression analysis was conducted between EC and the other parameters to determine if EC can be used as a surrogate for other water quality parameters.

## **RESULTS AND DISCUSSION**

A total of 38 water samples were collected bimonthly from the drainage outlet (sump) and analyzed for 38 water quality parameters by the North Dakota Department of Health Environmental Analysis Laboratory following standard EPA procedures (Jia et al., 2012). All water quality parameters were determined for drainage and irrigation samples (38), drainage outflow water (23 samples), and subirrigation inflow water (15 samples). The parameters are grouped into different categories according to their characteristics. The average, maximum, and minimum chemical concentrations for all water samples, and average concentrations for drainage and irrigation are shown in Table 1.

Table 1. Summary of water quality of tile drainage outflow and subirrigation inflow

	Unit	All Water			Drainage	Irrigation
		Average	Max	Min	Average	Average
Boron	ug/L	550	901	107	437	700
Aluminum	ug/L	941	3070	73.0	1156	1190
Manganese	mg/L	0.06	0.26	0.00	0.05	0.08
Iron	mg/L	1.90	26.2	0.00	2.51	1.01
Sodium	mg/L	279	862	42.2	356	167
Magnesium	mg/L	298	1210	6.10	485	22.7
Potassium	mg/L	3.54	16.4	0.00	3.81	3.17
Calcium	mg/L	241	493	38.8	371	45.4
Ammonia	mg/L	1.40	4.16	0.00	0.15	3.23
Nitrate + Nitrite	mg/L	5.74	22.3	0.00	8.77	0.77
Kjeldahl nitrogen	mg/L	2.07	4.74	0.00	0.95	3.80
Total nitrogen	mg/L	7.65	22.1	2.67	9.69	4.53
Beryllium	ug/L	0.55	12.1	0.00	0.86	0.00
Chromium	ug/L	2.11	15.4	0.00	3.32	0.00
Nickel	ug/L	6.57	17.7	0.00	10.2	0.96
Copper	ug/L	5.71	28.0	0.00	8.81	0.90
Zinc	ug/L	59.1	290	0.00	80.4	26.1
Arsenic	ug/L	1.85	26.6	0.00	2.91	0.00
Selenium	ug/L	16.7	84.4	0.00	26.3	0.00
Silver	ug/L	3.32	48.3	0.00	5.21	0.00
Cadmium	ug/L	0.00	0.00	0.00	0.00	0.00
Antimony	ug/L	0.00	0.00	0.00	0.00	0.00
Barium	ug/L	48.7	167	0.00	54.0	40.6
Thallium	ug/L	0.10	2.22	0.00	0.16	0.00
Lead	ug/L	0.35	5.67	0.00	0.55	0.00
pH		7.55	8.28	6.63	7.37	7.82
Carbonate	mg/L	0.00	0.00	0.00	0.00	0.00
Bicarbonate	mg/L	384	464	132	368	408
Hydroxide	mg/L	0.00	0.00	0.00	0.00	0.00
Alkalinity	mg/L	315	380	109	302	335
Hardness total		1917	6150	143	3033	207
Phosphorus	mg/L	0.33	0.84	0.00	0.15	0.61
Sulfate as SO <sub>4</sub>	mg/L	1966	6550	140	3143	162
Chloride	mg/L	25.5	37.4	8.64	19.6	34.6
% Sodium	%	37.8	73.2	13.8	20.5	63.2
SAR		3.70	6.74	0.90	2.76	5.08
Total dissolved solids	mg/L	2932	9330	572	4494	641
Electrical conductivity	umhos/cm	3298	8520	914	4755	1065

Key water quality parameters with the highest number of samples and ranges were chosen to compare with the EC values. Simple linear relationships were developed for drainage, irrigation, and both water samples and their R-square values are shown in Table 2.

Table 2. Linear regression  $R^2$  values between EC and key water quality parameters

	Unit	All	Drainage	Irrigation
Boron	ug/L	0.19	0.00	0.12
Aluminum	ug/L	0.00	0.18	0.88
Sodium	mg/L	0.83	0.89	0.25
Magnesium	mg/L	0.95	0.92	0.09
Calcium	mg/L	0.85	0.52	0.48
Nitrate + Nitrite	mg/L	0.63	0.33	0.08
Nitrogen (total)	mg/L	0.52	0.37	0.01
Zinc	ug/L	0.29	0.20	0.02
Selenium	ug/L	0.32	0.10	0.00
Barium	ug/L	0.00	0.08	0.00
pH		0.10	0.17	0.14
Hardness total		0.99	0.96	0.23
Phosphorus	mg/L	0.67	0.24	0.00
Sulfate as SO <sub>4</sub>	mg/L	0.99	0.98	0.41
Chloride	mg/L	0.49	0.04	0.05
Percent Exchangeable Sodium	%	0.66	0.02	0.03
Total Dissolved Solids	mg/L	1.00	0.99	0.63

From Table 2, we can see that not all parameters analyzed showed strong relationships with EC. Trace metals and micronutrients, possibly due to their low detection values, are not large enough to impact the EC values, and therefore, showed a weak or no relationship with the EC values. Dominant ions, such as sulfate and magnesium, showed strong linear relationships with EC values, with  $R^2$  values 0.99 and 0.95, respectively. The major nutrient parameters (nitrate and phosphorus) showed a weak relationship with EC, possibly because of their low concentrations, which were not large enough to influence the EC values. Since nutrient loss from the field is one of the major concerns in the environment, we found the best relationship between EC and nitrate + nitrite with an  $R^2$  value of 0.63 was for all water samples, instead of drainage or irrigation water only. This is probably due to the fact that the groundwater used for irrigation has a small number of water samples, and showed a narrow EC range from 974 to 1130 umhos/cm (Table 1). The chemical concentrations in the irrigation water are fairly constant, and are not affected by EC values. It is not surprising to see that a weak or no relationship can be found between the key water quality parameters and the EC values during the subirrigation period. After eliminating the chemical concentrations at the lower EC range in the irrigation water, the relationships for drainage water are decreased for most

parameters, except for sodium. The larger number of water samples and greater range of concentration are the main reasons for the improved relationship when considering both drainage and irrigation waters. These relationships will be helpful when determining the source of water. However, when determining the nutrient load discharged to surface waters, the relationship for drainage water only should be used. Overall, EC proved to be a good surrogate for the major cations and anions, and nutrients, and is indeed the “most widely used means” to evaluate water quality of surface water systems (Hem, 2005).

Linear relationships between dominant cations (e.g. magnesium, calcium, sodium, and exchangeable sodium), and dominant anions and nutrient parameters (e.g. sulfate, nitrate + nitrite, phosphorus, and total dissolved solids) and EC values for all water samples are plotted in Figure 2 and 3. In general, they were linear, but biased at the higher end due to the nature of the EC measurement or EC sensor errors (Hem, 2005). The strong linear relationship between EC and magnesium and sulfate indicate that they are the dominant cation and anion in the drainage water samples.

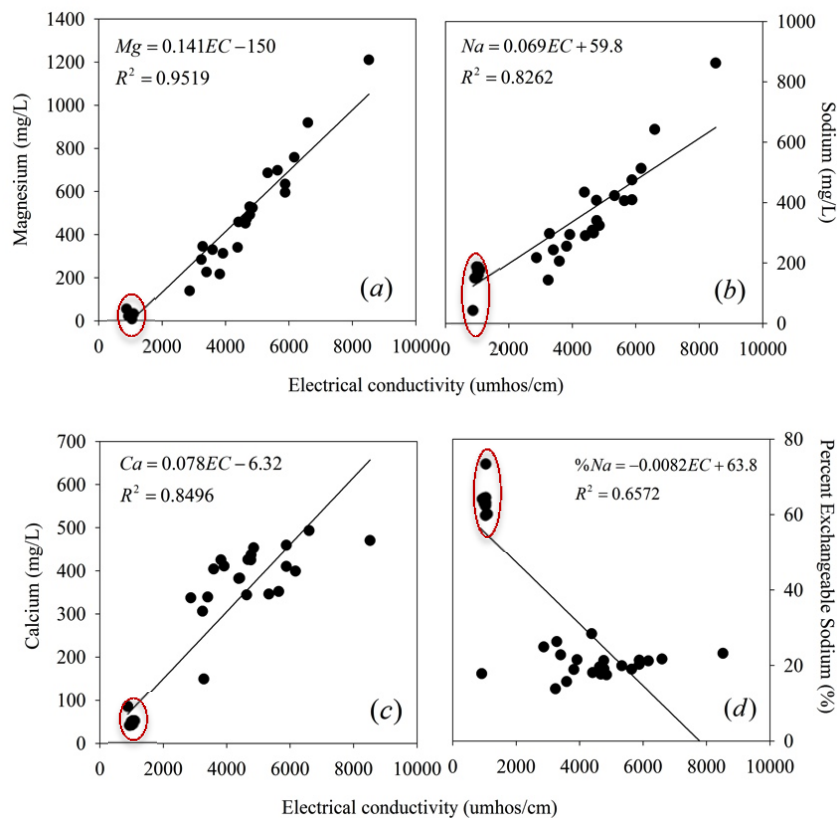


Figure 2. Linear relationship between electrical conductivity and magnesium (a), sodium (b), calcium (c), and percentage of exchangeable sodium (d) for all water samples. Red circles indicate irrigation water source.

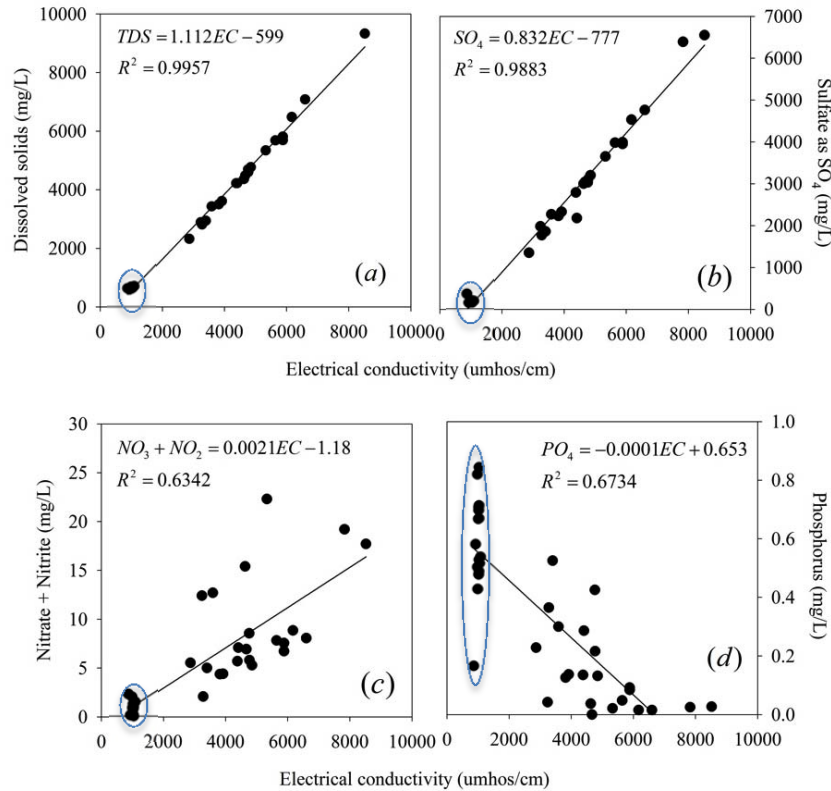


Figure 3. Linear relationship between electrical conductivity and total dissolved solids (a), sulfate (b), nitrate + nitrite (c), and phosphorus (d) for all water samples. Blue circles indicate irrigation water source.

The irrigation water is from groundwater and has a better water quality, except for phosphorus and exchangeable sodium percentage. The EC values for the irrigation water are all clustered near 1000 umhos/cm, and weighted at one end of the curves as they were circled in Figure 2 and 3. Therefore, the major reasons for the large EC range (up to 8520 umhos/cm) are primarily due to the concentration variation of the drainage water. Magnesium, sodium, calcium, sulfate, and nitrate + nitrite concentrations increase with increasing EC, indicating that they are higher in the drainage water. However, phosphorus and percent sodium decrease with increasing EC, showing that these two parameters are higher in the subirrigation water, similar to the results in Jia et al. (2012). Sodium concentration was low for a low EC (subirrigation water), but the percent of exchangeable sodium was high at low EC in the subirrigation water. However, note that the exchangeable sodium percentage is nearly constant for the varying EC of the drainage water (figure 4). This indicates the concentration relationship of the major mineral constituents of the drainage water remains relatively constant and is not dependent on the value of the total dissolved solids or EC. Special attention should be paid to the relatively high exchangeable sodium in the subirrigation water, which may influence the soil physical properties and soil structure in the future (Fausey and Baker, 2003).

The linear relationships for the drainage outflow only are plotted in Figure 4 and 5 for cations and anions, respectively.

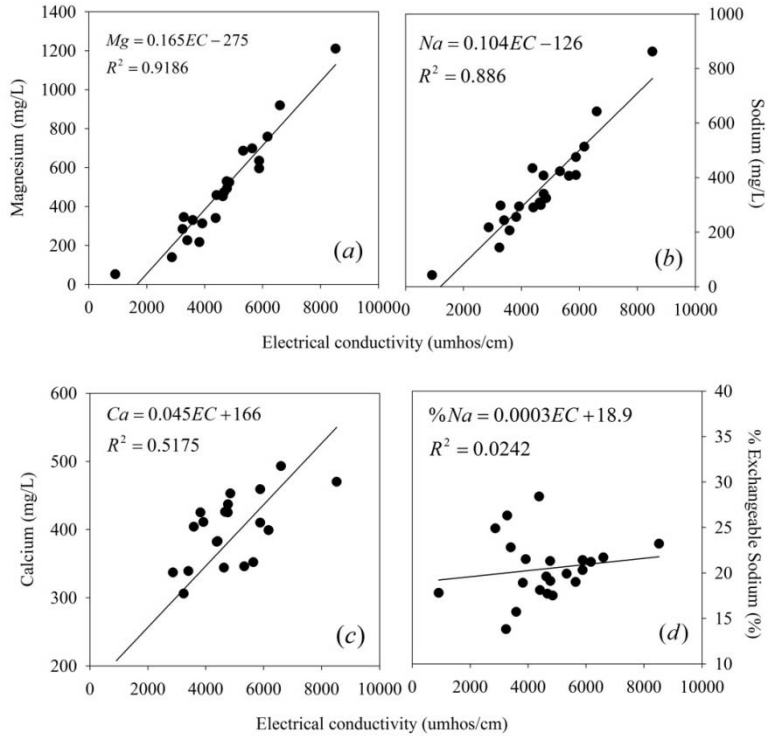


Figure 4. Linear relationship between electrical conductivity and magnesium (a), sodium (b), calcium (c), and percentage of exchangeable sodium (d) for drainage outflow.

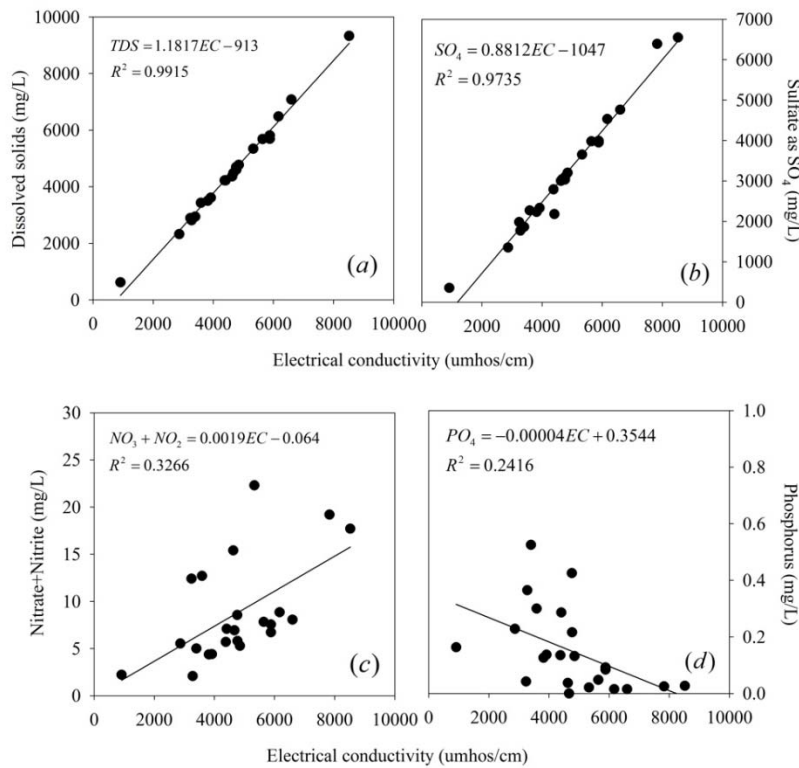


Figure 5. Linear relationship between electrical conductivity and total dissolved solids (a), sulfate (b), nitrate + nitrite (c), and phosphorus (d) for drainage outflow.

Because nitrate + nitrite release from tile drainage field is a major concern in agricultural water management practices, a prediction of nitrate + nitrite concentration is most needed. After removing the measurements for irrigation water, no relationship between EC and nitrate + nitrite and phosphorus can be found, with R-square values less than 0.5. The findings in this study are about the same as others have found (Gali et al., 2012).

The ultimate goal for predicting key water quality parameters with EC is to help in estimating the total nutrient load that is released from the drainage outlet or added to the field through subirrigation application. Because of the low concentrations for nutrient parameters, it is impossible to estimate their values. However, the EC values can be used to estimate the concentration of the dominant ions. Figure 6 shows the EC and sulfate concentration associated with drainage and subirrigation daily flow, where the daily outflow was calculated using the method outlined by Scherer and Jia (2010). Figure 7 shows the major cations, sodium, calcium, and magnesium associated with drainage and subirrigation daily flow.

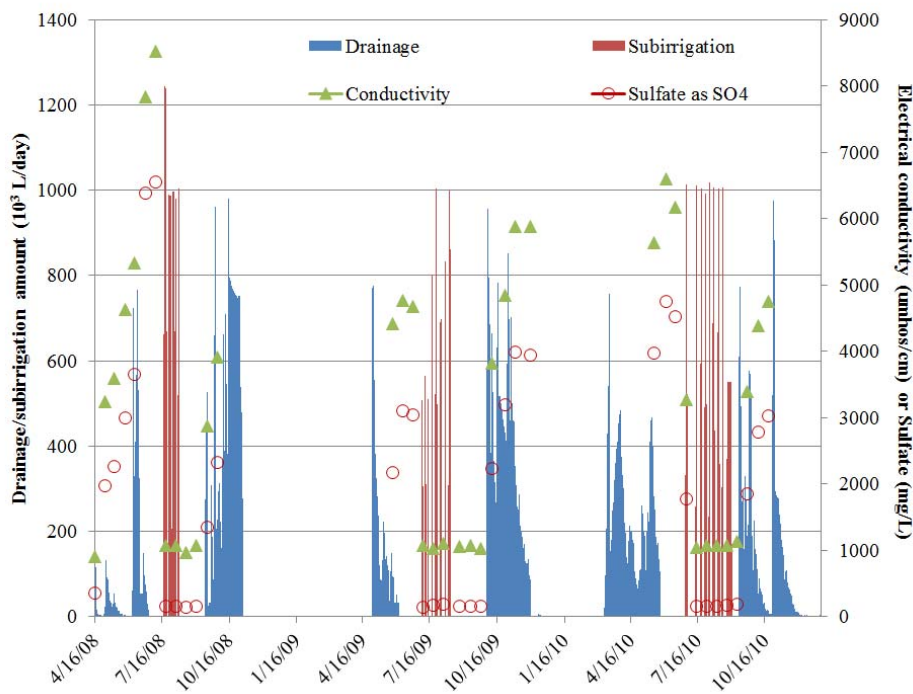


Figure 6. Daily drainage and subirrigation volumes related to electrical conductivity and sulfate concentration.

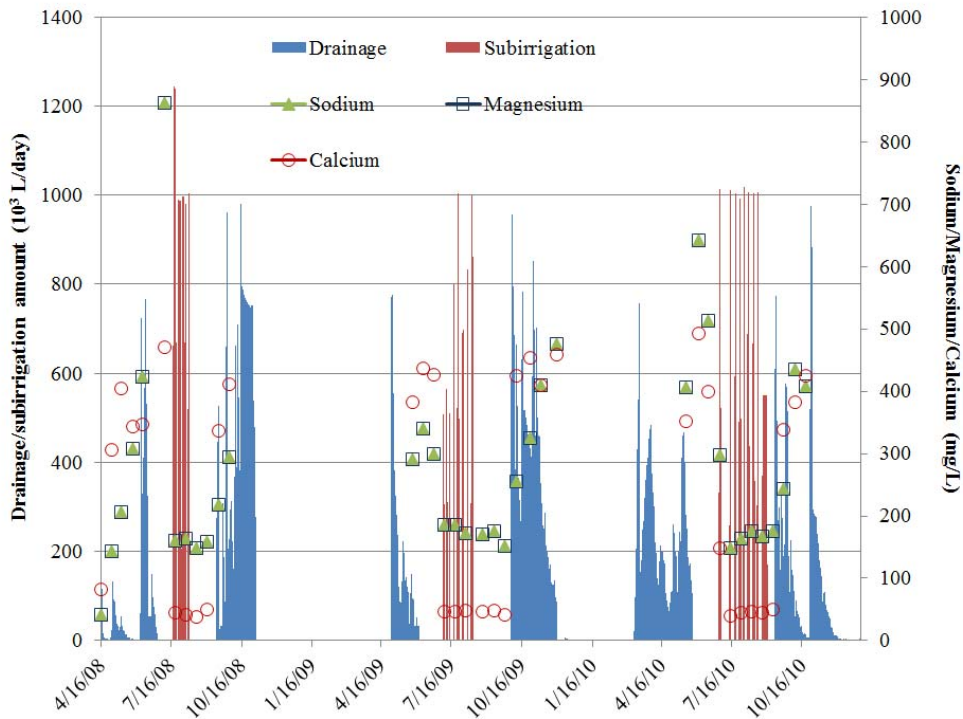


Figure 7. Sodium, magnesium, and calcium concentration compared with daily drainage and subirrigation volumes.

**CONCLUSION**

Strong relationships have been found between the electrical conductivity and the dominant cations and anions (salts parameters) using linear regression analysis of all 38 water samples collected at the outlet structure with  $R^2 > 0.90$ . Weak relationships were found between the electrical conductivity and nutrient parameters, with  $R^2 = 0.63$  for nitrate + nitrite and  $R^2 = 0.65$  for phosphorus. The electrical conductivity in the drainage outflow was relatively higher, indicated that salts and nitrate + nitrite were leaching out from the field. Strong relationships were developed between electrical conductivity and dominant ions for drainage outflow, but no relationship could be found with nutrient parameters because their low concentrations in the water samples. The electrical conductivity of the groundwater used for subirrigation was lower but the phosphorus concentration and exchangeable sodium were higher than in the drainage outflow. A clear threshold exists for most key water quality parameters between the two water sources, which can be used to separate water management practices according to water sources. In the future, a statistical analysis on principal components needs to be conducted to identify the key water quality parameters, instead of simple grouping based on the authors' personal experience. Other surrogates, such as total dissolved solids and pH values, should be considered to predict the nutrients concentrations and loads.

### ACKNOWLEDGEMENTS

Our appreciation goes to the landowner at Fairmount, ND, for providing his highly productive land for this research. The funding for the project was provided by USDA CSREES 2008-35102-19253, USDA NRCS 68-6633-8-0056, the North Dakota Agricultural Experiment Station, the North Dakota State Water Commission, and the North Dakota Department of Health. The authors wish to thank Mr. Dongqing Lin and Ms. Deb Baer for their technical support. Mention of trade names is for information purpose only and does not imply endorsement by the authors.

### REFERENCES

- ASAE Standard S526, Soil and Water Engineering Terminology. 2012. American Society of Agricultural and Biosystems Engineering, St. Joseph, MI.
- Fausey, N. R., and B. J. Baker. 2003. Effects of subirrigation on soil properties. ASABE Paper No. 032086. St. Joseph, Mich. ASABE.
- Gali, R. K., M. L. Soupier, and M. J. Helmers. 2012. Electrical conductivity as a tool to estimate chemical properties of drainage water quality in the Des Moines Lobe, Iowa. ASABE Paper No. 12-1338083. St. Joseph, Mich. ASABE.
- Gibson, G., R. Carlson, J. Simpson, E. Smeltzer, J. Gerritson, S. Chapra, S. Heiskary, J. Jones, and R. Kennedy. 2000. Nutrient Criteria Technical Guidance Manual: Lakes and Reservoirs. Washington, D.C., United States Environmental Protection Agency: Office of Water and Office of Science and Technology.
- Gilliam, J. W., J. L. Baker, and K. R. Reddy. 1999. Water quality effects of drainage in humid regions. In *Agricultural Drainage*, 801-830. R. W. Skaggs and J. van Schilfhaarde, eds. Madison, Wisc.: SSSA.
- Hayashi, M., T. Vogt, L. Machler, and M. Schirmer. 2012. Diurnal fluctuations of electrical conductivity in a pre-alpine river: effects of photosynthesis and groundwater exchange. *Journal of Hydrology* 450-451: 93-104.
- Hem, J. D. 2005. Study and interpretation of the chemical characteristics of natural water. U.S. Geological Survey Water-Supply Paper 1473. University Press of the Pacific, Honolulu, Hawaii.
- Iwanyshyn, M., M.C. Ryan, and A. Chu. 2009. Cost-effective approach for continuous major ion and nutrient concentration estimation in a river. *J. Env. Eng.* 135(4):218-224.
- Jayawardane, N. S., T. K. Biswas, J. Blackwell, and F. J. Cook. 2001. Management of salinity and sodicity in a land FILTER system, for treating saline wastewater on a saline-sodic soil. *Aus. J. Soil Res.* 39:1247-1258.

Jia, X., T.M. DeSutter, Z. Lin, W.M. Schuh, and D.D. Steele. 2012. Subsurface drainage and subirrigation effects on water quality in southeast North Dakota. *Transactions of the ASABE* 55(5): 1757-1769.

Marttila, H., and B. Klove. 2012. Use of turbidity measurements to estimate suspended solids and nutrient loads from peatland forestry drainage. *J. of Irrigation and Drainage* 138(12): 1088-1096.

Miguntanna, N. S., P. Egodawatta, S. Kokot, and A. Goonetilleke. 2010. Determination of a set of surrogate parameters to assess urban stormwater quality. *Science of the Total Environment* 408: 6251-6259.

Pellerin, B. A., W. M. Wollheim, X. Feng, and C. J. Vorosmarty. 2008. The application of electrical conductivity as a tracer of hydrograph separation in urban catchments. *Hydro. Proc.* 22:1810-1818.

Rijal, I., X. Jia, X. Zhang, D. D. Steele, T. F. Scherer, and A. Akyuz. 2012. Effects of subsurface drainage on evapotranspiration for corn and soybean in Southeast North Dakota. *J. of Irrigation and Drainage* 138(12): 1060-1067.

Scherer, T. F., and X. Jia. 2010. A simple method to measure the flow rate and volume from tile drainage pump stations. *Applied Engineering in Agriculture* 26 (1):79-83.

Smeti, E. M., N. C. Thanasoulis, E.S. Lytras, P.C. Tzoumerkas, and S. K. Golfopoulos. 2009. Treated water quality assurance and description of distribution networks by multivariate chemometrics. *Water Research* 43: 4676-4684.

Tan, C. S., C. F. Drury, J. D. Gaynor, T. W. Welacky, and W. D. Reynolds. 2002. Effect of tillage and water table control on evapotranspiration, surface runoff, tile drainage and soil water content under maize on a clay loam soil. *Agric. Water Manage.* 54(3):173-188.

Wilson, R. 2009. Winterkill. North Dakota Game & Fish Department. *North Dakota Outdoors*: 16-19.



# **GRASSLAND BYPASS PROJECT TREATMENT TECHNIQUES FOR REDUCTION OF SALT DISCHARGE TO THE SAN JOAQUIN RIVER**

Joseph C. McGahan<sup>1</sup>  
Dennis Falaschi<sup>2</sup>

## **ABSTRACT**

Agricultural subsurface drainwater discharges from the Grassland Drainage Area (a 90,000 acre productive farming area in the Firebaugh and Dos Palos area in the central San Joaquin Valley of California), for the period of 1995 to 2012 have dramatically declined. The Grassland Bypass Project began in 1997. The volume of drainage has been reduced significantly compared to pre-project (1995) discharges:

- Discharge volume (acre feet) has been reduced by 82%
- Selenium load has been reduced by 94%
- Salt load has been reduced by 84%
- Boron load has been reduced by 73%

The Project has been declared a success story related to meeting the selenium load limits for the San Joaquin River by the US Environmental Protection Agency. As a result of the Project's success the California State Water Resources Control Board removed several water bodies from its impaired waters list for selenium, including Salt Slough (10 miles) in 2008 and three segments of the San Joaquin River in 2010.

The reduction in salt discharges amounts to approximately 17% of the total salt discharge from the San Joaquin River into the Sacramento-San Joaquin River Delta as measured at Vernalis.

The Grassland Bypass Project is continually meeting monthly and annual selenium load targets for the project. Annual load targets have been met every year since 1999 and monthly targets have been met every month except for a few isolated instances when high rainfall occurred. This is being accomplished by management practices within the drainage area and the reuse of drainage water on salt-tolerant crops.

## **INTRODUCTION**

Management of subsurface drainage high in salts and other constituents has been a problem in the San Joaquin Valley since the 1960's or before. There have been many state and federal efforts to deal with this problem over the years. One of the most recent programs was the San Joaquin Valley Drainage Program completed in the late 1980's (SJVDA 1990). This study identified various methods to deal with the discharge of subsurface drainage water high in salt and other constituents. Within the Grassland

---

<sup>1</sup> President, Summers Engineering, P. O. Box 1122, Hanford, CA 93232; jmcgahan@summerseng.com.

<sup>2</sup> General Manager, Panoche Drainage District, Pacheco Water District, Charleston Drainage District, 52027 W. Althea Ave., Firebaugh, CA 93622; dfalaschi@aol.com.

Drainage Area (see **Figure 1**) it was recommended that the drainage issues be managed jointly among the various partners in the area. The Grassland Bypass Project is the project that was developed over the years to deal with the issue within the Grassland Drainage Area.

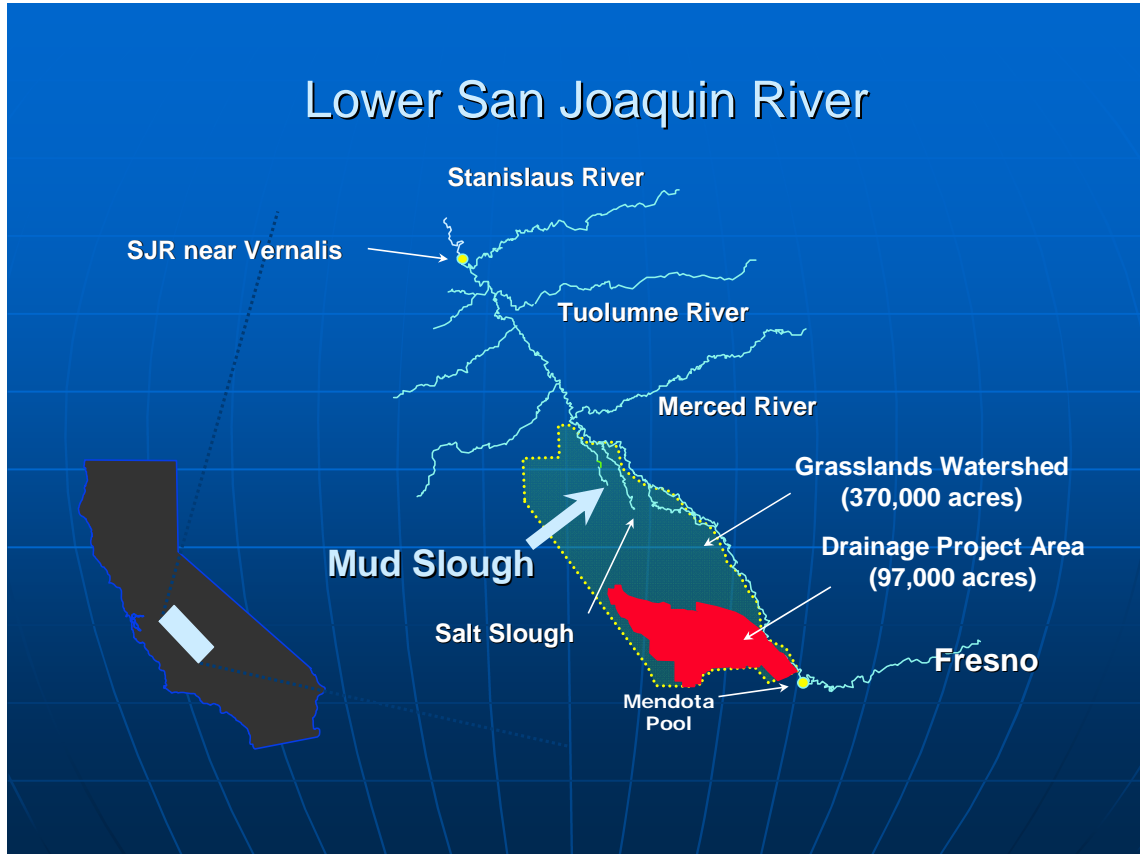


Figure 1. Area Map

### GRASSLAND BYPASS PROJECT

The Grassland Bypass Project (see **Figure 2**) is an innovative program that was designed to improve water quality in the channels used to deliver water to wetland areas. Prior to the Project, subsurface drainage water was conveyed through those channels in route to the San Joaquin River and limited their availability to deliver high-quality habitat supplies. The Project consolidates subsurface drainage flows on a regional basis and utilizes a portion of the federal San Luis Drain to convey the flows around the habitat areas.

Negotiations between the San Luis & Delta-Mendota Water Authority and the U S Bureau of Reclamation to utilize a portion of the San Luis Drain for the Project commenced in 1988. Stakeholders included in the process were: U.S. Environmental Protection Agency, U.S. Fish & Wildlife Service, California Department of Fish and Game, the Central Valley Regional Water Quality Control Board, Environmental Defense, Contra Costa County and Contra Costa Water District. In late 1995,

environmental documentation for the first five years was completed and the Use Agreement was signed.

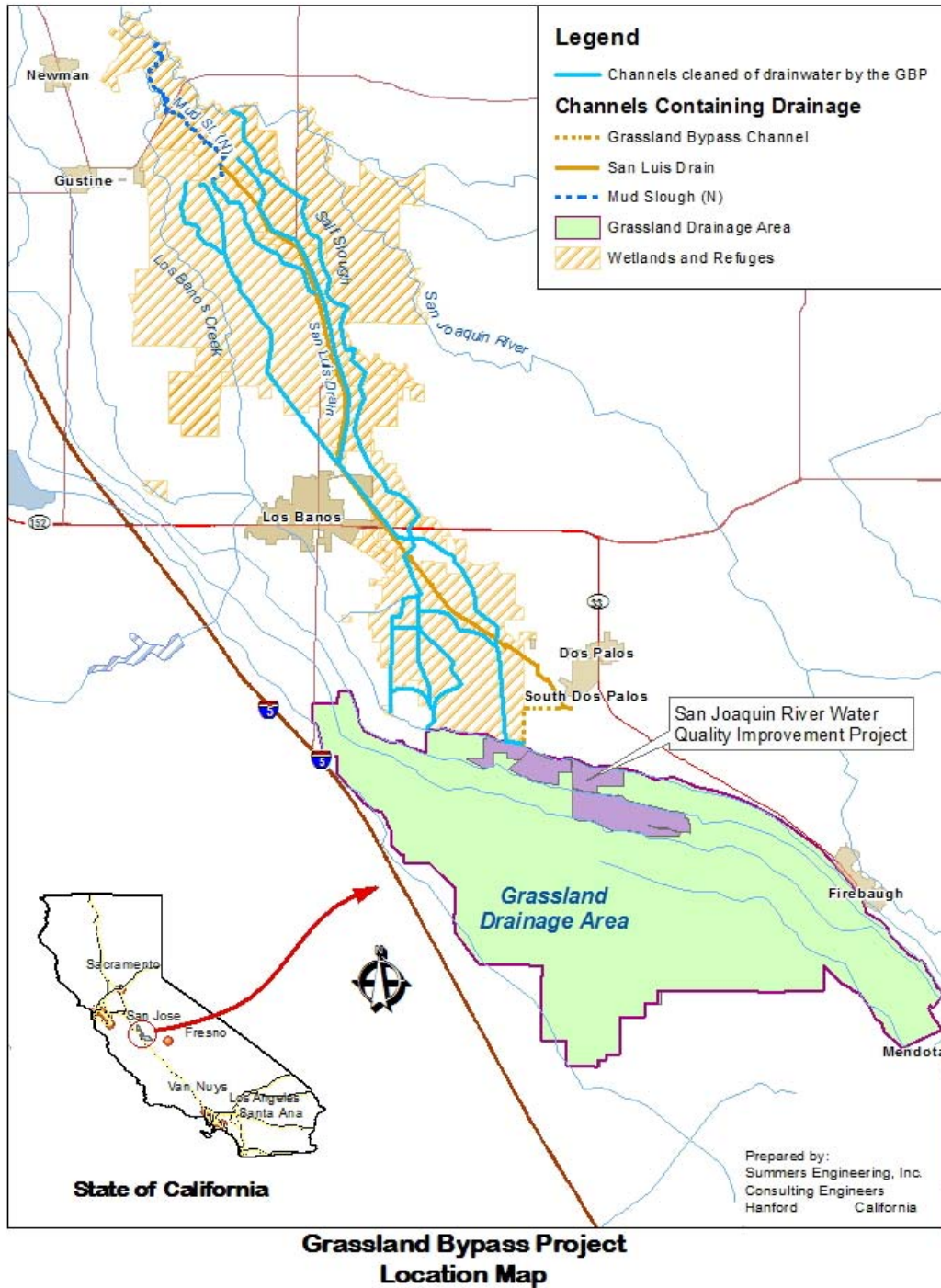


Figure 2. Grassland Bypass Project Location Map

Discharge through the project began in September 1996. In September 2001, the Use Agreement was extended for another 8 years and 3 months (through December 2009).

An Environmental Impact Report/Environmental Impact Statement was completed and on September 7, 2001 the Central Valley Regional Water Quality Control Board issued new Waste Discharge Requirements. Other items completed to support the continued use were a Biological Assessment/Biological Opinion, a selenium Total Maximum Monthly Load (TMML) report submitted by the Regional Board to EPA and a continued monitoring program. The new Use Agreement contained continued reductions in selenium and salinity discharge.

In 2007 negotiations renewed to extend the Use Agreement for a period of time up to December 2019 to allow the final measures to be implemented to reduce the discharge of sub-surface drainage water from the Grassland Drainage Area. An EIS/EIR was completed for that time extension. CEQA for the project was adopted on October 8, 2009. A biological opinion was issued on December 18, 2009 and the USBR adopted the Record of Decision on December 21, 2010. Steps ongoing include coordination with the Regional Water Quality Control Board for a Basin Plan Amendment and issuance of new Waste Discharge Requirements.

### **DRAINAGE MANAGEMENT COMPONENTS**

In 2003, the agricultural entities within the region developed a drainage plan to manage drainage discharges and meet compliance requirements. This plan identified four effective projects to manage and reduce drainage discharge through the Grassland Bypass Project. These include source control projects such as irrigation and infrastructure improvements to reduce the overall subsurface drainage production, groundwater management to lower the perched water level, drainage reuse to reduce the volume of drain water through the irrigation of salt tolerant crops, and drainage treatment to remove the salt and dissolved minerals. The ultimate goal of this plan will be to eliminate agricultural drainage discharge from the Grassland Drainage Area. **Figure 3** shows a schematic of the impact of each of the drainage solution components.

#### **Source Control Projects**

Source control projects are projects that can reduce the volume of water contributing to subsurface drainage production usually by reducing deep percolation. Source control projects can usually be divided into two categories: irrigation improvements and distribution infrastructure improvements.

Irrigation improvement projects include converting from a low efficiency irrigation system (such as furrow irrigation) to a high efficiency system (such as drip or micro sprinklers). The State of California and the local districts have made financial assistance (in the form of grants and low interest loans) available to growers as an incentive to convert from conventional irrigation practices to high efficiency drip irrigation (and similar systems).

Since the beginning of the Grassland Bypass Project, more than 45,000 acres within the Grassland Drainage Area have converted to high efficiency irrigation systems.

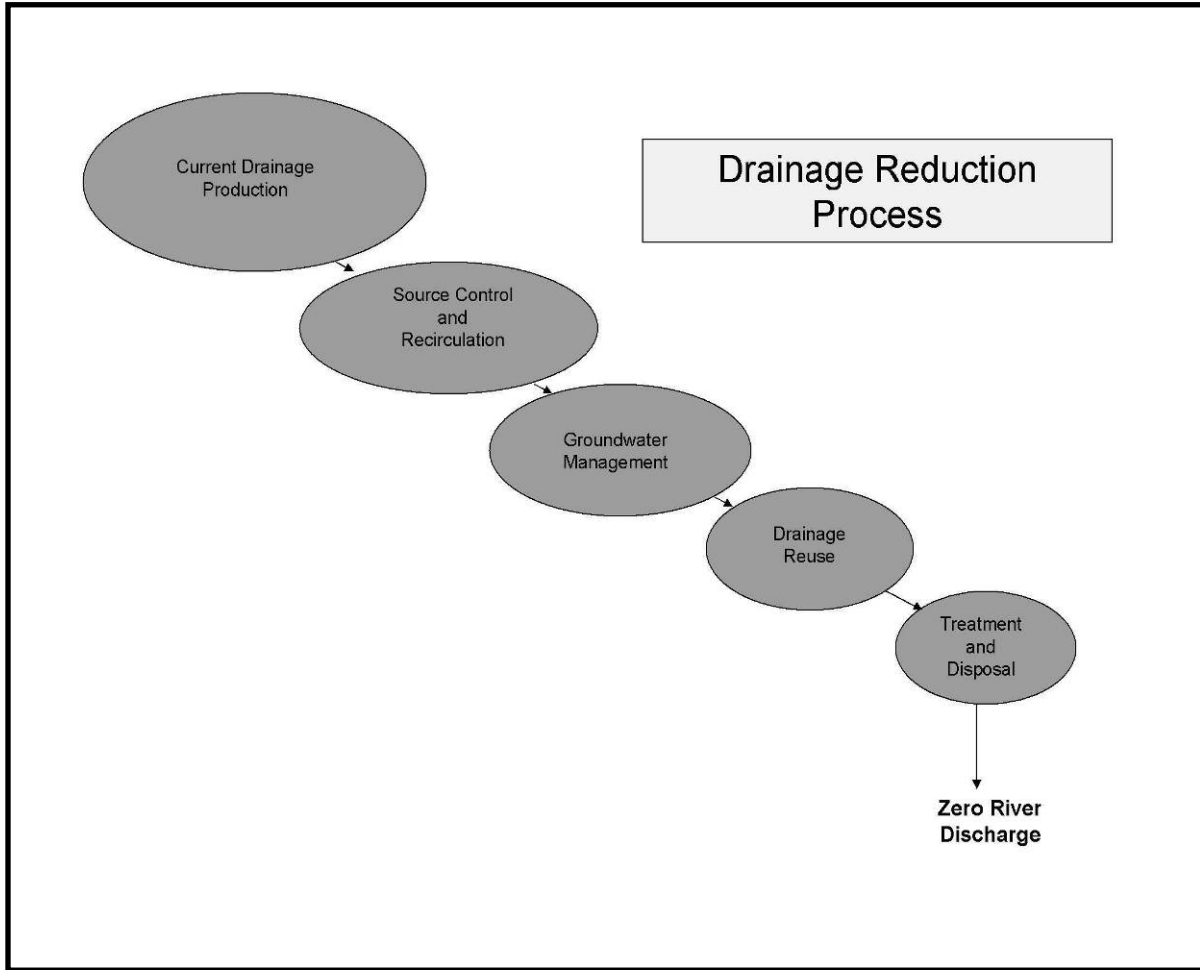


Figure 3. Drainage Solution Components

Distribution infrastructure improvement projects typically include the replacement of an unlined irrigation canal with a concrete lined channel or pipeline. Unlined channels within the Grassland Drainage Area can contribute more than 200 acre feet of seepage per year for each unlined mile. More than 30 miles of unlined canals have been lined or converted to pipelines since the beginning of the Grassland Bypass Project.

### **Drainage Recirculation**

Drainage recirculation is the process of redirecting drain water back into the irrigation system and it is one of the first drainage management tools implemented by the Grassland Area Farmers. Virtually all of the districts within the Grassland Drainage Area have some capacity for recirculation. Drainage recirculation is carefully monitored to maintain a blended water quality sufficient for agricultural use.

### Groundwater Management

A study performed in 2002, by the San Joaquin River Exchange Contractor's Water Authority (Exchange Contractor's) and the U.S. Bureau of Reclamation indicated that the pumping of strategically placed wells pumping in the unconfined aquifer below the confining clay known as the Corcoran Clay) could lower the perched water table and reduce the discharge of nearby subsurface drainage systems. A portion of the funding provided through a state grant program to improve water quality (Proposition 50) has been allocated to the installation of these wells, with about seven wells completed in to date.

### Drainage Reuse

One of the main management methods used to reduce drainage discharges is reuse – a process by which drain water is collected and reused as an irrigation source for salt tolerant crops. In 2001, 4,000 acres of marginal ground were purchased to become what is known as the San Joaquin River Water Quality Improvement Project or SJRIP for short. In 2007 this was expanded to 6,000 acres and was planted with a variety of salt tolerant crops including Jose Tall Wheatgrass, Bermuda grass, and salt tolerant varieties of alfalfa. In 2011, 21,600 acre feet of agricultural drainage water were used for irrigation in the Reuse Area. This neatly farmed Reuse Area continues to provide drainage service for 90,000 plus acres of productive farmland in Panoche Drainage District, Pacheco Water District, Charleston Drainage District, Firebaugh Canal Water District and Camp 13 Drainage District. Plans are underway to expand the Reuse Area to at least 8,000 acres with the goal of accomplishing zero discharge of agriculture related drainage to the San Joaquin River.

Drainage reuse began in the Grassland Drainage Area in 1998, when Panoche Drainage District began applying drain water to pasture fields. Some of the fields within the SJRIP have been irrigated with drain water since the start of the project, more than 10 years ago. **Figure 4** shows a planting of Jose Tall Wheatgrass in one of those fields.

The SJRIP has now evolved into a 6,000 acre area with six crop varieties ranging from alfalfa (moderately salt tolerant) to paspalum grass (a halophyte). Currently, about 5,500 acres of the SJRIP are developed to receive drain water.

Drainage reuse has been an extremely effective tool in reducing the volume of drainage water discharged from the Grassland Drainage Area but it is not without challenges. Because of the saline nature of the water applied, soil salinity needs to be carefully managed to prevent salt buildup in the root zone. Subsurface drainage systems have been installed on about 1700 acres, with plans to install the subsurface drainage systems in most of the SJRIP. Soil salinity is also managed through rotation where fields are fallowed or irrigated with fresh water for a season. Once the SJRIP is fully developed, the estimated drainage capacity of the project will be between 20,000 and 30,000 acre feet annually, provided the drain water is available for reuse when it is needed.



Figure 4. Planting of Jose Tall Wheatgrass in the SJRIP

### **Drainage Treatment/Disposal**

The application of saline drain water for irrigation on the SJRIP will result in some subsurface drain water generated by the drainage systems. Careful design of the drainage systems and irrigation management will minimize the volume of water generated; however it will be too saline for reuse and will need to be managed in some other form. Currently, the Grassland Area farmers are researching methods to treat this water, generating a usable treated product and a dry waste that can be easily managed. If it turns out that drainage treatment is not affordable, other methods of managing the reuse area soil salinity will need to be pursued. These would likely include field rotation and periodic fallowing with periodic leaching and may require further expansion of the SJRIP. Pilot treatment projects are in various stages of completion within the project area.

USBR Pilot Treatment Plant. The U.S. Bureau of Reclamation in cooperation with the Panoche Drainage District are in the final stages of preparing for construction for their pilot treatment plant to demonstrate Reclamation's preferred treatment method under the San Luis Drainage Feature Re-evaluation. It is anticipated this plant will come on line in by early 2014. Other pilot processes are also being tested including membrane monitoring, selenium removal and solar condensation.

UCLA Project. Smart Integrated Membrane System (SIMS): This project will test a SIMS module on a UF/RO membrane system and test operational capabilities while treating subsurface drain water from the SJRIP. The SIMS module monitors the rate of scaling on a representative membrane and initiates the backwash cycle before a drop in pressure is measured, improving the operation of the membranes as well as their lifespan. The system will be housed in a typical 40' container, and will have a flow rate of approximately 25 gpm. The pilot system is expected to operate on the SJRIP for approximately 3 months.

ADS Project. The ADS Project will use a proprietary technology to remove selenium from subsurface drain water generated by the SJRIP to levels below 5 ppb (the current water quality objective for selenium in wetlands is 2 ppb and for the San Joaquin River 5 ppb). The flow rate for this system will be between 3 and 5 gpm. The project is expected to operate on the SJRIP for approximately 3 months.

Water FX Project. The Water FX project will use solar energy and a refrigerant to condense drainwater from the SJRIP. The pilot system will include a solar collection component and a water condensation component, with a peak flow capacity of approximately 20 gpm. This system will not require any external energy source.

### **IMPACT OF THE GRASSLAND BYPASS PROJECT ON WATER SUPPLY**

Implementation of the Grassland Bypass Project has resulted in significant reduction in salt loading to the San Joaquin River (see **Table 1**). Water quality objectives in the San Joaquin River are set at Vernalis (See **Figure 1**) through the San Joaquin River Basin Plan adopted by the State Water Resources Control Board. These objectives are 1,000 uS/cm (microsiemens per centimeter) in the winter months (September – March) and 700 uS/cm in the summer months (April – August). The U.S. Bureau of Reclamation has the responsibility to release water from federal sources (such as New Melones Reservoir) to dilute flows in the San Joaquin River to meet these objectives. An analysis in the Grassland Bypass Project Annual Report 2008-2009 indicates that about 273,440 acre-feet of fresh water would have been required to dilute the average annual volume of drainage water from the Grassland Drainage Area to meet the Vernalis standard. During the period of the project though 2009 the theoretical annual volume of water needed to dilute the drainage water from the Grassland Drainage Area was reduced 40 percent to less than 164,000 acre-feet, a reduction of over 100,000 acre-feet. In 2009 the dilution amount required was 60,580 acre-feet or a reduction from the pre-project average of over 200,000 acre-feet. This amounts to a significant savings of water that can be used for other purposes.

### **SUMMARY**

The Grassland Bypass Project has been successful in reducing the volume of subsurface drain water discharged from the 100,000 acre Grassland Drainage Area while maintaining viable farming within the region. In 1995, prior to the Grassland Bypass Project, more than 57,000 acre feet of drain water were discharged through the wetland

channels. This not only impacted the water quality of the San Joaquin River system but exposed waterfowl attracted to the Grassland area wetlands to elevated levels of selenium and other constituents. The Grassland Bypass Project eliminated drainage discharge into the wetland channels and consolidated all of the drainage within the Grassland Drainage Area into one channel. By 2012, the volume of discharged drain water was reduced from more than 57,500 acre feet to about 10,500 (an 82% reduction in discharge). Similar reductions occur in the discharged load of selenium, salt, and boron. **Table 1** shows the annual reduction in drainage discharge and associated constituent load.

Although the success of the Grassland Bypass Project in reducing drainage discharge is evident, future water quality objectives will require near zero discharge from the Grassland Drainage Area. Full implementation of the solution components developed by the Grassland Area Farmers will be necessary to achieve this. Significant progress towards that end has been made:

- Drainage recirculation systems have been installed in nearly all of the Grassland Drainage Area districts.
- 5,500 acres of reuse are has been planted to salt tolerant crops – capable of reusing more than 20,000 acre feet of drainage annually.
- About 45% of the farmed acreage has converted been to high efficiency irrigation with many growers planning on installing new systems in coming years.
- Several wells have been installed in strategic locations to help lower the local perched water table.

Table 1. Constituent Load Reductions

	WY 95	WY 96	WY 97	WY 98	WY 99	WY 00	WY 01	WY 02	WY 03
Volume (AF)	57,574	52,978	39,856	49,289	32,317	31,342	28,235	28,358	27,345
Se (lbs)	11,875	10,034	7,096	9,118	5,124	4,603	4,377	3,939	4,032
Salt (tons)	237,530	197,526	172,602	213,533	149,081	139,303	142,415	128,411	126,500
B (1,000 lbs)	868	723	753	983	630	619	423	544	554
Se (ppm)	0.076	0.070	0.066	0.068	0.058	0.054	0.057	0.051	0.054
Salt (µmhos/cm)	4,102	3,707	4,306	4,308	4,587	4,420	5,016	4,503	4,600
Boron (ppm)	5.5	5.0	7.0	7.3	7.2	7.3	5.5	7.1	7.5

	WY 04	WY 05	WY 06	WY 07	WY 08	WY 09	WY 10	WY 11	WY 12	Reduction from WY 95 to WY 12
Volume (AF)	27,640	29,957	25,995	18,531	15,665	13,166	14,529	18,513	10,486	82%
Se (lbs)	3,860	4,305	3,563	2,554	1,736	1,264	1,577	2,067	741	94%
Salt (tons)	121,138	138,908	119,646	79,094	66,254	55,556	67,661	87,537	38,400	84%
B (1,000 lbs)	530	585	539	278	269	233	315	440	241	72%
Se (ppm)	0.051	0.053	0.050	0.051	0.041	0.035	0.040	0.041	0.026	
Salt (µmhos/cm)	4,358	4,611	4,577	4,244	4,206	4,196	4,631	4,702	3,642	
Boron (ppm)	7.1	7.2	7.6	5.5	6.3	6.5	8.0	8.7	8.5	

However, in order to eliminate discharge completely, all of these solution components need to be fully developed. In particular, the full 6,000 acres of the SJRIP need to be planted to salt tolerant crops and necessary infrastructure to deliver drain water to the

project needs to be constructed. In addition to that, a successful treatment process (or some other method to manage soil salinity) needs to be developed to full-scale to sustain long-term use of the SJRIP.

#### REFERENCES

San Joaquin Valley Drainage Program, A Management Plan for Agricultural Subsurface Drainage and Related Problems on the Westside of the San Joaquin Valley, September 1990

San Francisco Estuary Institute, Grassland Bypass Project Annual Report 2008-2009, <http://www.sfei.org/gbp/reports>

# THE ROLE OF AGRICULTURE IN ATMOSPHERIC NITROGEN DEPOSITION IN THE CHESAPEAKE BAY WATERSHED

William F. Ritter<sup>1</sup>

## ABSTRACT

The Chesapeake Bay is one of the major estuaries in the U.S. There are six major basins within the Chesapeake Bay watershed. These are the Potomac, Susquehanna, Rapahannock, York, James, and Patuxent basins. Agriculture is the largest contributor of nitrogen delivered to the Bay. Atmospheric deposition accounts for 33% of the nitrogen load delivered to the Bay in an average hydrologic year either through direct deposition on the tidal waters or deposition on land and transport to the Bay. Agricultural deposition accounts for 6% of the nitrogen load delivered to the Bay. Dairy and broilers account for the largest percentage of ammonia emissions from agriculture. Diet manipulation has the potential to reduce ammonia emissions from 15-25% in dairy cows, swine and poultry. Direct injection of manure is the most efficient method for reducing ammonia emissions during land application of manure. Dairy farms have the potential of reducing ammonia emissions by over 50% by implementing a combination of manure management and precision feeding practices.

## INTRODUCTION

The Chesapeake Bay watershed has a land area of approximately 180,000 km<sup>2</sup>, and a total water surface area of 9,890 km<sup>2</sup>. Of this water surface area, 390 km<sup>2</sup> are tidal fresh water, 9,190 km<sup>2</sup> are a mixing zone of fresh and salt waters, and 300 km<sup>2</sup> are salt water. The Bay is rather shallow, with a mean depth of 10 m. The Bay watershed consists of land area in Virginia, Maryland, West Virginia, Delaware, Pennsylvania, New York and the District of Columbia. There are six major basins within the Chesapeake Bay watershed. These are the Potomac, Susquehanna, Rapahannock, York, James, and Patuxent basins. These basins supply 90% of the flow to the Chesapeake Bay watershed. The Susquehanna River alone drains 43% of the watershed and contributes nearly 50% of the freshwater. Agriculture is the largest contributor of nonpoint source nutrients. Agriculture varies widely across the watershed. The western part of the watershed is dominated by small and medium sized dairy farms and grass-based cow-calf operations.

Dairy farms are also concentrated in southeastern Pennsylvania and in the New York portion of the watershed. Poultry production is concentrated on the Delmarva Peninsula, in the Shenandoah Valley of Virginia and southeastern Pennsylvania. Swine production is concentrated in southern Virginia and southern Pennsylvania. Corn, soybeans, wheat, hay, pasture, fruit and vegetables are the major crops grown in the watershed. The original 1987 Bay Agreement called for nutrient load reductions in each basin, with further nutrient load reductions being called for in the 2000 agreement. Because of the

---

<sup>1</sup> Bioresources Engineering Department, University of Delaware, Newark, DE, 19716  
Tel: 302-831-2468, Fax: 302-831-2469, E-mail: [writter@udel.edu](mailto:writter@udel.edu)

failure to meet past cleanup goals, the EPA was under a court order to complete a TMDL. EPA released the final TMDL for the Chesapeake Bay in December 2010.

### ATMOSPHERIC DEPOSITION INPUTS

Atmospheric loads of nitrogen are from chemically oxidized forms of nitrogen in the form of nitrogen oxides ( $\text{NO}_x$ ) and from reduced forms of nitrogen deposition in the form of ammonia ( $\text{NH}_3$ ). The oxidized forms of nitrogen deposition originate from atmospheric conditions of high heat and pressure and are formed from eutrophically inert diatomic atmospheric nitrogen. The principle sources of nitrogen oxides are air emissions from industrial boilers, electric power plants and the transportation industry internal combustion engines. Ammonia sources occur primarily from agriculture and include: volatilization of ammonia from manures and emissions from ammonia based fertilizers.

The Chesapeake Bay Airshed (CPA) Model is used to estimate nitrogen deposition to the Bay watershed either by depositing directly onto the Bay's tidal surface waters or onto the surrounding Bay watershed. The model is a combination of a regression model of wet deposition (Grimm and Lynch, 2005) and a continental-scale air quality model of North America called the CMAQ (Community Multiscale Air Quality model) for estimation of dry deposition (Hameedi et al., 2007). The regression model provides hourly wet deposition loads to each land segment on the basis of each land segment's rainfall. The model used data from 39 National Atmospheric Deposition Program monitoring stations to form a regression of wetfall deposition for the simulation period from 1985-2005 over the entire watershed. The CMAQ model covers the entire North American continent at a 36 km x 36 km grid scale. A 12 km x 12 km grid scale is used over the Chesapeake Bay watershed. The model needs hourly emissions estimates and meteorological data in every grid and a set of pollutant concentrations to initialize the model and to specify concentrations along the modeling domain boundaries. The CMAQ model airshed for the Chesapeake Bay covers 17 states, 2 provinces for a total of 1,547,000  $\text{km}^2$ .

The Chesapeake Bay Airshed model provides input to the Phase 5.3 Chesapeake Bay Watershed Model (Bay Watershed Model) and the Chesapeake Bay Water Quality and Sediment Transport Model (Bay Water Quality Model). The nitrogen outputs from the CPA Model affect the nitrogen input from atmospheric deposition to the Bay Watershed Model. The Bay Watershed Model, in turn, transports total nitrogen, phosphorus and sediment from all the different sources to the Bay Water Quality Model. The Bay Water Quality Model, in turn, simulates the effects of the nitrogen, phosphorus and sediment loads generated by the Bay Watershed Model and the effect of direct atmospheric deposition on the Bay water quality. The linkage between the models is illustrated in Figure 1 (EPA, 2011).

The nitrogen loads from different sources to the Bay generated by the Phase 4 Chesapeake Bay Watershed Model for an average hydrologic year are shown in Figure 2. Air sources account for about 33 % of the total nitrogen load delivered to the Bay by depositing directly onto the tidal surface waters of the Bay or falling on the watershed and being transported to the Bay. Direct deposition onto tidal waters is estimated to be 6

to 8 % of the total nitrogen load delivered to the Bay. The nitrogen deposited onto the Bay land surface and subsequently transported to the Bay accounts for 26 to 28 % of the total nitrogen load delivered to the Bay. Agricultural atmospheric deposition accounts for about 6 % of the total nitrogen load delivered to the Bay.

Between 1985 and 2005, the simulation period of the Bay Watershed Model for the TMDL, atmospheric deposition loads of nitrate ( $\text{NO}_x$ ) decreased by about 30 % (EPA, 2011). Most of the reduction was due to point sources air emissions by electrical power generating plants and cars and trucks. Average ammonia deposition loads have followed the trend of overall manure loads in the watershed, which have increased. Ammonia deposition is very site specific with increased poultry production occurring on the Eastern Shore and Shenandoah basins and a reduction of dairy farms in the northern part of the watershed.

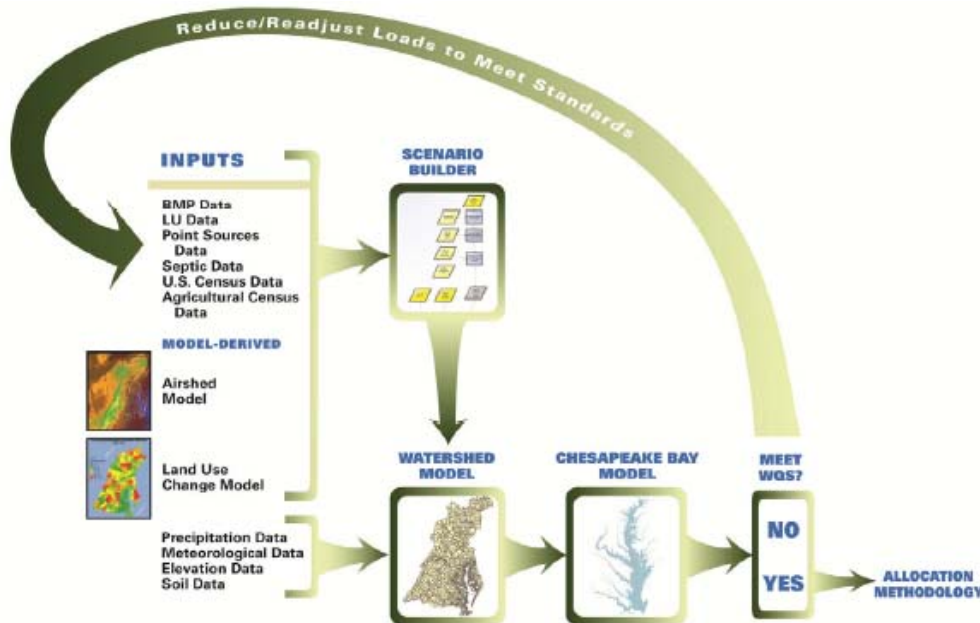


Figure 1. Chesapeake Bay TMDL Modeling Framework

### AMMONIA PRODUCTION

Agriculture is responsible for over three-fourths of the  $\text{NH}_3$  emissions in the U.S..(Bittman and Mikkelsen, 2009). Livestock accounts for 71 % and fertilizers account for 19 % of the emissions. The greatest  $\text{NH}_3$  losses from animal production typically come from animal confinement buildings and during land application of manure. Losses also come from animal grazing and manure storage.

Livestock and poultry consume a considerable amount of protein and other N compounds with their feed. The conversion of dietary N to animal product is very inefficient and 50 to 80 % of the N consumed can be excreted in the manure (Arogo et al., 2001). The

primary sources of  $\text{NH}_3$  in livestock and poultry production are urea and uric acid. In poultry more than 70 % of the N excreted is uric acid. Urea and uric acid are converted to total ammoniacal nitrogen ( $\text{TAN} = \text{NH}_4^+ + \text{NH}_3$ ), by hydrolysis. Substantial conversion takes place in hours after the manure is excreted and is influenced by temperature, pH and moisture content. Depending upon pH, ammonia exists as an ammonium ion ( $\text{NH}_4^+$ ) or as ammonia ( $\text{NH}_3$ ). Ammonia volatilization from aqueous solutions depends upon a number of factors, including TAN concentration, pH, temperature, wind speed, chemical and microbial activity, diffusion and convective transport, and gas transfer at the boundary layer between the emitting surface and the atmosphere (Arogo et al., 2001).

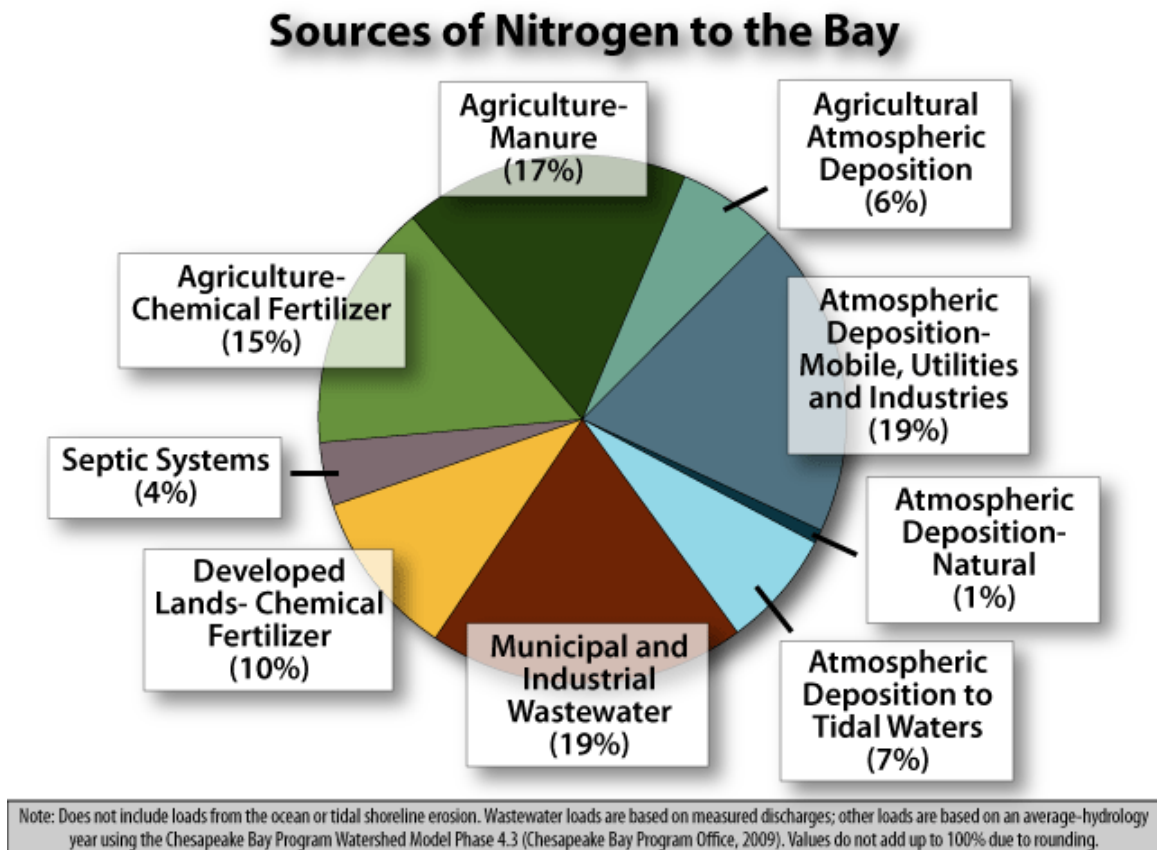


Figure 2. Sources of Nitrogen Delivered to Chesapeake Bay

EPA estimated ammonia emissions from animal operations for the EPA's National Emissions Inventory (NEI) for each county in the U.S. (EPA, 2005). They considered ammonia emissions from, housing, production area and land application of manure. They based their estimates on county census livestock and poultry data and emission factors from different manure management practices and sources. The percent nitrogen lost as ammonia for beef, dairy, swine and poultry for their emissions inventory are presented in Table 1.

The ammonia emission factors used by EPA were used to estimate ammonia emissions in the Chesapeake Bay watershed. Livestock and poultry numbers were estimated from the

latest state and county agricultural statistics data (NASS, 2012) for Delaware, Maryland, Pennsylvania, New York, Virginia and West Virginia and from the Delmarva Poultry Industry broiler production data (DPI, 2012). Manure production rates and nitrogen content for dairy, swine, broilers, turkey and layers were taken from the ASABE standard “Manure Production and Characteristics” (ASABE, 2012). The annual ammonia estimates for swine, dairy, broilers, layers and turkeys are presented in Table 2. The total annual ammonia emissions are estimated to be  $66.0 \times 10^6$  kg. The largest annual emissions are from broilers and dairy cows. Ammonia emissions are quite variable in the watershed because of the concentration of livestock and poultry production. Dairy production is concentrated in New York state and southeastern Pennsylvania, while broiler production is concentrated on the Delmarva Peninsula and the Shenandoah Valley of Virginia.

Table 1. Summary of Nitrogen Lost as Ammonia from Livestock and Poultry

Animal Groups	Percent Nitrogen Lost As Ammonia			
	Housing Area	Production Area	Land Application	Total
Dairy	11	14	13	38
Beef	10	0	3	12
Poultry	31	5	15	31
Swine	20	24	10	63

Table 2. Estimated Annual Ammonia Emissions from Livestock and Poultry in the Chesapeake Bay Watershed

Animal Group	Ammonia Emissions (kg/yr)
Dairy	$28.7 \times 10^6$
Swine	$8.7 \times 10^6$
Layers	$5.9 \times 10^6$
Turkeys	$6.5 \times 10^6$
Broilers	$22.6 \times 10^6$

There is considerable variation in ammonia emission factors in the literature for dairy, poultry and swine. This can be expected because of different climate, housing and manure management practices. Chitikela and Ritter (2004) estimated the annual ammonia emissions from broilers in Delaware were approximately  $8.7 \times 10^6$  kg/yr if a feeding period of 50 days is assumed before the birds are marketed. This ammonia emission rate is based upon 257 million broilers. Ullman et al (2003) estimated that each broiler contributed 19 g NH<sub>3</sub> to the atmosphere in Delaware. Based upon the 257 million birds marketed, this would give annual ammonia emissions of  $4.9 \times 10^6$  kg. Precipitation ammonia concentration increased 60% from 1981-2001 at Lewis, Delaware which parallels the growth of the poultry industry on the Delmarva Peninsula (Ullman et al., 2003). Using Chitikela and Ritter ammonia emission rates, the annual ammonia emissions for broilers for the entire Chesapeake Bay watershed would be  $28.4 \times 10^6$  kg based upon 840 million birds marketed. The 2008 EPA National Emission Inventory gives the total ammonia emissions from livestock and poultry for Delaware, Maryland,

Pennsylvania, Virginia and West Virginia as  $127 \times 10^6$  kg/yr (EPA, 2010), while the total in Table 2 is  $72.4 \times 10^6$  kg/yr. Table 2 does not include estimates for beef cattle, but includes the New York state portion of the watershed. Beef cattle ammonia emission rates are lower than dairy, swine or poultry and are not that prevalent in the Chesapeake Bay watershed. The 2002 EPA National Emission Inventory gives the total ammonia emissions from livestock and poultry for New York state of  $37.4 \times 10^6$  kg/yr with  $31.3 \times 10^6$  kg/yr coming from the dairy industry with New York having 670,000 dairy cows (Chase, 2011). Today New York counties in the Chesapeake Bay watershed have about 400,000 dairy cows. Using the ammonia emission factor to calculate the data in Table 2, the ammonia emissions from the New York portion of the watershed would be  $12.8 \times 10^6$  kg/yr. Using the 2002 EPA emission rate, the ammonia emissions would be  $18.7 \times 10^6$  kg/yr for New York State. The yearly ammonia emission factors from the National Air Emissions Monitoring study ranged from 12.7 to 16.3 kg/co (Gooch, 2010). If the emission factor of 16.3 kg/cow is used in the Chesapeake Bay watershed, the ammonia emissions from dairy cattle would be  $14.7 \times 10^6$  kg/yr, which is about half of the estimate in Table 2 for dairy cattle. Aneja et al. (2008) reported annual ammonia emission factors used around the world for dairy cattle range from 20.4 to 38.0 kg/cow/yr. Using an emission factor of 38.0 kg/cow, the annual ammonia emissions from dairy cattle for the Chesapeake Bay watershed would be  $34.2 \times 10^6$  kg/yr.

## CONTROL OF AMMONIA EMISSIONS

### Poultry

Ammonia volatilization is not only an environmental concern, but it affects the production process and the health of the birds. Strategies for controlling ammonia in poultry production include ventilation, dietary manipulation and manure management (Ritz et al., 2004). Increased ventilation rates improve air quality in the house but translate into releasing more ammonia to the environment. In recent years, a number of growers have been planting trees around their poultry houses to filter out the dust and ammonia emitted from the ventilation fans.

The most common method used in broiler and turkey production to reduce ammonia volatilization is to treat the litter with an acidifying agent such as alum (aluminum sulfate) or ferrous sulfate. Armstrong et al. (2003) investigated three levels of liquid alum litter treatment and compared them with no treatment in 4 different broiler houses. Alum application rates of 1.64 and 2.46 L/m<sup>2</sup> were effective in maintaining in-house ammonia concentrations below 25 ppm for the first 3 weeks of the grow-out. Odor and moisture absorbents, which are typically clay based products containing zeolites, are sometimes used (Ritz et al, 2004). By lowering the moisture of the litter or manure, absorbents inhibit the microbial activity associated with ammonia formation and volatilization.

Wheeler et al. (2003) found ammonia emissions were low in houses where the litter was replaced after every flock. If the ammonia emissions start to be regulated in the poultry industry, growers may be forced to replace litter after every

flock. This may be one of the only methods that would reduce ammonia emissions below regulatory limits, if EPA starts regulating ammonia emissions from poultry operations. Feeding reduced protein diets can reduce the nitrogen content of the manure and result in less ammonia volatilization. Other diet manipulation strategies that can be used include feed formulation based upon amino acid requirements rather than crude protein, optimizing the amino acid profile with bird requirements, phased feeding for current growth and production, selection of feed ingredients with low nutrient variability and use of feed enzymes and additives (Ritz et al., 2004).

### Swine

In the Chesapeake Bay watershed, swine are raised in enclosed buildings or on open lots with shelter. In most cases manure is handled as a liquid or semi-solid. For open lots either an earthen manure storage basin or anaerobic lagoon is used. The manure may be scraped or flushed into the storage basin or lagoon. Hogs in enclosed buildings are raised on solid or slotted floors. Slotted floors are commonly associated with under-floor deep storage pits or with shallow collection pits that are mechanically scraped or hydraulically flushed or gravity drained to outside storage structures or lagoons. Solid floors may be bedded for solid manure handling or may be used with gutters that provide for hydraulic handling of the manure.

In Pennsylvania most of the nursery and grower-finish facilities generally have a deep pit under totally slotted floors (Kephart, 2000). Sow units almost always have shallow pits with outside storage. In Virginia hogs producers are more likely to use open lots than in Pennsylvania. Anaerobic lagoons and flushing systems are used more in Virginia and other southeastern states.

Researchers have attempted modification of the nutrient content of pig diets in order to enable more effective utilization of dietary nutrients and reduce losses through excretion. Various different strategies have been experimented with, among which crude protein content of the diet is decreased. Lenis (1989) suggested modification of diet by examining the protein/amino acid balance to control emissions of N into the atmosphere. Therefore formulating diets according to the protein requirements could reduce N excretion by about 6%. An even greater reduction in N excretion could be achieved by mixing a feed rich in protein and minerals with an energy rich feed in a changing ratio during the fattening phase. Lowering the protein levels in pig diet and supplementing with synthetic amino acids like lysine, methionine, threonine, and tryptophan could result in about 25% reduction in N excretion by increasing efficiency of N utilization without any harmful effects (Lenis, 1989).

Sometimes feed additives used in feed may also have the additional benefit of increased nutrient utilization and reduced excretion. One such additive for swine is ractopamine hydrochloride (RAC), a  $\beta$  adrenergic agonist used to increase the amount of quality lean pork per carcass by directing nutrients away from fat and improve production efficiency. It also enhances feed efficiency and increases growth rate, which means less feed required for lean growth and fewer days to market and less manure. Sutton et al. (2002)

used RAC in a series of experiments with swine. RAC reduced average manure output by 3.9% and average nitrogen N reduction via excretion by 10.7%. When a lower crude protein CP diet containing RAC was used, nitrogen excretion was reduced by 34.7%.

In the swine industry, ammonia is lost from anaerobic lagoons, manure storage systems and during land application of manure. The simplest way to control ammonia emissions from storage and treatment units open to the atmosphere is to use a physical cover to contain the emissions. Impermeable floating covers on anaerobic swine lagoons can reduce ammonia emissions by almost 100%. A thin layer of vegetable oil or soybean oil on manure slurries can significantly reduce ammonia emissions, since ammonia is not soluble in oil. Heber et al. (2005) evaluated the efficacy of soybean oil sprinkling on ammonia emissions in tunnel ventilated swine finishing barns. The oil treated barn resulted in 40% less ammonia emissions than the control barns. Permeable covers such as straw, corn stalks, peat moss, foam or geotextile fabric will also reduce ammonia emissions from manure storages. Reduction rates may vary from 30 to 90% depending upon the type of cover and the thickness of the cover (Ndegwa et al., 2007). Impermeable covers are generally more effective than permeable covers in ammonia mitigation from manure storage systems, but generally cost more. The clean-up and removal of the material left behind when the useful life of the cover is over is also important to consider.

Removing ammonia from the ventilated air of swine buildings is also feasible using filters or scrubbers (water and acid). A wide range of efficiencies (9-100%) have been reported in the literature and a number of materials such as wood chips, compost, coconut peels, bark-wood and perlite have been used as filter material. The practical application of these devices is limited due to the high cost and technical problems due to dust, especially in poultry and swine housing (Ndegwa et al., 2007).

### **Dairy**

Housing and management practices can lower ammonia emissions in the dairy industry. by reducing the contact between the urine and solid manure. The type of bedding can affect ammonia emissions. In one study, the lowest ammonia emissions occurred when pine shavings were used. When shredded newspaper, straw and recycled manure solids were used as bedding the ammonia emissions increased (Chase, 2011). Powell et al. (2011) found applying tannin directly on the housing floor lowered ammonia emissions by 19%. Separating urine and feces is another way of reducing ammonia emissions. Using sloped floors with a urine collection tube in free-stall barns is one method of achieving this. Free-stall barns using flushing can use solid separators to separate the solids, which can then be composted. Ndegwa et al. (2007) found all urine-feces segregation methods evaluated and reviewed reduced ammonia emission by 50% for swine and cattle.

Feed and diet manipulation is another way to reduce ammonia emissions. Research studies have examined the relationship between ration crude protein, rumen degradability protein (RDP), N intake and ammonia emissions. A key factor related to ammonia emissions is the quantity of urinary N and urinary urea N. Research has shown when crude protein is decreased in the diet, urinary urea-N decreases and ammonia emission

are reduced (Chase, 2011). Ammonia emissions will also increase as diet metabolizable protein increases.

Significant amounts of ammonia volatilization occur when manure is surface applied to cropland or pasture. Direct injection or tillage shortly after applying the manure will increase the ammonia utilization of crops. Direct injection has shown to decrease ammonia emissions by 47-100% (Ndegwa et al., 2007).

There are opportunities to lower ammonia emissions significantly on a whole farm basis in the dairy industry. Jonker et al., (2002) did a process based model study of a dairy farm with 320 milking and dry cows and 290 replacement heifers with herd milk production of 11,800 kg/cow/y. They found precision feeding reduced ammonia emissions by 22% from the baseline while precision feeding plus soil incorporation of the manure reduced ammonia emissions by 48% and precision feeding, plus lagoon cover and soil incorporation decreased ammonia emissions by 65%. The baseline ammonia emissions were 30,050 kg/yr

### **CONCLUSION**

Air emission account for 33% of the nitrogen load delivered to the Chesapeake Bay either by deposition on the land and transport to the Bay or by direct deposition on the tidal waters of the Bay.

Agricultural atmospheric deposition accounts for about 6 % of the total nitrogen load delivered to the Bay.

Dairy and broilers account for the largest percentage of ammonia emissions from livestock and poultry in the watershed.

Diet manipulation has the potential to reduce ammonia emissions from 15-25% in dairy cows, swine and poultry.

Permeable and impermeable covers on manure storage and treatment systems can reduce ammonia emissions by 30-100%

Direct injection of manure is the most efficient method for reducing ammonia emissions during land application of manure.

Dairy farms have the potential of reducing ammonia emissions by over 50% by implementing a combination of manure management and precision feeding practices.

### **REFERENCES**

American Society of Agricultural and Biological Engineers. 2012. Manure production and characteristics. ASABE Standard D384.2. ASABE, St. Joseph, MI.

- Aneja, V.P., J. Blunder, K. James, W. Scjlesinger, R. Knighton, W. Gilliam and G. Jennings. 2008. Ammonia assessment from agriculture: U.S. status and needs. *J. of Environmental Quality*, 37:515-521.
- Armstrong, K.A., Burns, R.J. Walker, F.R. Wilhelm, L. R. and Ramon, D.R. (2003). Ammonia concentrations in poultry broiler production units treated with liquid alum. In: *Air Pollution From Agricultural Operations*, ASAE, St. Joseph, MI. pp. 116-122. ASAE, St. Joseph, MI. Paper No. 01-4094.
- Argo, J., P.W. Westerman, A.J. Heber, W.P. Rabarge and J.J. Clausen. 2001. Ammonia in animal production: A review. ASAE, St. Joseph, MI. Paper No. 01-4089.
- Bittman, S. and R. Mikkelsen. 2009. Ammonia emissions from agricultural operations: Livestock. *Better Crops*, Vol. 93, No. 7.
- Chase, L.E. 2011 Ammonia emissions from dairy operations-what do we know? Proc. Cornell Nutr. Conf., Syracuse, NY.
- Chitikela, S.R. and W.F. Ritter. 2004.. Ammonia emissions from poultry operations in the state of Delaware: A critical review, estimation and fate. Proceedings of EWRI/ASCE World Water and Environmental Congress, June 27-July 1, 2004, Salt Lake City, UT. CD-ROM.
- Delmarva Poultry Industry. 2012. Delmarva meat chickens, soybeans and corn production and use. DPI, Georgetown DE. Fact Sheet. Available at <http://www.dpichicken.org/>
- Gooch, C. 2010. National air emissions monitoring study – dairy component initial findings. Proc. Cornell Nutr. Conf., Syracuse, NY. 5 pgs
- Grimm, J.W., and J.A. Lynch. 2005. Improved daily precipitation nitrate and ammonium concentration models for the Chesapeake Bay Watershed. *Environmental Pollution* 135(2005):445–455.
- Heber A J; Tao P C; Ni J Q; Lim T T; Schmidt A M (2005). Air emissions from two swine finishing building with flushing: ammonia characteristics. Proceedings of the Seventh International Animal Environment Symposium, Beijing, China. ASABE, St. Joseph, MI.
- .Hameedi, J., H. Paerl, M. Kennish, and D. Whitall. 2007. Nitrogen deposition in U.S. coastal bays and estuaries. *Journal of the Air and Waste Management Association*. December 2007.
- Jonker, J. S., P. R. Hagenstein, R. G. Flocchini and C. K. Baer. 2002. Nutrient management effects on air emissions: examining best management practices through a process-based model to estimate air emissions from animal feeding operations. Proc. Cornell Nutr. Conf., Syracuse, NY. pp:99-108.

- Kephart, K. 2000. Manure management on swine farms: Practices and risks. In: Proceedings of Managing Nutrients and Pathogens from Animal Agriculture, March 28-30, 2000, Camp Hill, PA. NRAES, Cornell University, Ithaca, NY. NRAES-130. pp 119-123.
- Lenis, N. P. 1989. Lower nitrogen excretion in pig husbandry by feeding: Current and future possibilities. Netherlands J. of Animal Sci., 37:61-70.
- National Agricultural Statistics Service. 2012. Annual state statistical data. Available at <http://www.nass.usda.gov/>
- Ndegwa, P. M., A.N. Hristov, J. Arogo and R.E. Sheffield. 2007. A review of ammonia emissions mitigation techniques for concentrated animal feeding operations. Available at [http://www.ag.iastate.edu/wastemgmt/Mitigation\\_Conference\\_proceedings/CD\\_proceedings/Invited\\_Papers/Ndegwa\\_Emissions\\_Techniques.pdf](http://www.ag.iastate.edu/wastemgmt/Mitigation_Conference_proceedings/CD_proceedings/Invited_Papers/Ndegwa_Emissions_Techniques.pdf)
- Powell, J. M., M. J. Aquerre and M. A. Wattiaux. 2011. Tannin extracts abate ammonia emissions from simulated dairy barn floors. J. Environ. Qual. 40:907-914.
- Ritz, C.W., B.D. Fairchild and M.F. Lacy. 2004. Implications of ammonia production and emissions from commercial poultry facilities: A review. J. of applied Poultry Science, 35; 683-692.
- Sutton et al. 2001. Manipulation of animal diet to affect manure production composition and odors: State of the science. Proceedings of International Symposium Addressing Animal Production and Environmental Issues, Oct. 3-5, 2001, Raleigh, NC. CD-ROM
- Ullman, W.J., Wong, J.W., Scudlark, J.R., Madsen, J.M., Krantz, D.E., Andres, A.S. and McKenna, T.E. 2003. Nutrient inputs as a stressor and net nutrient flux as an indicator of stress response in Delaware's Inland Bays ecosystem. University of Delaware, College of Marine Studies, Newark, DE. Technical report submitted to EPA.
- USEPA. 2011. Chesapeake Bay TMDL Available at <http://www.epa.gov/reg3wapd/tmdl/chesapeakebay/tmd/exec.html>. EPA, Washington, DC
- USEPA. 2010. EPA National emissions inventory. Available at <http://www.epa.gov/ttn/chief/net/2008inventory.htm>.
- USEPA. 2005. National emission inventory – ammonia emissions from animal husbandry operations. Revised draft report. <http://www.epa.gov/ttn/chief/ap42/ch09/index.html>
- Wheeler, E.F., Zajackowski, J.L., Topper, P., Gates, R., Xin, H., Casey, K. and Liany, Y. 2003. Characterizing ammonia emissions from broiler houses. ASAE, St. Joseph, MI. Paper No. NABEC 03-026.



# **THE USE OF RECYCLED WATER FOR IRRIGATION OF TURF AND LANDSCAPE PLANTS: A COMPARISON OF THE CURRENT STATE REGULATIONS FOR WATER REUSE**

Anastasia E. M. Chirnside<sup>1</sup>  
Stephanie Hahn<sup>2</sup>

## **ABSTRACT**

Water scarcity and water quality issues across the country are increasing the demand and acceptance by consumers for the use of recycled water. Agricultural and landscape irrigation is the largest user of water resources. Therefore, it is no surprise that the most common type of water reuse has been for crop irrigation and landscape irrigation in urban areas. As the demand for recycled water increases, the need for regulations and recommendations to ensure human safety and to minimize adverse environmental impacts becomes apparent. At the federal level, the Environmental Protection Agency has issued voluntary guidelines that suggest the level of treatment, the minimum quality for reuse, and the type of monitoring required.

Even though benefits of promoting wastewater reuse as a means of supplementing existing water resources have been recognized by most state legislatures in the United States during the last quarter of the twentieth century, several states still do not have any regulations or guidelines. Currently, thirty states, including Arizona, California, Colorado, Florida, Nevada, and Texas, have developed comprehensive regulations. Although criteria vary among the states that have developed regulations, the general idea that increasing levels of human exposure calls for increasing levels of treatment remains constant. Nevertheless, the lack of state-level regulations for reclaimed water has hindered the development of state programs that advocate water reuse as a water resources conservation strategy.

This work outlines the current state regulations for water reuse and outlines the differences in the required quality of recycled wastewater among states.

## **INTRODUCTION**

Benjamin Franklin once said, “We will never know the true value of water until the well runs dry.” This statement has never been more poignant than it is now, as water reuse is one of the hottest and most talked about issues in the water industry today (Sundstrom, 2006). More than two billion gallons of water are reused daily for various applications throughout the United States, and it is estimated that the reused water volume is growing at a rate of fifteen percent per year (Morgan, 2009). Major reuse projects have been operational for over a decade, but is it too little too late? There have been indications of the utilization of wastewater for agricultural irrigation that extend back to about five thousand years (Asano and Levine, 1996). By the year 2015, it is estimated that thirty-six

---

<sup>1</sup> University of Delaware, 531 South College Ave., Newark, DE 19716, aemc@udel.edu

<sup>2</sup> University of Delaware, 301 DuPont Hall, Newark, DE 19716, hahn@udel.edu

states will face serious water shortages. In fact, due to rapid urbanization and mega-city development, water demand is expected to soon outpace water supply in mega-cities like Los Angeles (Morgan, 2009). Even though water scarcity is more of an issue in drier areas, it is increasingly becoming a greater problem in other various areas across the nation, e.g. southeastern U.S. Many communities and industries face water shortages, deteriorating water quality, and greater demands as a result of events like continuous population growth, tourism, recreational use, drought, sea-water intrusion, and industrial expansion.

Water reuse offers an essential, feasible, and drought-proof solution for managing limited resources. The use of recycled water is beneficial because it is abundant and reliable; provides protection against drought; conserves highly treated, expensive potable water; diversifies sources of water supply; and reduces the need to develop new water supplies that are costly. Specifically, the benefits of using recycled water for irrigation include an increase in crop yields, protection against frost damage, and a reduction in the need for full application chemical fertilizers because recycled water usually contains enough essential nutrients for crops to supply a large portion of a crops needs, including nitrogen, phosphorus, potassium, zinc, boron, and sulfur. The irrigated crop beneficially utilizes the nutrients in the discharge as fertilizers in irrigation applications (Bahri and Lazarova, 2005). Wastewater reuse decreases the amount of nutrient-rich wastewater that is discharged into environmentally stressed surface waters.

Development of programs for planned reuse of wastewater within the United States began in the early part of the twentieth century. The state of California declared its first reuse regulations in 1918 during the “Great Sanitary Awakening” (1850-1950), and some of the earliest water reuse systems were developed to provide water for irrigation with projects carried out in both Arizona and California in the late 1920s. The United States Environmental Protection Agency (EPA) first published guidelines for water reuse in 1980, intending to provide guidance for utilities and regulatory agencies in the United States, particularly in states where standards did not exist or were being revised or expanded (Asano and Levine, 1996). The guidelines were published in order to aid states in the planning, implementation, and monitoring of water reuse systems. Since the first set of guidelines, the EPA has published a new set every twelve years (1980, 1992, and 2004). In September of 2012, the EPA released the most current update of the guidelines, which addresses the new applications and advances in treatment technologies, and incorporates an approach for integrated water management where nonconventional sources of water are included in holistic water management planning. The updated guide also incorporates information found in the National Research Council’s (NRC) Water Science and Technology Board report, *Water Reuse: Potential for Expanding the Nation’s Water Supply Through Reuse of Municipal Wastewater* (NRC, 2012). The current publication promotes the development of state water reuse programs that not only set regulations and/or guidelines but develop programs that encourage water reuse development.

Even though benefits of promoting wastewater reuse as a means of supplementing water resources have been recognized by most state legislatures in the United States during the

last quarter of the twentieth century, several states still do not have any regulations or guidelines. In 2002, Connecticut, Kentucky, Louisiana, Maine, Minnesota, Mississippi, New Hampshire and Rhode Island did not have regulations or guidelines for wastewater reuse. By 2012, Minnesota has developed guidelines for water reuse. Mississippi has issued regulations for wastewater disposal with incidental coverage of water reuse. Currently, thirty states and 1 U. S. territory have developed comprehensive regulations and 15 states have guidelines or design standards that govern water reuse. Although criteria vary among the states that have developed regulations, the general idea that increasing levels of human exposure calls for increasing levels of treatment remains constant.

### **OBJECTIVES**

The overall objective of this work is to outline the current state regulations for water reuse and outline the differences in the required quality of recycled wastewater between states.

### **METHODOLOGY**

The paper is a review of the scientific literature in order to define the current state regulations for water reuse, outline the differences in the quality of recycled wastewater among states, and define types of uses for recycled water.

### **RESULTS AND DISCUSSION**

Recycled water is used for landscape irrigation, mostly for golf courses, but also for schoolyards, parks, athletic fields, cemeteries, nurseries, roadside vegetation, and some residential areas. Water scarcity and water quality issues across the country are increasing the demand and acceptance by consumers for the use of recycled water. However, as the demand for recycled water increases, the need for regulations and recommendations to ensure human safety and to minimize adverse environmental impacts becomes apparent. The most critical objective in all reuse programs is to ensure that public health is not jeopardized by the use of reclaimed water. Luckily, to date, there have not been any confirmed cases of infectious disease resulting from the use of treated recycled water in the United States. Other objectives in treating recycled water must also be satisfied, such as preventing environmental degradation, avoiding public nuisance, and meeting user requirements. According to the EPA (2004), protection of public health is achieved by: (1) reducing or eliminating concentrations of pathogenic bacteria, parasites, and enteric viruses in the reclaimed water, (2) controlling chemical constituents in reclaimed water, and/or (3) limiting public exposure (contact, inhalation, ingestion) to reclaimed water. The degree of treatment required and the extent of necessary monitoring depend on the specific applications of recycled water. The level of human exposure in reclaimed water projects may vary significantly with the corresponding variation in the potential for health risks. In general, irrigation systems are categorized according to the potential degree of human exposure. Where more human exposure is likely to occur in a reuse application, the reclaimed water should be treated more

thoroughly prior to its use. Also, a higher degree of treatment is required for the irrigation of crops that are consumed uncooked. Contrarily, where public access to a reuse site can be restricted causing less exposure, a lower level of treatment may be satisfactory, as long as the health of a worker is not compromised. Table 1 displays the suggested general water recycling treatment and uses based on Guidelines for Water Reuse developed by the EPA (Morgan, 2009).

Table 1. Suggested Water Recycling Treatment and Uses

<b>Primary Treatment</b>	<b>Secondary Treatment</b>	<b>Advanced Treatment</b>
Sedimentation	Biological oxidation or disinfection	Chemical coagulation, filtration or advanced disinfection
<b>Water Use</b>	<b>Water Use</b>	<b>Water Use</b>
No uses recommended at this level	Irrigation of orchards and vineyards Non-food crop irrigation Restricted Landscape watering Groundwater recharge of nonpotable aquifer Industrial cooling	Landscape or golf course irrigation Toilet flushing Vehicle washing Food crop irrigation Indirect potable reuse (i.e., groundwater recharge of potable water source)

There are regions throughout the United States where reuse is practiced more often than it is in other regions. For example, water-limited states such as Arizona, California, Florida, and Texas practice reuse extensively, which is why well-developed water reclamation and reuse regulations have been established in these states. Generally, as expected, irrigation with reclaimed water is adequately practiced in the dry western and southwestern states of the United States. Nonetheless, the advantages of water reclamation and reuse have been recognized in other regions of the country as well. As previously mentioned, thirty of the fifty states have reuse regulations. Even though the western and southwestern states have traditionally had their regulations set in place, regulations from Arkansas, Idaho, Utah, and Oregon are fairly recent. Southern and mid-Atlantic states have generally developed their regulations more recently, including the states of Massachusetts, Virginia, New Jersey and North Carolina, whose regulations have been created within the past five years. The majority of the states that do not have any reuse regulations or guidelines lie within the New England region of the United States.

Following the development of California's "Title 22" regulation, which was one of the most widely publicized and innovative reuse projects that addressed the quality of reclaimed wastewater, the development of reliable wastewater treatment systems to produce irrigation water and ensure the production of agricultural crops while still protecting public health resulted from two milestone studies conducted in California during the 1970s and 1980s:

### **The Pomona Virus Study**

The Pomona Virus Study was conducted by the Sanitation Districts of Los Angeles County in an effort to determine the degree of treatment that was necessary to minimize potential transmission of waterborne diseases via surface water. During low flow conditions in California streams, the control of microbiological impacts from discharge of wastewater effluents cannot be achieved by mixing and dilution alone due to the inadequate receiving of water quantities. Wastewater discharges must meet demanding requirements in accordance with the California Wastewater Reclamation Criteria in order to protect swimmers from health risks associated with exposure to undiluted effluents. According to Title 22, the specified “complete treatment” system consisted of chemical coagulation, sedimentation, and filtration. The Pomona Virus Study was initiated to evaluate the effectiveness of using alternative tertiary treatment systems instead of the “complete treatment” for virus removal under controlled conditions. The study also demonstrated that the direct filtration or carbon absorption achieved pathogen removal efficiency equivalent to the “complete treatment” system. Virus removal results verified that secondary effluent treatment by either direct filtration or activated carbon followed by adequate disinfection could be used to provide microbiologically safe effluent that is satisfactory for discharge into unrestricted recreational impoundments. This established the virus removal capabilities of tertiary treatment systems. This study also noted the importance in realizing that safe implementation of wastewater reuse in the developed world depends on the reliable control of enteric viruses. Such viruses represent a major health concern due to the possibility of infection from exposure to low doses and the lack of routine, cost-effective methods for the detection and quantification of viruses.

### **The Monterey Wastewater Reclamation Study for Agriculture**

The Monterey Wastewater Reclamation Study for Agriculture was a 7.2 million dollar field-scale project that lasted for ten years. This project was designed to evaluate the safety and feasibility of using reclaimed municipal wastewater to irrigate food crops that may be consumed raw. During the first 5 years, several baseline studies were performed in order to determine the uniformity of the soil within the experimental plots and to ensure the safety of downwind areas from aerosols produced during irrigation with the effluent. The five-year field portion of the study began in late 1980 and continued through 1985. During this time, a perennial crop of artichokes was grown, along with the rotating crops of celery, broccoli, lettuce, and cauliflower. A randomized complete block experimental design within a split plot allowed for the evaluation of 3 water types and 4 fertilization rates. Test plots were irrigated using effluent from two parallel municipal wastewater tertiary treatment process trains; one consisting of the Title 22 process required by California for treatment of wastewater used in irrigating food crops and the other process using filtration resulting in a less treated effluent. The control plots were irrigated with local well water. Three separate irrigation systems were constructed to supply the different effluents to each of the main plots. The systems consisted of an underground distribution system with portable aluminum pipes for both sprinkler and furrow irrigation. Extensive microbiological and chemical analyses of water, soil, and plant tissue samples were conducted during the field studies, and investigations centered

on the virus survival on crops and in soils within the field. During the five-year field study, no naturally-occurring animal viruses were recovered from chlorinated effluent discharged from either of the two tertiary treatment systems. In fact, during the course of the study, no animal viruses were detected in any crop and soil samples. Based on virological, bacteriological, and chemical results from sampled vegetable tissues, the safety of irrigation with filtered effluent was comparable to the use of local well water. Results following the five-year field study showed few statistically significant differences in measured soil or plant parameters traceable to the different water types. Another benefit from this study was evidence that the yields of annual crops irrigated with reclaimed wastewater were significantly higher than yields produced from irrigation using local well water. (Visit [www.mrwpc.org](http://www.mrwpc.org) for current information on this water reuse project.)

These two cases are both considered to be milestone cases in the development of reliable wastewater treatment systems because they both resulted in many benefits. For one, both studies provided conclusive evidence that effective virus removal can be accomplished through alternative tertiary treatment systems. Also, both demonstrated conclusively that virtually pathogen-free effluents could be produced from municipal wastewater by means of tertiary treatment and extended disinfection with chlorine. A major result of both studies was the reliable scientific demonstration that even food crops consumed uncooked could be successfully irrigated with reclaimed municipal wastewater without adverse environmental or health effects. The two studies also demonstrated the lower cost alternatives for the production of reclaimed wastewater for irrigation purposes. The cost of producing filtered effluent after the secondary treatment was estimated to be six cents per cubic meter, excluding conveyance and pumping costs. Lastly, each study served to provide a technical basis for the start of the development of regulations and guidelines to ensure the protection of public health in the use of reclaimed wastewater for irrigation (Asano and Levine, 1996). These studies are just two of several landmark studies that emphasized direct nonpotable reuse applications and have provided a sound technical basis for safe use of reclaimed wastewater.

Each state has its own legislative department responsible for creating the water reuse regulations or guidelines, with the objectives of such regulations varying considerably among states. Thirty-two states have developed regulations or guidelines that encourage water reuse as a water resources conservation strategy (Table 2). Twelve states have regulations or guidelines that focus on land treatment for wastewater-derived effluent that promotes disposal rather than reuse (EPA, 2012). Currently, Kentucky, Louisiana, Maine, New Hampshire, New York and Connecticut do not have any regulations or guidelines but may allow reuse on a case-by-case basis.

Florida's regulations are created by Florida Association of Counties (FAC). The FAC represents counties on a range of important issues before the state legislature, the governor and Cabinet, various state agencies, commissions, and the courts (Florida Association of Counties, 2009). California Department of Public Health (CDPH) is responsible for California's reuse regulations. This department focuses on optimizing the health and well-being of Californians (State of California, 2010). The regulations in

Texas are dependent on the Texas Commission on Environmental Quality (TCEQ). The TCEQ’s mission is to protect Texas’ human and natural resources consistent with sustainable economic development through keeping the air clean, the water clean, and the management of waste safe (Texas Commission on Environmental Quality, 2011). The state of Arizona relies on the Arizona Department of Environmental Quality (ADEQ) for its reuse regulations. Their focus is on the protection and enhancement of public health, welfare, and the environment within the state (ADEQ, 2011). Lastly, the Colorado Department of Public Health and Environment commits to protect and preserve the health and environment of the people of Colorado (Colorado Department of Public Health and Environment, 2011).

Table 2. State Programs for Water Reuse versus Wastewater Disposal

<b>States with Regulations That Promote Reuse</b>
Arizona, California, Colorado, Delaware, Florida, Idaho, Illinois, Iowa, Massachusetts, Missouri, Montana, Nevada, New Jersey, North Carolina, Oklahoma, Oregon, South Carolina, Texas, Utah, Vermont, Virginia, Wyoming
<b>States with Guidelines That Promote Reuse</b>
Georgia, Hawaii, Maryland, Minnesota, New Mexico, North Dakota, Ohio, Pennsylvania, Rhode Island, Washington
<b>States with Regulations for Wastewater Disposal</b>
Alaska, Arkansas, Indiana, Michigan, Mississippi, Nebraska, West Virginia, Wisconsin
<b>States with Guidelines for Wastewater Disposal</b>
Alabama, Kansas, South Dakota, Tennessee

Each of these organizations has created regulations for the unrestricted uses of reclaimed water where human contact is likely (e.g., parks, schoolyards, residential irrigation, etc.). Overall, the treatment of municipal wastewater is typically designed to meet water quality objectives based on particulate matter (Total Suspended Solids (TSS) or turbidity), organic content (Biochemical Oxygen Demand [BOD]), biological indicators (e.g., total or fecal coliforms, *Escherichia coli*, helminth eggs, enteroviruses), nutrient levels (Nitrogen and Phosphorus), and, in some cases, chlorine residues (Bahri and Lazarova, 1962). However, it is also important to note that many states evaluate particular types of water reuse on a case-by-case basis. Specific regulations for these five states according to the EPA (2004) are included in Table 3. Notice that California is the only state that uses total coliform as an indicator organism, where the other four states use fecal coliform. In addition, Florida is the only state that requires monitoring for TSS to determine particulate levels. The other states use turbidity.

Northeastern states are also operating water reuse systems within places like residential buildings, community developments, and on golf courses. The Solaire and Tribeca Green buildings in Battery Park City, New York City, utilize an underground piping system, which enables them to recycle and deliver wastewater for the irrigation of roof gardens

Table 3. Specific State Regulations for Wastewater Reuse

Table 2: Unrestricted Reuse	
State	Regulations
Florida	<p>At a minimum, secondary treatment, filtration, and high-level disinfection:</p> <ul style="list-style-type: none"> <li>-5 mg/l total suspended solids (TSS) in a single sample to be achieved prior to disinfection</li> <li>-20 mg/l (Carbonaceous Biochemical Oxygen Demand)CBOD<sub>5</sub></li> <li>-Continuous on-line monitoring of turbidity prior to disinfection</li> <li>-Monitoring for <i>Giardia</i> and <i>Cryptosporidium</i> based on treatment plant capacity               <ul style="list-style-type: none"> <li>-≥ 1 mgd, sampling one time during each 2-year period</li> <li>-&lt; 1 mgd, sampling one time during each 5-year period</li> </ul> </li> <li>-samples to be taken immediately following disinfection process</li> <li>-Fecal coliform               <ul style="list-style-type: none"> <li>-75% of samples below detection</li> <li>-25/100 ml (maximum)</li> </ul> </li> </ul>
California	<p>Oxidation, coagulation, filtration, and disinfection:</p> <ul style="list-style-type: none"> <li>-Chlorine following filtration CT ≥ 450 mg-min./l at all times with ≥ 90 minutes modal contact time, based on peak dry weather flow (PDWF); or</li> <li>-Process that inactivates and/or removes 99.999% plaque-forming units of F-specific bacteriophage MS2, or polio virus</li> </ul> <p>Total Coliform:</p> <ul style="list-style-type: none"> <li>-2.2/100 ml (7-day median)</li> <li>-&lt; 23/100 ml (not to exceed in more than one sample in any 30-day period)</li> <li>-240/100 ml (maximum any one sample)</li> </ul> <p>Filtered recycled wastewater</p> <ul style="list-style-type: none"> <li>-filtered wastewater coagulated and passed through natural undisturbed soils or filter bed media               <ul style="list-style-type: none"> <li>-Turbidity: &lt; 2 NTU average daily; &lt; 5 NTU for &gt; 95% time within 24-hr; &lt; 10 NTU max</li> </ul> </li> <li>-System has either automatic chemical feed or means for flow diversion for fouled wastewater effluent: if &gt; 5 NTU for more than 15 minutes</li> </ul>
Texas	<p>Type I Reclaimed Water on a 30-day average to have a quality of:</p> <ul style="list-style-type: none"> <li>-5 mg/l BOD<sub>5</sub> or CBOD<sub>5</sub></li> <li>-10 mg/l for landscape impoundment</li> <li>-20 cfu/100 ml (avg.): <i>E. coli</i> or Fecal Coliform; &lt; 75 cfu/100 ml (max. single grab)</li> <li>-4 cfu/100 ml (avg.): Enterococci; 9 cfu/100 ml (max. single grab)</li> <li>-Turbidity: 3 NTU</li> </ul>
Arizona	<ul style="list-style-type: none"> <li>-Secondary treatment with filtration and disinfection</li> <li>-Turbidity prior to disinfection: ≤ 2 NTU (avg. daily); ≤ 5 NTU (max)</li> <li>-Fecal coliform post disinfection: none detectable in 4 of last 7 daily samples; 23/100 ml (single sample maximum)</li> <li>-If using alternative treatment to get to Class A: enteric virus non-detectable in 4 of last 7 daily samples</li> </ul>
Colorado	<p>Landscape irrigation:</p> <ul style="list-style-type: none"> <li>-Oxidized, filtered, and disinfected</li> <li>-<i>E. coli</i> : 126/100 ml (monthly average); 235/100 ml (single sample maximum in any calendar month)</li> <li>-Turbidity: not to exceed 3 NTU (monthly average); not to exceed 5 NTU in more than 5% of the individual analytical results (any calendar month)</li> </ul>

and an adjacent park, as well as other nonpotable uses. Tribeca Green's potable water needs are reduced by nearly half due to them reusing wastewater for nonpotable applications. In New Jersey, The Homestead at Mansfield, which is an active adult residential development, is connected to a wastewater treatment plant. Their water reuse system provides up to 250,000 gallons per day (gpd) of reclaimed water which is used to irrigate landscaped spaces at personal residences and open common areas. The Hawk Pointe Golf Course in Washington, New Jersey, uses reclaimed and treated wastewater to

supply the abundant volumes of water required to irrigate the course (Morgan, 2009). More wastewater is used for irrigation on golf courses today than ever before. There are more than 150 golf courses irrigated with reclaimed water in California and Florida alone (The USGA, 1997). The United States Golf Association (USGA) has developed new grasses to use on golf courses, like buffalograss, that require less use of pesticides, fertilizers, and water. The USGA has also sponsored research to continue to produce new grasses that require less water, pesticides, and fertilizer so that such grasses can be used on golf courses, sports fields, and home lawns. As a result of past USGA research, golf courses use half the water they did ten years ago. The USGA staff helps superintendents conserve water by making better decisions about when to water their courses and how to use technology that improves irrigation precision (The USGA, 2009).

### **CONCLUSIONS**

There has been significant progress made in regard to developing technical approaches in producing good quality and reliable water sources from reclaimed wastewater. Overall, the formation of planned wastewater reclamation, recycling, and reuse in water resource systems reflects increasing societal demands for water, technological advancements, public acceptance, and improved understanding of public health risks. However, there is still work to be done on individual levels within the community, state, and even the nation. It is crucial that the value of water be communicated to consumers. Individuals must realize that the reuse of wastewater cannot solve scarcity issues alone, even though it is an essential part of a sustainable approach toward managing water resources; they must learn how to conserve water. Community leaders should perform a public outreach in an effort to educate consumers about wastewater and answer to any public safety and/or cost concerns. Within a community, wastewater and water agencies must collaborate to set policies and develop system and facility plans in order to make the most of water recycling opportunities. If these issues can be improved upon, more communities would look to finance water reuse for cost-effective, environmentally friendly, and safe water resource management.

Research is still needed to resolve issues related to reuse criteria. Key concepts for further research and efforts include, but are not limited to: an assessment of health risks associated with trace contaminants in reclaimed water, improved monitoring techniques to evaluate microbiological quality, real-time on-line monitoring of parameters of concern, improved removal of wastewater particles to increase the effectiveness of disinfection, the effect of reclaimed water storage systems on water quality, and the evaluation of the fate of microbiological, chemical, and organic contaminants in reclaimed water (Asano and Levine, 1996). The development and implementation of water reuse projects are still problematic because of some major constraints like economic viability, the lack of infrastructure for distribution, the availability of funding, sensitive health and environmental issues, and public acceptance. Solutions for such issues will continue to be sought after by utilities, municipalities, and the industrial private sector.

## ACKNOWLEDGEMENTS

Funding provided by DE Water Resources Center, University of Delaware, Newark, DE.

## REFERENCES

- ADEQ. "About Us." 2011. Azdeq.gov. 1 May 2011  
<<http://www.azdeq.gov/function/about/index.html>>.
- Asano, L. and A. D. Levine. 1996. "Wastewater Reclamation, Recycling and Reuse: Past, Present, and Future." *Water Science Technology*: 33(10-11): 1-14.
- Bahri, A. and V. Lazarova. Water Reuse for Irrigation: Agriculture, Landscapes, and Turf Grass. Boca Raton: CRC Press, 2005.
- Colorado Department of Public Health and Environment. "About the Department." 2011. Cdphe.state.co.us. 1 May 2011 <<http://www.cdphe.state.co.us/about.html>>.
- Florida Association of Counties. "About FAC." 2009. Fl-counties.com. 1 May 2011  
<[http://www.fl-counties.com/Pages/About\\_FAC.aspx](http://www.fl-counties.com/Pages/About_FAC.aspx)>.
- Morgan, Wayne. "Reuse on the Rise." *Water and Wastes Digest*, March 2009: 26-27.
- State of California. "About Us." 2010. Cdph.ca.gov. 1 May 2011  
<<http://www.cdph.ca.gov/Pages/AboutUs.aspx>>.
- Sundstrom, Glen. "What's Driving Reuse." *Environmental Protection*, Sept. 2006: 22.
- Texas Commission on Environmental Quality. "About the TCEQ." 2011. Tceq.texas.gov. 1 May 2011 <<http://www.tceq.texas.gov/about>>.
- The USGA. Wastewater Reuse for Golf Course Irrigation. Boca Raton: CRC Press, 1997.
- The USGA. "Key Environmental Messages." 2009. Usga.org. 20 March 2011  
<[http://www.usga.org/course\\_care/articles/environment/general/Key-Environmental-Messages/](http://www.usga.org/course_care/articles/environment/general/Key-Environmental-Messages/)>.
- US. EPA (2004). Guidelines for Water Reuse. EPA/625/R-04/108, US. Environmental Protection Agency, Center for Environmental Research Information, Cincinnati, Ohio.
- US. EPA (2012). Guidelines for Water Reuse. EPA/600/R-12/618, US. Environmental Protection Agency, Office of Wastewater Management, and National Risk Management Research Laboratory, Office of Research and Development, Cincinnati, Ohio.

# ESTIMATING PRODUCTION AND CROP WATER USE OF DEFICIT IRRIGATED CROPS

Thomas J Trout<sup>1</sup>  
Kendall DeJonge<sup>2</sup>

## ABSTRACT

Sustaining irrigated agriculture with limited water supplies requires maximizing productivity per unit of water. Relationships between crop production and water consumed are basic information required to maximize productivity. This information can be used to determine if deficit irrigation is economically desirable and how to best manage limited water supplies. Field trials of corn, sunflower, dry bean, and wheat production with six levels of water application were used to develop water production functions based on consumptive use and to better understand water timing effects and crop responses to stress. Initial results indicate linear relationships between yield and crop ET and transpiration. The field data are being used to improve and validate crop models so they can be used to generalize the field results for other climate and soil characteristics.

## INTRODUCTION

Irrigation water supplies in the Central Plains and much of the western U.S. are declining. Supplies originally developed for irrigated agriculture are being diverted to growing urban areas and for ecosystem restoration. Groundwater use in many areas must decrease if we are to reduce depletion of this valuable resource. Temperature increases due to climate change will likely reduce the mountain snowpack accumulation that is critical to surface water supplies. Irrigated agriculture will very likely have less water available in the future than it had in the past. Sustaining irrigated agriculture will require increasing the economic productivity per unit of water.

Past studies have shown that the reduction in yield is often less than the reduction in irrigation water applied - for example, a 30% reduction in irrigation may result in only a 10% reduction in yield (Zang, 2003). This means the marginal productivity of irrigation water applied tends to be low when water application is near full irrigation. However, as the water deficit increases, higher marginal productivity may result either from higher efficiency of water applications (less deep percolation, runoff, and evaporation losses from irrigation and better use of precipitation), or from a physiological response in plants that increases productivity per unit water consumed when water is limited. Increasing marginal productivity of water with deficit irrigation indicates that deficit irrigation may be a way to maximize economic returns per unit irrigation water.

---

<sup>1</sup> USDA Agricultural Research Service, Water Management Research Unit, Fort Collins, CO; 970-492-7419; Thomas.trout@ars.usda.gov

<sup>2</sup> USDA Agricultural Research Service, Water Management Research Unit, Fort Collins, CO; 970-492-7417; Kendall.DeJonge@ars.usda.gov.

Past studies have also shown that yield relationships based on water consumption or evapotranspiration are often linear (Doorenbos et al., 1986). This implies that the marginal productivity of the water is constant and deficit irrigation may be no more productive per unit water consumed than full irrigation. If this is the case, where deep percolation and runoff losses can be reused and have value, full irrigation on a reduced irrigated area may provide higher economic returns for the watershed. In many western watersheds, water is effectively reused, and in fact, reuse of irrigation water return flows is the legal water right of downstream users. For example, Colorado water law allows only the estimated consumptively used portion of a water supply to be transferred to other uses; the return flows must be maintained for downstream users.

Thus, it is critical to understand the water balance and water law in a watershed to establish the value of water for crop production and means to maximize irrigation productivity. Improved irrigation efficiency is not likely to produce much “new” water because it results primarily in a reduction of return flows rather than a reduction in ET, and even deficit irrigation is economically viable only if the marginal productivity of consumed water increases substantially.

Although many limited irrigation studies have been carried out in the Central Plains and around the world, we feel there continues to be a need for more information on crop responses to deficit irrigation. So, in 2008, USDA-ARS began a field study of the water productivity of 4 common Central Plains crops under a wide range of irrigation levels from fully irrigated to about 40% of full irrigation. We are measuring ET of the crops under each of these conditions and seeking ways to maximize productivity per unit water consumed. We also strive to better understand and predict the responses of the crops to deficit irrigation so that limited irrigation water can be scheduled and managed to maximize yields.

## METHODS

A 50 acre research farm northeast of Greeley, CO — the Limited Irrigation Research Farm, or LIRF — was developed to enable the precision water control and field measurements required to accurately measure ET of field crops. The predominately sandy-loam soils and good groundwater well are ideal for irrigation research.

Four crops — field corn, sunflower (oil), dry beans (pinto), and winter wheat were rotated through research fields on the farm. Crops are planted, fertilized, and managed for maximum production under fully-irrigated conditions, but are irrigated at 6 levels that range from fully irrigated to about 40% of the fully irrigated amount. Deficit irrigations are timed to maximize production – usually by allowing relatively higher stress during early vegetative and late maturity stages and applying extra water to reduce stress during reproductive stages.

Each crop field was divided into 4 replications in which the 6 irrigation treatments were randomized. Water was regulated, measured, and delivered to 12 row (30 ft) x 140 ft



Figure 1. Aerial view of the water productivity plots at LIRF in 2008. Crops from left to right are beans, wheat, sunflower, and corn. Lower fields contain Bowen Ratio instrumentation.

plot. We applied irrigation water with drip irrigation tubes placed on the soil surface in each crop row to insure that the water was applied uniformly. This was essential to be able to complete the water balance. Figure 1 shows an aerial view of the research fields in 2008.

A CoAgMet (Colorado Agricultural Meteorological Network) automated weather station was installed on the farm near the center of a 1 acre grass plot. Hourly weather data from the station were used to calculate ASCE Standardized Penman-Monteith alfalfa reference evapotranspiration (ET<sub>r</sub>). Soil water content between 6 inch and 7 ft depth was measured by a neutron probe from an access tube in the center of each plot. Soil water content in the surface 6 inches was measured with a portable TDR system (MiniTrase, SoilMoisture, Inc., Santa Barbara, CA). Soil evaporation was estimated based on techniques described in Allen et al. (1998). Basal crop coefficients were adapted from Table 8.8 in Allen et al. (2007) based on full cover date. Irrigations were scheduled using both predicted soil water depletions based on ET<sub>r</sub> measurements, and measured soil water depletion.

Plant measurements were taken periodically to determine crop responses to the water levels. We recorded plant growth stage and measured canopy cover with digital cameras. The digital cameras along with spectral radiometers and an infrared thermometer were mounted on a “high boy” mobile platform and driven through the plots weekly (Figure 2). Indicators of crop water stress such as stomatal conductance and leaf water potential were measured periodically. Canopy temperature was measured continuously with stationary infrared thermometers and periodically with the mobile platform (Bausch et al., 2010). At the end of the season, seed yield and quality as well as total biomass were

measured from each plot. On two fields on the farm, crop ET was measured with energy balance instruments (Bowen Ratio method) for well-watered crops. These measurements allow crop coefficients to be estimated for the crops. On other fields on the farm, we are cooperating with Colorado State University faculty to test wheat and dry bean varieties under varying irrigation levels.

An important part of the research is to extend the results beyond the climate and soils at LIRF. We are working with the ARS Agricultural Systems Research group to use this field data to improve and validate crop models. Once we have confidence in the models, we can estimate crop water use and yields over a wide range of conditions.



Figure 2. High Boy reflectance tractor measuring canopy reflectance and temperature.

## RESULTS

Table 1 summarizes the overall results for the four crops in terms of water requirements and productivity. For comparison, productivity is listed in terms of pounds of grain produced per inch of water consumed, or evapotranspiration, often referred to as water use efficiency. Water consumption includes rainfall and irrigation but deducts any water lost to runoff or deep percolation. Corn, although a fairly high water user, is the most efficient at converting water to biomass and grain. Sunflower uses a little less water than corn and tends to utilize any available water efficiently because of its vigorous rooting system. Winter wheat uses about the same amount of water as sunflower. Because wheat matures early, it can be a good rotation crop if well capacity or late season water supply is limited. Pinto beans use less water than the other crops studied because of the

shorter season. Our beans were grown on 30 inch rows which result in a little lower water use and yields than if planted in narrower rows.

Table 1. Water productivity and total water requirements of 4 crops

<i>Crop</i>	<i>Water Productivity</i>	<i>Total Water Requirements</i>
Corn	500 lb per ac-in (9 bu)	23 inches
Sunflower	185 lb per ac-in	19 inches
Winter Wheat	290 lb per ac-in (5 bu)	19 inches
Pinto Beans	180 lb per ac-in	14 inches

We will summarize the four years of corn (Dekalb DKC52-59 (VT3)) results in more detail. Figure 3 shows the seasonal water balance for the 2011 corn crop for the 6 irrigation treatments. Precipitation was all stored in the root zone except for the 100% and 85% irrigation treatments which lost about 1” and ½” to deep percolation, respectively. All treatments ended the season with a little more water in soil storage than at the beginning. The irrigation applications varied between 17 – 6 in. With deep percolation and storage changes, the ET varied between 25 – 14 in. In other years, ET of the fully-irrigated crop averaged 23 in. and of the most stressed crop, 13 in. Irrigations were timed such that plant water stress for the deficit irrigation levels was least between tasseling and soft dough (growth stages VT to R4).

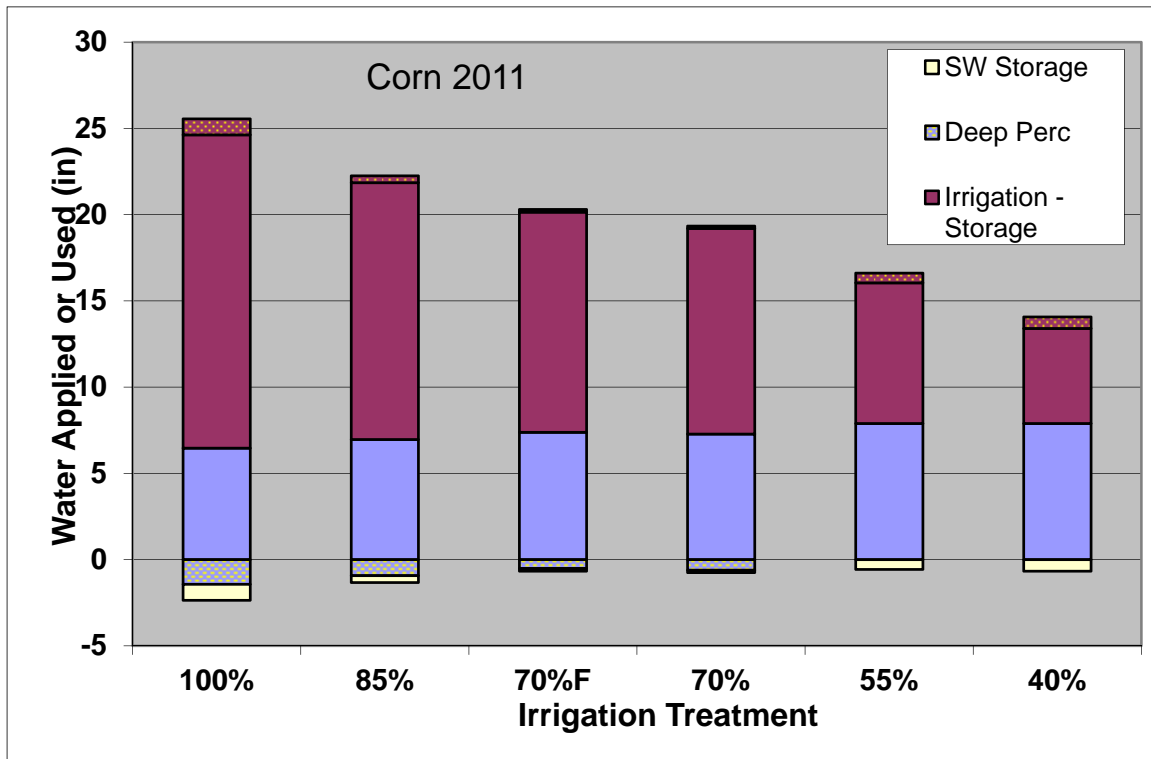


Figure 3. Water balance for the 2011 corn crop showing precipitation, irrigation, and seasonal soil water storage changes. Bars below zero represent additions to storage or deep percolation losses. Dotted areas represent irrigation or precipitation stored or percolated.



Figure 4. Comparison of corn growth condition on Aug 4, 2008 just before tasseling. Rows at the left and background are fully irrigated; rows at right are the lowest irrigation level.



(a) Full irrigation: 91% ground cover (b) Low irrigation: 63% ground cover

Figure 5. Overhead photos showing corn canopy on Aug 1, 2008.

The wide range of irrigation applications resulted in substantial differences in crop growth. Figures 4 and 5 show a comparison of plant height and ground cover in early August, 2008 as the corn was beginning to tassel.

Figure 6 shows the yield:water relationship for corn for each year. Grain yields varied from over 200 bu/ac at full irrigation to under 100 bu/ac at low irrigation and biomass was about double grain yields. Hail damage in 2009 resulted in about 15% lower grain yields but little difference in total biomass. The reason for the relatively low yield with full irrigation in 2010 is not known. Harvest index (the portion of total biomass that is grain) ranged from 50 – 60% and did not vary with irrigation level.

The water production function based on applied irrigation water is fairly flat at full irrigation and curves downward as the water application decreases, showing that the decrease in yield for each unit decrease in water applied is relatively small when the deficit is small, but the rate of yield decrease gets larger as the deficit increases. This means that the marginal productivity of irrigation water (additional yield per unit additional water) is relatively low near full irrigation, showing the potential benefit to the farmer of reducing irrigation and transferring water to higher-valued uses. The water use efficiency, or productivity per unit of irrigation water applied, increases from about 12 bu/ac per inch of water applied at full irrigation to about 20 bu/ac/in when irrigation is reduced by 50%. This is because irrigation is more efficient, precipitation is more effectively used by the crop, and the crop extracts more water from the soil.

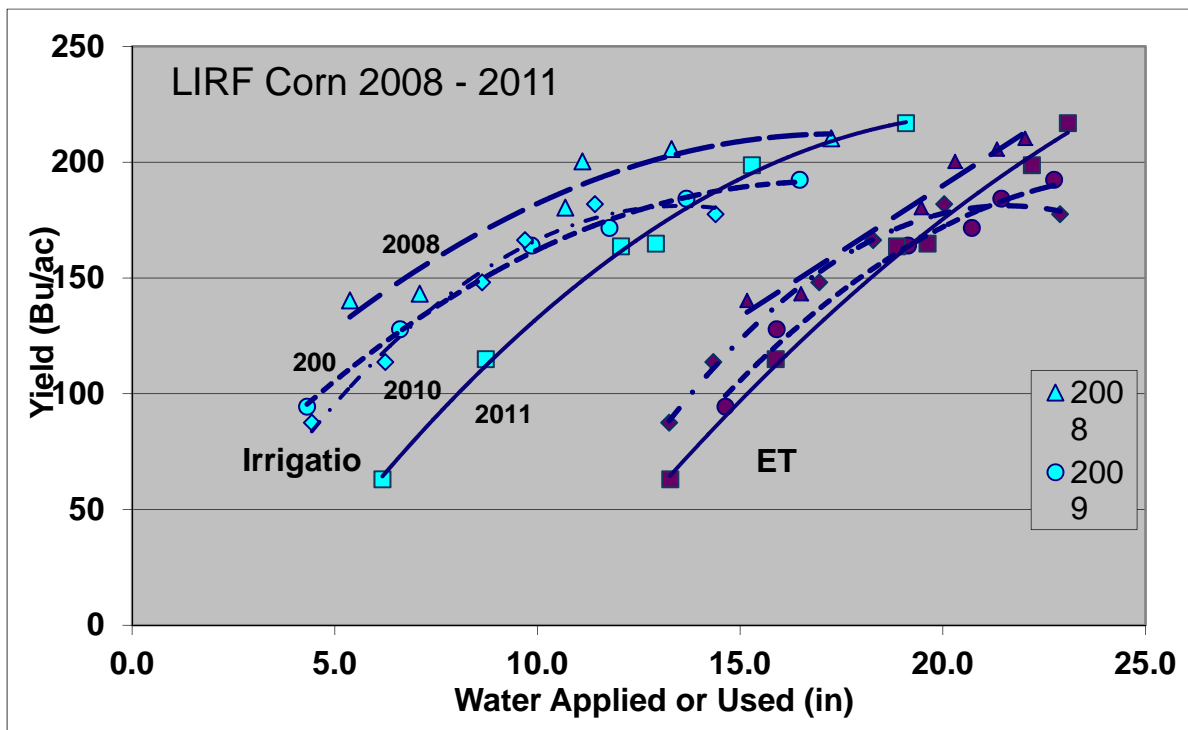


Figure 6. Water production functions for 2008 - 2012 corn at LIRF. Blue symbols are yield vs. irrigation water applied; purple symbols are yield vs ET. Yields are plotted relative to irrigation amount (Irr) and crop ET.

However, the water production function for grain yield based consumptive use or ET (the right curves in Fig 6) moves to the right and is relatively straight. This implies that the corn is equally efficient in its use of every additional unit of water consumed. The water use efficiency in terms of ET is about 9 bu/ac/in at full irrigation. This is smaller than when based on irrigation water because it also counts precipitation used by the crop. The water use efficiency based on ET stays relatively constant for deficits up to about 15%, and then decreases. Because corn requires about 12" of water to produce any yield, the water use efficiency declines with deficit irrigation.

These results imply that nearly all of the increase in the water use efficiency of irrigation water with deficit irrigation results from more effective use of precipitation, increased irrigation efficiency, and increased use of stored soil water, or conversely, the lower marginal value of water near full irrigation is due to inefficient use of rainfall and irrigation water. The marginal value of applied water near full irrigation would be even smaller with less efficient irrigation systems since more of the applied water would be lost to runoff, deep percolation, and possibly surface evaporation.

These results also imply that, based on consumptive use, there would be little or no yield benefit to deficit irrigation compared to fully irrigating only a portion of the land. In fact, fully irrigating less land would likely provide the highest economic returns due to lower production costs.

These results show the importance of developing water production functions based on the correct unit of water. If water value is based on cost of the water supply (eg. pumping costs from a well), then productivity based on applied water is important. However, for the purpose of transferring consumptive use savings, the productivity must be based on water consumed. The value of limited irrigation based on consumptive use savings will likely be less, and if the crop is efficient at converting increased consumptive use to yield, there may be no economic benefit to limited irrigation.

## CONCLUSION

Although the marginal productivity of applied water will generally increase with decreasing irrigation amounts, the marginal productivity of ET tends to be constant. Thus, in watersheds where return flows are effectively used downstream, deficit irrigation may not increase overall irrigated production in the watershed and may not be economically viable for farmers.

## REFERENCES

Allen, R.G., L.S. Pereira, D.Raes, and M. Smith. 1998. Crop evapotranspiration: guidelines for computing crop water requirements. FAO Irrigation and Drainage paper # 56. FAO, Rome.

Allen, R.G., J.L. Wright, W.O. Pruitt, L.S. Pereira, M.E. Jensen. 2007. Water Requirements. Ch 8 in G.J. Hoffman, R.G. Evans, M.E. Jensen, D.L. Martin, and R.L. Elliott (eds) Design and Operation of Farm Irrigation Systems (2nd Ed). ASABE, St. Joseph, MI.

Bausch, W., T.J. Trout and G. Buchleiter. 2010. Evapotranspiration estimates for deficit irrigated crops. In Proceedings of the 5th Decennial National Irrigation Symposium. Phoenix, AZ. Dec 5 – 8, 2010. ASABE, St. Joseph, MI.

Doorenbos, J. and A.H. Kassam. 1986. Yield Response to Water. Irrigation and Drainage Paper #33, FAO, Rome.

Zang, H. 2003. Improving water productivity through deficit irrigation: examples from Syria, the North China Plain and Oregon. Ch 19 in Kinje, J.W., R. Barker, and D. Molden (eds). Water Productivity in Agriculture: Limits and Opportunities for Improvement. CABI Publishing. Wallingford, UK.



# POTENTIAL NUTRIENT TRADING IN THE CHESAPEAKE BAY WATERSHED TO MEET TMDL NUTRIENT LOAD REDUCTIONS

William F. Ritter<sup>1</sup>

## ABSTRACT

The Chesapeake Bay is one of the major estuaries in the U.S. There are six major basins within the Chesapeake Bay watershed. These are the Potomac, Susquehanna, Rapahannock, York, James, and Patuxent basins. These basins supply 90% of the flow to the Chesapeake Bay. The Susquehanna River alone drains 43% of the watershed and contributes nearly 50% of the freshwater. Agriculture is the largest contributor of nonpoint source nutrients. With the EPA TMDL issued in December 2010, each state was required to develop further nutrient load reductions than those set in the 2000 Bay Agreement. One potential way to reduce nutrient loads further is by nutrient trading. Since livestock and poultry are the largest sources of N and P in the watershed, further reductions in nutrient loads from animal agriculture will have to be developed.

Maryland, Pennsylvania, Virginia and West Virginia have developed nutrient trading programs as part of their Tributary Strategy Nutrient Load Reduction programs. Virginia was the first state to establish the framework for nutrient trading followed by Pennsylvania. All four states allow wastewater treatment plants to purchase credits from agricultural nonpoint sources. For property owner to generate nutrient credits they must first of all install Best Management Practices (BMPs) to meet their baseline nutrient load reductions. Cost share money cannot be used to install BMPs to generate credits. Wastewater treatment plants in Virginia, Pennsylvania and West Virginia can purchase credits to meet their load limits. All treatment plants in Maryland must install enhanced nutrient removal technology to meet permit requirements. They can purchase credits if they want to expand,

## INTRODUCTION

The Chesapeake Bay watershed has a land area of approximately 180,000 km<sup>2</sup>, and a total water surface area of 9,890 km<sup>2</sup>. Of this water surface area, 390 km<sup>2</sup> are tidal fresh water, 9,190 km<sup>2</sup> are a mixing zone of fresh and salt waters, and 300 km<sup>2</sup> are salt water. The Bay is rather shallow, with a mean depth of 10 m. The Bay watershed consists of land area in Virginia, Maryland, West Virginia, Delaware, Pennsylvania, New York and the District of Columbia. There are six major basins within the Chesapeake Bay watershed. These are the Potomac, Susquehanna, Rapahannock, York, James, and Patuxent basins. These basins supply 90% of the flow to the Chesapeake Bay. The Susquehanna River alone drains 43% of the watershed and contributes nearly 50% of the freshwater. Agriculture is the largest contributor of nonpoint source nutrients and varies widely across the watershed. The western part of the watershed is dominated by small and medium sized dairy farms and grass-based cow-calf operations. Dairy farms are also

---

<sup>1</sup>. Bioresources Engineering Department, University of Delaware, Newark, DE, 19716  
Tel: 302-831-2468, Fax: 302-831-2469, E-mail: [writter@udel.edu](mailto:writter@udel.edu)

concentrated in southeastern Pennsylvania and in the New York portion of the watershed. Poultry production is concentrated on the Delmarva Peninsula, in the Shenandoah Valley of Virginia and southeastern Pennsylvania. Swine production is concentrated in southern Virginia and southern Pennsylvania. Corn, soybeans, wheat, hay, pasture, fruit and vegetables are the major crops grown in the watershed.

The original 1987 Bay Agreement called for nutrient load reductions in each basin, with further nutrient load reductions being called for in the 2000 Agreement. Because of the failure to meet past cleanup goals, the U.S. Environmental Protection Agency (EPA) was under a court order to complete a total daily maximum load (TMDL) for nutrients. The EPA released the final TMDL for the Chesapeake Bay in December 2010.

### **CHESAPEAKE BAY TMDL**

The overall process of developing the Chesapeake Bay TMDL had four steps (EPA, 2011):

1. EPA defined 19 major river basin and jurisdictional target and allocations were set using the Phase 5.3 Chesapeake Bay Watershed model. The allocations for nitrogen, phosphorus and sediment were reported to the jurisdictions in July and August, 2010.
2. Each jurisdiction developed a Phase I watershed implementation plan (WIP) that described how it would achieve the target allocations for nitrogen, phosphorus, and sediment that were assigned in Step 1. Each jurisdiction developed sub-allocations to assign to individual significant wastewater treatment plant (WWTP) point sources, aggregate non-significant WWTPs, urban stormwater, and confined animal feeding operations (CAFO) point sources; and nonpoint source sectors draining to each of the 92 segments of the Chesapeake Bay and its tidal tributaries and also developed implementation strategies to achieve the sub-allocations..
3. EPA evaluated each jurisdiction's proposed sub-allocations and implementation strategies in its final Phase I WIP to determine whether allocations would be met.
4. EPA established an allocation scenario for the final Chesapeake Bay TMDL on the basis of all seven Bay jurisdictions' final Phase I WIPs and refinements EPA made thereto, and supplemented by more than 14,000 comments from the public during a formal public review of the draft TMDL

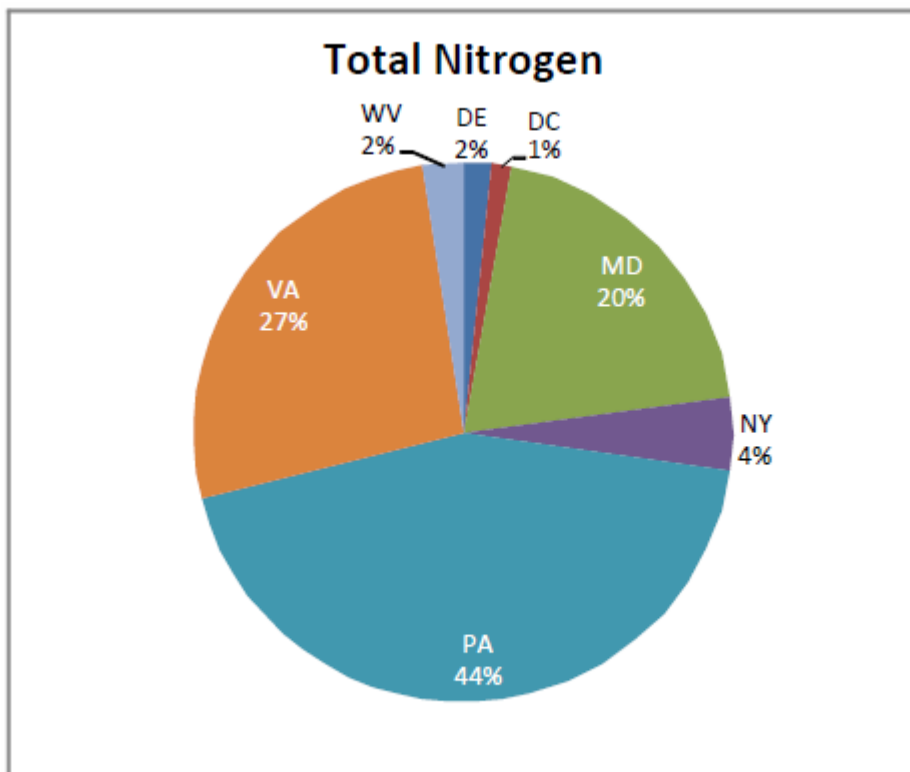
Bay jurisdictions submitted their Phase II WIPs in December 2011. The Phase II WIPs are expected to provide the strategies necessary to have practices in place by 2017 that would result in 60 % of the necessary nitrogen, phosphorus, and sediment reductions needed by 2025 based on the 2010 final TMDL. EPA will use these planning targets when assessing 2-year milestone progress toward meeting the 2017 interim goal.

The final TMDL allocations and total 2009 nitrogen and phosphorus loads for each sector are presented in Table 1 and the 2009 percent nitrogen and phosphorus loads from each jurisdiction are presented in Figures 1 and 2.

Agriculture is the contributing largest source of nitrogen and phosphorus with approximately 44 percent of the nitrogen and phosphorus loads and accounts for 22 percent of the land use. The Bay watershed has over 87,000 farms and 2.63 million hectares of cropland.

Table 1. Nitrogen and Phosphorus 2009 and TMDL Loads

	2009 N Load kg x10 <sup>6</sup> /yr	TMDL N Load kg x10 <sup>6</sup> /yr	2009 P Load kg x10 <sup>6</sup> /yr	TMDL P Load kg x10 <sup>6</sup> /yr
Agriculture	49.6	31.5	3.3	2.3
Urban RO	9.3	7.1	1.1	0.8
Point Source	24.1	17.7	1.9	1.4
Septic	5.0	3.8	0	0
Forest	22.4	23.1	1.1	1.1
Atm Deposit	1.1	1.2	0.1	0.1
Total	111.5	84.4	7.5	5.7



Source: Phase 5.3 Chesapeake Bay Watershed Model 2009 Scenario

Figure 1. 2009 Nitrogen Loads from Different Jurisdictions

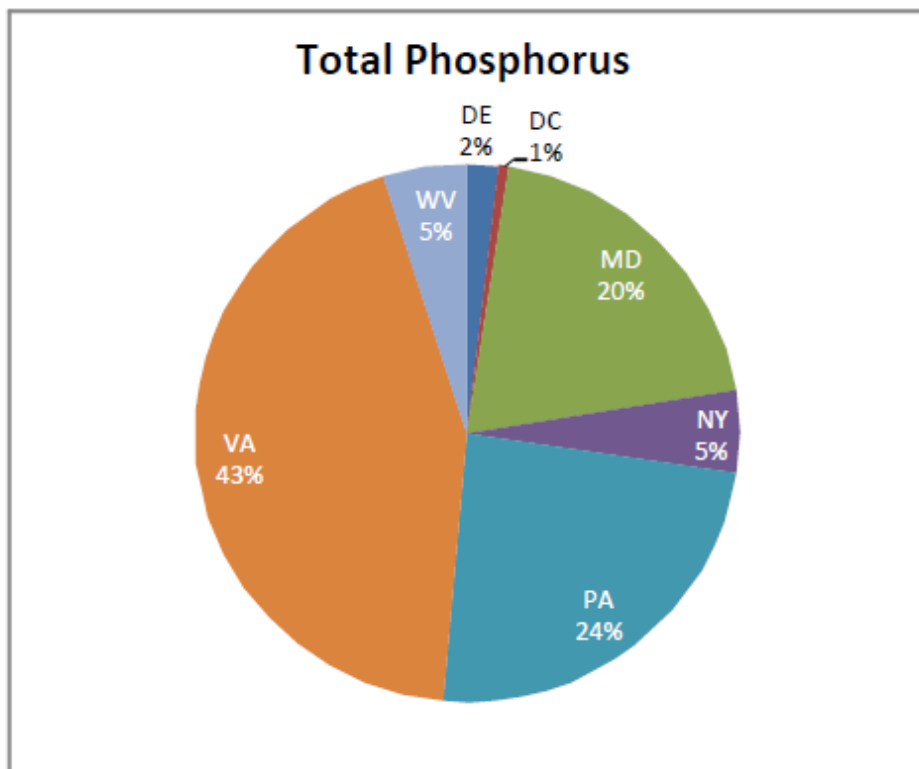
**MECHANISMS USED IN WATER QUALITY TRADING PROGRAMS**

It is important to realize that not all pollution control policy mechanisms are equal. A broad range of policy options are available when designing a program to tackle water

pollution. Many programs are designed to incorporate multiple strategies with ideas taken from old policies combined with new and untested ideas. Through the history of U.S. environmental policy, the following mechanisms have emerged, which can all be incorporated into a water quality trading program:

1. Permits and command and control regulations such as National Permit Discharge Elimination System (NPDES) permits.
2. Taxes and fees where the polluter pays for pollutant discharge.
3. Public fund purchases such as agricultural conservation programs.
4. Offsets between point and nonpoint source pollution.
5. Market trading.

Cole and Ritter (2010) reviewed a total of 40 water quality trading programs. Only about 15% could be considered as successful. Although there are many factors affecting the success of water quality trading, they can be broken up into four general categories; Sound Economics, Sound Planning and Administrative Structure, Sound Legal Backing and Sound Environmental Improvement. A total of 32 factors were identified from reviewing the 40 programs. Some of the identified factors overlap two or more of the categories. These interrelationships are shown in Figure 3.



Source: Phase 5.3 Chesapeake Bay Watershed Model 2009 Scenario  
Figure 2. 2009 Phosphorus Loads from Different Jurisdictions

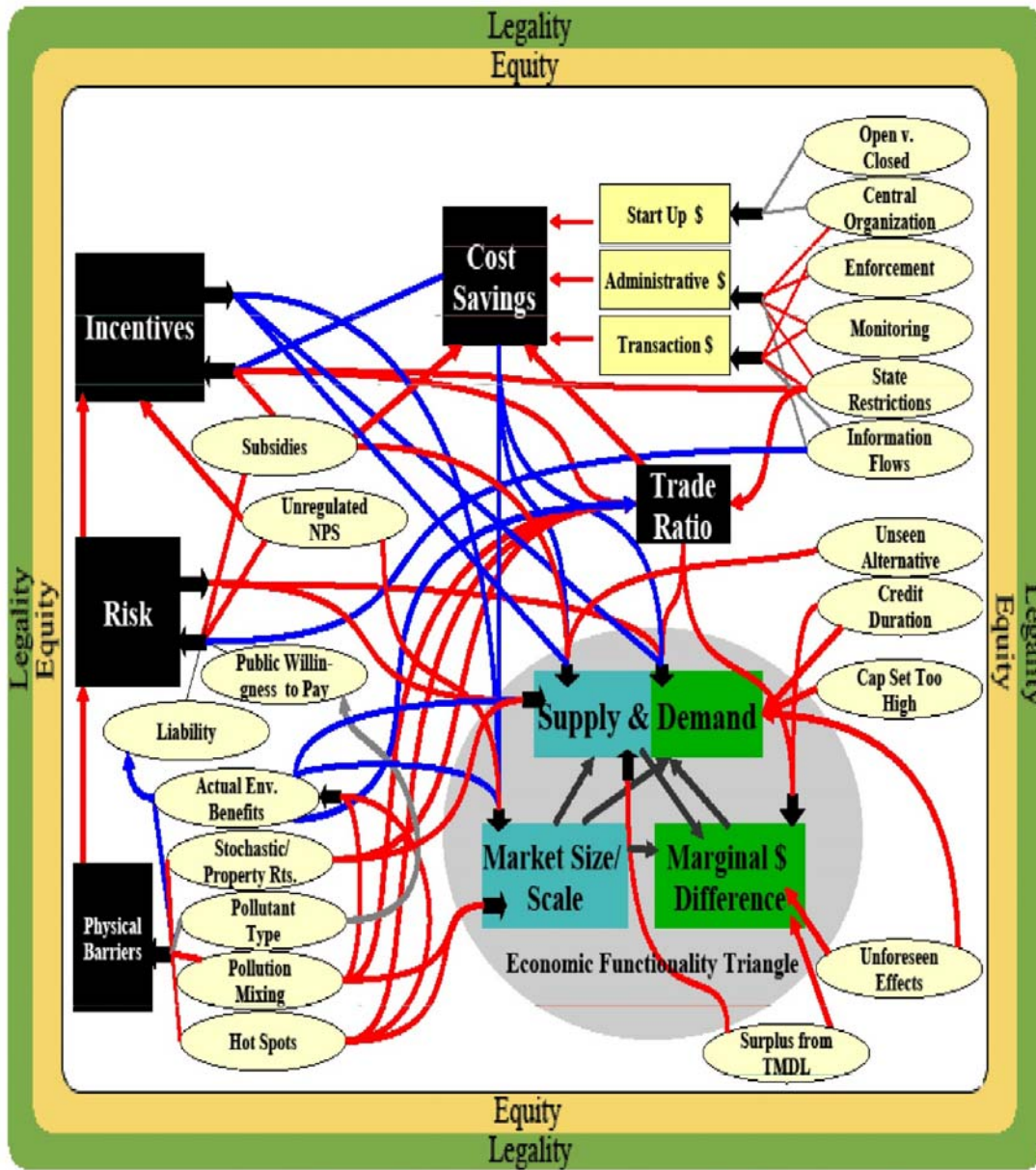


Figure 3. Interrelationship of Factors Affecting Nutrient Trading

**MARYLAND’S NUTRIENT TRADING PROGRAM**

In 2008, Maryland’s Department of the Environment (MDE) issued a policy document that represented the start of Phase I of the State’s nutrient trading program (MDE, 2008). The document described the purpose and form of nutrient trading in Maryland. It allowed for wastewater treatment plants in Maryland to trade with other wastewater treatment plants in the State.

As part of the Tributary Strategy Statewide Implementation Plan all significant wastewater treatment plants had to upgrade to state of the art enhanced nutrient removal

(ENR) technology to meet permit requirements of 4.0 mg/L total nitrogen and 0.3 mg/L total phosphorus and maintain the nutrient load caps for all point sources. If plants want to expand they can go to land application or buy nutrient credits from other point or nonpoint sources or upgrade minor point sources to ENR.

In 2008, Maryland Department of Agriculture (MDA) issued Phase II guidelines for the generation of agricultural nonpoint source nutrient credits (MDA, 2008). The following key principles apply to agricultural nutrient trading credits in Maryland.

1. Any generator of agricultural nonpoint source credits must demonstrate they have met the baseline water quality requirements of their watershed.
2. All agricultural generators must be in compliance with all local, state, federal laws, regulations and programs.
3. Those portions of BMPs funded by federal or state cost share cannot be used to generate credits during the life span of the project.
4. Credits cannot be generated for the purchase and idling of whole or substantial portions of farms to provide nutrient credits off site.
5. Trades must result in a net decrease in loads.
6. An agricultural practice can only generate credits once it is installed.

Tradable credits can be generated by any agronomic, land conversion or structural practice which will reduce the nutrient loadings below the baseline. Credits will be determined using BMP efficiency rates used by the Chesapeake Bay Program. Baseline loadings must achieve the stricter of nutrient load reductions called for in the tributary strategies or the load reductions called for in an applicable TMDL for the watershed in question.

The MDA uses a central Trading Registry to post, track and market agricultural credits once they are certified. Users can manage and post credits and manage offers from buyers through their account. Credits can only be applied to offsets in the year in which they are generated and cannot be banked for future use. If a BMP generates an average of 15 credits per year and has a life of span of five years, no more than 15 credits can be used as an offset each year and 75 credits could not be applied in the fifth year.

### **PENNSYLVANIA'S NUTRIENT TRADING PROGRAM**

Pennsylvania Department of Environmental Protection (DEP) issued the guidance document in December 2006 entitled "Final Trading of Nutrient and Sediment Reduction Credits-Policy and Guidelines" (No. 392-0900-001, December 2006) as it relates to the Chesapeake Bay (PADEP, 2006). The purpose of the program was to ease the cost of wastewater treatment plants upgrading to reduce nutrient discharges. On October 9, 2010, the Department published its nutrient trading regulation, 25 Pa. Code § 96.8, entitled "Use of Offsets and Tradable Credits From Pollution Reduction Activities in the Chesapeake Bay Watershed," in the Pennsylvania Bulletin. See, 40 Pa. B. 5790. The regulation became effective that day.

Nutrient credits can only be generated after a generator demonstrates compliance with the baseline. The regulation specifies procedural requirements to ensure that credits are calculated correctly and accomplish pollutant reductions. Specifically, before credits can be applied to effluent limits they must be certified, verified, and registered. A person who wishes to generate credits shall submit to DEP a written request for certification of the pollutant reduction activity. A request for certification is typically submitted before a person conducts the pollutant reduction activity. The Department will publish notice of receipt of a certification request in the Pennsylvania Bulletin for an informal 30-day public comment period. During this 30-day period, a team will review the request for technical acceptability, and consistency with program requirements.

The Department may only certify the pollutant reduction activity that will generate credits for use to meet permit effluent limits for the compliance period(s) for which they are certified, verified and registered. Also, the Department will certify a pollutant reduction activity contingent upon conditions to ensure that the program requirements will be satisfied. Certification serves as DEP's final determination of the amount of credits that the pollutant reduction activity may generate. If the Department certifies a pollutant reduction activity, the Department will publish notice of the action in the Pennsylvania Bulletin, which begins a 30-day appeal period,

A key component of the Department's certification decision is a review of the "verification" plan included in the certification request. A verification plan explains how verification will occur. Verification can take a number of forms, but regardless of the form it must demonstrate that the pollutant reduction activity was implemented as described in the certification. Verification is a condition of registration. Registration is the Department's accounting mechanism to track verified credits before they are used to comply with the NPDES permit effluent limits.

On July 22, 2010 the Pennsylvania Infrastructure Investment Authority (PENNVEST), in cooperation with DEP, announced its inaugural step in the creation of a Nutrient Credit Clearinghouse within the Chesapeake Bay watershed in Pennsylvania. The Nutrient Credit Clearinghouse is a component of Pennsylvania's Nutrient Credit Trading Program to encourage the trading of nutrient credits. Regulated public and private wastewater treatment plants, as well as developers and others, may purchase nutrient credits from PENNVEST, who in turn will purchase credits from credit generators and aggregators. These transactions occur through periodic credit auctions as well as through bilateral agreements. To reduce risks to market participants and to ensure a stable marketplace, PENNVEST serves as a Clearinghouse in which credit buyers and sellers contract with PENNVEST rather than directly with each other. In this way, PENNVEST reduces the market risk otherwise facing buyers and sellers, which in turn creates a more viable and robust nutrient credit trading market in Pennsylvania.

### **VIRGINIA'S NUTRIENT TRADING PROGRAM**

The Virginia legislature authorized legislation in 2005 for nutrient trading that involved a general watershed permit. Article 4.02 of the Code of Virginia established the

Chesapeake Bay Watershed Nutrient Credit Exchange Program. The final regulation was approved by the State Water Control Board at its September 6, 2006 meeting. The nutrient trading program was part of Virginia's Tributary Strategy program. The general watershed permit established the framework for market based point source credit trading program under which 125 significant dischargers must comply with the tributary strategy load reductions. The general watershed permit expired December 31, 2012, but was renewed for another five years and incorporated waste load allocations of the Chesapeake bay TMDL (CBP, 2012). Existing wastewater treatment plants who participate in the program must purchase their credits from other point sources. New and expanding plants must install the best technology for nutrient removal and obtain offsets for 100 percent of their nutrient discharge. The offsets must be obtained from nonpoint sources. A brief comparison of Virginia's program with other states is presented in Table 2 (Branosky et al., 2011).

To generate credits for trading from agricultural nonpoint sources, the property must implement the following 5 BMPs that are appropriate for the farming operation to meet baseline loads.

- Soil conservation plan
- Nutrient management plan
- Cover crops
- Livestock stream exclusion with 11 m buffers
- 11 m riparian buffers

To generate credits the following BMPs can be installed.

- Continuous no-till
- Early planting date cover crops
- 15 percent N fertilizer reduction on corn
- Wider than 11 m buffer for livestock stream exclusion
- Wider than 11 m riparian buffers

Virginia established the Virginia Nutrient Credit Exchange Association which is a voluntary association of owners of 73 regulated municipal wastewater treatment plants and industrial facilities discharging nitrogen and phosphorus within the Chesapeake Bay watershed. The purpose of the Exchange is to coordinate and facilitate nutrient credit trading among its members with the goal of improving water quality in the Chesapeake Bay watershed efficiently and cost-effectively.

### **SUPPLY AND DEMAND OF CREDITS**

Selman et al. (2010) analyzed the existing and developing nutrient trading markets in the Chesapeake Bay region. The analysis examined both the short-term and long-term demand for credits. The short-term demand will be generated by wastewater treatment plants that need credits to meet their permit requirements. Eventually these treatment plants may opt to install technology upgrades or obtain other types of permanent offsets. Long-term demand will come from population growth which will generate the need for wastewater treatment plants to expand or new plants to be constructed. All the trading basins in West Virginia and Pennsylvania will experience a short-term demand for

nutrient credits. The demand will be such that credits from point sources will not meet the demand. Wastewater treatment plants will have to obtain credits from agricultural nonpoint sources. By 2030 many of the wastewater treatment plants are expected to exceed 80 to 100 percent of their existing design flow capacity. Nonpoint sources will supply most of the credits along with other offset methods approved by the states such as septic hook-ups or minor facility upgrades. The vast majority of credits will come from agricultural nonpoint sources. One of the challenges with agricultural nonpoint source credits will be that agriculture will have to meet their baseline for the TMDL

There will likely be a geographical mismatch between potential supply of nonpoint source credits and the demand for credits within trading basins. This will result in the need for interbasin-interstate water quality trading. This would produce a more stable and reliable supply of credits. Also encouraging agricultural innovative practices for nutrient reduction that are on the horizon like precision agriculture and animal feed manipulation could generate more credits from agriculture.

Table 2. Comparison of States Nutrient Trading Programs

Feature	Maryland	Pennsylvania	Virginia	West Virginia
<b>Pollutants that can be traded<sup>a</sup></b>	<ul style="list-style-type: none"> <li>Nitrogen</li> <li>Phosphorus</li> <li>Sediment</li> </ul>	<ul style="list-style-type: none"> <li>Nitrogen</li> <li>Phosphorus</li> <li>Sediment</li> </ul>	<ul style="list-style-type: none"> <li>Nitrogen</li> <li>Phosphorus</li> </ul>	<ul style="list-style-type: none"> <li>Nitrogen</li> <li>Phosphorus</li> <li>Sediment</li> </ul>
<b>Eligible market participants</b>	<ul style="list-style-type: none"> <li>Agricultural operations</li> <li>Nonsignificant point sources</li> <li>Other landowners</li> <li>Significant point sources</li> <li>Third parties</li> </ul>	<ul style="list-style-type: none"> <li>Nonpoint sources (e.g., agricultural operations, other landowners)</li> <li>Nonsignificant point sources</li> <li>Significant point sources</li> <li>Third parties</li> </ul>	<ul style="list-style-type: none"> <li>Agricultural operations</li> <li>Construction stormwater projects</li> <li>Nonsignificant point sources</li> <li>Other landowners</li> <li>Significant point sources</li> <li>Third parties</li> </ul>	<ul style="list-style-type: none"> <li>Agricultural operations</li> <li>Nonsignificant point sources<sup>b</sup></li> <li>Other landowners</li> <li>Significant point sources<sup>b</sup></li> <li>Third parties</li> </ul>
<b>General eligibility requirements for credit purchases</b>	<ul style="list-style-type: none"> <li>Existing significant point sources must have ENR in operation before purchasing credits or offsets.</li> <li>Point sources accommodate growth by purchasing offsets generated by point or non-point sources.</li> </ul>	<ul style="list-style-type: none"> <li>Existing point sources may purchase credits generated by point or nonpoint sources to meet annual load limits subject to additional conditions of NPDES permits.</li> </ul>	<ul style="list-style-type: none"> <li>Existing point sources may purchase credits generated by other point sources to meet annual load limits subject to additional conditions of NPDES permits.</li> <li>Point sources accommodate growth by purchasing offsets in the form of WLAs from other point sources or offsets from nonpoint sources.</li> </ul>	<ul style="list-style-type: none"> <li>Existing point sources must have NPDES permits and may purchase credits generated by point or nonpoint sources to meet annual load limits subject to conditions of the permits.</li> </ul>
<b>General eligibility requirements for credit and/or offset sales</b>	<ul style="list-style-type: none"> <li>Significant point sources must have ENR in operation before selling credits.</li> <li>WLA cannot be sold until it has been adopted in a NPDES permit through the public review process.</li> <li>Nonsignificant point sources must have annual load limits for nutrients.<sup>c</sup></li> <li>Sellers must meet baseline requirements.</li> <li>Facilities trading excess credits based on excess capacity must demonstrate consistency with water and sewerage plans.</li> </ul>	<ul style="list-style-type: none"> <li>Sellers must meet baseline and applicable threshold requirements before selling credits.</li> </ul>	<ul style="list-style-type: none"> <li>WLAs or compliance credits and offsets cannot be sold unless the facility for which the WLA was granted has been constructed and is operating.</li> <li>Sellers must meet baseline requirements before selling offsets.</li> </ul>	<ul style="list-style-type: none"> <li>Point sources must have NPDES permits that contain annual load limits for nutrients and/or sediment.</li> <li>Sellers must meet baseline requirements before selling credits.</li> </ul>

### SUMMARY

The following summary statements can be made from examining the potential for nutrient trading in the Chesapeake Bay watershed:

1. Maryland, Pennsylvania, Virginia and West Virginia have had nutrient trading programs established for a number of years.
2. To date the nutrient trading activity has been relatively light.
3. Virginia, West Virginia and Pennsylvania allow wastewater treatment plants to meet permit requirements by purchasing credits.
4. All significant wastewater treatment plants in Maryland have to install enhanced nutrient removal technology to meet permit requirements and can only purchase credits for expansion capacity.
5. Most of the long-term nutrient credit demand will be met by agricultural nonpoint source credits.
6. There will be a geographical mismatch between demand for nonpoint source credits and the supply of nonpoint source credits. This problem can be overcome by interbasin-interstate nutrient trading.

### REFERENCES

Branosky, C., C. Jones and M. Selman. 2011. Comparison Tables Of State Nutrient Trading Programs In The Chesapeake Bay Watershed. World Resources Institute, Washington, DC. WRI Fact Sheet.

Chesapeake Bay Program. 2012 Virginia's Nutrient Trading And Offset Program Review Observations. EPA, CBP, Annapolis MD. Final Report 2-17-2012. Available at [www.chesapeakebay.net/channel\\_files/17761/va\\_final\\_report.pdf](http://www.chesapeakebay.net/channel_files/17761/va_final_report.pdf).

Cole, P. and W.F. Ritter. 2010. A Conceptual Framework For Assessing The Success Of Water Quality Trading Programs. Proceedings of ASCE World Environmental and Water Resources Congress, May 23-26, 2010, Providence, RI. CD-ROM.

Maryland Department Of Agriculture. 2008. Maryland Policy for Nutrient Cap Management And Trading In Maryland's Chesapeake Bay Watershed Phase II- Guidelines For The Generation Of Agricultural Nonpoint Source Nutrient Credits. Maryland Department of Agriculture, Annapolis, MD. April, 2010.

Maryland Department Of Environment. 2008. Maryland Policy For Nutrient Cap Management And Trading In Maryland's Chesapeake Bay Watershed. Maryland Department Of Environment, Annapolis, MD. April, 2008.

Pennsylvania Department of Environmental Protection. 2006. Final Trading of Nutrient And Sediment Reduction Credits--Policy and Guidelines. Doc No.392-09000-001. December 30, 2006. [http://www.dep.state.pa.us/river/river\\_trading.htm](http://www.dep.state.pa.us/river/river_trading.htm)

Selman, M., E. Sprague, S Walker and B. Kittler. 2010. Nutrient Trading In The Chesapeake Bay Region; An Analysis Of Supply And Demand. Pinchot Institute, Washington, DC. March, 2010.

U.S. Environmental Protection Agency. 2011. Chesapeake Bay TMDL Available at <http://www.epa.gov/reg3wapd/tmdl/chesapeakebay/tmd/exec.html>. EPA, Washington, DC.



# WHAT HAPPENS IF THE CANAL BREAKS? TOOLS FOR ESTIMATING CANAL-BREACH FLOOD HYDROGRAPHS

Tony L. Wahl<sup>1</sup>

## ABSTRACT

A program of physical model tests and numerical unsteady-flow simulations has led to the development of appraisal-level tools for predicting the characteristics of floods caused by the breaching of homogeneous canal embankments. The procedures yield estimates of the time needed for initiation and development of a breach, the magnitude of the peak outflow, and the duration of the recession limb of the flood hydrograph. These tools can help water managers identify canal reaches that have the potential to produce floods with serious consequences. This can aid emergency management planning and help to prioritize the need for more detailed investigations. This paper demonstrates the use of the procedures and illustrates the importance of key input parameters, especially the erodibility of the soil in the embankment. The method has not yet been tested against real-world canal failures.

## INTRODUCTION

The Bureau of Reclamation (Reclamation) is responsible for more than 8,000 miles of irrigation canals in the western U.S., and failures of canal embankments have occurred periodically throughout its history. When these canals were constructed, the adjacent lands were primarily agricultural or undeveloped. Development of these lands has led to greater interest in understanding the potential impacts and consequences of canal embankment failures on surrounding areas. Threats to canals include animal burrows, tree roots, penetrations by turnout pipes and utilities, embankment and foundation issues, seismic events, internal erosion under static loading, hydrologic events, and operational incidents.

Numerical modeling of breach outflows and downstream flooding can be used to evaluate potential consequences of a canal breach. To facilitate appraisal-level investigations of Reclamation's canal inventory, a research program was undertaken to study the canal breach process and develop tools for predicting canal breach outflow hydrographs (Wahl and Lentz 2011). This work included both physical hydraulic modeling of the erosion and breaching processes and numerical modeling of transient canal behavior during a hypothetical breach event. Results from these studies were used to develop procedures for estimating breach initiation and breach enlargement rates and associated canal breach outflows. This paper illustrates the use of these procedures and demonstrates the sensitivity of results to key input parameters.

---

<sup>1</sup> Hydraulic Engineer, Bureau of Reclamation, Hydraulic Investigations and Laboratory Services, Denver, CO, 303-445-2155, [twahl@usbr.gov](mailto:twahl@usbr.gov).

## BACKGROUND

Although canal breaches have occurred throughout history, there have been remarkably few efforts to generalize experiences from these events. Prior to this study, there was no guidance specific to canals for predicting breach parameters or breach outflow hydrographs. Dun (2007) provided the most notable prior work on the hydraulics of a canal breach in a study of a navigation canal that failed in the United Kingdom in 2004. Dun concluded that the hydraulics of canal breaches were significantly different from breaches of traditional dams and storage reservoirs. For a traditional dam breach, outflow is typically limited by the breach geometry and the reservoir storage, but for a canal breach, outflow is also limited by the conveyance capacity of the reaches of canal that deliver water to the breach site.

Nearly all canal embankments contain soils that may be conducive to headcut development during erosion. Even canal embankment soils that do not demonstrate plasticity contain enough fine materials to resist seepage loss of water and thus exhibit enough apparent cohesion to allow headcuts to develop. Recognizing this general characteristic, the typical stages of a canal breach can be described as follows:

1. Initial overtopping of the embankment, or development of a defect in an embankment that allows erosive flow through the embankment or foundation (typically described as internal erosion or “piping”).
2. Development of a headcut that begins on the downstream (outer) slope of the embankment and migrates upstream toward the canal. In this stage, erosion is primarily taking place downstream from the section (the hydraulic control) that controls the outflow rate. The breach outflow rate is small and normal canal flow can continue past the developing breach site.
3. Migration of the headcut through the hydraulic control, which enlarges the control section rapidly and allows a dramatic increase in outflow. As the breach enlarges during this stage, the size of the breach and the water level maintained in the canal are the primary factors determining the outflow rate. In this phase, the breach outflow becomes so large that flow reverses in the canal reach that was initially downstream from the breach site.
4. The breach eventually enlarges to the point that the hydraulic control shifts from the breach opening to the two canal sections. Critical-depth flow occurs in the leg of the canal upstream from the breach and also in the leg of the canal downstream from the breach. The breach may continue to widen, but the outflow rate cannot increase. As the canal drains, the flow rate through the two critical sections drops and the breach outflow rate is reduced.

One potential modification of this staged breach process is a situation in which the embankment is weak enough to allow the overtopping channel or initial pipe to enlarge so rapidly that steps 2 and 3 are not distinct from one another but are effectively combined into one step in which erosion and enlargement of the hydraulic control section

occurs simultaneously with headcut development and advance. This would not change the hydraulic control shift that still occurs during the last step of the process.

The research studies carried out at Reclamation have focused on the last three steps of the process outlined above. These studies assumed that the occurrence of the first step in the process is given; there has been no attempt to model the initiation of piping, which is a complex process that can occur through a large variety of specific mechanisms (e.g., Von Thun 1996; Engemoen 2012). These studies have also been based on the conservative assumption that there is no intervention, such as early shutdown of the canal or closing of check gates at the upstream and downstream ends of a reach experiencing a breach event. This provides results that are appropriate for the worst-case scenario of a breach that develops so rapidly that intervention is not possible.

### PHYSICAL MODELING

Physical modeling to support this research was described in detail by Wahl and Lentz (2011). The facility used in the hydraulics laboratory (Figure 1) recreated a typical canal flow situation prior to development of a breach. Water could be provided into both ends of a non-erodible canal with an erodible test section in the middle. Each test started with normal canal flow past the test embankment, and as the breach developed, the flow into both ends of the model canal was increased to maintain boundary conditions at the breach site that were representative of a fast-developing breach in a long canal reach (i.e., a relatively steady canal water surface). The upper limit of inflow provided to each end of the canal was the theoretical critical-flow discharge capacity of the canal sections.

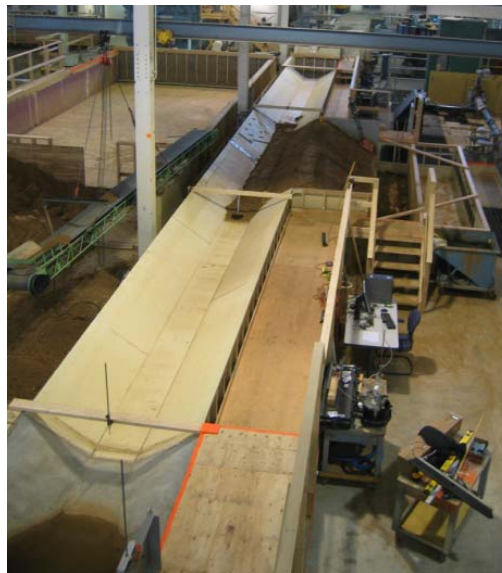


Figure 1. Overview of canal breach model test facility, looking in the upstream direction.

The three tested embankments were constructed in the model as simulated fill sections in a canal reach that is elevated above the surrounding landscape. Soil used to construct the embankments was a silty sand (SM) obtained from a local landscape materials supplier.

To simulate the wide range of erodibility properties that can occur in real canal embankments, we varied both the water content at compaction and the level of compaction effort. The test soil contained about 10% clay fines and exhibited some plasticity ( $PI=5$ ), so its erodibility was sensitive to the placement conditions. The erodibility of each test embankment was measured during embankment construction and after the completion of each breach test using submerged jet testing (Hanson and Cook 2004; ASTM D5852). Across three breach tests, the erodibility of the embankments varied by about three orders of magnitude as indicated by detachment rate coefficients obtained from the jet tests.

The breach tests exhibited three canal breach development scenarios, all initiated by erosion through a pre-formed pipe in the embankment (a #4 rebar embedded in the embankment and removed to start the test). The first test with a well-compacted and erosion-resistant embankment produced a very slow headcut migration and breach widening process, without a sudden and catastrophic breach outflow. This test was representative of a scenario in which there would likely be adequate time to shut down the canal and reduce the severity of the breach outflow. The second test demonstrated the breach behavior of a poorly-compacted and very erodible embankment, with rapid headcut development, headcut migration, and breach widening. The third test illustrated an intermediate situation in which the embankment was very erodible, but the initial pipe was located so high in the embankment that flow through it was small and initial headcut development and migration were slow. However, when the headcut finally migrated into the canal prism, failure and breach widening were nearly as rapid as that seen in the second test.

Data collected from the three tests were used to relate the soil erodibility parameters (detachment rate coefficient and critical shear stress) and hydraulic attack (estimated shear stresses and energy dissipation rates) to observed headcut migration and breach widening rates. The relations between these variables were found to be consistent with observations from breach testing of traditional embankment dams (Hunt et al. 2005; Temple et al. 2005; Hanson et al. 2011). This led to the development of simplified mathematical models for predicting headcut advance, piping hole enlargement, and breach widening rates. The first two models are relevant to estimating the time required for *breach initiation* (the time preceding headcut advance through the hydraulic control), which affects the amount of time available for detection of a breach in progress and warning of the downstream population at risk. The last model can be used to estimate the rate of breach enlargement after breach initiation has been completed.

### NUMERICAL MODELING

The physical model tests provide a means to predict how a breach will develop. The other significant question is what breach outflow hydrograph will be produced through this opening. This is dependent on both the characteristics of the breach and the transient behavior of the water within the canal reach in which the breach occurs, since drawdown of the canal and development of a varying water surface profile in the canal will change the head acting on the breach opening and the amount of flow that can be delivered to the breach site. To quantify these effects, one-dimensional unsteady flow modeling was

undertaken using HEC-RAS (Wahl and Lentz 2011). Numerous canal breach scenarios were simulated with varying canal sizes, breach times, canal reach lengths, and breach locations within the canal reach. This led to the development of dimensionless relationships that yield estimates of breach hydrograph parameters (peak outflow and recession time) as a function of breach development time, breach location within the canal reach, and canal hydraulic properties.

### CANAL BREACH OUTFLOW PREDICTION PROCEDURE

The essential characteristics of a canal breach hydrograph are the time required for breach initiation, the time required for breach development, and the resulting breach outflow hydrograph. The hydrograph may be defined by the peak outflow magnitude, the time at which peak outflow occurs, and the time required for the hydrograph to recede. The physical embankment breach tests and HEC-RAS modeling conducted in this research project provide a basis for estimating all of these characteristics of a canal breach event.

#### Breach Initiation

Breach initiation may take place through one or a combination of three different processes: headcut advance caused by overtopping flow; headcut advance due to flow through an existing piping channel that is not enlarging significantly; or continuous enlargement of an existing piping defect. Models for all three processes were developed (Wahl and Lentz 2011), but only the first two based on headcutting are presented here, as they are believed to be more reliable at this time.

Breach Initiation by Headcut Advance due to Overtopping Flow. Consider the canal embankment shown in Figure 2, which is depicted as a fill section deeper than the canal prism. Flow overtops the embankment with head  $H_{ov}$ . The unit discharge over the embankment can be estimated from a broad-crested weir equation as  $q=2.6H_{ov}^{1.5}$  with  $H_{ov}$  in ft and  $q$  in  $\text{ft}^3/\text{s}/\text{ft}$ . Assuming that headcutting initiates at the toe of the embankment, the time for breach initiation is the time required for the headcut to advance the distance  $L$  back to the upstream edge of the embankment crest. The headcut advance rate can be estimated from (Temple et al. 2005)

$$\frac{dX}{dt} = C(qH_h)^{1/3} \quad (1)$$

where:

- $dX/dt$  = headcut advance rate (ft/hr);
- $C$  = headcut advance rate coefficient ( $\text{s}^{1/3}/\text{hr}$ );
- $q$  = unit discharge ( $\text{ft}^3/\text{s}/\text{ft}$ ); and
- $H_h$  = headcut height (ft).

Hanson et al. (2011) showed (and the physical hydraulic model testing of canal breaches confirmed) that  $C$  can be estimated as  $C=0.44k_d$ , with  $k_d$  being the detachment rate coefficient obtained from a submerged jet erosion test with units of  $\text{ft}/\text{hr}/\text{psf}$ . In the event

that a jet test is unavailable, values of  $k_d$  may be estimated using Table 1 (Hanson et al. 2011) which relates  $k_d$  to the clay content, compaction effort, and water content of the soil during compaction (relative to the optimum water content that yields maximum dry density during a compaction test). Note that this table gives values of  $k_d$  in metric units, but they may be converted using the factor shown with the table.

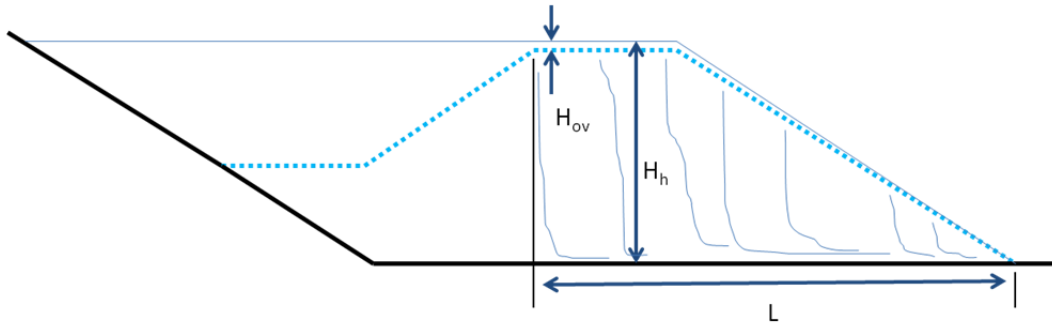


Figure 2. Canal embankment parameters for estimating headcut advance rate due to overtopping flow.

Combining these equations, the time for breach initiation in hours is:

$$t_{\text{initiation}} = \frac{L}{(0.44k_d)(2.6H_{\text{ov}}^{1.5}H_h)^{1/3}} \tag{2}$$

where:

- $L$  = required headcut advance distance, from toe of exterior slope (ft);
- $H_h$  = potential height of headcut (ft);
- $H_{\text{ov}}$  = overtopping head (ft); and
- $k_d$  = detachment rate coefficient (ft/hr/psf).

One could argue that the headcut should be assumed to initiate at the top of the slope to conservatively shorten the migration distance required, but in that case the head acting on the headcut would be initially small. The headcut would eventually deepen to approach  $H_h$ , and it is believed that the time required for this to occur is comparable to the time needed for headcut migration from the toe back to the head of the slope.

Table 1. — Approximate values of  $k_d$  in  $\text{cm}^3/(\text{N}\cdot\text{s})$  as a function of compaction conditions and % clay (Hanson et al. 2011). [1  $\text{cm}^3/(\text{N}\cdot\text{s}) = 0.5655 \text{ ft/hr/psf}$ ]

% Clay ( $<0.002 \text{ mm}$ )	Modified Compaction (56,250 ft-lb/ft <sup>3</sup> )		Standard Compaction (12,375 ft-lb/ft <sup>3</sup> )		Low Compaction (2,475 ft-lb/ft <sup>3</sup> )	
	$\geq\text{Opt WC}\%$	$<\text{Opt WC}\%$	$\geq\text{Opt WC}\%$	$<\text{Opt WC}\%$	$\geq\text{Opt WC}\%$	$<\text{Opt WC}\%$
	Erodibility, $k_d$ , $\text{cm}^3/(\text{N}\cdot\text{s})$					
>25	0.05	0.5	0.1	1	0.2	2
14-25	0.5	5	1	10	2	20
8-13	5	50	10	100	20	200
0-7	50	200	100	400	200	800

Breach Initiation by Headcut Advance due to Piping Flow. Analysis of this case is similar to the previous situation, except that the overtopping flow is replaced by orifice flow through a piping defect in the embankment. The elevation of this defect and its diameter and length must be specified to allow estimation of the flow rate through the pipe. The starting diameter should be a practical value relating to the size of piping defect that might prompt notice of the piping condition by project personnel and begin the cycle of potential operational responses to a canal emergency. The key variables are illustrated in Figure 3.

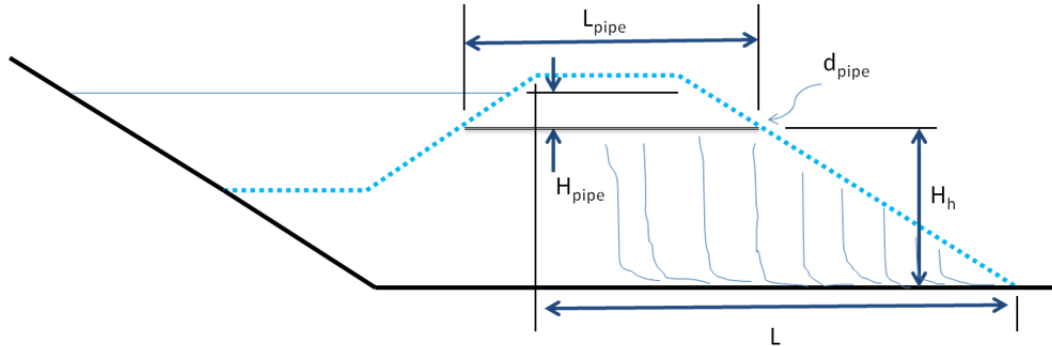


Figure 3. Canal embankment parameters for estimating headcut advance rate due to piping flow.

The flow rate through the pipe can be estimated by applying the energy equation

$$Q = \frac{\pi(d_{\text{pipe}})^2 \sqrt{2gH_{\text{pipe}}}}{4 \sqrt{1 + f \frac{L_{\text{pipe}}}{d_{\text{pipe}}}}} \quad (3)$$

where:

- $Q$  = discharge (ft<sup>3</sup>/s);
- $d_{\text{pipe}}$  = pipe diameter (ft);
- $g$  = acceleration due to gravity (ft/s<sup>2</sup>);
- $H_{\text{pipe}}$  = head across pipe (ft);
- $f$  = friction factor, assumed to be 0.05 for a relatively rough pipe interior; and
- $L_{\text{pipe}}$  = length of pipe (ft).

The unit discharge effective in advancing the headcut can then be estimated by converting the flow through the round pipe into the unit discharge of an equivalent square jet,  $q = (\pi/4)^{1/2}(Q/d_{\text{pipe}}) = 0.886Q/d_{\text{pipe}}$ . The time required for headcut advance is then computed as

$$t_{\text{initiation}} = \frac{L}{(0.44k_d)(0.886QH_h/d_{\text{pipe}})^{1/3}} \quad (4)$$

Note that the distance  $L$  is shown in Figure 3 as the distance to the upstream crest, not the full distance to the upstream end of the pipe. This leads to a shorter, more conservative estimate of the breach initiation time and is consistent with the observed behavior of the test embankments, which seemed to experience collapse of the bridge over the pipe at about the time that headcutting reached the upstream side of the crest.

Breach Initiation by Pipe Enlargement. A model for pipe enlargement was developed by Wahl and Lentz (2011), but was extremely sensitive to the values of  $k_d$  and the critical shear stress of the soil,  $\tau_c$ , as well as the choice of a starting condition for the piping erosion analysis. The model may be of interest for future research.

Breach Development. The breach development phase is characterized by headcut advancement through the upstream (canal side) slope of the embankment down to its toe, followed by widening of the breach in both directions until the breach becomes wide enough that it no longer serves as the hydraulic control. At this point, control of the flow shifts to the critical-flow sections that will exist in the upstream and downstream canals. For purposes of this appraisal-level model, the period of headcut advance into the canal is assumed to be short compared to the time for breach widening and is incorporated into the estimate of the widening time by assuming that widening begins from a breach width of zero. The breach is assumed to have vertical sidewalls during the widening phase and a rectangular cross-section, as observed in physical model tests and real embankment failures.

To estimate the breach development time, it is necessary to first define the ending condition for this phase. We need to determine the maximum theoretical flow that can be provided to the breach site by the upstream and downstream canals. This is accomplished by iteratively solving a system of three equations applying to critical flow (Clemmens et al. 2001):

$$Q = \sqrt{\frac{gA_c^3}{T_c}} \quad (5)$$

$$y_c = H_1 - \frac{A_c}{2T_c} \quad (6)$$

$$H_1 = h_1 + \frac{Q^2}{2gA_1^2} \quad (7)$$

where:

$y_c$  = critical depth,

$A_c$  = area of the critical section,

$T_c$  = top width of the critical section,

$h_1$  = normal flow depth in the canal,

$H_1$  = total energy head in the canal at normal flow, and

$A_1$  = area of the canal at normal depth.

For the design normal-depth flow condition of the canal, the flow depth  $h_1$  is known and a value of  $H_1$  can be computed using Eq. 7. Next, assume a starting value for critical depth,  $y_c$ , such as  $y_c=0.7H_1$ . For this critical depth, the cross-sectional area,  $A_c$ , and top width,  $T_c$ , of the canal may be computed. The critical discharge can then be computed from Eq. 5 and a refined estimate of  $y_c$  computed with Eq. 6.  $H_1$  should be kept constant, so the iteration between Eqs. 7 and 8 is continued until convergence is obtained. The maximum theoretical breach outflow,  $Q_{c,max}$ , will be two times the critical discharge computed with Eq. 5, assuming that both canals have the same cross section. This flow must pass through the breach opening in the canal embankment, and we will assume again that it does so in a critical-flow condition. The critical flow depth through the rectangular breach opening will be estimated as  $(2/3)y_n$ , where  $y_n$  is the normal depth of flow in the canal. (This is a crude estimation that ignores any head loss that occurs in the canal as flow approaches the breach). For a rectangular channel, the critical flow depth is  $y_c=(q^2/g)^{1/3}$ , so the unit discharge at the end of breach widening is  $q=[(2y_n/3)^3g]^{1/2}$  and the final width of the breach is

$$b_{\max} = \frac{Q_{c,\max}}{\sqrt{\left(\frac{2y_n}{3}\right)^3 g}} \quad (8)$$

The breach widening rate is estimated using a relation developed by Hunt et al. (2005) and confirmed in the physical model tests discussed previously.

$$\frac{db}{dt} = 2k_d [0.7\gamma_w g (y_c^{1/3} n / 1.49)^2 - \tau_c] \quad (9)$$

where  $db/dt$  is the change in breach width per unit time, the constant 1.49 comes from the Manning equation in English units, and Manning's  $n$  is taken to be 0.020 in the breach opening. With the final breach width and widening rates known, the time required for breach widening is

$$t_f = \frac{b_{\max}}{2k_d [0.7\gamma_w g (y_c^{1/3} n / 1.49)^2 - \tau_c]} \quad (10)$$

The critical shear stress,  $\tau_c$ , may be assumed to be zero to obtain a conservatively short estimate of the breach widening time. Once the breach widening time is estimated, it is converted to a dimensionless quantity,  $t_{\hat{f}}^* = t_f / t_{\text{ref}}$ , with  $t_{\text{ref}}$  being a reference time based on the hydraulic depth of the canal,  $D$ , and the wave celerity,  $c$

$$t_{\text{ref}} = \frac{D}{c} = \frac{D}{\sqrt{Dg}} = \sqrt{D/g} \quad (11)$$

In this equation the hydraulic depth,  $D$ , is defined to be the canal flow area divided by the wetted top width, and  $g$  is the acceleration due to gravity.

Numerical modeling of hypothetical canal failures (Wahl and Lentz 2011) was used to develop relations for predicting the dimensionless peak outflow,  $Q^*_{\text{peak}} = Q_{\text{peak}}/Q_{c,\text{max}}$ . Figure 4 shows the dimensionless peak outflow versus the dimensionless breach development time. Data points at or just below the upper envelope curve come from simulations in which the hypothetical breach site is a long distance upstream from the next downstream check structure along the canal, so there is a significant volume of water in the downstream canal that can drain back upstream to add to the breach outflow. Points lying well below the envelope curve are for simulations in which the breach site was closer to the downstream end of the canal reach. Figure 5 shows the percentage of the envelope value that was actually developed as a function of the dimensionless distance from the breach site to the downstream end of the reach. Note that the curve shown in Figure 5 is modified from that shown in Wahl and Lentz (2011) so that the curve passes through 50% at a dimensionless distance of 1. Thus, if the breach is located very near the downstream end of the reach, then the downstream channel is short and contributes almost nothing to the peak outflow, so the maximum possible outflow is 50% of the value obtained from the envelope curve. Note also that in the numerical simulations the distance from the breach to the upstream end of the canal reach had much less effect on the peak outflow than did the downstream distance. Combining the two relations shown on these figures produces one equation for estimating the peak outflow:

$$Q_{\text{peak}} = Q_{c,\text{max}} (Q^*_{\text{peak}}) = Q_{c,\text{max}} \frac{1.9}{(t^*_f)^{1/6}} \left[ 1 - \frac{0.5}{(L^*_{\text{ds}})^{1/4}} \right] \quad (12)$$

where  $t^*_f$  is the dimensionless breach development time defined earlier and  $L^*_{\text{ds}}$  is the downstream canal reach length nondimensionalized by the hydraulic radius,  $L_{\text{ds}}/R_h$ . The value of  $L^*_{\text{ds}}$  is never allowed to be less than 1.

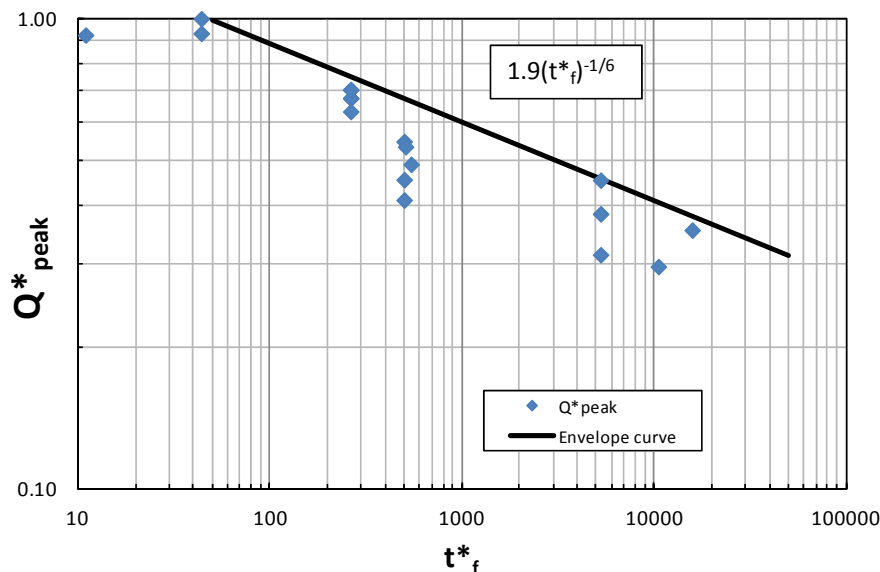


Figure 4. Dimensionless peak outflow from hypothetical canal breaches as a function of dimensionless breach development time.

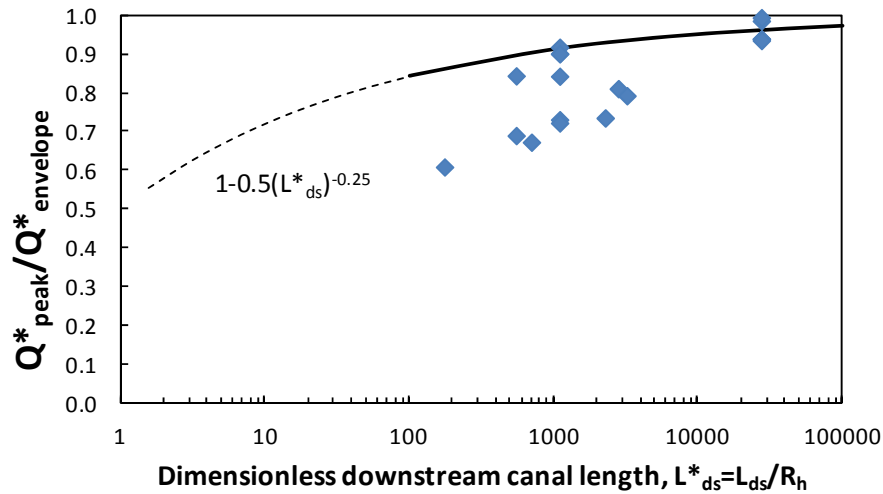


Figure 5. Effect of downstream canal reach length on peak breach outflow.  $L_{ds}$  is the length of the downstream canal and  $R_h$  is the hydraulic radius.

The peak discharge is assumed to occur at the end of the breach widening phase. The other parameter of significant interest is the time required for the breach outflow to recede back toward the normal canal flow rate. (Since we assume that the canal is not shut down during a hypothetical “fast” breach, the canal continues to supply water from upstream at the normal rate.) To describe the recession curve, the duration for the flow to drop back to a flow rate of  $Q_{normal} + 0.5(Q_{peak} - Q_{normal})$  can be estimated with Eq. 13 (Wahl and Lentz 2011), which defines the curve shown in Figure 6.

$$t_{recession} = \frac{123}{t_f^{*0.66}} t_f \tag{13}$$

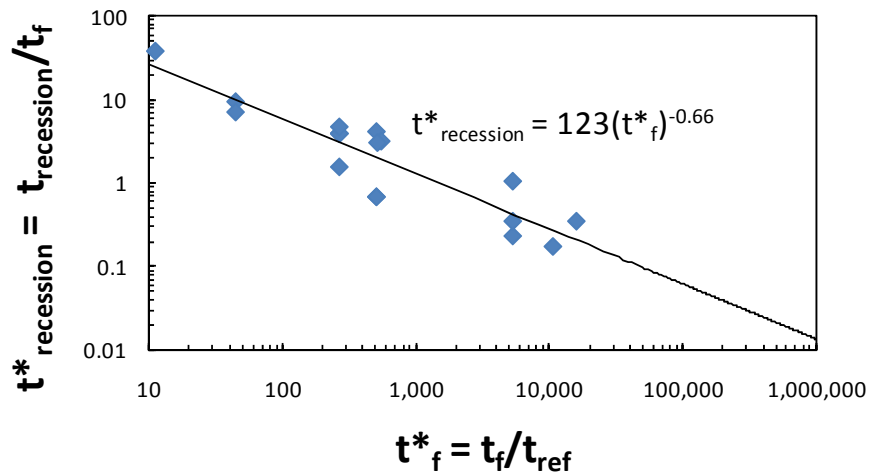


Figure 6. Hydrograph recession time as a function of breach development time.

### SPREADSHEET MODEL

The set of equations described above has been programmed into a spreadsheet model that allows a user to describe the canal properties, the embankment dimensions, and the embankment materials, and then estimate breach initiation time, breach development time, and the breach outflow hydrograph. The next step in the development of this tool is to validate it against actual canal failures. This will require case studies with the necessary input data and good estimates of the actual breach outflow hydrograph.

### EXAMPLE APPLICATION

To illustrate the use of the procedures described in this paper, consider a hypothetical example as follows:

- Earthen canal with design discharge of 800 ft<sup>3</sup>/s;
- Canal cross section in the reach of interest is trapezoidal with 15 ft base width, 2:1 (H:V) side slopes, bed slope = 0.000379 (2 ft/mile), and Manning's  $n = 0.028$ . Normal depth of flow for the design discharge is 8.32 ft.
- The canal reach being considered is a 3-mi-long fill section, with gated check structures at each end of the reach. The check structures are assumed to remain at their normal operating positions during a breach event (worst-case, very rapid breach scenario).
- The canal embankments on both sides of the canal are 15 ft tall from land-side toe to crest, and the freeboard between the crest and the normal operating water surface is 2 ft. The crest width is 16 ft, and the external embankment slope is 2:1.
- The embankment is constructed from a silty sand (SM) with 4% clay. The embankment was constructed in about 1910 and is believed to have been compacted by animal traffic (low compaction effort) at a water content that was equal to or wetter than optimum.
- Locations of greatest concern are near the downstream end of the reach and about 1 mile upstream from the downstream check structure. Several homes are located near the toe of the embankment at each of these locations.

The canal was operated for two years at a reduced discharge of 500 ft<sup>3</sup>/s, and the flow depth during this time was only 6.61 ft. When the canal is returned to service this year at the original design flow rate, a potential failure mode is piping through muskrat burrows located at the water line corresponding to the previous years' operations (3.71 ft below the embankment crest). We will assume that a muskrat burrow has a starting diameter of 2 inches and passes straight through the embankment.

Before considering specific breach locations and material parameters, we can use Eqs. 5-7 to compute the maximum theoretical peak outflow, which will be the reference discharge for any breach scenario. The maximum critical-flow discharge in one canal

reach is  $2054 \text{ ft}^3/\text{s}$ , before the canal drains significantly, and thus, the maximum theoretical breach outflow is  $Q_{c,max} = 4108 \text{ ft}^3/\text{s}$ .

Soil erodibility parameters are estimated by referring to Table 1. For the compaction conditions described, the table suggests  $k_d = 200 \text{ cm}^3/(\text{N-s}) = 113.1 \text{ ft/hr/psf}$ . We will assume that the critical shear stress for this material is 0 psf. Applying the equations describing the model for headcut advance caused by flow through the pipe (muskrat hole), the initial flow through the pipe is 32 GPM, and the time needed for breach initiation is 34 minutes. For comparison, a scenario in which the canal is misoperated so that the banks are overtopped by 3 inches yields a breach initiation time of 33 min. If we return to the piping scenario and the initial pipe is raised 1 ft higher in the embankment, the breach initiation time increases to 38 min; if lowered by 1 ft the time reduces to 33 min, so the result is relatively insensitive to the initial pipe elevation.

The breach widening phase of the process is analyzed next. The breach widening rate is estimated to be 181 ft/hr, using Eq. 9. The maximum breach width needed to release the theoretical peak outflow previously calculated is only 55 ft, so the time needed for breach widening is only 18.4 min.

To predict the peak outflow from the breach, we must select a location for the breach. We consider two possible locations, one at the end of the reach ( $L_{ds}=5 \text{ ft}$ ;  $L^*_{ds}=1$ ), and the second located 1 mile upstream from the end of the reach ( $L^*_{ds}\approx 1000$ ). Applying Eqs. 11-12 we obtain a peak outflow of  $1050 \text{ ft}^3/\text{s}$  at the downstream site and  $1910 \text{ ft}^3/\text{s}$  at the upstream site.

To test the sensitivity of the results to the soil erodibility parameters, let us revisit Table 1 and assume that the embankments were compacted dry of optimum. This changes the estimated value of  $k_d$  to  $800 \text{ cm}^3/(\text{N-s})$ , or  $452 \text{ ft/hr/psf}$ . Assuming again that the piping failure initiates at 3.71 ft below the embankment crest, the breach initiation time is now reduced to 8.5 min and the breach widening time is only 4.6 min. The peak outflow for a breach at the downstream end of the reach is increased to  $1320 \text{ ft}^3/\text{s}$  and the peak outflow for a breach 1 mile upstream is  $2410 \text{ ft}^3/\text{s}$ . Figure 7 shows a predicted breach hydrograph for this latter case. The figure includes a plot of the estimated product of flow depth and velocity (DV) at the breach opening. This parameter can be useful for assessing the lethality of the flood and its potential to cause property damage, although if the flood is able to spread rapidly downstream from the breach, the DV values will drop accordingly and the potential for damage will diminish. A one or two-dimensional flood routing simulation may be needed to predict inundation depths and flooding severity at a distance from the breach site.

Table 2 summarizes results for the scenarios discussed above, and one other involving an assumption that the embankment was constructed with standard compaction effort near optimum water content.

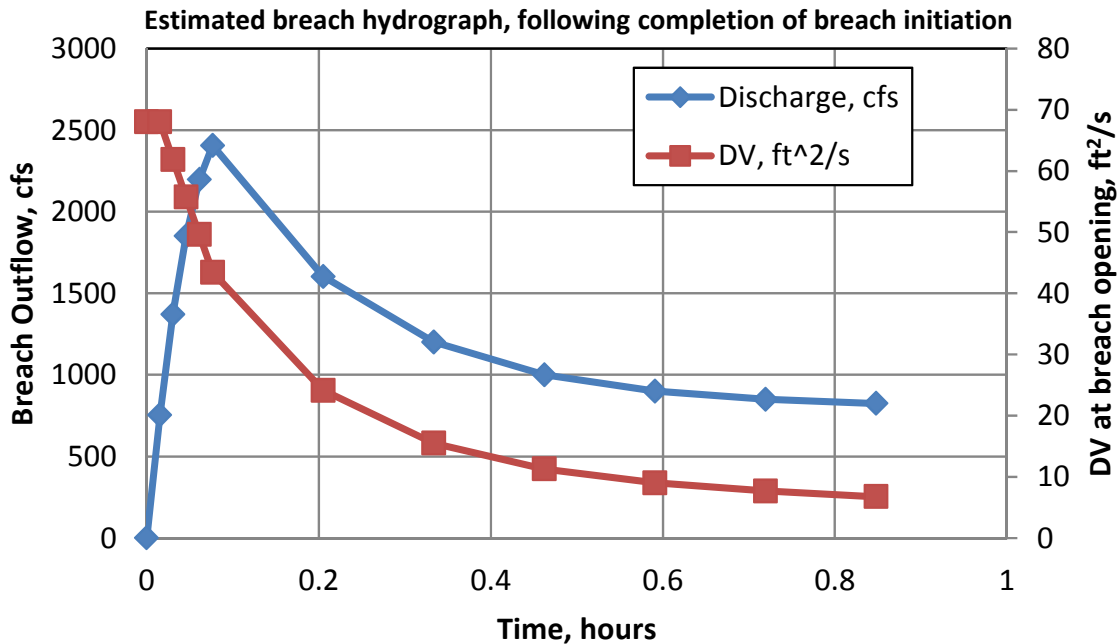


Figure 7. Predicted breach outflow hydrograph for the hypothetical example.

Table 2. Hypothetical canal breach hydrograph predictions.

Embankment compaction	Failure initiation	$k_d$ (ft/hr/psf)	Breach initiation time (min)	Widening time to reach peak outflow (min)	Peak outflow if breach at downstream end (ft <sup>3</sup> /s)	Peak outflow if breach is 1 mile upstream (ft <sup>3</sup> /s)
Low effort, optimum water content	Headcut advance due to flow through 2" animal burrow pipe 3.71 ft below embankment crest	113.1	34	18.4	1050	1910
	Overtopping by 3"	113.1	33			
Low effort, dry	Headcut advance due to piping	452	8.5	4.6	1320	2410
Standard effort, optimum water content	Headcut advance due to piping	56.6	68	37	930	1700

## CONCLUSIONS

Prediction of canal breach outflow hydrographs requires modeling of both breach development processes and the transient response of the canal. Physical model testing and analytical work has produced methods for estimating breach initiation time, breach development time and breach width. Numerical modeling of canal and breach dynamics has produced relations for predicting breach outflow hydrograph characteristics as a function of breach development time and breach location within a canal pool relative to nearby check structures that regulate the canal flow. These components have been assembled to create an integrated mathematical model that can be used to make appraisal-

level estimates of canal breach outflow hydrographs as a function of canal hydraulic properties and embankment material properties. The method has not yet been tested against real-world canal failures.

### REFERENCES

ASTM, 2003. Annual Book of ASTM Standards, Section 4: Construction, Vol. 04.08. Philadelphia, Pa.: ASTM.

Dun, R.W.A., 2007. An improved understanding of canal hydraulics and flood risk from breach failures. *Water and Environment Journal*. 21(1): 9-18.

Engemoen, W. 2012. Reclamation's processes for evaluating potential internal erosion concerns in embankment dams. 6<sup>th</sup> International Conference on Scour and Erosion, August 27-31, 2012, Paris, France.

Hanson, G.J., and K.R. Cook, 2004. Apparatus, test procedures, and analytical methods to measure soil erodibility *in situ*. *Applied Engineering in Agriculture*, 20(4):455-462.

Hanson, G.J., D.M. Temple, S.L. Hunt, and R.D. Tejral, 2011. Development and characterization of soil material parameters for embankment breach. *Applied Engineering in Agriculture*, 27(4):587-595.

Temple, D.M., G.J. Hanson, M.L. Neilsen, and K.R. Cook. 2005. Simplified breach analysis for homogeneous embankments: Part 1. Background and model components. In *Technologies to Enhance Dam Safety and the Environment*, Proceedings of the Annual Meeting of the United States Society on Dams, Denver, Colorado, 151-161.

Von Thun, J.L., 1996. Understanding piping and seepage failures - the no. 1 dam safety problem in the west. ASDSO West Regional Conference, April 14-16, 1996, Lake Tahoe, NV.

Wahl, T.L. and D.J. Lentz, 2011. *Physical hydraulic modeling of canal breaches*, Hydraulic Laboratory Report HL-2011-09, U.S. Dept. of the Interior, Bureau of Reclamation, Denver, CO.

Wahl, T.L., 2012. Numerical modeling to predict canal breach outflow hydrographs. 2012 World Environmental and Water Resources Congress, Environmental and Water Resources Institute of the American Society of Civil Engineers, Albuquerque, NM, May 20-24, 2012.



# HURRICANE KATRINA: ITS IMPACTS TO THE MIDDLE RIO GRANDE REGION OF NEW MEXICO

Subhas K. Shah, P.E.<sup>1</sup>  
Ray A. Gomez, P.E.<sup>2</sup>  
Dr. Kristoph Kinzli, P.E.<sup>3</sup>

## ABSTRACT

Hurricane Katrina was the most costly hurricane in U.S. history and the impacts to the City of New Orleans and surrounding areas were national news for many months. Less well known is how Katrina resulted in nationwide changes to the evaluation of flood control. These changes have been costly for many communities, and have been clearly felt in the Middle Rio Grande Region of New Mexico, where rainfall is scant and the Rio Grande runs dry due to water scarcity.

The failure of flood control structures, including levees to hold back flooding caused by Hurricane Katrina, prompted the United States Army Corp of Engineers (USACE) to re-evaluate and implement new levee standards for construction, maintenance, and certification. Since the implementation of these new levee standards, the Middle Rio Grande Conservancy District (MRGCD) in cooperation with other local governmental agencies has reconstructed 3.2 miles of the Albuquerque West Levee at a cost of \$6 million over a two year period. The MRGCD levee maintenance costs have increased to comply with new USACE guidelines for vegetation management. The USACE, MRGCD, New Mexico Interstate Stream Commission (NMISC) and other governmental agencies are working cooperatively to plan the reconstruction of 43 miles of the San Acacia to Bosque Del Apache Unit Levee. Construction of Phase 1 is anticipated to begin in September 2013 and proposes reconstruction of approximately 3 miles of levee at an estimated cost of \$11.9 million.

Seven years after Hurricane Katrina, the MRGCD continues its efforts to maintain and reconstruct now unacceptable levees to comply with new USACE standards. Ultimately, these efforts will require millions of dollars to bring the Middle Rio Grande Region into compliance with these new standards.

---

<sup>1</sup> Chief Engineer, CEO, Middle Rio Grande Conservancy District, Albuquerque, NM; shah@mrgcd.com

<sup>2</sup> Assistant Engineer, Middle Rio Grande Conservancy District, Albuquerque, NM; ray@mrgcd.com

<sup>3</sup> Assistant Professor, Department of Environmental and Civil Engineering, Florida Gulf Coast University, Fort Myers, FL; [kkinzli@fgcu.edu](mailto:kkinzli@fgcu.edu) (Corresponding author)

## INTRODUCTION

### **The Middle Rio Grande Conservancy District (MRGCD)**

The MRGCD is a political subdivision of the State of New Mexico that was formed by the Conservancy Act of 1923 to provide irrigation, drainage and flood protection in the Middle Rio Grande Valley. Under the unitary classification system all property owners within the benefited areas of the MRGCD pay ad-valorem assessment and additionally, those who use irrigation water, pay a water service charge. The MRGCD is governed by an elected seven member board of directors who serve staggered four year terms. The MRGCD encompasses four counties within central New Mexico; Sandoval, Bernalillo, Valencia, and Socorro. Three members are elected from Bernalillo County the most populous county, one each from Sandoval, Valencia, and Socorro counties, and one member is elected at-large.

The MRGCD boundaries extend along a 150 mile stretch of river valley known as the Middle Rio Grande Valley (Figure 1). The Rio Grande is the predominant river in the State of New Mexico. The MRGCD's jurisdictional boundary extends from Cochiti Dam to the Bosque Del Apache National Wildlife Refuge and the boundary width varies approximately 0 to 7 miles east and west of the Rio Grande. The river valley is home to an abundance of plant and animal life, which thrives in the regional cottonwood forest growing along the banks of the Rio Grande. This forest is commonly referred to as the "Bosque" and is the largest cottonwood forest in the United States. The Bosque and Rio Grande are unique given that they meander through the valley and encompass several urban communities, including Albuquerque, the largest city in New Mexico. The MRGCD diverts water from the Rio Grande at four different dam diversions to serve agricultural lands.

New Mexico's climate is considered an arid desert. June to September is typically considered the monsoon season with an average annual precipitation of roughly 9 inches. Rain events are typically short in duration, but often very intense and can cause local flooding. Earthen levees along the Rio Grande restrict flood events to a defined floodway channel. These earthen levees were initially constructed by the MRGCD in the early 1930's. Prior to those initial levees, the Rio Grande was uncontrolled and communities along the Rio Grande were frequently flooded. In the early 1920's, periodic uncontrolled floods and an aggrading river caused 70 percent of the river valley to be waterlogged and unsuitable for development.

### **MRGCD Levees**

A major portion of the flood protection work done by the MRGCD was to construct the initial system of earthen levees. This occurred simultaneously with the construction of the riverside drain network. Excavation of the riverside drains provided the earth material for levees between the riverside drain and river channel. Today these levees are referred to as spoil bank levees and are assumed to be structurally unsafe; though they have provided flood protection to the Middle Rio Grande Valley for over 80 years. The

MRGCD today continues to operate and maintain 400 miles of drains, 250 miles of levees, and 800 miles of irrigation facilities.

### **Flood Control Reservoirs**

Flood control facilities also exist upstream of the Middle Rio Grande Valley in the form of storage reservoirs. El Vado Reservoir is owned and was constructed by the MRGCD in 1935. El Vado has a total storage capacity of 196,500 acre-feet and is located about 160 miles north of Albuquerque on the Rio Chama, a major tributary of the Rio Grande. The primary purpose of El Vado is to store supplemental water for irrigation delivery to agricultural lands within the MRGCD. Today El Vado, operated by the Bureau of Reclamation (BOR), includes specific flood control requirements. Water operations help sustain the endangered Rio Grande Silvery Minnow, and other wildlife and plant life; including the Rio Grande Bosque. El Vado operations also provide recreation activities such as kayaking, fishing, and white water rafting.

Abiquiu Reservoir was constructed for flood protection by the USACE in 1963 on the Rio Chama about 30 miles downstream of El Vado and has a capacity of 1,192,800 ac-ft. A secondary purpose is now storage of San Juan Chama Project Water, which is imported from Colorado, across the Continental Divide, to New Mexico. The Albuquerque Bernalillo County Water Utility Authority (ABCWUA) and other San Juan Chama Project contractors can store as much as 180,000 ac-ft of project water in the reservoir. ABCWUA typically stores approximately 48,000 ac-ft of project water annually, which is used to supplement City of Albuquerque drinking water.

A third reservoir was constructed on the main stem of the Rio Grande within the Pueblo of Cochiti, the north end of the Middle Rio Grande Valley. Cochiti Reservoir is a USACE project, completed in 1975. Its primary purpose is flood protection and sediment control. Cochiti is a large reservoir, potentially detaining up to 582,000 ac-ft during flood control operations. Under normal operations, only a small pool of about 50,000 ac-ft is maintained for sediment control and recreation. Through the combination of these reservoirs, a very substantial amount of flood storage has been developed above the Middle Rio Grande Valley since the original construction of the MRGCD levee system.

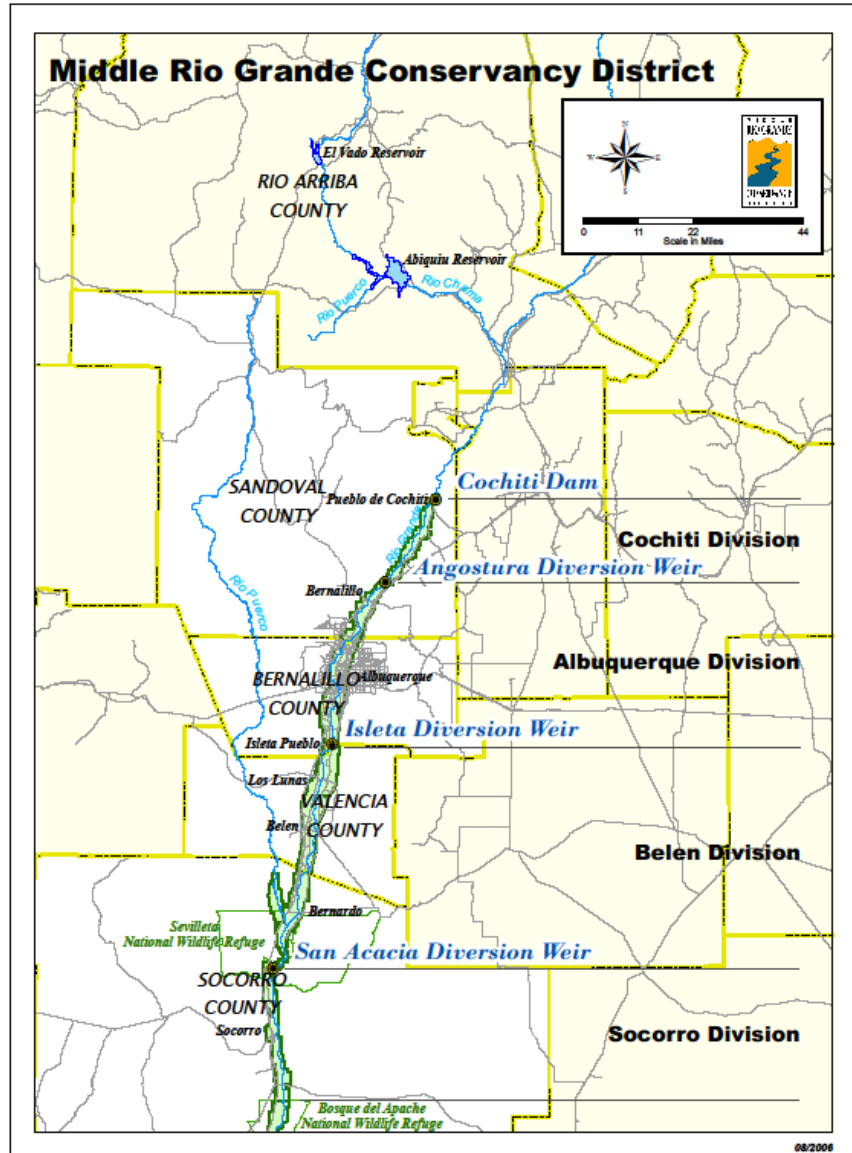


Figure 1. The Middle Rio Grande Conservancy District in Central New Mexico

### USACE LEVEE INVOLVEMENT

In 1950, the USACE received authorization and funding to design and construct new levees to protect the City of Albuquerque. The USACE considered the existing spoil bank levees unsuitable because they did not meet the engineering and construction standards for that time. The project removed approximately 30 miles of spoil bank levees, replacing them with newly engineered levees. The USACE levee projects were identified as: Albuquerque Tie Back Levee Unit Phase 1 East, Albuquerque Levee Unit 2 East, Albuquerque Levee Unit Phase 3 East, and Albuquerque Levee Unit Phase 3 West (Figure 2). The Corrales Levee Unit was completed in 1997. This levee is approximately 10.6 miles long and provides flood protection to the Village of Corrales west of the Rio Grande.

The levees constructed by the USACE are periodically inspected and the minor deficiencies are corrected by the local sponsor. The USACE last certified the engineered levees that were designed and constructed by them in 2005. Under new criteria, the USACE has refused to certify any levees that were designed, constructed and financed by them.

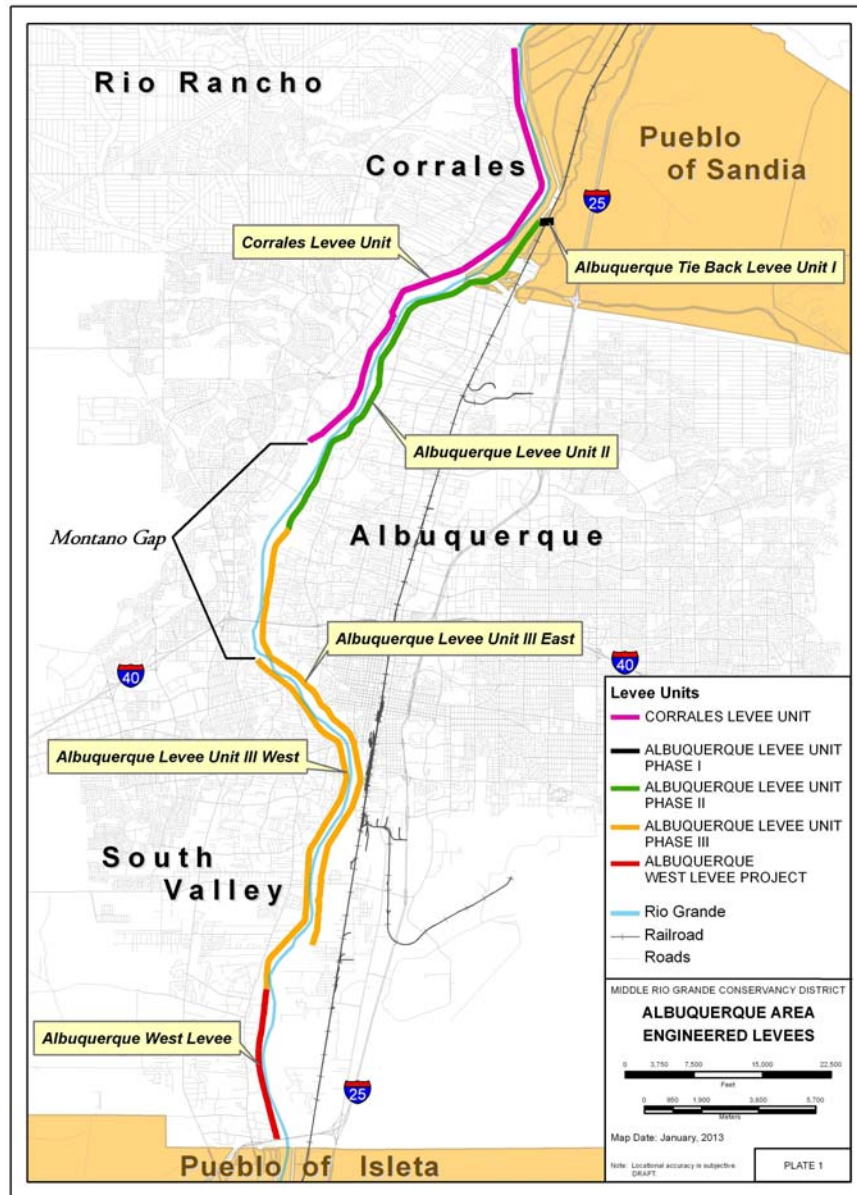


Figure 2. USACE Levee Projects in the MRGCD

### HURRICANE KATRINA

On August 23, 2005, the National Oceanic & Atmospheric Administration (NOAA) reported a tropical depression over the Bahamas. The following day NOAA reported a well-defined band of storm clouds wrapping around in a circular storm center with winds approaching 40 miles per hour. The storm was named Tropical Storm Katrina. As Tropical Storm Katrina continued to be tracked, the storm moved in a northwest direction towards southern Florida. On August 25th Tropical Storm Katrina was upgraded to a Category 1 hurricane with maximum sustained winds near 75 miles per hour. The hurricane crossed southern Florida with reports of minor flooding.

NOAA continued to track Hurricane Katrina as it moved from Florida into the Gulf of Mexico. Once in the Gulf of Mexico the hurricane increased in size and strength. On August 28th Hurricane Katrina was upgraded to a Category 5 hurricane with winds blowing at 175 miles per hour. As Katrina approached the Gulf Coast States of Louisiana and Alabama, the storm weakened to a Category 3 storm before making landfall along the Louisiana and Mississippi coastline the morning of August 29th. Gulfport and Biloxi Mississippi were devastated as hurricane winds and flooding pounded the coastline. Levees protecting New Orleans were breached causing the city to be flooded. Citizens living in these communities lost their homes, and many lost their lives. Those who survived were given refuge in the New Orleans Convention Center and the Superdome. The National Guard assisted with evacuations from flooded communities and emergency responders and volunteers from across the nation deployed to flooded areas, offering their assistance.

The damage brought by Hurricane Katrina to the Gulf Coast states was unprecedented. The USACE indicated approximately 80 percent of New Orleans was flooded to depths exceeding 15 feet. Storm surge and heavy rains caused major levee breaches and 169 miles of a 350 mile levee system protecting New Orleans and surrounding communities was compromised. It was determined pump stations, intended to protect New Orleans from significant flooding, did not operate at their capacity due to loss of power and damage to the pump motors as a result of floodwaters.

As the floodwaters from Hurricane Katrina increased above levee system capacities, massive levee failures were reported by the national media. The levee system had been designed and constructed by the USACE, and maintained by local sponsors. The local New Orleans government was criticized for poor emergency response before and after the hurricane. Blame was leveled at the USACE for levee failures, and critics questioned the integrity of the New Orleans levee system. An Interagency Performance Evaluation Task Force (IPET) was convened to find scientific and engineering answers to the levee failures. The IPET was selected by the Chief of the USACE and was comprised of 50 different organizations including recognized experts, numerous governmental agencies, universities and private sector firms. The IPET report concluded the flooding by Hurricane Katrina had caused 50 major levee breaches, four caused by foundation failure and the remainder by overtopping and scour. Due to the massive failure of the New

Orleans levee system, the USACE adopted new levee standards to prevent such destruction in the future.

## HURRICANE KATRINA STRIKES NEW MEXICO

### Initial Assessment

The long reaching effects of Hurricane Katrina were first recognized when the USACE published a news release on February 1, 2007 identifying 25 locations of unacceptably maintained levees along the Middle Rio Grande. Unacceptable ratings were a result of one or more deficient conditions, which included animal burrows, erosion, tree growth within newly established vegetation free zones, movement of floodwalls or faulty culvert conditions and age of levees. Levees across the nation were identified as receiving unacceptable ratings including the *"Albuquerque Unit, Middle Rio Grande Levees"*.

The USACE formally contacted the MRGCD by letter on March 6, 2007. The letter noted,

*"Since the catastrophic New Orleans levee failures during Hurricane Katrina, the USACE has initiated a National Levee Inventory and Assessment Program to identify public risks associated with levee systems across the nation. As per March 2004, Middle Rio Grande Bosque Levee Preliminary Assessment Report, and subsequent March 22-23, 2004, inspection under the Inspection of Completed Works Program, the USACE established a poor rating for the Albuquerque Unit, Middle Rio Grande levee system"*.

The USACE indicated the rating was based on the fact that the Middle Rio Grande Levee System is over 50 years old and has reached the end of its design life, requiring major rehabilitation and/or replacement. The maintenance of the levee system was not the critical issue. The poor rating was based solely on age and new stringent design, construction, and inspection standards.

Although maintenance was not the underlying issue, the USACE offered to provide a one time "maintenance deficiency correction period" of up to one year to comply with their new levee standards or face removal from the USACE Rehabilitation and Inspection Program (PL84-99). If the Albuquerque Levees were removed from PL84-99, these levees would be ineligible for federal assistance for repair or rehabilitation if damaged by storm event or other natural disaster. The MRGCD was suddenly faced with the difficult and problematic task of compliance with new USACE post-Katrina levee standards, specifications and guidelines. The specifications and guidelines for vegetation management on levees were new and they had not yet been published. Further consequences of Hurricane Katrina were felt in the Middle Rio Grande Region when USACE threatened potential removal of Albuquerque levees from PL84-99.

### **Initial Response**

The inspection and assessment report evaluated the Albuquerque Tie Back Levee Unit Phase 1, Albuquerque Levee Unit 2, Albuquerque Levee Unit Phase 3 East & West, and Corrales Levee Unit. These levees provide the City of Albuquerque with flood protection from flooding of the Rio Grande up to the 270 year storm event (42,000 cfs). Three specific deficiencies and recommendations were identified:

- 1) The riverside drain located adjacent to the landside of the levee was identified as a levee instability problem due to hydrostatic uplift, and concerns of possible uncontrolled seepage and piping of the levee foundation material. The USACE recommended relocating the riverside drain from its present location, which is approximately 40 feet from the toe of levee, to a minimum of 300 feet from the levee toe. As an alternate, an appropriate sized reinforced concrete drainage system might be constructed to replace the riverside drain.
- 2) Woody vegetation within the Bosque should be cleared from the levee footprint; including 50 feet beyond the toe of levee.
- 3) Unprotected levee embankments are susceptible to erosion, more drought tolerant grasses should be planted on levee side slopes and the riverside levee slope should be armored with rip-rap or possibly soil cement.

The specified deficiencies and corrective recommendations were determined by MRGCD to have the following impacts:

- 1) Relocating the riverside drains would require purchase and or condemnation of properties adjacent to the levees. Additionally, placing the riverside drains in a concrete pipe drainage system along all 43 miles of engineered levee would require new levee design, new maintenance requirements, and USACE approval. The continued maintenance of the open channel riverside drains, per USACE guidelines, would be more cost effective with present MRGCD maintenance practice.
- 2) Removing woody vegetation within the Bosque, 50 feet beyond the riverside levee toe, would impact approximately 260 acres of cottonwood forest. All species of wildlife found in the Bosque including the endangered Southwestern Willow Fly Catcher could be affected making this a very unpopular proposal to the MRGCD, United States Fish and Wildlife Service, and other governmental agencies and environmental groups. The removal of trees 50 feet beyond the levee footprint was arbitrary and no scientific information could be provided to substantiate this kind of tree removal.
- 3) Protecting and maintaining levee slopes from erosion and animal burrows have continued to be MRGCD standard maintenance practice.

### **USACE MANDATES NEW LEVEE STANDARDS**

The USACE on April 10, 2009 published "Guidelines for Landscaping, Planting, and Vegetation Management at Levees, Floodwalls, Embankment Dams, and Appurtenant

Structures". These new guidelines provide minimum clearance for landscape and vegetation management adjacent to MRGCD levees. The guidelines required Vegetation Free Zones, which measured the width of the levee footprint plus 15 feet beyond the landside toe of levee, and 15 feet beyond the riverside toe of levee. Vegetation Free Zones require woody vegetation to be removed and the growth of perennial grasses encouraged to minimize levee erosion. These new levee guidelines were inconsistent with USACE guidelines that were established for the Corrales Levee Unit in 1997. Those guidelines required a 3 foot vegetation free zone, not 15 feet. Removing any woody vegetation within the Middle Rio Grande Valley's unique cottonwood forest, beyond the present 3 foot Vegetation Free Zone, was viewed by the general public as environmentally damaging, and possibly detrimental wildlife including the endangered Southwest Willow Flycatcher.

### **FEMA DE-CERTIFICATION**

The Federal Emergency Management Agency (FEMA) is responsible for administering the National Flood Insurance Program (NFIP). FEMA provides flood hazard data and maps across the country. Up to date flood hazard information and maps are needed to identify flood hazard locations to support the purchase of flood insurance. On August 22, 2005, FEMA issued Procedure Memorandum No. 34 (PM 34) Interim Guidance for Studies Including Levees. The purpose of PM 34 was to help clarify the responsibility of community officials or other parties seeking recognition of a levee by providing documentation regarding levee design, operation and maintenance, inspection reports, and an engineer's certification that the levee system is capable of containing the 100 year storm event. This documentation would be used to aid in, "properly assessing how to handle levee mapping issues". FEMA recognized the role of levees and their condition for determining Flood Insurance Rate Maps (FIRMs). FEMA was concerned that the condition of many levees had not been assessed since FIRM'S were produced more than 30 years ago. As a result, FEMA initiated the new study to gain a better understanding of the actual flood risks for citizens living and working behind levees nationwide.

On February 16, 2007, FEMA contacted Bernalillo County, the City of Albuquerque and the MRGCD indicating they had initiated a study to update FIRMs for Bernalillo County. The FIRMs were to be revised to a digital format (DFIRMs) which would eventually provide a seamless coverage across the county. FEMA hoped the DFIRMs would provide reliable, easy to use, and readily available information regarding flood hazards within the county.

FEMA's efforts to produce DFIRM's in Bernalillo County identified a 3.2 mile stretch of spoil bank levee located on the west side of the Rio Grande and north of Isleta Pueblo that lacked certification by the USACE and MRGCD. This stretch of levee became known as the Albuquerque West Levee. For FEMA to continue to show the levee providing flood protection, the MRGCD would be required to provide data and documentation for meeting the certification requirements of 44 CFR 65.10. After researching levee plans and records, it was determined that the 3.2 miles of levee were not part of the USACE engineered levee system. FEMA considered it a spoil bank levee.

The spoil bank levee did not comply with the requirements of 44 CFR 65.10. Therefore, revised mapping could not show the levee providing flood protection from the 100 year storm event. FEMA issued new DFIRM's in September 2008, which did not acknowledge the spoil bank levee as providing any flood protection, and expanded the flood plain to encompass approximately 2,600 acres outside the levee; well outside of historic river channel. By stroke of a bureaucratic pen, approximately 1,500 property owners in the Albuquerque's South Valley suddenly were living in the Rio Grande floodplain. The result was devastating to property owners with mortgages, who were now required to purchase expensive flood insurance during economically difficult times even though the existing levees provided flood protection to those properties for over 80 years.

### **MRGCD RESPONSE**

#### **An Intergovernmental Task Force**

The Middle Rio Grande Levee Task Force (LTF) was created on March 3, 2009 in response to New Mexico State Senate Memorial 18. The Memorial requested the MRGCD, in cooperation with the Mid-Region Council of Governments (MRCOG), to convene a task force to study the status of the levees within the Middle Rio Grande Region. A report was presented by the MRGCD and MRCOG to the New Mexico State Legislature Water and Natural Resources Committee and impacted entities on November 2009.

The LTF continues to invite discussion with the USACE and FEMA pertaining to new levee standards, certifications, vegetation management guidelines on levees and new flood plain mapping efforts. The LTF prepared estimated costs and project status of levee projects based on new USACE levee standards and FEMA's efforts to revise FIRM's. The information presented will hopefully aid lawmakers and interested parties in understanding the significant rehabilitation work required to comply with new levee standards and certifications. Table 1 summarizes the cost and project status for levees affected by the new USACE levee standards. As can be seen from Table 1, the LTF identified Levee Projects in excess of \$470 million required to provide full compliance with new USACE and FEMA guidelines. Hurricane Katrina proved to be very costly for the citizens of the New Mexico.

Table 1. Current Middle Rio Grande Levee Project Summary

Project	Congressional Authorization	Estimated Cost	Local Cost Requirement (%) *	Status
Town of Bernalillo	Yes	\$11,700,000	50% & 35%	** Feasibility phase is underway
MRG Mountain View, Isleta, Belen	Yes	\$170,000,000	25%	Feasibility Study is presently underway. \$1 million dollars has been cost shared by the MRGCD & USACE
Albuquerque Levees includes the Montano Gap	No	\$120,000,000	TBD	**
San Acacia to Bosque del Apache	Yes	170,000,000	12.5%	Construction is scheduled to begin 2013
Total		\$471,700,000		
* Cost sharing requirement includes a minimum cash requirement of 5% of the total project cost; remaining cost share may be cash and or in-kind services				
** Requires 50% cost sharing for feasibility phase; 35% cost sharing for construction phase				

## CONCLUSION

Seven years after Hurricane Katrina devastated the Gulf Coast States, the MRGCD continues to feel the effects of a hurricane which changed the way levees and other flood control structures are looked at by the USACE and FEMA. Existing levees have successfully protected the Middle Rio Grande region for over 80 years since their initial construction. During that time, a large amount of upstream flood storage capacity has been developed in the basin, greatly reducing the magnitude of potential flood flows through the Rio Grande Valley. Regardless of need, new levee guidelines and flood plain mapping efforts have required MRGCD to spend millions of taxpayer dollars for the continued maintenance and rehabilitation of the levee system under its jurisdiction. Future levee projects within the Middle Rio Grande Region will require an estimated \$471,700,000 to provide flood protection, which complies with these new USACE and FEMA standards. Undoubtedly, rehabilitation of the Middle Rio Grande Levee System and other levee systems across the nation will likely require federal funding assistance through the USACE and local governments being required to cost share. Obtaining federal assistance could become competitive leaving some projects on hold until federal funds become available.

**ACKNOWLEDGEMENTS**

Figures were prepared by Doug Strech, Middle Rio Grande Conservancy District Geographic Information Systems Manager.

**REFERENCES**

Federal Emergency Management Agency: [www.fema.gov](http://www.fema.gov)

Middle Rio Grande Conservancy District: Engineering Department Files and Correspondence.

NOAA Home Page – Hurricane Katrina: <http://www.katrina.noaa.gov/>

US Army Corps of Engineers New Orleans District: [www.mvn.usace.army.mil](http://www.mvn.usace.army.mil)

## UNIQUE METHODOLOGY FOR DETERMINING PONDING FLOODPLAINS ALONG IRRIGATION CANAL EMBANKMENTS

Brian Wahlin, Ph.D., P.E., D.WRE<sup>1</sup>

Brent Travis, Ph.D., P.E., D.WRE<sup>2</sup>

Riley Asburry, P.E., CFM<sup>3</sup>

Kathryn Gross, CFM<sup>4</sup>

### ABSTRACT

Many irrigation districts are dealing with urbanization issues due to rapid urban growth. Floodplain management is one of the urbanization issues that irrigation district must deal with. Irrigation canals can alter the discharge into Federal Emergency Management Agency (FEMA) floodplains. In addition, flood waters can pond against canal embankments, creating ponding areas that could be mapped as FEMA regulated floodplains. Unfortunately, modeling these ponding floodplains is often complicated by an existing drainage network consisting of intricately connected ponding areas, retention basins, storm drains, and outlet weirs. To avoid this complication, many ponding areas are depicted simply as buffer zones along the canal embankment. Recently, the Flood Control District of Maricopa County (FCDMC) worked with WEST Consultants, Inc. (WEST) to delineate ponding along the Highline Canal in the Town of Guadalupe, which is located in the Phoenix metropolitan area. The challenge of determining the ponding areas along the canal embankment was met by creating a unique unsteady HEC-RAS model that directly accounted for all flow splits and reversals and predicted the high water ponding surfaces needed for the floodplain delineation. Using HEC-RAS rather than more complicated modeling efforts reduced the cost as well as the time to complete the project. The finalized floodplain was subsequently approved by FEMA. The success of the project indicates that the developed methodology would be very useful for similar future projects.

### INTRODUCTION

For good reasons, many agriculture areas are located in floodplains. First, floodplains are located near rivers, which provide water for irrigation. Second, the river channel naturally meanders through the valley floor and over time deposits sand, silt and other soil-forming material, especially during floods. These deposits provide fertile soil for agricultural production. In turn, the use of floodplain land for agriculture allows the land to continue to provide beneficial functions to society. The Federal Emergency

---

<sup>1</sup> WEST Consultants, Inc., 8950 S. 52<sup>nd</sup> Street, Suite 210, Tempe, AZ 85284, 480-345-2155, [bwahlin@westconsultants.com](mailto:bwahlin@westconsultants.com)

<sup>2</sup> WEST Consultants, Inc., 8950 S. 52<sup>nd</sup> Street, Suite 210, Tempe, AZ 85284, 480-345-2155, [btravis@westconsultants.com](mailto:btravis@westconsultants.com)

<sup>3</sup> WEST Consultants, Inc., 8950 S. 52<sup>nd</sup> Street, Suite 210, Tempe, AZ 85284, 480-345-2155, [rasburry@westconsultants.com](mailto:rasburry@westconsultants.com)

<sup>4</sup> Flood Control District of Maricopa County, 2801 W. Durango Street, Phoenix, AZ 85009, 602-506-4837, [kag@mail.maricopa.gov](mailto:kag@mail.maricopa.gov)

Management Agency (FEMA) describes three types of “natural and beneficial functions” of floodplains that warrant protection (Federal Emergency Management Agency, 2002):

- 1 *Impact on Flooding.* Flood waters can spread over a large area of flat open agricultural land. This reduces flood velocities and provides water storage to reduce flood depths downstream, which in turn reduces flood damage risks to downstream communities.
- 2 *Water Quality.* Water quality is improved in floodplains where vegetative cover prevents soil erosion and acts as a filter for runoff and overbank flows.
- 3 *Groundwater Recharge.* Floodplains can act as recharge areas for groundwater and provide habitat for diverse species of flora and fauna.

Flood insurance in the United States is provided primarily by the federal government via the National Flood Insurance Program (NFIP), in partnership with private insurers and servicing contractors. Prior to the NFIP, private-sector insurance companies had viewed the risk of flood events as uninsurable. Thus, Congress passed the National Flood Insurance Act of 1968 (NFIA) to provide a means by which the risk of flood could be insured in the United States. This act created the NFIP, a mechanism by which the federal government could act as the insurer. From its inception, the NFIP has been guided by its three foundations (Flood Insurance Subcommittee, 2011):

- 1 *Flood Risk Identification.* Mapping the flood risks of each community and publishing the Flood Insurance Rate Maps (FIRMs).
- 2 *Floodplain Management.* Promulgating minimum building and flood plain management standards and encouraging communities to exceed the minimum standards.
- 3 *Flood Insurance.* Providing a mechanism for individuals to prefund the risk of flood losses.

Through the NFIP, FEMA regulates development in areas subject to flooding from a base flood, which is typically taken as the flood that has a 1% chance of occurring in any given year. The area inundated by the base flood is referred as a Special Flood Hazard Area (SFHA). Homeowners are required to purchase flood insurance if they live in a SFHA.

In the 1970s and 1980s, FEMA determined the extents of base floodplains for many communities and published these floodplains on FIRMs. Many of these early floodplain maps developed by FEMA were based on approximate studies. In addition, many communities, such as rural farming communities, did not have floodplain maps developed early on because they were located in areas of low population or low potential for significant financial losses due to flooding. On these early FIRMs, many agricultural levees were mapped as protecting areas (essentially removing them from being in a SFHA).

In 2001, the Map Modernization Program was initiated by FEMA to update FIRMs that had become outdated. Also, as urbanization has occurred into these rural areas, FEMA

has attempted to map areas that were previously not mapped to reflect the changing demographics. As a result, many agricultural areas have had new changes to the FIRMs in their area, which may result in an increase in flood insurance requirements or the introduction of the requirement to buy flood insurance.

In addition, many agricultural levees were constructed without engineering documentation supporting the level protection provided by the levee. FEMA now requires stringent documentation on the engineering for a levee in order for it to offer protection from flooding. The cost of certifying a levee for FEMA is typically more than irrigation districts can afford. Thus, many of these old agricultural levees were assumed to not exist and many farming communities were placed in SFHA.

One potential area of flooding that is often overlooked is flooding that can occur from ponding against a canal embankment. FEMA designates SFHA that are a result from ponding as Zone AH floodplains (detailed studies) or Zone A floodplains (approximate studies). Much like the certification of a levee, determining the extents of flooding due to ponding against canal embankments can be an expensive engineering effort.

The mapping of any area into an SFHA can be controversial since it typically involves requiring residents to purchase flood insurance. This is especially true in agricultural areas, where residents cannot afford to purchase flood insurance or certify their levees. The purpose of this paper is not to explore the controversial aspects of FEMA floodplain mapping. Instead, the purpose of this paper is to discuss a simplified methodology that can be used to map floodplains for ponding areas against canal embankments.

### **FLOODPLAINS AGAINST CANAL EMBANKMENTS**

Traditionally, ponding areas against canal embankments were modeled utilizing a hydrologic program, such as HEC-1 or HEC-HMS. Such hydrologic programs are designed to simulate the precipitation-runoff processes of watershed systems. These programs can be used to describe the hydrology for a wide variety of conditions, including large river basin water supply and flood hydrology as well as small urban or natural watershed runoff. The output of such programs is hydrographs of flows at various locations throughout the watershed. These hydrographs can then be used directly or in conjunction with other software for studies of water availability, urban drainage, flow forecasting, future urbanization impact, reservoir spillway design, flood damage reduction, systems operation, and, in this case, floodplain mapping and regulation.

To set up the hydrologic model, the study area is divided up into smaller areas called basins based on topography and drainage features of the land. Hydrologic parameters, such as infiltration, soil type, and land use, are then defined for each of these basins. Precipitation that falls on the study area is determined by the National Oceanic and Atmospheric Administration (NOAA) Atlas 14 (National Oceanic and Atmospheric Administration, 2006). The return interval and length of storm taken from NOAA Atlas 14 is typically assumed to be either a 100-year, 6-hour storm or a 100-year, 24-hour storm. In many cases, both events are calculated and the worst case floodplain is

mapped. The output from hydrologic models is hydrographs of flows. To map floodplains against canal embankments, these hydrographs are integrated to determine the total volume of water that would pond against the canal.

Once the initial hydrologic modeling is complete, the areas with significant potential of ponding can be identified. Upon identifying the areas of potential ponding, an elevation-storage relationship is developed for each ponding area using the topography and ArcGIS software. For each elevation in the ponding relationship, the storage capacity is determined using the volume calculation capability of ArcGIS software. An example ponding area shown on a topographic map appears in Figure 1. Note that the blue outline does not depict the extent of flooding; it depicts the overall extents of where ponding may occur. An example elevation-storage table appears in Table 1.

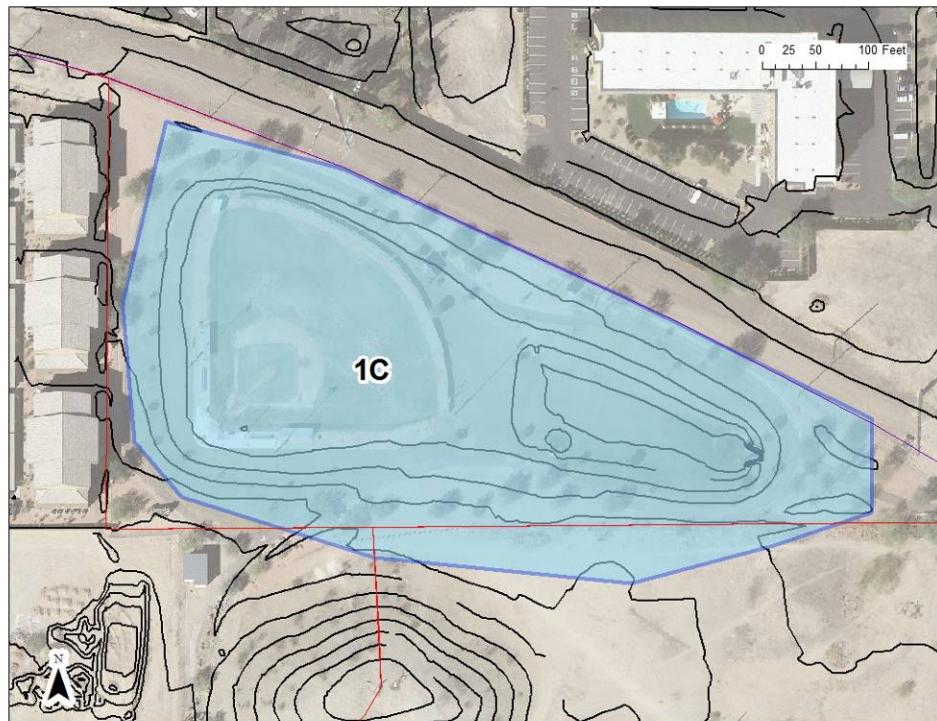


Figure 1. Example Ponding Area

Table 1. Example Elevation-Storage Table

Stage (ft)	1217	1218	1219	1220	1221	1222	1223	1224	1225	1226
Storage (ac-ft)	0.00	0.05	0.30	0.65	1.17	2.66	4.84	7.34	10.43	14.06

Using the total volume that will pond in a given ponding area and the elevation-storage relationships, the depth of ponding in each ponding area is then determined using ArcGIS software. This depth and the topography are then used to determine the horizontal extent of the floodplain in the ponded area. A typical FEMA FIRM panel showing floodplains resulting from ponding against a canal embankment is shown in Figure 2. Note that these

floodplains are designated as Zone A floodplains, which indicates that they were developed using approximate methods and not the methods described here.

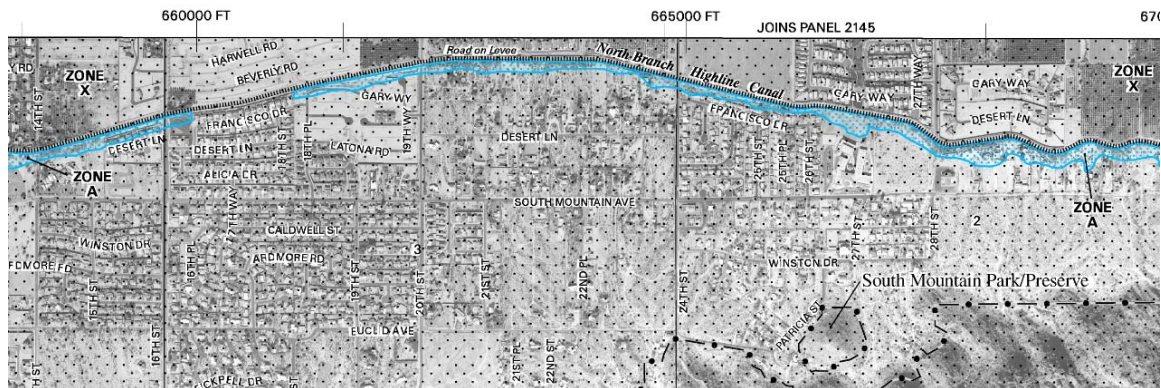


Figure 2. Typical FEMA Map Showing Floodplains Resulting from Ponding against a Canal Embankment

Difficulties arise using this method when the individual ponding areas are not isolated. That is, if there are a series of possible ponding areas along the canal embankment that are separated by high areas, such as a roads or other variations in the topography. In this case, the volume of water that flows into one ponding area may fill and overtop the ponding area and spill, or weir, into an adjacent ponding area. When this happens, the depth of ponding (and the horizontal extent of ponding) is dependent not only on the volume of water coming into the ponding area but also the physical characteristics of the high area separating the two ponding areas as well as the depth of water in the adjacent ponding areas. As a further complication, water may overtop the canal embankment and spill into the canal itself.

Another similar situation occurs if there is a culvert or storm drain that connects one ponding area to another.

In terms of the hydrologic model used, this means that water from one basin in the model exits that basin and enters another one. To accomplish this, the hydrologic model must be modified to allow the diversion of water from one ponding area to another. However, because the depths of water of the individual ponding areas are not known ahead of time, an iterative procedure is needed. The hydrologic model is set up with an assumed split of flow between on ponding area and adjacent ponding area. The ponding extents are then determined using ArcGIS software as described above. If the assumed split between the basins does not agree with the mapped floodplains, then the hydrologic model is adjusted and re-run. This process is repeated until the assumed split and the mapped floodplains produce similar results. This iterative process is time consuming and complex, especially if there are many possible connections between the ponding areas.

If there is a culvert or storm drain that allows water from one ponding area to be transferred to another ponding area, a similar iterative procedure is needed.

### NEW METHODOLOGY

A new methodology was developed to overcome the difficulties involved with the iterative procedure typically used to map floodplains against canal embankments.

As discussed above, water can move several different ways in ponding area against a canal embankment. Most typically, water can:

1. Flow into the ponding area from the upstream drainage area;
2. Flow along the canal embankment itself;
3. Weir flow into an adjacent ponding area;
4. Weir flow into the canal itself; or
5. Flow into a culvert or storm drain.

In researching this issue, it was determined that flow characteristics of these ponding areas are similar to the flow characteristics of a side channel spillway used for dams (US Bureau of Reclamation, 1987). A side channel spillway is a spillway whose control weir is placed alongside and approximately parallel to the upper portion of the spillway discharge channel. Flow over the crest falls into a narrow trough opposite the weir, turns approximately 90 degrees, and then continues into the main discharge channel (US Bureau of Reclamation, 1987).

A schematic diagram of a side channel spillway is shown in Figure 3. Similarities between the side channel spillway and the ponding areas in canals are obvious. Water can flow into the trench from the upstream drainage area. Water can flow along the base of the canal in the trench. Water can weir flow into the canal. Weirs could be added at the upstream and downstream end of the trench to allow for weir flow into an adjacent ponding area. Culverts or storm drains could also be added.

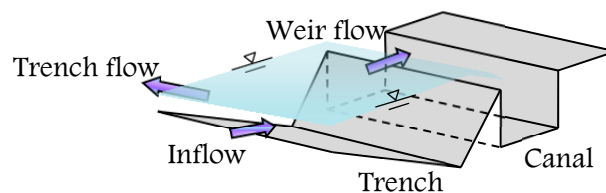


Figure 3. Schematic of a Side Channel Spillway

Using an approach similar to the side channel spillway eliminates the need for numerous iterations in developing floodplains against canal embankments. While this analysis can be done using a simple spreadsheet, this methodology for determining floodplains would not be approved by FEMA. After brainstorming, it was determined that the ponding areas against the canal embankments could be modeled using the hydraulic model HEC-RAS. Typically, HEC-RAS is used to model the hydraulics of riverine systems and not ponding areas. However, there is a feature in HEC-RAS that can be used to model ponding areas called Storage Areas. In unsteady HEC-RAS, Storage Areas are used to model off-channel ponding areas that exchange water with the main channel or other

Storage Areas. This water exchange can occur via weir flow, culvert flow, or hydrologic routing. Thus, the Storage Areas in HEC-RAS have all the necessary components to model ponding areas against canal embankments. Water can flow into the main canal or adjacent ponding areas via weir flow. Water can also exit the Storage Area through culverts. Water enters the Storage Area from a hydrograph, which would be determined from the hydrologic model (e.g., HEC-1 or HEC-HMS).

Thus, the ponding against a canal embankment can be quickly modeled using an unsteady HEC-RAS model that consists entirely of Storage Areas and connections between these Storage Areas. HEC-RAS automatically calculates the amount of water entering and leaving the Storage Areas, eliminating the need for the iterative process described above. Note that the hydrologic model (e.g., HEC-1 or HEC-HMS) is still needed to determine the amount of volume that enters the Storage Area from a storm event. Even though this methodology requires the creation of a separate hydraulics model, there is still a significant savings in effort to map the floodplains. In the case study described below, the HEC-RAS model and preliminary floodplains were created in about one day. It was estimated that it would have taken about two weeks to accomplish the same result using the traditional iterative approach.

## CASE STUDY

This methodology was utilized for a Floodplain Delineation Study (FDS) for the Town of Guadalupe, Arizona. The study was commissioned by the Flood Control District of Maricopa County (FCDMC), the agency that is responsible for regulating floodplains in the Town of Guadalupe.

### **Background on the Town of Guadalupe**

The Town of Guadalupe is located in the Phoenix metropolitan area (see Figure 4). It was founded in 1900 by Yaqui Indians and continues to be the center of Yaqui culture to this day. This small town of just over 5,000 people occupies only 0.8 square miles. It is bordered by the City of Tempe on the north, east, and south as well as the City of Phoenix on the west. The Highline Lateral, which is operated by the Salt River Project (SRP) runs along the eastern edge of the Town of Guadalupe and forms the border between Guadalupe and Tempe. The general slope of the land is to the northeast in the northern half of the Town and to the east and southeast in the southern end of the Town. No off-site flows enter the Town of Guadalupe in the 100-year event. Thus, rain that falls onto the Town of Guadalupe generally flows towards the east and ponds against the Highline Lateral.

In the past, FEMA mapped the ponding area against the Highline Lateral simply as a 150-foot buffer from the canal banks (see Figure 5). These were mapped as Zone A, which indicates the floodplains were determined using approximate methods. The FCDMC and WEST updated this approximate floodplain limit with detailed floodplains that more accurately depict the ponding along the embankment of the Highline Lateral. The updated floodplains are now mapped as Zone AH floodplains, which mean they were

developed using detailed study methods. The study area is outlined in red as shown in Figure 4 and does not quite cover the entire Town of Guadalupe.

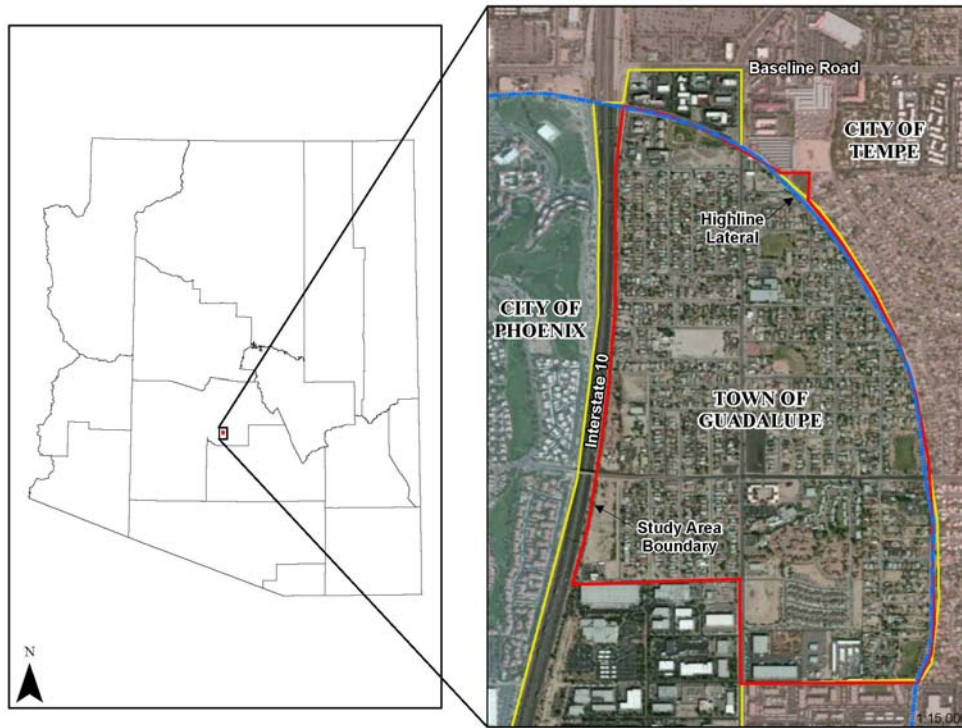


Figure 4. Location Map for Case Study



Figure 5. Effective Floodplains along the Highline Lateral

### **Hydrologic Model**

Approximate basin boundaries and flow paths for the hydrology model were delineated within ArcGIS using the topographic data, survey data, and aerial photographs. HEC-1 was used to develop a hydrologic model for the area. Both the 100-year, 6-hour and the 100-year, 24-hour storms were analyzed based on the NOAA Atlas 14 rainfall data (National Oceanic and Atmospheric Administration, 2006). Locations of potential ponding along the canal were located, concentration points were placed in those locations and the HEC-1 model was programmed to output hydrographs at each of these locations.

The study area was divided up into small subbasins. The initial basins generated in ArcGIS clearly showed the flow directions and approximate high and low areas throughout the study area. The final subbasin boundaries were decided based on the available topography, survey data, and through site visits by WEST and FCDMC personnel. The boundaries of the natural subbasins are influenced by the presence of the roadways and the canal. The subbasin boundaries are shown in Figure 6.

The areas with significant potential of ponding were identified after initial runs of the HEC-1 models (see Figure 7). Upon identifying the areas of potential ponding, an elevation-storage relationship was developed for each area using topographic data in ArcGIS (see Figure 1). For each elevation in the ponding relationship, the storage capacity was determined using the volume calculation capability of ArcGIS (see Table 1).

Ponding relationships were developed between each ponding area in HEC-RAS. HEC-RAS was used because of its ability to correctly balance flows over weirs and through pipes simultaneously. Hydrographs were extracted from HEC-1 at each ponding area and were referenced as flow files in HEC-RAS. The storage area connections consist of weirs, pipes, or a combination of both. Most ponding areas have three weirs, one on the north side, one on the south side, and one on the east side. The north and south weirs represent spilling from one pond to another, and the weir on the east side represents spill from the ponding area into the canal. The 10-year storm drain system was represented using the culvert routines in the storage area connections. Additional storage area connections were created with a culvert and an artificially high weir to represent drainage storm drain pipe connections between certain ponds.

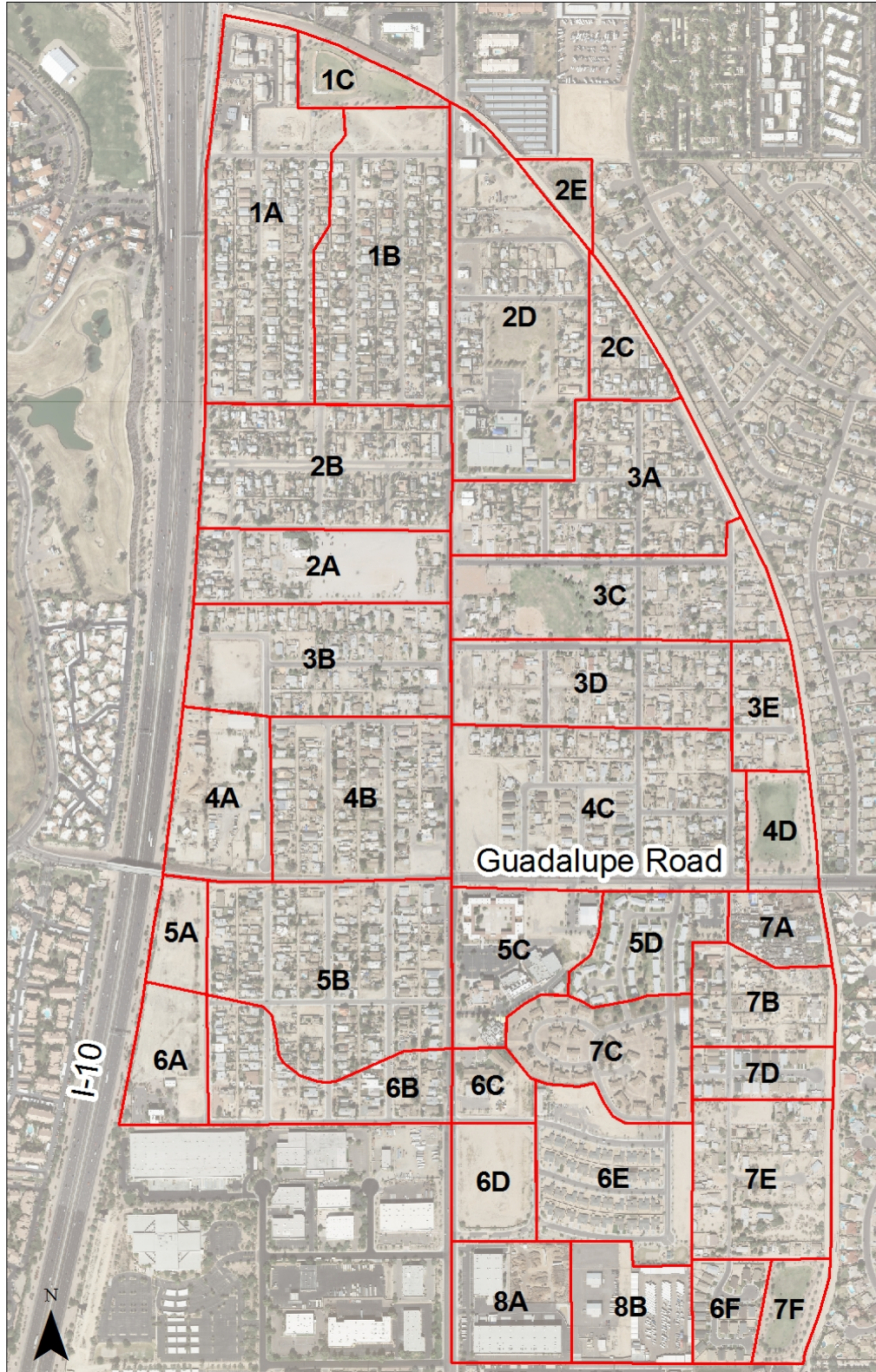


Figure 6. Subbasins Used in the HEC-1 Model for the Town of Guadalupe

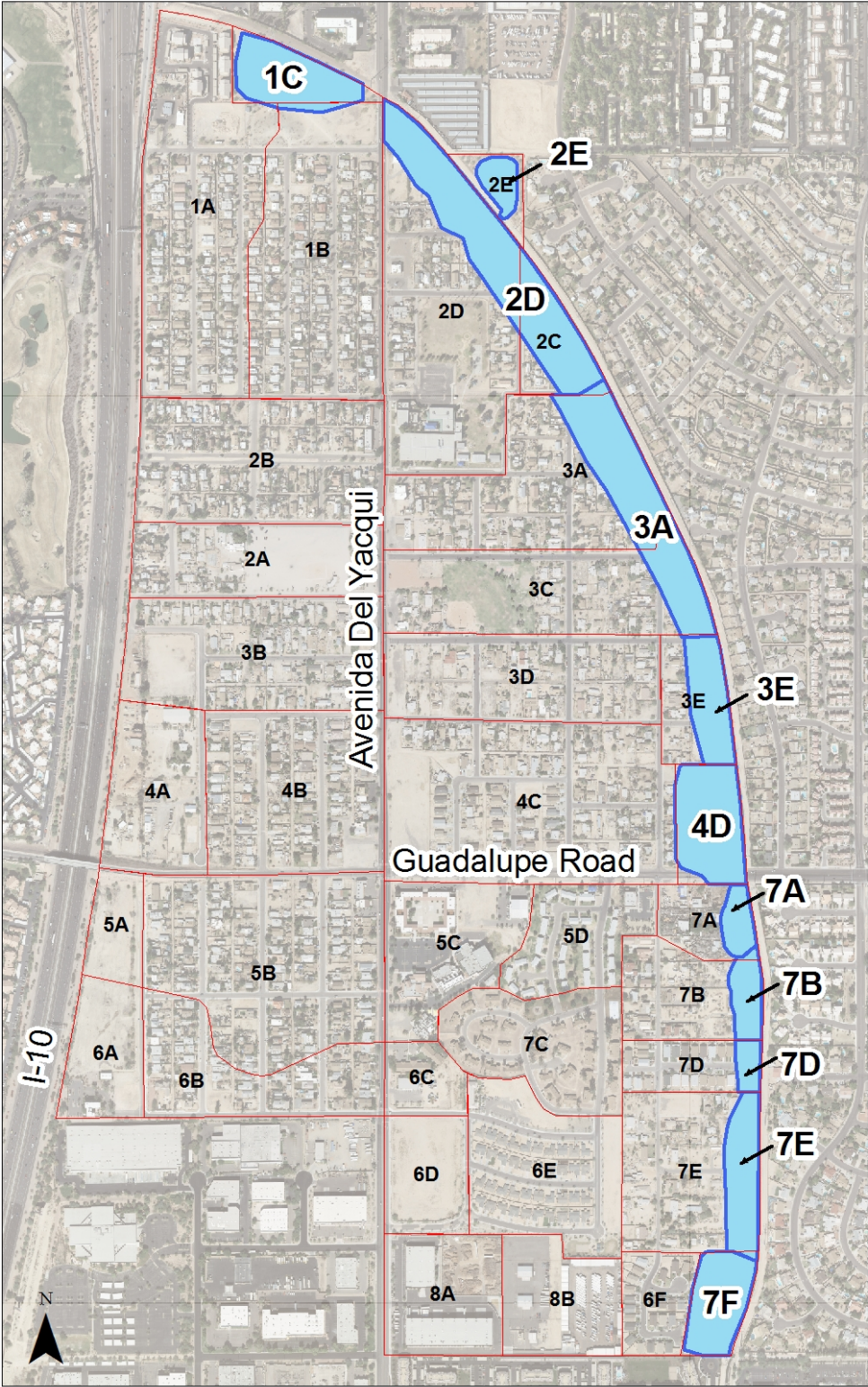


Figure 7. Areas of Potential Ponding along the Highline Lateral

The Highline Lateral is lined with elevated berms running parallel to the canal with the top of the berm located few feet above the existing surrounding ground. The existing topography in the study area is such that the storm water runoff from flood events would flow towards the canal and there is a potential for flooding on the upstream side of the canals as shown in Figure 8. As a result, floodplain delineations are based on ponding areas rather than flow conveyance. The existing conditions indicate that the runoff from the watershed tends to collect in low-lying areas adjacent to the canal and has the potential to overtop the berms and enter the canal. Since some of the low lying areas with ponding potential are not well defined, the probability also exists that the ponding areas may join together or spill laterally into each other. For this purpose the water surface elevations for each ponding area was computed in HEC-RAS using storage areas with weir connections between each ponding area and between the ponding areas and the canal.

An unsteady HEC-RAS model was created to represent the ponding areas. Each ponding area was represented with a Storage Area in HEC-RAS. The hydrographs from HEC-1 were read into HEC-RAS at each Storage Area corresponding to the same concentration point in HEC-1. The resulting water-surface elevations at each ponding location were then mapped in ArcGIS based on the location of the concentration points and the surface elevation of the topography. This procedure was repeated for both the 24-hour storm and the 6-hour storm to identify the worst case scenario for mapping the Zone AH floodplains.

As a result, the floodplain delineations were based on the water-surface elevations computed using the HEC-RAS hydraulic model and mapped using the topography. The weir dimensions and characteristics were determined using ArcGIS and the topography.

The updated floodplains for the Town of Guadalupe are shown in Figure 9. These new floodplains are more realistic of the potential for flooding than the previous 150-foot buffer floodplains. The updated floodplain maps were documented and submitted to FEMA for approval. FEMA recently accepted the proposed floodplain revisions.



Figure 8. Rainwater Ponding against the Highline Lateral



Figure 9. Updated Floodplains

## CONCLUSION

Flood waters can pond against canal embankments, creating ponding areas that could be mapped as FEMA regulated floodplains. Unfortunately, modeling these ponding floodplains is often complicated by an existing drainage network consisting of intricately connected ponding areas, retention basins, storm drains, and outlet weirs. Historically, procedures utilized to map the floodplains against canal embankments involved a tedious iterative process.

A unique methodology was developed to map the floodplains against canal embankments. This methodology eliminates the lengthy iterative procedure typically needed for these types of studies. The methodology involves the creation of a hydrologic model to determine the flood flows into the ponding areas. In addition, a unique hydraulic model consisting of only Storage Areas was created. This Storage-Area-only model can easily model the complex hydraulics of the ponding areas. This methodology was successfully utilized to develop the floodplains ponding against the Highline Lateral in the Town of Guadalupe.

## REFERENCES

Federal Emergency Management Agency. (2002). *National Flood Insurance Program Community Rating System, CRS Coordinator's Manual*.

Flood Insurance Subcommittee. (2011). *The National Flood Insurance Program: Past, Present. . . and Future?* Washington D.C.: American Academy of Actuaries.

National Oceanic and Atmospheric Administration. (2006). *NOAA Atlas 14: Precipitation-Frequency Atlas of the United States*. NOAA.

US Bureau of Reclamation. (1987). *Design of Small Dams*. Washington DC: US Department of the Interior.

# POTENTIAL SAVINGS OF WATER AND NUTRIENTS FOR THE BEAR RIVER CANAL COMPANY

Jonna D. van Opstal<sup>1</sup>  
Christopher M.U. Neale<sup>2</sup>

## ABSTRACT

Water savings in irrigated agriculture can be significant under certain conditions as irrigated agriculture is the largest consumer of water in the Western US. In a state such as Utah, where the water supply is limited, it is essential to find methods of saving water while maintaining high productivity. Crop productivity in irrigated agricultural areas is influenced by both effective irrigation and fertilizer application. Proper management of these factors can result in water conservation and the reduction of nutrient pollution from agricultural runoff. For this study, an irrigation district in Northern Utah was selected as a case study. Remote sensing with satellite and airborne imagery was used in an energy balance algorithm to provide crop evapotranspiration (ET) and water use estimates for the study area. These results will indicate the potential water savings for the irrigation district if changes in canal operations and water deliveries are made. Additionally, water quality measurements for conductivity, nitrate, ammonium and orthophosphate concentrations were performed on both irrigation and drainage water for a selected lateral in the irrigation district. The different components of the solute balance were estimated for an irrigation season and provided insight on potential fertilizer leaching. The study of the water and solute balance of this system, could lead to improvements in farming practices with the goal of achieving a higher productivity and simultaneously conserve water and nutrients.

## INTRODUCTION

The Western US is characterized as being predominantly semi-arid to arid. Summers are generally warm and dry and most of the annual precipitation is in the form of winter snowfall. Utah is amongst the driest states of the nation. Due to a rapidly growing population, the state is urged to evaluate water usage and potential savings among competing interests. The largest user of water in Utah is the agricultural sector. During the growing season, farmers are dependent on irrigation from streams and reservoirs to achieve sufficient crop production. However, recent years have shown that surface water sources are becoming less reliable and are decreasing in quantity, which is echoed by climate models (Barnett, Adam, and Lettenmaier 2005). Additionally, the source of irrigation water, namely the rivers and reservoirs show a trend of water quality deterioration. This will potentially create two major issues for agricultural water use: firstly, irrigation water will contain high nutrient concentrations and cause weed growth in irrigation canals; and secondly, crop fertilization needs to be managed to prevent high

---

<sup>1</sup> PhD student, Irrigation Engineering Div., Civil and Environmental Engineering Dept., Utah State University, Logan, Utah; j.van\_opstal@aggiemail.usu.edu

<sup>2</sup> Professor, Irrigation Engineering Div., Civil and Environmental Engineering Dept., Utah State University, Logan, Utah; christopher.neale@usu.edu

nutrient concentrations in agricultural runoff. In Utah several streams are classified as impaired due to deteriorating water quality, and require measures to be taken to reduce non-point loadings of nutrients (Sehlke and Jacobson 2005).

The Bear River Canal Company (BRCC) is an agricultural irrigation area located in Northern Utah with the main town being Tremonton ( $41^{\circ}42'N$ ,  $112^{\circ}10'W$ ). This area already presents several of the typical issues occurring in other agricultural regions of Western US: water resources are limited and unpredictable, and water quality of surface waters is deteriorating. A Total Maximum Daily Load (TMDL) exists for the Bear River to reduce the high phosphorus (P) concentrations (Allred and Judd 2002). Additionally, the Bear River Basin is becoming more populated resulting in a higher water demand for municipal use. These issues altogether require decisions to be made considering water allocations and water quality management (Sehlke and Jacobson 2005).

Spatial analysis tools aid water managers in evaluating the water issues and locating the key problem areas. Geographical Information Systems (GIS) mapping tools are useful for data integrations (Romanelli et al. 2012). Remote sensing is a powerful research tool, providing insight on the spatial variability of, for example, crop cover and evapotranspiration (ET). This information is provided to decision-makers such as water managers, users and policy makers (Bastiaanssen, Molden, and Makin 2000). Remote sensing is used in several cases for estimating the water consumption of irrigated areas including agricultural and riparian vegetation. It has been shown to be very precise in the estimation of ET and is a reliable input for the water balance of an agricultural area (Taghvaeian and Neale 2011).

These GIS mapping tools are used in this study to evaluate water and nutrient management of the BRCC. The water demand and irrigation efficiency throughout the command area will be determined using the images and maps generated from remote sensing. Additionally, measurements of water quality parameters from samples of irrigation and drainage water from a selected lateral in the BRCC are compared with the water demand for that lateral providing insight on both the spatial and temporal variation in quality throughout the irrigation season.

## METHODOLOGY

### Description of Study Area

The BRCC is located in Northern Utah and the main stream in this area is the Bear River. The Bear River has a length of nearly 800 km and the watershed is about 19,500 km<sup>2</sup>. The agricultural sector is the largest consumer of the river water at 94% (Toth et al. 2010). The BRCC is part of the Lower Bear River watershed and its drainage water ends up in the Migratory Bird Refuge and eventually in the Great Salt Lake. Irrigation water for the BRCC is diverted at and measured downstream of Cutler Dam.

The BRCC consists of main canals and laterals (Figure 1.). The command area is 26,500 ha. The main crops are alfalfa, wheat, maize and hay, which are grown and harvested in

the summer months (May to September). The majority of the irrigators practice basin or border surface irrigation. The soils are mainly silty loam and silty clay loam soils, with seven main soil classifications covering the irrigated area. The average annual precipitation is 413 mm of which, on average, 69 mm falls in the summer months; the annual reference  $ET_0$  is 1368 mm. (Lecina et al. 2011).

Irrigation is performed through a fixed schedule rotating the flow through several head gates within the laterals. This schedule is developed and can be modified by the BRCC manager. A recent study (Lecina et al. 2009) used a simulation model to evaluate the rotation schedule and irrigation time. It was estimated that water savings of up to 27% can be obtained if the irrigation schedule is modified by cutting off the irrigation application sooner.

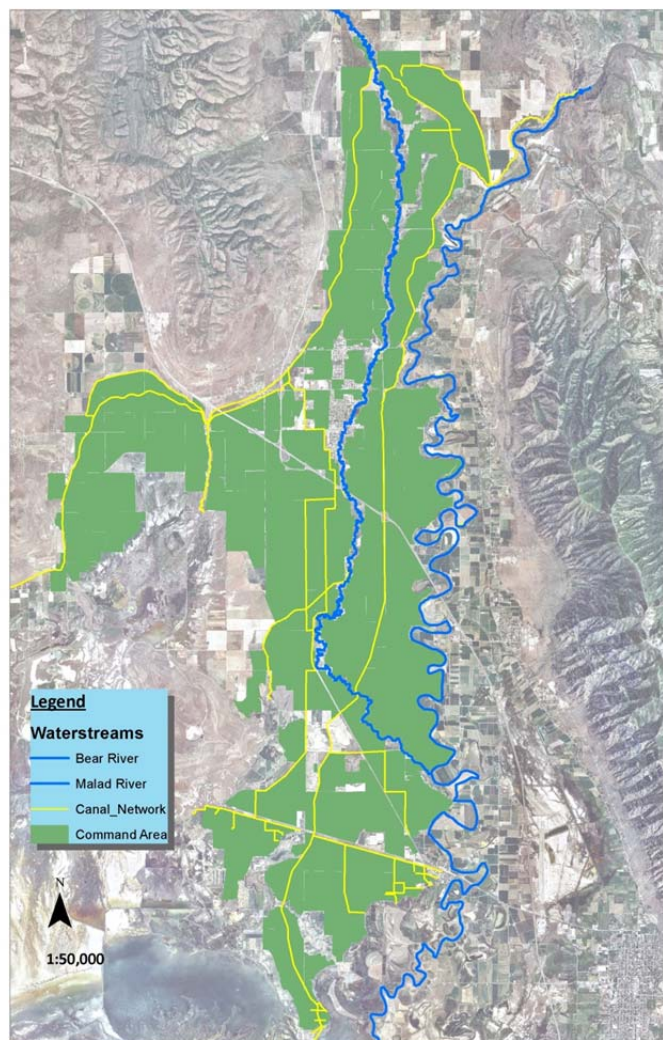


Figure 1. BRCC command area and canal system

### Remote Sensing Images

The remote sensing images were taken from the MODIS satellite imagery with pixel size 250 m or 500 m depending on the bandwidth. Images were taken from the USGS/NASA data pool site<sup>3</sup>, which provides images with atmospheric corrections. The images were obtained for the 2012 irrigation season. Images were selected for cloudless conditions and smokeless skies, which was challenging due to the smoke caused by wildfires in the region. Additionally, images with a small viewing angle were selected. The dates chosen for this study are presented in Table 1.

Table 1. MODIS image dates, solar and sensor zenith angle in degrees

Date	Day of Year	Solar zenith	Sensor zenith
13-May-12	134	26.34	4.945
21-Jun-12	173	22.04	6.17
7-Jul-12	189	23.22	6.25
24-Aug-12	237	33.55	6.5
9-Sep-12	253	38.67	6.55

### SEBAL

The model used for estimating ET is the Surface Energy Balance Algorithm for Land (SEBAL). This model was developed and published in Bastiaanssen et al. (1998). It has been successfully used in several large-scale irrigation areas under different climate regimes (Bastiaanssen et al. 1998).

SEBAL is based on the energy balance equation

$$R_n = G + H + LE \quad (1)$$

$R_n$  = Net radiation

$G$  = Soil heat flux

$H$  = Sensible heat flux

$LE$  = Latent heat flux

All components of the energy balance are expressed in units  $W/m^2$ . The different equations used in this process are described in the manual for SEBAL (Waters et al. 2002). Typical for SEBAL is the calculation of the sensible heat flux using a 'hot' and a 'cold' pixel. It requires skill and the guidelines from the manual (Waters et al. 2002) to do this correctly. The entire SEBAL process was performed in Earth Resources Data Analysis System (ERDAS) Imagine version 2011 using the model-maker tools. The weather data were taken from a weather station at Tremonton, which is in the center of the command area and gives a good representation for the rest of the area.

<sup>3</sup> [https://lpdaac.usgs.gov/products/modis\\_products\\_table](https://lpdaac.usgs.gov/products/modis_products_table)

**Water Quality Samples**

For the evaluation of water quality in the irrigation and drainage water, a lateral from the BRCC was selected namely Iowa String. It is located in the center of the BRCC command area and consists of a lateral canal of 6.8 km length; with an area of 12.5 km<sup>2</sup>, as shown in figure 2.

The water sampling locations were chosen along the canal at different head gates, in the drainage canal at the end of a head gate and at Sulphur Creek, which is the main drainage canal for several agricultural areas. The samples were taken on three dates throughout the irrigation season: 11<sup>th</sup> July, 6<sup>th</sup> August and 27<sup>th</sup> August 2012. The parameters evaluated from these samples were pH, EC [dS/m], Ortho-phosphate, Nitrate-N and Ammonium-N. The analysis of results were studied in the software R version 2.15.1

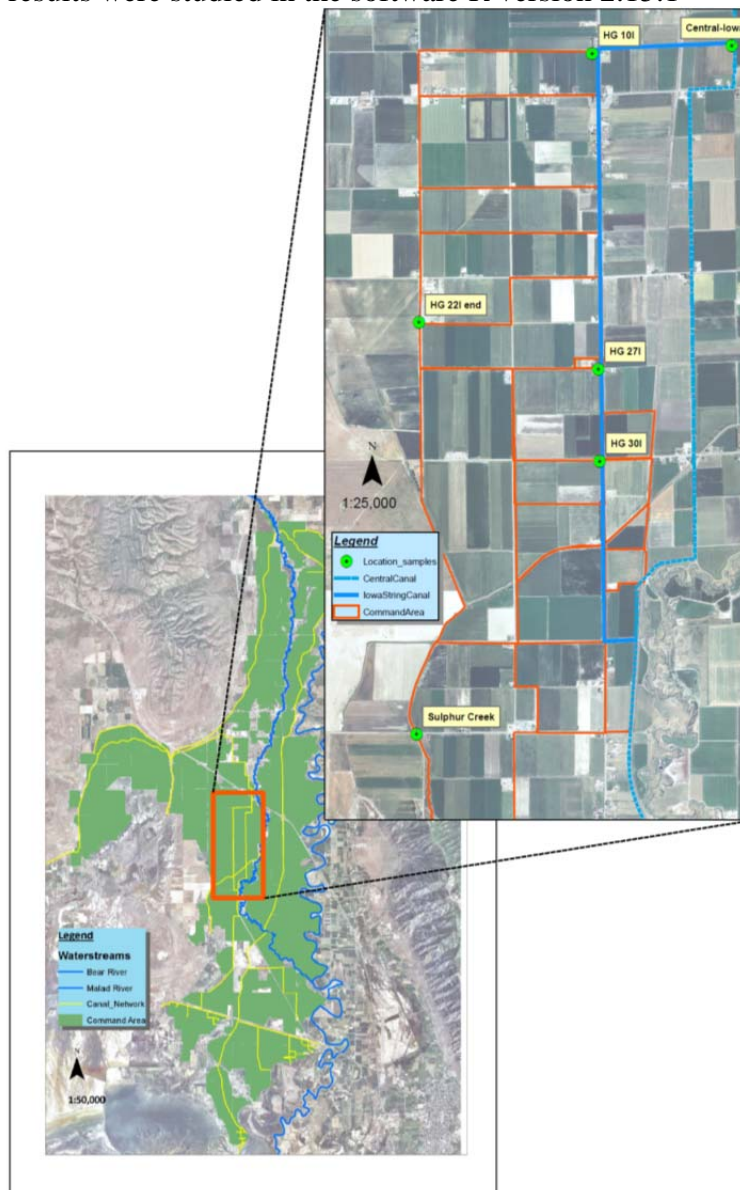


Figure 2. Location of water sampling on the Iowa String lateral

## RESULTS AND DISCUSSION

### Evapotranspiration Estimation

The ET estimates for the five satellite images are shown in figure 3. June and July are the peak irrigation months, where ET values are higher throughout the command area. Crop cover and warm temperatures cause water demand and thus ET values to be high during these months. At the end of August most crops are harvested except alfalfa, which usually produces another harvest in September.

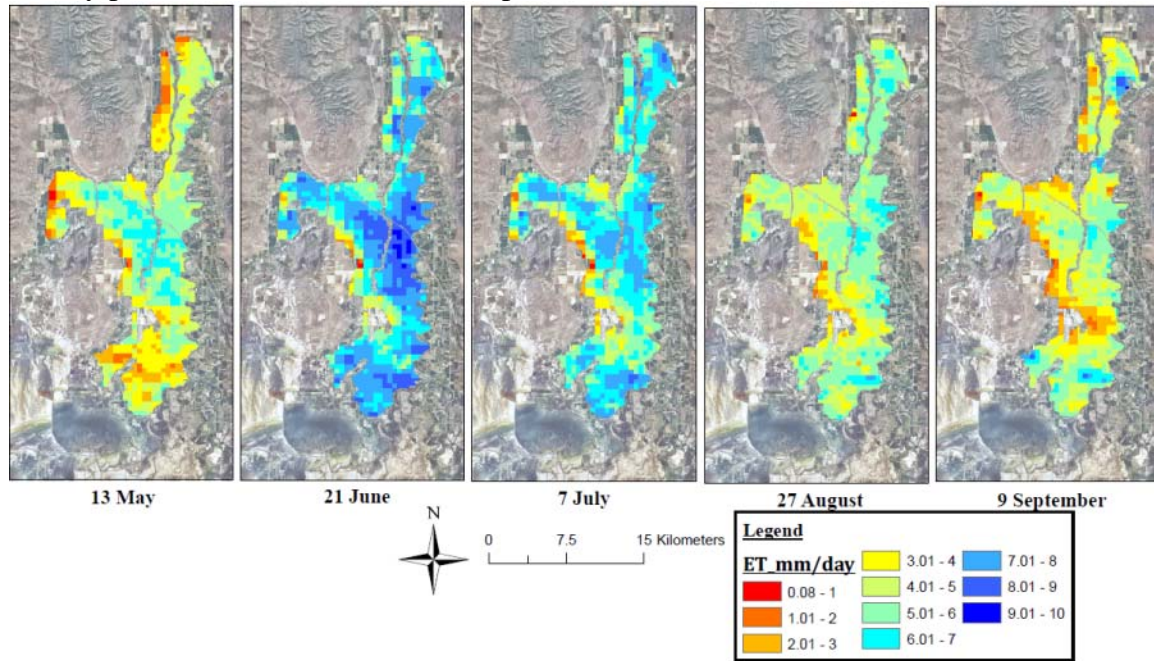


Figure 3. Results from SEBAL ET calculation for the BRCC command area using MODIS imagery

The results for each satellite overpass date can be extrapolated to an estimated ET value for each day in between using the crop coefficient. For the Iowa String command area (location indicated in figure 2), the average crop coefficient was calculated and is shown in figure 4. A polynomial fit was used to extrapolate the values to a predicted average crop coefficient throughout the irrigation season. The crop coefficient and the potential ET as measured at the Tremonton weather station, gives a prediction of daily ET values as shown in figure 5. These results show higher ET values during the peak of the irrigation season in June and July.

The total ET for the BRCC command area was also calculated in a similar fashion and is shown in figure 6. This is compared with the irrigation diversions to the main canal of the BRCC. For the 2012 irrigation season the total volume of irrigation water diverted was 1135 mm; the total ET for the growing season was estimated to be 784 mm. This results in an irrigation efficiency for the entire BRCC irrigation system of 69%, calculated as the volume of water consumed as crop ET divided by volume of water supplied to command area.

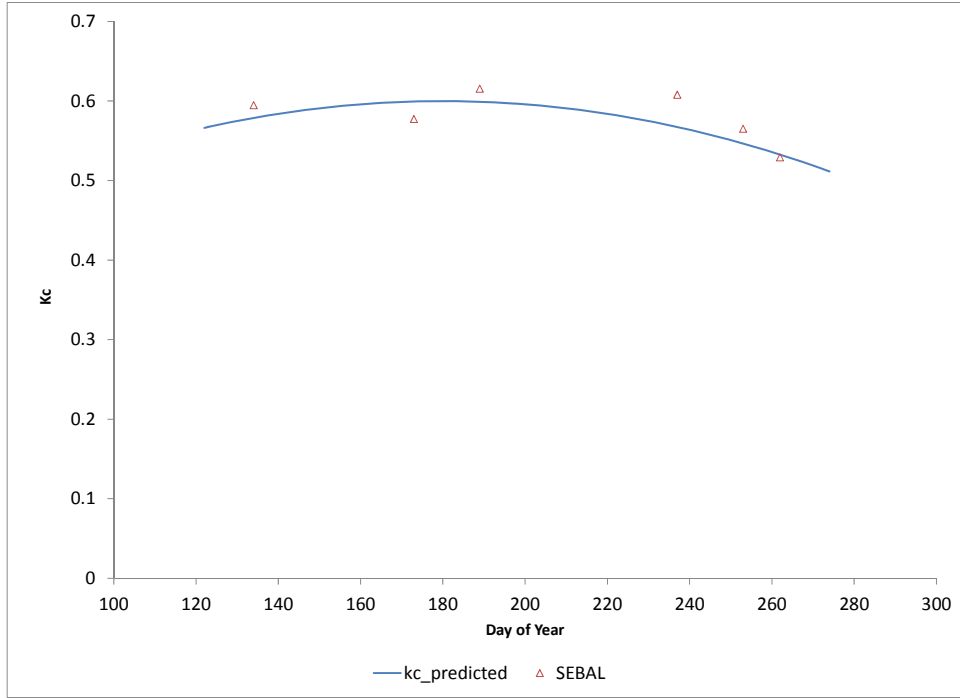


Figure 4. Crop coefficient predicted for the Iowa String command area

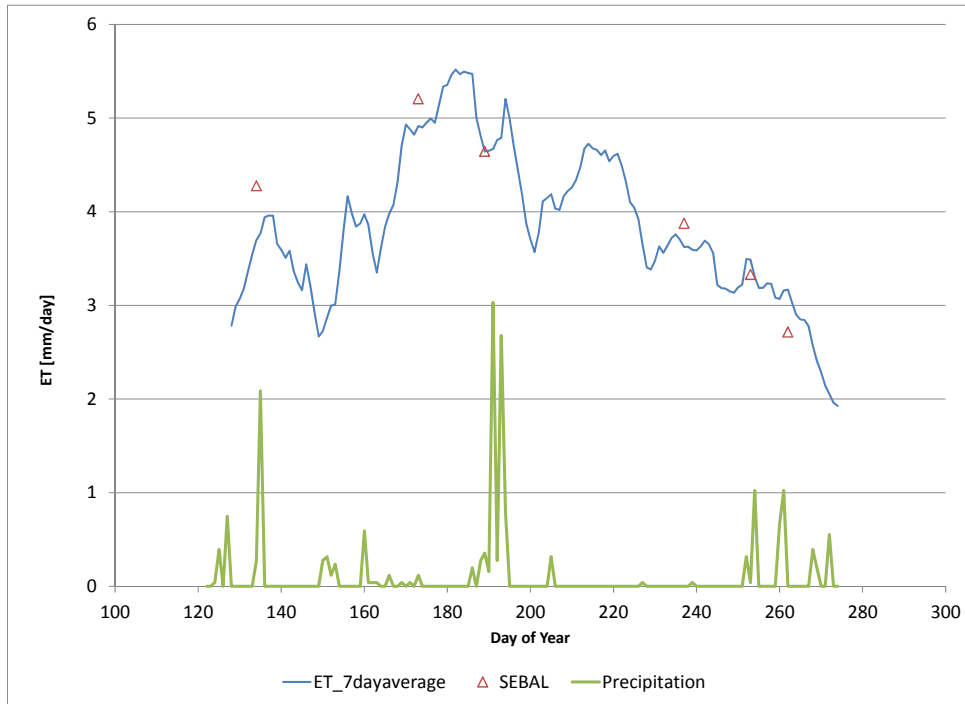


Figure 5. Moving 7-day average of estimated ET for Iowa String command area

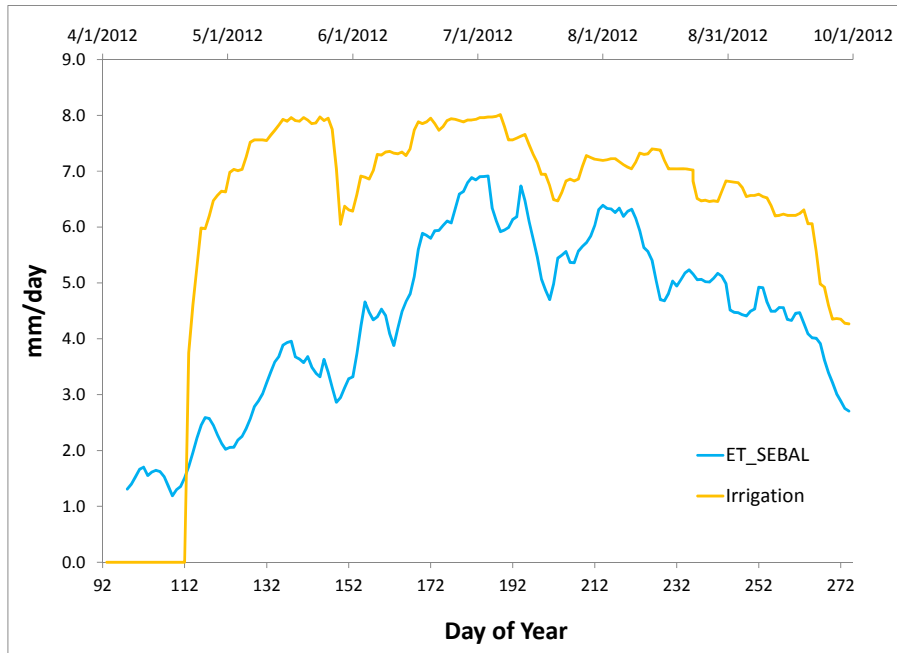


Figure 6. ET and irrigation diversions for the BRCC command area

### Water Quality

Results for the water quality sampling analysis of irrigation and drainage water are shown in figure 7. The first sample date was during the peak of the irrigation season as indicated in figure 5, when ET was highest. However, no significant statistical differences were found between the three sampling dates. This was due to the low degrees of freedom with a limited number of samples and is a recurring issue in several water quality studies.

From figure 7 it is observed that differences in quality parameters between the drainage and irrigation water were measured. In particular, the electrical conductivity (EC) of Sulphur Creek, which contains drainage water, is higher as compared to the EC of the irrigation water. The phosphorus (P) concentrations are variable in the irrigation water for the first sampling date, at the peak of the irrigation season. At the end of the growing season the irrigation water had a low and similar P concentration at the different points along the Iowa String lateral. Note that the P concentration in the irrigation water is above the desired limit of 0.075 mg/L as determined by the TMDL for in-stream P concentration (Allred and Judd 2002). Therefore it is not surprising that the drainage water will considerably exceed the targeted in-stream P concentration. For nitrogen (N) the difference between irrigation and drainage water vary for ammonium ( $\text{NH}_4^+$ ) and nitrate ( $\text{NO}_3^-$ ). During the peak of the irrigation season the  $\text{NO}_3^-$  concentration is higher in drainage water than in irrigation water. This trend shifts to the  $\text{NH}_4^+$  concentration, which is higher at the end of the season for drainage water.

Overall, the results for P and  $\text{NO}_3^-$  indicate that agricultural runoff during the peak of the irrigation season contains a higher concentration of these constituents. As was previously found, the irrigation efficiency is 69%, which indicates that there are losses to runoff,

amongst others. Fertilizer management can be adapted to ensure a good balance between irrigation timing and fertilizer application.

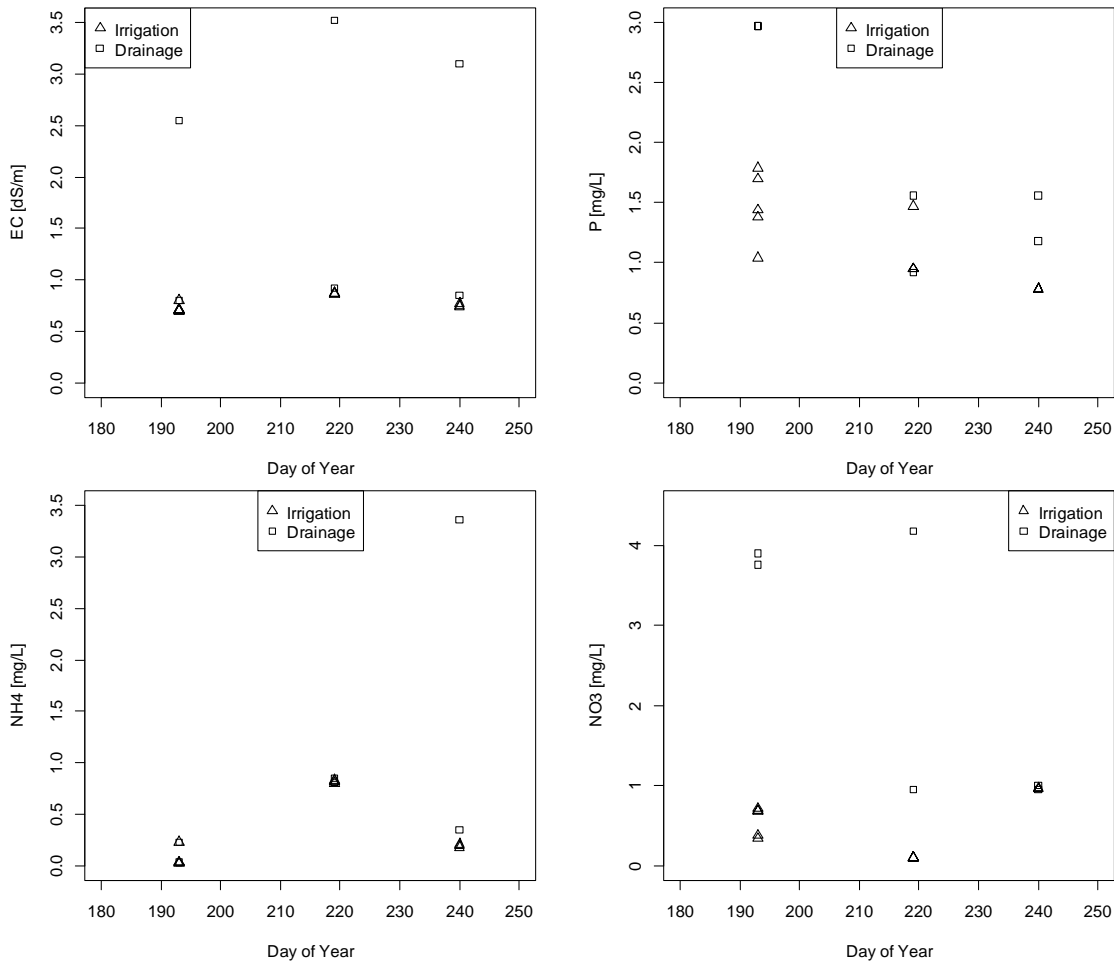


Figure 7. Results for samples of irrigation and drainage water for EC, P, NH4 and NO3

### CONCLUSION

In this study the use of spatial analysis tools such as GIS and remote sensing have proven to be useful in creating insights of an irrigation area. It provides several representations of an agricultural area indicating the spatial variance of ET and thus water demand throughout the area. Also, temporal variation of ET was presented using images at different dates throughout the irrigation season.

ET was estimated by the model SEBAL to evaluate irrigation water demand for the BRCC. The calculated irrigation efficiency for the entire irrigation system was 69%, calculated with consumed crop ET divided by volume of water supplied. This performance indicates that water is lost to runoff and other components.

The water quality of the agricultural drainage was evaluated. It was found that the P and NO<sub>3</sub><sup>-</sup> concentrations are higher in the drainage water during peak irrigation season. The P concentration in the irrigation water varies largely along the lateral and is higher than the targeted in-stream P concentration 0.075 mg/L. The conductivity of the irrigation and drainage water was similar, except Sulphur Creek, which has a higher conductivity. Nutrient savings can be achieved with an adapted fertilizer management.

### ACKNOWLEDGEMENTS

This project is financed and supported by the Utah Water Research Laboratory in Logan, Utah and the Utah State Agricultural Experiment Station. Additionally the authors acknowledge the assistance of Dr. Saleh Taghvaeian and Prof. Bethany Neilson.

### REFERENCES

- Allred, Michael, and Harry Lewis Judd. 2002. *Lower Bear River Watershed Restoration Action Strategy*.
- Barnett, T P, J C Adam, and D P Lettenmaier. 2005. "Potential impacts of a warming climate on water availability in snow-dominated regions." *Nature* 438(7066): 303–9.
- Bastiaanssen, W G M, M. Menenti, R.a. Feddes, and A.a.M. Holtslag. 1998. "A remote sensing surface energy balance algorithm for land (SEBAL). 1. Formulation." *Journal of Hydrology* 212-213: 198–212.
- Bastiaanssen, W G M, D J Molden, and I W Makin. 2000. "Remote sensing for irrigated agriculture: examples from research and possible applications." *Agricultural Water Management* 46(2): 137–155.
- Bastiaanssen, W.G.M., H. Pelgrum, J. Wang, Y. Ma, J.F. Moreno, G.J. Roerink, and T. van der Wal. 1998. "A remote sensing surface energy balance algorithm for land (SEBAL) 2.Validation." *Journal of Hydrology* 212-213: 213–229.
- Lecina, S, C.M.U. Neale, G.P. Merkley, and C.a.C. Dos Santos. 2009. "Increasing field work productivity in irrigation evaluation processes through use of combined irrigation models." *World Environmental and Water Resources Congress*: 4250–4262.
- Lecina, S., C.M.U. Neale, G.P. Merkley, and C.a.C. Dos Santos. 2011. "Irrigation evaluation based on performance analysis and water accounting at the Bear River Irrigation Project (U.S.A.)." *Agricultural Water Management* 98(9): 1349–1363.
- Romanelli, Asunción, María Lourdes Lima, Orlando Mauricio Quiroz Londoño, Daniel Emilio Martínez, and Héctor Enrique Massone. 2012. "A GIS-based assessment of groundwater suitability for irrigation purposes in flat areas of the wet Pampa plain, Argentina." *Environmental management* 50(3): 490–503.

Sehlke, Gerald, and Jake Jacobson. 2005. "System dynamics modeling of transboundary systems: the bear river basin model." *Ground water* 43(5): 722–30.

Taghvaeian, Saleh, and Christopher M.U. Neale. 2011. "Water balance of irrigated areas: a remote sensing approach." *Hydrological Processes* 25(26): 4132–4141.

Toth, Richard E., T.C. Edwards, A.L. Perschon, and D.C. White. 2010. *Bear River Watershed: It's role in maintaining the Bear River Migratory Bird Refuge*.

Waters, Ralph, Richard G. Allen, M. Tasumi, Ricardo Trezza, and Wim G.M Bastiaanssen. 2002. 1–98 *SEBAL - Idaho implementation*.



# **USING 21<sup>ST</sup> CENTURY TECHNOLOGY TO GROW ONE OF THE EARTH'S MOST RENEWABLE RESOURCES — TREES, ON 10,440 HECTARES OF DRIP IRRIGATED TREE FARM.**

Nabil Mohamed<sup>1</sup>

## **ABSTRACT**

On one of the world largest contiguous drip irrigated farms, 21<sup>st</sup> Century technology assists to efficiently and economically produce fiber from one of the earth's most renewable resource – trees. At this Greenwood Resources Boardman Tree Farm in Eastern Oregon, US, these trees are grown in a sustainable and eco-friendly manner.

Boardman Tree Farm (BTF) has one of the most advanced large-scale I-SCADA (Irrigation Supervisory and Data Acquisition) systems in the US. It also has an innovative Advance Scientific Irrigation Management (ASIM) system which utilizes evapotranspiration and total growing degree days modeling. BTF's unique Advanced Hydraulic Balanced Irrigation Scheduling (AHBIS) program enables the I-SCADA system to be a truly “stand-alone” system. The I-SCADA system can be remotely controlled by mobile devices, has “auto-control” functionality for hydraulic emergencies and more than 1,400 sensors and 1,800 controls.

Other areas being developed are on-farm energy generation, mitigating high power demand spikes for local power utility, large scale irrigation system real-time hydraulic modeling, recharging of ground water and reservoir storage for a local irrigation district and electric utility.

Other 21<sup>st</sup> Century technologies in use are terrestrial Laser Imaging Detection and Ranging (LIDAR) for tree yield inventory, satellite imagery with tree growth differential mapping, breeding drought resistant trees to lower irrigation power costs and the use of cloud computing.

Boardman Tree Farm goal is to develop an economically sustainable agricultural system that produces fiber for bio-chemicals, bio-fuels, bio-energy, paper, veneer and solid wood products. Using 21<sup>st</sup> Century technology BTF hopes to remain productive in the long run.

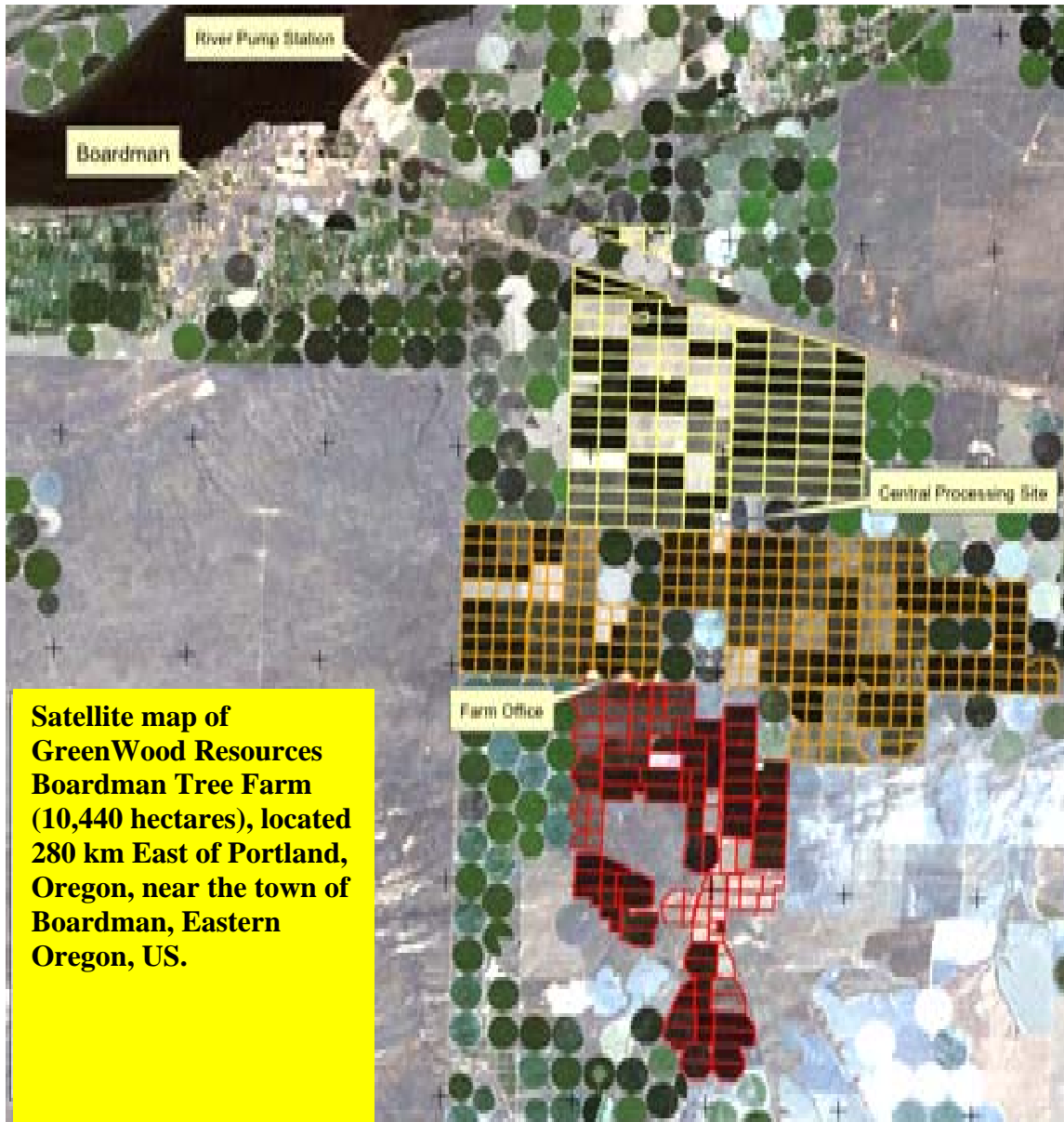
## **INTRODUCTION**

Imagine a 10,440 hectare drip irrigated tree farm that has 1,000 km of buried mainline, 30,622 km of drip line and 34 pump stations with 110 pumps, in an area more arid than the Kalahari Desert in Africa. Add 21<sup>st</sup> Century automation technology with 1,400 sensors and 1,800 controls to irrigate day and night and this very large sized farm can be operated with minimal need of humans. In case things go wrong, add sophisticated algorithms and programs to provide “smarts” for the computer to handle detrimental hydraulic situations. Just to feel being in control, add remote access to the irrigation

---

<sup>1</sup>Water & Energy Resource Engineer, Greenwood Resources Boardman Tree Farm, 77200 Poleline Road, Boardman, OR 97818, [nabil.mohamed@gwrglobal.com](mailto:nabil.mohamed@gwrglobal.com), [www.grgreenwoodresources.com](http://www.grgreenwoodresources.com)

automation system so that no matter where, or which mobile device, one can remotely override the computer. Now you have just imagined a large sized irrigated “dream” farm. Actually this “dream” farm does exist and is known as the GreenWood Resources Boardman Tree Farm (GWR BTF) located in Eastern Oregon US. See Figure 1 for the layout of the farm.



**Satellite map of  
GreenWood Resources  
Boardman Tree Farm  
(10,440 hectares), located  
280 km East of Portland,  
Oregon, near the town of  
Boardman, Eastern  
Oregon, US.**

Figure 1. Satellite location map of GreenWood Resources Boardman Tree Farm.

### **BOARDMAN TREE FARM (BTF) FACTS**

Boardman Tree Farm (BTF) covers 104 square km planted with nearly 9,000,000 Pacific Albus (Hybrid Poplar) trees on 10,440 ha. In addition to the trees, there are 2,225 ha of

various high value crops including organic crops under pivot irrigation, but on non-GWR ownership. The extensive irrigation pipe network consists of 1,000 km of buried pipe, 4 to 183 cm in diameter. Both the trees and the pivot crops are irrigated by 34 pump stations with 110 pumps. Single pump capacities range from 1,900 lpm to 121,000 lpm with pump motors ranging in size from 22 to 746 kW. BTF's peak pumping capability of 28,420 kW can deliver in excess of 852,000 lpm with a capacity to produce 1,226,000,000 lpd. This very large volume of water is fed via nearly 27,000,000 drip emitters to the trees through 30,622 km of drip line, which is about  $\frac{3}{4}$  the circumference of the earth. The 250 sand media filters in the irrigation system gives BTF one of the largest concentrations of operational sand media filters in the world. BTF's 10,440 hectares makes it the world's largest irrigated fiber farm and one of the largest contiguous drip irrigated farms in the world. BTF is also a world leader in large-scale drip irrigation efficiency.

## **BOARDMAN TREE FARM AND ITS USE OF 21<sup>ST</sup> CENTURY TECHNOLOGY**

### **Advanced Scientific Irrigation Management (ASIM) System.**

Boardman Tree Farm uses the best practices of an Advanced Scientific Irrigation Management (ASIM) system for accurately predicting future water demands for each age group of trees. This water demand predication utilizes localized Hybrid Poplar crop models, 25 years historical local AgriMet hourly weather data for evapotranspiration (ET) and growing degree days, multiple independent local extended weather forecasts and real-time soil moisture sensors. Due to the huge energy cost to pump, the operational objective is to pump only what the trees need.

Using in-house and special customized programs, irrigation schedules are created and transferred to the I-SCADA system for implementation into the many Remote Terminal Units (RTU's) in the field. The I-SCADA system computer displays the new schedule and keeps track of its real-time operation as it progresses. Each field has three soil moisture sensors at three different soil depths and these can be reviewed in real-time by irrigation personnel. Irrigation schedule modifications are made when unpredicted weather events occur, or other conditions dictate a change in irrigation.

The ASIM and I-SCADA systems combination allows BTF to replace daily the ET losses, thereby allowing optimum daily soil moistures around the root zone. This daily replacement of lost soil water produces exceptional high growth in the trees. Measured height growth rates during peak growth have ranged in excess of five centimeters a day and growth rings of more than four centimeters wide are common. This high growth and ET has consequently lead to high evaporative cooling. Interestingly this high evaporative cooling over 10,440 hectares acres was observed by NASA's based thermal satellite to show an incredible cooling effect of the irrigated trees in comparison to the surrounding pristine sage brush habitat. Documented cooling ranged as high as 12 degrees Centigrade, similar to the temperature difference between a rainforest and the desert. The large area of healthy fast-growing trees at BTF, favorably impacts neighboring towns and farms by

increasing humidity and moderating temperatures of the semi-arid zone of Eastern Oregon (Figure 2).

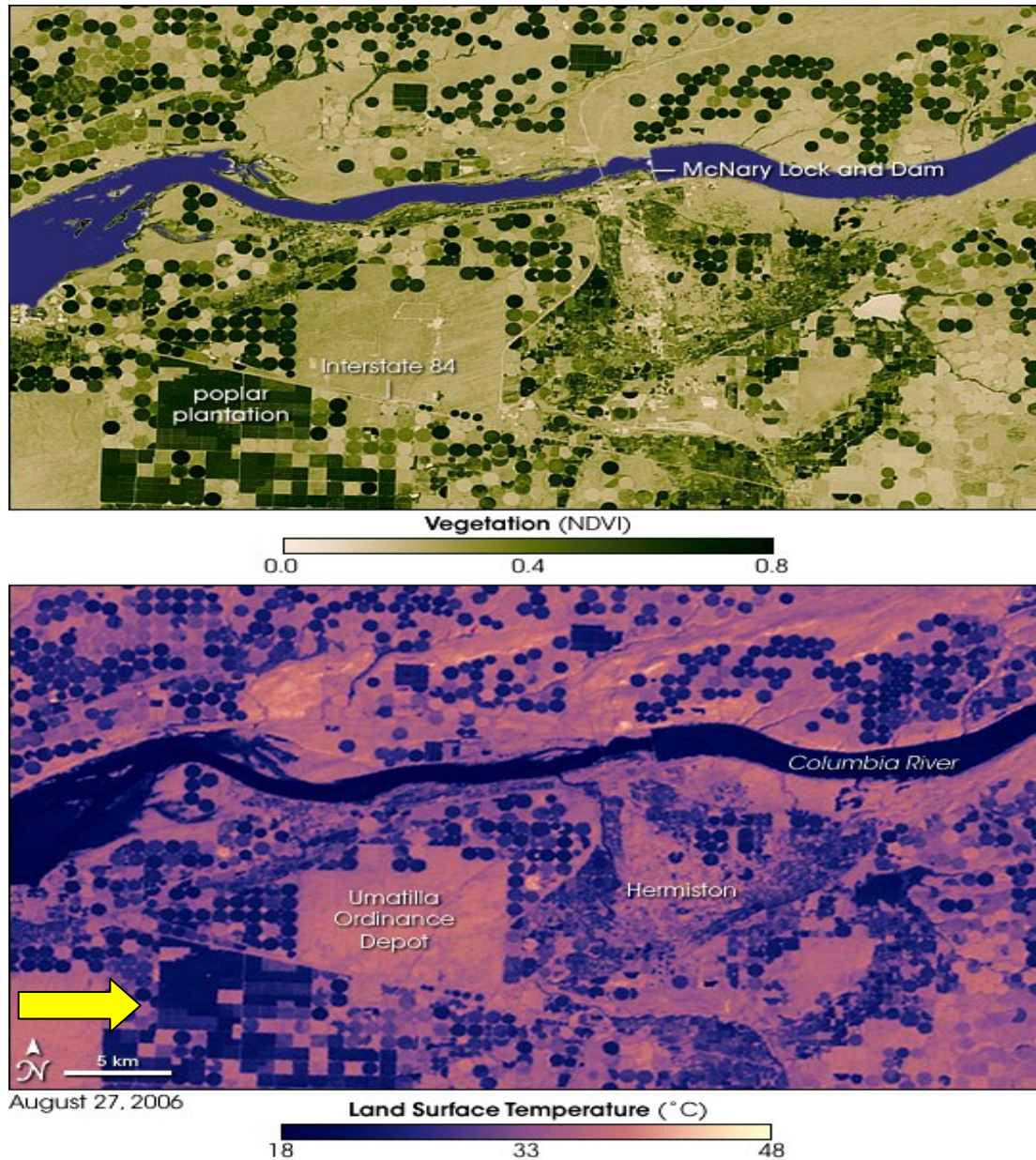


Figure 2. NASA Satellite image of Greenwood Resources Boardman Tree (Poplar) Farm (Plantation) showing vegetative growth and surface temperature variation on irrigated and non-irrigated lands.

### Irrigation Supervisory Control and Data Acquisition (I-SCADA) System

BTF uses one of the nations most advanced and sophisticated Irrigation Supervisory Control and Data Acquisition (I-SCADA) systems to achieve an on-farm irrigation application efficiency surpassed by no other large-scale irrigated farm in the nation, even

possibly the world. This I-SCADA system provides BTF the ability to “spoon feed” the trees with desired amounts of water and fertilizer four times a day at different rates on each irrigation cycle.

The BTF I-SCADA system controls and monitors 250 pumps, 370 irrigation blocks, 1,254 automated valves and 46 center pivots. There are nearly 1,400 sensors and 1,800 controls in this system. I-SCADA system consists of two master processors, three computer servers and one Operator Interface Terminal (OIT) workstation computer, installed with Human Machine Interface (HMI) software, all interacting together with the 153 RTU's (Figure 3). All communications to the RTU's are done by multi-spread spectrum radio telemetry on two totally independent licensed radio frequencies. This I-SCADA system is designed to remotely control valve(s) or pump(s) within a radius of 30 km from the OIT at the office. All I-SCADA system's remote field actions occur within two seconds of operator command, with full control acknowledgement within five seconds of command initialization from the OIT.



Figure 3. BTF I-SCADA System Field Remote Terminal Unit (RTU)

Irrigation system operations can be remotely, or manually, programmed and stored at multiple locations on the I-SCADA system such as the OIT, master processors and the RTU's. I-SCADA system's real-time data are stored on a sequential database. Some data are stored every minute, plotted for trends and analyzed to improve BTF irrigation performance and methodologies.

I-SCADA system can be controlled by remote devices from any location that has either an internet, or cell coverage. This system is accessible, via Virtual Private Network (VPN), which also creates a virtual backup image in case of server failure. All field RTU's can work independently of the office master processor, so as to enable the BTF irrigation system to work even when the office computer systems are non-functional. BTF's I-SCADA system is truly a "stand-alone" system that can in extreme hydraulic situations use sophisticated auto shut-off programs to independently shut down pumps, or fields, to mitigate a hydraulic problem and so maintain system integrity. This is combined with an extensive real-time alarm/pager system to alert operators of an irrigation situation that would adversely affect irrigation performance, or efficiency.

Complex localized programming at each block level enables hydraulic self recovery of the irrigation system in case of partial loss of pumps or pumps stations. This self recovery allows partial irrigation to occur, minimizing the downtime effects of an irrigation system crisis. Use of extensive real-time flow and pressure monitoring and trending at pump station and block levels, enables high irrigation uniformity efficiencies and optimizes irrigation system performance.

Power usage per unit water pumped for each pump station with real-time power monitoring and algorithms are built into the OIT. Use of Variable Frequency Drive (VFD) motors, real-time innovative pump selection OIT guide for single or multiple pump operations, combined with on-line pump testing; all collectively help improve BTF's irrigation pumping energy efficiencies.

Besides providing reliable operations of the BTF irrigation system, I-SCADA system is programed to protect and serve the non-GWR customers. One example is the monitoring of flows from underground mainlines that run below high cash crop fields. This allows a preemptive shut-down of the mainline, via I-SCADA system auto- controls, in case leak(s) are detected. This and other critical I-SCADA system auto-functionalities are very essential because BTF's irrigation system provides water to 2,225 hectares of neighboring farms that grow very high-value crops, such as mint, onions, corn, potatoes and organic crops.

Presently BTF's I-SCADA system is being expanded by another 14 RTU's to automate additional 3,000 hectares of trees. Also as cloud computing is still new at GWR and has just recently been implemented into BTF operations; its migration into the I-SCADA system and its database will take some time.

### **Advance Hydraulic Balanced Irrigation Scheduling (AHBIS) Program**

BTF uses an original and innovative methodology of creating individual block schedule regime that leads to a smooth and steady pump station hydraulic operation. This methodology is incorporated into a customized highly sophisticated Advance Hydraulic Balanced Irrigation Scheduling (AHBIS) program which optimizes irrigation schedule regimes, such that no pump changes are necessary during a period of a particular irrigation schedule regime. With no pump changes, leads to a steady irrigation canal

withdrawal rate, greatly assisting the irrigation district to maintain efficient canal operations. All this allows the operation of a very large and complex irrigation system without the use of expensive and complex pump automation programs.

The AHBIS methodology improves pumping energy efficiency with tangible pump energy savings, decreases irrigation system wear and greatly improves human resource allocations. Interesting to note is that operating one of the world's largest contiguous drip irrigated farm 24/7 during the irrigation season, takes BTF only one part-time manager, one engineer, one water quality and three pump technicians with three field assistants. A total of only nine persons make up the full BTF irrigation team.

With AHBIS program's ability to provide a "smooth" hydraulic operation of the BTF irrigation system, makes it "easy" on the hardware of the system and lessens the burden to the irrigation team members. The irrigation team members then only have to interact with the I-SCADA system when the system remotely alarms them. This hydraulically smooth operation is what enables the I-SCADA system to become a true stand-alone system.

AHBIS program generates an I-SCADA system operational code file for each irrigation schedule change. The code file has 12,000 individual block six-day irrigation schedules with random daily irrigation start times and it is hydraulically balanced. The I-SCADA system and AHBIS program interaction allows BTF to micromanage irrigation scheduling at the individual 16 to 28 ha block level to within +/- a minute, for a high precision and accurate irrigation of the Pacific Albus trees. This precise scheduling is very important, as any additional minute of irrigation at each of the 370 irrigation blocks would easily add up to nearly six hours of unnecessary and costly irrigation.

### **Drip Irrigation Technology**

BTF's use of an innovative and an award winning design for closed-loop drip irrigation systems, together with pressure compensated emitters, achieves the highest irrigation application and uniformity efficiencies at minimum pump energy costs. Automated system flushing of the drip lines can be programmed and scheduled days in advance, much the same way as an irrigation schedule. Additional features of BTF drip operations allow "Flush Filling" at flush pressures when the empty drips lines are filled at the start of irrigation. Also an RTU program allows BTF to conduct a unique drip operation, known as "desilting", by pausing irrigation for a couple of minutes, that moves sediment in the drip line to the outer edges and also purges the emitters.

### **Irrigation Simulator (IrSim) Hydraulic Model**

A MathLab/Simulink based customized hydraulic simulator program that interacts with BTF's I-SCADA database to update actual and modeled reality of hydraulic operations at BTF. This use of an IrSim Hydraulic Model is to potentially enable irrigation at operational minimum pressures, leading to improved pump energy efficiency and decreased pump energy costs.

### **Satellite and Aerial Imagery and in-house Geographic Information System (GIS)**

Satellite and aerial Near-Infrared images are used to assist in improving irrigation uniformity efficiencies, monitor tree and vegetation growth, disease and crop loss evaluation. Complex algorithms generate growth differential between the two different periods of satellite imagery and graphically lay out the growth patterns that have, or have not, occurred at BTF in the time span of these two satellite passes. It enables BTF to easily and accurately monitor growth of all crops and other vegetation like noxious weeds, on its large farm. A very active GWR GIS department assists in acquiring the satellite and aerial images and is also active in the field GIS layout for tree planting, inventory, harvest hauling roads and general national and international mapping for GWR.

### **Ground Water Recharge**

The BTF's irrigation system also provides river water, during excess winter and spring runoffs, to the water recharge project's basin at the edge of its property. Additionally, during certain periods of the irrigation season, "excess" BTF water is bypassed through a complex piping configuration to the recharge basin (Figure 4). This recharge project's goal is to reverse the declining water table in the area and so allow the local farmers to grow high value crops to improve the economical returns in the region. These regional ground water recharge projects are expected to generate more than \$300,000,000 of new economic growth in the local area.



Figure 4. BTF Ground Water Recharge RTU and "Bypass" manifold

### **Bio-Energy, Bio-Fuels and Bio-Chemicals.**

BTF's irrigation system provides water to other non-tree high yield fiber crops such as switch grass for bio-energy and bio-chemicals and Aronda Donax (Giant cane), after torrefaction, for bio-fuel to substitute, or replace, coal for a local coal-fired electric plant. Some of the tree fiber produced by BTF is used as primary source for the conversions into aviation fuel, ethanol, biochemicals like methyl acetate, acetic acid and for bio-plastics production. These conversions are done by non-GWR companies using very high ended 21<sup>st</sup> Century technologies that are still at research levels. Other technologies like

using acetogenic bacteria from termites, to break down cellulose, are now being upsized in a small industrial plant close to BTF. This new patented process using termite bacteria involves a 100 % fermentation process that produces cellulosic ethanol from wood chips, without producing carbon dioxide. This efficient process, combined with fiber from high yielding, fast growing BTF trees, potentially yields per hectare five times the ethanol yield of corn, and at a production cost estimate of less than one dollar per gallon of ethanol.

### **Water Rights and Use.**

BTF runs an innovative and creative water rights program to irrigate only a 120 cm zone on either side of the three meter tree rows and maintain a center 60 cm wide dry zone strip in the middle of the row strips. This enables BTF to efficiently transfer the water rights of the pervious circular pivot ground to the newly converted rectangular drip irrigated field. This also involves a very intensive real-time soil moisture monitoring program with regular reporting to the State to comply with regulations. Annual temporary transfer of water rights to other users, or locations, from fields that are not planted, due to late season harvest, is potentially a very lucrative option for BTF.

### **Power Grid Demand Balance.**

With 28,420 kW under immediate control of I-SCADA system, it provides potentially a powerful ability for BTF to assist the local and regional electric utilities to manage the high peak demand for power during the summer. Additionally, when there is excess power available on the grid, especially during the spring runoff and high wind power generation, river water can potentially be pumped into a reservoir on BTF for latter use.

### **Terrestrial Laser Imaging Detection and Ranging (LIDAR)**

BTF's uses terrestrial LIDAR, which provides 1,000,000 points of tree form measurements per second, for inventory and harvest purposes (Figure 5). Also on BTF properties is located one of the largest hardwood sawmill in the US. This state-of-art sawmill incorporates this LIDAR data with its scanner data. Then, through complex programs and algorithms, this combined information is used by the sawmill's computers, together with a value-added component, to direct the automated mill saws to make the best cuts on the log to return the maximum dollar value from each log. This process is greatly assisted by the use of a sophisticated curve gang saw that can cut a sinusoidal shaped log at an angle, to provide improved recovery and superior quality lumber.



Figure 5. Terrestrial LIDAR mapping tree form at GWR BTF.

### **Evapotranspiration Adjustment for Water Demand**

Complex programming at the ASIM and I-SCADA systems allows implementation on a farm-level scale, or individual fields, any percent of deficit irrigation to lower irrigation pumping costs and “over” irrigation to increase yield and provide an early harvest due to early maturation.

### **Breeding and Cloning Technology**

GWR is the foremost company in high level breeding and cloning of Hybrid Poplar and has one of the most advanced hybrid poplar breeding and research stations in the world. From these breeding stations originates the best planting material in the form of high-yielding, fast-growing, disease and pest resistant trees. Using carbon isotope discrimination for selection of drought resistant clone varieties, which when planted at BTF will potentially lower irrigation electrical costs and save water. Additionally breeding is ongoing to produce Hybrid Poplar trees that have lower lignin wood content for efficient bio-fuel and bio-chemical production. Breeding is also on-going for the increased demand for high-yielding, fast-growing planting material for international tree plantations in various regions of the world.

### **On-farm Energy Generation**

BTF has participated in wind power evaluation and other on-farm energy generation for any potential in replacing some of its high-pump energy usage. Because of BTF's large size and a climate that is sunny and cloud free for most of the year, solar power is a very viable option. Low-head hydro energy generating potential also exists in the many miles of irrigation district canal that run through BTF.

### **Other Technologies and Practices in Place or Planned**

BTF has invested in cement mortar lining all steel mainlines to extend the useful life of the pipe by at least another 25 years, and lower the friction losses and thus the energy required moving water through the system. Huge pump energy savings are derived from this extensive and costly modification.

BTF plans to provide cooling water to local data centers and food processors. As BTF pumps water from the Columbia River, from a zone that provides a constant 12 degrees Centigrade water, it offers a cheap alternative source of cooling for the local industry.

BTF's zero-waste and ecofriendly policy where all wood wastes, including planer saw dust, are incorporated back into the soil, or made into products for sale e.g. saw dust is being extruded into pellets for wood stove burning and pressed water excluded from veneer board processing is applied back to the trees on the farm.

Multiple million dollar investment into huge "fish-friendly" river screens that are specifically designed to minimize the inrush velocity of water into BTF's river intake pipes. These huge river screens can be auto-cleaned from a program inbuilt into BTF's I-SCADA system.

Intensive BTF Insect Pest Management (IPM) that prioritizes prevention, monitoring and non-chemical control methods. BTF's wildlife management program is also set to enhance habitat, manage for beneficial species and protect rare species, therefore BTF dedicates 10% of the farm to native habitat. BTF was the first plantation in North America to achieve Forest Stewardship Council Certification (FSC) and has been recognized as a fully sustainable fiber supplier and a well-managed plantation.

## CONCLUSION

By using 21<sup>st</sup> Century technology, GreenWood Resources Boardman Tree Farm is a working real-world model on how technology can enable Agroforestry to efficiently and economically produce fiber from one of the earth's most renewable resource – trees and other fiber crops. It is even a greater achievement when it is done on a sustainable and eco-friendly manner.

BTF produces one of the highest fiber yields in the US by 1) Planting genetically best (high-yielding, fast-growing, disease and pest resistant) tree material suited to that particular environment; and 2) Using sophisticated I-SCADA, AHBIS, ASIM systems and other advanced programs and practices to grow trees in an eco-friendly way using water and energy resources efficiently.

Ground water recharge from excess winter and spring runoff, growing high yield fiber plants for torrefaction process to replace coal in a power plant, potentially assisting local utility in high peak demand control, all provide a large social-economical foot print for BTF.

BTF's goal is to develop an economically sustainable agricultural system that can remain productive in the long run and produces fiber for bio-chemical, bio-fuel, bio-energy, paper, veneer and solid wood products. The adoption of 21<sup>st</sup> Century technology has been the key element that allows BTF to achieve its goal.

## ACKNOWLEDGEMENT

Appreciation is extended to the GreenWood Resources Inc. and its Boardman Tree Farm Team, whose members devote tireless efforts in seeking higher levels of efficiency in producing low cost, sustainable and eco-friendly fiber and wood products.

## REFERENCES

GWR Boardman Tree Farm internal reports and documents.

Mildrexler, D.J., Zhao, M., and Running, S.W. (2006, October 26). Where are the hottest spots on Earth? *EOS*, 87(43), 461-467. <http://earthobservatory.nasa.gov/Newsroom/NewImages/images.php3>.

Mohamed, N. 2010. Interaction of Advanced Scientific irrigation Management (ASIM) with I-SCADA System for Efficient and Sustainable production of Fiber on 10,360 Hectares. USCID SCADA and Technology Conference, Fort Collins, Colorado.

Mohamed, N. 2010. Utilizing a Vast and Complex Wireless Communication Network in a Sustainable "Bio System" for the Production of Fiber for use in BioEnergy, Paper and Solid Wood. XVII<sup>th</sup> World congress of the International Commission of Agricultural

Engineering (CIGR), Proceedings of the 2010 World Congress on Computers in Agriculture and Natural Resources (WCCA), Quebec, Cañada.

Mohamed, N. 2010. The Role of I-SCADA System and Specialized Software in Energy and Water Efficiency on a 104 km<sup>2</sup> (40 ml<sup>2</sup>) Large-Scale Drip Irrigated Agro-Forestry Farm, USA. Beijing University of Forestry, China & Proceedings of the 2009 World Congress on Computers in Agriculture and Natural Resources (WCCA), Reno, Nevada

Mohamed, N. 2008. Sustainable “Green” Fiber and Energy Production on 29 000 acres of Drip Irrigated Tree Farms. High Efficiency Irrigations Systems Consultants (HEISCON), Lahore, Pakistan & 2008 ASABE PNW, Boise, Idaho.

Mohamed, N. 2008. Real Time Energy and Pumping Efficiency Monitoring for Irrigation. Umatilla Electric Cooperative (UEC), Hermiston, Oregon.

Mohamed, N. 2007. Use of Sophisticated State-of-Art SCADA System for very Efficient Automated Irrigation Operations on 22,070 acres of Agro forestry, USCID Water Management conference, Denver, Colorado.

Mohamed, N. 2006. Use of “Hydraulic Balanced Irrigation Schedule (HBIS)” optimization program to cost effectively irrigate a very large scale Tree Farm of 7 007 ha (17 300 acres). ASAE Paper No. 062321. ASAE AIM, Portland, Oregon.

Mohamed, N. 2005. Use of sophisticated SCADA System for Automated Irrigation Operations on 9,140 ha of Agroforest and Crops. ASABE PNW Paper No. Oral 05-2001. ASABE PNW. Lethbridge, Alberta, Cañada.

Mohamed, N. 2005. High ‘Tech’ Farm Automation for solid desert wood production. American Society of Agricultural and Biological Engineers (ASABE) Resource, September 2005, vol. 12 No. 7, pg. 10.

Mohamed, N. 2003. Use of State-of-Art Technologies to Irrigate a Very Large-Scale Drip Irrigated “Fiber Farm. ASAE Paper No. 0238613. ASAE AIM. Las Vegas, Nevada.

Mohamed, N. 2000. Facing the Challenges of Producing “Desert Wood” on a Very Large Scale Drip Project. ASAE Paper No. PNW 2000-03. ASAE PNW. Richland, Washington.



# MOBILE CANAL CONTROL, AN AUTOMATIC ADMINISTRATION SYSTEM FOR MANUAL CANAL OPERATIONS USING SMART-PHONE TECHNOLOGY

Peter-Jules van Overloop<sup>1</sup>  
Rick Kuijten<sup>2</sup>  
Wouter Jan Klerk<sup>3</sup>  
Meinte Vierstra<sup>4</sup>

## ABSTRACT

In many irrigation districts around the world, canal operators fulfill a pivotal role in the process of water delivery to farmers and are an important link between management and these end-users. Although skilled in their job, there are factors which make operators less effective as they could be: measurement inaccuracies cause less-accurate water delivery and since administration is mainly done by paperwork, managers often have limited insight in the work of their operators, which could hamper their ability to justify certain decisions or prove they meet the water conservation goals and laws. Mobile Canal Control, a smart-phone based technique to measure water level and gate positions could provide a tool to support operators in their job. Image processing and pattern recognition applied to pictures taken at the local control sites can reduce measurement errors and by automatically storing images and water data in a central database, the amount of paperwork necessary for administration can be reduced enormously. It also gives farmers the ability to get a more accountable billing of their water use. Moreover, Mobile Canal Control can provide managers with the necessary background information that justify decisions taken in the field and help them achieving their conservation goals, resulting in a more accurate and more accountable water delivery.

## INTRODUCTION

Many irrigation canals in the world are manually operated by employees of irrigation districts that travel along the canal making changes to the gates in order to deliver water to farmers [Burt 1999]. Throughout the world different names are used for this person, for example ditch tender, zanjero, canalero. In this work the description 'canal operator' is used. These canal operators have a pivotal role in the entire process of water delivery as they are the link between the management and the end-users [van der Zaag & Rap 2012]. There is no question about their skills in the task they perform [Vos 2005], [Vos & Vincent 2011], yet the pivotal role makes it hard to frame their work in the management and accountability of an irrigation district [Skogerboe et al. 1998]. The latter is becoming

---

<sup>1</sup> Delft University of Technology, Stevinweg 1, 2628 CN, Delft, The Netherlands, +31-620368817, p.j.vanoverloop@citg.tudelft.nl.

<sup>2</sup> Water Board De Dommel, Bosscheweg 56, 5283 WB, Boxtel, The Netherlands, +31-411618618, rkuijten@dommel.nl.

<sup>3</sup> Delft University of Technology, Stevinweg 1, 2628 CN, Delft, The Netherlands, +31-152781646, w.j.klerk@gmail.com.

<sup>4</sup> Mobile Canal Control, Stippelzegge 14, 2498 CC, Den Haag, The Netherlands, +31-15-7009727, m.vierstra@mobilecanalcontrol.com.

more and more important because of the new conservation goals [Cooley et al. 2010] and laws, such as the Water Conservation Act of 2009 in the United States of America.

Figure 1 shows the position of the canal operator in the water delivery framework. To make the role position as clear as possible the terms ‘manager’ and ‘farmer’ are employed for the persons in the other layers of the framework.

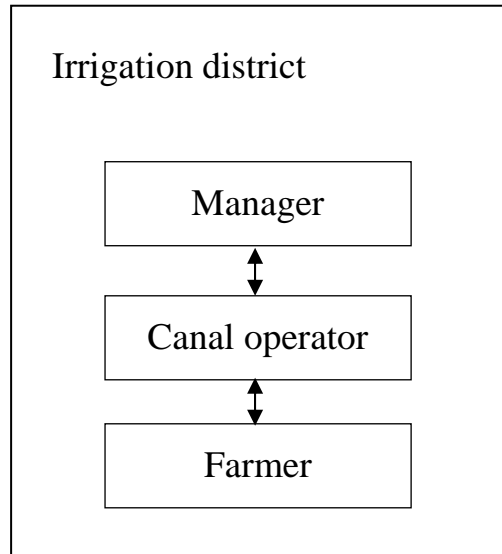


Figure 1. Position of canal operator within irrigation district

This paper discusses the pivotal role of the canal operator and a technical innovation that may be useful to improve the integration of the operator in the management and accountability of the irrigation district.

### MANUAL OPERATIONS OF IRRIGATION CANALS

In many irrigation districts, the following water delivery procedure often applies [Clemmens et al. 1994]:

- An order for a certain amount of water is made during working hours one day in advance of the actual delivery. In most districts this is done by a telephone call from the farmer to the manager in the irrigation district office (see Figure 2) or an order submitted online. Although there is usually another layer between manager and canal operator that is responsible for taking the orders, for simplicity reasons, this person is considered responsible for proper management of the water delivery, so referred to as manager;
- In the early morning, at the office, all required deliveries are taken over by the canal operator and this person makes a schedule for where to implement changes to the canal structures. If necessary, the schedule is discussed with the manager;
- The canal operator starts at the beginning of the canal to change the head flow and travels along the canal to make the changes at the intermediate and turnout gates. The gates are opened or closed manually with a certain displacement which is

verified with a local or portable ruler, e.g. a spring ruler or a measuring rod (see Figure 3). In terms of control theory [Vandevogte 1990] this way of implementing an action would be considered feedforward control. For determining the gate opening, tables and a calculator such as given in Figure 4, may be utilized. When the turnout gates to the farm lands need to be opened, there is often a check with the farmer if this person is ready to receive the water. It often happens that the moment of delivery needs to be shifted and the canal operator decides to deviate from the schedule. All deliveries and changes to the schedule are written on pieces of paper and kept for administrative purposes later that day (see Figure 5);

- The canal operator travels back along the canal and visits the gates again in order to make corrections to the situation. The operator determines the water level visually from a staff gauge or a portable ruler and corrects on the difference between the desired level and the measured one. In control theory this would be considered feedback control;
- It may require a number of runs forth and back along the canal before a new acceptable steady state is reached;
- The previous steps need to be repeated when the water delivery needs to be shut off or changed again;
- At the end of the shift, the canal operator returns to the office, gathers all pieces of paper and fills out an administration form in the computer from which the farmers can be charged for the water.

282 (R5 5-87)

APPLICATION FOR WATER

Date OCT 7 4 2012 Account No. \_\_\_\_\_

Time 11:15 AM  
PM

Division SW

Starting not earlier than 2.5 (Date)

please deliver \_\_\_\_\_ 2 Second Feet

from WPI Canal

through Delivery Gate No. 34

Delivery is required for 24 1 days,

to irrigate 103

of Tract \_\_\_\_\_ Sec. \_\_\_\_\_ T. \_\_\_\_\_ S., R. \_\_\_\_\_ E.

Owner's name \_\_\_\_\_

By \_\_\_\_\_ (Authorized Agent)

Telephone No. \_\_\_\_\_ (For District Notification of Scheduled Delivery)

Figure 2. Water order as registered at irrigation district



Figure 3. Flow change made to an undershot gate and verified using a measuring rod

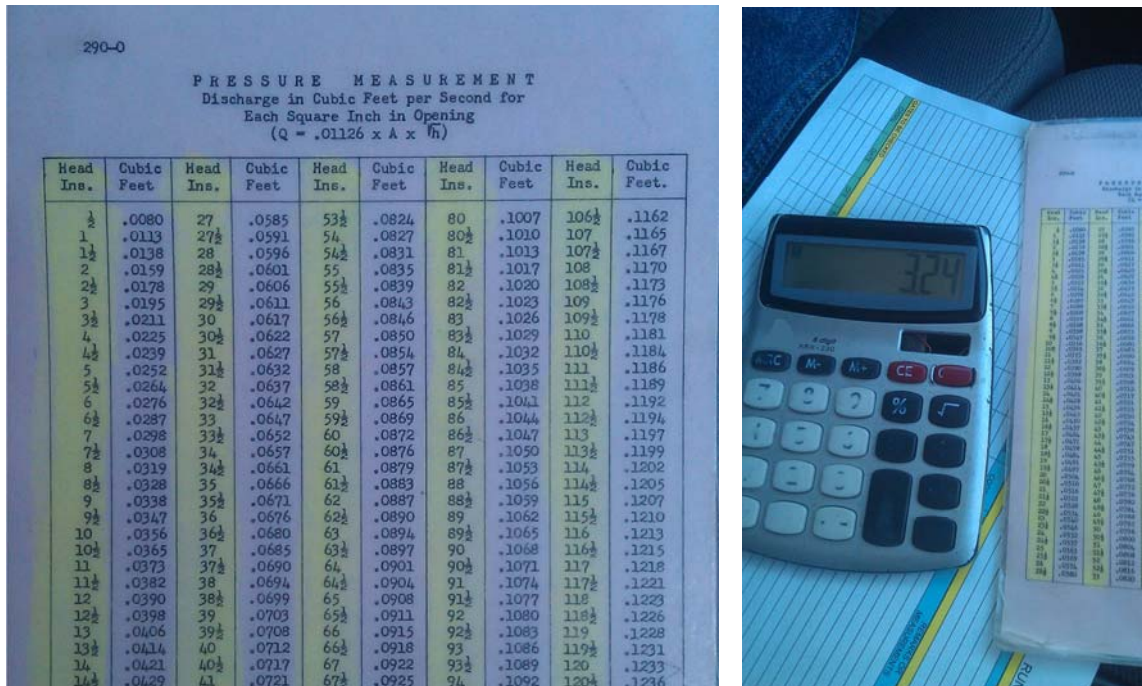


Figure 4. Manual computations of flows to be delivered



Figure 5. Manual administration of delivered flows

Two types of issues can be pointed out in this way of managing water delivery. The first one is related to the accuracy of the delivery and the second issue relates to the pivotal role of the canal operator.

### WATER DELIVERY ACCURACY

Canal operators are usually very experienced in knowing how to operate the gates and route the water from source to the users [Clemmens et al. 1994], [Godaliyadda et al. 1999], [Vos 2005], [Vos & Vincent 2011], [van der Zaag & Rap 2012]. Still, at every site, the operator can only use local information of the water levels and flows. Certain influences at other locations that may influence the situation at a later stage cannot be anticipated on. Changes in weather conditions or sudden changes of the in- or outflows that were not communicated the day before, may cause the water delivery to be less accurate as would be possible compared to the situation when this kind of information would have been available to the operator. This can lead to undesirable situations in regions facing scarcity of water [Clemmens et al. 1994].

Another source of inaccuracy in the water delivery is the visual reading of the water level and gate position. A Gage Repeatability & Reproducibility field test [Tennant 2001] done at a water board in The Netherlands shows that the standard deviation in reading a water level, even by experienced operators, is in the order of a centimetre, and moreover different operators have different performances. Table 1 gives the results of the test. The data was taken from three experienced operators at 12 locations measuring the water level using three different measuring tools: spring ruler, measuring rod and the local staff gauge attached to the canal wall. High percentages of the Repeatability number means that, using the measurement tool and method, it is not easy to determine a consistent value even by one and the same person that repeats the task, while higher values for the Reproducibility number means that different persons often find different measured values for the same actual value.

Table 1. Test results of reading the water variables using different devices by multiple experienced operators

	Gage R&R	Repeatability	Reproducibility	Standard deviation	95% Reliability
	%	%	%	m	M
Spring ruler	0.5	0.3	0.4	0.0037	0.0074
Measuring rod	2.2	2.0	0.8	0.0084	0.0168
Staff gauge	0.2	0.2	0.1	0.0028	0.0056

It can be seen that the task of reading the water levels (from which the flows are calculated) can be considered accurate and reproducible for experienced canal operators when using a spring ruler or a staff gauge. In that case, the accuracy is in the order of 6 to 7 millimetres or a quarter of an inch. For the measuring rod, the accuracy is 17 millimetres or two thirds of an inch.

Another test, where these water level values were manually entered in a portable computer and later, from this device, manually entered in a central system gave another 9 mm (or 0.36 inch) standard deviation and so a 18 mm (or 0.71 inch) 95% reliability interval compared to the actual values. This test was executed using 197 water level readings.

It is common to take in at least 10% more water than is actually ordered in order to always have enough water in the canal to compensate for inaccuracies in delivery, one of them being the above mentioned measurement inaccuracies. This water can be considered as water loss and especially in districts with water conservation goals and policies this is possibly preventable by adding more accuracy to measurements and the way these are entered in the central administration system.

### PIVOTAL ROLE OF CANAL OPERATOR

Another issue with the manual operations is that the entire water delivery depends on the information that the canal operator shares with the other layers in the water delivery process (see Figure 1). Although the amounts of water delivered are written on paper, the decisions taken during the day are not transparent. In hindsight, this makes it hard for the manager to justify certain events to the outside world and proof that the irrigation district complies with the water conservation laws. At the other end of the delivery process, the farmers may have a desire to have an increased flexibility in the delivery and are inclined to push the canal operator for more unrequested changes. In [Clemmens et al. 1994], [Vos 2005], [Vos & Vincent 2011] and [van der Zaag & Rap 2012] there are examples presented of farmers imposing pressure on the canal operator in personal interactions to deliver more water to them. At present, it is hard to find out about these incidents, as there is no objective registration of the decisions made by the operator.

### MOBILE CANAL CONTROL

A recent smart-phone based technology may be a tool to support the canal operator in his water delivery task (see Figure 6). The idea is that the operator is equipped with a smart-phone with a special app. With this app the operator takes pictures of a water level and gate at every site and these pictures are sent to a web-based central server and stored in a database together with location and time. Using appropriate image processing and pattern recognition software the water level and gate position are read from the picture and these values are stored in the database as well. These measurements allow for a direct administration from local site to an administration form, without the intermediate steps of visual reading, writing on paper and entering in the computer. This leads to a faster and more reproducible procedure which is less prone to human errors. At present, the accuracy of the technology in reading and automatically registering the water variables is in the order of 5 millimetres (or 0.20 inch).

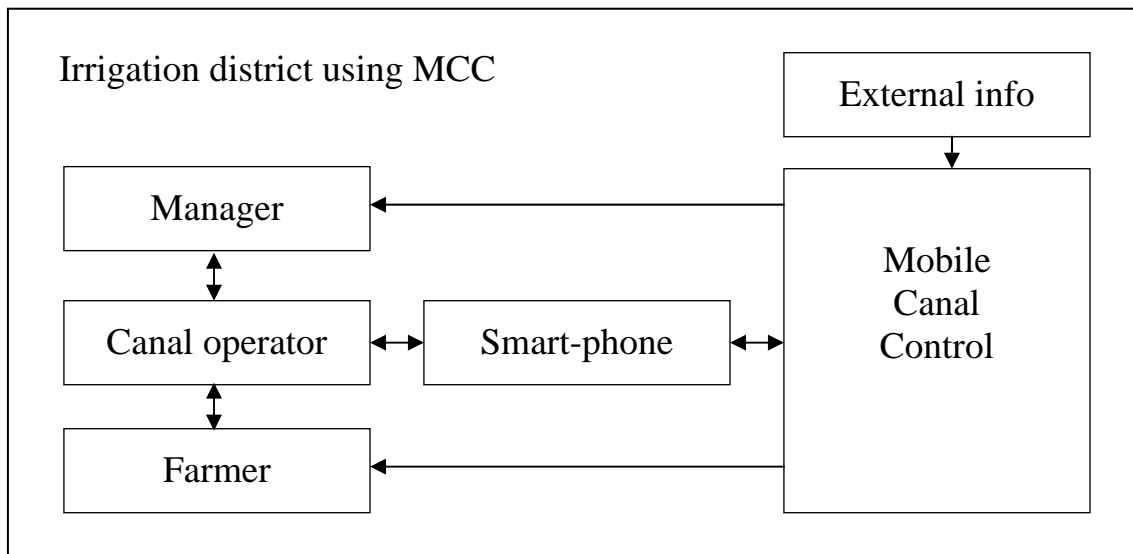


Figure 6. Position of canal operator within the irrigation district using the Mobile Canal Control administration system

The manager has access to real-time measurements and is not only depending on spoken communication with the canal operator anymore. The farmer receives a more accurate and accountable billing for the water delivered, while the operator is relieved from the administrative paperwork.

The system is setup to be able to communicate more information to the canal operator. External influences, such as weather conditions or sudden unscheduled demands, can be included. This can be used to advise the operator to change the schedule through the two-way communication of the app on the smart-phone. In this way, the system can also be configured as decision support system or centralized control system.

The procedure of water delivery can be condensed to:

- The orders are submitted online by the farmers. The manager checks for possible conflicts. This would allow for a shorter notice times for farmers to order water, which results in a higher flexibility of water delivery;
- The canal operator starts with a run and, when arriving at a location, receives a message on the smart phone how much flow needs to be imposed at that location;
- The operator implements the change manually;
- The operator takes a picture of the water level and gate (see Figure 7). The picture and measured water level and computed flow are send to the central system and automatically administrated;
- The operator continues with the runs, arrives at other locations and repeats the local procedure until all changes are implemented. No administrative tasks need to be fulfilled after the runs.



Figure 7. Canal operator using smart phone technology for measuring and automatic administration of water levels and flows

## CONCLUSION

The pivotal role of a canal operator is having a dominant influence on the water delivery in irrigation districts making the process non-transparent and less accurate as it could be. By using modern-day smart-phone technology, as used in Mobile Canal Control, the

situation for manager, farmer and canal operator can be improved. The manager gets more insight in the way the operator implements control actions, the farmer gets a billing for water that is more accountable, while in support of the operator, the administrative paperwork is automated.

### REFERENCES

- Burt, C.M., 'Current Canal Modernization from an International Perspective', Proceedings USCID-Workshop, Phoenix, Arizona, 1999.
- Clemmens, A. J., Sloan, G., & Schuurmans, J., 'Canal-control needs: Example. Journal of Irrigation and Drainage Engineering', 1994.
- Cooley, H., Christian-Smith, J., Gleick, P. H., Cohen, M. J., Heberger, M., 'California's Next Million Acre-Feet: Saving Water, Energy, and Money', Report Pacific Institute, 2010.
- Godaliyadda, G. G. A., Renault, D., Hemakumara, H. M., Makin, I. W., 'Strategies to improve manual operation of irrigation systems in Sri Lanka', Irrigation and Drainage Systems, 1999.
- Skogerboe, G. V., Habib, Z., Pongput, K., Vehmeyer, P. W., and Khan, A.H., 'Canal Modernization In The Indus Basin Irrigation System', International Meeting on Modernization of Irrigation System Operations, Information Techniques for Irrigation Systems, Aurangabad-Maharashtra-India, 1998.
- Tennant, G., 'SIX SIGMA: SPC and TQM in Manufacturing and Services', Gower Publishing Ltd., 2001.
- Vandevogte, J., 'Feedback control systems', Prentice hall, New Jersey, 1990.
- Vos, J., 'Understanding water delivery performance in a large scale irrigation system in Peru', Journal of Irrigation and Drainage, 2005.
- Vos, J., Vincent, L., 'Volumetric water control in a large-scale open canal irrigation system with many smallholders: The case of Chancay-Lambayeque in Peru', Agricultural Water Management, 2011.
- Zaag, P. van der, Rap, E., 'The pivotal role of canal operators in irrigation schemes: the case of the canalero', Journal of Irrigation and Drainage, 2012.



# REGULATING RESERVOIR AND LATERAL IMPROVEMENTS RESULT IN SPILLAGE REDUCTION

Bryan Thoreson<sup>1</sup>  
Rick Massa<sup>2</sup>  
Tommy Ostrowski<sup>3</sup>

## ABSTRACT

The Orland Unit Water Users Association (OUWUA or Association) delivers irrigation water to about 20,000 acres in northern California. The Association is modernizing its distribution system to improve water delivery efficiency and flexibility. In the spring of 2012, OUWUA completed construction of a regulating reservoir and lateral improvements facilitating re-routing of flow fluctuations along Lateral 210 to the regulating reservoir where these flows can be re-regulated.

This paper describes the improvements and reports the spillage reduction results achieved during the first year of operation. Additionally, the actual operation and spillage reduction results are compared and contrasted with estimates developed through the verification-based modernization planning technique.

## INTRODUCTION

The Orland Unit Water Users Association (OUWUA or Association) recognizes the need for system modernization to improve water use efficiency and is aggressively following a conceptual modernization plan. OUWUA is utilizing a strategy of re-routing flow fluctuations along main canals to points where these flows can be re-regulated. These re-regulating points are either regulating reservoirs or discharge points to the Tehama-Colusa Canal (TCC) where OUWUA receives credit to offset its Stony Creek diversions<sup>4</sup>.

Primary goals identified by the OUWUA include replacing obsolete structures, increasing water delivery flexibility, and increasing conveyance efficiency. Among other benefits, the improved levels of service made possible through modernization will ensure continued use of renewable surface water supplies, reducing the incidence of farmers converting to readily available groundwater supplies. This, in turn, will protect local groundwater supplies for use in dry periods.

---

<sup>1</sup> Principal Engineer, Davids Engineering, Inc. 1772 Picasso Ave, Suite A, Davis, CA 95618, 530-757-6107 ext.105; bryan@davidsengineering.com.

<sup>2</sup> Project Manager, Orland Water Users Association, 828 Eighth Street, Orland, CA 95963, 530-865-4126; rmassa@ouwua.net.

<sup>3</sup> Assistant Engineer, Davids Engineering, Inc. 1772 Picasso Ave, Suite A, Davis, CA 95618, 530-757-6107 ext.108; tommy@davidsengineering.com.

<sup>4</sup> Upon completion of Black Butte Reservoir in 1964, the United States and the Orland Unit Water Users' Association entered into a contract providing for the exchange of water. In present Black Butte water accounting, OUWUA discharges into the TC Canal are credited against (CVP) supplies diverted from Black Butte Reservoir.

Regulating reservoirs are an important part of OUWUA's modernization plans because they minimize system spillage while enabling system operators to provide additional delivery flexibility to growers. Through improved surface water service, these reservoirs help the Association accomplish its conjunctive water management goals and improve local and regional water supply reliability.

Proposition 50, the Water Security, Clean Drinking Water, Coastal and Beach Protection Act of 2002 passed by California voters provides funds to assist agencies improve water use efficiency. This grant program implements California Water Code Chapter 7, Section 79550 (g) of Proposition 50 and provided the funds for both the Feasibility Investigation utilizing verification-based modernization planning (Thoreson and Massa, 2009) and the implementation of the regulating reservoir and related lateral improvements completed in 2012.

Verification-based modernization planning is "a tool to improve the irrigation system modernization planning process and to effectively monitor the post-project effects on system performance" (Burns, J.I., et al., 2000). The aforementioned Proposition 50 grant program requires monitoring of post-project system performance with annual reports for five years following project completion. This paper will describe the OUWUA physical and institutional setting, the regulating reservoir and lateral improvements, the water conservation estimate and the verified water conservation resulting from the first year of operation.

### PHYSICAL AND INSTITUTIONAL SETTING

The Orland Project (or Project), constructed between 1907 and 1918 and operated and maintained by the Orland Unit Water Users Association (OUWUA or Association), irrigates about 20,000 acres in northern Glenn County (Figure 1). The Project diverts roughly 100,000 acre-feet (AF) of water from Stony Creek in most years, shortages occur only in the driest years. One hundred and forty miles of mostly concrete lined canals distribute water into six "beats" (ditch tender service areas). Beats One, Two, Three and Four are served by the Southside system via direct Stony Creek diversions at Black Butte Dam into the South Canal. The Southside system serves roughly two-thirds of the Project area. Beats Five and Six are served by the Northside system via direct diversions from Stony Creek into the North Canal at the North Diversion, a diversion dam located approximately four miles downstream of Black Butte Dam.

Beats One, Two and Three are independent units receiving water at diversion points on the South Canal. The South Canal terminates at the head of Beat Four and becomes Lateral 40 with all remaining water designated for Beat Four deliveries. Beats Five and Six serve roughly one-third of the Project on the north side of Stony Creek. Beat Five receives water from the North Canal via sub-lateral turnouts with the remaining water passing through to Beat Six. Beat Two covers the largest area and serves the most water users (Table 1).

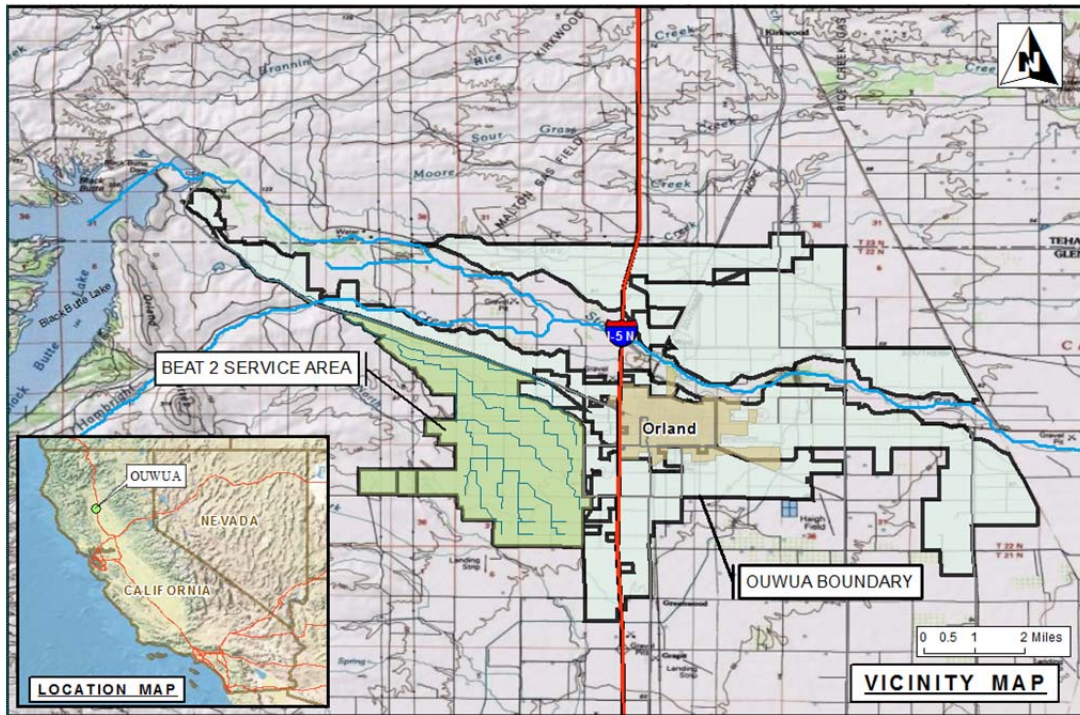


Figure 1. Location of the Orland Project in Northern California.

Table 1. Irrigated Area, Water Users, Canal Branches and Lengths for OUWUA Beats.

Beat No.	Irrigated Area, acres	Number of Water Users	Number of Canal Branches	Total Canal Length, miles	Average Irrigated Field Size, acres
Beat 1	1,323	70	6	17.6	19
Beat 2	4,492	179	11	24.6	25
Beat 3	2,091	200	19	21.6	11
Beat 4	2,586	128	16	27.3	20
Beat 5	2,031	80	9	15.7	25
Beat 6	3,455	125	9	19.7	28

Irrigation water is distributed in open, upstream controlled canals and ditches on a rotation pattern – specifically, a “head” of water is passed from one grower to the next on a 24/7 basis throughout the irrigation season. Rotational irrigation deliveries generally result in over-irrigation in the spring and fall and under-irrigation in the summer. Consequently, yields are less than optimum, causing an increasing number of growers to convert from surface irrigation with Project water to drip irrigation systems supplied by private groundwater wells.

Because parcel sizes are generally small (averaging 18 acres) and delivery flows are large (six to 12 cfs), water is typically passed from one grower to the next every few hours. These frequent flow changes cannot be made with perfect timing and accuracy, resulting in high canal spillage due to the lack of regulating storage in the distribution system.

The Army Corps of Engineers (USACOE), the operating entity of Black Butte Dam, receives water orders from OUWUA for the North and South Canal and regulates the flows downstream from the Black Butte Reservoir accordingly. OUWUA is generally restricted to two orders per day, one at 7 am and one at 1 pm during the irrigation season. Due to the inability to reduce Black Butte heading flows in the late afternoon or evening, water is sometimes spilled throughout the night when an irrigation “run” is finished, or when an irrigator is unable to take the water. Under certain conditions in dry years, OUWUA can petition for an additional water order change at 6 pm. This additional water order change helps to reduce spillage, but still leaves a substantial period throughout the night where delivery shutoffs result in system spillage.

This paper describes the regulating reservoir and lateral improvements design and construction, the reservoir operational procedures, and the water savings estimate developed using the verification modernization planning method.

### **REGULATING RESERVOIR AND LATERAL IMPROVEMENTS**

Thoreson and Massa (2009) describe the Feasibility Investigation utilizing verification-based modernization planning that selected Beat 2 for a regulating reservoir and associated lateral improvements with spillage reduction as the primary objective. Achieving spillage reduction while simultaneously improving, or at least maintaining, existing service levels requires an integrated lateral and reservoir control strategy. Flow changes must be passed down Lateral 210 to the reservoir and from the reservoir to the lateral spill, known as Beck’s Spill, without significantly changing delivery flows to growers and sublaterals along the way.

Six 2-bay long crested weirs (LCW), 14 single bay long crested weirs, one flap gate and one automated slide gate were constructed at existing check structures on Lateral 210 (Figure 2). These improved check structures were designed to maintain delivery flow rates to growers and sublaterals within plus/minus five percent when the passing flow rate changed plus or minus 12 cfs (one head). Automated overshot gates with flow measurement and the capability to remotely program flow changes were installed at the head of Lateral 210 and at the headings of sublaterals 220, 212, 230 and 214. Automated overshot gates were also installed at a flow control point in Lateral 210 at the reservoir inlet and at the two reservoir outlets.

The Beat 2 improvements incorporate elements of both localized and remote upstream and downstream control to effectively reduce spillage while improving delivery service. Automated system features are monitored and controlled through a Supervisory Control and Data Acquisition (SCADA) system that utilizes a spread-spectrum radio network to transfer critical data and commands. In addition to the main office control, the Beat 2 operator has a truck-mounted laptop that has complete access and control of all automated system features.

Achieving significant spillage reduction depends on developing a sound, integrated canal and reservoir control strategy. The reservoir was located approximately two-thirds of the

way down Lateral 210 so that sufficient irrigation demand remains downstream of the reservoir to effectively use the water re-regulated by the reservoir.

All LCWs along Lateral 210 are downstream-facing one or two bay convergent structures with removable stop logs at the downstream end for sediment flushing. Figure 3 shows a two-bay LCW during construction. The more constant upstream water levels resulting from new long crested weirs (Figure 4) have resulted in steadier delivery flows enhancing delivery service and facilitating improved on-farm water management. The LCWs also require fewer changes to check settings, thus simplifying operations.

Eight Rubicon FlumeGates (Figure 5) are located along Lateral 210 to provide flow rate control to sublaterals, while a Rubicon SlipGate is installed at one location where the canal transitions into a short length of buried pipeline. Because of the short distance to the closest upstream delivery, this compact undershot style gate utilizes an externally mounted acoustic water level sensor to enable automatic upstream water level control. The FlumeGates allow the ditch tender to make accurate flow changes and remotely program changes when needed. This is especially important at night. A flexible and efficient distribution system is only possible with accurate and readily available measurement and control over the inputs and outputs (total inflow and spill). Flow control into the Lateral 210 system is remotely automated through two parallel FlumeGates installed in a modified structure at its turnout on the South Canal.

Both styles of automated gates are powered by attached solar panels, and provide automated, local and remote control of the operation objective (level or flow control), and the set point (level or flow rate). Remote control and remote monitoring is available through the Association's SCADA system.

Orland Project Regulating Reservoir Construction

- |               |                      |                           |                                  |
|---------------|----------------------|---------------------------|----------------------------------|
| Reservoir     | Structures           | Flume Gate (C-3.3)        | Long Crested Weir, 2 Bay (C-3.5) |
| Beat 2 Canals | Automated Slide Gate | Flap Gate                 | Measurement Device               |
| Other Canals  | Broad Crested Weir   | Long Crested Weir (C-3.4) | No Improvement                   |
| Raise Banks   |                      |                           |                                  |

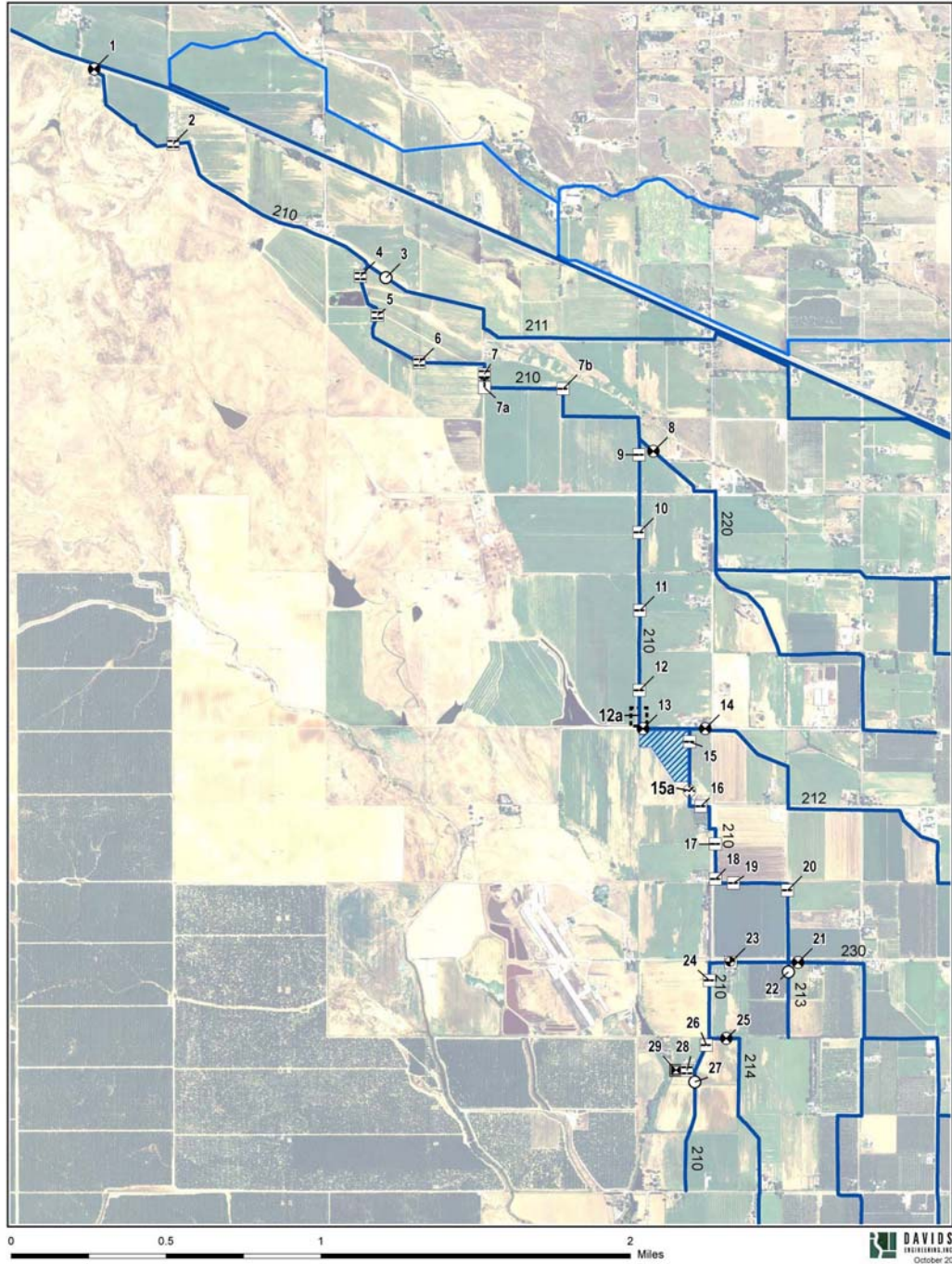


Figure 2. Beat 2 Improvements on Lateral 210.



Figure 3. Two-Bay Long-Crested Weir in Lateral 210 during Construction. Adjustable Boards Will Be Attached to Form the Weir Crest.



Figure 4. One-Bay Long-Crested Weir in Operation.



Figure 5. Automated Overshot Gate Installed at the Heading of Sub-Lateral 212.

One of the FlumeGates is positioned in Lateral 210 just downstream of the reservoir inlet weir to pass flow fluctuations to the reservoir and reregulate the passing flowrate for downstream deliveries. Flow rates in excess of the downstream demand pass over the side-spill weir and flow by gravity to the reservoir. The 35 foot weir length allows for the passing of a large flow rate with minimal change in head, thus minimizing the affects to upstream deliveries.

The regulating reservoir has a total capacity of 49.5 acre-feet with approximately 44 acre-feet of operational capacity and 5 acre-feet of dead storage. The earthen embankments are constructed to provide 2 feet of freeboard at maximum capacity. A reinforced concrete access ramp allows for periodic cleaning and maintenance of the reservoir floor. The reservoir side-slopes are lined with fiber-reinforced 3" thick concrete. Based on research by Burt, C.M., et.al. (2010) that showed reductions in canal seepage through compaction, the earthen floor was extensively compacted to a minimum of 95 percent of relative dry density to a depth of 1 foot in effort to minimize seepage. Post irrigation season ponding tests (conducted in October 2012) showed that reservoir seepage averaged 0.10 feet/day.

The reservoir (Figure 6) features a gravity flow inlet structure and two automated outlet gates that gravity discharge to Lateral 212 and Lateral 210. The Lateral 212 outlet provides another area where reservoir water can be used. This is important to ensure that the downstream demand on the reservoir is sufficient to use all the water re-regulated by the reservoir. The Lateral 210 outlet can be controlled automatically depending on the

spill sensed at Becks Spill. Becks Spill is located approximately 1.6 miles downstream from the reservoir and is the destination for all operational spillage in Lateral 210.



Figure 6. Regulating Reservoir with the Lateral 210 Outlet in Foreground, and Reservoir Inlet in Background.

At Becks Spill, a ramp flume measures spill flows after they have passed over the top of a long crested weir, located just upstream of the ramp flume. Water level measurements upstream of the LCW and flow rate measurements at the ramp flume serve as the spillage indicators for adjustment of reservoir discharges into Lateral 210 through a project-specific control algorithm.

The reservoir outlet gate to Lateral 210 is designed to adjust inflow into the portion of canal downstream of the reservoir in response to these spillage indicators. At a minimum, reservoir outflow will account for approximately 5 cubic feet per second (CFS) of the downstream water order so that, if spillage occurs, the canal flow can be reduced by adjusting the outlet gate. A target spillage rate of 2 CFS was initially set to ensure that no deliveries are being shorted. This target spillage rate will be reduced as operation experience is gained. If spill *flow* measured at the ramp flume is high, the reservoir outlet gate to Lateral 210 will decrease the inflow to the canal.

Additionally, the Beck's Spill controller is equipped with a timer that can be set to temporarily suspend the control logic from controlling the reservoir outlet gate and allow the operator to make outlet gate changes independent of spillage. The controller will reset to automated spillage control after the set delay time has elapsed.

The reservoir and the aforementioned canal improvements provide improved service levels in two ways: by providing additional deliveries outside of the normal rotation on

an arranged basis; and, by providing users the option of changing the quantity of ordered flows and durations within the normal rotation. There are two cases when providing additional deliveries outside of the normal rotation could benefit a farmer. Farming practices, for instance, hay drying, can preclude a grower from receiving water within the normal rotation. Current OUWUA policies encourage ditch tenders to “fit” the grower back into the rotation at the “earliest opportunity.” The grower may have to wait until the next rotation for delivery causing decreased crop productivity, or conversely, take two irrigation deliveries closely in time and resulting in over-irrigation—an inefficient use of water. Although Beat 2 will continue to operate primarily on a rotation schedule, reservoir storage will increase the opportunities to provide water to growers outside of the normal rotation. This flexibility allows the farmer to more closely match deliveries to demands and cultural practices of the crop, thereby increasing on-farm water utilization and facilitating improved on-farm water management.

The reservoir also provides growers with the ability to order flows and durations that are compatible with more efficient irrigation methods. Operations typically provide a set flow and duration based on acreage. This operations practice is most compatible with flood irrigation. The ability to provide more flexible flows and durations will ensure the OUWUA can continue to meet the service needs of those growers who switch from flood irrigation to drip or micro-spray to take advantage of the benefits provided by these irrigation technologies. Since the completion of the regulating reservoir, the additional flexibility has prompted several growers along the Lateral 210 system to install surface-water supplied pressurized irrigation systems. OUWUA has additionally facilitated this by allowing delivery structure modifications (Figure 7) that facilitate these on-farm improvements.



Figure 7. Modified delivery structure to allow pressurized on-farm system. A booster pump intake and a rotating self-cleaning filter will be installed in the pictured sump to supply a new orchard (beyond).

#### **WATER CONSERVATION ESTIMATE AND 2012 WATER CONSERVATION**

Following the verification-based modernization planning process and the Spillage Reduction and Monitoring Protocol (2007), a water balance was prepared and flow paths were targeted for conservation. These flow paths, in decreasing order of priority, are measured flows at Beck's Spill (location where spillage from Beat 2 is measured), unmeasured spillage from sublaterals and tailwater from irrigated lands. With the project, water that would have either spilled through Beck's spill or from sublaterals would be stored in the regulating reservoir. In addition, growers would be able to reduce tailwater by shutting off delivery when irrigation is complete, with the remaining unused water being conveyed to, and stored in, the reservoir.

The total spillage volumes for the 2005 and 2006 irrigation seasons at Beck's Spill were 2,900 and 2,600 acre-feet, respectively. Verification-based planning requires estimating the changes to the targeted flow paths. The 2006 pre-project record was considered representative of future spillage magnitudes if the project was not constructed, and thus assumed to be the without-project spillage volume. With-project spillage volumes were estimated using a spreadsheet model to simulate reservoir operations on a 15-minute time-step. The simulations indicated that the annual spillage volume at Beck's spill could be reduced by 1,871 acre-feet. During the 2012 irrigation season, the total volume spilled at Beck's Spill was 1,131 acre-feet. This is a measured spillage reduction of 1,469 (2,600 – 1,131).

Unrecorded spillage from sublaterals in the Beat 2 canal system was estimated to be 1,882 acre-feet. The reservoir and related automation was estimated to capture 945 acre-feet of this spillage. Based on an analysis of SCADA data, the remote flow rate changes on sublateral headings, made possible by the project, were estimated to reduce unrecorded spillage by 825 acre-feet.

On-farm water savings were expected to be modest, resulting from improved surface irrigation practices and from the more rapid conversion from surface irrigation to pressurized irrigation enabled by the reservoir. Together these effects were estimated to eventually, over a period of years, reduce tailwater by 661 acre-feet. By assuming an average one percent reduction of tailwater across the Beat 2 area, the with-project savings is 158 acre-feet.

The total estimated spillage and delivery reduction was 3,500 acre-feet. Evaporation and seepage losses from the reservoir must be deducted from the estimated spillage and delivery reduction. Deducting these losses and rounding to the nearest one hundred acre-feet leads to an expected project savings of 3,400 acre-feet (Table 2). Based on confidence intervals estimated for the OUWUA Beat 2 water balance, a 95 percent confidence interval of 30 percent is established for these savings (Clemmens and Burt 1997). This can be interpreted as being 95 percent confident that the project savings will fall between 2,380 and 4,420 acre-feet with an expected value of 3,400 acre-feet.

Based on the average seepage rate from seepage tests performed in April and October, seepage from the reservoir was estimated to be 394 acre-feet over the 2012 irrigation season. Due to siltation deposition over the irrigation season, the seepage rate in October was much less than the April seepage rate. Based on the October seepage test, seepage from the reservoir is estimated to be 150 AF of water due over a typical 180 day future irrigation season. After deducting the seepage "loss," or groundwater recharge, and evaporation from the conserved water, the actual 2012 irrigation season water conservation estimate is 2,100 acre-feet (Table 3). This water savings estimate is just below the lower end of the range of savings as defined by the confidence interval analysis. As operator proficiency with the new tools increases and growers become more aware of the possibilities, conservation is expected to increase in future years.

Table 2. Estimated Annual Average Project Water Conservation.

Targeted Flow Path	Without Project, (AF)	With-project, (AF)	Flow Path Reduction, (AF)	95% Confidence Interval
Spillage at Beck's Spill	2,600	729	1,871	7%
Unrecorded Spillage to irrigated lands	1,882	937	945	96%
Tailwater from irrigated lands	3,165	2,504	661	64%
Reduced Deliveries (Reservoir area)	23	0	23	10%
<b>Total Conserved Water</b>			3,500	25%
New Flow Paths with Reservoir				
Reservoir Evaporation	0	28	-28	30%
Reservoir Seepage	0	29	-29	50%
Reservoir Spillage	0	8	-8	10%
<b>Total New Flow Paths (Losses)</b>			-65	0%
<b>Total Conserved Water (Rounded to the nearest 100 acre-feet)</b>			3,400	30%

Table 3. Actual 2012 Project Water Conservation Estimate.

Targeted Flow Path	Flow Path Reduction, acre-feet	95% Confidence Interval
Spillage at Beck's Spill	1,469	12%
Unrecorded Spillage	825	5%
Tailwater from irrigated lands	161	96%
Reduced Deliveries (Reservoir area)	23	10%
<b>Total Conserved Water</b>	2,478	10%
New Flow Paths with Reservoir		
Reservoir Evaporation	-19	25%
Reservoir Seepage	-394	20%
<b>Total New Flow Paths (Losses)</b>	-413	19%
<b>Total Conserved Water (Rounded to the nearest 100 acre-feet)</b>	2,100	12%

### SUMMARY

A regulating reservoir and associated lateral improvements were constructed in OUWUA Beat 2 service area on Lateral 210. The improvements included a 49.5 acre-foot regulating reservoir, 20 LCWs, eight automated overshot gates, one flap gate, and one

automated slide gate. A verification-based modernization planning process estimated these improvements would save 3,400 acre-feet with a confidence interval of 30 percent. Grant funds were obtained and the regulating reservoir and associated lateral improvements were constructed. The 2012 irrigation season was the first year of operation with the regulating reservoir and associated lateral improvements. The first year of operation was expected to be a learning experience with the resulting water conservation expected to be less than estimated. Due to excessive spillage the first month of operation as the operator was adjusting to the tools available, the water conservation obtained through reduction of spillage at Beck's spill was about 300 acre-feet less than the estimate. The reduction in unrecorded spillage and tailwater was about 623 acre-feet less than the estimate. These savings are expected to increase as more growers learn to utilize the additional delivery flexibility provided. Also, as many growers will convert to drip/micro systems, on-farm tailwater reductions will increase. The total estimated savings was within the 95 percent confidence interval estimated.

### REFERENCES

- Burns, J.I., Davids, G.G., Dimmitt, A.K., and Keller, J. (2000). Verification-based Planning for Modernizing Irrigation Systems. Proceedings of the U.S. Committee on Irrigation and Drainage Conference on Irrigation and Drainage in the New Millennium. Denver, Colorado. 2000. pp. 51-63.
- Burt, C.M., Orvis, S. and Alexander, N. (2010). Canal seepage reduction by soil compaction *Journal of Irrigation and Drainage Engineering*. 136(7), 479-485.
- Clemmens, A.J. and Burt, C.M. (1997). Accuracy of Irrigation Efficiency Estimates. *Journal of Irrigation and Drainage Engineering*. 123(6), 443-453.
- Spillage Reduction Monitoring and Verification. (2007).  
[http://www.agwatercouncil.org/images/stories/monitoring\\_and\\_verification\\_spillage\\_reduction.pdf](http://www.agwatercouncil.org/images/stories/monitoring_and_verification_spillage_reduction.pdf)
- Thoreson, B.P. and Massa, R. (2009). Orland Unit Water Users Association Regulating Reservoir, an Example of Verification-Based Modernization Planning. U.S. Committee on Irrigation and Drainage Irrigation District Specialty Conference. Irrigation District Sustainability — Strategies to Meet the Challenges. Reno, Nevada June 3-6, 2009.

# DEVELOPMENT OF A WEB-BASED GIS MANAGEMENT SYSTEM FOR AGRICULTURAL AUTHORITIES IN IRAQ

Gabriele Bonaiti, Ph.D.<sup>1</sup>

Dave Flahive<sup>2</sup>

Guy Fipps, Ph.D., P.E.<sup>3</sup>

## ABSTRACT

A Geographic Information System (GIS) is a technological tool for comprehending geography and making decisions in any discipline. In agriculture, GIS is playing an increasing role by helping farmers increase production, reduce costs, and manage land and water more efficiently. In collaboration with USAID, Texas A&M University implemented a program aimed at providing direct support to the Ministry of Agriculture in implementing GIS as a data management and planning tool. Training was provided to personnel in GIS methods and procedures, and assistance offered in planning and implementing the overall GIS program.

Much of GIS implementation has to do with the proper construction of databases with required information structured in such a way to be compatible with GIS products. Therefore, technical assistance was provided in the construction and reformatting of databases. In addition, technical expertise was also provided to implement web-based GIS and data tools for internal use or presentation with the public.

In this paper we describe the phases of the work done, and some examples of the results obtained. In the first phase an assessment was conducted to develop a detailed work plan on the degree of technical assistance and training required. This assessment included elements such as goals and scope of project, GIS and database capabilities of Iraqi cooperators, software/hardware and internet resources available to cooperators, existing data and data organization. In a second phase, Iraqi cooperators and USAID personnel were involved in the implementation of the GIS. In this phase training was also provided in basic and advanced GIS, database software and data management, and use and maintenance of the completed GIS system.

---

<sup>1</sup> Extension Program Specialist, Department of Biological and Agricultural Engineering, 2117 Texas A&M University, College Station, Texas 77843-2117, [gbonaiti@ag.tamu.edu](mailto:gbonaiti@ag.tamu.edu)

<sup>2</sup> System Analyst, Department of Biological and Agricultural Engineering, 2117 Texas A&M University, College Station, Texas 77843-2117, [david@4honline.com](mailto:david@4honline.com)

<sup>3</sup> Professor and Extension Agricultural Engineer, Department of Biological and Agricultural Engineering, 2117 Texas A&M University, College Station, Texas 77843-2117, [g-fipps@tamu.edu](mailto:g-fipps@tamu.edu)

## INTRODUCTION

Texas A&M University assisted the Ministry of Agriculture, Iraq National Program for the preparation of Agro-ecological Zoning System maps Department (AEZ), to initiate an online GIS program. Training was provided to personnel as needed in GIS methods and procedures, and assistance was offered in planning and implementing the overall GIS program. Technical expertise was also provided to implement web-based products. The activity was part of the USAID-Inma Agribusiness Program, which is a comprehensive program funded by the United States Agency for International Development (USAID) to support the development of agribusinesses and agricultural markets in Iraq. Inma means "growth" in Arabic.

The objectives of the project were:

- Conduct a preliminary analysis of the current organization, and identify the goals and scope of project
- Provide training to Iraqi cooperators on basic GIS skills needed for project
- Work with Iraqi cooperators and Inma personnel on implementation of the GIS

Focus of current analysis was on GIS and database capabilities of Iraqi cooperators; software, hardware and internet resources available to cooperators; existing data and GIS available; database system including software and data organization; Web-based products needed.

## PRELIMINARY ANALYSIS

Several meetings at the USAID-INMA Monsur compound in Baghdad, and one visit at the AEZ office premises were organized to conduct an analysis of the current organization and to plan the activity. People participating to one or more meetings included all AEZ personnel, the local ESRI software provider Atlas GIS and Surveying System Company (Atlas), and Inma personnel.

The AEZ Department was constituted in 2010, with a crew of 15 people with various background (ex. Agronomist, Computer Science and Statistical, data entry and analysis responsibilities). Personnel had GIS experience ranging 3-7 years. Available data include land-use and land-cover classification maps, crop suitability maps, and temperature maps. Part of the GIS database and maps were created from a previous project that the Ministry of Agriculture carried out in 2005. AEZ current focus is to contribute improving management of water issues in Iraq, to identify soil salinity using satellite imagery, and to create land crop maps based on desertification.

The software utilized is Excel and ArcGIS version 9.3. Personal computers are not connected to a local network which would allow file sharing between computers; each person works independently. Back up of files is carried out monthly from each computer using a mobile external unit. A training room exists with several machines connected to a server with installed software such as ArcGIS Server 9.3 Advance Enterprise and Microsoft SQL Server 2005 Enterprise. The server is not currently in use.

The identified main interests are:

- Move to use of a real database (ex. SQL)
- Connect all computers
- Develop GIS advanced skills and image processing
- Create a website to be used for internal or public use

### TRAINING AND GIS IMPLEMENTATION

Based on the collected information a 3-weeks training was conducted on advanced GIS. Thirteen people from the Ministry of Agriculture in Baghdad were trained: 7 people from the AEZ Department, and 6 people from the Engineering Department/Department of Planning and Follow-up. The training program was agreed with AEZ personnel, and classes were taught by Atlas at their training center. Training was given in 4 components: advanced GIS, ArcGIS server, multiuser geodatabase, and image processing. The ESRI Arcgis server was identified as a key component of the training, considering also that it was already installed in their server. Some of the benefits of using ESRI Arcgis server are to allow sharing resources, like maps, and to access the GIS functionalities embedded in them. Trainees completed successfully all training, practiced on how to use also their own data, and showed interest on all classes.

A website called “AEZ-GIS Online” (<http://aez-gisonline.org/>) was set up to host an Iraqi Online GIS Demonstration. The demonstration includes data provided by the AEZ personnel on existing completed projects. Data was provided as SHP files and XLS files on: 1) Land use/Land cover maps for the Middle Tigris area, 2) monthly average temperature in Iraq for several years and meteorological stations, including interpolations for the entire Iraq territory, 3) Soil Suitability map for wheat in North Iraq, and 4) Soil Suitability map for wheat in Baghdad. All published information is currently hosted in our server in Texas, but can be at any time moved to the AEZ server, once it is functioning correctly. The website is organized in three components:

- The home web page, which welcomes to the “Iraqi Online GIS Demonstration” and lists the available “Project demonstration” for the online GIS mapping (Fig. 1)
- The “Esri ArcGIS Map Server” demonstration, which uses an Esri ArcGIS Map Server to directly publish the maps' SHP files into an online presentable format (Fig. 2). A possible fee-based use of these ArcGIS Map Server services is as ArcGIS Online Map, which provides several display and interactive features, including a choice of base maps (Fig. 3).

- The “Google Maps with KML overlay” demonstration, which uses Google Map API to overlay a KML export of the SHP files onto the Google map (Fig. 4 and 5). KML is an XML-based format used in Google map, and SHP files are converted into KML export using a tool from the ArcToolBox in ArcMap. The final export is KMZ, which is a compressed KML and which works as well in Google map. SHP files exported as KML/KMZ can be in any projection, and will be re-projected automatically in the Latitude/Longitude projection using the WGS 84 Auto datum.

In order to move toward a database management system, we provided and installed in the AEZ server the Cisco Firewall and one upgrade to ArcGIS Server Enterprise Advanced Up to Four Cores, version 10. Other preliminary steps were identified in collaboration with the AEZ personnel, including getting an IP address and setup a network among computers. For security reasons visits to the AEZ office were limited and working using a remote desktop was not possible; therefore at the end of the project the setup of the network and the construction of the database were not completed.

### CONCLUSIONS

The program provided a preliminary analysis of database and GIS capabilities at the Iraqi AEZ Department, together with a list of main interests. While GIS skills resulted fairly advanced, computers and database setup are basic and need improvement. Interviewed personnel agreed on this analysis, and expressed interest in specific GIS advanced training (image processing) and in opening a public website.

Training was an important part of the program, and was agreed with the AEZ Department and a local Esri software provider. All personnel involved in GIS analysis completed a 3-weeks advanced training successfully. The implementation component of our program included exchanging completed project data, creating a new “AEZ-GIS Online” website, and hosting several online GIS demonstrations using the collected data. To give a wider view of online GIS capabilities, we demonstrated two options, directly publishing SHP files with Esri ArcGIS Map Server, and overlaying KLM export of SHP files using Google Map API.

For security reasons it was organized only one visit to the AEZ office, and working using a remote desktop was not possible. Therefore some related activities were slowed down and in some cases not completed. Assisted by the local Esri software provider, we managed to provide and install a Cisco Firewall and an upgrade to ArcGIS Server Enterprise, but we could not setup the database and complete the ArcGIS Server registration. Online GIS services are therefore currently hosted in our server in Texas.

AEZ-GIS Online Project Demonstrations ▾

## Welcome to the Iraqi Online GIS Demonstration

We have demonstrated two different options available for the online GIS mapping. The first option is using ESRI ArcGIS Map Server to directly integrate the maps' SHP files into an online presentable format. The second option is using Google Map API to overlay a KML export of the SHP files onto the Google map.

[ESRI ArcGIS Map Server](#)  
[Google Maps with KML overlay](#)

© 2012 Iraq AEZ-GIS Project Contact Webmaster

Figure 1. Home web page welcoming to the “Iraqi Online GIS Demonstration” and listing the available “Project demonstration” for the online GIS mapping (<http://aez-gisonline.org/>)

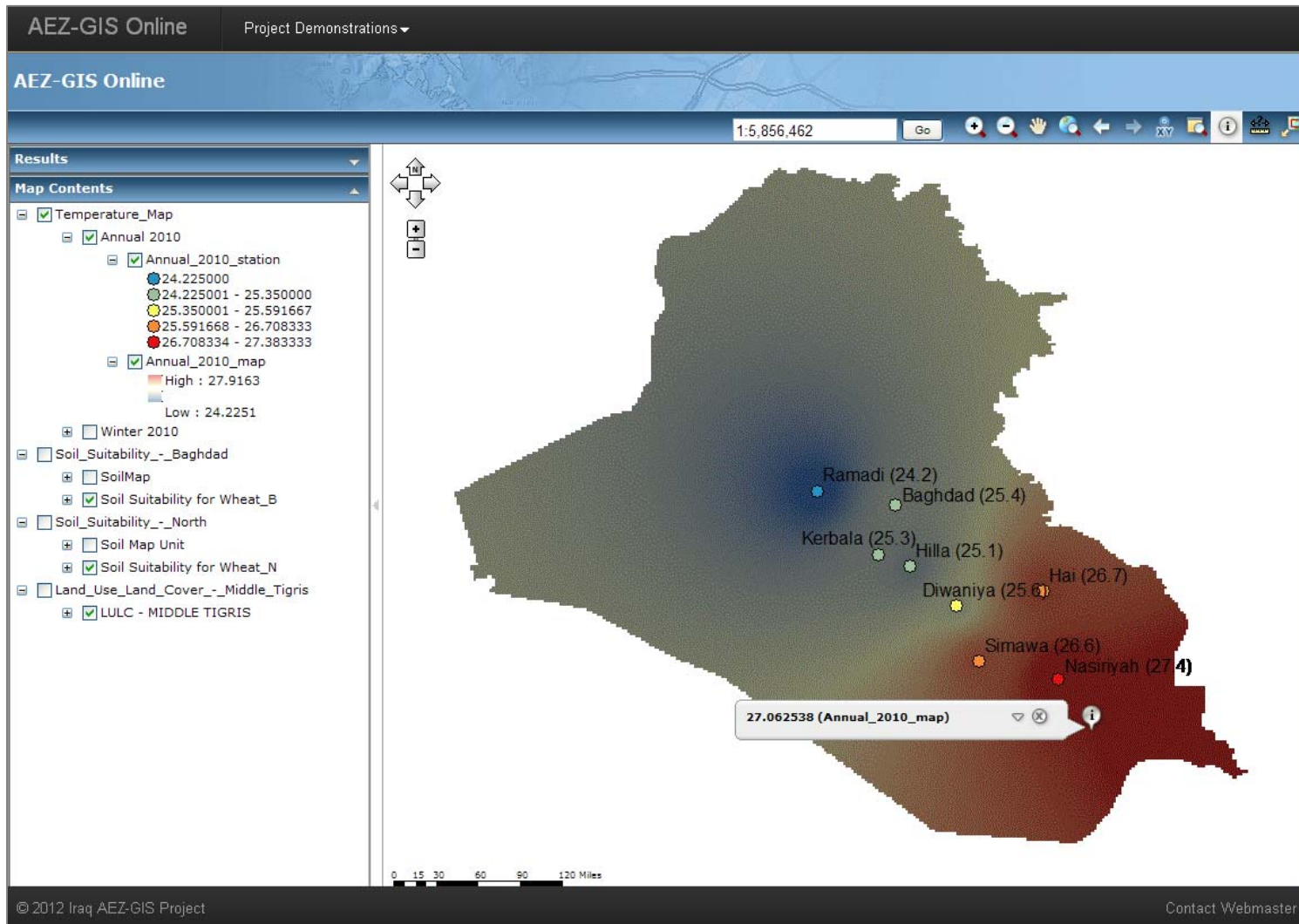


Figure 2. Esri ArcGIS Map Server demonstration. Web application showing the 2010 annual temperature average map service

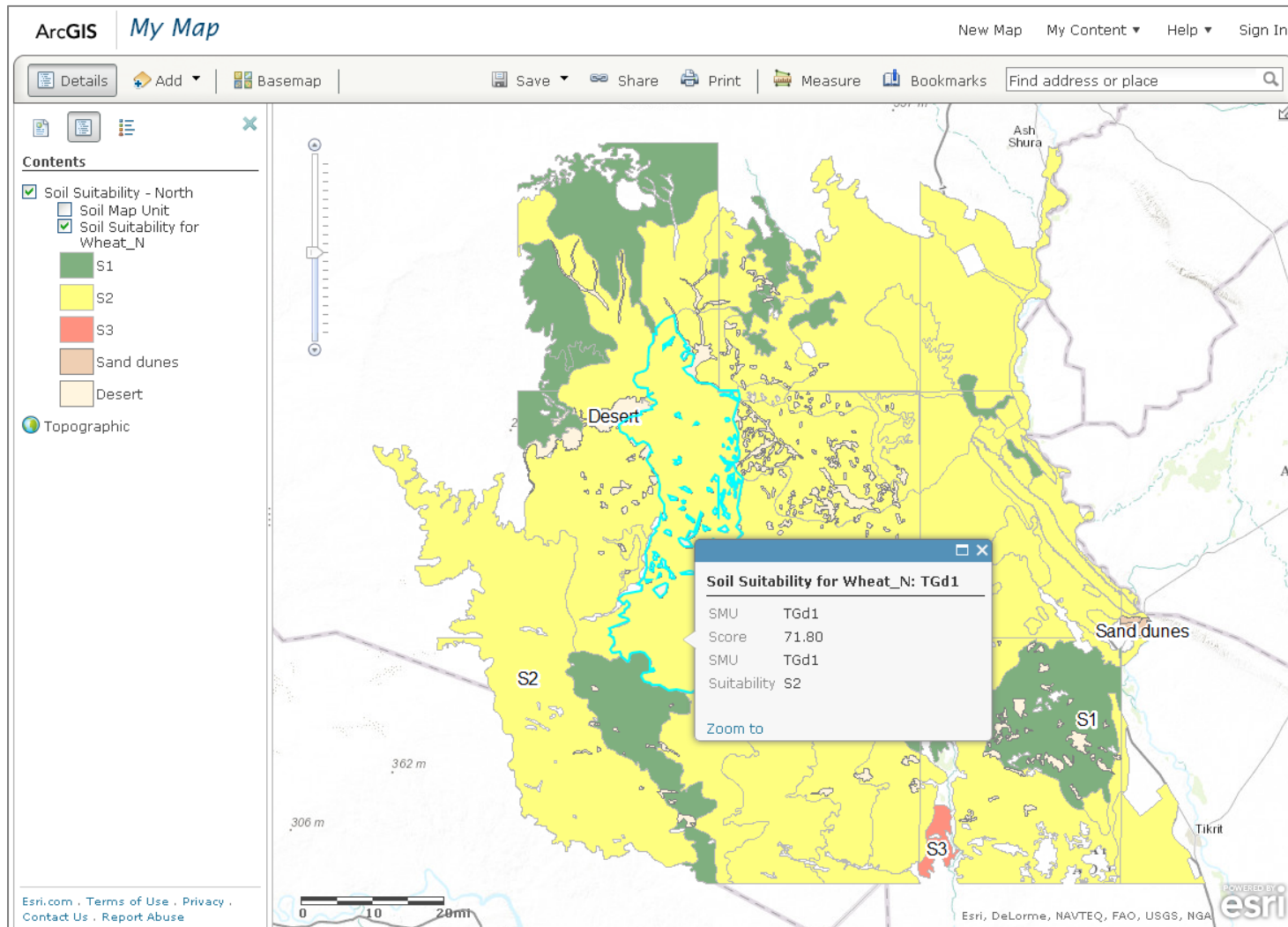


Figure 3. Proposed use of the Esri ArcGIS Map Server services as ArcGIS Online Map

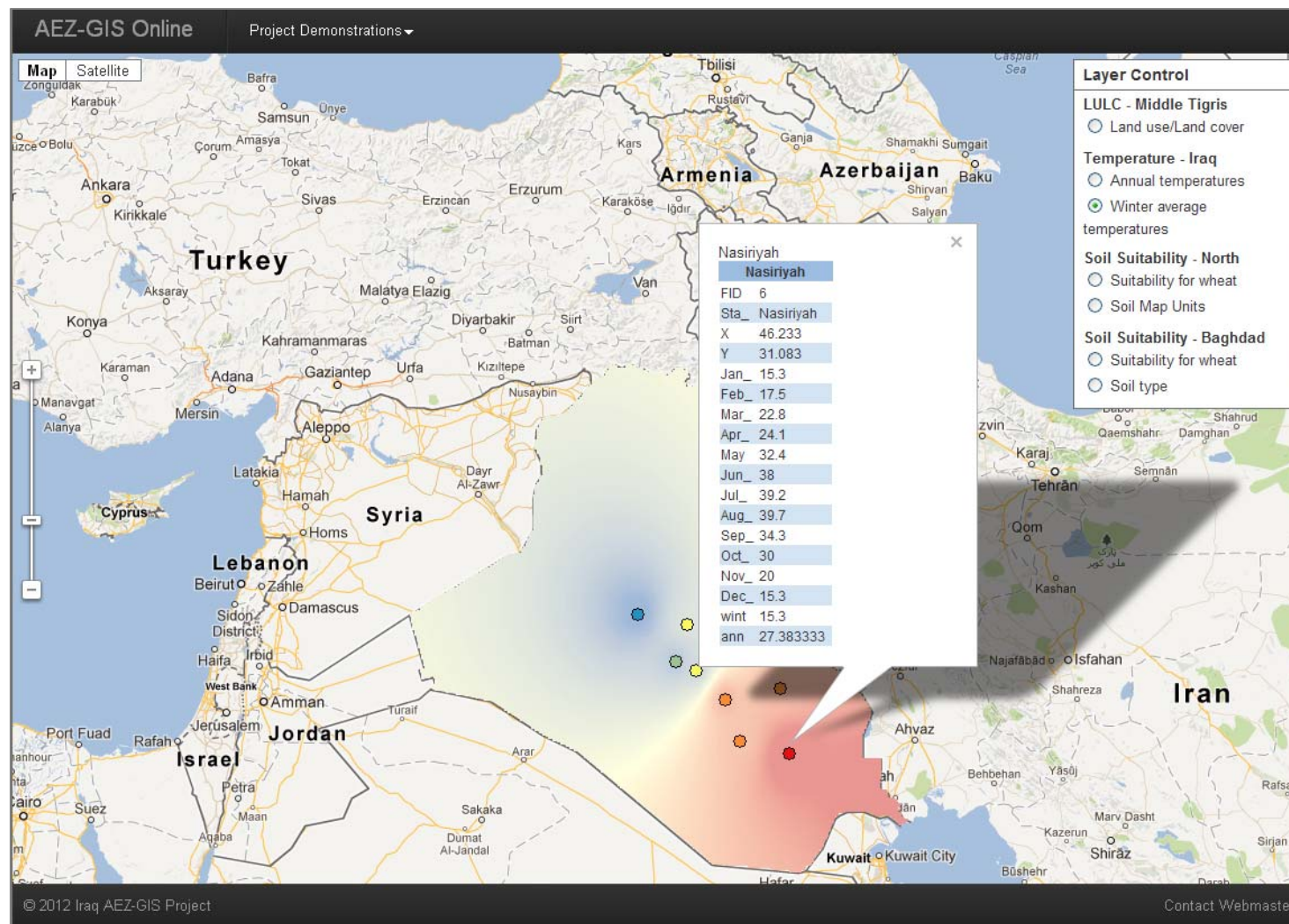


Figure 4. Google Maps with KML overlay demonstration. Layer showing the 2010 Winter average temperature map

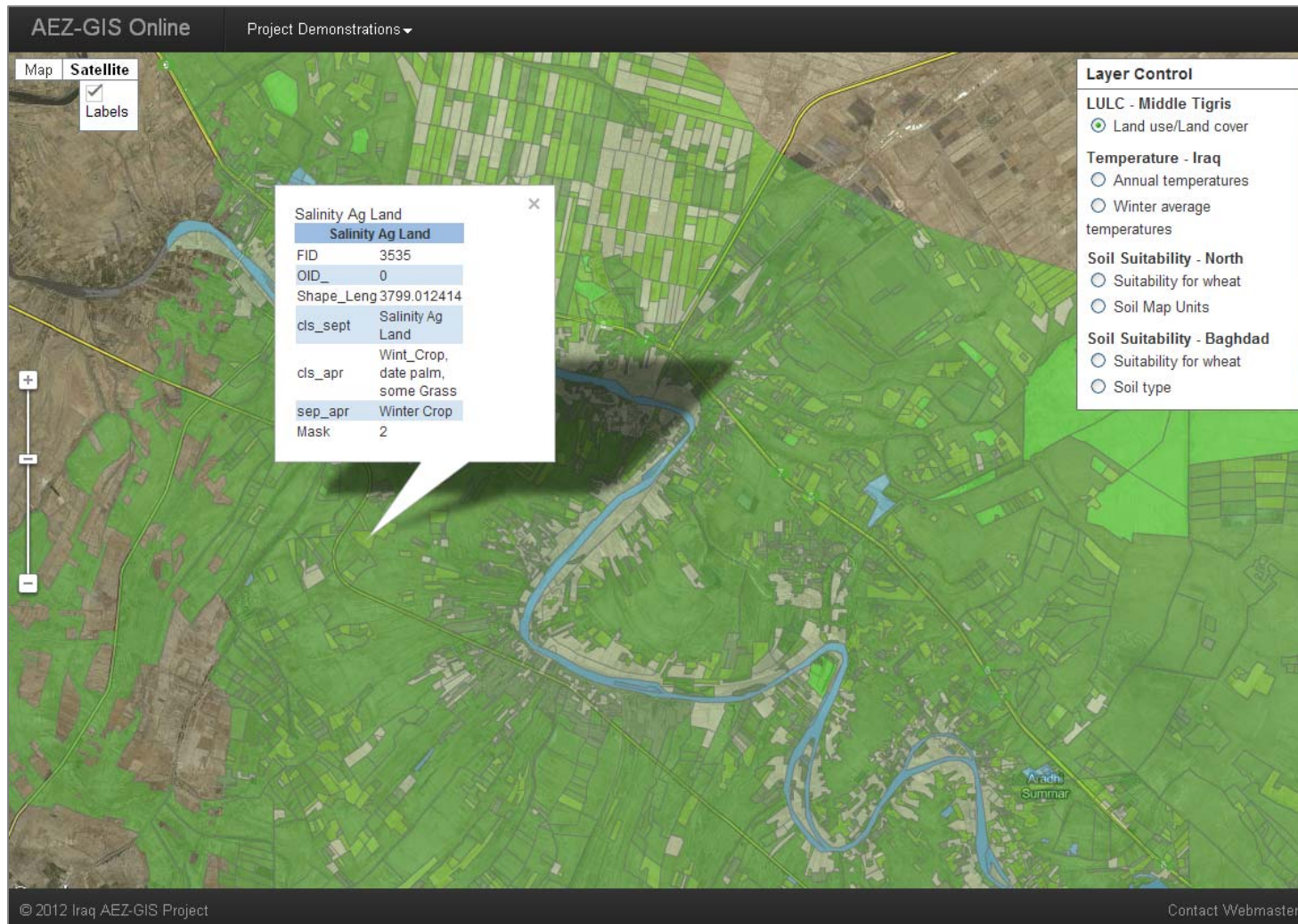


Figure 5. Google Maps with KML overlay demonstration. Layer showing the Land Use/Land Cover map created within the Middle Tigris Project



# **“SPOT” MEASUREMENTS OF FLOW RATE CAN BE “GOOD ENOUGH” FOR CALIFORNIA’S HEIGHTENING AGRICULTURAL MEASUREMENT REQUIREMENTS**

Jeffrey C. Davids, P.E.<sup>1</sup>  
Brandon A. Ertis, E.I.T.<sup>2</sup>  
Sean P. Early<sup>3</sup>  
Lewis E. Bair, P.E.<sup>4</sup>

## **ABSTRACT**

Gathering accurate farm-gate delivery measurement data in response to the Agricultural Water Measurement regulation, or California Code of Regulations Title 23 Section 597 (CCR 23 §597) is a challenging task for many of California’s agricultural water suppliers. Managing flow data for the purposes of (1) billing in part by volume and (2) providing aggregate reports to the State can be an equally onerous task. Additionally, many agricultural water purveyors are questioning if the cost of installing permanent measurement devices at each farm-gate is necessary to meet the volumetric accuracy requirements stated in CCR 23 §597.

In this paper, we briefly summarize the requirements of CCR 23 §597. An accuracy analysis performed in support of a laboratory volumetric accuracy certification for the RemoteTracker, as required by CCR 23 §597, is then presented. Embedded within the accuracy analysis is an examination of water level data from multiple irrigation districts located in California to assess the impacts of water level fluctuations on volumetric accuracy resulting from “spot” flow measurements (as opposed to continuously logging devices).

## **INTRODUCTION**

From an agricultural water purveyor’s perspective, the primary benefits of measurement at the farm turnout level are (1) the ability to precisely control and (2) accurately account for the amount of water being delivered to each customer. However, the cost<sup>5</sup> of fully implementing a measurement program on the farm turnout level by installing a permanent flow measurement device at every turnout in many cases outweighs the benefits. A method of decreasing costs in order to equalize the cost-benefit ratio is to find an alternative to installing a permanent flow measurement device at every farm

---

<sup>1</sup> H2oTech|RemoteTracker, 1771 Modoc Drive, Chico, CA 95928, (530) 588-3064, [jeff@h2otechonline.com](mailto:jeff@h2otechonline.com)

<sup>2</sup> H2oTech|RemoteTracker, 1771 Modoc Drive, Chico, CA 95928, (530) 588-3207, [brandon@h2otechonline.com](mailto:brandon@h2otechonline.com)

<sup>3</sup> Richvale Irrigation District, 1193 Richvale Highway, Richvale, CA 95974, (530) 882-4243 [rid@pulsarco.com](mailto:rid@pulsarco.com)

<sup>4</sup> Reclamation District No. 108, 975 Wilson Bend Road, Grimes, CA 95950, (530) 437-2221, [lbair@rd108.org](mailto:lbair@rd108.org)

<sup>5</sup> The use of cost here includes initial capital, operational and maintenance expenditures.

turnout. Aside from the case of flow automation of the farm turnout<sup>6</sup>, the control (i.e. flow setting) of the farm turnout (or gate) is accomplished manually by district staff. It is during this period of manually setting the gate that accurate flow measurement is required for precise flow control. In other words, accurate flow measurement on a manually controlled gate provides no benefit towards the control of deliveries, with the exception of when district personnel are on site (i.e. at the gate).

Therefore, if the first of the two primary benefits of measurement (i.e. flow setting) can be accomplished by “spot” measurements while the operator is on site, the discussion then becomes centered on whether “spot” flow measurements can provide accurate volumetric delivery data. This paper focuses on developing a volumetric accuracy analysis that shows that “spot” measurements with the RemoteTracker are sufficiently accurate for volumetric accounting, and more specifically, a laboratory certification in accordance with the requirements of California Code of Regulations Section 597 (CCR 23 §597). In order to lay the foundation for the accuracy analysis, we first present a summary of CCR 23 §597. We then provide an overview of the measurement principles of the RemoteTracker, and some initial results from field, laboratory and pilot testing.

### **CALIFORNIA CODE OF REGULATIONS SECTION 597 (CCR 23 §597)**

#### **General**

Senate Bill X7-7 (the “Water Conservation Act”) was enacted in November 2009, requiring all water suppliers to increase water use efficiency. Agricultural water suppliers with irrigated areas above 25,000 acres were mandated to prepare and adopt agricultural water management plans by December 31, 2012, and update those plans by December 31, 2015, and every 5 years thereafter. The Water Conservation Act included Water Code Section 10608.48(i)(1) directing the California Department of Water Resources to adopt regulations providing for a range of options that agricultural water suppliers may use to implement volumetric measurement of farm turnout (i.e. farm-gate or turnout) water deliveries. The resulting regulation, California Code of Regulations Title 23 Division 2 Chapter 5.1 Article 2 Section 597 et seq. (CCR 23 §597), requires that, on or before July 31, 2012, agricultural water suppliers subject to the law shall measure the volume of water delivered to customers with sufficient accuracy to:

- Enable reporting of aggregated farm turnout delivery data to the State; and
- Adopt a pricing structure based at least in part on the quantity of water delivered.

CCR 23 §597 requires that existing farm turnouts like those in the District have a measurement accuracy of  $\pm 12$  percent by volume, meaning that the measured volume of water delivered at each farm turnout must be no greater than 12 percent more, or 12 percent less, than the actual volume delivered. Additionally, any new or replacement measurement devices installed must be accurate to within:

---

<sup>6</sup> In most cases in the Western United States, cost prohibits flow automation of farm turnouts from being a viable option.

- $\pm 5$  percent by volume in the laboratory if using a laboratory certification;
- $\pm 10$  percent by volume in the field if using a non-laboratory certification

The regulation requires that an accuracy certification be performed by either: (1) field testing of a random and statistically representative sample of existing farm turnouts, (2) field inspections and analysis of every existing farm turnout, with the testing or inspections documented by a registered engineer, or (3) a laboratory certification.

## **REMOTETRACKER MEASUREMENT DEVICE**

### **System Overview**

The RemoteTracker is an integrated turnout flow measurement, data management and volumetric accounting system developed by H2oTech specifically for agricultural water suppliers. The RemoteTracker system is comprised of (1) a wirelessly controlled water velocity sensor, (2) a ruggedized tablet PC in the operator's vehicle and (3) a database running on a file server connected to the internet. The user interface on the tablet PC enables operators to view real time flow data from the wirelessly water velocity sensor (WWVS) via a Bluetooth radio connection while adjusting flows at the turnout gate. Data is automatically transferred over a wireless wide area network (WWAN) to a centralized file server at the district headquarters where it is automatically loaded into a custom database application. The database performs quality control and quality assurance procedures on the data and then develops daily volumes for each delivery point within the district.

The WWVS is held in place at a precise location at the pipe outlet by an aluminum or stainless steel mounting bracket. The user interface, shown in Figure 1, was designed with simplicity and ease of use in mind. If ‘Auto Locate’ is selected, the program automatically populates the three site identification pull-downs at the top of the screen. If the operator needs to select a different site, the pull-downs can be manually changed. The site selection hierarchy is a three digit abbreviation of ‘Operator Route’ (i.e. ride, beat or division) on the left, a three digit abbreviation of ‘Canal’ in the middle and site name on the right. The last measured flow and any pending orders are shown on the ‘Home’ tab. Many useful reports, including (1) Delivery History, (2) Pending Orders, (3) Fulfilled Orders and (4) Canal Management are available on the ‘Reports’ tab. These reports can be sorted at any spatial or temporal scale. The cloud based data management framework allows water order and delivery data collected by any operator to be automatically available for viewing by other operators or management staff in a matter of minutes.

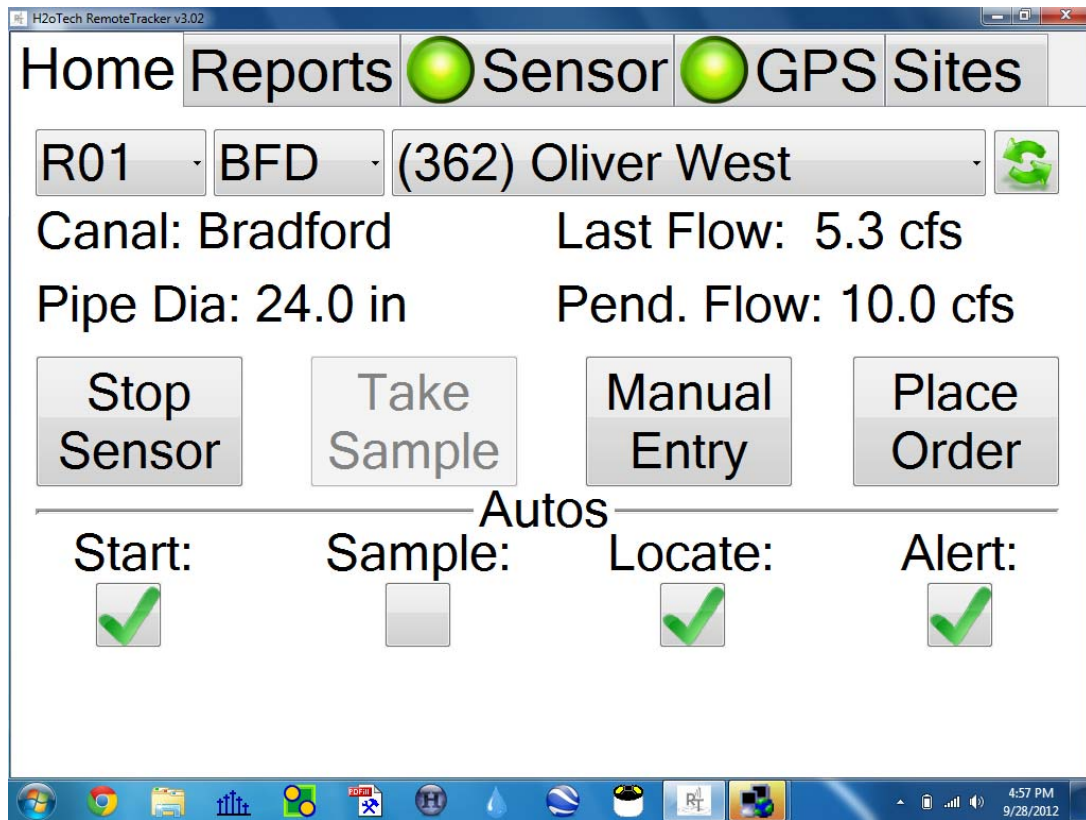


Figure 1. RemoteTracker User Interface - Home Tab Shown

Davids et al. (2012) provide a more detailed description of the RemoteTracker principles of operation, initial field verification, laboratory verification and district piloting results.

### REMOTETRACKER ACCURACY ANALYSIS FOR VOLUMETRIC CONVERSION

Accuracy mandates established by CCR 23 §597 apply to delivery volume and not instantaneous flow rate or velocity. CCR 23 §597.4(e)(3)(B) states, “For devices that measure velocity only, the documentation shall describe protocols associated with the measurement of the cross-sectional area of flow and duration of water delivery...”. This document provides descriptions of the protocols associated with the measurement of (1) average velocity, (2) cross-sectional area of flow and (3) duration of delivery, in addition to the corresponding accuracies associated with each measurement.

Because the RemoteTracker WWVS measures water velocity only, Equation 1 suggested in CCR 23 597.4(e)(3)(B) is used to calculate volume.

$$V = V * A * \Delta t \quad (1)$$

Where the variables are defined as:

- $V$ : Volume
- $V$ : Average Velocity
- $A$ : Cross-Section Flow Area
- $\Delta t$ : Duration of Delivery

This relative accuracy analysis assumes:

- 3 cubic foot per second (cfs) maintenance delivery
- A 24 inch inner diameter delivery pipe
- Normal distribution of measurement errors

A 3 cfs delivery was selected because it represents the lower range of agricultural water delivery rates and accuracy is harder to achieve at low flows. A 24 inch pipe is the average turnout pipe size within most agricultural districts. These assumptions lead to the listed variables having the values presented below.

- $V_{RT}$  = RemoteTracker Velocity Measurement = 1.00 ft/s
- $V_{Avg}^*$  = Average Velocity of the pipe at the time of the RemoteTracker spot measurement = 0.95 ft/s (determined by correlation with measured velocity; see Davids et al. 2012)
- $D$  = Pipe Diameter = 2.00 ft
- $A$  = Cross-Section Flow Area = 3.14 ft<sup>2</sup>

Based on the following analysis, the expected accuracy in volumetric measurements performed with the RemoteTracker system is ±4.6 percent.

Volumetric Accuracy. Analysis Overview. Volumetric accuracy of water deliveries consists of the accuracies in each of the following three components:

- Average Velocity ( $V_{Avg}$ )
- Cross-Section Flow Area ( $A$ )
- Duration of Delivery ( $\Delta t$ )

Assuming the input estimates to the three measured quantities above are uncorrelated, the total absolute accuracy is found using Equation 2 (NASA 2010 and NIST 2013).

$$\sigma_V = \pm \sqrt{\left(\frac{\partial V}{\partial V_{Avg}} \sigma_{V_{Avg}}\right)^2 + \left(\frac{\partial V}{\partial A} \sigma_A\right)^2 + \left(\frac{\partial V}{\partial \Delta t} \sigma_{\Delta t}\right)^2} \quad (2)$$

Where the variables are defined as:

- $V$ : Volume
- $V_{Avg}$ : Average Velocity
- $\Delta t$ : Duration of Delivery
- $\sigma$ : Absolute Accuracy (expressed in the units of the term in question)
- $U$ : Relative Accuracy (expressed as a percentage)

The total relative accuracy is:

$$U_V = \frac{\sigma_V}{V} = \pm \frac{1}{V} \sqrt{\left(\frac{\partial V}{\partial V_{Avg}} \sigma_{V_{Avg}}\right)^2 + \left(\frac{\partial V}{\partial A} \sigma_A\right)^2 + \left(\frac{\partial V}{\partial \Delta t} \sigma_{\Delta t}\right)^2} \quad (3)$$

$$U_V = \pm \sqrt{\frac{1}{V^2} \left( \left(\frac{\partial V}{\partial V_{Avg}} \sigma_{V_{Avg}}\right)^2 + \left(\frac{\partial V}{\partial A} \sigma_A\right)^2 + \left(\frac{\partial V}{\partial \Delta t} \sigma_{\Delta t}\right)^2 \right)}$$

Where the partial derivatives are:

$$\frac{\partial V}{\partial V_{Avg}} = A \Delta t, \quad \frac{\partial V}{\partial A} = V_{Avg} \Delta t, \quad \frac{\partial V}{\partial \Delta t} = V_{Avg} A$$

Substituting in the solutions to the partial derivatives:

$$U_V = \pm \sqrt{\frac{1}{V^2} \left( (A \Delta t \sigma_{V_{Avg}})^2 + (V_{Avg} \Delta t \sigma_A)^2 + (V_{Avg} A \sigma_{\Delta t})^2 \right)}$$

$$U_V = \pm \sqrt{\left(\frac{A \Delta t \sigma_{V_{Avg}}}{V}\right)^2 + \left(\frac{V_{Avg} \Delta t \sigma_A}{V}\right)^2 + \left(\frac{V_{Avg} A \sigma_{\Delta t}}{V}\right)^2}$$

$$U_V = \pm \sqrt{\left(\frac{\sigma_{V_{Avg}}}{V_{Avg}}\right)^2 + \left(\frac{\sigma_A}{A}\right)^2 + \left(\frac{\sigma_{\Delta t}}{\Delta t}\right)^2}$$

This becomes:

$$U_V = \pm \sqrt{(U_{V_{Avg}})^2 + (U_A)^2 + (U_{\Delta t})^2} \quad (4)$$

Based on Equation 4, the relative accuracies of Average Velocity, Cross-Section Flow Area, and Duration of Delivery are required. The following sections detail their determination.

Relative Accuracy in Velocity. The following bullet points provide protocols for the collection of water velocity data.

- The RemoteTracker WWVS will be deployed in the delivery pipe outfall so that the sample volume is located in the center of the delivery pipe
- Water velocities will be collected with the RemoteTracker WWVS at:
  - The start of all delivery events
  - After any changes in delivery events
- Shutoffs will be recorded on the RemoteTracker user interface with the “Record Shutoff” button at the time the gate is closed

The accuracies in average velocity consist of three parts:

1.  $\sigma_{V_{RT}}$ : Accuracy of RemoteTracker velocity measurements
2.  $\sigma_{V_{Avg}^*}$ : Accuracy due to the process of correlating RemoteTracker velocity measured at the pipe center and the average velocity of the pipe at the time of the RemoteTracker spot measurement<sup>7</sup>
3.  $\sigma_{\Delta V_T}$ : Accuracy due to the difference between the average velocity at the time of the RemoteTracker spot measurement and the actual average velocity for the duration of the delivery (i.e. change in velocity over time)

The average velocity relative accuracy is:

$$U_{V_{Avg}} = \pm \frac{\sigma_{V_{Avg}}}{V_{Avg}} \tag{5}$$

Where the variables are defined as:

- $V_{Avg}$ : Average Velocity
- $U_{V_{Avg}}$ : Relative Velocity Accuracy
- $\sigma_{V_{Avg}}$ : Absolute Velocity Accuracy

The average velocity of the entire irrigation event is the summation of the average velocity at the time of observation and the average change in velocity throughout the remainder of the event due to water level fluctuations.

---

<sup>7</sup> Average velocity at the time of the RemoteTracker spot measurement ( $V_{Avg}^*$ ) represents a snapshot of the average water velocity in a delivery pipe at the time of the RemoteTracker measurement.

$$V_{Avg} = V_{Avg} * + \Delta V_T \quad (6)$$

Where the variables are defined as:

- $V_{Avg}$ : Average Velocity
- $V_{Avg} *$ : Average Velocity at the time of the RemoteTracker spot measurement
- $\Delta V_T$ : Average Change in Velocity over time

Therefore:

$$\sigma_{V_{Avg}} = \pm \sqrt{\left(\frac{\partial V_{Avg}}{\partial V_{Avg} *} \sigma_{V_{Avg} *}\right)^2 + \left(\frac{\partial V_{Avg}}{\partial \Delta V_T} \sigma_{\Delta V_T}\right)^2} \quad (7)$$

Where the partial derivatives are:

$$\frac{\partial V_{Avg}}{\partial V_{Avg} *} = 1, \quad \frac{\partial V_{Avg}}{\partial \Delta V_T} = 1$$

Substituting in the solutions to the partial derivatives:

$$\sigma_{V_{Avg}} = \pm \sqrt{(\sigma_{V_{Avg} *})^2 + (\sigma_{\Delta V_T})^2} \quad (8)$$

The following subsections present (1) the accuracy of the RemoteTracker velocity measurements, (2) the accuracy of the average velocity at the time of the RemoteTracker spot measurements ( $\sigma_{V_{Avg} *}$ ) and (3) the accuracy in the change in average velocity over time ( $\sigma_{\Delta V_T}$ ).

### **Accuracy of Remote Tracker Velocity Measurement**

The RemoteTracker system uses a SonTek ADV for water velocity measurements. The SonTek ADV technical specifications sheet lists a velocity measurement error of 0.01 or 1.0% (SonTek 2006). Therefore,  $\sigma_{V_{RT}}$  is equal to 0.010 ft/s, or 1.0% of 1.00 ft/s ( $V_D$ ).

### **Accuracy of the Average Velocity at the Time of the RemoteTracker Spot Measurement**

The average velocity is computed as the product of the velocity measured by the RemoteTracker and the coefficient correlating the RemoteTracker velocity measurement to the average velocity at the time of the RemoteTracker spot measurement.

$$V_{Avg}^* = CV_{RT} \quad (9)$$

Where the variables are defined as:

- $V_{Avg}^*$ : Average velocity at the time of the RemoteTracker spot measurement
- $C$ : Coefficient correlating the RemoteTracker velocity measurement to the average velocity at the time of the RemoteTracker spot measurement, which is equal to 0.95 (Davids et al. 2012)
- $V_{RT}$ : RemoteTracker velocity measurement

Therefore:

$$\sigma_{V_{Avg}^*} = \pm \sqrt{\left(\frac{\partial V_{Avg}^*}{\partial C} \sigma_C\right)^2 + \left(\frac{\partial V_{Avg}^*}{\partial V_{RT}} \sigma_{V_{RT}}\right)^2} \quad (10)$$

Where the partial derivatives are:

$$\frac{\partial V_{Avg}^*}{\partial C} = V_{RT}, \frac{\partial V_{Avg}^*}{\partial V_{RT}} = C$$

Substituting in the solutions to the partial derivatives:

$$\sigma_{V_{Avg}^*} = \pm \sqrt{(V_{RT} \sigma_C)^2 + (C \sigma_{V_{RT}})^2} \quad (11)$$

Based on water velocity data collected, the average error introduced by converting the RemoteTracker velocity measurement to the average velocity at the time of the RemoteTracker spot measurement ( $\sigma_C$ ) is 0.014 or 1.4%.

Inserting the determined values into Equation 11:

$$\sigma_{V_{Avg}^*} = \pm \sqrt{(1.0 * 0.014)^2 + (0.95 * 0.010)^2} = \pm 0.017 \text{ ft/s}$$

**Accuracy of the Change in Velocity over Time (Impact of Canal Water Level Fluctuation on Volumetric Measurement Accuracy)**

A Microsoft Access database was developed to assess the accuracy in the change in velocity over time based on nearly one million real water level records from 27 different sites from multiple irrigation districts spanning five irrigation seasons. Based on the orifice equation, the change in velocity through an orifice is solely a function of changes in head (or difference between upstream and downstream water level). Only water level data from the typical irrigation season (i.e. May through August) was used. It was assumed that measurements of head were performed every three days.

The difference between the head observed every three days and the actual average of the 15 minute data during the three day period was computed for each 15 minute record and then averaged over the reporting period (i.e. one month). Equation 16 was used to calculate the change in velocity over time ( $\Delta V_T$ ) for each three day period. The initial observed head ( $h_*$ ) was assumed to be 0.5 feet to simulate a low head delivery. A low head was chosen because water level fluctuations impact the velocity of low head deliveries more significantly than high head deliveries.

Rearranging Equation 6:

$$\Delta V_T = V_{Avg} - V_{Avg} * \quad (12)$$

From the orifice equation (King 1963):

$$V = C(2gh)^{0.5} \quad (13)$$

Where the variables are defined as:

- $V$ : Velocity
- $C$ : Discharge Coefficient
- $g$ : Gravitational Constant
- $h$ : Head

Orifice gates in most agricultural water districts operate under submerged conditions (i.e. not free flow conditions). As upstream canal water levels fluctuate, the flow through the orifice would theoretically vary as a function of the changes in canal water level to the one-half power. However, since the orifice gates are submerged, the hydraulically connected downstream water level also varies together with the upstream canal water level. This provides a damping effect on the overall change in velocity due to upstream water level fluctuations. The California Polytechnic State University at San Luis Obispo Irrigation Training and Research Center (ITRC) suggest using a power of 0.38 in the orifice equation to simulate the damping effect of submergence for a range of downstream channel conditions (Burt and Geer 2012).

$$V = C(2gh)^{0.38} \quad (14)$$

Substituting values:

$$\Delta V_T = C(2gh_{avg})^{0.38} - C(2gh_*)^{0.38} \quad (15)$$

Where the variables are defined as:

- $h_{avg}$ : Average Head
- $h_*$ : Initial Observed Head

Factoring:

$$\Delta V_T = C(2g)^{0.38}((h_{avg})^{0.38} - (h_*)^{0.38})$$

Substituting values:

$$\Delta V_T = C(2g)^{0.38}((h_* + \Delta h_{avg})^{0.38} - (h_*)^{0.38}) \tag{16}$$

Where the variables are defined as:

- $\Delta h_{avg}$  = average change in head

Since the volumetric reporting mandates apply to a monthly or bi-monthly basis (California Water Code §531.10(a)), the change in velocity over time was then averaged on a monthly time step. The average of the absolute values of each of the average monthly changes in velocity over time was taken across all 27 sites. Largely due to the fact that water level fluctuations are normally distributed, the results of the hydraulic database model suggest that the average change in velocity over time due to water level fluctuation is:

$$\sigma_{\Delta V_T} = \pm 0.031 \text{ ft/s}$$

Inserting the calculated values into Equation A-8, the average velocity accuracy is:

$$\sigma_{V_{Avg}} = \pm \sqrt{(0.017)^2 + (0.031)^2} = 0.035 \text{ ft/s}$$

The relative accuracy of the average velocity is:

$$U_{V_{Avg}} = \pm \frac{\sigma_{V_{Avg}}}{V_{Avg}} = \pm \frac{0.035 \text{ ft/s}}{0.95 \text{ ft/s}} = \pm 0.037 \text{ or } 3.7\%$$

**Relative Accuracy in Cross-Section Flow Area**

The following bullet points provide protocols for the collection of cross-section flow area data.

- The cross-section flow area will be calculated by measuring the inner diameter of the delivery pipe at the location of the water velocity measurement and using Equation 18 to calculate area from inner diameter
- Inner pipe diameters will be measured with best professional practices when the pipe is dry

The accuracy in the inner pipe diameter measurement is assumed to be 0.02 feet (or 1/4 inch). The relative accuracy due to area is:

$$U_A = \pm \frac{\sigma_A}{A} \quad (17)$$

The correlation between diameter and area is:

$$A = \frac{\pi D^2}{4} \quad (18)$$

Where the variables are defined as:

- A: Cross-Section Flow Area
- $\pi$ : Pi
- D: Inner Diameter

The accuracy is:

$$\sigma_A = \pm \sqrt{\left(\frac{\partial A}{\partial D} \sigma_D\right)^2} \quad (19)$$

Where the partial derivative is equal to:

$$\frac{\partial A}{\partial D} = \frac{2\pi D}{4} = \frac{\pi D}{2}$$

The assumed pipe is 2.00 feet (24 inch) in diameter, giving an area of 3.142 ft<sup>2</sup>

$$\sigma_A = \pm \sqrt{\left(\frac{\partial A}{\partial D} \sigma_D\right)^2} = \sqrt{\left(\frac{\pi D}{2} 0.02\right)^2} = \sqrt{\left(\frac{\pi^2}{2} 0.02\right)^2} = \pm 0.063 \text{ ft}$$

The relative accuracy in the cross-section flow area is:

$$U_A = \pm \frac{\sigma_A}{A} = \pm \frac{0.063 \text{ ft}}{3.142 \text{ ft}} = \pm 0.020 \text{ or } 2.0\%$$

### **Relative Accuracy in Duration of Delivery**

The following bullet points provide protocols for the collection of duration of delivery data.

- The start time for delivery will be the date and time recorded in the RemoteTracker system when a velocity measurement is taken at the start of a delivery
- The stop time for delivery will be the date and time recorded in the RemoteTracker system when either:
  - “Record Shutoff” is pressed after a gate is closed at the end of a delivery
  - or

- A new velocity measurement is taken after a change in delivery flow rate is made

A conservative value for the duration of an irrigation event is assumed to be a period of 24 hours. The possible accuracy in duration measurement is considered to be 15 minutes for the startup and 15 minutes for the shutoff (or 0.25 hours for both). Realistically, the actual accuracy in duration is much smaller when using the RemoteTracker system since the operator is recording water velocity data on site when gate position changes are made. The relative accuracy due to duration of delivery is:

$$U_{\Delta t} = \pm \frac{\sigma_{\Delta t}}{\Delta t} \tag{20}$$

Where:

$$\Delta t = Et - St \tag{21}$$

Where the variables are defined as:

- $\Delta t$ : Duration of Delivery
- $St$ : Start Time
- $Et$ : End Time

The accuracy of the Duration of Delivery is:

$$\sigma_{\Delta t} = \pm \sqrt{\left(\frac{\partial \Delta t}{\partial St} \sigma_{St}\right)^2 + \left(\frac{\partial \Delta t}{\partial Et} \sigma_{Et}\right)^2} \tag{22}$$

Where the partial derivatives are equal to:

$$\frac{\partial \Delta t}{\partial St} = 1, \frac{\partial \Delta t}{\partial Et} = 1$$

$$\sigma_{\Delta t} = \pm \sqrt{(\sigma_{St})^2 + (\sigma_{Et})^2} = \sqrt{(0.25)^2 + (0.25)^2} = 0.35 \text{ hrs}$$

The relative accuracy in the duration of delivery is:

$$U_{\Delta t} = \pm \frac{\sigma_{\Delta t}}{\Delta t} = \pm \frac{0.35}{24} = \pm 0.015 \text{ or } 1.5\%$$

**Relative Accuracy in Volume**

As previously stated this relative accuracy assumes a 3 cfs maintenance delivery in a 24” pipe. Inserting the calculated relative accuracy value for each component into Equation 4, the relative accuracy is as follows:

$$U_V = \pm \sqrt{(U_{V_{Avg}})^2 + (U_A)^2 + (U_{\Delta t})^2}$$

$$U_V = \pm \sqrt{(.037)^2 + (.020)^2 + (.015)^2}$$

$U_V = \pm 0.045 \text{ or } \pm 4.5\%$
---

Based on the foregoing analysis and the resulting  $\pm 4.5\%$  accuracy in delivery volume determined for the RemoteTracker, the RemoteTracker complies with the  $\pm 5.0\%$  accuracy mandate in CCR 23 §597 for laboratory certification.

### CONCLUSION

The primary benefits of measurement at the farm turnout level are (1) the ability to precisely control and (2) accurately account for the amount of water being delivered to each customer. From the perspective of controlling delivery flow rates, accurate flow measurement on manually controlled gates is only utilized when district personnel are on site (i.e. at the gate). The volumetric accuracy analysis presented above suggests that the RemoteTracker complies with the  $\pm 5.0\%$  accuracy requirements in CCR 23 §597 for laboratory based accuracy certification. Analysis of water level fluctuations within this paper supports the conclusion of Burt and Geer (2012) that “the seasonal impact of fluctuating canal water levels is likely 0.0%, for all practical purposes.” Therefore, “spot” measurements of flow rate can be “good enough” for California’s heightening agricultural measurement requirements.

Initial field testing, laboratory testing and District piloting indicates that the RemoteTracker is technically viable and offers certain advantages relative to other measurement options. Based on the evidence provided herein, and the overall operational benefits realized by District operators, Reclamation District No. 108, Richvale Irrigation District and Biggs-West Gridley Water District have selected the RemoteTracker device to achieve the measurement accuracy standards of CCR 23 §597. The RemoteTracker’s advantages include:

- Accurate flow measurement during the period of setting or adjusting delivery flow rates
- Volumetric measurement accuracy sufficient for the laboratory certification requirements of CCR 23 §597
- Lower overall implementation costs than measurement methods requiring permanent devices at each delivery point
- No need for individual site calibration (but individual site configuration brackets are required)
- Simple measurement procedure requiring minimal staff training
- Automated data logging
- Automated transfer of data to centralized data server
- Feedback of delivery history to operators

- Orders management capabilities
- Can be integrated with automated water accounting and billing processes

### REFERENCES

Burt, C.M. and E. Geer “SBx7 Flow Rate Measurement Compliance for Agricultural Irrigation Districts,” Irrigation Training & Research Center, California Polytechnic State University, San Luis Obispo, California, 2012.

Dauids, J.C., G.G. Davids, L.E. Bair and E.A. Miller, “Creative, Accurate, and Cost-Effective Farm Gate Delivery Measurement Approaches,” United States Committee on Irrigation and Drainage Fall Conference Proceedings, 2012.

King, H.W. “Handbook of Hydraulics,” McGraw-Hill Book, New York, NY, 1963.

National Aeronautics and Space Administration (NASA), “Measurement Uncertainty Analysis Principles and Methods, NASA Measurement Quality Assurance Handbook - ANNEX 3,” <http://www.hq.nasa.gov/office/codeq/doctree/NHBK873919-3.pdf> 2010.

National Institute of Standards and Technology, “The NIST Reference on Constants, Units and Uncertainty - Uncertainty of Measurement Results,” <http://physics.nist.gov/cuu/Uncertainty/combination.html> , 2013.

Rantz, S.E. “Measurement and Computation of Streamflow,” U.S. Geological Survey Water Supply Paper 2175. U.S. Government Printing Office, Washington, DC, 1982. (Also available at <http://pubs.usgs.gov/wsp/wsp2175/>)

Thiede, M.V. and J.C. Davids, “Evaluation of Weir Boxes and Orifice Gates for Farm-Gate Delivery Measurement,” United States Committee on Irrigation and Drainage Fall Conference Proceedings, 2012.



# **COLORADO EXPERIENCE WITH DISCHARGE MEASUREMENTS AT PARSHALL FLUMES AND ASSESSMENT OF PARSHALL FLUME PERFORMANCE**

T. Ley, R. Stroud, B. Tyner, S. Veneman, G. Thrush, C. Bruner, D. Meyer, B. Boughton, L. Cunning, P. Tyler, M. Wild, B. Erosky, D. Ridnour, T. Arnett, M. Rusch, A. Gutierrez, C. Hart, G. Markus, S. Ditmars, L. Conner, J. Jaminet, A. Taillacq, J. Miller, B. Leavesley, P. DeArcos, D. Hutchens<sup>1</sup>

## **ABSTRACT**

The collective experience of the Colorado Division of Water Resources (CDWR) Hydrographic and Satellite Monitoring Branch with operational performance of Parshall flumes installed across Colorado during the last 10-12 years is summarized. Hundreds of discharge measurements have been made at Parshall flumes, ranging in size from 6-inch to 40-ft throat widths during this period. The purpose of these measurements is to continually assess Parshall flume measurement performance in order to provide accurate discharge data for water rights administration. Discharge measurements, along with systematic assessment of flume levelness, flow approach and exit conditions at the flume installation, and other factors, provide quantifiable checks on flume stage-discharge relationship (rating) performance. Causes of any significant departures of measured flow from the flume rating indicated flow and solutions for improved flow accuracy are presented. Several special case studies of flume performance issues are discussed.

## **BACKGROUND**

Colorado water law is based on the concept of “first in time, first in right”. As mining went through its boom and bust cycles in the mid to late 19<sup>th</sup> century, homesteading and development of agriculture followed closely behind. Prior to Colorado statehood in 1876, territorial laws were enacted allowing water to be taken from streams and rivers to lands “not adjoining the waterway”, as well as recognition of rights of way to transport water across lands not owned by the owners of the water right.

The Colorado Doctrine, or the Doctrine of Prior Appropriation, recognizes: a) those that put the water to use first are entitled to get their water first during periods of water shortage, and b) water is a separate property right that can be sold separately from the land. This is opposed to the Riparian Doctrine that ties water use rights to the ownership of lands adjacent to the river or stream. The codification of fundamental Colorado water law is found in Colorado’s 1876 Constitution, Article XVI, Sections 5, 6 and 7. These basically state: water within the State of Colorado is a public resource belonging to the citizens of the State; the right is recognized to divert unappropriated waters of any natural

---

<sup>1</sup> The authors are all employees of the Colorado Division of Water Resources (CDWR) Hydrography and Satellite Monitoring Branch.

Corresponding author: Thomas W. Ley, PhD, PE, Chief, Hydrography and Satellite Monitoring Branch, Colorado Division of Water Resources, 310 E. Abriendo, Suite B, Pueblo CO, 81004.

[thomas.ley@state.co.us](mailto:thomas.ley@state.co.us)

stream and apply that water to beneficial use with priority of appropriation determining who gets water first in times of shortage; and, the right is recognized to convey water across public, private and corporate lands upon payment of just compensation. In 1879, the Colorado legislature created a part of Colorado's present water administration system. It provided for the division of the State into ten water districts, nine of these in the South Platte valley and one in the Arkansas. The position of water commissioner was created with this legislation for the express purpose of allocating and distributing water according to the doctrine of prior appropriation. In 1881, the Colorado legislature established the Office of the State Hydraulic Engineer. The purpose of this office was to assist in carrying out the provisions of certain portions of the irrigation laws passed at the same session, and to obtain important information by means of surveys and observations. Primary responsibility was the administration of water rights according to the prior appropriation doctrine, by maintaining a list of water rights, on each stream, in order of priority. The priority of a water right is determined by both when the water was first diverted and put to a beneficial use and when the right was decreed by the district court. Additionally, the State Engineer (among other duties): *"shall make, or cause to be made, careful measurements and calculations of the maximum and minimum flow in cubic feet per second, of water in each stream from which water shall be drawn for irrigation, as may be best for affording information for irrigating purposes; commencing with those streams most used for irrigation..."*.

These two early pieces of legislation formed the basis of the system of water administration still in use today: measurements of the amount of water in rivers and streams over time provide the data needed and used by water commissioners to administer water rights according to the State's Constitution. In 1883, Colorado's second State Engineer, E.S. Nettleton, designed and developed the Colorado Current Meter, cups or vanes rotating in a horizontal plane around a vertical axis, the speed of rotation of which could be directly related to the velocity of water impinging on the vanes. This advance greatly improved the ability to accurately measure stream discharge, and the design is the basis of the Price AA current meter still widely used today. In 1884, Nettleton designed and developed a stream stage recorder for use at stream gage stations to collect continuous records of stream stage, which could be used to compute records of streamflow. The State Engineer's Office established some of Colorado's earliest stream gage stations during this period: Cache la Poudre at the Canyon Mouth (1881) and actually the oldest continuous operational streamgage in the US; Arkansas River at Canon City (1888); and, Rio Grande near Del Norte (1889); All are still operated by the CDWR.

More recently, in 1969, the State legislature passed the Colorado Water Rights Determination and Administration Act. This legislation created the Colorado Division of Water Resources (CDWR) as part of the Department of Natural Resources. The State Engineer's Office was incorporated as the CDWR. CDWR is empowered to administer all surface and ground water rights throughout the state and ensure that water is administered according the State Constitution, court decrees and well permits. CDWR employs approximately 280 professional engineers, geologists, hydrologists, information technology professionals, technicians, and support staff to administer water rights, to

evaluate and issue water well permits, monitor stream flow and water use, inspect dams and wells for construction and safety, maintain databases of Colorado water information, represent Colorado in interstate water compact proceedings, evaluate impacts of and necessary mitigation for various water use activities, educate the public, and numerous other responsibilities.

Significant development has transpired over the 137 years since Colorado became a State, including development of major urban centers (particularly on the Front Range), economic development, and agricultural development. Interstate compacts and agreements were developed describing how water, which has its source in Colorado, would be shared with downstream States. By the later decades of the 20<sup>th</sup> century, heavy stress on Colorado's limited water supply and on administration of that water supply was being experienced. Population growth has resulted in greater domestic demand for both surface and ground water. Increasingly complex water court decrees, augmentation plans, exchanges, etc. have been developed and executed. Colorado water administrators are experiencing greater and greater need for timely and accurate water resources data at more and more locations statewide.

### **THE CDWR HYDROGRAPHY AND SATELLITE MONITORING BRANCH**

The Colorado State Engineer has general supervisory control over measurement, record-keeping, and distribution of the public waters of the State. Within CDWR, the State Engineer charges the Hydrography and Satellite Monitoring Branch with streamflow measurement and monitoring responsibility. This involves the collection and dissemination of accurate, high quality 'real-time' surface water (stream and reservoir) data to support the water rights administration mission of the agency. The Branch currently operates and maintains over 530 satellite-telemetered gage stations throughout Colorado, and coordinates with the USGS, and other State and Federal agencies that operate approximately an additional 390 gage stations in the State. Primary objectives of this work are: 1) to conduct streamflow measurements at streamgaging sites along the State's natural rivers and creeks, and at major ditch and canal diversions, and, 2) to operate and maintain a water resources data collection (at key gage stations) and telemetry system to provide accurate near real-time water supply data to water administration decision makers. This latter effort is known as the Colorado Satellite-Linked Water Resources Monitoring System (SMS) and is fully described by Ley et al. (2010). Water level (stage) sensing and satellite telemetry equipment at gages on the network are visited on a regular basis. Stage sensor calibration checks are made to ensure accurate data, and equipment is checked to help minimize operational downtime and missing data. Flow measurements are performed on rivers, streams, creeks, major ditch and canal diversions to maintain accurate stage-discharge relationships at the gage station sites.

The CDWR Hydrographic Program employs standard operating procedures used for streamflow measurement; gage station design, construction, operation and maintenance; and streamflow record development that are directly attributable to US Geological Survey standards and protocols (Rantz et al., 1982; Sauer and Turnipseed, 2010;

Turnipseed and Sauer, 2010). Discharge measurements are made using conventional vertical axis Price AA and pygmy current meters, and hydroacoustics technology (acoustic Doppler current profilers and both fixed and wading rod mounted acoustic Doppler velocimeters).

Maintaining accurate real-time data requires expenditure of considerable manpower resources to ensure that remote gage station hardware and sensors remain in calibration, and the stage-discharge relationships accurately reflect current channel/control conditions. Since important real-time water administration decisions are made based on the available data, the Hydrographic Branch's calibration efforts are rigorous. State hydrographers are located in each of the 7 major river basins in Colorado. They visit gage stations as frequently as every week, but generally at two to four week intervals. Over 4,000 discharge measurements are made and saved in a digital database annually. Raw and processed gage station data are available to users at the Colorado Surface Water Conditions web site ([www.dwr.state.co.us](http://www.dwr.state.co.us)). This website provides users with current surface water conditions (streamflow and reservoir storage), and provisional, historical data in graphic and tabular formats. A touch tone telephone-based application called WaterTalk, an automated water information phone line is also available to users to access streamflow data at user selected stream gages.

### **WATER MEASUREMENT AT PRIMARY DIVERSION STRUCTURES**

The majority of the large, senior water rights in Colorado belong to irrigation companies. These rights are also often the calling right in the administration of a water district. These diversion rights can significantly affect mainstem and tributary stream flows. Dozens of major irrigation diversions are monitored by the SMS, and in large part these diversion are measured using Parshall flumes.

Trans-basin diversions (from one river basin drainage to another) and transmountain diversions (from one side of the Continental Divide to the other) must be carefully measured and monitored. Such diversions are obviously of major interest to water users in the source basin as well as to water right holders exercising the diversion rights in the receiving basin. Over 40 such transmountain diversions and trans-basin diversions are monitored by the SMS, and again, in large part these diversions are measured using Parshall flumes.

#### **Parshall Flumes**

The Parshall flume was developed in the early 20<sup>th</sup> century by Ralph Parshall and others at (then) Colorado A&M College (Parshall, 1936; Parshall, 1953). Parshall flumes have been employed extensively throughout Colorado to measure irrigation water diversions and deliveries, and are one of the most widely used water measurement devices in the world. The Parshall flume is characterized as a short-throated, critical depth flume. Flow control is achieved in a converging section from the flume entrance to the throat, in which flow accelerates from tranquil, sub-critical velocity to critical velocity at the flume throat. The accelerating, curvilinear flow to the flume throat and the non-geometric similitude among sizes required a unique stage-discharge relationship to be empirically

developed for each flume size. Under free flow conditions, a single upstream head measurement at a specific location in the converging flume section is used to compute flow. Parshall conducted a large number of flume calibration studies to develop free flow ratings for various flume sizes at the Colorado State College Hydraulics lab in Ft Collins Colorado and at an outdoor lab near Bellevue about 8 miles northwest of Ft Collins. The flume stage-discharge relationships or rating equations (Parshall, 1936 and 1953; USBR, 2001 and elsewhere) are reported to be accurate to within  $\pm 3\text{-}5\%$  of the true flow only under several stringent design, construction, installation, and operating conditions. These include:

- careful fabrication or construction to given structural dimensions for each flume size
- approach channel design and maintenance such that:
  - length of straight and unobstructed channel upstream, with mild slope, is at least 10 times the channel width
  - channel upstream of the structure should be both wider and deeper than the flume entrance cross section
  - stilling pool should be created and maintained in this upstream section (15-18 inches deeper than the flume crest) so that water flow is tranquil (smooth surface) and slow
  - transition from upstream channel bed to flume floor (no shallower than 1:4 slope) should be provided
  - wing walls from channel section to flume entry no shallower than  $45^\circ$  transition
  - upstream pool should be kept free of weeds and trash; sediment should be routinely removed
- flume floor in the converging section to the flume throat must be installed and maintained level laterally and longitudinally
- free outfall flow conditions meaning the flume crest elevation is designed and installed based on engineering analysis of channel geometry, slope, and design flow; and maintenance of downstream flow channel conditions to ensure no more than 70% submergence for flumes from 1 to 8 feet in size and no more than 80% submergence for flume sizes of 10 feet and larger
- head measurement (staff gage or stilling well intakes) must be correctly positioned vertically (staff reads zero and stilling well intake invert at the flume floor), and longitudinally along the flume converging section wall ( $\frac{2}{3}A$  upstream from the flume crest, where A is the converging section sidewall length, as measured along the wall and not axially in the flume)
- maintenance of the integrity of the flume (corrosion of metal, concrete spalling, etc.) to minimize deviations in cross sectional flow area and roughness from design conditions
- maintenance of the integrity of the flume installation to eliminate leaks past sidewalls or under the flume
- attention to transient maintenance issues such as moss and other aquatic vegetative growth in the flume, debris in the flume, and debris/vegetation in the up- and downstream channel, all of which can affect cross-sectional flow area and roughness deviations from design conditions, or cause backwater into the flume throat and flume submergence greater than specified for free flow conditions.

Several laboratory and field studies have been conducted to evaluate Parshall flume performance when these conditions are not met. Effects of longitudinal and lateral flume settlement, with and without submerged outfall conditions, on measured flume discharge versus indicated (i.e., determined from rating) flume discharge for flumes up to 2-foot throat widths were studied in the Hydraulics Lab at Colorado State University (Genovez et al., 1993; Abt et al., 1994; Abt et al., 1995). Correction and adjustment procedures were developed.

Abt and Ruth (1997) presented and discussed field assessments of 66 Parshall flumes ranging in size from 9-inch to 6-foot throat widths (there was one 12-ft flume in the study) installed around Colorado. Integrity of the flume construction and installation, including levelness, and operating conditions, such as approach and outfall conditions were assessed. Flume submergence and flow rate were also determined. A wide variety of issues were found. Rated discharge was compared with corrected discharge, where flow corrections were applied for lateral and longitudinal settlement and submergence based on Genovez et al (1993), Abt et al (1994), Abt et al (1995). In 59 percent of the flumes assessed, the rating indicated discharge was less than corrected discharge, i.e., more water delivered than indicated. Abt and Ruth (1997) also report 41 percent of the flumes assessed were measuring flow beyond  $\pm 5$  percent of the corrected flow. Independent measurements of actual flow at the sites studied were apparently not made.

Heiner et al. (2011) reported results of an assessment of 70 Utah flow measurement structures, 50 of which were Parshall flumes ranging in size from 2 ft to 12 ft throat widths. Again, a wide variety of issues were found ranging from settling to poor approach flow to improper stage measurement to vegetation/debris and sediment problems. Only 15 of the 50 Parshall flumes were found to measure flow within  $\pm 5$  percent of the indicated flow.

In this paper, we report on the field operational performance of over 220 Parshall flume installations across Colorado used for measuring mainstem river, tributary, and creek diversions; and trans-basin and transmountain diversions. Flume size ranges from 6-inch to 40-ft throat widths. Flume performance is assessed by on-site inspection of the flume installation, settling (as determined by differential leveling), improper approach conditions, and independent discharge measurements of stream flow.

## METHODS

Discharge measurement summary data were obtained from the CDWR discharge measurement database for all measurements made at Parshall flume gage stations by CDWR hydrographers over approximately the last 12 years. In a few cases, measurement summaries dating back to the 1980's have been hand entered, and were also included in this analysis. Stage-discharge relationships (rating curves) used at these gages, whether the standard Parshall flume rating for the given flume size, or a custom rating based in part on the standard Parshall flume rating, were also obtained. The discharge measurements were categorized by flume size. The measurement shift and percent difference from the rating were computed for each measurement:

$$\text{Shift (ft)} = \text{Rating GH for Measured Q} - \text{Observed GH} \quad (1)$$

$$\% \text{ difference} = [(\text{Measured Q} - \text{Rating Q}) / \text{Rating Q}] \times 100 \quad (2)$$

where GH is gage height (ft), Measured Q is independent measurement of discharge (cfs), and Rating Q is the indicated discharge (cfs) from the flume rating at the observed gage height.

All measurements for a given flume size were plotted against the standard flume rating curve for that flume size. Note that while discharge is the dependent variable, the standard convention of plotting discharge as the abscissa and stage as the ordinate is used here. Measurements with positive (+) shifts, indicating the actual flow is greater than the rated flow at the measured gage height, plot to the right of the rating curve, while measurements with negative (-) shifts, indicating the actual flow is less than the rated flow at the measured gage height, plot to the left of the rating curve.

At artificial controls such as Parshall flumes, shifts to the rating may be caused by all of the factors discussed in the previous section. The sign of the shift, (+) or (-), is a result of whether the affecting factor causes observed gage height to be greater or less than the rating gage height for the measured flow. For example, moss or other aquatic vegetative growth on the flume floor in the converging section effectively causes increased gage height for a given discharge and thus results in a negative shift. Conversely, upstream approach conditions which result in excess approach velocities (no provision for stilling of flow to tranquil conditions) typically result in positive shifts since flow velocity through the flume is faster than conditions under which flume ratings were developed. Shift adjustments to the rating, essentially a new or “re-calibrated” rating, may be applied temporarily, such as for the conditions of transient aquatic vegetation growth. Or, the shifts may be consistent to one side of the standard rating, and relatively stable, such as in the case of some poor approach channel designs, in which case, a semi-permanent variable stage-shift relationship is developed and applied. In such cases, this essentially becomes a custom rating for the flume.

Measurement percent difference from the standard rating is an indicator of whether the flume is measuring within expected accuracy ( $\pm 3-5\%$ ) and whether remedial procedures need to be implemented ranging from complete physical refurbishment of the installation to development and application of a variable stage-shift relationship to improve measurement accuracy. Discharge measurement accuracy ratings used by CDWR are based on USGS methods (Turnipseed and Sauer, 2010). Measurements are rated good (within 5% of the true flow), fair (within from 5% to 8% of the true flow), and poor (greater than 8% from the true flow).

## DISCUSSION OF RESULTS

A total of 4,228 independent discharge measurements at 223 flume installations across Colorado are summarized in Table 1. The results in Table 1 are broken down by number of sites and number of measurements analyzed for each flume size. The range of observed gage heights and measured discharges represented by the independent

measurements is given. The last three columns of Table 1 break the number of measurements into measurement percent difference categories: good (<5% from true flow), fair (5% to 8%), and poor (more than 8%).

Table 1. Summary of discharge measurements made by CDWR Hydrographers during approximately 1999 to present at various size Parshall flumes across Colorado.

Flume Size	No. of Sites	Measurements			% Difference from Rating		
		Number	Gage Height Range (ft)	Discharge Range (cfs)	No. of Measurements		
					<5%	5-8%	>8%
6-inch	2	3	0.37-0.89	0.47-1.76	1	0	2
9-inch	2	6	0.17-1.04	0.18-3.23	4	1	1
1-ft	6	32	0.13-1.04	0.14-4.75	8	3	21
18-inch	6	15	0.39-1.14	1.17-5.48	3	2	10
2-ft	23	434	0.01-1.32	0.05-12.9	123	67	244
30-inch	7	131	0.01-1.08	0.03-11.3	48	19	64
3-ft	24	168	0.04-1.87	0.15-27.7	15	15	138
4-ft	32	540	0.15-2.28	0.87-60.6	176	85	279
5-ft	23	363	0.13-2.78	0.62-96.6	97	52	214
6-ft	19	254	0.03-2.90	0.05-131	100	41	113
7-ft	2	2	0.70-1.47	14.4-46.8	0	0	2
8-ft	20	325	0.21-4.65	3.53-412	201	50	74
10-ft	11	89	0.02-2.71	0.24-192	62	7	20
12-ft	19	487	0.20-5.01	2.57-627	298	91	98
15-ft	15	790	0.15-5.51	3.15-976	416	118	256
20-ft	4	59	0.16-3.10	2.95-487	23	23	13
25-ft	4	253	0.20-3.01	6.07-572	181	47	25
30-ft	3	275	0.24-4.82	12.0-1610	166	49	60
40-ft	1	2	1.03-1.82	161-386	2	0	0
<b>Total</b>	223	4228			1924	670	1634

Table 1 shows that for 45% of the discharge measurements, the flumes were found to be operating within 5% of the rating indicated flow. In such instances, unless there is a consistent trend in the shift from the rating, typically no shift adjustment is considered necessary nor applied. If, however, there is a consistent trend in the sign and magnitude of the shift as determined by calibration measurements, then a shift will be developed and applied to improve overall flume measurement accuracy. For approximately 16% of the measurements, flumes were found to be operating within 5% to 8% of the standard rating. And, in 39% of the measurements, the flume was operating more than 8% from the standard rating. In these last two categories, shifts will typically be applied and further calibration measurements are often scheduled and flume inspections undertaken to determine the root causes of the flume measurement deviations.

Summary results shown in the last three columns of Table 1 indicate the smaller flume sizes included in this summary (up to 6 ft throat widths) tended to operate with greater deviation from the standard rating, and thus greater potential for compromised measurement accuracy. For the smaller flume sizes (up to 6-ft throat widths), an average of approximately 56% of discharge measurements show the flumes are operating greater than 8% from the standard rating. For the larger flumes in this summary (8 ft and larger throats) better measurement accuracy was found. An average of approximately 60% of the discharge measurements show these flumes are operating within 5% of the standard rating. Several factors contribute to this result, including for example: random discharge measurement errors will be a larger percentage of the smaller flows measured at the smaller flume sites, smaller flumes tend to be lighter (smaller mass) installations and potentially more prone to frost heaving and settling, discharge errors in small flumes due to even small lateral or longitudinal settling will be a larger percentage of measured flows than for the same amount of settling in a large flume.

Discharge measurements included in this analysis are plotted with the standard Parshall flume rating curve in Figures 1-16 for each flume size (with the exception of the 6-inch, 7-ft and 40-ft flumes, for which there were only a few available measurements). [Note: all figures are found at the end of the paper, following the References] A quick visual assessment of these rating curve plots reveals:

- In Figures 1 through 9, for flume sizes up to 6-ft throats, the larger measurement deviation from the standard rating (as discussed above regarding Table 1) is readily apparent when compared to Figures 11-16 for the larger flume sizes, which illustrate much less measurement variability from the standard rating. Documented submerged flow measurements are readily apparent in Figures 2, 7, 8, and 10 (blue symbols circled in a blue oval) and illustrate the large measurement error that occurs when the flume is under submergence and only a single upstream head measurement is made. The blue symbols are the actual measured flow and are considerably less than the discharge computed using the measurement gage height with the standard rating equation or table. At one time in history it was standard practice in Colorado to design and install Parshall flumes to operate under submerged flow in order to reduce head loss across the structure, minimize upstream channel size, and reduce operational overtopping of upstream channels. This is no longer considered good engineering practice in Colorado and flumes are expected to be installed, operated and maintained for free-flow conditions.
- In Figure 4 (2-ft), Figure 6, (3-ft), Figure 9 (6-ft), Figure 10 (8-ft), some discharge measurements show a curvilinear (concave down) trend plotting to the right of the standard rating (positive shifts) as discharge and gage height decrease. This result is typically caused by a drop in the effective point of zero flow of the flume, i.e., settling, spalling, etc., which, for the measured gage height results in a larger flow than indicated by the standard rating.
- Less apparent, but still evident in a few cases, is the opposite effect, where heaving of the flume or some other factor (increased surface roughness, aquatic vegetative growth, etc.) have caused an increase in the effective point of zero flow and measurements plot with a curvilinear (concave up) trend versus the standard rating.

- In a several instances of the larger flumes, some discharge measurements show a curvilinear (concave down) trend plotting to the right of the standard rating (positive shifts) at higher discharges and gage heights. This result is typically caused by high approach velocities in the upstream approach channel and in the flume entrance section.

### CASE STUDIES

The CDWR Hydrography and Satellite Monitoring Branch performs discharge measurements and systematic assessments of flume installation and operating conditions to document quantifiable checks on flume measurement performance. As data are gathered and evaluated, causes of departures of measured flow from the flow indicated by the flume rating, whether these departures are ephemeral or long term, and solutions for improved flow accuracy are formulated. Often, flume installations must be physically refurbished to improve measurement accuracy to desired levels. In other cases, shifts to the rating may be temporary in nature and measurement accuracy is improved by application of measurement shifts to the rating (temporary ratings) over identified periods of time when the flume performance was affected. In yet other cases, the data and evaluations may suggest the flume performance has been altered in some semi-permanent way and a custom rating is developed and maintained to provide improved measurement accuracy. Following are several brief example case studies illustrating flume performance issues and solutions implemented.

#### **Effects of Aquatic Vegetation Growth in the Flume**

Figure 16 shows discharge measurements made at 3 different 30-ft Parshall flumes. The measurements for Site No. 1-30 are highlighted with gold symbols. This flume is subject to considerable moss growth in the flume converging section and crest, particularly at lower gage heights (<1.00 ft) and flows. Such flow conditions typically occur in mid to late summer at this site, under high air temperature and warmer water temperature conditions. The consistent plotting of the measurements above and to the left of the standard rating illustrates the small negative shifts which occur due to the moss growth. Real time measurement accuracy of the flume is improved by applying small negative shift adjustments to the real time gage height data prior to computing flow. Such adjustments are applied and removed as site conditions change, i.e., cleaning of the moss from the flume floor, subsequent re-growth, etc. This is obviously a very dynamic situation and requires considerable attention in order to maintain measurement accuracy. Flume owners (and of the water diverted) are typically keen to keep such affected structures clean to avoid getting reduced credit and less water diverted.

#### **High Approach Velocities/Poor Approach Conditions**

Site 12-15 is a transmountain diversion gage at the downstream end of a tunnel under the Continental Divide through which water is diverted from the Colorado River drainage basin to the Arkansas River drainage basin. The measurement structure can be described as a standard, concrete, 15 foot Parshall flume and is located approximately 90 feet

downstream of the mouth of the tunnel. The approach channel from the mouth of the tunnel to the flume is a concrete rectangular section. The channel section gradually increases in width from the width of the tunnel mouth to a width of approximately 25 feet over a distance of about 70 feet. This is followed by approximately 20 feet of channel having a constant 25-foot width. This constant width section ends at the flume entrance. The floor of the approach channel is flat. There is no provision over this 90-foot reach for a deeper channel section prior to the flume entrance, or any other channel modifications to help still the flow to the recommended tranquil flow conditions. Approach velocities to the flume above a stage of 3.00 ft are high, exceeding an average of 4 ft/s at the flume entrance. Previous experiences with such poor, high velocity approach flow conditions at other flumes have shown such flumes operate with a positive shift to the standard flume rating, i.e., at higher flows the flume passes more water than the standard flume rating suggests for the given gage height. Parshall (1936) reported results of limited tests conducted at the Bellevue lab in which the approach velocity to a 2 ft flume was varied. He found that discharge through the 2-ft flume was not significantly affected when approach velocities were nearly 3 times the approach velocity for standard conditions of about 1 ft/s.

A series of high flow (650-950 cfs) measurements have been made over the past 10 years at Site 12-15. These measurements show a consistent departure from the rating. A high velocity “thread” of water in the center section of the approach channel at the flume entrance and shaped like the tunnel is evident (Figure 17) for these high flows. The high flow measurements have been used to build and further refine a variable stage-shift relationship (for stages above about 2.70 ft), which, when applied to the standard flume rating results in a custom rating for the flume. The custom flume rating is shown in Figure 18. For gage heights above 2.70 ft, 19 measurements showed a percent difference from the standard 15 ft Parshall flume rating ranging from 3.2% to 10% and averaging 7.2%. Against the custom rating, these same 19 measurements showed a percent difference ranging from -3.5 to 4.7% and averaging 0.93%. Calibration efforts continue in order to better define the range of stage where the flume departs significantly from the standard rating.

#### **Apparent Changes to Flume Effective Point of Zero Flow**

Sites 2-4 and 17-6 are transmountain diversion gages. Water is diverted from the Colorado River drainage basin and carried by open ditch to the Arkansas River drainage basin. The measurement structure at Site 2-4 is a standard, steel 4 foot Parshall flume, while at Site 17-6 it is a standard, concrete 6 foot Parshall flume. Approach and outfall channel conditions are good at both locations.

A series of discharge measurements made over the past 13 years at Site 2-4 have shown (and continue to show) that the flume operates with a nearly constant negative shift of -0.03 ft over the range of stage measured. These discharge measurements have been used to build variable stage-shift relationship or custom rating for the flume. Measurements, the custom flume rating (blue line), and the standard 4-ft flume rating (red line) are plotted in Figure 19. Measurements showed a percent difference from the standard 4 ft

Parshall flume rating ranging from -3.6% to -24% and averaging -11%. Against the custom rating, these same measurements showed a percent difference ranging from -3.8 to 2.7% and averaging 0.19%. The negative shift from the standard rating to the custom rating is attributed to an effective increase in the flume's point of zero flow caused by corrosion and deposits on the steel floor resulting in increased roughness and water surface elevation.

The opposite is the case at Site 17-6, where a series of discharge measurements made over the past 14 years at the site have shown (and continue to show) that the flume operates with a nearly constant positive shift of 0.04 ft over the range of stage measured. These discharge measurements have been used to build variable stage-shift relationship or custom rating for the flume. Measurements, the custom flume rating (blue line), and the standard 6-ft flume rating (red line) are plotted in Figure 20. Measurements showed a percent difference from the standard 6 ft Parshall flume rating ranging from 3.3% to 40.2% and averaging 14.1%. Against the custom rating, these same measurements showed a percent difference ranging from -2.7 to 1.5% and averaging -0.14%. The positive shift from the standard rating to the custom rating is attributed to an effective decrease in the flume's point of zero flow caused by some spalling and erosion on the flume floor resulting in an effective decrease in water surface at the same flow level compared to the standard rating.

Site 21-2 is a 2 foot steel Parshall flume on a small creek. The flume is not level laterally. At the staff gage-stilling well intake transect, the floor at the right side (stilling well side) is approximately 0.06 ft lower than the flume floor at the left side (staff gage side). There is also a small downward tilt from flume entrance to throat. Backwater is not an issue, but approach conditions vary from due to scour in the channel above the flume due to higher flows during snowmelt runoff, and aquatic vegetation growth during low flow periods causing slow water and deposition in the approach. The site requires continuous work on the approach channel. The gage is operated using the staff gage as the primary reference gage, and combined with the lateral slope in the flume, this results in a small additional unaccounted area of flow relative to the flume's standard condition, resulting in positive shifts to the rating. Discharge measurements made at Site 21-2 are plotted with a standard 2-ft Parshall rating in Figure 21. The concave downward trend in the measurements is consistent with the additional unaccounted flow area and the fact that this additional area essentially means the point of zero flow for this structure has effectively dropped to a slightly lower stage. The extra unaccounted flow area can be used to develop a geometrically (area) corrected custom rating. The corrected rating is plotted as a blue line in Figure 21. The geometric correction in this case is equivalent to a +0.02 ft shift to the standard rating, or, an effective reduction of the point of zero flow by 0.02 ft. Measurements plotted in Figure 21 show the flume operating at an average of 30.2% difference from the standard 2-ft Parshall rating. Against the custom (geometrically corrected) rating, the flume is now operating at an average 7.4% difference from the custom rating. Variable approach channel conditions, measurement errors and variability due to shallow depths and slow velocities at low flows, and the slight longitudinal tilt are remaining factors causing deviations from the custom rating.

### **Abnormal Vertical Velocity Profile**

Site 2-15 is another transmountain diversion gage which measures waters diverted from the Colorado River basin to the South Platte River basin. The measurement structure is a concrete 15 foot Parshall flume in good condition. Water exiting the transmission tunnel enters a 0.5 acre stilling reservoir before entering the Parshall flume on the opposite side of this reservoir, some 300 feet away. The stilling reservoir provides tranquil, laminar approach flow conditions. The immediate approach channel is devoid of accumulated sediment and has a greater than 1:4 slope. Geometric and differential level analysis of the flume did not show any significant deviations nor lateral or longitudinal levelness issues.

Discharge measurements at this site are made using a bridge crane above the standard  $H_a$  location. Both standard and individually rated Price AA current meters have been used. They are suspended on either a C50-lb or C75-lb Columbus weight. Section depths are obtained using a sectional rod, reducing systematic depth measurement errors resulting from downstream drift of the current meter and weight. Discharge measurements have consistently shown a positive shift from the standard rating with larger deviations at higher stages. These observations are consistent with mass balance computations made on the reservoirs associated with this gage. The positive shifts to the rating are attributed to two factors that result in a vertical velocity profile at the measurement section that is nearly uniform with depth compared to the standard 1/6 power law vertical velocity profile: 1) an abnormal wing wall configuration where the wing walls from the channel section to the flume section, upstream of segment D (Parshall, 1953), are at a shallower than  $45^\circ$  angle with respect to the flume mouth and the wing wall tapers from an approximate  $60^\circ$  slope at its extreme upstream end to vertical at the flume entrance section, and 2) the floor of the flume has been coated with an epoxy paint-like coating that greatly reduces roughness and reduces adherence of aquatic vegetation. The combined effect of two these factors is an overall higher average velocity with reduced floor and sidewall friction effects as water enters the flume. The typical vertical and lateral velocity distribution measured at a higher flow and stage at Site 2-15 is shown in Figure 22. Note the range in velocities, and then compare to Figure 17 where floor and sidewall effects are apparent and a much wider range of velocities was measured. Discharge measurements continue to be made periodically, as well as at targeted stages, to better map deviations away from the rating with the ultimate goal of developing a custom rating for this site. Due to operational practices, duplicative measurements throughout the full range in stage experienced are difficult to obtain at this site.

### **High Approach Velocities: Approach Channel and Flume Degradation**

Site 11-15 is a stream delivery quantification point for a large irrigation water conveyance system distributing waters across several sub-basins tributary to the South Platte River. The flume is a concrete 15 foot Parshall flume in fair condition. In the upstream channel, flow exits from a tunnel approximately 0.25 miles upstream from the flume, higher up on a hillside. From this point, the channel drops down a steep gradient chute into the flume's forebay, which includes a stilling basin section, that is deeper and

wider (transitioning from 10 feet to 25 feet wide over 50 linear feet) than the flume. However, the volume of the stilling basin is insufficient to effectively dissipate energy in the high velocity, surging flow produced by the drop chute. The flume has also been coated with an anti-spall paint, reducing friction losses through the flume, adding to the high approach velocity condition.

A custom rating accounting for high approach velocities was developed and had been used at this site for better than 30 years. Measurements made over the last several years, and especially those made from 2010 to present, have shown a negative shift or shift to the left of the custom rating of -1.6% to -5.4%. This denotes a reduction in the water delivered for a given stage. Visual inspection of the flume floor and walls showed areas where the anti-spall coating has been worn off, areas of rough concrete, and some areas of spalled concrete. These visual observations are consistent with the discharge measurement results indicating increased friction losses along the degrading concrete bottom and walls. Differential levels run on the Parshall flume in 2012 showed the flume is level and the primary reference gage is correct. A new rating has been developed. It plots to the left of the custom rating but still to the right of the standard 15 foot Parshall flume rating.

### SUMMARY AND CONCLUSIONS

The CDWR Hydrography and Satellite Monitoring Branch operates and maintains over 530 stream gages around Colorado to provide accurate real-time stream flow data in support of the water rights administration mission of the agency. Included among these gages are hundreds of Parshall flumes used for water measurement at diversions. Over 4200 discharge measurements made at 223 Parshall flumes across Colorado, ranging in size from 6-inch to 40-ft throat widths, were compared to standard flume stage discharge relationships. CDWR Hydrographers proactively inspect, assess physical conditions, and perform discharge measurements at flume sites. The results are used to design interventions for improving and maintaining flume measurement accuracy. Interventions range from complete removal and replacement of the measurement structure, to channel and/or flume floor modifications to eliminate submergence, to temporary and permanent custom rating development and implementation, to increased discharge measurement frequency. This program provides quantifiable checks on short and long term adequacy of standard and custom flume stage-discharge relationships. Several case studies of flume performance issues illustrating causes of departures of measured flow from the flume rating indicated flow and solutions for improved flow accuracy were presented and discussed.

This proactive program vividly shows that one cannot just simply install and walk away from an open channel water measurement structure such as a Parshall flume and expect accurate flow measurement. The following conclusions are made:

- Care needs to be taken when designing, installing, or constructing Parshall flumes. Strict adherence to standard Parshall flume dimensions is required for standard ratings to apply.
- Upstream approach channel conditions, in which smooth, tranquil flow into the flume entrance is developed and maintained, are required for standard ratings to

apply. Deviations from standard installation considerations can have varied and significant effects on Parshall flume measurement accuracy.

- Elevation setting of the flume crest must be carefully designed and downstream exit channel conditions must be maintained to eliminate flume submergence (or keep within allowable limits). Flow measurement error using a single upstream head measurement when a flume is operating submerged is significant.
- Physical problems and deficiencies may develop over time, such as flume floor levelness, increased surface roughness, development of abnormal velocity profiles, etc., and can significantly affect flume performance.
- Site evaluations and visual observations taking into consideration overall installation conditions and specific installation deficiencies are good predictors of the direction of Parshall flume measurement bias (under or over measurement). The magnitude of the bias can only be determined with a systematic program of independent discharge measurements.
- Development and application of custom Parshall flume ratings (temporary or permanent) is often warranted as a result of flume inspections and independent measurement. Such interventions were shown to improve flume measurement accuracy.

Although not explicitly included in this paper, CDWR staff have similar inspection, evaluation and measurement experience at other types of water measurement structures, including Cipoletti, rectangular, v-notch and other sharp crested weirs, broad crested weirs, long-throated flumes, cutthroat flumes, and submerged orifices with similar results and conclusions. All open channel water measurement structures require frequent maintenance, physical inspection and evaluation, and periodic independent discharge measurements to verify the structure is operating within design parameters and that expected measurement accuracies are being achieved.

### ACKNOWLEDGMENTS

The authors, all current staff members of the CDWR Hydrography and Satellite Monitoring Branch, have each been involved with Parshall flume operational performance assessment in Colorado for several years. They hereby wish to acknowledge the contributions and efforts of many other past and present CDWR staff who have measured and evaluated Parshall flumes in Colorado.

### REFERENCES

- Abt, S., A. Genovez, and B. Florentin, 1994. Correction for Settlement in Submerged Parshall Flumes. *Jour. of Irrigation and Drainage Engineering* 120(3):676-82, 1994. Amer Soc. of Civil Engineers, Reston VA.
- Abt, S., C.B. Florentin, A. Genovez, and B. Ruth, 1995. Settlement and Submergence Adjustments for Parshall Flume. *Jour. of Irrigation and Drainage Engineering* 121(5):317-21. Amer Soc. of Civil Engineers, Reston VA.
- Abt, S. and B. Ruth, 1997. Flume Condition Assessment in Colorado. *Jour. of the American Water Resources Association* 33(1):71-77. Amer. Water Resources Assoc., Middleburg VA.

Genovez, A., S. Abt, B. Florentin, and A. Garton, 1993. Correction for Settlement of Parshall Flume”, *Jour. of Irrigation and Drainage Engineering* 119(6):1081-91. Amer Soc. of Civil Engineers, Reston VA.

Heiner, B., S. Barfuss, and M. Johnson, 2011. Conditional Assessment of Flow Measurement Accuracy. *Jour. of Irrigation and Drainage Engineering* 137(6):367-374. Amer Soc. of Civil Engineers, Reston VA.

Ley, T.W., P. DeArcos, R. Stroud, and D. Hutchens, 2010. The Colorado Satellite-Linked Water Resources Monitoring System: 25 Years Later. *Proceedings of the USCID Conference: Meeting Irrigation Demands in a Water-Challenged Environment*, Sept 28-Oct 1, 2010, Ft Collins, CO.

Parshall, R.L., 1936. The Parshall Measuring Flume. Bulletin 423, Colorado Experiment Station, Colorado State College, Ft. Collins CO.

Parshall, R.L., 1953. Parshall Flumes of Large Size. Bulletin 426-A. Colorado Agricultural Experiment Station, Colorado Agricultural and Mechanical College, Ft. Collins CO.

Rantz, S.E. et al., 1982. Measurement and Computation of Streamflow. USGS Water Supply Paper 2175. USGS, Reston VA. 2 volumes.

Sauer, V. and P. Turnipseed, 2010. Stage Measurement at Gaging Stations. USGS Manual TM3-A7. USGS, Reston VA. 45 p. (Also available at <http://pubs.usgs.gov/tm/tm3-a7/>.)

Turnipseed, P. and V. Sauer, 2010. Discharge Measurements at Gaging Stations. USGS Manual TM3-A8. USGS, Reston VA. 87 p. (Also available at <http://pubs.usgs.gov/tm/tm3-a8/>.)

USBR, 2001. Water Measurement Manual. 3<sup>rd</sup> Edition. US Bureau of Reclamation, US Dept of the Interior. U.S. Government Printing Office, Washington, DC (Also available at [www.usbr.gov/pmts/hydraulics\\_lab/pubs/wmm/](http://www.usbr.gov/pmts/hydraulics_lab/pubs/wmm/)).

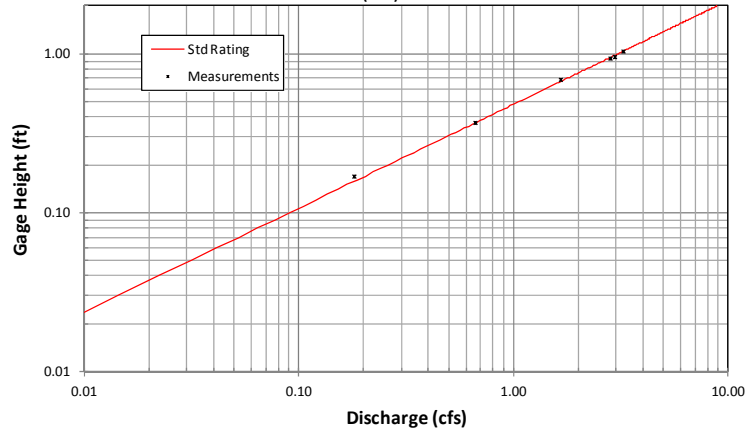


Figure 1. Discharge measurements (n=6) at standard 9-inch Parshall flume plotted with standard rating.

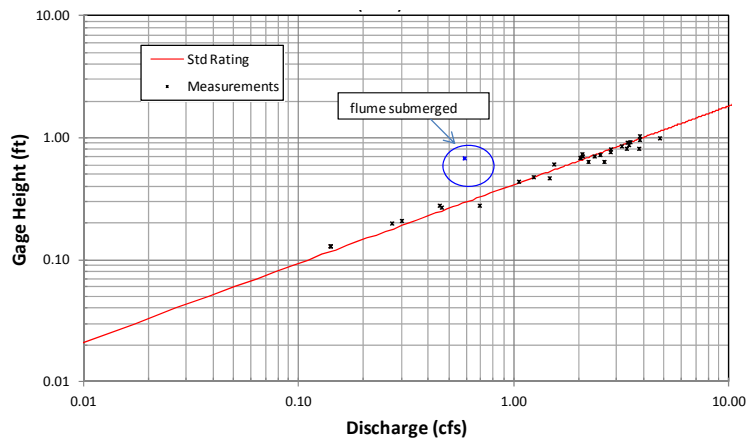


Figure 2. Discharge measurements (n=32) at standard 1-foot Parshall flume plotted with standard rating.

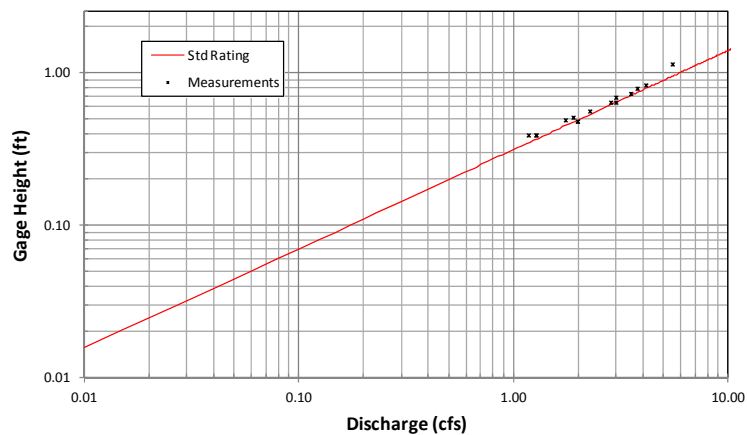


Figure 3. Discharge measurements (n=15) at standard 1.5-foot Parshall flume plotted with standard rating.

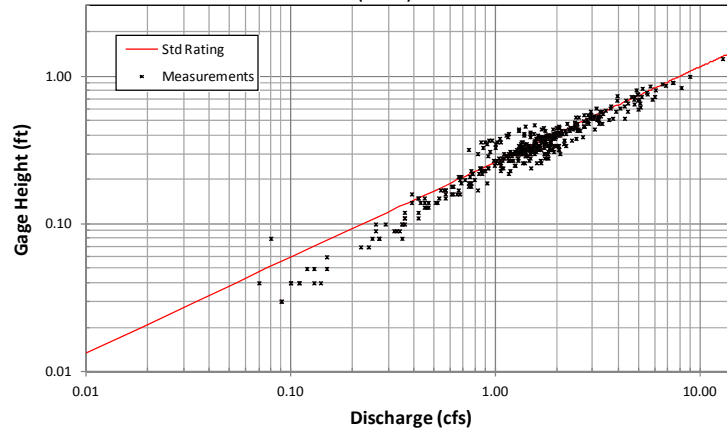


Figure 4. Discharge measurements (n=434) at standard 2-foot Parshall flume plotted with standard rating.

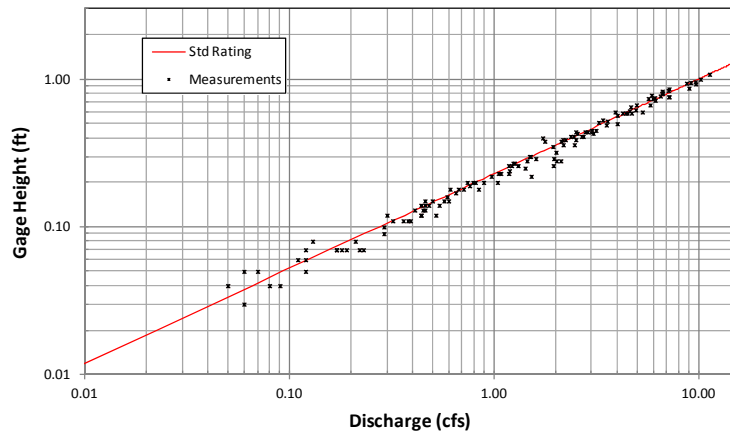


Figure 5. Discharge measurements (n=131) at standard 2.5-foot Parshall flume plotted with standard rating.

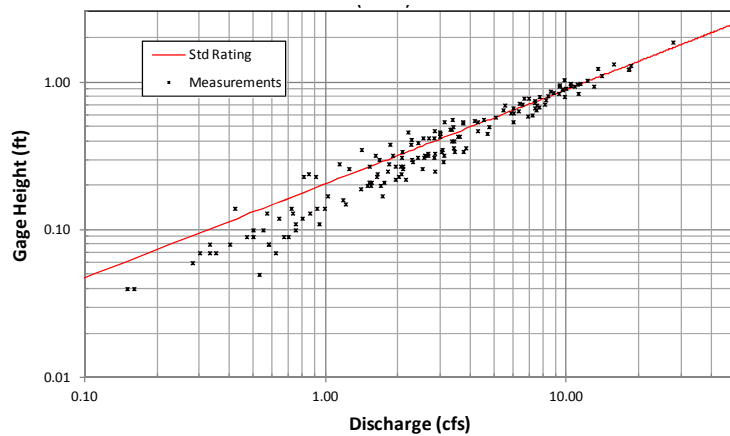


Figure 6. Discharge measurements (n=168) at standard 3-foot Parshall flume plotted with standard rating.

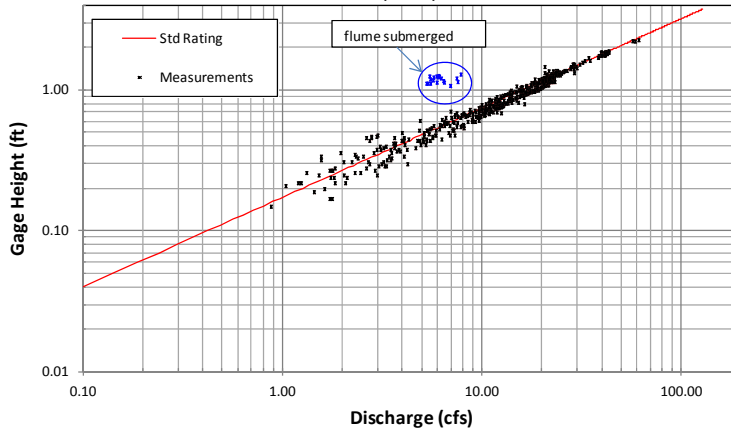


Figure 7. Discharge measurements (n=540) at standard 4-foot Parshall flume plotted with standard rating.

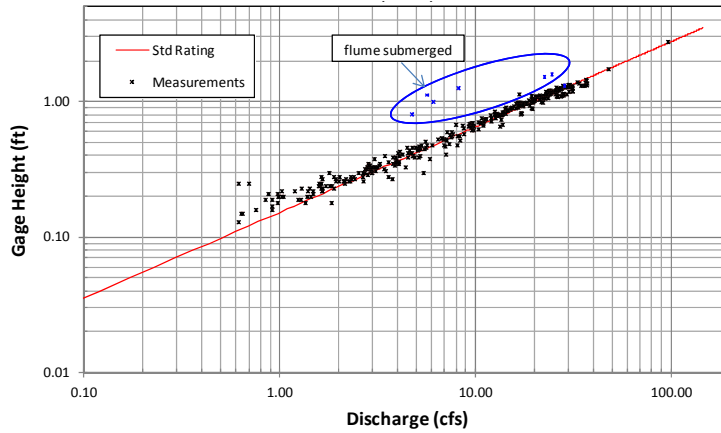


Figure 8. Discharge measurements (n=363) at standard 5-foot Parshall flume plotted with standard rating.

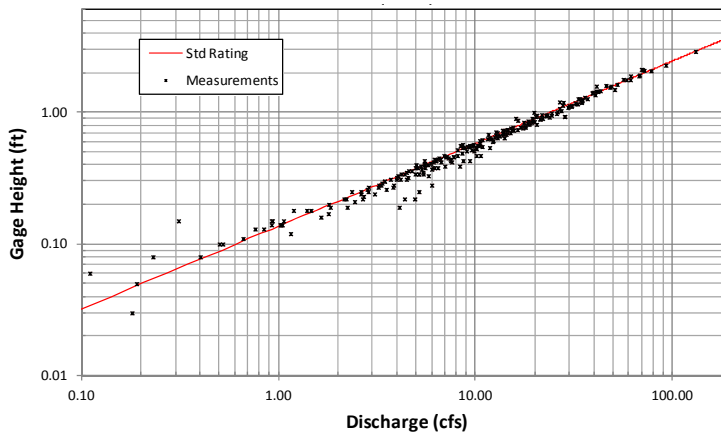


Figure 9. Discharge measurements (n=254) at standard 6-foot Parshall flume plotted with standard rating.

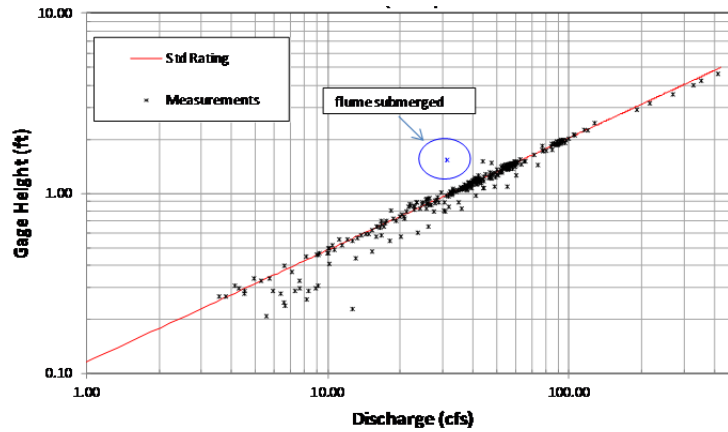


Figure 10. Discharge measurements (n=325) at standard 8-foot Parshall flume plotted with standard rating.

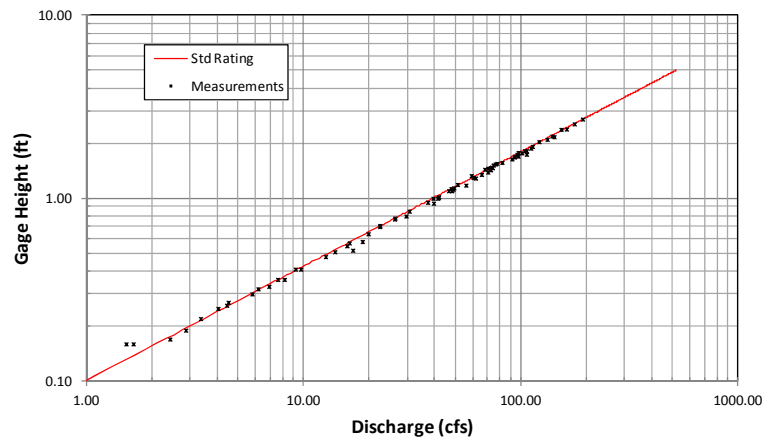


Figure 11. Discharge measurements (n=89) at standard 10-foot Parshall flume plotted with standard rating.

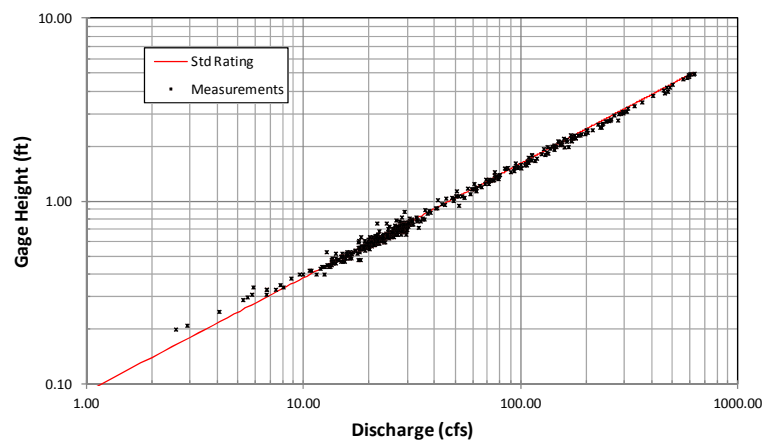


Figure 12. Discharge measurements (n=487) at standard 12-foot Parshall flume plotted with standard rating.

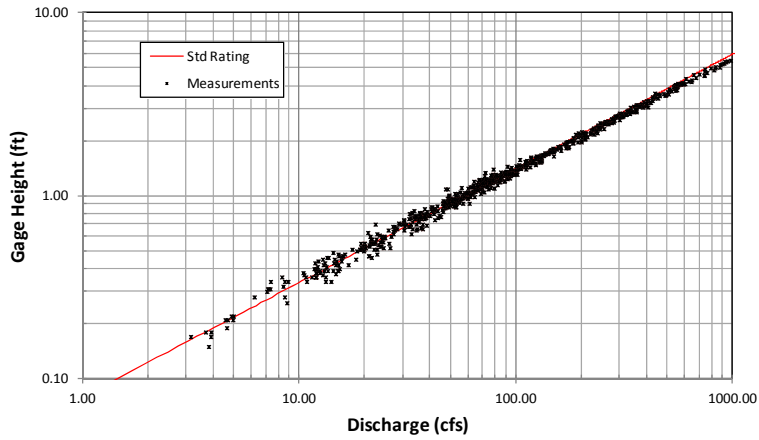


Figure 13. Discharge measurements at (n=790) standard 15-foot Parshall flume plotted with standard rating.

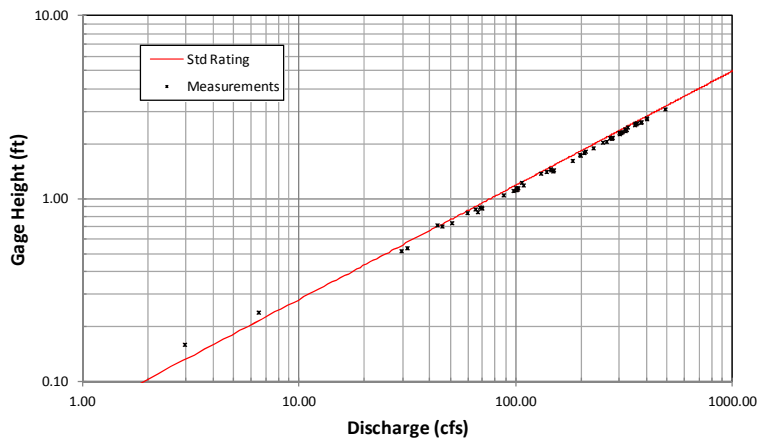


Figure 14. Discharge measurements (n=59) at standard 20-foot Parshall flume plotted with standard rating.

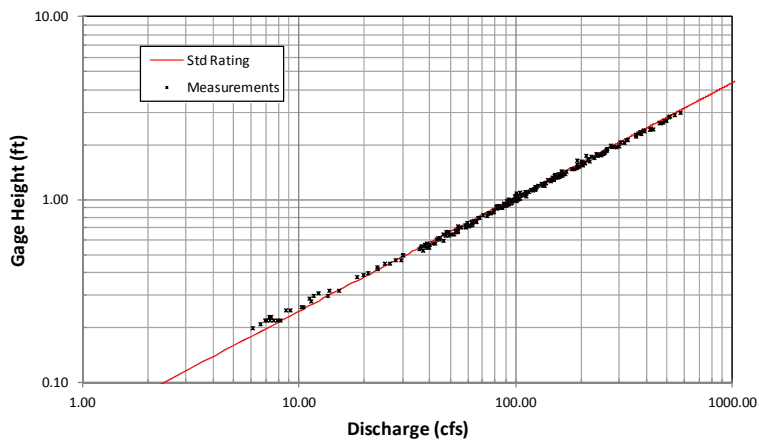


Figure 15. Discharge measurements (n=253) at standard 25-foot Parshall flume plotted with standard rating.

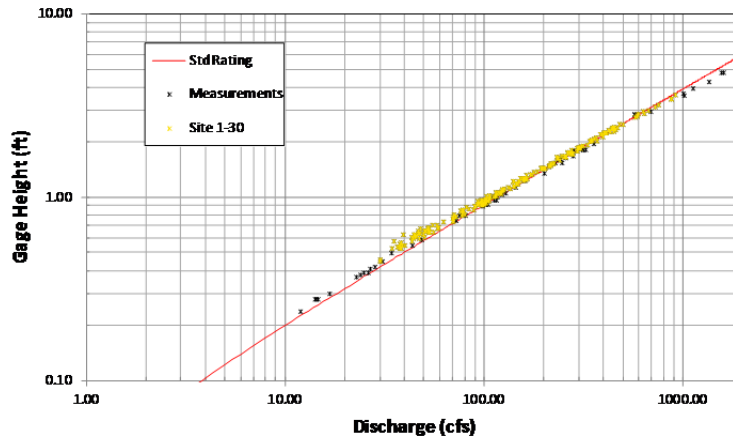


Figure 16. Discharge measurements (n=275) at standard 30-foot Parshall flume plotted with standard rating.

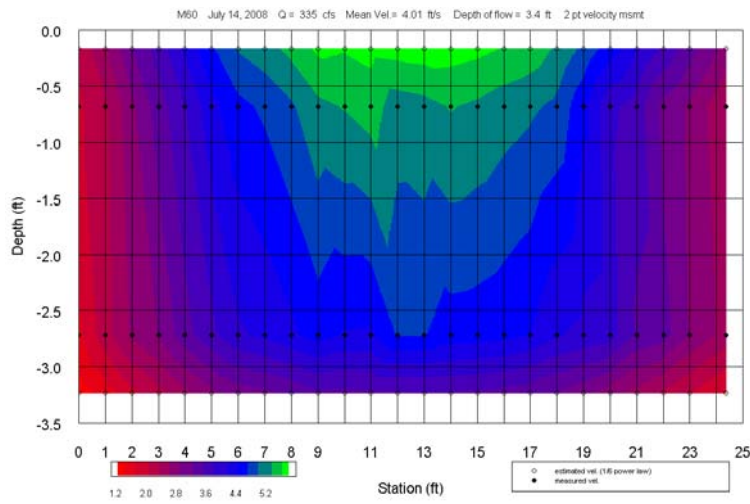


Figure 17a. Velocity distribution for measurement 60 (335 cfs) at Site 12-15.

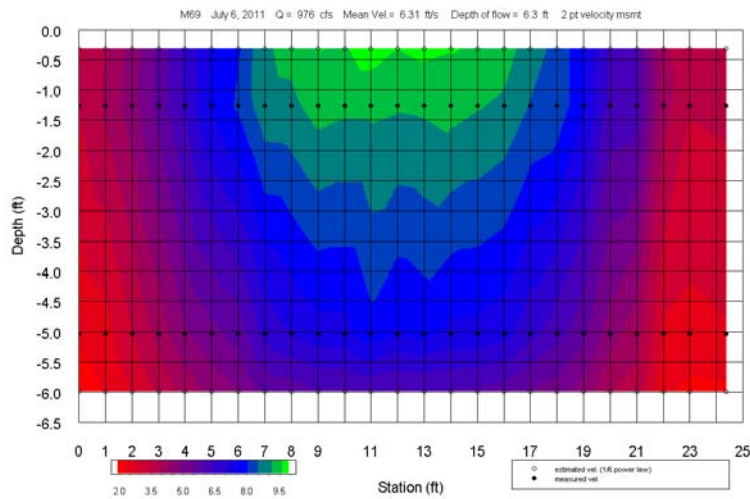


Figure 17b. Velocity distribution for measurement 69 (976 cfs) at Site 12-15.

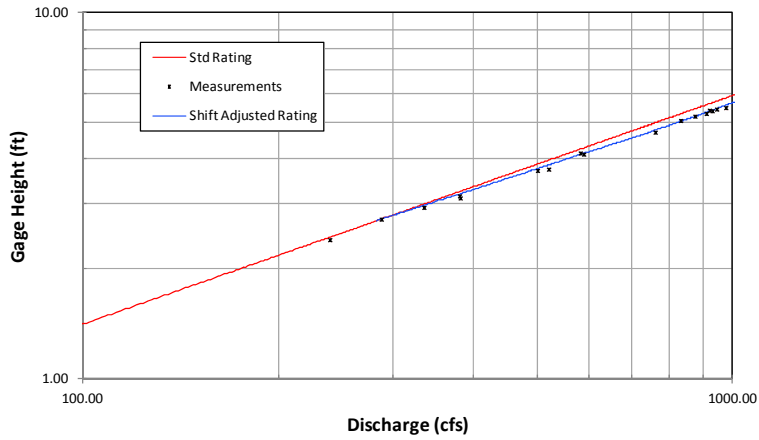


Figure 18. Custom (shift-adjusted) rating at Site 12-15 as defined by discharge measurements compared to standard 15-foot Parshall flume rating.

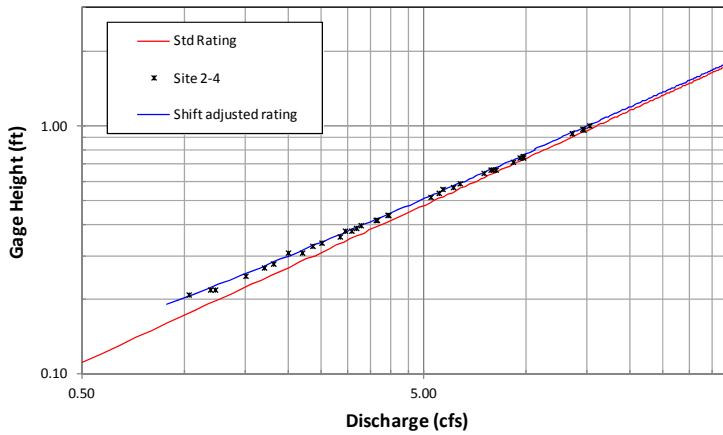


Figure 19. Custom (shift-adjusted) rating at Site 2-4 as defined by discharge measurements compared to standard 4-ft Parshall flume rating.

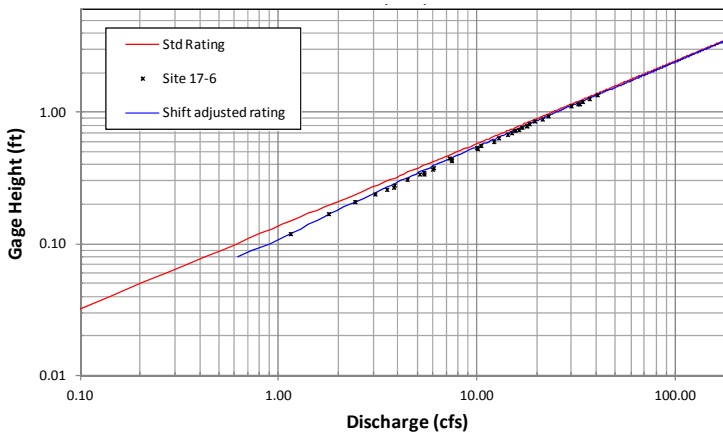


Figure 20. Custom (shift-adjusted) rating at Site 17-6 as defined by discharge measurements compared to standard 6-ft Parshall flume rating.

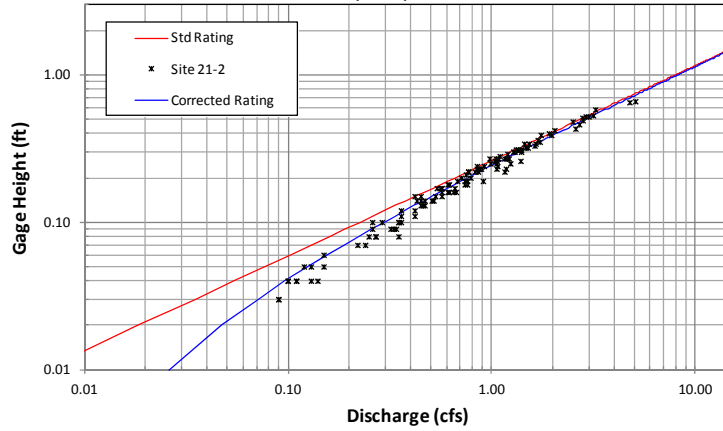


Figure 21. Custom (geometrically corrected) rating at Site 21-2 as defined by discharge measurements compared to standard 2-ft Parshall flume rating.

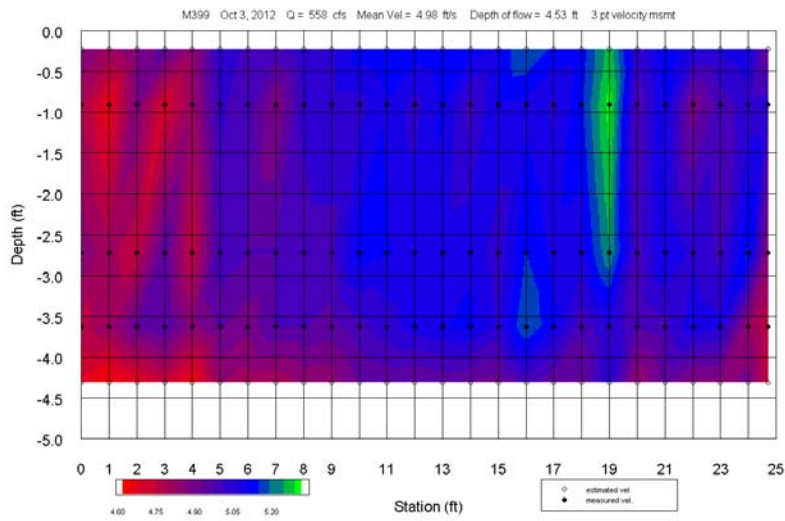


Figure 22. Velocity distribution for measurement 399 (558 cfs) at Site 2-15 showing little sidewall and floor friction effects on velocity.

# LONG-THROATED FLUME MEASUREMENT ACCURACY VERIFICATION AND HEAD LOSS CALCULATION

Guanghua Guan<sup>1</sup>  
Changde Wang<sup>2</sup>  
Albert J. Clemmens<sup>3</sup>

## ABSTRACT

Long-throated flume has been widely used as a flow measurement structure in irrigation channel systems. Measurement accuracy of this flume is based on an accurate prediction of head-loss. A series of experiments were carried out in China to verify the effectiveness of this structure. The results of these experiments showed that current theoretical model predicts larger discharges than measured values. We suggest that this is caused by a local head loss (energy-conversion loss) at the upstream converting section, which has been ignored. Based on experimental data and analysis, this paper introduced a local head loss  $\Delta H'_b$  which is applied to the head loss of the upstream transition. For side contraction of 1:2 and 1:3, this paper recommends the local head loss parameter to be 0.136 and 0.066 times the change in velocity head, respectively. With this new energy loss, calculation accuracy is significantly improved for long-throated flumes with side contractions.

## INTRODUCTION

One major approach to improve irrigation system management is to precisely measure the amount of water that has been delivered and used. Since the early 1900s, engineers and researchers have been seeking measurement structures that can retain simple relationships between upstream water-level and discharge. Among all kinds of structures, long-throated flume has been proved to be both effective and economical (Bos, 1975 & 1984). It is convenient for irrigation systems and even can be made portable (Raza et al., 2007). Long-throated flume has a throat section in which the streamlines run parallel over a short distance. This unique feature enables low head loss, high accuracy and high modular limit. Also the designing process is fairly simple with the software *WinFlume* (Wahl et al., 2001). Replogle (1975) proposed a mathematic model for discharge calculation of various kinds of measurement structures. It is claimed that this model was accurate to within 2% based on the results of laboratory studies (Replogle, 1975, Bos et al., 1984, Clemmens et al. 2010, Wahl et al., 2001b). Additional errors are associated with errors in measured water level, which can also be improved by proper design of stilling well (Wojciech et al. 2012). When the calibration error is combined with the measurement error, the resulting accuracy of the measurement can be lower than 5%.

---

<sup>1</sup> Associate Professor, State Key Laboratory of Water Resources and Hydropower Engineering Science, Wuhan University, 8# South Donghu Road, Wuhan, Hubei Province, China, 430072. GGH@whu.edu.cn

<sup>2</sup> Professor, State Key Laboratory of Water Resources and Hydropower Engineering Science, Wuhan University, 8# South Donghu Road, Wuhan, Hubei Province, China, 430072.

<sup>3</sup> Senior Hydraulic Engineer, WEST Consultants, Inc., 8950 South 52nd street, suite 210, Tempe, AZ 85284-1043.

In order to introduce long-throated flume to China and advocate it countrywide, laboratory experiments were carried out to verify the effectiveness of this structure and improve the accuracy of field calibration.

### REPLOGLE MATHEMATIC MODEL

The theoretical calculation process of long-throated flume is based on an iterative procedure (Clemmens et al, 2001). Terminology used in this calculation can be found in Figure 1, and meanings of symbols are listed in NOTATIONS at end of paper.

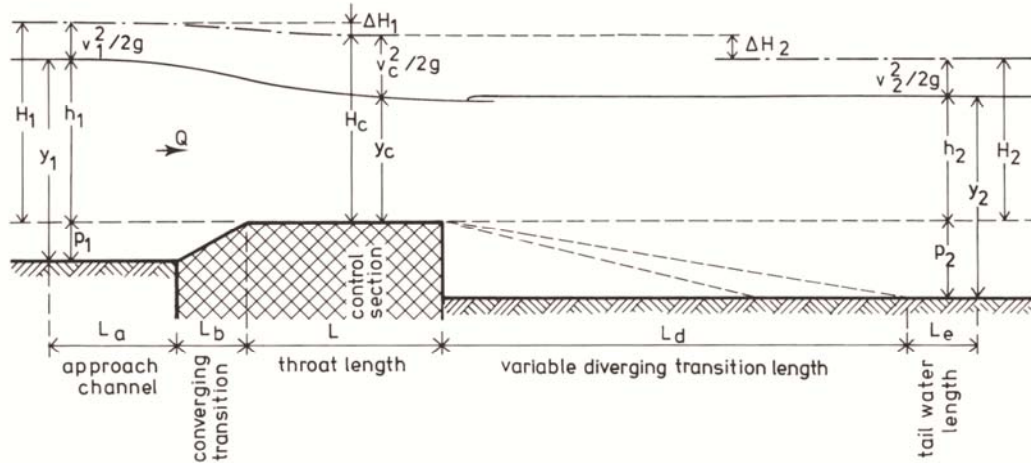


Figure 1. Illustration of terminology related to flume head loss (Clemmens et al, 2001)

Total energy loss across this structure is considered to be combined by three parts due to different reason of energy loss (Clemmens et al, 2001):

- The head loss between upstream head measurement section (gauging station) and the control section in the throat ( $\Delta H_1$ );
- Friction loss between the control section and the section where  $h_2$  could be measured ( $\Delta H_f$ );
- The losses due to conversion over the downstream transition ( $\Delta H_2 - \Delta H_f$ );

Because critical flow exists at the throat section, discharge is a function water level across the throat ( $y_c$ ):

$$Q = \sqrt{\frac{gA_c^3}{B_c}} \quad (1)$$

Here,  $A_c$  is the crossing area of critical flow and  $B_c$  is the width of critical flow water surface, they are all function of the water level  $y_c$  at the throat section, which is actually not easy to measure. Usually the water level at the approaching channel  $h_1$  is measured and energy equation between entrance and throat section is used to calculate  $y_c$ :

$$H_1 = h_1 + \frac{\alpha_1 v_1^2}{2g} = y_c + \frac{\alpha_c v_c^2}{2g} + \Delta H_1 = H_c + \Delta H_1 \quad (2)$$

$\Delta H_1$  is the head loss between entrance and throat section ( $\Delta H_1$ ):

$$\Delta H_1 = \Delta H_a + \Delta H_b + \Delta H_L \quad (3)$$

So, in order to get accurate assumption of discharge, one must be able to calculate the head loss properly. Because the head loss is also a function of  $y_c$ , this solving procedure becomes an interactive loop:

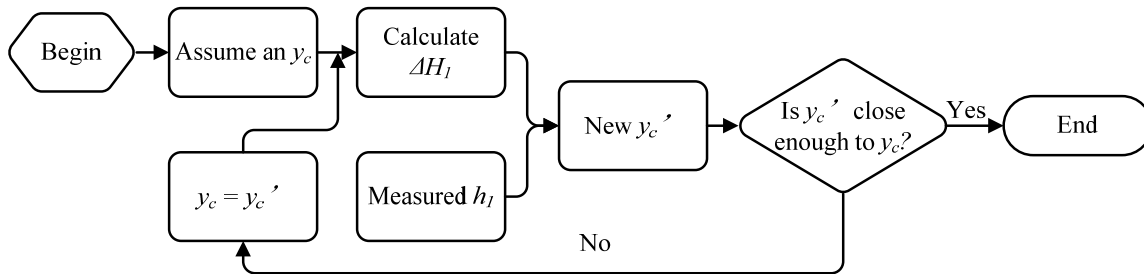


Figure 2. Critical depth calculation for long-throated flume

Replogle’s head loss equation (Bos et al, 1984) is based on boundary layer theory,  $\Delta H_1$  is considered to be combined by the following sections (Eq. 3):

- 1) The head loss in the throat  $\Delta H_L$ ;
- 2) The head loss in the approach channel  $\Delta H_a$ ;
- 3) Head loss in converging section  $\Delta H_b$ ;

In this model, friction loss is considered in all sections listed above. But the local head loss (conversion loss) is only covered in the head loss across the downstream ( $\Delta H_2$ ). This means that only local head loss at the downstream section is considered while the local head loss at the upstream contraction section has been ignored. If there is only vertical contraction at the upstream converging section, due to low velocity distribution on the bottom, the local head loss is not remarkable. But when there is side contraction, the side wall will play blocking force on the flow and local head loss would be more outstanding. Although this head loss is not a large share of the total loss, it will always leads to larger calculated flow.

This procedure is included in the *WinFlume* program (T. I. Wahl et al, 2001b), so *WinFlume* is able to make this calibration automatically.

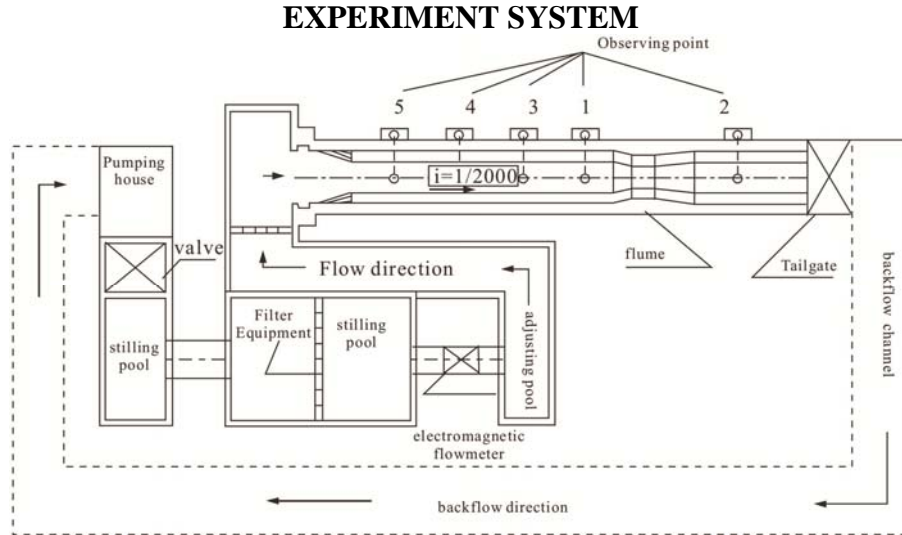


Figure 3. Layout of experiment system.

Layout of the experiment system is shown in Figure 3, the total canal length is 45m with 28m on upstream side and 17m on downstream side. A photo of this system can be found in Figure 4. Approaching channel and tail water channel is prismatic with the same cross section shown in Figure 5. The canal is lined with concrete and roughness  $n$  is assumed to be 0.017.



Figure 4. A photo of experiment system

Concerning accuracy and effectiveness of these experiments, large scale model and highly accurate measurement equipment are employed in this laboratory research. A canal system of 45m long was constructed with bottom slop of 1/2000. Electromagnetic flow-meter, IFS4000 (SGAIC, 2006), is used to measure flow with accuracy of  $\pm 0.5\%$  and needle gauge is used to measure water level with accuracy of  $\pm 0.1\text{mm}$ . Series of experiments with different vertical and side converging rate were performed for analyses and comparisons.

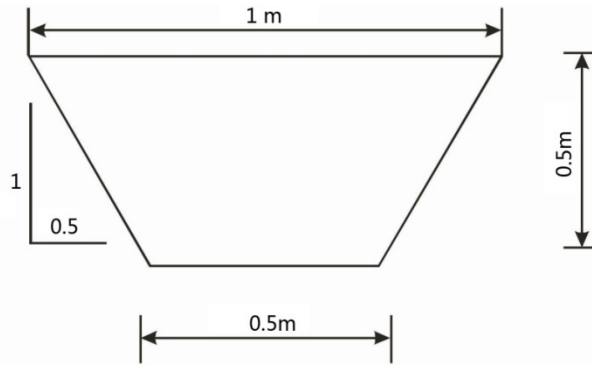


Figure 5. Canal cross section parameter.

In this experiment, three sets of flume are used:

- 1) 5 trapezoid flumes with only side contraction;
- 2) 5 trapezoid flumes with only vertical contraction;
- 3) 2 flumes with both side and vertical contractions, one with a trapezoid cross section and one with a U shape cross section.

For the five flumes with only side-contractions, four upstream converging rate (length to width: 2, 2.5, 3, 4) are used, and downstream side expansion rate remains unchanged  $EM'=6$ . Width of these flumes throat section are all  $0.18m$ . An extra set of model is created from the set with upstream converging rate of 3, by cutting-off half-length of the downstream converging section. Detail of these models can be found in Figure 6. Approaching canal bottom width are all  $0.5m$  and throat width of all flumes are  $0.18m$ , different converging rate is made by changing the length of converging section ( $L_b$ ). The corresponding parameters are shown in Table 1.

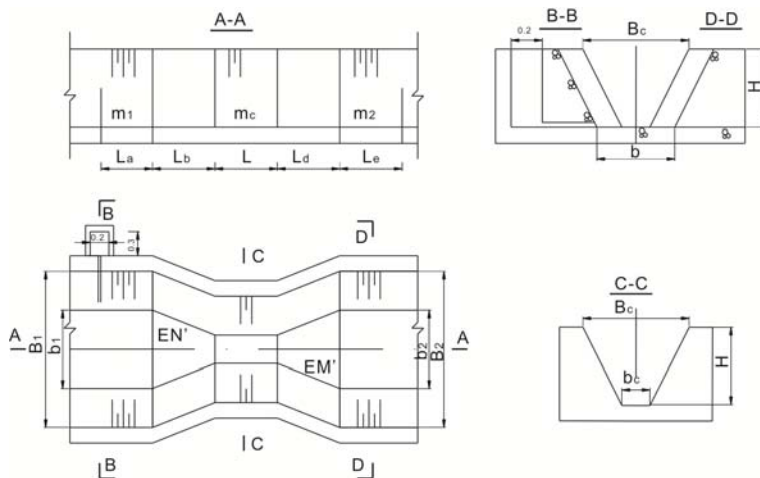


Figure 6. Flumes with only side contraction

Table 1. Parameter for flumes with only side converge

parameter	Model 1	Model 2	Model 3	Model 4	Model 5
	EN'=2.5	EN'=2	EN'=3	EN'=3	EN'=4
$L_a$ (m)	0.25	0.33	0.17	0.17	0.01
$L_b$ (m)	<b>0.40</b>	<b>0.32</b>	<b>0.48</b>	<b>0.48</b>	<b>0.64</b>
$L$ (m)	0.55	0.55	0.55	0.55	0.55
$L_d$ (m)	0.96	0.96	0.96	0.48	0.96
$L_e$ (m)	3.39	3.39	3.39	3.87	3.39
$EM'$	1:6	1:6	1:6	1:6	1:6
$bI$ (m)	0.5	0.5	0.5	0.5	0.5
$m_1$	0.5:1	0.5:1	0.5:1	0.5:1	0.5:1
$b_c$ (m)	0.18	0.18	0.18	0.18	0.18
$m_c$	0.5:1	0.5:1	0.5:1	0.5:1	0.5:1
$b_2$ (m)	0.5	0.5	0.5	0.5	0.5
$m_2$	0.5:1	0.5:1	0.5:1	0.5:1	0.5:1

For vertical contraction experiments, the sill height is  $p_1 = p_2 = 0.2m$ . Four upstream vertical-converging rate (2, 2.5, 3, 4) are used, and downstream vertical converging rate remains unchanged  $EM=6$ . An extra set of model is created from the set with vertical-converging rate of 3, by cutting-off half-length of the downstream shrink section. Parameters of these flumes are shown in Table 2.

Table 2. Parameter for flumes with only vertical converge

parameter	Model 1	Model 2	Model 3	Model 4	Model 5
	EN=2.5	EN=2	EN=3	EN=3	EN=4
$L_a$ (m)	0.5	0.6	0.4	0.4	0.2
$L_b$ (m)	<b>0.5</b>	<b>0.4</b>	<b>0.6</b>	<b>0.6</b>	<b>0.8</b>
$L$ (m)	0.31	0.31	0.31	0.31	0.31
$L_d$ (m)	1.20	1.20	1.20	0.60	1.20
$L_e$ (m)	2.35	2.35	2.35	2.95	2.35
$EM$	1:6	1:6	1:6	1:6	1:6
$bI$ (m)	0.5	0.5	0.5	0.5	0.5
$m_1$	0.5:1	0.5:1	0.5:1	0.5:1	0.5:1
$b_c$ (m)	0.70	0.70	0.70	0.70	0.70
$m_c$	0.5:1	0.5:1	0.5:1	0.5:1	0.5:1
$b_2$ (m)	0.5	0.5	0.5	0.5	0.5
$m_2$	0.5:1	0.5:1	0.5:1	0.5:1	0.5:1

For flumes with side and vertical converge, both trapezoid and U shape cross section are tested. Details of the model are shown in Figure 7, and parameters are in Table 3.

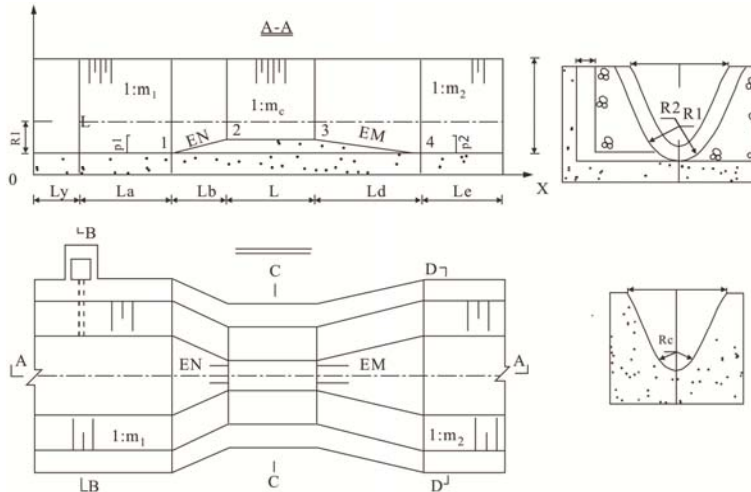


Figure 7. U shape long-throated flume with both side and vertical contraction

Table 3. Parameter for flumes with both side and vertical converge (m)

parameter	trapezoid shape flume	U shape flume
$L_a(m)$	0.64	0.57
$L_b(m)$	0.36	0.36
$L(m)$	0.43	0.58
$L_d(m)$	0.72	0.72
$L_c(m)$	2.63	2.63
$EM$	1:6	1:6
$b_1(m)$	0.5	0.5
$m_1$	0.5:1	0.5:1
$b_c(m)$	0.38	----
$m_c$	0.5:1	0.5:1
$b_2(m)$	0.5	0.5
$m_2$	0.5:1	0.5:1
$P_1$	0.2	0.2

**EXPERIMENTAL RESULTS AND ANALYSES**

Comparisons between calculated and measured discharge ( $Q_R$  and  $Q_T$ , respectively) are shown in Figure 8. In this figure, error is  $\frac{(Q_R - Q_T)}{Q_T} \times 100\%$  and  $H_1/L$  is the upstream water head divided by length of the throat. In this figure, all models with side contraction (Side  $EN'=2$ , Side  $EN'=2.5$ , Side  $EN'=3$ , Side  $EN'=3'$ , Side  $EN'=4$ ) are shown. The model “Side  $EN'=3$ ” refers to the one with half length of the downstream shrinking section. At the same time, Figure8 also presents those models with vertical converging rate of 3 (shown in the figure by ‘vertical’) and U shape flume with both side and vertical converging rate of 3 (shown in the figure by ‘side and vertical’).

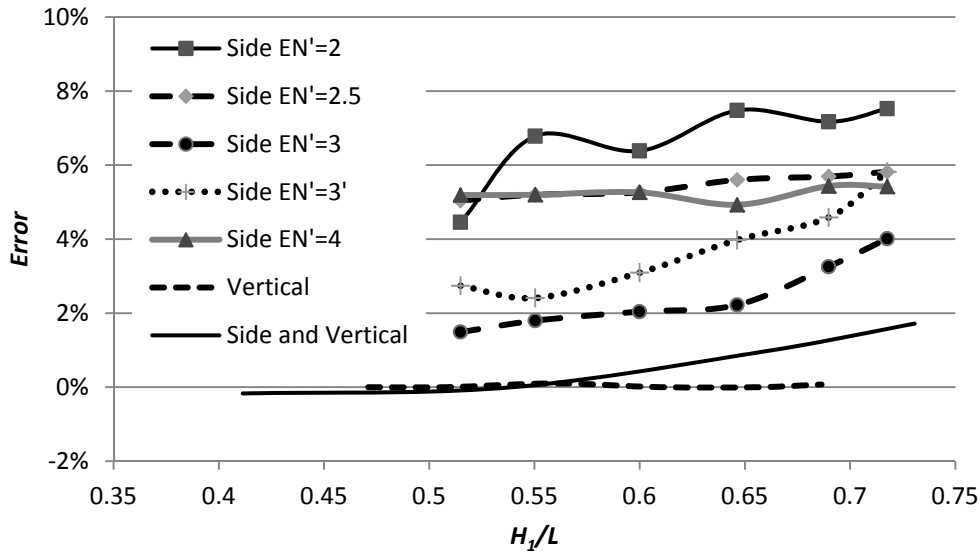


Figure 8. Measured discharge error for different model

It can be easily seen that the model with only side converge has relatively high error while the one with only vertical has almost none. At the same time, calculated discharge is always larger than measured value, this implies that some local head loss (conversion loss) is ignored so that the calculated total head loss is smaller than actual value. Similar results can be found for other tested converging rate.

### THE MODIFICATION OF THE HEAD LOSS EQUATION

With side contraction, the separation zone would occur where the converging transition intersects with the start of the flume throat. In the model described in Clemmens et al 2010, velocity at this section this is labeled as  $v_b$ . The head loss of the upstream transition section ( $\Delta H_b$ ), flow in this area is considered to be turbulent flow, so  $C_F$  is 0.00235 and the head loss equation is as following:

$$\Delta H_b = \frac{0.00235L_b}{4g} \left[ \frac{v_1^2}{R_1} + \frac{v_b^2}{R_b} \right] \quad (4)$$

As mentioned before, side contraction at this section will play blocking force on the flow thus local head loss is formed. So there should be one more head loss, the local head loss at converging section ( $\Delta H'_b$ ). In order to get a reasonable assumption of  $\Delta H'_b$ , firstly we define an ideal head loss ( $\Delta H'_{b-opt}$ ) to perform perfect match of measured discharge. Based on the source code in BOS M. G. (1975), we developed a routine by *MATLAB* (MathWorks 2000) to calculate  $\Delta H'_{b-opt}$ , the results are listed in Table 4.

Table 4. Extra head loss needed to perform a perfect calibration for side converge

$\Delta H'_{b-opt}$	Side converge rate			
	Upstream water level	1:2	1:2.5	1:3
0.2832	0.00549	0.00621	0.00146	0.00627
0.3027	0.00927	0.00708	0.00230	0.00695
0.3300	0.01005	0.00838	0.00354	0.00825
0.3555	0.01328	0.01038	0.00501	0.00920
0.3794	0.01453	0.01211	0.00805	0.01155
0.3974	0.01640	0.01353	0.01043	0.01273

This energy loss is caused by side contraction and it varies with energy head between approaching canal and throat section. Head loss across downstream expansion section in Repologle’s model (Clemmens et al, 2001) is calculated from the velocity difference between throat and downstream section:

$$\Delta H_2 - \Delta H_f = \frac{\xi(v_c - v_2)^2}{2g} \tag{5}$$

As described by Chow (1959), energy head between entrance and throat section  $\Delta h_v$  ( $\Delta H_v = \frac{v_c^2}{2g} - \frac{v_1^2}{2g}$ ) is used in this paper to build relationship between local head loss and flow condition. A parameter  $c_i$  is introduced in equation (5) to calculation this local head loss:

$$\Delta H'_b = c_i \left[ \frac{v_c^2}{2g} - \frac{v_1^2}{2g} \right] = c_i \Delta h_v \tag{6}$$

And the head loss  $\Delta H_1$  in equation (3) becomes:

$$\Delta H_1 = \Delta H_a + \Delta H_b + \Delta H'_b + \Delta H_L \tag{7}$$

In order to get proper assumption of  $c_i$  value, a computer program was developed by *MATLAB* (MathWorks 2000). In this program discharge calculation procedure was written as a function with the input of  $c_i$  value, and if there is no correction  $c_i$  should be zero. Then a main routine will try different  $c_i$  value to and find a best one to minimize the quadratic mean deviation of all experiment data.

According to the measurement of this paper,  $c_i$  value for side contraction rate 1:2, 1:3 and 1:4 is 0.136, 0.066 and 0.124 respectively. After this modification, the calculation accuracy is increased from 7.5% to be within 3%. See detailed data in Table 5.

Table 5. The compare of calculation and measurement after modification

model	Side converge 1:2			Side converge 1:3		
	$h_i$	$Q_R$	$Q_T$	Error×%	$Q_R$	$Q_T$
0.2832	0.0699	0.0718	-2.69	0.0723	0.0739	-2.21
0.3027	0.0794	0.0796	-0.24	0.0821	0.0835	-1.68
0.3300	0.0938	0.094	-0.18	0.0970	0.098	-0.99
0.3555	0.1085	0.107	1.41	0.1123	0.1125	-0.22
0.3794	0.1234	0.1213	1.71	0.1276	0.1259	1.37
0.3974	0.1335	0.1302	2.47	0.1381	0.1346	2.54

Side contraction rate will influence  $c_i$  value dramatically. If side contraction is sharp (1:2), the resistance force placed by the boundary is large, so the head loss is large and  $c_i$  value is large (0.136). In the other hand, if contraction rate is 1:3, this resistance is weaker thus  $c_i$  value is smaller (0.066).

For the side contraction of 1:4,  $c_i$  value should be even smaller than 0.066 but here we got the value of 0.124. That's because this value and even the measurement of side contraction 1:4 is not reliable. In this series of experiment, gaging station is much too close to the contraction section (see  $L_a$  value in Table 1 for side contraction 1:4). Here this distance is only 0.01m, so the measured water level is greatly influenced by the curving profile caused by the contraction. As a result, this paper recommends  $c_i$  value for side contraction rate 1:2 and 1:3 to be 0.136 and 0.066 respectively. And we believe  $c_i$  value for 1:4 should be between 0.066 and 0.05.

Because this modification is made just for flumes with side contraction, those with bottom contraction will not need this modification. For flumes with side and bottom contraction, the measurement data shows that calculation accuracy can reach 2%, so we believe no modification will be necessary.

## CONCLUSION

Results of the experiments verified that long-throated flume is an effective flow-measurement structure with simple shape, low head loss, high modular limit, high robustness and accuracy. It should be advocated in most irrigation canal systems.

Based upon test results, modification is made to the original head loss equation to further increase the calculation accuracy. A local head loss parameter  $\Delta H'_b$  is introduced to original model, and a local head loss parameter  $c_i$  is used to calculate this head loss from the energy head between entrance and throat section  $\Delta h_v$ . In this paper the recommended  $c_i$  value for side contraction rate 1:2 and 1:3 is 0.136 and 0.066 respectively. With the modified method, for flumes with only side converging, calculation error is deduced from 7.53% to 2.69%.

## ACKNOWLEDGEMENTS

This work was partially supported by National Natural Science Foundation of China (No. 51009108) on the "Coupling ID model and resonance filter algorithm study for open-

channel water delivery control system”, and Doctoral Found of Ministry of Education of China (No. 20090141120029) on “Centralized ID modeling and LQR Controller design on canal system”

## REFERENCES

Ackers P., and Harrison A. J. M. (1963). “Critical depth flumes for flow measurements in open channels”. *Hydraulic Research Paper No. 5*, department of Industrial and Scientific Research. Hydraulic Research Station, Wallingford, Berkshire, England. 50pp

Ali Raza, Muhammad Latif, and Ghulam Nabi (2007). “Fabrication and Evaluation of a Portable Long-throated Flume”, *Irrig. And Drain*. Vol. 56, No.5, 565-575.

Clemmens, A. J, Replogle J. A, Bos, M. G, (1984). “Rectangular measuring flumes for lined and earthen channels”, *Journal of Irrigation and Drainage Engineering, ASCE* Vol. 110, No. 2, June 1984, 121-131.

Clemmens, A. J., Replogle, J. A., and Reinink, Y. 1990. Field predictability of flume and weir operating conditions. *Journal of Hydraulic Engineering, ASCE*, Vol. 116, No. 1, January, 1990, 102-118.

Clemmens, A. J., Wahl, T. L., Bos, M. G., and Replogle, J. A. 2001. Water measurement with flumes and weirs. Water Resouces Publications, Highlands Ranch, CO 382 pp.

French Richard H. (1987). “Open-Channel hydraulics”, *McGRAW-HILL Book Company*.

MathWorks. (2000). *MATLAB user's guide: Version 6*, MathWorks, Natick, Mass.

Replogle, J. A. 1975. Critical flow flumes with complex cross section. In: *Irrigation and Drainage in an Age of Competition for Resources*. Specialty Conference Proceedings, American Society of Civil Engineers, Logan, Utah, Aug. 13-15, pp. 366-388.

Kline S. J. et al (1967). “The Structure of Turbulent Boundary Layers”. *J. Fluid Mech. ASCE*, Vol.30, 714-773.

Kim H. T., Kline S. J, and Reynolds W. C., (1971). “The production of Turbulence near a smooth Wall in a Turbulent Boundary layer”. *J. Fluid Mech. ASCE*, Vol. 50, 133-160.

BOS M. G. (1975). “Discharge Measurement Structures”, *International Institute for Land Reclamation and Improvement (ILRI)*.

BOS M. G., Replogle J. A., Clemmens A. J. (1984). “Flow measuring flumes for open channel systems”, *John Wiley & Sons, Inc*.

SGAIC (2006), IFS4000:

<http://www.transmitters.co.kr/measurement.file/flowmeter/ifs4000.htm>

U.S. Department of the Interior Bureau of Reclamation (2001). “Water Measurement Manual”, *U.S. Government Printing Office, Washington, DC.*

V. T. Chow (1959), “Open-Channel Hydraulics”. *McGraw-Hill Book Co.*, New York, NY.

Wahl T. I., Clemmens A. J., Replogle J. A., Bos M. G. (2001a). “WinFlume User’s Manual” *U.S. Bureau of Reclamation, Denver, Colorado.*

Wahl T. I., Clemmens A. J., Replogle J. A., Bos M. G. (2001b). “Winflume: Windows-Based Software for the Design of Long-Throated Measuring Flumes” *U.S. Bureau of Reclamation, Denver, Colorado.*

Wojciech D., Urszula P. (2012) “Improvements in flow rate measurements by flumes”, *Journal of Hydraulic Engineering, ASCE* , Vol. 138, No. 8, August 1, 2012.

### NOTATIONS

Symbol	Definition	Unit
$c_i$	Local head loss parameter for side contraction	-
$C_F$	Boundary layer friction coefficient	-
$EN$	Upstream vertical converging rate	-
$EN'$	Upstream side converging rate	-
$EM$	Downstream vertical shrink rate	-
$EM'$	Downstream side shrink rate	-
$g$	Acceleration due to gravity	m/s <sup>2</sup>
$H_1$	Approaching water head above the flume	m
$H_2$	Downstream water head	m
$H_c$	Water head at the throat section	m
$h_1$	Upstream flow head referenced to throat sill	m
$h_2$	Downstream flow head referenced to throat sill	m
$\Delta H_1$	The head loss across the upstream canal	m
$\Delta H_2$	The head loss across the downstream canal	m
$\Delta H_f$	Friction loss across the downstream canal	m
$\Delta H_L$	The head loss across the throat	m
$\Delta H_a$	The head loss across the approach canal	m
$\Delta H_b$	Friction head loss at the converging section of upstream canal	m
$\Delta H'_b$	Local head loss at the converging section of upstream canal	m

$\Delta H'_{b-opt}$	Extra head loss needed for perfect match of measurement	m
$\Delta H_v$	Energy head between entrance and throat section	m
$i$	Bottom slope rate of the canal	-
$L$	Flume length	m
$L_a$	Distance from gauging station to start of converging transition	m
$L_b$	Length of upstream converging section	m
$L_d$	Length of diverging transition	m
$L_e$	Length of tail water channel from transition of fully developed flow	m
$n$	Relative roughness	-
$p_1$	Upstream sill height relative to channel bottom	m
$p_2$	Downstream sill height relative to channel bottom	m
$Q_R$	Calculated discharge	m <sup>3</sup> /s
$Q_T$	Measured discharge	m <sup>3</sup> /s
$R_1$	Upstream measuring gage hydraulic radius	m
$R_b$	Flume upstream converging section hydraulic radius	m
$v_1$	Upstream measuring gage average flow velocity	m/s
$v_2$	Downstream average flow velocity	m/s
$v_c$	Average velocity at throat	m/s
$v_b$	Flume upstream converging section average flow velocity	m/s
$y_1$	Actual water depth at approaching channel	m
$y_2$	Actual water depth at downstream channel	m
$y_c$	Water level at throat section	m



# THE USE OF LOW-COST PNEUMATIC SENSORS FOR WATER LEVEL DETECTION IN PERMANENT STREAM GAUGE STATIONS

Kristoph-Dietrich Kinzli<sup>1</sup>  
David Gensler<sup>2</sup>  
Matthew Martinez<sup>3</sup>  
Aaron Morris<sup>4</sup>  
Zach Wohlpart<sup>5</sup>

## ABSTRACT

Permanent stream gauge stations are a common feature on irrigation projects worldwide, and their use is rapidly increasing. Modern iterations of these stations typically consist of an enclosure, a power supply, electronic data recording and/or communication equipment, and sensor(s). The sensor must typically produce an electrical representation of water level at the station, and be responsive to changes in that water, while maintaining a high level of resolution. The sensor is the connection between an uncertain physical environment and the electrical environment. As a result, sensors are generally the most troublesome component, and may easily introduce corrosion, electrical interference, and other potentially damaging influences to the other components of the station.

One technology currently available for water level sensors is pneumatic detection. A gas is allowed to exit from a small orifice located below the water surface, and the pressure required for gas to flow from this system is measured, providing an indication of the water head above the orifice. The primary advantage of this type of sensor is to provide physical separation of electrical components from the water, and if the orifice tubing is non-conductive, electrical isolation may also be achieved. Pneumatic sensors are also highly advantageous in systems with high silt or debris loads

Surface water irrigation facilities water levels are often less than 1-2 meters, requiring low pressures (< 200mB) for pneumatic measurement, which allows for the construction of simple low-cost pneumatic sensors. The cost of these sensors has fallen in recent years and is competitive with submersible pressure sensors of similar range and resolution. This paper presents the construction and use of these sensors, their suitability for use on irrigation canals, and a comparison of their performance with two types of low cost submersible pressure sensors.

---

<sup>1</sup>Assistant Professor, Department of Environmental and Civil Engineering, Florida Gulf Coast University, Fort Myers, FL; [kkinzli@fgcu.edu](mailto:kkinzli@fgcu.edu) (Corresponding author)

<sup>2</sup>Water Operations Manager, Middle Rio Grande Conservancy District, Albuquerque, NM  
[dgersler@mrgcd.com](mailto:dgensler@mrgcd.com)

<sup>3</sup>Hydrology Technician, Middle Rio Grande Conservancy District, Albuquerque, NM  
[mmartinez@mrgcd.com](mailto:mmartinez@mrgcd.com)

<sup>4</sup>Undergraduate Research Assistant, Department of Environmental and Civil Engineering, Florida Gulf Coast University, Fort Myers, FL, [apmorris5105@eagle.fgcu.edu](mailto:apmorris5105@eagle.fgcu.edu)

<sup>5</sup>Undergraduate Research Assistant, Department of Environmental and Civil Engineering, Florida Gulf Coast University, Fort Myers, FL, [zjwohlpa@eagle.fgcu.edu](mailto:zjwohlpa@eagle.fgcu.edu)

## INTRODUCTION

It seems quite plausible to surmise that the stream gauge was invented by the second man to begin irrigating a field using river water. Once two users attempted to utilize a common resource, it became necessary to apportion the resource between them, and some form of measurement was needed. Water level or stage, became a vital piece of information, along with the volume of water in the stream available for distribution. The historical importance of stream gauges is evident throughout the ancient world. Of the remaining ancient stream gages, one of the best known is the nilometer on Roda Island near Cairo, Egypt (Figure 1) dating back to 860 AD. The design of the nilometer is instantly recognizable to modern engineers, hydrologists, and water managers and consists of a stilling well, conduits connecting to the stream flow (the Nile River), and a simple sensor. The sensor is a calibrated column, and water level of the Nile can be visually evaluated. At particular levels it was known that water could enter specific canals, and flow volume was related qualitatively in terms of economic success.



Figure 1. The sensor (graduated stone pillar) in the Roda Nilometer. Similar gages dating back to 3000 BC can be found throughout Egypt. (Photo taken by author).

Remarkably stream gauging today has many similarities to the nilometer. Stream flow volume is still derived from stage and some form of sensor is required to evaluate water level. The ancient priests of Egypt read the water level from a graduated pillar and inscribed the value on papyrus. In modern times an electronic sensor supplies a variable output value that is recorded in a digital format. Our modern devices may prove inferior to the ancient ways. Many of those ancient inscriptions survive today, producing streamflow records for the Nile going back thousands of years. One must wonder if our digital recordings of river and canal conditions will persist for even a fraction of that time. It is interesting to note that the motivation for the nilometer was to levy taxes on the populace. Low flow resulted in an expectation of low crop yield, and a reduction in

taxes to be paid. A high flow increased yield, and farmers were thus expected to pay a greater annual tax. In modern times a vast number of stream gauges are operated to demonstrate the volume of water delivered, and hence the revenue due from users to those who distribute the water.

In ancient stream gauges the sensor was elegantly simple, consisting of marks carved in stone that were visually inspected and recorded. Conversely, the sensor in modern stream gauges is complex and generally the weakest link. It is required to translate vertical changes in water level into an output signal, and often involves considerable expense. The information age has resulted in stream gauging data becoming widely available over the internet. Water levels and flow rates of natural and man-made channels are expected to be instantly available and this mandates the use of electrical and electronic components. Unfortunately, water and damp stilling wells tend to be challenging environments for electronic devices. A wide variety of stage sensors have been developed over the years to deal with these difficult conditions.

### SENSOR TYPES

Aside from the staff gauge and a pair of eyes, the simplest sensor has traditionally been the float/cable. Rudimentary versions of these probably existed in ancient times, perhaps being ropes, logs, and stones. When the United States Geological Survey developed standard techniques, a float, steel tape (or wire cable), pulley, and weight, made an effective mechanism to produce an analog record by moving pens on paper. Vertical movement of water surface in a stilling well could thus be translated into mechanical motion at the top of a stilling well. The float/pulley/tape/weight is durable and low cost, but a few obvious drawbacks are apparent. Error can be introduced due to the mass of the tape, and the proportion of mass on either the float or weight side. Corrosion, deposits, vegetation, or floating debris can change the effective mass or surface area of the float. There is a limit to movement, and mechanical friction and inertia may influence readings, or cause failure of the mechanism. At the top, the device used to translate movement of the float into analog or digital values has also been a weakness. Early analog versions were extremely reliable, but were costly and could not readily produce a signal suitable for electrical transmission. A variety of devices were later developed to adapt these for electronic output, but at added cost and complexity.

Around 1950 the “shaft encoder” was developed, which dispensed with the clockwork analog devices and translated rotational motion of the pulley shaft directly into electrical output. The simplest versions of these utilize a potentiometer or rheostat, with the pulley mounted directly on the shaft. Many irrigation projects and even individual irrigators have built these in-house from low-cost components. While often tending to be fragile and having somewhat poor performance, they are a practical solution and used in many locales. More complicated versions are commercially available, and generally have a bearing-supported shaft with more sophisticated electronic components for greater durability and performance. Electrical encoders are of the absolute variety, meaning there is a specific output signal associated with any given position on the shaft. The optical encoder is yet another improvement for performance which has appeared,

allowing greater accuracy as a perforated disc or similar switching system allows very regularly spaced switching of the signal, and circuitry in the device counts the number of state changes. The optical device is inherently a relative encoder, meaning it starts counting from whatever point power is first applied. To cause it to function as an absolute encoder, mandatory for stream gauge usage, it must use some digital conversions to remember what point it was at when power was removed. While this is not difficult to do in the age of microchips, a problem occurs with this type of encoder should movement of the shaft occur when power is off. The encoder must then be recalibrated each time power is applied.

### **Submersible Sensors**

Submersible pressure sensors have gained increasing acceptance as a reasonable low-cost compromise and are widely used. These sensors use the piezo-electric properties of a material to vary a current through that material depending on the pressure applied. Pressure results from the column of water above the sensor head. The deeper the water, the more pressure is applied, and typically the greater the current that is passed through the sensor. Less expensive versions commonly produce a current output (4-20 milliamps) or a voltage output (0-5vdc) as analog signals. More advanced models use internal circuitry to convert the analog signal to a digital output such as SDI-12 or MODBUS. These are absolute sensors, in that they produce a specific output signal for any given depth of water. They are also advantageous in that power consumption is generally small, and they can be powered off when not actively making a measurement. When switching back on, warm-up time to stability is usually quite short (10-20 milliseconds). Drawbacks for their use are a degree of fragility, buildup of mineral deposits or corrosion around the sensor area, and risk of plugging from sediment. Many also tend to experience electronic drift over time, and may be sensitive to water temperature changes. However the biggest difficulty with the submersible transducer is clear in its name. Sensitive electronic components are submerged, often to a considerable depth, and sealing water out is challenging. No matter how well sealed the housing is, there must be a passageway for electrical cabling to enter the device. In order to measure pressure relative to atmospheric pressure, a conduit to the surface (vent tube) must exist as well. Even when liquid is effectively sealed out, condensation in the vent tube can still result in enough moisture entering the transducer to cause failure. In spite of these difficulties, many irrigation projects make wide use of submersible pressure sensors because of their relatively low cost and ease of installation and maintenance.

A myriad of other sensors exist. Capacitance sensors have existed for a long time, and have been used effectively in some areas. Acoustic sensors have been used on rivers and irrigation systems, and have the great advantage of no parts contacting water, although they have problems owing to temperature and humidity affecting the speed at which sound travels through air. Recently sensors have been developed which use radar waves reflected off the surface of the water to measure stage, though these are costly. However sensing of water level (or pressure) is performed, it is certain that there will be compromises. A truly perfect sensor has yet to be invented.

### Pneumatic Sensors

Around 1963 the USGS developed a pneumatic sensor system for stream gauge use (Hardison and Martin, 1963). Due to their habit of steadily releasing a slow, steady stream of bubbles into the water, they quickly came to be referred to as bubbler gauges. The bubbler was developed in response to difficulties in constructing and maintaining stilling wells at many sites in natural streams, particularly those which experienced constant lateral movement leaving stilling wells isolated from flow, or those with high flood and debris potential, that resulted in loss of equipment. The bubbler was a way in which a small piece of tubing could be led to the water. If the channel migrated away from the sensor, the tubing could be extended, or simply relocated to a better place. In floods, the tubing might be ripped away and lost, but it was a low cost item to sacrifice and could be quickly replaced when the waters receded. The bubbler could be installed in a conventional stilling well if desired, but it allowed for direct measurement of stage in many streams and canals without the construction of a stilling well. Thus it was advantageous for locations where stilling well construction was costly or impractical. The deletion of stilling wells became even more attractive after the development of electronic recording devices that were capable of averaging multiple readings, digitally “stilling” the water surface.

The underlying principle of the bubbler gauge is that gas pressure in the gauge’s tubing will be equivalent to the pressure exerted by the column of water above the discharge point of the tubing. The very simple principle becomes rapidly complicated by the reality of maintaining a supply of gas under a higher pressure than the expected maximum water level can exert, and accurately detecting the pressure in the discharge tubing. The traditional USGS system utilized tanks of high pressure nitrogen and an array of manifolds and regulators to provide a very slow and steady delivery of nitrogen gas to the discharge tubing, producing a slow regular release of gas bubbles and maintaining steady pressure in the tubing. Reading pressure in the tubing was accomplished with a precise sloped manometer filled with mercury. These early USGS bubblers were complex, and maintaining them properly was difficult for technicians. There was also the potential for contamination from mercury. However they produced reliable measurements, with the only real drawback being that the nitrogen tanks required regular replacement.

Over time, the original design evolved considerably. Mercury manometers have been gradually replaced with electronic pressure sensors. Small air compressors and storage tanks have replaced many of the old nitrogen tanks. These are packaged by a number of commercial suppliers into self-contained bubbler sensor systems, incorporating the compressor, air storage, pressure sensor, and data recording device in one integrated component. Commercial sensor systems have proven well-built and reliable, but are costly (\$3000-\$5000). They utilize compressors maintaining a small reservoir of pressurized air, and due to the high pressure of the stored air relative to the required discharge tubing pressure, have moderately high electrical power requirements (20-25 ma)

### DEVELOPMENT OF A LOW-COST PNEUMATIC (LCP) SENSOR

Development of a relatively low-cost alternative to existing pneumatic sensors emerged as an offshoot of testing and calibration of venturi flumes for flow measurement at the USBR Water Resources Research Laboratory (WRRL) in 2006. At that time, researchers were exploring multiple methods of correcting these flumes for varying degrees of submergence, requiring pressure measurements to be made at multiple locations as water passed through the structures. Various pressure taps were used on laboratory models, connecting to stilling wells equipped with hook-type point gauges and vernier scales allowing water levels to be detected to within 0.35mm (0.001'). Eventually it was determined from this effort that pressure measurements made at three distinct locations could successfully be used to correct the flumes for high levels (up to 95%) of submergence. Because the differences in pressure between the three locations could be quite small a very high level of accuracy was required, and a significant source of potential error could be eliminated by using a single sensor for all three measurements. Initially this was done by manually connecting tubing from the three locations to a single pneumatic sensor. It was realized early in the research that if this work were to result in practical field applications, a sensor with a manifold and electrical switching capabilities would be needed.

Existing commercial devices were relatively costly, but it was apparent the much of the cost was due to their being smart devices. Though capable of providing simple analog outputs, all included on-board electronics to enable them to operate as stand-alone units. While this enabled them to do the purposes they were designed for, it resulted in redundant electronic intelligence that provided no enhancement in the functionality sought for the project and came at significant cost. It was believed that a functional sensor could be created with little more than a small air compressor and a sensing element. Implicit in the design of the sensor was that a brief addition of gas (air) to the line would very quickly equilibrate within the sensor plumbing to a pressure equivalent to the pressure exerted by water above the discharge point (orifice) of the system, allowing for simple plumbing without any gas flow regulators. Electrically operated solenoid valves could automatically connect the single sensing element with the appropriate pressure point to be measured. WRRL constructed prototypes of this design using available low cost components (Figure 2).

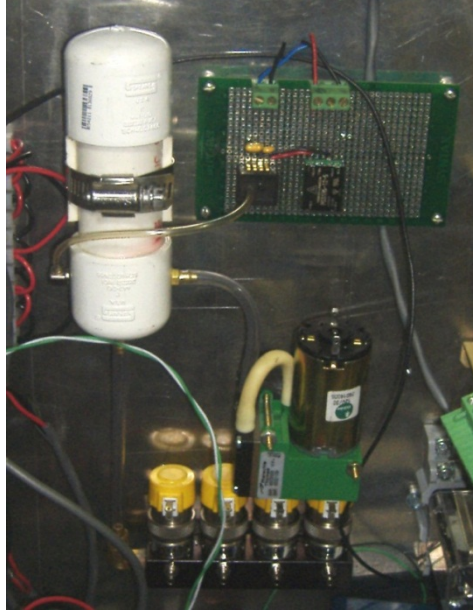


Figure 2. Prototype LCP sensor at WRRL (courtesy of Tom Gill)

Researchers engaged the assistance of Control Design , Inc. (CDI) to produce a small run of complete LCP sensor units using the components that had been identified. CDI produced a printed circuit board suitable for mounting the components and simplifying wiring connections. The sensor used a single source of pressurized air that could be directed to three separate pressure lines via electrical solenoids and a manifold. A single pressure sensor was incorporated which could detect pressure in any line selected.

Initial field tests were conducted in Yuma, Arizona on measurement structures in canals of the Yuma County Water Users in 2009. The tests at Yuma were primarily oriented towards verifying laboratory conclusions about submerged flow measurement correction in 443enture flumes. However it also proved to be a practical test of the utility of the LCP sensor. An ADCP was used alongside the flume tests at Yuma to verify rates of flow, confirming the ability to do submergence correction calculations for the flumes by measuring pressure at multiple locations, and incidentally evaluating the effectiveness of the LCP sensor. Based on the successful use of the sensor at Yuma, CDI began offering its production commercially.

### **Specifications of the Low Cost Pneumatic Sensor**

The LCP sensor is assembled from readily available off-the-shelf components. The unit is constructed around a Thomas model 8003055 compressor. This small precision air supply is capable of producing 3.0 l/min or a maximum pressure of 2000 millibar (mb) (30 psi). Stream gauge applications, at least those typical of irrigation canal settings, rarely encounter water depths greater than 2 meters (6.5 ft), so the compressor is quite under-stressed generating no more than 200 mb (2.9 psi). At this pressure, the compressor is able to produce about 2.6 l/min. The compressor is powered by a 12vdc sealed-bearing electric motor consuming 8.5 watts at 3000 rpm.

Pressure sensing is accomplished by a Honeywell ASDX series sensor. These are available in a wide variety of pressure sensing ranges, from as little as 25 mB (0.36 psi) to 7000mB (100 psi). Commonly used on the CDI LCP sensor are 70 mB, and 350 mB (0-1, and 0-5 psi) ranges. Higher pressure ranges are available if needed, though the 200mB unit appears particularly well suited for most canal settings. Several units are currently in use to measure pressure in discharge piping from pumped wells. The sensor element requires a stable 5vdc power supply (optional 3.3 vdc). Output from the sensor is then typically 0.5-4.5 vdc. The sensor is designed to be mounted on a printed circuit board. Generally the pneumatic sensor is equipped with a single pressure sensor, though it is possible to use two different sensors and switch ranges when necessary via an electrically controlled manifold valve. The CDI unit allows for installation of two pressure sensors on a single board, selected by jumpers. Overpressure range of the pressure sensor is 2x the chosen pressure range, a significant concern for installations that could potentially see ice formation. A pressure relief valve could potentially be used to protect the sensor from overpressure if desired. The sensor is temperature compensated, and able to withstand environments ranging from -50 C to 105 C. The sensing unit itself is relatively low cost (<\$40.00) and may be readily replaced if damaged.

A one way check valve is used just downstream of the compressor, preventing any loss of pressure through the stilled compressor. A T fitting connects the compressor and checkvalve to the orifice (bubbler) line in one direction, and the pressure sensor in the other. A small metal chamber is installed between the orifice line and the pressure sensor. The purpose of this chamber is to provide a damping effect on pressure surges reaching the sensor, which was found to be advantageous during laboratory testing and allows pressure to stabilize more quickly. The chamber typically used is a Clippard AVT-17-2 32.8 cc (2.0 cubic inch) volume tank. For higher pressures or long discharge lines, a larger 49.2 cc (3.0 cu in.) chamber is used.

The above components comprise the air supply and sensor system for a single output pneumatic sensor. Simple 1/8 inch plastic tubing is used for connections. The orifice line may be any suitably durable small diameter tubing. Fittings should be high quality and carefully assembled to be leak-free. The connection to the pressure sensor is 1/16 tubing, requiring a reduction fitting from the volume chamber. The commercially available CDI unit uses stainless steel Clippard fittings throughout. Optionally, a manifold may be added to allow for sensing pressures of multiple orifice lines. For the CDI product Clippard EV-2M-12 solenoid valves are used, mounted on a Clippard manifold. This allows the compressor and sensor to be connected to 1, 2, 3, or 4 orifice lines.

The CDI product uses a printed circuit board both for wiring of the components, and to provide a convenient mechanism for physical mounting. Additional components of the pneumatic sensor are a few assorted small electronic parts (capacitors and diodes) related to protecting the other devices, and a connector for wiring inputs and outputs. The result is a compact sensor unit easily installed at most locations (Figure 3). Size of the completed CDI product is approximately 140mm x 170mm x 40mm (5.5' x 6.75" x 1.5")



Figure 3. CDI LCP sensor showing components. (3 output version with solenoid valves and manifold).

Power consumption of the complete unit is minimal. When not actively making a measurement, the board is completely switched off and power consumption is zero. The compressor itself uses a considerable amount of power when running, but a measurement requires the compressor to run only 0.1 sec. Set up to collect a single pressure measurement on a 15 minute cycle, power consumption is equivalent to a steady drain of less than 3.5ma/hr. An installation using the solenoid valves to measure three separate locations on a 15 minute cycle would result in power consumption equivalent to a steady drain of less than 12ma/hr.

### Use of the Pneumatic Sensor

While the sensor is potentially capable of operating as a constant bubbler and generating an analog electrical output, doing so in the absence of pressure regulation and more complex plumbing would not be sensible in terms of power consumption. Unlike early USGS pneumatic sensors, and modern commercially available units which use a regulator to deliver a small flow of pressurized gas to the orifice line, the CDI sensor does not require a regulator on the orifice line. Instead the compressor is cycled very briefly any time a measurement is to be made. Since it is expected that the output will be converted by a data-logger or other such device into digital form, practical operation is to use the same device for control of the compressor (and switch orifice lines if desired).

The data-logger used with this pneumatic sensor is thus required to have the ability to turn power on/off to the compressor, and the pressure sensor as well, if maximum efficiency is desired. Many modern dataloggers now have these types of input/output capability, as well as flexible programming potential. The units tested for this report, and those presented as examples of field installations, use programmable (RP-52 BASIC) CDI Radio Terminal Units (RTU) to control the sensor. These units program in BASIC

(RP-52 BASIC). To read the sensor the program triggers an approximately 0.1 second burst of power to the compressor, which cycles briefly, slightly increasing pressure in the orifice line and forcing a small volume of gas (5 ml) from the orifice. The pressure in the line then quickly stabilizes at a pressure equivalent to the head of water above the submerged orifice. The program then pauses briefly (1 second), before beginning to evaluate pressure.

The brief surge in pressure and the absence of a regulator require care when evaluating pressure readings. It must be verified that pressure in the line has indeed stabilized after the compressor has cycled. To accomplish this, a series of 10 sequential samplings of the analog output from the pressure sensor are made. All values are converted to a digital format and temporarily stored. The initial reading is then compared with the average of the 10 readings. If outside of a user specified tolerance, the measurement is rejected and the process is repeated. In the present iteration, about 25% of initial readings are rejected, though this could be improved either by increasing the acceptable tolerance (currently equivalent to 0.3mb (0.01')), or increasing the pause after compressor shutdown and before sensor sampling is initiated. On very rare occasions (less than 1%) a third measurement cycle may be required. It appears that use of the mouse valves to select orifice lines may be associated with most, if not all of these rejected initial readings. The current program opens the mouse valve and cycles the compressor simultaneously, but it may be necessary to operate the mouse valve with a slightly different timing than the compressor and this could decrease the incidence of rejection of initial readings. Physical properties of the orifice line tubing (length/diameter) and the size of the volume chamber will also have an effect on time to stabilization, and should be considered by the user. Orifice line runs of up to 20 m are in use by the authors. At least one user is reportedly having success with an orifice line run of about 450 m.

Once the RTU has verified a successful measurement cycle, the digital pressure value is converted using slope and offset to a recognizable engineering value (meters, or feet, of water depth) and permanently stored. It may then be either retrieved via telemetry (built-in radio/modem in the CDI unit) or manually collected. In the example currently used for this report, a wide range of parameters, including duration of compressor run (0.1s), pause before first pressure reading (1s), number of pressure readings to average (10), tolerance between first reading and average (0.01'), sensor slope (.00352), sensor offset (-1.4418), and engineering offset are set in the program as variables. However, the user is free to adjust these parameters to other values, or create an entirely different program if desired. Any programmable controller capable of generating switch closures to cycle the pump/sensor (or operate mouse valves, if needed) and accepting an analog voltage input could be used with the pneumatic sensor.

### **USE OF LCP SENSORS IN THE MIDDLE RIO GRANDE CONSERVANCY DISTRICT**

A number of LCP sensors are currently in use at the Middle Rio Grande Conservancy District (MRGCD). The first was installed in May 2011 (Figure 4). At this location two separate channels, the Corrales Wasteway and the Lower Corrales Drain, are in close

proximity to each other, allowing a single gauge to monitor both facilities. A gauge with a submersible pressure sensor had existed for some time on the Corrales Wasteway, but had been a poor performer due to frequent drying/wetting cycles, sediment, and growth of algal mats on the floor of the structure. In particular the regular complete drying of the wasteway seemed to result in almost constant drift of the submersible sensor, requiring constant adjustment of the engineering offset value. The Lower Corrales Drain had not previously been measured.



Figure 4. LCP Gauge for Corrales Wasteway and Lower Corrales Drain. The wasteway is the concrete channel and the drain passes below.

Construction of the new gauge utilized a CDI 110 RTU operating a CDI CD103 LCP sensor with 3 outputs. One output was terminated on the concrete floor of the Corrales wasteway structure just before it drops to the Rio Grande (Figure 5). The second output was terminated on the upstream wall of a concrete flood control structure in the Lower Corrales Drain just before it empties to the Rio Grande, and which was expected to provide hydraulic control for the gauge. The third output was not used. Both of these gauges have worked well since installation. It has been learned that the concrete control structure in the drain can and does become partially submerged, so a planned improvement for this gauge is to construct a long throated flume and use the third output to make a downstream pressure measurement for submergence correction.



Figure 5. LCP sensor orifice affixed to Corrales Wasteway. The small plastic tube is protected by PVC.

Another installation was made on the Atrisco Drain Outfall in October 2011 (Figure 6). In this case a single output CDI CD103 LCP sensor was used, along with the CD110 RTU (Figure 7) for control and telemetry. Similar to above, the orifice line was terminated on the upstream face of a concrete flood control structure. This installation has operated flawlessly since completion (Figure 8)



Figure 6. LCP sensor gauge at Atrisco Drain



Figure 7. Internal components of gauge at Atrisco Drain



Figure 8. LCP sensor “bubbling” during measurement cycle

Additional installations were made over the winter of 2011/2012 in two canals. The first of these, the San Antonio Lateral (Figure 9), involved a single output sensor, with an orifice line terminating on the concrete sloping (1.5:1) wall of the canal approximately 0.1 meter below the elevation of a small ramp flume. The previous installation at this location had used a submersible pressure transducer, but fine clay deposits upstream of the flume had a tendency to foul the sensor. Since replacement with the pneumatic sensor, no further difficulties have been encountered with this gauge, and the orifice has remained clear of sediment. The second gauge installed in a canal was on the Socorro Main South Canal. Much like the other canal, this location was also equipped with a ramp flume and the nose of the submersible pressure transducer frequently became solidly plugged with clay. A three outlet LCP sensor was used since it was known that a downstream check structure occasionally submerged this flume, and correction would be necessary whenever the downstream structure was in use. This installation has also worked well and has not experienced any plugging of the orifice lines.

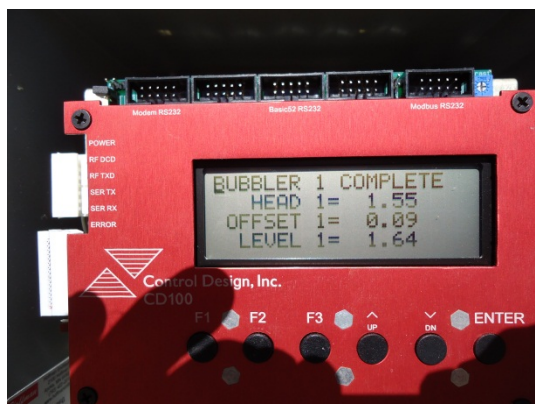


Figure 9. LCP completing a measurement cycle and displaying stage on LCD screen for the San Antonio Lateral

Additional installations are being made over winter 2012/13 for use during the 2013 irrigation season. In all cases, installation is completed in less than one day. Materials cost can be seen in Table 1.

Table 1. Material costs for instrumentation with LCP sensor (all costs in \$)

	Single Output	Multiple Output
Sensor (CDI CD103 LCP “bubbler”)	600.00	800.00
RTU (CDI CD110 controller/modem/radio)	1700.00	1700.00
Battery(s), 26AH+12AH	80.00	80.00
Antenna/cable/connectors	150.00	150.00
Solar panel, 20 watt	170.00	170.00
Gauge Housing (shop fabricated)	100.00	100.00
Lock (“hockey puck”) and Hasp	60.00	60.00
Enameled Staff	40.00	40.00
<u>Misc tubing/pvc/connectors</u>	<u>50.00</u>	<u>50.00</u>
Total	2950.00	3150.00

The materials cost for MRGCD to construct a single telemetry equipped gauging station using an LCP sensor is about \$3000. This is virtually identical to the cost of building a similar station using a submersible pressure sensor (\$600) mounted to the wall of the canal. Greater economy is realized for sites where a stilling well might otherwise be necessary. At sites featuring multiple gauges (2 or 3 canals in close proximity), the multiple output sensor (\$800) has a distinct cost advantage over the purchase of multiple submersible pressure sensors (2-\$1200, 3-\$1800)

In addition to the MRGCD, and the previously mentioned work at Yuma County WUA, the LCP sensor is currently in use at several other irrigation projects. Within New Mexico the Elephant Butte Irrigation District has employed several, and Carlsbad Irrigation District is currently installing their first units. Elsewhere the Mohave Valley IDD in California, Farwell and Sargent Irrigation districts in Nebraska, and South Platte Ditch Company in Colorado are currently using the LCP sensor. Most of the installations

involve measurement of water levels through flumes, although MVIDD and EBID also are using the LCP sensor to measure flow in pipes discharging from wells.

### LABORATORY PERFORMANCE EVALUATION

Of course there is little advantage to cost saving if the device does not perform the job intended, and to an acceptable level. Accordingly, a series of tests for the LCP sensor described here were devised. Tests were performed by the Civil Engineering department at Florida Gulf Coast University (FGCU). For comparison purposes, commercially available submersible pressure sensors from two different manufacturers were also subjected to the same test procedure. These were referred to as submersible sensor #1 (HOBO U20) supplied by Onset Computer Corp. of Bourne, Massachusetts; and submersible #2 (INW-PS9800) supplied by Instrumentation Northwest of Kirkland, Washington. Both of these submersible pressure sensors are comparable in cost (\$500-\$600) to the commercially available version of the LCP sensor (\$600).

FGCU students and faculty constructed a test apparatus (Figure 10). This apparatus consisted of large diameter PVC tube over 10 feet (3m) in length. The tube was mounted vertically to provide a column of water for testing. At the bottom of the tube an elbow was attached creating a manifold in which sensors could be installed for testing. The manifold was carefully constructed to ensure that all installed sensors were at precisely the same elevation relative to the water column. Sensors were installed using a laser level to insure that all three were at the exact same elevation. A series of small holes were drilled along the length of the vertical PVC tube, at precise 1.00 foot (0.3048m) intervals above the sensor manifold.

To test a particular type of sensor, three examples of that sensor were installed in the manifold and the mounting holes sealed. The vertical tube was then filled completely with water. The entire apparatus was then carefully laser leveled and adjusted prior to beginning each test. To begin testing, the uppermost hole in the vertical tube was unplugged, allowing water to drain by gravity to an elevation 10.00 feet (3.048m) above the sensor manifold. A series of measurements were then made at 1 minute intervals for each sensor, ranging from a minimum of 22 to a maximum of 30 total measurements from each sensor at a particular water level. Groups of three sensors were tested simultaneously. After all measurements were collected at 10.00 feet (3.048m), the next lower hole was unplugged, allowing water in the tube to drain to the 9.00 feet (2.727m) level, and the process of collecting measurements from the sensors was repeated. The process continued through successive iterations until measurements had been collected from all water levels down to and including 1.00 feet (0.3048m) above the sensor manifold.



Figure 10. Sensor test apparatus showing manifold

Measurements were collected from the sensors through electronic means, converting the electrical signal output of the sensors to appropriate engineering values. Measurements were collected from LCP sensors and INW submersible pressure sensors using a Control Design CD110 programmable controller. Measurements were only collected from depths of 5 feet and below for the INW sensor as this was the limit of the sensors. The CD110 unit was programmed with scale and offset values derived from the electrical properties of the sensors and physical properties of water.

In the case of the LCP sensor, a scale factor of (0.00352), and an offset of (-1.4418) were used, based on the following parameters:

Pressure range: 0-5 psig, 1 psi=2.3068' water, 0-11.534' water

Electrical output: 0.5-4.5vdc, 16 bit A-D, 5 vdc into 4096 units, 0.001221vdc/unit

Outputs: 0psig=0.5v/0.001221=409; 5 psig=4.5v/0.001221=3686

Range=(3686-409)=3277

Scale=(11.534/3277)=0.00352

Offset=(-409)\*(0.00352)= (-1.44)

For the INW sensor, a scale factor of (0.001408) and an offset of (0) were used.

Pressure range: 0-2.5 psig, 1 psi=2.3068' water, 0-5.77' water

Electrical output: 4-20ma, 16 bit A-D 16 ma into 4096 units, 0.003906ma/unit

Outputs: 0psig=((4ma/0.003906)-1024\*)=0; 2.5 psig=((20ma/0.003906)-1024\*)=4095

\*note: CDI units internally adjust 4-20ma sensors to zero during AD conversion (-1024)

Range=(0-4095)=4096

Scale=(5.77/4096)=0.001408

Offset=(0)\*(0.001408)=0

Measurements from the HOBO submersible pressure sensor were collected as final engineering values directly from the sensor using a laptop computer. The HOBO scale and offset values are pre-programmed by the manufacturer and it is unclear if they are electrical/physical derived values, or have been determined by the manufacturer from empirical testing.

All measurements collected were tabulated in a spreadsheet for evaluation. A summary of the results is provided in Table 2. In the summary, the mean was computed from the entire set of measurements (n=22-30) from a particular sensor at a particular water depth. For convenience, the height of the water column above the installed sensor location is noted simply as “water depth”.

Table 2. Summarized test results for all sensors

Test Column	Pneumatic Sensor			Submersible 1			Submersible 2			
	Sensor1	Sensor 2	Sensor 3	(HOBO)	Sensor 1	Sensor 2	(INW)	Sensor 1	Sensor 2	Sensor 3
Water Depth	(ft)	(ft)	(ft)	(ft)	(ft)	(ft)	(ft)	(ft)	(ft)	(ft)
1.00	1.065	1.035	1.023	1.035	0.974	1.009	1.025	1.036	1.045	
2.00	2.051	2.018	1.995	2.051	1.985	2.017	2.005	2.016	2.030	
3.00	3.029	3.004	2.982	3.028	2.960	2.994	2.989	3.003	3.018	
4.00	4.008	3.984	3.955	4.025	3.954	4.000	3.978	3.993	4.012	
5.00	5.009	5.000	4.946	5.022	4.951	4.984	4.966	4.983	5.002	
6.00	5.990	5.999	5.918	6.028	5.948	5.991	--	--	--	
7.00	6.966	6.973	6.898	7.015	6.949	6.978	--	--	--	
8.00	7.950	7.958	7.867	8.012	7.939	7.968	--	--	--	
9.00	8.932	8.950	8.858	9.025	8.948	8.971	--	--	--	
10.00	9.925	9.945	9.832	10.000	9.923	9.944	--	--	--	

The LCP sensors measurements from each water depth produced standard deviations ranging from 0.004 feet to 0.017 feet. With the exception of a single sensor at the 9.00 feet depth (0.017) all standard deviations were effectively equivalent to 0.01 feet or less. This resulted in a very tight clustering of data near the expected result. For comparison, the HOBO sensors produced standard deviations ranging from 0.003 feet to 0.008 feet. INW sensor results produced standard deviations ranging from 0.001 feet to 0.007 feet. The standard deviations of all sensors were very small, and well within the 0.006 feet that represents the practical resolution limits of the test apparatus.

The slightly greater standard deviation seen by the LCP sensor may have been the result of releasing a small pulse of air into the water column tube, destabilizing the water surface. Although the water surface appeared to quickly calm after the pulse, the small diameter of the tube and limited volume probably resulted in a slight instability (waves) of the water column. Since the submersible pressure sensors do not introduce air to the water column and have no moving components, they would not result in such effects. If

the LCP sensor were installed in a volumetrically large chamber, such as a stilling well, or an open canal or other body of water, this effect would be minimized.

Within groups of the same type of sensor, there were slight differences in performance between individual sensors. Particularly with the LCP and the HOBO sensors, there was one of each type that produced slightly lower values than the other two. This could be readily corrected with an adjustment to the sensor offset if using the LCP, or through post-processing of the output from the HOBO sensor. These differences are evident when comparing across all mean sensor values (Figure 11).

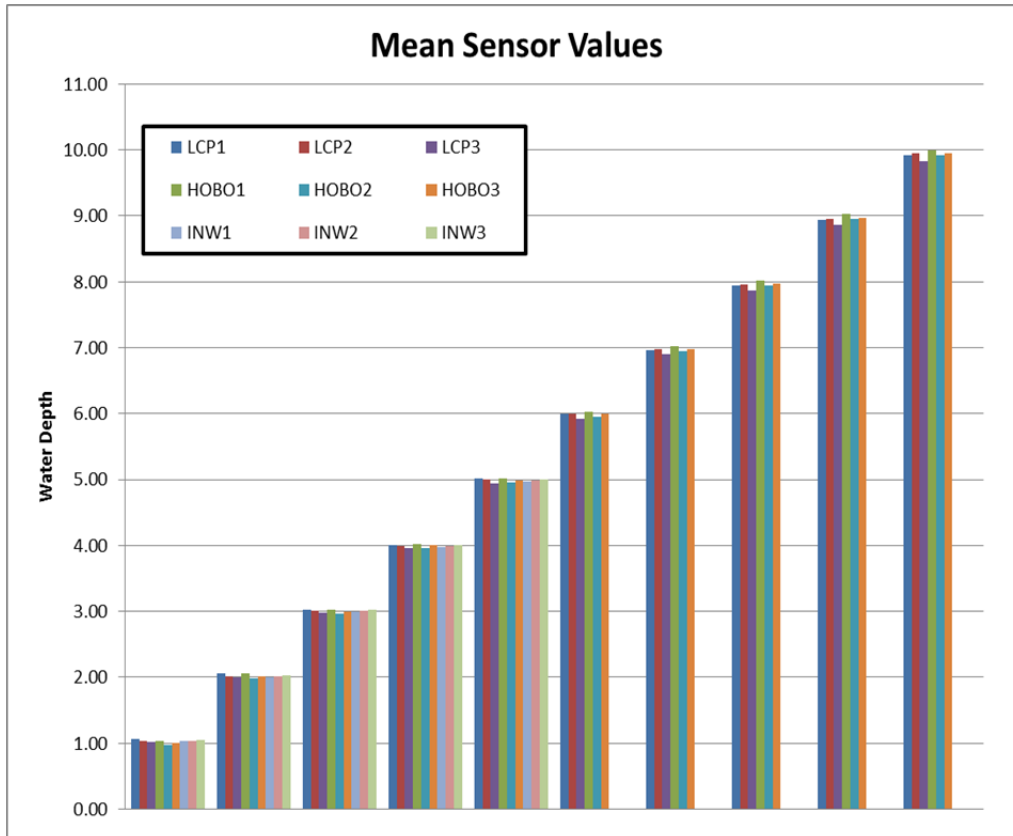


Figure 11. Comparison of mean sensor values

Both the LCP sensors and the INW sensors demonstrated a slight but noticeable drift away from the expected value with increased water depth. Since the electrical outputs of both sensors increase with increasing water depth, this is attributable to the scale factor used. An empirical recalibration of the scale and offset factors used for the LCP sensors in this test to 0.00356 and -1.51 respectively would have yielded even better results. A similar recalibration could readily be done for the INW sensor.

Particularly in the case of the offset value, it would be reasonable to determine this individually for each sensor. In fact, during practical use of these sensors at the MRGCD, the programming used in the CDI units to operate the sensors incorporates a zeroing mechanism for when the sensor is first installed, that effectively creates a unique

offset for each sensor. During field visits to these gauges, calibration is checked by technicians and can be adjusted if necessary. To date it has not been necessary to make any adjustments subsequent to the initial calibration.

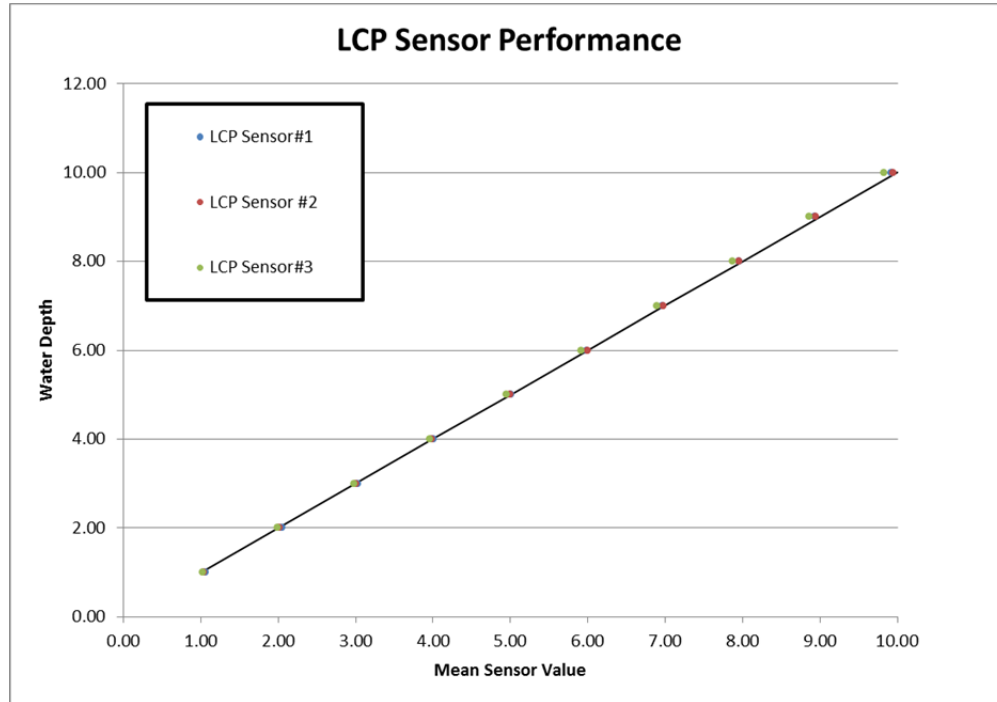


Figure 12. LCP sensor measurements plotted against ideal water depth

The LCP sensor performed quite well (Figure 12) in measuring water levels in the test column. Values from all 3 LCP sensors tested plot so closely together that the differences are very difficult to discern. The slight trend away from the expected value with increasing water depth is evident from the plot, but would be readily corrected by a slight increase to the scaling factor.

## CONCLUSION

The use of the LCP sensor is a practical alternative to the use of submersible pressure sensors in many applications. The components used in these sensors are readily available and adequately rugged for use in the settings typically encountered along irrigation canals. Performance of a commercially available version of this sensor was equivalent to that of similarly priced submersible pressure sensors. Installation using pneumatic sensors is often considerably simplified over other types of sensors. The only component of the pneumatic sensor in contact with water; or exposed to damage from sediment, debris, or vandals; is low cost, easily replaceable small diameter tubing. The LCP uses commercially available off-the-shelf components, which can be readily replaced should they fail or be damaged. The ability to sense multiple pressure heads with a single sensor

opens additional opportunity for cost savings over other sensor types. This sensor shows promise and long term in field studies of its performance should be conducted.

#### **ACKNOWLEDGEMENTS**

The authors would also like to acknowledge Dr. Thomas Gill for his resourcefulness in developing the LCP; Mr. Jim Conley for moving it to commercial production; and Mr. Mark Chew of Florida Gulf Coast University for his assistance in developing the testing apparatus.

#### **REFERENCES**

Hardison, C.H., and Martin, R.O.R., 1963, Water-supply characteristics of streams in the Delaware River basin and southern New Jersey: U.S. Geological Survey Water-Supply Paper 1669-N, 45 p.

# EVENT-DRIVEN HIERARCHICAL CONTROL OF IRRIGATION CANALS

Anna Sadowska<sup>1</sup>  
Bart De Schutter<sup>2</sup>  
Peter-Jules van Overloop<sup>3</sup>

## ABSTRACT

We present a novel, simple and cost-effective strategy for control of irrigation canals to aid water deliveries to the users through the canal. The method enhances water deliveries through the canal by incorporating, alongside local PI controllers maintaining water levels in each canal pool at some predefined setpoints, a higher-layer centralized controller. The purpose of that centralized controller is to coordinate the local controllers by modifying the setpoints in individual pools. This speeds up the delivery process so that water is available to users faster than when only local controllers are used. Because the higher-layer centralized controller is invoked only when deliveries are requested and in normal operating conditions the canal is maintained merely by the local upstream PI controllers, the method is computationally efficient and resilient to temporary communication failures. We use Time Instant Optimization Model Predictive Control as the main control framework to design the higher-layer centralized controller and present a simulation study to illustrate the method proposed in this paper.

## INTRODUCTION

Irrigation canals are open channels that transport water through the land from a source (a river or a reservoir) to users (farmers) for the purpose of irrigation of crops (Chow, 1959). They consist of a number of pools that are interconnected with one another in a cascade by hydraulic structures (e.g. gates) that control water flow between neighboring pools. Considering the vast importance of irrigation canals in agriculture, it is a crucial task to be able to control the water flow through a canal efficiently and effectively, and ideally with minimal resources involved.

There are numerous methods proposed in the literature to control water flow in irrigation canals (Malaterre and Baume, 1998; Rutz et al., 1998; Malaterre, 2007; Weyer, 2008). Some rely on manual controlling of the gates by a human operator. These methods, however, may fail to provide a sufficiently good performance due to many variables describing the state of the canal that the operator may need to account for, which ultimately may prove intractable. An alternative to manual operation of gates in a canal is automatic control where the gates between individual pools are controlled automatically employing various types of feedforward or feedback controllers (Van Overloop, 2006; Schuurmans, 1997). In general, the functioning of feedforward controllers depends entirely on the internal model of the system that a controller uses. Then, knowing external inputs affecting the system, a feedforward controller calculates the appropriate control

---

<sup>1</sup> Delft Center for Systems and Control, Delft University of Technology, email: A.D.Sadowska@tudelft.nl

<sup>2</sup> Delft Center for Systems and Control, Delft University of Technology, email: B.DeSchutter@tudelft.nl

<sup>3</sup> Water Resources Management, Delft University of Technology, email: J.A.T.M.vanOverloop@tudelft.nl

inputs by verifying the effect of the disturbances on the model. In contrast, feedback controllers act in response to actual measured signals (e.g. water levels) and according to pre-specified rules, they set up the control inputs to counteract any disturbances given the observed effect of the disturbances on the system.

Controllers can be classified as centralized when there is a central governing entity that takes into account the state of the whole canal and calculates control inputs for all canal pools according to the information available (Malaterre, 2007; Sepúlveda Toepfer, 2007). The main advantage of centralized controllers is the fact that they have access to global information regarding the canal and thus see the broad picture of the situation. However, for large-scale problems centralized algorithms may require significant computational effort to produce results in a reasonable time due to many variables that they need to consider. On contrary, decentralized controllers use only local information. More specifically, to determine a suitable position of a gate in a pool, a controller takes into consideration the state of that particular canal pool and, possibly, the state of pools immediately upstream and downstream. Another kind of control algorithm using only local information are distributed controllers. They use inter-gate communication to find a control action that is not only satisfactory for themselves but also for the neighboring pools. Therefore, distributed controllers aim to obtain a solution that is of comparable quality to the solution that would be given by a centralized controller (Šiljak, 1991; Negenborn et al., 2009b). While in many dynamical systems it is beneficial to use distributed controllers, in the case of canal control it can be argued that in fact it is more advantageous to employ a centralized controller over a distributed controller due to the stationary nature of a canal and a large amount of communication between neighboring gates that may be needed for the gates to reach values of control actions suitable for all of them.

In practice, despite the benefits that sophisticated controllers can provide, very simple controllers are often used owing to their low cost and robust functioning. A very popular solution is the application of an upstream PI controller to control gate position locally in every canal pool (Litrico et al., 2003; Van Overloop et al., 2005; Litrico and Fromion, 2006; Litrico et al., 2007). PI controllers are feedback controllers that react to deviations in water levels with respect to some given setpoint (Åström and Hägglund, 1995). Since they do not depend on any particular model of the plant, they are widely used and in fact, when tuned properly, are able to provide a rather satisfactory performance.

In this paper we present a strategy to improve the performance of local PI controllers applied at individual gates for upstream control in order to facilitate water deliveries to users through irrigation canals. To that end we propose a hierarchical control structure, see Figure 1. Our proposed scheme is such that in normal operating conditions, only local PI controllers take care of the water flow in the canal. However, when any of the users announces a sudden delivery request, a higher hierarchy centralized controller steps in to coordinate the individual canal pools and thus enhance the delivery process. This centralized controller (hereafter called the Coordinator) uses Model Predictive Control tools to compute its control action and communicates it to the local sites only when changes are needed. Therefore, the alterations to the settings of the local sites are

infrequent. In such a way, the local controllers remain fully in charge of the canal when there are no deliveries requested and the centralized controller is used to help coordinating the deliveries only. By allowing the local PI controllers to take care of the canal and changing the settings of the local sites infrequently to aid a delivery, we make sure that even if the communication lines fail for some time, the control remains acceptable due to the PI controllers, which can control the canal independently of the Coordinator.

As said earlier, the Coordinator only acts in response to a new delivery request. Thus, it is event-triggered as opposed to time-triggered. To that end, we propose to use the Time Instant Optimization (Van Ekeren et al., 2011), which allows to define how many times the setpoint may be changed and essentially optimize the switching time instants.

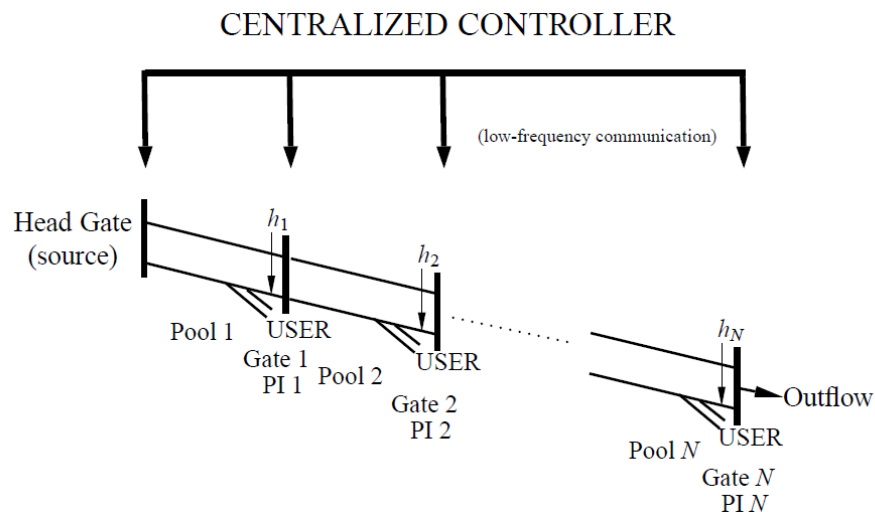


Figure 1. A schematic of the hierarchical controller proposed in the paper.

The rationale behind the application of the higher-layer centralized controller is as follows. When a delivery is requested and only local PI controllers are in use, it may take a considerable amount of time before water is available to users due to the time that is needed for water to travel from the source to the user. In particular, when only PI controllers operate and water is requested by one of the users, the required volume is released from the head gate. Then, as that extra amount of water reaches pool  $i$ , the local PI controller reacts to an increased water level and pushes it towards the subsequent pool  $i+1$ . This situation is repeated until water reaches the user. Therefore, depending on the distance between the head gate and the user, the delay may be significant. While the Coordinator cannot change the internal property of the canal of how long it takes for water to travel between the head gate and any single pool, the way the Coordinator works is to coordinate the local sites and by changing the setpoints in the pools, the Coordinator makes the water available to the user quicker than it would be without the Coordinator. Importantly, one of the main advantages of the way the Coordinator works is that it performs its job with minimal possible disruption to further parts of the canal. For example, if some base flow is needed for downstream users, the Coordinator aims at preserving that flow as closely as possible.

The idea of altering setpoints was previously proposed for power networks in (Negenborn et al., 2009a) where a supervisory control problem to prevent voltage collapse in the network was considered. Prominently, however, the supervisory controller provides new setpoints after each run of the optimizer, which is undesirable in our system because of the restriction of how much and how often the Coordinator can interfere with the local sites. For water systems, the concept of changing setpoints and hierarchical control structure was studied in (Zafra-Cabeza et al., 2011) for the purpose of risk management. In particular, various risk factors were defined: operational, financial, political and others. Considering these risk factors, the functioning of the higher hierarchy controller is to adapt the setpoints when needed to minimize the risk exposure. This control layer as well as the lower layer control are both realized employing the MPC strategy. Moreover, the lower layer controllers are distributed and thus, arguably, a significant volume of communication between individual controllers might be needed for the controllers to reach consensus on what control actions to apply. In addition, the scheme proposed in (Zafra-Cabeza et al., 2011) allows to change the setpoints freely in terms of frequency, which does not comply with our system's requirements.

The outline of this paper is as follows. In the next section we give some preliminaries regarding the topic: we present the dynamic model of the canal as well as present the main concepts of Model Predictive Control and Time Instant Optimization. Then, the hierarchical controller is introduced and, in the following section, its functioning is illustrated in a simulation study. After that we give our concluding remarks.

## PRELIMINARIES

### Model of an irrigation canal

In this section we present a dynamical model of a canal. We assume that the canal consists of  $N$  pools. Due to gravitational forces, water in a canal flows from upstream pools to downstream pools. The flow of water in a canal can be modeled using nonlinear partial differential equations, the so-called Saint Venant's equations (Chow, 1959; Van Overloop, 2006; Malaterre and Baume, 1998):

$$\begin{aligned} \frac{\partial Q}{\partial x} + \frac{\partial A}{\partial t} &= q_{\text{lat}}, \\ \frac{\partial Q}{\partial t} + \frac{\partial}{\partial x} \left( \frac{Q^2}{A} \right) + gA \frac{\partial h}{\partial x} + \frac{gQ|Q|}{C^2 RA} &= 0. \end{aligned} \quad (1)$$

In the formula,  $Q$  denotes the flow,  $x$  is the longitudinal distance,  $A$  is the cross section area,  $t$  is time,  $q_{\text{lat}}$  is the unitary lateral inflow or outflow,  $g$  is the gravitational acceleration,  $h$  is the water height,  $R$  is the hydraulic radius and  $C$  is the Chézy constant, see (Chow, 1959; Van Overloop, 2006; Malaterre and Baume, 1998) for details. Unfortunately, the Saint Venant's equations are not suitable to be used for the purpose of real-time canal control due to their high complexity. However, by discretizing and linearizing the model, we obtain a simplified model that proves to be more efficient for control. For pool  $i = 1, \dots, N$  the model reads

$$h_i(k+1) = A_i h_i(k) + B_{ui} u_i(k) + B_{di} d_i(k), \quad (2)$$

where  $k$  is the discrete time step counter,  $h_i$  denotes water level at the end of pool  $i$ ,  $u_i$  is the control input denoting the outflow from the canal,  $d_i$  is a disturbance inflow or outflow, and  $A_i$ ,  $B_{ui}$  and  $B_{di}$  are suitable matrices. In particular, assuming an upstream control, we end up with a model of the form

$$h_i(k+1) = h_i(k) + \frac{T_m}{c_i} (u_{i-1}(k - k_{di}) - u_i(k) + d_i(k) + g_i(k)), \quad (3)$$

in which  $T_m$  denotes the sampling period (equal for all pools),  $c_i$  is the surface area, and  $k_{di}$  is a time delay (in control steps) representing the time required for an inflow from upstream gate  $i-1$  to influence the water level in pool  $i$ . Clearly, for  $i=1$ , the inflow is the flow from the head gate. Moreover,  $d_i(k)$  denotes a water offtake from the canal due to a request made by the user and  $g_i(k)$  is a known disturbance in the pool  $i$  due to for instance rainfall.

As mentioned earlier in the paper, local PI controllers are employed throughout the canal to control the water level immediately upstream of each gate. Taking that into consideration, each canal pool  $i \in \{1, \dots, N\}$  is described with the following discrete-time model

$$\begin{aligned} h_i(k+1) &= h_i(k) + \frac{T_m}{c_i} (u_{i-1}(k - k_{di}) - u_i(k) + d_i(k) + g_i(k)), \\ u_i(k) &= u_i(k-1) + K_{pi} (e_i(k) - e_i(k-1)) + K_{li} e_i(k), \quad (\text{PI controller}) \\ u_0(k) &= Q_s(k), \\ e_i(k) &= h_i(k) - h_i^{\text{ref}}(k), \end{aligned} \quad (4)$$

where  $e_i$  denotes the deviation between the water level in Pool  $i$  and a given setpoint for that pool,  $h_i^{\text{ref}}$ , and  $Q_s$  denotes the inflow from the head gate. Note that in (4) the local PI controllers are already incorporated. In that sense, (4) represents the closed-loop dynamics of the pools  $i=1, \dots, N$  in terms of the local controllers  $u_i$ . However, these dynamics are subject to control inputs from the Coordinator as shown in due course.

### **Model Predictive Control**

In this section we briefly recall the concept of Model Predictive Control (Maciejowski, 2002; Camacho and Bordons, 1999), which is used in this paper to develop the controller. Model Predictive Control, also known as Receding Horizon Control, is a very powerful tool due to, amongst others, its ability to take care of state and control input constraints and to deal with multivariable systems. It is a type of optimal controller that at each time step uses current measurements and the internal model of the plant to obtain state predictions  $x(k+1|k), \dots, x(k+N_p|k)$  for the following  $N_p$  steps. These predictions are then used to evaluate a given objective function

$J(x(k+1|k), \dots, x(k+N_p|k), u(k|k), \dots, u(k+N_p-1|k))$ . The objective of MPC is to find a suitable sequence of control actions over the whole prediction horizon  $u(k|k), \dots, u(k+N_p-1|k)$  minimizing the cost function. Here  $x(k+j|k)$  denotes the state prediction for time  $k+j$  obtained at time  $k$  and  $u(k+j|k)$  denotes the optimal control found by the optimizer at time  $k$  to be applied at time  $k+j$ . Once the sequence of optimal controls over the prediction horizon is found, the first control action  $u(k|k)$  from the sequence is applied to the plant and the process is repeated at next time step  $k+1$  looking again  $N_p$  steps into the future and using new information as it comes along.

### **Time Instant Optimization**

Time instant optimization is an approach to MPC that was first introduced in (De Schutter and De Moor, 1998) for optimal traffic control. For water systems the idea of optimizing time instants was primarily proposed for discontinuous on/off hydraulic structures in (Van Ekeren et al., 2011). Note that in classical MPC for on/off structures it needs to be decided at each step whether the structure should be switched on or off at every time from the current moment up to the time  $N_p$  steps ahead. Therefore, the problem results in  $N_p$  binary control variables and as a result the problem may turn out to be impracticable to solve numerically. An alternative is to decide how many on/off switches are allowed for the next  $N_p$  steps and optimize when the switching time instants are to occur. Hence, the optimization problem redefined using the rationale of TIO-MPC reduces the number of control variables thus making the problem more viable computationally.

## **HIERARCHICAL CONTROLLER DESIGN**

In this section we introduce the hierarchical centralized controller to coordinate the local PI controllers and thus enhance the water delivery process. It is assumed that a single delivery request is described by its volume per second and time instants when the delivery should start and finish. For example, a request can be made for  $0.1\text{m}^3/\text{s}$  to start in 1 hour and last for 30 min. For the time being, to present our concept in a simplified way, we also assume that no overlapping of the requests of individual users is allowed.

The Coordinator coordinates the water deliveries to the users by controlling the water flow through the head gate as well as by manipulating the reference levels in individual canal pools at appropriate times when it is needed. In other words, the Coordinator provides the local controllers with a block-shaped setpoint profile: it finds a modified value of the setpoint and time instants when this modified value should be switched on and back off to return to the normal operating value of the setpoint. Examples of possible setpoint profiles are given in Figure 2. Importantly, because of the nature of the profile found by the Coordinator, the Coordinator only needs to communicate twice to each local site: once to provide the changed value of the setpoint at the time of change and later when the setpoint should return to the normal level. This is an essential feature because it

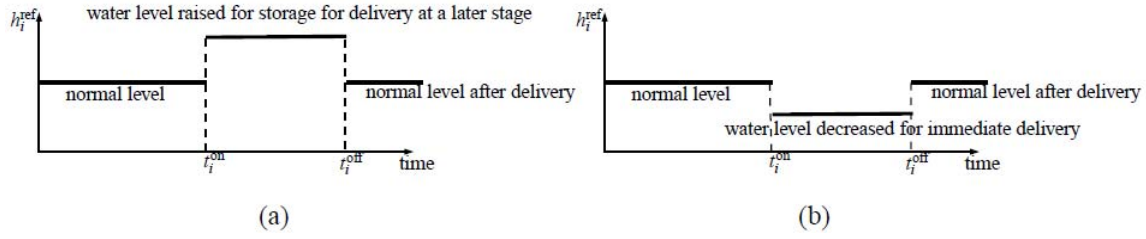


Figure 2. Possible setpoint profiles provided by the Coordinator.

implies that there is no need for frequent interference with the operation of local sites.

Following this introduction, the control inputs to be found by the Coordinator are

$$U_s = \begin{pmatrix} \bar{Q}_{S,\text{demand},s} \\ H_s^{\text{ref,delivery}} \\ T_s^{\text{on}} \\ T_s^{\text{off}} \end{pmatrix}. \quad (5)$$

Here,  $s \in \mathbb{N}$  is the delivery counter, which is incremented every time the Coordinator is activated. Moreover,  $\bar{Q}_{S,\text{demand},s}$  denotes a profile of the extra flow from the head gate to the first pool for the whole prediction horizon  $N_p \in \mathbb{N}$  needed for delivery  $s$ , i.e.

$$\bar{Q}_{S,\text{demand},s} = (Q_{S,\text{demand},s}(0), \dots, Q_{S,\text{demand},s}(N_p - 1))^T. \quad (6)$$

From  $Q_{S,\text{demand},s}(j)$ ,  $j = 0, \dots, N_p - 1$ , we can determine the overall flow from the head gate to be used in (4) as

$$Q_S(k_{\text{active},s} + jA_c + i) = Q_{S,\text{base}} + Q_{S,\text{demand},s}(j), \quad (7)$$

where  $Q_{S,\text{base}}$  denotes the base flow in the canal and  $i = 0, \dots, A_c - 1$ . Here, we use  $A_c = T_c / T_m \in \mathbb{N}$ , in which  $T_c$  is the length of the control cycle of the Coordinator, which is a multiple of the sampling time of the model  $T_m$ . Moreover,  $k_{\text{active},s} \in \mathbb{N}$  denotes the Coordinator's activation time step for the  $s^{\text{th}}$  delivery defined as

$$k_{\text{active},s} = \left\lceil \frac{t_{\text{active},s}}{T_m} \right\rceil, \quad (8)$$

where  $\lceil x \rceil$  denotes the ceiling function. By the above definition,  $t_{\text{active},s} \leq k_{\text{active},s} T_m$ , where  $t_{\text{active},s}$  is the activation time of the Coordinator.

Further control inputs in (5) are

$$\begin{aligned} H_s^{\text{ref,delivery}} &= (h_{1,s}^{\text{ref,delivery}}, \dots, h_{N,s}^{\text{ref,delivery}})^T, \\ T_s^{\text{on}} &= (t_{1,s}^{\text{on}}, \dots, t_{N,s}^{\text{on}})^T, \\ T_s^{\text{off}} &= (t_{1,s}^{\text{off}}, \dots, t_{N,s}^{\text{off}})^T, \end{aligned} \quad (9)$$

where  $h_{i,s}^{\text{ref,delivery}} \in \mathbb{R}$ , and where in the spirit of TIO-MPC,  $t_{i,s}^{\text{on}} \in \mathbb{R}$  and  $t_{i,s}^{\text{off}} \in \mathbb{R}$  are the switching time instants such that

$$h_i^{\text{ref}}(k) = \begin{cases} h_i^{\text{ref,normal}} & \text{if } k \leq k_{i,s}^{\text{on}} \text{ or } k \geq k_{i,s}^{\text{off}}, \\ h_{i,s}^{\text{ref,delivery}} & \text{otherwise,} \end{cases} \quad (10)$$

in which  $k_{i,s}^{\text{on}}$  and  $k_{i,s}^{\text{off}}$  are discrete-time equivalents of the continuous variables  $t_{i,s}^{\text{on}}$  and  $t_{i,s}^{\text{off}}$  given certain model sampling time  $T_m$ :

$$k_{i,s}^{\text{on}} = \left\lceil \frac{t_{i,s}^{\text{on}}}{T_m} \right\rceil \quad \text{and} \quad k_{i,s}^{\text{off}} = \left\lceil \frac{t_{i,s}^{\text{off}}}{T_m} \right\rceil, \quad (11)$$

where  $\lceil x \rceil$  denotes the value of  $x$  rounded to the nearest integer. Moreover,  $h_i^{\text{ref,normal}}$  is the normal operating level of the setpoint in canal pool  $i$ .

In view of the above, the cost function that the Coordinator minimizes once triggered is

$$J_s \quad (12)$$

$$= \alpha \sum_{j=1}^{A_c N_p} \left( u_N(k_{\text{active},s} + j - 1) - Q_{S,\text{base}} \right) \quad (13)$$

$$+ \sum_{i=1}^N \sum_{j=1}^{A_c N_p} \left[ \gamma_1 \left( \max(h_i(k_{\text{active},s} + j) - h_i^{\text{max,des}}, 0) \right)^2 \right. \quad (14)$$

$$\left. + \gamma_2 \left( \min(h_i(k_{\text{active},s} + j) + h_i^{\text{min,des}}, 0) \right)^2 \right] \quad (15)$$

$$+ \sum_{i=1}^N \sum_{j=1}^{A_c N_p} \beta \left( h_i(k_{\text{active},s} + j) - h_i^{\text{ref}}(k_{\text{active},s} + j) \right)^2 \quad (16)$$

$$+ \sum_{i=1}^N \mu \left( h_i^{\text{ref,normal}} - h_i^{\text{ref}}(k_{\text{active},s} + N_p A_c - 1) \right)^2, \quad (17)$$

in which  $\alpha$ ,  $\gamma_1$ ,  $\gamma_2$ , and  $\beta$  are positive weighting coefficients, and  $u_N$  denotes flow through gate  $N$ .

In the cost function  $J_s$ , the term (13) penalizes any deviations in flow through the last gate of the canal with respect to the value of the base flow  $Q_{S,\text{base}}$  as it is required that the flow through the last gate to further parts of the canal behind the  $N$  pools should always be as close as possible to some given  $Q_{S,\text{base}}$ . The terms (14) and (15) penalizes control actions resulting in the water levels violating the upper and lower bounds. Note that the values  $h_i^{\text{max,des}}$  and  $h_i^{\text{min,des}}$  denote desired operating upper and lower bounds; actual physical bounds stemming from canal geometry are less strict and are imposed as hard constraints (see (18) below). Furthermore, the term (16) penalizes any deviations of the water levels from their desired levels and the term (17) poses a penalty on the final value of the reference levels so that after the delivery has been finished, the reference levels return to normal.

The hard constraints are as follows

$$h_i^{\min} \leq h_i(\ell) \leq h_i^{\max}, \quad (\ell = k_{\text{active},s} + 1, \dots, k_{\text{active},s} + N_p A_c), \quad (18)$$

$$h_i^{\min} \leq h_{i,s}^{\text{ref,delivery}} \leq h_i^{\max}, \quad (19)$$

$$t_{i,s}^{\text{off}} \geq t_{i,s}^{\text{on}} + T_m, \quad (20)$$

$$t_{i,s}^{\text{on}} \geq k_{\text{active},s} T_m, \quad (21)$$

$$Q_{S,\text{demand},s}(n) \geq 0, \quad (n = 0, \dots, N_p - 1), \quad (22)$$

$$0 \leq Q_S(m) \leq Q_{\text{capacity}}, \quad (m = k_{\text{active},s}, \dots, k_{\text{active},s} + N_p A_c - 1), \quad (23)$$

for all  $i \in \{1, \dots, N\}$ . The meaning of constraints (18) and (19) is that the water levels as well as the modified setpoints chosen by the Coordinator need to remain within safety bounds to avoid the risk of flooding or drying out the canal. Constraints (20) and (21) limit the possible choices of the switching time instants in that the first switch must not occur before the time  $k_{\text{active},s} T_m$  when the Coordinator is activated for the  $s^{\text{th}}$  delivery and the second switch must occur strictly after the first one. In addition, the last two constraints, (22) and (23), give restrictions on possible values of  $Q_{S,\text{demand},s}$ . In particular, this extra flow needs to be nonnegative and together with the base flow, the overall flow must not exceed the maximum capacity of the head gate. Furthermore, Equation (10) can also be treated as a hard constraint defining that in between the switches the setpoint may not change.

Since the Coordinator only works in response to requested offtakes, its triggering condition can be described as follows. The Coordinator optimizes (12) subject to constraints (10) and (18)–(23) when it learns about a new delivery. In particular, we assume that the Coordinator remains inactive until the trigger switches it on (when a delivery  $s$  is requested). Then the Coordinator finds suitable values  $U_s$ , i.e. a profile  $\bar{Q}_{S,\text{demand},s}$ , the switching time instants  $T_s^{\text{on}}$  and  $T_s^{\text{off}}$  and the modified setpoints  $H_s^{\text{ref,delivery}}$ . Assuming a long enough prediction horizon  $N_p$ , no overlapping requests, and a strictly deterministic case, the Coordinator performs the optimization only once per delivery. Therefore, after finding the suitable control action  $U_s$  for delivery  $s$ , the Coordinator is switched off until a new delivery  $s+1$  comes along. Note that we also require that the time between any two activations of the Coordinator is at least  $T_{\text{min}}$  so the changes to the local settings are not too often. The time  $T_{\text{min}}$  represents the minimal reactivation time of the Coordinator and is a multiple of the sampling time  $T_m$ . It may be viewed as a design parameter that can be chosen according to the requirements of a particular system. It is also required that before the Coordinator can be reactivated for delivery  $s+1$ , all setpoints changed for delivery  $s$  need to return back to their normal levels.

The functioning of the system governed by the Coordinator for  $t \in (0, T_f)$  can be illustrated by the following algorithm:

- (1)  $s=0$ ,
- (2)  $k=1$ ,
- (3) if a new delivery is requested, go to (4), otherwise go to (6),
- (4) if  $k \geq k_{\text{active},s-1} + T_{\text{min}}/T_m$  and for all  $i$ ,  $k \geq k_{i,s-1}^{\text{off}}$ ,  
     set  $s=s+1$  and go to (5); otherwise go to (6),
- (5) solve the MPC problem,
- (6)  $k=k+1$ ,
- (7) wait until  $t=kT_m$ ,
- (8) if  $t < T_f$  go to (3), otherwise stop.

### SIMULATION STUDY

This section illustrates the method introduced in the paper by simulations. For the sake of clarity of presentation, we use a canal consisting of 5 pools. The sampling period of the model is  $T_m=1$  min and the sampling time of the Coordinator is  $T_c=5$  min. For all pools we use  $K_{P_i}=3.6$  and  $K_{I_i}=0.2$ . This chosen by fine tuning to be the proportional and integral gains of the upstream PI controllers. Moreover, the weighting coefficients used to evaluate the cost function (12) are  $\alpha=10$ ,  $\beta=5$ ,  $\gamma_1=\gamma_2=1$ , and  $\mu=3$ .

The surface areas of the pools are (in square meters): 397, 653, 503, 1530, and 1614. Furthermore, the delays in all pools before an inflow from a pool immediately upstream affects water levels at the end of the pool are: 7, 10, 3, 1, and 9 steps, respectively. The prediction horizon in our simulations is  $N_p=120$  simulation steps, which is equivalent to 24 control cycles of the Coordinator. This number is chosen to enable the Coordinator to verify how its actions would affect the whole canal given internal delays in each canal pool.

We start the simulation from steady state in which water height in all pools is equal to  $h_i(0) = -0.6$  m and the flow is  $u_i(0) = 1.5$  m<sup>3</sup>/s. The initial flow from the head gate is 1.5 m<sup>3</sup>/s and that base flow should be maintained throughout the simulation. Note that water levels are given as negative numbers since the coordinate frame used in the simulations is assumed to be located at the ground level. Thus, water levels in the canal with respect to that coordinate frame are negative numbers.

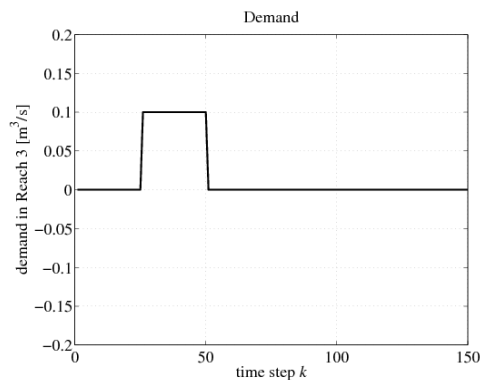


Figure 3. Demand profile in Pool 3.

The simple demand chosen to illustrate how the hierarchical centralized controller works is such that from  $k = 25$  until  $k = 50$  there is an outflow from Pool 3 of  $0.1 \text{ m}^3/\text{s}$ , see Figure 3. Note that in the classical way when only local PI controllers operate, an offtake in Pool 3 would require an announcement at least 20 steps before the actual offtake can be done. Recall that with only local PI controllers, water is delivered to the user by adding the required amount of water from the head gate to the first pool and waiting for local controllers to transport it to Pool 3. However, in the hierarchical control settings the Coordinator only finds out about the delivery requested 5 steps ahead (at  $k = 20$ ) and yet, as shown below, it is still able to realize it. In the future, we will also formally consider the extreme case when no notice period is required and offtakes can be announced and immediately realized, e.g. in the case of emergency etc.

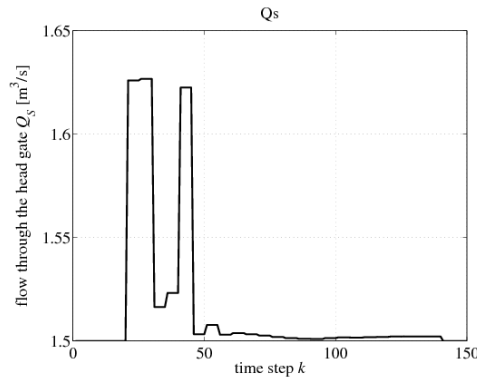


Figure 4. Inflow from the head gate.

Simulation results are given in Figures 4-6. In particular, in Figure 4 we present the profile of flow from the head gate as found by the Coordinator. In Figure 5 we show how the setpoints are changed by the Coordinator for all pools. We see that the setpoints of Pools 1 and 2 are lowered before the offtake starts soon after the Coordinator is activated (i.e. just after  $k = 20$ ). That means that water can be released from these pools and made available for the delivery in Pool 3. This is an important observation because since it takes 20 steps to deliver water from the head gate to Pool 3, it would be impossible to merely use water from the head gate for the delivery since there is not enough time to transport that water to Pool 3. However, by the changed setpoints in Pool 1 and Pool 2, water can be delivered timely without disturbing the rest of the canal. We also see that the setpoint in Pool 3 is increased a little, which allows to store water released from Pool 1 in Pool 2 in Pool 3 for a delivery in that pool a few moments later. Moreover, notice that the setpoints also change in Pools 4 and 5, yet when looking at the scale, we immediately see that this change is minor. While there are no deliveries in these pools, changes can be explained by the objective of the Coordinator to maintain the flow through the fifth gate of the canal as close as possible to the given base flow. Hence, by also modifying the setpoints in Pools 4 and 5, the Coordinator has more means to meet this objective. Indeed, Figure 6 shows that the deviation in flow through the fifth gate is minor, thus demonstrating that the delivery is accomplished with minimal disruption to the remaining part of the canal and confirming good performance yielded by the Coordinator.

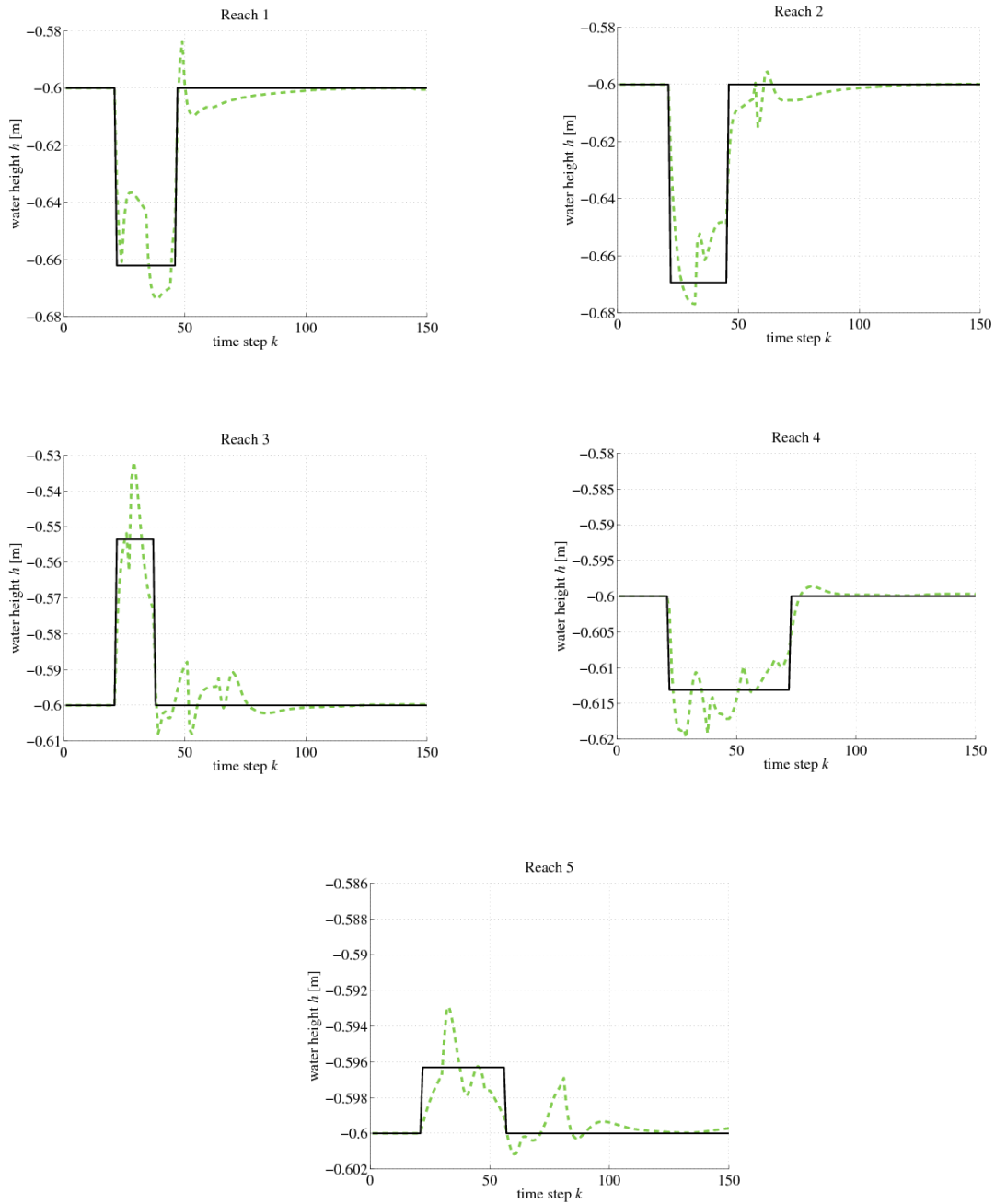


Figure 5. Water levels (dashed line) and setpoint (solid line) for each pool.

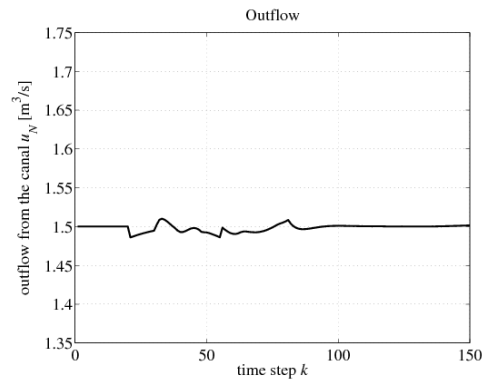


Figure 6. Outflow from the fifth pool.

## CONCLUSIONS

We have showed a new hierarchical control method to tackle water deliveries to farmers through an irrigation canal. The method is simple because it mainly relies on the application of local PI controllers at each gate to control water levels upstream of the gate. However, to boost the performance of the local PI controllers and allow faster deliveries, we have proposed a higher-layer centralized controller – the Coordinator – whose job is to coordinate the local controllers and hence enable shorter times before an offtake can be made after it has been announced. To that end, Time Instant Optimization was used within the framework of Model Predictive Control. The findings of the paper are illustrated by simulation results demonstrating the effectiveness of the method.

Because the model of the canal used is linear, in our work we assume a proportional relation between water level and volume in the pools. As, in reality, volume is a nonlinear function of the water level, there may be corrections necessary to the imposed inflow at the head gate. This can be done by using Volume Compensation as in (Bautista and Clemmens, 2005) or by employing a nonlinear internal model in MPC in future applications. Our future work will also include tests on a more accurate model of an actual irrigation canal and its local controllers, possibly accounting for nonlinearities, measurement noise, and unmodeled dynamics. Moreover, we will also extend the method to allow for overlapping deliveries and analyze the performance of sudden schedule changes (without any lead time) to make the method more universal and applicable in the field.

## ACKNOWLEDGEMENTS

Research supported by the European Union Seventh Framework Programme [FP7/2007-2013] under grant agreement no. 257462 HYCON2 Network of Excellence.

## REFERENCES

K. J. Åström and T. Hägglund. *PID Controllers: Theory, Design, and Tuning*. Instrument Society of America, Research Triangle Park, NC, 1995.

E. Bautista and A. Clemmens. Volume compensation method for routing irrigation canal demand changes. *Journal of Irrigation and Drainage Engineering*, 131(6):494–503, 2005.

E.F. Camacho and Carlos Bordons. *Model predictive control*. Springer, Berlin Heidelberg, 1999.

V. T. Chow. *Open-Channel Hydraulics*. McGraw-Hill Civil Engineering. McGraw-Hill, London, 1959.

B. De Schutter and B. De Moor. Optimal traffic light control for a single intersection. *European Journal of Control*, 4(3):260–276, 1998.

J. M. Maciejowski. *Predictive Control with Constraints*. Prentice Hall, Essex, England, 2002.

P.-O. Malaterre and J.-P. Baume. Modeling and regulation of irrigation canals: existing applications and ongoing researches. In *IEEE International Conference on Systems, Man, and Cybernetics*, volume 4, pages 3850–3855, 1998.

P.-O. Malaterre. Control of irrigation canals: why and how? In *International Workshop on Numerical Modelling of Hydrodynamics for Water Resources*, pages 271–293, 2007.

R. R. Negenborn, S. Leirens, B. De Schutter, and J. Hellendoorn. Supervisory nonlinear MPC for emergency voltage control using pattern search. *Control Engineering Practice*, 17(7):841–848, 2009.

R. R. Negenborn, P. J. van Overloop, T. Keviczky, and B. De Schutter. Distributed model predictive control for irrigation canals. *Networks and Heterogeneous Media*, 4(2):359–380, 2009.

V.M. Rutz, C. Ruiz, and L. Ramirez. Predictive control in irrigation canal operation. In *Proceedings of the 2011 IEEE International Conference on Systems, Man, and Cybernetics*, volume 4, pages 3897–3901, 1998.

C. Sepúlveda Toepfer. *Instrumentation, Model Identification and Control of an Experimental Irrigation Canal*. PhD thesis, Universitat Politècnica de Catalunya, Spain, 2007.

D. D. Šiljak. *Decentralized Control of Complex Systems*. Academic Press, Boston, Massachusetts, 1991.

E. Weyer. Control of irrigation channels. *IEEE Transactions on Control Systems Technology*, 16(4):664–675, 2008.

A. Zafra-Cabeza, J. M. Maestre, M. A. Ridao, E. F. Camacho, and L. Sanchez.

Hierarchical distributed model predictive control for risk mitigation: An irrigation canal case study. In *Proceedings of the 2011 American Control Conference*, pages 3172–3177, 2011.



# A PROTOTYPE AUTOMATED SURFACE IRRIGATION SYSTEM

Tom Gill<sup>1</sup>  
Dale Lentz<sup>2</sup>  
Khaled Bali<sup>3</sup>

## ABSTRACT

Engineers from the U.S. Bureau of Reclamation are working in cooperation with staff at the University of California Desert Research and Extension Center (DREC) near Holtville, California, in development of an automated surface irrigation system. The system will utilize measured inflow along with the observed advance rate of surface-applied irrigation water to determine appropriate cut-off times for transition of flow from one field section to the next. The objective for the automation scheme will be to apply a sufficient volume to fully irrigate each field section while limiting runoff flows. A wireless communication network will link the primary control unit with gate controllers, field advance sensors, and a runoff monitoring station. The project will include multiple flow control technologies at field turnouts to be evaluated based on functional reliability and cost effectiveness. The communications, monitoring, and control network is being configured using solar charged power. The project is on schedule for automated operation beginning in early 2013.

## BACKGROUND

This project follows a previous effort initiated in 2008 to develop and field test a prototype automated surface irrigation system in Imperial Valley operated by a private cooperating farm. The scope of the earlier effort was the attempt to automate the open canal delivery system at an eighty acre field set up for border irrigation divided into twelve border sections. At this site water was delivered to each border section via three port openings imbedded in the side of a concrete lined canal. The existing port openings were a style common to many field canals in the vicinity, equipped with manually operated slide gates. A rod attached to the slide gates was pulled up to open the ports and pushed down to close the ports. A cam on the lower end of the rod needed to be rotated toward the gate leaf by twisting the handle on top of the rod to seal the gate against a steel ring imbedded in the concrete lining formed the perimeter of the port opening. Figure 1 shows a hand-operated port gate in a concrete lined canal.

For the earlier project modified port gates operated by electric linear actuators were designed and installed that attempted to mimic the gate movement and gate sealing functions of the hand operated port gates requiring both linear and rotational motion. All gate operating actuators were controlled from a central control unit linked via a hard wired network to each gate site. Before the automation components of the system could

---

<sup>1</sup> Hydraulic Engineer, US Bureau of Reclamation, Denver CO, tgill@usbr.gov

<sup>2</sup> Hydraulic Engineer, US Bureau of Reclamation, Denver CO, dlentz@usbr.gov

<sup>3</sup> Irrigation/Water Management Advisor and County Director, University of California Desert Research and Extension Center, Holtville CA, kmbali@ucdavis.edu

be tested, robust performance of the motorized gates needed to be achieved. Unfortunately problems encountered in operation of the modified gate systems along with shortcomings exposed in the power linkage configuration proved too great to overcome given the limits of staff time and funding allocations available for the project. Figure 2 shows the motorized configuration used for the port gates in the previous project.



Figure 1. Hand-operated Port Gate



Figure 2. Motorized Port Gate

Key points taken from this unsuccessful effort include:

- A future prototype developed on a more limited scale would enable device and system modifications to be put in place within manageable staff time and funding budgets

- Locating a prototype system at a site where it would be operated by research project team members would be appropriate for development of an untested technology
- Identification of cost effective flow control structures that can be readily and reliably operated using electrical devices is imperative
- A system that can be transported from one site and reinstalled at a new site as lease agreements change would enhance the attractiveness of the technology in an area (Imperial Valley) where much of the irrigated land is operated by tenant farmers

**DREC FIELD TEST AND DEMONSTRATION CONFIGURATION**

A border-irrigated plot made available at the University of California Desert Research and Extension Center (DREC) farm has initially been set up with four border sections, each served by a single turnout from the concrete lined field canal. Run length of the border sections is approximately 1200 ft. and border width is 60 ft. [Field slope =0.15%] Figure 3 shows the field site layout.

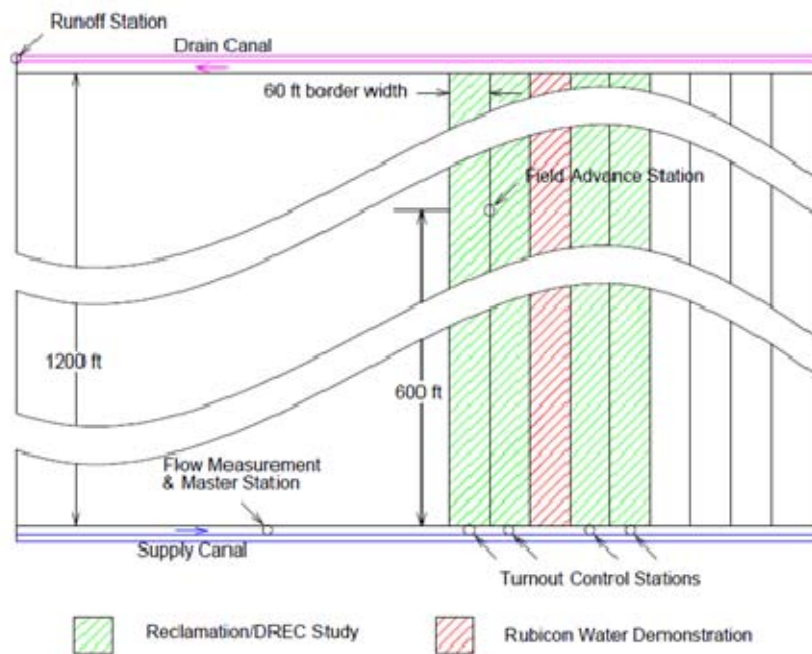


Figure 3. Sketch of the Field Demonstration Site Layout

Multiple border sections are available for use by the project at the site. In the initial configuration equipment has been installed by the Reclamation/DREC team in three of the border sections – each featuring a different turnout control device. An additional turnout control device currently under development by the Reclamation/DREC team will be added in a fourth border section in early 2013. Along with the Reclamation/DREC project there is a border section equipped with a turnout control device and an automation system developed by Rubicon Water. The Rubicon Water equipment is operated

independently from the Reclamation/DREC system. The focus of this paper is the development of the Reclamation/DREC prototype system.

The Reclamation/DREC prototype features five types of stations. All stations are equipped with similar programmable control units with integral data radios. The master unit is located along the supply canal and measures discharge being delivered to the flow at a long-throated flume. The flume is subject to excessive submergence due to checking up the canal for irrigation so flow is measured by making level measurements at both the approach and throat sections of the flume and using the venturi solution to calculate discharge, (Gill & Niblack, 2009). The master station is also able to measure water level in the canal downstream from the flume. This measurement is utilized to determine whether the canal has filled before flow is turned out to the first border section. Measured flows and operational data during an irrigation cycle are logged on-site at the master station. Figure 4 and Figure 5 show the master station as the flume was being modified.



Figure 4. Flume Modification at Master Station



Figure 5. Modified Long-Throated Flume

The crest of the ramp-type long-throated flume was raised four inches and a downstream ramp was added to improve measurement capability under excessive high tail water conditions. A two-location level measurement system (water levels at the flume approach and crest sections) was installed using two stilling wells with valved lines between each stilling well and canal tap. A valved line also links the two stilling wells. [The stilling wells are the taller risers seen in the background of Figure 4. The three shorter risers are valve access tubes.] A third stilling well was later added downstream of the flume to monitor when the canal has filled sufficiently for an irrigation to begin.

Turnout control stations are located at each border station turnout. The master station directs each turnout station to open the flow control device in the border section when irrigation is being initiated. When sufficient water has been applied to the border section the master station directs the turnout section to close the flow control device. Turnout control stations are also equipped with two toggle switches. An On-On toggle is a selector switch which allows an operator to select automated or manual operation. When the selector switch is in the manual position, the turnout may be manually operated using the second toggle switch. The manual operation toggle is a momentary (On)-Off-(On) switch that defaults to the off position when not being in the open or close positions. All stations are powered by solar charged 12 volt batteries. The turnout technologies installed have modest energy requirements compatible with solar charged operation.

The field advance sensing station is located at the midpoint of the field length in the direction of travel of irrigation water (see Figure 3). The primary function of the field advance station sensing station is to determine when the irrigation water has reached the half-way point of the traverse from upper to lower end of the border section. This is accomplished by linking a conductivity “water sensor” placed near the center of the width of the border section with the radio/control unit.

A secondary function of the advance sensing station is to monitor soil moisture conditions between irrigations. Soil moisture sensors may be installed at one or more depths in the border section are linked to the radio/control unit at the stations. Soil moisture readings may be taken at user-defined intervals and logged on-site. At a minimum, one field advance station is required for the system to monitor the advance rate of water applied to the first border section being watered. In the DREC layout, a field advance station is located on the ridged boundary of two border sections. Water sensors located in both adjacent border sections are linked to the station radio/control unit.

The fourth type of station in this system is a field runoff measurement station. For the test site layout, field runoff from all border sections enters a concrete lined runoff canal and is conveyed to the edge of the field where it passes through a standard Imperial Irrigation District (IID) runoff weir box into the IID drainage collection network. A water level sensor monitoring water level at the weir box is linked to a radio/control unit at this site. Flow over the weir is calculated at 60 second intervals and logged on-site.

The fifth type of station is a base station at the DREC office that is linked to a PC. The base is capable of communicating with each of the other stations, either using software loaded on the PC, or directly from the base radio/control unit following on-screen

prompts and user keypad inputs. Under normal operations, the PC software will be operated in the “auto poll” mode. This will direct the periodic collection of logged data from the master station, the field sensing station and from the runoff monitoring station. This information is then written to files on the PC hard drive. The system can be configured so that operating commands or modifications to programming parameters can be put into effect remotely from the office base.

### **AUTOMATED OPERATION OF THE DREC SITE**

Irrigation of the Reclamation/DREC equipped border sections is initiated by turning flow into the field supply canal. The master unit at the measurement flume will determine when a measurable flow is passing the flume and will monitor the flow rate and the downstream water level until the canal has filled sufficiently to start the irrigation. The master unit uses the on-board real-time clock to establish the irrigation start time which is logged in an on-board data register.

To initiate the irrigation, a message is wirelessly transmitted to the radio/control unit at the flow control station in the first border section directing it to open. A second message is transmitted almost simultaneously to the radio/control advance station directing it to begin monitoring the surface water advance sensor. After flow into the first border section has been initiated, measurements of flow crossing the flume are taken at a user defined interval (i.e. one to three minutes). The measured flow rate is multiplied by the time interval to calculate an incremental volume for the time interval which becomes the initial value for a totalized volume variable which is also logged and updated with each measurement cycle.

At the border section flow control station a relay that opens the flow control device is turned on when directions have been received from the master unit. Depending on the type of flow control device installed at the border, the “open” relay may be energized for a specified time interval, or may be energized until a position indicator on the flow control device provides feedback that the device is fully open. After switching off current to the “open” relay the flow control station will be inactive until a command to close off flow to the border section is received from the master station. Then a second “close” relay will be energized for a pre-set time interval or until feedback from a position sensor indicates that the flow control device is closed.

When the field advance sensing station has received direction from the master unit, the station will monitor the surface water sensor at 60 second intervals until the arrival of irrigation flow is detected. The field sensing station then transmits an indicator to the master station that the surface water advance has arrived at the border section mid-point.

At the time feedback from the field advance station is received, the master station program will note the totalized volume delivered to the border section up to that point in time and calculate the additional applied volume needed to fully irrigate the border section. The additional volume is added to the totalized volume already applied to determine a target total volume. When the target volume is reached, the master station

will communicate the initiation of flow in the next border section and shut off of flow into the first section.

For sites where only one border section is equipped with an advance sensing station, the applied volume total target value derived during irrigation of the initially irrigated section would be used as the target for remaining border sections. [Obviously the single advance station configuration of this system would be applicable only for multiple border sections of the same dimensions field, slope and common soil properties.] In the Reclamation/DREC prototype configuration, the advance sensing station is positioned and instrumented to monitor advance on two adjacent border sections. For the prototype, irrigation of the second border section is essentially a repeat of the process described for irrigation of the initial border section. The volume total target derived for irrigation of the second section would be volume target used for additional border sections.

### **PROTOTYPE TURNOUT CONTROL STRUCTURES**

As noted in the background section of this paper, the difficulties that were encountered in efforts to motorize existing turnout structures in our earlier project proved fatal to that effort. Complete stoppage of flow when field turnout flow control devices are in closed position is necessary to prevent ponded conditions along the upper end of the field from persisting. Exposure to extended ponding conditions may result in stunting or death of the exposed plants. A key facet of the current project is identification of multiple turnout flow control alternatives that work reliably and are affordable.

Figure 6 and Figure 7 show one of the pre-existing “alfalfa” valve turnouts at the DREC site that are being modified or replaced for this project. The alfalfa valves are installed in the concrete lined canal. When the valves are opened water passes through a concrete pipe through the canal bank and is discharged into the field. The three initially installed flow control systems devised for this project move the flow control function from the entrance of the culvert pipes through the canal bank to the outlet end of the pipes.



Figure 6. “Alfalfa” Valve Field Turnout



Figure 7. Concrete Pipe Outlet from Canal

Each flow control device currently installed in the project meets these criteria following:

- Can be transitioned between open and fully closed by simple mechanical actions with a tolerance range in achieving fully closed state
- Cost effective for irrigation systems with multiple turnouts
- Can readily be operated with solar charged power
- Can be installed with limited modification to existing facilities

A pinch valve system was developed and tested by the DREC staff. A section of flexible irrigation tubing is housed inside a section of rigid PVC pipe. A “stopper” attached to a linear actuator passes through a slot cut in the top half of the PVC pipe and “pinches” the flex tubing against the lower half of the PVC pipe to stop flow. To turn on flow the linear actuator raises the stopper and the flexible tube opens up. Figures 8 and 9 show the pinch valve prototype.



Figure 8. Pinch Valve in Closed Position



Figure 9. Stopper Raised in Open Position

A tip-up valve system that also utilizes flexible irrigation tube was developed and tested at the Reclamation Hydraulics Laboratory in Denver CO. A short segment of rigid PVC pipe is installed in the end of a section of the flexible tube. Rigid arms are attached to either side of the PVC segment. The other ends of the rigid arms are hinge mounted to a lifting frame. A linear actuator attached to the hinge arms and to the lifting frame can then raise PVC pipe segment at the discharge end of the flexible tube above the canal level to stop flow or lower the discharge end to ground level to turn flow into the border section. Figure 10 and Figure 11 show the tip-up valve in laboratory tests.



Figure 10. Tip-up Valve in Closed Position



Figure 11. Tip-up Valve in Open Position

Another turnout flow control system developed and tested at the Reclamation Hydraulics Laboratory is a hydraulically operated valve. This system is a box with an inflow port in one side and an outflow port in the bottom. A cylindrical tank moves down and up inside the box over the outflow port as the tank is alternatively filled or drained. Flow into or out of the cylinder is controlled by an electric motor valve. Vertical rods installed in the box constrain motion of the cylinder so that it raised and lowers directly above the outflow port. Figure 12 and Figure 13 show the hydraulically operated valve system.



Figure 12. Hydraulic Valve in Laboratory Test



Figure 13. Hydraulic Valve Field Installation

A fourth flow control system is currently under development at the Reclamation Hydraulics Laboratory. This device will utilize a rotating frame that raises and lowers a flexible gate made of tarp material. Laboratory test photos of this system are shown in Figure 14 and Figure 15.



Figure 14. Flexible Turnout Gate (lowered)



Figure 15. Flexible Turnout Gate (raised)

This flow control device – operated using a linear actuator – is being designed as a “drop-in” system that is installed in stop-log type slots in a rectangular opening. The “drop-in” configuration whereby the gate structure is installed stop-log type slots formed in a concrete opening will simplify installation tasks and would enable gates be moved from site to site.

Two possible installation configurations are envisioned for the flexible turnout gate. A section of lining and canal bank can be removed to construct a rectangular opening with installation slots in the side of the canal. Alternatively, at sites currently equipped with control gates installed on the canal lining and culvert pipes to convey flow through the canal bank (see Figures 6 & 7), a concrete structure with a rectangular opening with “drop-in” installation slots could be constructed at the exit end of the culvert. The previously used gates would be removed (or left open) and control of flow would be transferred from the entrance to the exit end of the culverts. Installation of a prototype flexible turnout gate at the DREC site is scheduled for March, 2013.

### **AUTOMATION LOGIC**

The cracking clay soils at DREC which are prevalent in much of Imperial Valley experience minimal infiltration after initial wetting. The volume of water retained in the soil during an irrigation thus approximately represents the volume of the cracks that have formed in the soil, (Grismer and Tod, 1994). For a near constant inflow rate delivered at the border section turnout, an appropriate cut-off time for the border section may be calculated as a function of the time measured for the irrigation front to travel a known distance (i.e. to a field advance sensing station).

The minimal infiltration after initial wetting associated with the clay soil means the volume water requirement needed to fully irrigate a border section would be minimally impacted by varying turnout flow rate. For sites where the available inflow rate may be subject to variation, the inflow rate measurement capability inherent in the Reclamation/DREC prototype allows the automation scheme to be operated as a function the delivered volume needed to reach the field advance sensing station. Field research has shown that runoff can be reduced to as little as two percent of the infiltrated volume by stopping application of water to a border section when the appropriate amount of water has been applied (Bali et.al. 2010).

### **PROJECT STATUS**

As this paper is being submitted, turnout automation stations and prototype turnout flow control devices have been installed in three border sections at the demonstration site. These prototype flow control devices have been successfully operated in manual mode since being installed. Instrumentation and programming for the field advance and soil moisture sensing station was tested at the DREC field site in January of 2013.

The currently installed turnout control devices were operated via manual toggle switches during for irrigation of a 2012 sudangrass crop and appear to be performing robustly.

Sudangrass will again be planted at the DREC test site in 2013. The project team expects to be able initiate automated operations in March of 2013.

#### REFERENCES

Bali, K.M., Hanson B.R., and Sanden B.L. (2010). "Improving Flood Irrigation Management in Alfalfa". *Proceedings, 2010 California Alfalfa and Forage Symposium and Corn/Cereal Silage Conference, Visalia CA, 1-2 Dec, 2010*. UC Cooperative Extension, Plant Sciences Department, University of California Davis, CA 95616

Bali, K., Grismer, M., and Tod, I. (2001). "Reduced-Runoff Irrigation of Alfalfa in Imperial Valley, California." *Journal of Irrigation and Drainage Engineering*, 127(3), 123–130.

Gill, T. and Niblack, M. (2009). "Flow measurement with Long-Throated Flumes Under Uncertain Submergence". *US Bureau of Reclamation Hydraulics Laboratory Publications*. PAP-987.

Grismer, M. E. and Tod, I. C. (1994). "Field Procedure Helps Calculate Irrigation Time for Cracking Clay Soils" *California Agriculture*, 48(5), 33-36.

# ON-FARM IRRIGATION EFFICIENCY IN NEW MEXICO'S LOWER RIO GRANDE

Rasool Ahadi<sup>1</sup>  
Zohrab Samani<sup>2</sup>  
Rhonda Skaggs<sup>3</sup>

## ABSTRACT

On-farm irrigation efficiency, defined as the ratio of water consumed by a crop to water applied to the crop, is an important indicator of irrigation system performance. High irrigation efficiencies in agriculture indicate that much of the water applied to a field actually contributes to crop production. Low irrigation efficiencies may mean that a large portion of applied water is lost for crop production, although the water may contribute to aquifer recharge or be used downstream. Irrigation efficiency is used in economic analysis when selecting an irrigation system design and in irrigation management. Estimates of irrigation efficiency are also used in water rights adjudication and administration, with decrees and policy decisions frequently founded on single values of on-farm efficiency which are assumed to represent conditions on dozens or hundreds of fields. Measuring on-farm irrigation efficiency on multiple farms throughout a basin is time consuming and costly. However, single value assumptions of on-farm irrigation efficiency are legally and hydrologically risky, and do not capture real-world spatial and temporal variability in on-farm irrigation conditions.

This paper describes a process to evaluate on-farm irrigation efficiency in New Mexico's Lower Rio Grande (LRG) watershed using a combination of remote sensing and ground level measurements. On-farm irrigation efficiency was evaluated for three major crops in the LRG. The results of on-farm irrigation efficiency evaluation of 152 alfalfa fields, 189 pecan fields and 38 cotton fields showed that the average on-farm irrigation efficiency was 64%, with on-farm irrigation efficiency values ranging from 11% to 95%.

## INTRODUCTION

This study involved three major steps. The first step was to estimate alfalfa, pecan, and cotton evapotranspiration (ET) on LRG fields in 2008 using the Regional ET Estimation Model (REEM) (Samani et al. 2009; Samani et al. 2007a; Samani et al. 2006). The second step was to estimate groundwater and surface water applied to individual LRG fields or orchards in 2008. The third step was calculation of on-farm irrigation efficiencies for individual fields or orchards. The three stages of the study are described below.

---

<sup>1</sup> Former Graduate Student, Civil Engineering, New Mexico State University, Las Cruces, NM, USA.

<sup>2</sup> Professor, Civil Engineering, New Mexico State University, Las Cruces, NM, USA, zsamani@nmsu.edu.

<sup>3</sup> Professor, Agricultural Economics, New Mexico State University, Las Cruces, NM, USA, rskaggs@nmsu.edu.

### Remotely Sensed Estimation of Field-Level ET

The Regional ET Estimation Model (REEM) was used to calculate daily ET for various agricultural fields in the LRG in 2008. REEM is based on the surface energy balance similar to that presented by Bastiaanssen (1995) and Allen, Tasumi, and Trezza (2007) with the latent heat flux (LE) determined as a residual of the surface energy equation:

$$LE = R_n - G - H \quad (1)$$

where, LE is the latent heat flux,  $R_n$  is the net radiation flux at the surface, G is the soil heat flux and H is the sensible heat flux .

Daily net radiation over the crop canopy was calculated using methodology developed by Samani et al. (2007b) as:

$$R_n = R_{ni} \left( \frac{R_s}{R_{si}} \right) \left( \frac{T_a}{T_i} \right)^4 \quad (2)$$

where,  $R_n$  is the daily net radiation in MJ/m<sup>2</sup>/day,  $R_{ni}$  is instantaneous net radiation (W/m<sup>2</sup>),  $R_s$  is daily short wave solar radiation (MJ/m<sup>2</sup>/day),  $R_{si}$  is the instantaneous short wave solar radiation (W/m<sup>2</sup>),  $T_a$  is average daily temperature in Kelvins (K), and  $T_i$  is the instantaneous air temperature (K).

Instantaneous net radiation ( $R_{ni}$ ) was calculated by subtracting all outgoing radiant fluxes from all incoming radiant fluxes as described in the following equation

$$R_{ni} = (1 - \alpha)R_{si} + RL \downarrow - RL \uparrow - (1 - \epsilon_o)RL \downarrow \quad (3)$$

where,  $RL \downarrow$  is instantaneous incoming long wave radiation (W/m<sup>2</sup>),  $RL \uparrow$  is instantaneous outgoing long wave radiation (W/m<sup>2</sup>),  $\alpha$  is surface albedo (dimensionless), and  $\epsilon_o$  is surface emissivity (dimensionless).

The instantaneous sensible heat flux ( $H_i$ ) was calculated by combining the aerodynamic equation with Monin-Obukhov similarity theory. The aerodynamic equation

$$H_i = \rho_a C_p \frac{dT}{r_{ah}} \quad (4)$$

where,  $\rho_a$  is the air density (kg/m<sup>3</sup>),  $C_p$  is specific heat of air (1004 J/kg/K), dT is the difference between aerodynamic surface temperature and the air temperature (K),  $r_{ah}$  is

the aerodynamic surface resistance.  $dT$  is calculated using a linear function described by Bastiaanssen (1995):

$$dT = aT_s + b \quad (5)$$

where,  $a$  and  $b$  are calibration constants that are empirically determined on daily basis by using reference extreme points on the ground. Calibration of this equation was accomplished using two points on the ground where  $dT$  values can be calculated from sensible heat ( $H_i$ ) fluxes using the aerodynamic equation. In this study, two sensible heat values were used. One sensible heat value was measured over a pecan orchard using a one-propeller eddy covariance (OPEC) system. The orchard was a mature, well-watered pecan orchard which extended more than five km in the predominant wind direction.

The other sensible heat value was estimated for a dry fallow field with no vegetation by setting instantaneous latent heat ( $LE_i$ ) equal to zero and estimating instantaneous  $R_{ni}$  and ground flux  $G_i$ . The  $H_i$  value for the dry field was then calculated as a residual of the energy balance as:

$$H_i = R_{ni} - G_i \quad (6)$$

The instantaneous ground flux ( $G_i$ ) was estimated using an equation developed by Samani et al. (2006) where the ratio of  $G_i$  to  $R_{ni}$  is calculated as a function of Normalized Difference Vegetation Index (NDVI):

$$\frac{G_i}{R_{ni}} = 0.26e^{(-1.97NDVI)} \quad (7)$$

Daily ET and crop coefficient ( $K_c$ ) were calculated for crops in the LRG watershed using 11 satellite images from Landsat-5 and Landsat-7 during 2008. A crop classification survey conducted by the New Mexico OSE in 2008 made it possible to calculate crop ET for individual fields throughout the basin.

Daily ET and  $K_c$  values were developed for each pixel for the days in which satellite images were available. The daily  $K_c$  values combined with daily standardized reference  $ET_{sz}$  were used to interpolate  $K_c$  values and to calculate daily ET for each pixel. The ET values for each pixel were then integrated within each shape files representing a field, to calculate average ET of each field for each day of the growing season. The ET values for the growing season were summed to calculate seasonal ET values for each field. Using these procedures, growing season ET was estimated for 751 alfalfa fields, 1375 pecan orchards, and 577 cotton fields in the LRG in 2008.

### Calculation of Water Deliveries

Groundwater pumping records from the New Mexico Office of the State Engineer (OSE) and surface water delivery records from the Elephant Butte Irrigation District (EBID) provided data for water applied on LRG farms. Fields receiving water from one or more wells serving other fields or fields combined with other parcels in irrigation district records were excluded from the data because it was impossible to determine the amount of water applied to a specific parcel of land. Segregated fields with dedicated or unique water delivery data were matched to field-level ET estimates for the same fields. The study found 152 alfalfa fields, 189 pecan orchards, and 38 cotton fields with groundwater and/or surface water delivery data that could be isolated to only one field or orchard.

### Calculation of On-Farm Irrigation Efficiencies

Farm-level irrigation efficiency calculations were performed for the 152 alfalfa fields, 189 pecan orchards, and 38 cotton fields with dedicated irrigation wells and /or unique EBID water delivery records. These are the three primary LRG crops and comprise about 80% of LRG irrigated acreage.

On-farm irrigation efficiency for individual fields or orchards was calculated using the equation

$$\text{Eff} = (\text{ET} - \text{Re}) / \text{FD} \quad (8)$$

where Eff is on-farm irrigation efficiency, ET (mm) is seasonal evapotranspiration estimated using the procedures outlined above, Re is effective precipitation during the growing season, and FD is field delivery (e.g., the sum of applied groundwater and applied surface water).

Effective precipitation was calculated monthly for each field using monthly ET and monthly precipitation values for each field based on an equation provided by USDA-SCS (1967)

$$\text{Re} = 25.4x(0.70917[Rt / 25.4]^{0.82416} - 0.11556)x(10^{0.02426(\frac{\text{ETm}}{25.4})}) \quad (9)$$

where Re is effective monthly precipitation in mm, Rt is total monthly precipitation in mm and ETm is cumulative monthly evapotranspiration in mm. If rainfall (Rt) was less than 1.85 mm, Re was set equal to zero. The net irrigation application was assumed to be 76 mm (3 inches). To calculate the FD, groundwater pumping records from the OSE were combined with EBID surface water delivery records for individual fields or parcels.

## RESULTS

Table 1 shows the range of on-farm irrigation efficiencies and average on-farm irrigation efficiencies for alfalfa, pecans, and cotton fields in the LRG in 2008.

Table 1. Summary of average seasonal irrigation efficiency for alfalfa, pecans, and cotton, New Mexico's Lower Rio Grande Valley, 2008.

Crop	Estimated Irrigation Efficiency (%)		Number of fields
	Range	Average	
Alfalfa	11.0 – 95.0	65.1	152
Pecans	14.5 – 95.0	59.7	189
Cotton	11.0 – 95.0	76.3	38

Examination of individual LRG fields in the study area reveal that low irrigation efficiency is often associated with sandy soil, long runs, low flow rates, undersized turnouts, and poor irrigation management. However, high irrigation efficiency values for LRG fields do not necessarily reflect good water management, because they are often the result of deficit irrigation (Al-Jamal, Sammis and Jones. 1997) and unaccounted for groundwater contribution to ET. Previous research in the region has found little correlation between irrigation efficiency and quality of overall pecan orchard management (Sammis, Mexal and Miller. 2004).

The weighted average (by land area) farm-level irrigation efficiency for all three LRG crops in 2008 was 64%. By comparison, Wilson (1998) estimated 60% average on-farm irrigation efficiency in the region, using cropping pattern data, estimated consumptive use, and on-farm water delivery records. In this study, we also estimated weighted average LRG irrigation efficiencies for 2010 and 2011 using the same procedures outlined above for 2008. Average seasonal irrigation efficiencies for the three crops were 66% and 65% for 2010 and 2011, respectively.

## DISCUSSION AND CONCLUSION

The results of this study show that average on-farm irrigation efficiency in the LRG basin is between 64-66% with average of 64.7%. While the average on-farm efficiency is within the range of what can be expected from surface irrigation techniques, there is significant spatial variability in irrigation efficiency between fields and farms. The low efficiency values can be attributed to design as well as management factors; and high efficiency does not necessarily imply a well-managed field or orchard.

The LRG basin is currently going through water rights adjudication. A recent agreement and subsequent court order have established a farm delivery requirement (FDR) of 4.5 acre-ft per acre per year, with an assumed consumptive irrigation requirement (CIR) of 4.0 acre-ft per acre per year for all crops. Thus, the assumed on-farm irrigation efficiency is 88.9%. Irrigators also have the opportunity to claim an FDR of up to 5.5 acre-ft per acre per year if they can prove the historically higher water use. For farmers who intend to prove up the 5.5 FDR, the assumed on-farm irrigation efficiency is 72%. Neither of

these on-farm irrigation efficiencies is based on science or actual research. The CIR assumptions are also based on theoretical estimates of water use by healthy, disease-and-insect free, actively growing, well-watered, and overall well-managed crops produced under near-optimal conditions. These conditions, and the associated CIRs, characterize very few LRG fields and orchards (Skaggs et al. 2011; Samani, Skaggs and Longworth 2012). Essentially, LRG adjudication and water policymaking are being founded upon unreliable and unrealistic estimates of all the components used in measuring on-farm water use.

Documenting irrigation efficiency across a watershed provides a powerful tool for economic analysis of alternative irrigation and water policy schemes. Understanding irrigation efficiency within the LRG also has significant implications in defining adjudicated water duties and long term administration of water resources. As water becomes more valuable and scarce, some farmers will seek to irrigate more efficiently. The current average on-farm irrigation efficiency of 64% shows there is significant potential for improving on-farm efficiencies, and government supported cost-sharing conservation programs such as the Environmental Quality Incentives Program (EQIP) support investments in technologies that do so.

The results of this study indicate that the potential exists for LRG farmers to push on-farm efficiency up to 90-95% under different management scenarios or in response to economic incentives. This means that the current annual LRG depletion of approximately two acre-ft per acre has the potential to more than double with improved on-farm irrigation efficiency. Such an increase in depletion, due to technology and management changes, would completely disrupt the current hydrologic balance of the LRG basin and threaten sustainable groundwater supplies.

Reality-based water policymaking requires broad-scale, reality-based estimates of farm-level crop ET and farm-level irrigation efficiency. Remote sensing makes it possible to estimate irrigation efficiency on hundreds of fields and farms, and thus reflect the diverse conditions which characterize real-world crop production. The result is improved water resource accounting, accountability, and sustainability.

## REFERENCES

- Al-Jamal, M., T.W. Sammis and T. Jones. 1997. Nitrogen and chloride concentration in deep soil cores related to fertilization. *Agricultural Water Management* 34(1):1-16.
- Allen, R.G., M. Tasumi and R. Trezza. 2007. Satellite-Based Energy Balance for Mapping for Evapotranspiration with Internalized Calibration. *ASCE J. Irrig. and Drain. Engrg.* 133(4): 380-394.
- Bastiaanssen, W.G.M.. 1995. Regionalization of surface flux densities and moisture indicators in composite terrain: A remote sensing approach under clear skies in Mediterranean climates. Ph.D. dissertation, Landbouwniversiteit te Wageningen, The

Netherlands. Published as Report 109 of DLO Win and Staring Centre, Wageningen, The Netherlands.

Samani, Z., A.S. Bawazir, M. Bleiweiss, R. Skaggs and T. Schmugge. 2006. Estimating riparian ET through remote sensing. American Geophysical Union Fall Meeting, San Francisco, CA, Dec. 8, 2006.

Samani, Z., A.S. Bawazir, R. Skaggs, M. Bleiweiss, A. Piñon and V. Tran. 2007a. Water use by agricultural crops and riparian vegetation: An application of remote sensing technology. *J. of Contemporary Water Research & Education* 137: 8-13.

Samani, Z., A.S. Bawazir, M. Bleiweiss and R. Skaggs. 2007b. Estimating net radiation over vegetation canopy. *ASCE J. Irrig. and Drain. Engrg.* 133(4): 291-297.

Samani, Z., A.S. Bawazir, M. Bleiweiss, R. Skaggs, J. Longworth, V.D. Tran and A. Piñon. 2009. Using Remote Sensing to Evaluate the Spatial Variability of Evapotranspiration and Crop Coefficient in the Lower Rio Grande Valley, New Mexico. *Irrigation Science* 28:93-100.

Samani, Z., R. Skaggs and J. Longworth. Forthcoming 2013. Alfalfa Water Use and Crop Coefficients across the Watershed: From Theory to Practice. *Journal of Irrigation and Drainage Engineering*. Available online:  
<http://ascelibrary.org/doi/pdf/10.1061/%28ASCE%29IR.1943-4774.0000549>.

Sammis, T.W., J.G. Mexal and D. Miller. 2004. Evapotranspiration of flood-irrigated pecans. *Agricultural Water Management* 69(3): 179-190.

Skaggs, R., Z. Samani, A.S. Bawazir and M. Bleiweiss. 2011. The Convergence of Water Rights, Structural Change, Technology, and Hydrology: A Case Study of New Mexico's Lower Rio Grande. *Natural Resources Journal* 51(1): 95-117.

United States Department of Agriculture, Soil Conservation Service, Engineering Division. 1967. *Irrigation Water Requirements*, Technical Release No. 21, revised 1970.

Wilson, B.C. 1998 (8 April). *Quantification of irrigation water requirements Lower Rio Grande River Basin in Dona Ana and Sierra Counties, New Mexico*. New Mexico Office of the State Engineer.



# UNIQUE REPLOGLE FLUME INSTALLATIONS AT THE TRUCKEE CARSON IRRIGATION DISTRICT

Stuart Styles<sup>1</sup>  
Brandon Downing<sup>2</sup>  
Walter Winder<sup>3</sup>

## ABSTRACT

The Water Measurement Program (WMP) for Truckee Carson Irrigation District (TCID) began in 1997, when the Irrigation Training and Research Center (ITRC) of Cal Poly State University was asked to develop a volumetric measurement plan for TCID, funded by the U.S. Bureau of Reclamation, Mid-Pacific Region. This program was intended to develop and install reasonably accurate turnout delivery measurement techniques in the district. As part of the WMP, TCID was required to install a number of new open-channel measurement devices. TCID opted for the Replogle flume as its primary flow measurement device using the newly developed WinFlume computer program.

A few key problems prevented TCID from using the typical Replogle flume design that is used in most irrigation districts. For example, the majority of flow measurement sites were to be installed in earthen channels. In addition, the head loss available at each of the sites was relatively small for this type of structure. This required a new design where the cross section and the ramp portion of the flume had to be incorporated in the same construction package. The process used in the design and the unique aspects of construction used on these projects are documented in this paper.

## INTRODUCTION

With demand on worldwide water supplies continually increasing, it is necessary to find ways to both improve the efficiency of its use as well as promote conservation. In order to achieve these simultaneous goals, good water management is required that relies on effective and practical flow measurement. Flow measurement in canals can be a complicated problem that is often solved with the use of critical-flow devices. These devices measure the flow in sections of the canal that have been structured to create critical flow (Clemmens et al. 2001). Critical flow is maintained by assuring that any changes downstream of the critical flow point will not affect the upstream head. This allows the flow rate through the control section to be computed as a function of the upstream head (Clemmens et al. 2001). Many types of critical-flow devices have been utilized for decades, including sharp-crested weirs, broad-crested weirs, and different types of flumes. Some devices are better than others; one particularly effective device is the Replogle flume, technically known as a broad-crested weir but known in different

---

<sup>1</sup>Professor and Director, Irrigation Training and Research Center (ITRC). California Polytechnic State University (Cal Poly). San Luis Obispo, CA 93407-0730. (805) 756-5555. sstyles@calpoly.edu

<sup>2</sup>Engineering Technician, ITRC. Cal Poly. San Luis Obispo, CA 93407-0730. bpdowin@calpoly.edu

<sup>3</sup>Deputy District Manager, Truckee-Carson Irrigation District (TCID). Fallon NV 89406. (775) 423-2141. walt@tcid.org

regions as a “ramp flume”, “ramp weir”, “BCW”, “RBC flume” (short for the Replogle-Bos-Clemmens flume), “Burton flume”, or “long-throated flume”. The senior author worked with Dr. Replogle when the original design was developed and has used the term “Replogle” over the course of 30 years’ experience with these flumes and over 2,500 installations.

Some flow measurement devices are found to be relatively expensive to maintain, difficult to install, or costly to construct. Others have problems with accuracy. The hydraulic properties of the Parshall flume, for example, cause the accuracy of the measured flow rate to be greatly affected by the accuracy of installation and the constructed dimensions. Many of these devices are laboratory calibrated, so construction or installation errors cannot be easily evaluated, causing the accuracy of the measured flow rate to vary by installation.

### **Discussion of Advantages and Placement of Flumes**

The development of the Replogle flume has effectively addressed many of the problems stated above (Clemmens et al. 1984). Clemmens et al. (1984) describes the recommended design and installation of Replogle flumes as follows:

(1) The discharge for any prismatic-shaped flume can be computed from existing hydraulic theory to within +/-2% of the true discharge; (2) the flume cross section can have a wide variety of shapes; (3) head loss over the flume for a unique (upstream) head-discharge relationship is the lowest of known devices and can be estimated with sufficient accuracy from existing hydraulic theory; and (4) this type of flume is presently the least expensive structure that can measure flow accurately under similar hydraulic conditions.

In general, flow measuring flumes consist primarily of a contraction of the side walls, with the flume bottom being slightly lower, on-grade, or slightly higher than the existing channel bottom. For monitoring flow in irrigation canals, the writers have found that a bottom contraction has many advantages over the side contraction. A flume with a bottom contraction resembles a broad-crested weir but is shaped in such a way that it acts hydraulically like a long-throated flume. The advantages of this “modified” broad-crested weir over other long-throated flumes are: (1) Construction of a bottom sill is much simpler and less expensive than the construction of side walls; (2) the bottom width of the flume is much wider and thus construction tolerances on width are much greater; (3) the wider bottom provides good sediment transporting capabilities; and (4) the absolute head loss over the structure required for modular flow is low. If the water level downstream from the structure does not affect the head-discharge relationship, the flow is said to be modular. (Clemmens et al. 1984)

Clemmens et al. (1990) performed an experiment “to determine the effects of entrance and exit conditions on the discharge and required energy loss.” Flumes were tested with different entrance and exit ramp slopes, and different  $H_1/L$  ratios, where  $H_1$  is the sill

referenced energy head and  $L$  is the length of the throat. It was concluded that entrance slopes of 2:1 and 3:1 resulted in errors of 1-2%. These errors can be improved if the approach ramp at the throat was rounded. The necessity of having an exit ramp depended on the  $H_1/L$  ratio. Ratios up to 0.4 resulted in errors less than 1% using exit ramp slopes of 0:1 and 6:1. The error in discharge measurement increased at ratios higher than 0.4 for both exit ramp slopes; however, the 6:1 exit ramp slope had a lower percent error than the 0:1 exit ramp slope. Based on these tests and experience, the ITRC recommends to irrigation districts a standard design of a 3:1 approach slope with rounded entrance conditions and a 6:1 exit ramp slopes.

The placement of a Replogle flume in a canal is crucial for accuracy. Clemmens et al. (1987) developed a Froude number approach to designing flow measurement devices. This approach concentrated on “providing an appropriate Froude number in the approach channel for the passage of sediment and for producing a stable readable water surface at the head measurement station.” Three basic design requirements for critical-depth measuring devices need to be met for this approach to work:

- (1) The flume should provide enough constriction to flow so that it is unaffected by downstream backwater effects, but not so much that the upstream water level is too high at maximum flow;
- (2) the upstream channel Froude number should be high enough so that upstream water levels can be accurately measured;
- and (3) the flume should have acceptable sensitivity to flow changes and provide sufficient accuracy. (Clemmens et al. 1987)

The target value for the entrance condition is to have the Froude number be less than 0.5.

### **WinFlume Software Program, Version 1.06.0004**

The USBR developed software to design, analyze and run feasibility tests on proposed Replogle flumes. WinFlume is a Windows-based program that can be downloaded from the USBR’s website. Primary funding for the software was provided by the USBR’s Water Conservation Field Services Program. This software is essential to optimizing the Replogle flume installation and operation. With the development of the WinFlume program, users are able to create possible flume situations under various conditions. The ease of use and flexibility in design are some WinFlume’s advantages. Further design capabilities are discussed in the following methodologies (Wahl 2012).

### **TCID’s Use of Replogle Flumes**

Since 1997, TCID has installed many flow measurement devices in its canal systems, following the recommendations of the United States Bureau of Reclamation’s (USBR) *Water Measurement Manual*. The 3<sup>rd</sup> edition of the manual, published in 2001, states:

Long-throated flumes are coming into general use because they can be easily fitted into complex channel shapes as well as simple shapes. Long throated flumes have many advantages compared to other measuring devices, including Parshall

flumes. Long-throated flumes are more accurate, cost less, have better technical performance, and can be computer designed and calibrated. Thus, long-throated flumes are preferred over Parshall flumes for new installations. (USBR 2001)

In 2009, Dr. John Replogle, a consultant and retired USDA/ARS flow measurement expert, Tracy Vermeyen of the USBR Technical Service Center (TSC), and Dr. Charles Burt of ITRC, went to Fallon, Nevada to evaluate the Water Measurement Program for TCID. Table 1 shows the number and types of flow measurement devices that have been installed in the TCID service area as of 2009. The Replogle flume has been the most frequently used flow measurement device since the WMP was started. The conclusion from an independent review of these flow measurement experts was that “the broad-crested weir designs of TCID are of excellent design and construction overall” (ITRC 2010). Currently, in 2013, over 100 Replogle flumes have been installed in TCID canals.

Table 1. Number of Flow Measurement Devices Installed in TCID (ITRC, 2010)

Type of Measurement Device	# of Devices in 2009	Datalogger?
Broad-crested weir (a.k.a. “ramp”, “Replogle Flume”)	53	Yes
Weir	20	Some
Trapezoidal flume	13	Yes
Other (Parshall flume, rated pipe or section, propeller meter in a pipe)	8	Some

### ITRC METHODOLOGY

The Cal Poly ITRC developed a report on the basic design of Replogle flumes as a guideline for irrigation districts. According to this report, “one of the primary advantages of the Replogle flume is the capability to custom design and calibrate structures for unique operational and site requirements using the Windows-based computer program WinFlume” (ITRC 2002). The report provides a list of the steps for properly constructing a Replogle flume. These steps are summarized below.

#### Definition of the Existing Channel Conditions

The first design step is to select the proper site and determine the field conditions under which the flume must operate. The following characteristics of the installation should be established through site surveying and a thorough review of the conditions at high and low flows:

- Range of flows to be measured
- Freeboard requirement at maximum flow
- Access to the site for construction and subsequent measurement
- Influence of any downstream control structures, if any
- Uniform flow, Froude number
- Lining material and material used for flume construction (roughness coefficient)
- Cross-sectional dimensions and side slope

For design purposes for this size flume, it is usually necessary to measure the cross section of the canal at about four locations: the site where the flume will be, one location upstream of the site about 50 ft, and two downstream locations (at about 50 ft intervals). The survey data required at each location includes top of left bank, top of left concrete, invert at left toe, invert at centerline, invert at right toe, top of right concrete, and top of right bank.

In addition, the water level elevation in the canal should be surveyed at 100 ft intervals, for approximately 200 ft upstream and 300 ft downstream of the proposed site. This needs to be done at the maximum and minimum flows, with estimates made of the approximate flow rates.

The upstream and downstream channels should be investigated for possible flow restrictions including culverts, check structures, turnouts, etc. that might affect flows. The size and locations of these structures should be obtained.

It is critical that the backwater effects of downstream control structures, if any, be evaluated at the proposed flume location. To determine the potential impacts from submergence, the water level at the nearest downstream control structure should be raised to its highest point, while at low flow conditions, and then survey data of the water level obtained at the flume site.

### **Recommended Site Conditions, Location and Specifications**

Figure 1 shows a possible location for a Replogle flume. The following conditions should be met for accurate flow measurement:

- The Froude number of the approaching channel should not exceed 0.5. A Froude number closer to 0.2 is preferred.
- Note:  $H_{1\max}$  is the sill-referenced energy head at maximum flow
- There should be no high turbulent flow upstream of the structure for a distance of  $30H_{1\max}$

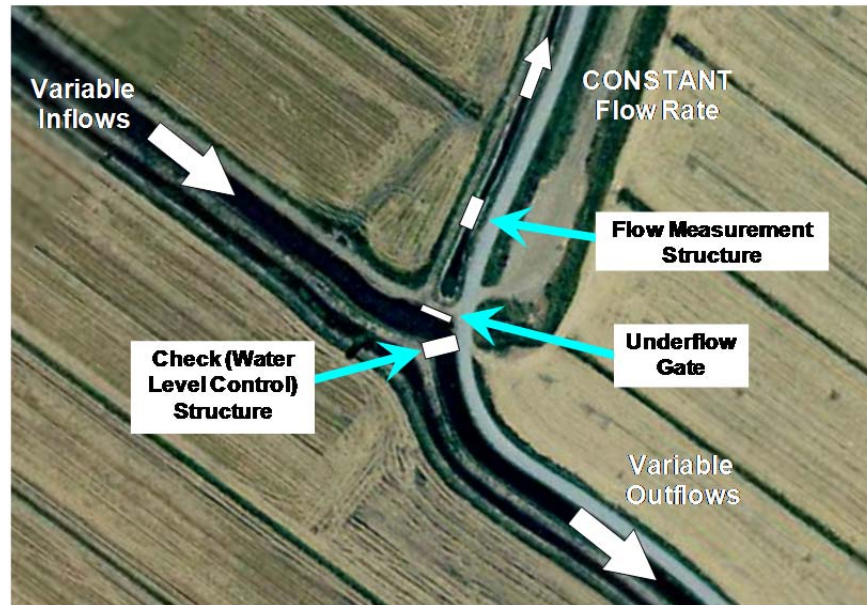


Figure 1. Customer (or lateral) turnout location for a Replogle flume

Method of contraction. Options of contractions include a bottom-only contraction or a side contraction using a change in slope of the vertical walls. The size and dimensions of these contractions can be determined using the WinFlume program. In rare cases, a side and a bottom contraction can be used. These types of designs are discouraged due to the constructability issues with a more complex cross-section.

Suggested flume dimensions. In order to properly design the length of the approach channel, converging transition, throat, and diverging transition, the sill-referenced energy head ( $H_1$ ) at maximum flow must be known. Once all of the parameters for the design are known, data can be entered into the WinFlume program for a design. When designing the flume in WinFlume, using a sill height of half the normal flow water depth is a good place to start. The height can be adjusted as long as a check for adequate submergence protection is done.

Head loss design criteria. Minimizing the head loss is a key issue for flow measurement in canals. Having a contraction helps avoid submergence but there cannot be so much contraction that the canal overtops. The amount of contraction needed depends on the height of the sill of the Replogle flume. It is important to verify that the design does not have any design errors flagged in the WinFlume software.

Head measurement method. Head measurement should be done with electronic water level sensors that are accurate within  $\pm 1/16$  inch. This is easily achievable with the availability of numerous pressure transducers and other measurement devices.

Flush pipe. A flush pipe should be installed at the bottom of the Replogle flume to prevent pooling when the canal is drained. The pipe should be flush with the concrete and be at least 4" in diameter for flows above 5 cubic feet per second. Typically, a PVC pipe is cut in half and two drains are installed.

Staff gage. WinFlume is able to print out a full scale staff gage that can be transferred to metal or plastic so it can handle outdoor conditions. A custom gage can be used or a simple staff gage can be used. The key to improving the volumetric accuracy on an installation is to have the water level monitored with a logger.

Verification of as-built dimensions. After the flume has been constructed, the as-built dimensions must be precisely measured and entered back into WinFlume so it can generate the proper discharge tables with the as-built dimensions.

ITRC has been recognized by Dr. Replogle as one of the key organizations to help with the field implementation of the Replogle flume measurement device. ITRC continues to recommend this device to irrigation districts in the US and internationally if the site conditions are appropriate.

### **TCID METHODOLOGY**

The Truckee Carson Irrigation District (TCID) has developed its own detailed protocols in designing and constructing Replogle flumes in its canals. Their protocols are outlined in the following paragraphs.

#### **Education of District Growers**

The first step of the process was that the district had to convince growers that Replogle flumes are a viable flow measurement device. TCID began by explaining to the growers how they work. This education of the growers on the meters has been the key to the successful acceptance of this device as a standard, robust measurement device. TCID staff has to be able to explain the device as a flow rate measurement device and also how the loggers allow TCID to record the flow rate over the time of an irrigation event.

#### **Meter to Measure Flow Rate**

Replogle flumes work as a flow meter by creating critical flow conditions as water passes through the sill of the flume. Critical flow condition means that for a single depth, there is a single flow rate associated with that depth. The speed of the water accelerates through the throat of the flume until critical flow is achieved at the sill of the flume. WinFlume is used to design the size of the flume and after it is constructed, the as-built dimensions are entered in the program and a staff gage is generated with the zero reference being the top of the sill. This staff gage can either have the flow rate measurement or the water level above the sill on it. If it is the water level above the sill, WinFlume also generates rating tables that give the flow rate over the flume with a given height that is read from the staff gage.

#### **Construction to Record Events**

TCID has a specific construction method for the Replogle flume. This paper focuses on the earth-lined canal application. WinFlume is used to determine the required

dimensions of the flume for the given application before construction is started. The first part of construction is to lay the foundation of the contraction. When the foundation is poured, vertical steel rebar is left extruded out of it to be used when the walls are poured. After the contraction section is built, water is run through it and the data set is re-run to ensure that putting a flume in the contraction will work. The Replogle flume is then constructed using the dimensions from WinFlume. As-built dimensions are then verified and the final calibration of the flume is done in WinFlume.

The installation process is described in detail below:

1. A detailed site evaluation is performed where the flume will be installed. The site evaluation consists of site survey data, high and low flows in the canal throughout the season, and the high water mark in the canal. All of these values are used to design an appropriate Replogle flume using WinFlume (Figure 2).

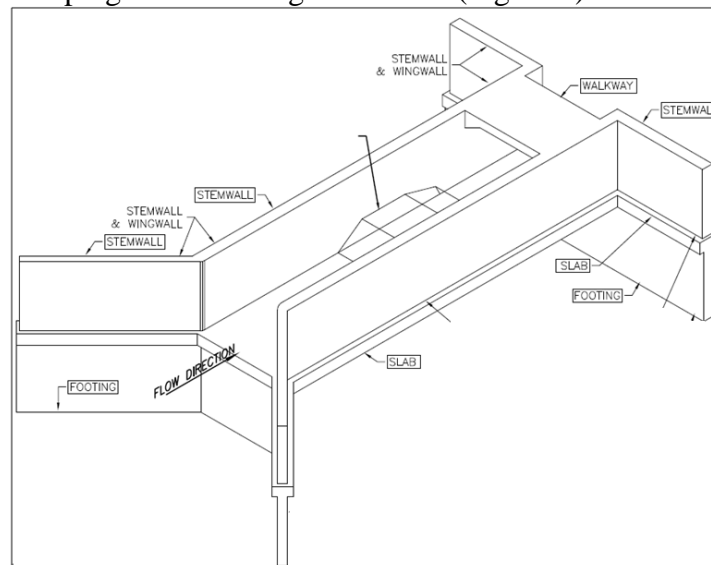


Figure 2. TCID's standard design for Replogle flumes

2. Cross section of the structure is built. TCID uses a set of standard-sized cross sections. Depending of the size and capacity of each canal, the widths and lengths of the cross sections range from 2ft to 10ft and 12ft to 36ft, respectively.
3. After cross section construction, water is run through the canal and the tail water data is recorded. This step is to ensure that putting a Replogle flume there will actually work. This is a **KEY** step in the process.
4. The tail water data obtained in step 3 is used to adjust the original dimensions of the Replogle flume in WinFlume, to make sure the flume will not submerge and to ensure accuracy of the flume.
5. After the flume has been carefully and accurately designed in WinFlume, the flume itself is finally constructed inside the cross section. This process takes TCID about 3-5 days. The canal must be drained and the cross section prepared to lay the concrete

forms for the flume, then the concrete is poured. Figures 3 and 4 show the construction of a cross section.



Figure 3. Framework and steel for the foundation



Figure 4. Vertical steel rebar to be used for the walls of the flume contraction

6. The as-built dimensions are measured and entered into WinFlume to obtain the proper staff gages to be used for the flume.
7. A final calibration is done and the accuracy of the flume is checked via current metering.



Figure 5. Standard TCID Replogle flume



Figure 6. Standard TCID Replogle flume with water flowing

## DISCUSSION

WinFlume. The USBR program has been a tremendous aid to the successful implementation of the Replogle Flume. The program is regularly updated and improved to help even the novice designer.

Water Measurement Program Review. As mentioned previously, Dr. John Replogle, Tracy Vermeyen, and Dr. Charles Burt visited TCID in 2009 to evaluate the devices that had been installed due to the WMP. During this trip 30 measurement sites were randomly selected and these experts evaluated their accuracy. They determined that “the existing Water Measurement Program, with some modifications, appears to be functional, reasonably accurate, and reasonably cost-effective to administer” (ITRC 2010). Some of these proposed modifications included:

- Develop a standardized procedure for verifying flow rates.
- Re-check the zero elevations/settings for its data collection at flumes and weirs, where errors are greater than 2%.

## CONCLUSIONS

In this decade-long project, ITRC and TCID have demonstrated that the Replogle flume is the preferable device for open channel flow measurement for this application. TCID has taken basic knowledge of the ITRC’s recommended flume design and modified it into its own device, fit for the district’s purposes. TCID’s conveyance of material to and education of farmers in the district is commendable. Enabling other entities to properly customize the Replogle flume design is a continuing goal of ITRC.

## REFERENCES

Clemmens, A.J., T.L. Wahl, M.G. Bos, and J.A. Replogle. 2001. *Water Measurement with Flumes and Weirs*. ILRI Publication 58, International Institute for Land Reclamation and Improvement, Wageningen, The Netherlands. 18 p.

Clemmens, A.J., J.A. Replogle, Y. Reinink. 1990. Field Predictability of Flume and Weir Operating Conditions. *Journal of Hydraulic Engineering*. 116:102-118.

Clemmens, A.J., M.G. Bos, and J.A. Replogle. 1987. Contraction Ratios for Weir and Flume Designs. *Journal of Irrigation and Drainage Engineering*. 113:420-424.

Clemmens, A.J., J.A. Replogle, M.G. Bos 1984, Rectangular Measuring Flumes for Lined and Earthen Channels. *Journal of Irrigation and Drainage Engineering*. 110:121-137.

Irrigation Training and Research Center (ITRC). 2002. Basic Design of Replogle Flumes. California Polytechnic State University (Cal Poly), San Luis Obispo, CA

Irrigation Training and Research Center (ITRC). 2010. Truckee-Carson Irrigation District: Water Delivery Measurement Program. California Polytechnic State University (Cal Poly), San Luis Obispo, CA

USBR Water Resources Research Laboratory. 2001. Water Measurement Manual. United States Bureau of Reclamation (USBR), U. S. Department of the Interior.

Wahl, T. L., A. J. Clemmens, J. A. Replogle, Bos, M.G. 2000. Winflume — Windows-Based Software for the Design of Long-Throated Measuring Flumes. 4th Decennial National Irrigation Symposium, ASABE, Phoenix, AZ, 1-9.

Wahl, L. T., A. J. Clemmens, M. G. Bos, J. A. Replogle. 2012. The WinFlume Home Page. US Department of the Interior, USBR.

[http://www.usbr.gov/pmts/hydraulics\\_lab/winflume/](http://www.usbr.gov/pmts/hydraulics_lab/winflume/)

